2013

Behavioural analysis of marine predator movements in relation to heterogeneous environments

Humphries, Nicolas Edmund

http://hdl.handle.net/10026.1/1571

Behavioural analysis of marine predator movements in relation to heterogeneous environments

by

Nicolas Edmund Humphries

A thesis submitted to the University of Plymouth
in partial fulfilment for the degree of

DOCTOR OF PHILOSOPHY

School of Marine Science and Engineering

Faculty of Science

In collaboration with the Marine Biological Association

February 2013

Behavioural analysis of marine predator movements in relation to heterogeneous environments

Nicolas Edmund Humphries

Abstract

An understanding of the spatio-temporal dynamics of marine predator populations is essential for the sustainable management of marine resources. Tagging studies are providing ever more information about the movements and migrations of marine predators and much has been learned about where these predators spend their time. However little is known about their underlying motivations, making it difficult to make predictions about how apex predators will respond to changing environments. While much progress has been made in behavioural ecology through the use of optimality models, in the marine environment the necessary costs and benefits are difficult to quantify making this approach less successful than with terrestrial studies. One aspect of foraging behaviour that has proved tractable however is the optimisation of random searches. Work by statistical physicists has shown that a specialised movement, known as Lévy flight, can optimise the rate of new prey patch encounters when new prey patches are beyond sensory range. The resulting Lévy flight foraging (LFF) hypothesis makes testable predictions about marine predator search behaviour that can be addressed with the theoretical and empirical studies that form the basis of this thesis.

Results presented here resolve the controversy surrounding the hypothesis, demonstrating the optimality of Lévy searches under a broader set of conditions than previously considered, including whether observed Lévy patterns are innate or emergent. Empirical studies provide robust evidence for the prevalence of Lévy search patterns in the movements of diverse marine pelagic predators such as sharks, tunas and billfish as well as in the foraging patterns of albatrosses, overturning a previous study. Predictions from the LFF hypothesis concerning fast moving prey are confirmed leading to simulation studies of ambush predator's activity patterns. Movement analysis is then applied to the assessment of by-catch mitigation efforts involving VMS data from long-liners and simulated sharks.

Contents

Figures

Tables

Acknowledgements

I am very grateful to Professor David Sims for giving me the opportunity to do the work presented in this thesis as part of the Behavioural Ecology group at the Marine Biological Association's Citadel Hill laboratory in Plymouth. David is an enthusiastic and inspirational group leader and I have greatly enjoyed and benefited from our wide-ranging discussions and his much appreciated encouragement. This work has been, and continues to be, both rewarding and enjoyable, and I look forward to our continuing collaboration.

While at the MBA I have been fortunate to work with many talented and knowledgeable people who have helped me considerably with this work and with my own professional development. Some have helped directly, by analysing data, others with helpful discussions, advice, or in feedback that has helped to further the development of the software developed to do much of the analysis in this thesis. The list is long, but in particular I would like to express my thanks to Viki Wearmouth, Jenifer Dyer, Cat Wilding, Stephen Cotterell, David Jacoby, Chris Bird and Lara Sousa.

Author's declaration

At no time during the registration for the degree of Doctor of Philosophy has the author been registered for any other University award without prior agreement of the Graduate Committee.

This study was financed with the aid of a studentship form the Natural Environment Research Council and carried out in collaboration with The Marine Biological Association of the UK.

Relevant scientific seminars and conferences were regularly attended at which work was often presented; external institutions were visited for consultation purposes and several papers prepared for publication.

Publications:

Humphries, N. E., N. Queiroz, J. R. M. Dyer, N. G. Pade, M. K. Musyl, K. M. Schaefer, D. W. Fuller, J. M. Brunnschweiler, T. K. Doyle, J. D. R. Houghton, G. C. Hays, C. S. Jones, L. R. Noble, V. J. Wearmouth, E. J. Southall, and D. W. Sims. 2010. Environmental context explains Lévy and Brownian movement patterns of marine predators. *Nature* **465**:1066-1069.

Humphries, N. E., H. Weimerskirch, N. Queiroz, E. J. Southall, and D. W. Sims. 2012. Foraging success of biological Lévy flights recorded in situ. *Proceedings of the National Academy of Sciences of the United States of America* **109**:7169-7174.

Presentations and Conferences Attended:

Humphries, N. E. and D. W. Sims. 2009. Modelling the movements and behaviour of sharks with Lévy statistics. Comparative Biochemistry and Physiology a-Molecular & Integrative Physiology 153A:S67-S67. SEB Glasgow.

Humphries, N. E., N. Queiroz, G. R. Mucientes, L. L. Sousa, and D. W. Sims. 2011. Assessing capture risk of pelagic fish by satellite-tracked long-line vessels and the effectiveness of Marine Protected Areas. Marine Protected Areas on the high seas, Institute of Zoology, Regents Park, London, NW1 4RY, UK.

Word count of main body of thesis: 66,458

Signed

Date

1 Introduction

The pressing concerns of over-fishing (Garstang 1900, Thurstan *et al.* 2010) and climate change (Brander 2010, Genner *et al.* 2010, Jennings and Brander 2010, Perry *et al.* 2010, Spencer *et al.* 2010) make careful management of the exploitation of marine predator populations increasingly important. Natural fish populations are typically managed as 'stocks', the implication being that stocks form independent manageable units; however fish are known to exhibit complex spatio-temporal dynamics (Block *et al.* 2011) which are likely to blur the boundaries imposed by human social and political institutions (Bailey 1997). For example thornback rays (*Raja clavata*) have been shown to perform seasonal migrations between the Southern North Sea and the Thames estuary, with rays moving into the estuary between March and April to spawn (Hunter *et al.* 2006). Similarly Atlantic cod (*Gadus morhua*) and plaice (*Pleuronectes platessa*) have also been shown to perform long distance seasonal migrations (Hunter *et al.* 2003, Righton *et al.* 2007). Evidence from long-line fisheries has identified sexual segregation of short fin mako sharks (*Isurus oxyrinchus*) at the large-scale in the South Pacific (Mucientes *et al.* 2009), whereas some animals, such as common skate (*Dipturis batis*), exhibit site fidelity to local areas (Wearmouth and Sims 2009). Complex movement dynamics such as these suggest that stocks are far from the independent units that management regimes assume them to be (Sumaila and Huang 2012) and therefore an understanding of the processes that structure natural fish populations is essential both to their sustainable management (Bailey 1997) and for the design of conservation efforts such as marine protected areas (Hyrenbach *et al.* 2000).

In the marine environment, and especially in the open ocean, however, it is difficult to observe individuals or even populations directly with any degree of spatial and temporal accuracy. Consequently much of what has been learnt regarding the large-scale movement of marine predators has been inferred from mark-recapture studies (Stevens 1976, 1990, Queiroz *et al.* 2005). Such studies can only provide information regarding the release and recapture locations and, because the recapture normally occurs via commercial fisheries, these data are known to be prone to significant biases (Bolle *et al.* 2005), furthermore if the fish move beyond the areas being regularly fished then they simply disappear from the study and nothing can be determined or inferred about their movements or distributions. Therefore only superficial knowledge exists concerning the spatio-temporal dynamics of the populations forming managed fish stocks. In addition mark-recapture studies cannot provide any information on the fine-scale movements in which animals are engaged during various behavioural activities such as foraging or diel changes in depth, or about habitat and thermal preferences and so provide little insight into their behavioural ecology. Important questions that have occupied terrestrial ecologists, such as site fidelity, habitat use or optimal foraging strategies have therefore proved much more difficult to study in the marine environment. These studies are further hampered by the dynamic nature of the marine environment which can lead to a patchy and often unpredictable distribution of resources (Zimmerman and Biggs 1999, Seki *et al.* 2001, Zainuddin *et al.* 2006). The first step in gaining a better understanding of how animals respond to this dynamic heterogeneous resource landscape is to gather more detailed information about their movements at all scales by using electronic tags, which now constitutes a thriving research field in itself known as animal biotelemetry or bio-logging (Sims 2010).

1.1 Electronic tags

Recent advances in electronics and miniaturisation of devices have made it possible to produce tags that can be attached to marine fish to measure and record environmental factors such as swimming depth, water temperature and ambient light over extended periods of time. Sea water, being conductive to electricity, makes radio-frequency (RF) transmission impossible over long distances. Therefore in the marine environment three categories of tag can be used: data logging/storage (or archival),

satellite transmitter or acoustic transmitter or transponder. Some examples are shown in Figure 1.

Data storage tags (DSTs) are relatively small, typically 20-30mm in length, and weigh only 1-2g in water. Some of the smallest tags record only pressure (swimming depth) and water temperature, whereas other tags can record depth, temperature and light with more advanced tags also having sensors for measuring magnetic field parameters or 3-axis accelerometers. Data are stored in non-volatile Flash memory until the tag is recovered at which point the data can be downloaded, even if the battery is exhausted. As long as the tag can be recovered then very large data sets of high resolution depth, temperature and light level measurements can be returned. Tags can be attached externally in a variety of ways, depending on the species (or size of the animal) or can be surgically inserted into a fish's peritoneal cavity, for example.

Satellite transmitter tags have the advantage that data can be returned without the need to recover the tag, but have the disadvantage that they only transmit in air, such as when the animal surfaces or when the tag is detached and floats at the surface. This type of tag is generally larger in size than the DSTs and they provide, in general, only low resolution or summary data transmitted via Argos polar-orbiting satellites, they are becoming smaller in size such that a wider range of species can now be tagged. However, these characteristics make them ideal for studying larger pelagic open ocean predators such as sharks and tunas. Satellite tags can be divided into two basic categories; tags that transmit continuously (when at the surface) to the Argos data collection system of satellites are known as Argos satellite transmitters or platform transmitter terminals (PTTs), e.g. SPOT (Smart Position-Only Transmitting) tags; and pop-off satellite-linked archival transmitters (PSATs) that record data for a pre-determined time and then pop-off, rise to the surface and transmit data via the Argos system, e.g. PAT (Pop-up Archival Transmitting) tags by Wildlife Computers. PSAT tags typically record summarised data which are then transmitted on surfacing, however the transmission depends on the serendipitous location of the polar-orbiting satellite and the length, strength and stability of the transmitted message and data are frequently incomplete as a consequence. If a PSAT tag is recovered then the archived data is available for download.

Acoustic transmitter tags produce sound energy that is received via a hydrophone to a decoding receiver. Tags can be tracked in the sea actively by a hydrophone on a ship, or passively by a fixed array of receivers, from which the data are later recovered. Tags (pingers) that generate an acoustic signal (or ping) can be attached to, or be surgically implanted, in fish and enable a receiver to identify the tag/fish and record the time of the ping. Typically an array of receivers is deployed on the surface (in the case of triangulating receivers) or the sea bed (for archival logging devices) to allow research into longer-term patterns of behaviour such as sexual segregation, social networks, migration or site fidelity (Sims *et al.* 2001, Simpfendorfer *et al.* 2002, Sims *et al.* 2006a, Jacoby *et al.* 2010).

A comprehensive review of tags and tagging techniques has been provided by Sims (Sims 2010, Chapter 8, p 351) and of shark tagging studies by Hammerschlag *et al.* (2011).

Figure 1: Example tag designs from Wildlife Computers
Top left Spot5; top right PAT MK-10; bottom TDR-Mk9.

1.1.1 *Horizontal (geographic) data*

It is evident that the types of data measured by tags are dependent on the tag type and that this logistical constraint influences the sorts of biological questions that can

be levelled, and the analyses that can be reliably supported, using such data. In the case of horizontal (geographic) data, the geographic location of a satellite tag using the Argos system is calculated from the Doppler shift in transmission carrier frequency observed by the satellite when the message is received from the transmitter on the tag. The system provides a location class code with each location estimate that indicates the size of the error field, which can range from 500-1500m radius for the lowest class (1) to < 250m for the best class (3). Tags equipped with Positioning System (GPS) receivers are able to encode GPS location data in the Argos message to give a G class message with positional error that can be < 50m depending on how many satellites can be acquired (Hazel 2009). Because locations can only be determined when a satellite passes within range of a transmitter, the number of locations per day is dependent on the satellite coverage, which is itself dependant on latitude. The polar orbiting satellites in the Argos constellation (which are usually satellites with other primary functions, such as the NOAA satellites but which are equipped with the Argos receivers) have best coverage at the poles and worst at the equator and any given satellite can be expected to pass the poles about 14 times per day. The low number of locations per day and the large error fields means that while such data are useful for knowing roughly where the tagged animal was on any given day it is not good enough to allow any investigation into short term behaviour or very fine-scale movements (Bradshaw *et al.* 2007). Even with high resolution location data problems can arise in the detailed analysis of the animal's movements. All recorded location data comprises a series of observed coordinates which approximate the animal's true movement path and the accuracy of a reconstructed (i.e. plotted) path will depend on the sampling frequency, with low sampling rates resulting in simpler paths where more complex behaviour (such as area restricted search) will be poorly represented. In many more recent studies it has become popular to use state-space models and Kalman filters to interpolate what are considered to be the most likely intermediate points along the path (e.g. Royer *et al.* 2005, Tremblay *et al.* 2006). The resulting, smoothed path might appear realistic, however it must be remembered that the interpolated points are simply best guesses and are subject to the parameters used in the state-space model. Consequently these reconstructed paths should, perhaps, be treated with caution.

1.1.2 Vertical (dive) data

DSTs and some satellite tags can store archival data which record a time series of measurements such as depth, light or temperature which are typically made at intervals of between 1 second and 1 hour. Satellite tags usually summarise the data into a series of histograms. While depth is usually recorded at the highest temporal resolution the other metrics, such as temperature, are often recorded at longer intervals (e.g. 5 minutes). Many tags can be configured to record high temporal resolution data for a specified length of time and then a lower rate subsequently, to maximise the overall data recorded by the tag. For instance, although the prime interest might require a few months of high resolution data, if the tag remains attached and the animal active, it is clearly very useful to obtain some lower resolution information over a longer time scale. Tags can usually be configured for different depth ranges, with deeper depths usually requiring some sacrifice of resolution; therefore a tag configured for high resolution (e.g. 4cm depth) will only record to 120m depth, while tags configured to record depths down to 1km or more typically have resolutions of around 0.5m. This is simply a consequence of the number of bits available to store each measurement and the scaling factor used to encode the measured depth value. There is a natural tendency to prefer data with high temporal and spatial resolution. However, very high temporal resolution data (i.e. of the order of 1 second) not only consumes much more of the tag's memory but can result in problems in analysis that are only solved by under-sampling the data (described further in Chapter 2). In fact in many studies comparatively low temporal resolution data is perfectly adequate, as illustrated in Figure 2, where little difference is discernible between data at 5 seconds or 15 minutes, despite the higher resolution requiring 180 times the data.

Although a dive time series is essentially a recording of one dimensional movement, a great deal of useful behavioural information can be obtained from the data using quite straightforward analysis. For example, habitat use, in terms of the water column, can be determined from a time-at-depth analysis. Figure 3 shows a simple histogram of binned depth data that reveals a pattern of habitat use where the animal, a blue shark (*Prionace glauca*), can be seen to spend the majority of its time either at, or just below the surface, or at deeper depths, around 570m. A daily profile of depth use for the same animal reveals diel vertical movements sometimes termed 'migrations' (DVM)

with daytime hours being spent at depth and night time spent near the surface. A daily profile of activity however shows that the animal is generally equally active (in terms of summed vertical displacements per hour) over the whole of the day (Figure 4).

While clearly very valuable, analyses such as these only provide a descriptive representation of some aspects of an animal's behaviour; they provide information on where and when the animal was, but not on what it is doing. In other words, while we might discover that a blue shark spends the daylight hours at depth, we do not know from the dive time series data what behaviour the shark is engaged in, whether it is searching for food (although this is likely), hiding from predators (less likely) or fulfilling some other function such as thermoregulation or searching for mates (see Queiroz *et al.* 2010). The problem of understanding the function or survival value of decisions leading to an observed behaviour has been approached in behavioural ecology through the use of optimality models (Stephens and Krebs 1987). These models are usually defined in terms of currencies, such as time or energy, which are then either maximised or minimised through decisions such as when to leave a prey patch. Typically these decisions are constrained by factors such as the prey handling time, the nutritional content of the prey or even, in some cases, the toxicity of the prey (Barnett *et al.* 2012). Bumblebees, for example, have been shown to adapt how many flowers they visit on a given plant depending on both local nectar availability and the profitability of the individual plant, in a manner that can be modelled well using the marginal value theorem (Dreisig 2012). However it is very difficult to know what currency an animal might be maximising (or minimising), and indeed these currencies and constraints are very difficult to define in the marine environment, even with telemetry devices. Hence, this reduces considerably the applicability of this conceptual framework to free-ranging animals such as marine vertebrates. One recent development in traditional optimal foraging theory that appears more tractable for studying in free-ranging animal behaviour, however, is that of random search strategies, which have been found to be optimal in certain situations. Theoretical and methodological developments in this area have led to an intriguing concept in ecology, the so-called Lévy flight foraging hypothesis.
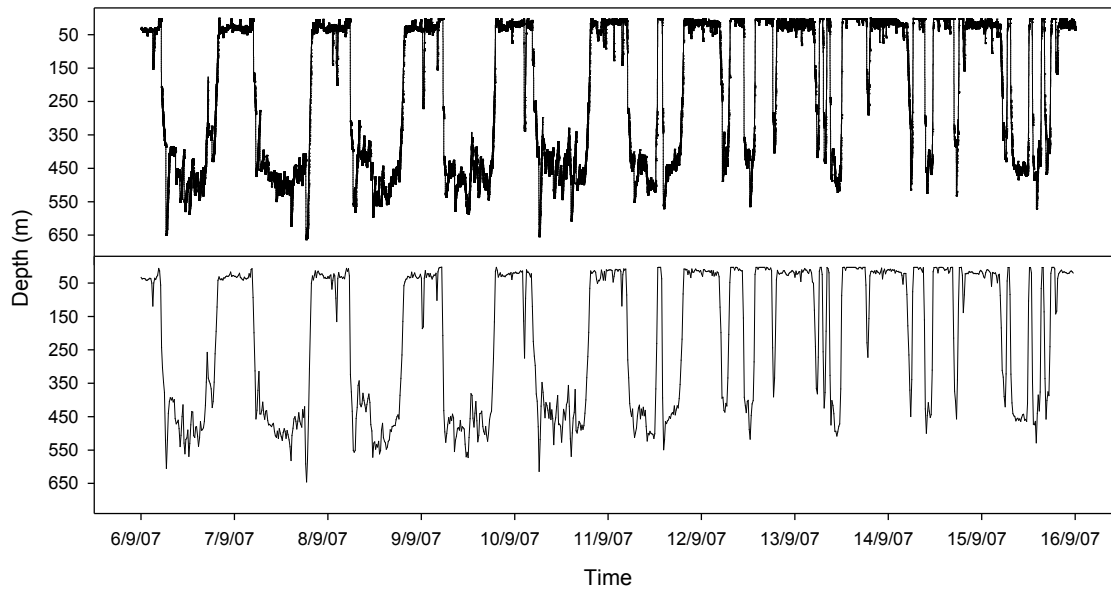
Figure 2: Depth time series from a blue shark

Upper panel shows data at a 5 second resolution, lower panel at 15 minutes. Despite the much lower resolution very little of the behavioural information has been lost, with changes in diel vertical migration and habitat use of the water column being clear.
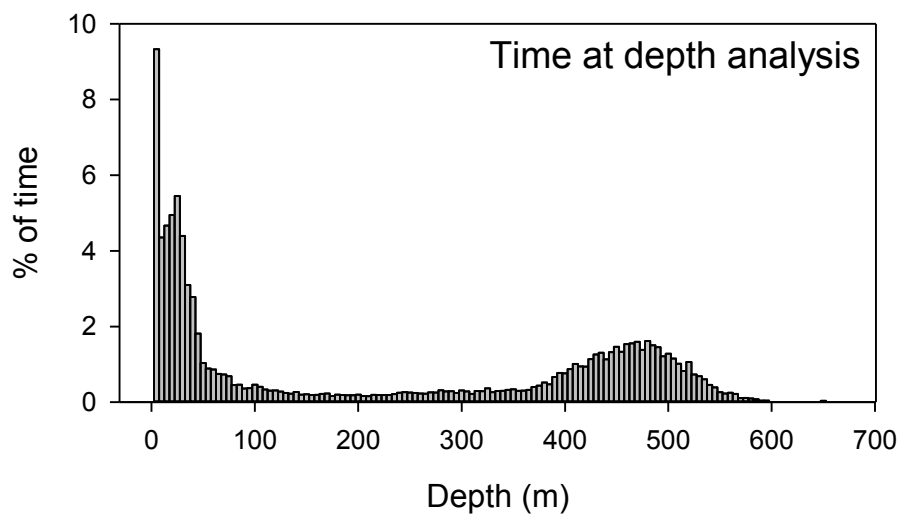
Figure 3: A time at depth analysis

Time at depth for a blue shark represented as a percentage of time spent at depths binned at 5m. The animal spends much of the time at, or just below, the surface and the remainder either at a depth of around 470m or commuting between the two.
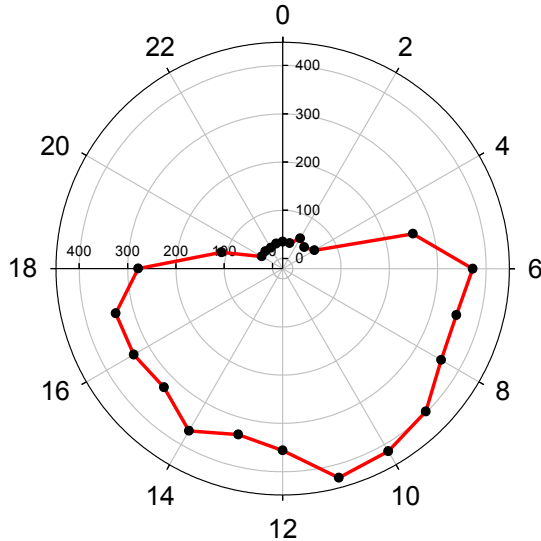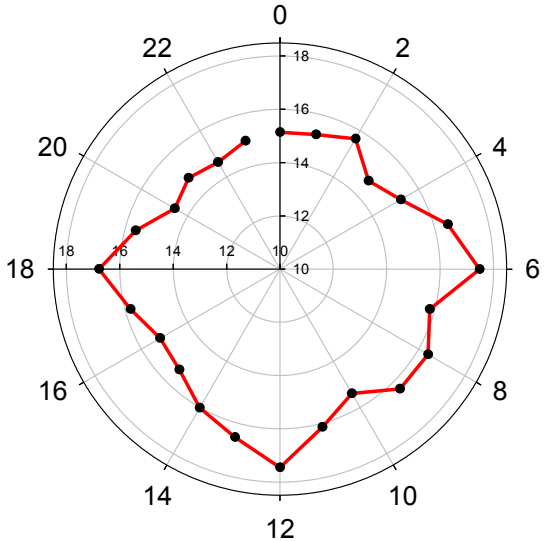
Figure 4: Depth and activity profiles

Time depth and time activity profiles for a blue shark showing that while there is a clear movement to deeper water during the day there is less change in the level of activity (as measured as the sum of move step-lengths i.e. total distance travelled per hour).

1.2 The Lévy flight foraging hypothesis

To find fresh resources all mobile animals must search new geographic locations if the precise location of those resources is unknown to the searcher. For example, a blue shark in the open ocean faces a significant search problem: new prey patches are sparsely distributed at distances well beyond sensory range, so in what direction and for how long should the shark swim to increase its chances of finding a new patch of prey? As biologists wishing to understand how such searches might be performed and optimised, we too face a significant challenge in putting the movement data obtained from electronic tags into a behavioural context. Recent work by statistical physicists on anomalous diffusion in a range of physical systems and latterly in biological systems by physicists and ecologists has provided a useful theoretical framework in the form of the Lévy flight foraging (LFF) hypothesis which seeks to gain some insight into what free-ranging animals are doing and why they might be doing it at specific times and places.

Early work by Shlesinger, Klafter *et al.* (e.g. 1990, 1993, 1993) demonstrated that a specialised random walk, known as a Lévy walk (or flight) had super-diffusive characteristics which results in particles diffusing further per unit time then would be expected if the particles moved with simple Brownian motion. Lévy flights describe a movement pattern characterised by many small steps connected by longer relocations,

with this pattern repeating at all scales, with step-lengths being drawn from a power-law distribution such that $P(l) \sim l^{\mu}$, with $1 < \mu \leq 3$ where l is the move step-length, and μ the power-law exponent. In other words, the probability of a step of given length is inversely proportional to its length, making short steps much more likely than long ones. This early theoretical work gained tentative empirical support in studies such as Coughlin *et al.* (1992) where fractal movement patterns were identified in the larvae of pink clown fish (*Amphiprion perideraion*) using novel computerised tracking cameras. Work by Cole (1995) investigated the fractal nature of the timing of movement in the fruit fly (*Drosophila melanogaster*) and presented the first simulated analysis of the optimality of a Lévy search compared to a Brownian random walk. However, the study focussed not on the effect of changing the exponent (μ), which was kept at the observed value of 1.37, but on the resilience of the advantage of Lévy movement under changing detection radii. The observation was clearly made, however, that Lévy movement increased the area explored compared to Brownian motion and so increased the rate of new prey patch encounters. The difference in area explored is illustrated in Figure 5 which compares a Brownian (exponential) forager with a Lévy forager, both of which have paths limited in length to 500 units. The tendency for the path of the Brownian forager to revisit the same areas greatly reduces the exploration of novel areas whereas the weak oversampling characteristics of the Lévy path increases the number of novel locations explored.
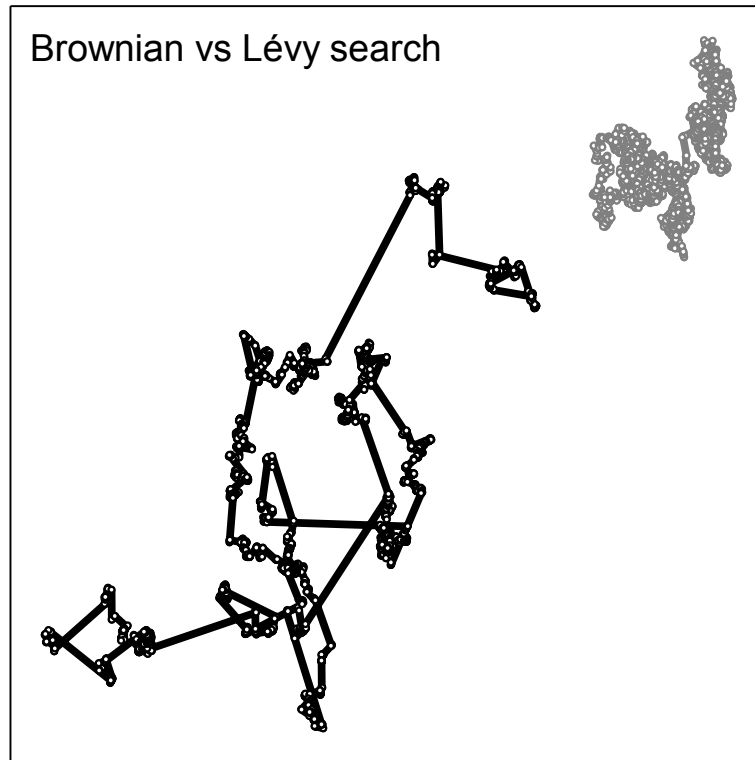
Figure 5: Swept area searched by a Brownian and a Lévy forager

Two simulated foraging paths each limited to a maximum length of 20000 units. Grey plot is Brownian (exponential, x_{min} = 1, λ = 0.148), black is Lévy (truncated Pareto, x_{min} = 1, μ = 2, x_{max} = 600. The area explored by the Lévy forager is more extensive than the Brownian forager, where the path can be seen to oversample previously visited areas.

The presence of Lévy flight search patterns in empirical data was brought to prominence by Viswanathan *et al.* (1996) in a study of wandering albatross (*Diomedea exulans*) foraging movements, where data recorded by wet-dry loggers attached to one of the bird's legs were used to calculate the number of 9s intervals per hour where the bird was considered to be in flight. Support for a Lévy flight pattern was provided by both logarithmic binning of the data as well as from calculation of the root mean square fluctuation, both of which suggested super-diffusive movements. In this case the result (i.e. the temporal scale invariance) was explained as arising from a scale invariant distribution of prey items at the surface of the ocean. This early work on Lévy searching led Viswanathan *et al.* to propose an early form of the Lévy flight foraging hypothesis (1999) where both mathematical analysis and numerical simulations were used to determine the efficiency of an idealised foraging model. In this model an animal has no prior knowledge of resource distribution, is able to revisit randomly distributed, stationary patches and is able to locate prey patches within a limited detection radius. This represents quite a realistic model of a foraging animal searching for sparse resources and has the advantage that it can be approximately solved

analytically, as well as allowing simulations. Both the analysis and the simulations showed foraging efficiency (i.e. targets visited per unit distance travelled) to be maximised when the step-lengths of the random walk followed an inverse power-law distribution (i.e. a Lévy distribution) with an exponent equal to -2.0, albeit only when prey targets were sparse. If prey was abundant then there was no effect on foraging efficiency by changing the exponent (μ) because the long step-lengths associated with Lévy walks do not arise when prey is more frequently encountered, truncating the step.

The proportion of longer relocations is dependent on the exponent (μ) with low values generating more long relocations and higher values more short steps such that a family of distributions arises ranging from almost ballistic ($\mu \rightarrow 1$) to Brownian in nature ($\mu \rightarrow 3$) (Figure 6). Lévy walks therefore have a scale invariant or fractal character and are linked to fractal geometry and anomalous diffusion phenomena (Shlesinger and Klafter 1986). Given the fractal nature of the natural world (Stanley 1992) it is perhaps unsurprising that animal movements should also be fractal in nature, and in fact this connection has been studied in many contexts (Dicke and Burrough 1988, Crist *et al.* 1992, Russell *et al.* 1992, Ritchie 1998). These early studies generally concentrate on the fractal dimension of the landscape (or environment) and the corresponding fractal nature of the animal movement path rather than specifically analysing the movement for Lévy distributed move step-lengths. However studies such as Russell *et al.* (1992) serve to highlight the fractal nature of prey distribution in the marine environment, where scale-free turbulent eddies were suggested to play an import role in the structuring of prey fields, e.g. calanoid copepods, which are the principal prey of the least auklet (*Aethia pusilla*) and the movement patterns of the predator were found to have a fractal dimension correlated with the prey. Many of the more recent studies also focus on characteristics such as tortuosity (or area restricted search, analysed using first passage time) rather than explicitly testing for movements that are approximated by an idealised Lévy walks (e.g. Fauchald and Tveraa 2003, Fritz *et al.* 2003, Pinaud and Weimerskirch 2005).
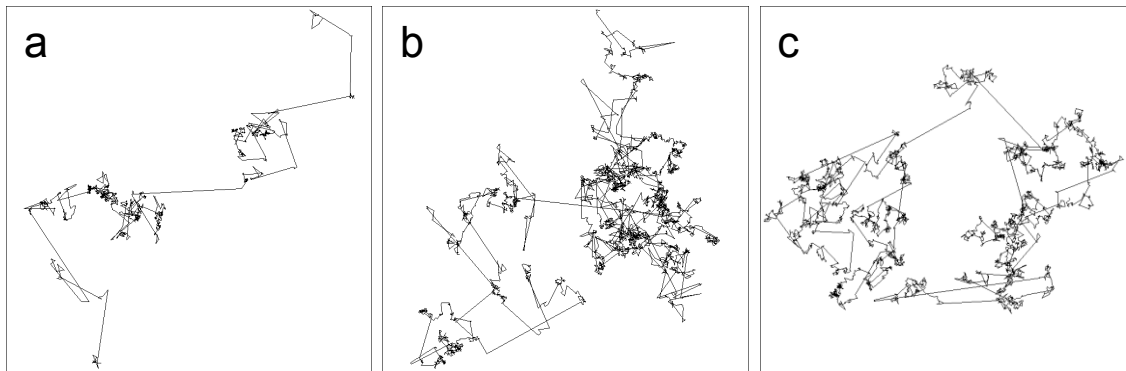
Figure 6: Example Lévy walks of 5000 steps from a truncated Pareto distribution
The characteristic pattern of clusters of small steps connected by longer relocations is clear, with the number of long steps reducing as the exponent (μ) increases. a) μ = 1.5; b) μ = 2.0; c) μ = 2.5;

A review and two further papers by Viswanathan (2000, 2001, 2002) and others such as da Luz (2001) extended the earlier work and further generalised the applicability of the LFF hypothesis to foraging situations in nature. Importantly it was shown that Lévy flight movement with μ = 2 is an optimum strategy in 1, 2 and 3 dimensions and is unaffected by short range correlations (Viswanathan *et al.* 2001). The latter is important because animals rarely perform 180° turns and therefore many recorded animal tracks naturally contain some degree of correlation.

The case of moving foragers and moving targets was also considered (Viswanathan *et al.* 2002). It was shown that Lévy movement is only advantageous when the target moves more slowly than the forager and is in effect stationary relative to the forager. With fast moving targets, or slow predators, Brownian movement is more efficient leading to the conclusion that:

> "*For such targets, the most efficient search strategy is not to move at all, because the preys will come by themselves! Hence, emerges the ambushing strategy*" [sic].

Therefore, the Lévy flight foraging hypothesis is only expected to hold true for relatively fast moving predators searching in resource sparse environments. The theoretical advantage of a Lévy flight pattern of movement in finding new prey patches, together with the early empirical support, has resulted in the LFF hypothesis being cast in an evolutionary context, which can be stated as: Since Lévy flights and walks can optimize search efficiencies; therefore natural selection should have led to adaptations for Lévy flight foraging.

This apparent new concept in behavioural ecology has, however, generated a great deal of controversy, with criticism being aimed at several aspects of the early empirical work. Firstly the original work on wandering albatross (Viswanathan *et al.* 1996) was

found by Edwards *et al.* (2007) to have methodological errors in the recording of the flight times of the birds (by the ecologists collecting the data), resulting in time spent resting on the nest being erroneously included as long flight times (by the physicists analysing these data). With these erroneous long steps removed Edwards *et al.* found that the data no longer fitted a power-law distribution and did not therefore represent Lévy flight. The statistical methodology used to identify power-law distributed step-lengths has also been criticised (Edwards *et al.* 2007, Sims *et al.* 2007, Edwards 2008). Studies, such as Viswanathan *et al.* (1996) and Sims *et al.* (2008a) relied principally upon a graphical technique, known as normalised logarithmic binning (LBN), to estimate the power-law exponent. In this method step-lengths are first binned into bins of width 2^k, the resulting frequencies are then divided by the bin width and total frequency in order to normalise them. The normalised frequencies and bin widths are then plotted on a log-log plot (Figure 7). The presence of a straight line identifies a power-law distribution and the slope, derived through least squares linear regression, estimates the exponent μ. Although this method had been shown to be easy to use, robust to noise and reasonably accurate (Sims *et al.* 2007) later studies have concluded that maximum likelihood estimation (MLE) should be the preferred method to estimate the exponent (Edwards 2008, White *et al.* 2008, Clauset *et al.* 2009). One advantage of MLE (which does not involve the binning of step-lengths) over LBN is that fewer step-lengths are required as all the observations are used, whereas with the LBN method sparse data can lead to empty bins resulting in inaccurate estimates and incorrect interpretation of results. Nevertheless, one disadvantage of the MLE method is that it only provides an estimate of the exponent's value and does not offer an indication of the goodness of fit, unlike LBN where the linear regression can provide both the r^2 and p values. However, MLE has the further advantage over LBN in that it can be used with distributions other than a pure power-law, such as truncated power-laws (e.g. truncated Pareto distribution) or exponential distributions (Figure 8), which then allows model comparison tests to be employed, such as log-likelihood ratios and Akaike Information Criteria (AIC) weights.
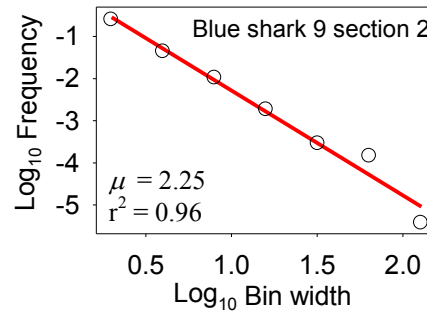
Figure 7: Normalised logarithmic binning plot of a blue shark track section

Black circles are binned frequencies; red line is least squares regression. The slope estimates the exponent, in this case 2.25, and r^2 gives some indication of how well the observations fit the distribution. In this case the data show a very good fit to a pure power-law.
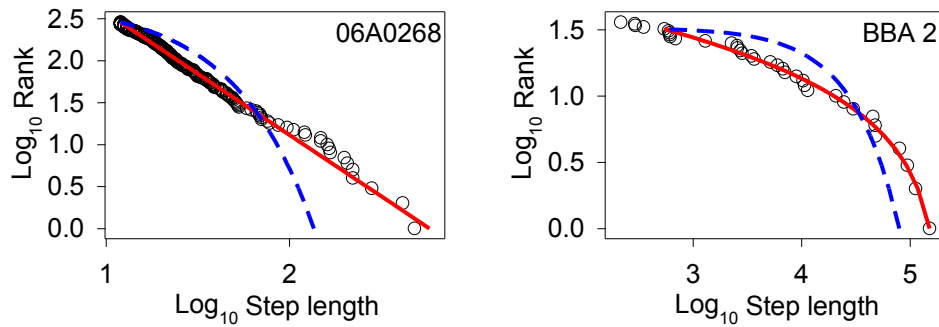
Figure 8: Example MLE plots

Left showing power-law (red) and exponential (dashed blue) fits to observed step-lengths (black circles), for archival data from a tracked blue shark, and *right* showing truncated Pareto (red) and exponential (dashed blue) fits to GPS-tracked movements of a black-browed albatross.

Other work has further questioned the statistical methods used, suggesting that Lévy distributions could be an artefact of the sampling rate employed (Plank and Codling 2009). These criticisms are levelled at the analysis of horizontal tracks, as recorded by GPS or Argos, and highlight a significant problem in the analysis of these data. The analysis of step-length distributions clearly requires the movement path to be divided into steps, where each step represents the distance between turning points. When originally recorded by, for example, a GPS device, the track will comprise a time series of locations spaced along the animal's true path at intervals dependent on the recording device. In the case of a GPS transmitter the interval might be between 1 and 10 seconds (Weimerskirch *et al.* 2007) and the resulting path will comprise many small correlated steps as the sampling frequency is much greater than the rate at which the animal actually changes direction. Furthermore, an animal such as an albatross does not perform movements that comprise straight-line relocations connected by turning points, but a complex curved swooping flight which does not submit to a simple turning point deconstruction (Richardson 2011). Any method used to determine steps and turning points from such a path is sensitive to the parameters used to identify a

turn (or path deviation)(Turchin 1998), leaving the resultant analysis open to the criticisms levelled by Plank and Codling (2009).

The controversy surrounding biological Lévy flights has tended to polarise the field with many studies falling into either a pro- or anti-Lévy camp. Since the original study by Viswanathan *et al.* (1996) there have been many empirical studies purporting to identify Lévy flight foraging behaviour in the movement patterns of many animals, including humans (Ramos-Fernandez *et al.* 2004, Brown *et al.* 2007, Sims *et al.* 2008a, Reynolds *et al.* 2009), and theoretical work seeking alternative explanations for the observed move step-length distributions (e.g. Benhamou 2007, Plank and James 2008). These alternative scenarios generally involve some form of correlated random walk with, in the study by Benichou *et al.* (2005), behavioural switching between searching and travelling. In this model a saltatory search is considered, with an animal exhibiting two phases of movement when searching: (i) a search phase with slow diffusive (i.e. Brownian) movement when the animal can detect targets and (ii) a fast, ballistic phase during which targets cannot be detected. Benichou *et al.* (2005) calculate that this model can be more efficient than Lévy flight models. However this seems intuitively to be a less realistic foraging model than that proposed by Viswanathan *et al.* (1999) since even ambush predators can detect targets while moving; furthermore, Benichou *et al.* (2005) presented no empirical evidence in support of their theoretical argument.

By contrast the Lévy flight model allows a range of movement patterns, simply by varying the exponent as described above (Figure 6). Another alternative, composite Brownian walks, have also been investigated by Benhamou (2007). In this scenario the searcher performs long runs when in sparse patches and shorter runs when in rich patches; the resulting path has a form very like that of a Lévy walk and again is reported as being more efficient. However it has been observed by Matthaus *et al.* (2011) that the switching requires the forager to be aware of whether the currently occupied patch is rich or sparse. Clearly the more information a searcher has about the environment the more a search can be optimised and the less like a random search it becomes. In addition the composite Brownian walk is simply another, albeit more complex, way to produce the same distribution of move step-lengths as a Lévy distribution and, consequently, a similar overall pattern.

Other studies have suggested that Lévy patterns appear through interactions with a fractal environment (Boyer *et al.* 2006, Miramontes *et al.* 2012) or even with simple, non-fractal environmental cues (Reynolds and Frye 2007, Guy *et al.* 2008, Reynolds 2008). However, empirical studies involving complex structured environments, such as rainforests, where resource availability is to some extent predictable, might be inappropriate for investigating Lévy searching, where the unpredictable location of sparse resources is a prerequisite. The lack of such complex environmental structuring and the dynamic nature of resource availability make the marine environment, in some respects, a much less contentious location for investigating the presence of movements similar to Lévy searching (Sims *et al.* 2008a). Therefore, given the apparent controversy surrounding the theoretical and empirical evidence for biological Lévy flights, it is necessary for a comprehensive study of the reliability and applicability of Lévy foraging models, and for new empirical results from in-depth analyses of the large datasets recorded by novel tag technologies attached to marine vertebrates including fish.

1.3 Objectives

The Lévy flight foraging hypothesis makes a number of predictions concerning the movements of marine predators that can be tested using the data obtained from electronic tags. Given the theoretical controversy, which could undermine the hypothesis altogether, the objectives will be as follows:

(1) To explore thoroughly the efficiency of Lévy foragers under a broader range of conditions than have been tested so far in the literature. Simulations with both stationary and moving prey will be considered as well as testing the predictions regarding ambush predation.

(2) The empirical evidence for the presence of Lévy movement patterns in marine pelagic predators will be tested using the largest database of animal movements so far collated for this purpose in conjunction with the use of robust statistical methods. The further prediction suggesting that Lévy flight is likely to be linked only to sparse prey fields will also be thoroughly examined. The same methods will be applied to the issue of whether albatrosses perform movements consistent with Lévy flights, which will be

reconsidered using high resolution GPS data, together with stomach temperature recorders for measuring prey capture and biomass.

(3) Finally, some of the problems associated with fisheries management and control of targeted and by-catch of large pelagic fish will be explored in a new analysis using vessel monitoring data from long-line fishing vessels; the potential impact of the fishing fleet under various by-catch mitigation measures will be assessed using a simulated prey field informed from the satellite-tracked movements of sharks. It is reasonable to assume that if large pelagic predators do exhibit complex spatial dynamics characterised by movement patterns consistent with optimal models, it will be necessary to explore management measures that can incorporate the type and scales of behaviour observed.

2 General methods

2.1 Maximum Likelihood Estimation and model selection

It is important to recognise that regardless of the computations performed to determine the best fitting distribution, it is essential to select candidate distributions that are meaningful in terms of the hypothesis being tested. In this study, the hypothesis being tested is the Lévy flight foraging hypothesis (LFF), where three distributions are relevant: power-law, exponential and truncated power-law. Exponential distributions produce move step-lengths with normal diffusion (i.e. Brownian movements), whereas power-laws produce super-diffusive movements, which have been shown previously to optimise encounter rates under conditions of sparse prey availability (Bartumeus *et al.* 2002). Because natural movement data is inevitably bounded, pure power-law fits are rare and therefore, in the first instance, only truncated power-law and exponential distributions were of interest. Other distributions may well exist that provide better fits to the data, but these would not be meaningful in terms of the hypothesis being tested and are therefore not considered further in this study.

2.1.1   Using MLE to estimate distribution parameters

The Maximum Likelihood Estimation (MLE) methodology employed was based on that described by Clauset *et al*. (2009) with, in most cases, truncated Pareto-Lévy (truncated power-law) and exponential distributions being tested. If the truncated power-law was found to be a particularly good fit then there is a case for also testing

the power-law, although this was found to be rare in biological data. The general methodology was to use the MLE equations to estimate the exponent from the dataset and to use an iterative technique to refine estimates of x_{min} and, in the case of the truncated Pareto distribution, x_{max}. First, the appropriate MLE equation was used to derive an exponent with the initial x_{min} parameter set to the minimum value found in the dataset. A best fit dataset was then generated using the estimated parameters and a Kolmogorov-Smirnov (KS) test was used to determine the goodness of fit (the KS D statistic) between the estimated distribution and the empirical data. To determine the best fit value for the x_{min} parameter the calculation was repeated with increasing values for x_{min} drawn from the dataset and with the data set subsequently reduced by the removal of all values < x_{min}. The value (and dataset) that resulted in the best (lowest) KS-D statistic was retained as the best fit value. When fitting a truncated Pareto distribution the method was repeated to derive a best fit value for the x_{max} parameter, so for the truncated Pareto distribution both the x_{min} and x_{max} parameters were fitted in the same way. There were two departures from the method as implemented in the program code given in Clauset *et al.* (2009). Firstly, once values for x_{min} and x_{max} had been derived, the dataset was reduced to include only values between those lower and upper bounds. The resulting dataset therefore contained only the step-lengths fitting the proposed distribution and it was this that was used to produce plots of $\log_{10}$ rank *vs* $\log_{10}$ step-length that were used to assess visually the goodness of fit; however, for purposes of clarity, the fitted distributions were plotted against the full set of observations so that the extent of the fit was evident. Secondly, rather than test all values in the dataset as possible candidates for x_{min} or x_{max}, the iterative search routine was halted once five consecutive worse fits had been found to avoid the problem of fitting to a very small sub-set of the data; a problem exacerbated by complex biological data and exponent estimation. The aim of fitting the lower and upper bounds was to find the distribution that best fit most of the data, rather than select a small sub-set of the data that was a very good fit to a particular distribution.

The MLE analysis requires two equations for each distribution to be tested. One is the MLE equation for the distribution and is used to estimate the exponent. The other is a random number generator (RNG) and is used to generate best-fit datasets. Table 1 gives the equations that were used for each distribution. The power-law MLE and the power-law and exponential RNG equations were obtained from Clauset *et al.* (2009),

the truncated Pareto MLE equation was from White *et al.* (2008) and the truncated Pareto RNG was from Kagan (2002). The MLE equation for the truncated Pareto distribution has no closed form solution and is therefore solved numerically by finding the value for $\hat{a}$ that minimises y in the equation:

$$y = \frac{-\overline{\ln x} - 1}{(-\hat{a} + 1)} + \frac{\left(x_{max}^{-\hat{a}+1} \ln x_{max} - x_{min}^{\hat{a}+1} \ln x_{min}\right)}{\left(x_{max}^{\hat{a}+1} - x_{min}^{\hat{a}+1}\right)}$$

<div align="right">Eqn 1</div>

Table 1: The MLE and RNG equations used in the analysis

In these equations a and λ are the exponents; n is the number of step-lengths; x_i an individual step-length.

	MLE equations
Power-law	$\hat{a} = 1 + n \left(\sum_{i=1}^{n} \ln \frac{x_i}{x_{min}}\right)^{-1}$
Exponential	$\hat{a} = 1 + n \left(\sum_{i=1}^{n} (x_i - x_{min})\right)^{-1}$
Truncated Pareto	$\overline{\ln x} = \frac{-1}{(\hat{\lambda} + 1)} + \frac{\left(x_{max}^{\hat{\lambda}+1} \ln x_{max} - x_{min}^{\hat{\lambda}+1} \ln x_{min}\right)}{\left(x_{max}^{\hat{\lambda}+1} - x_{min}^{\hat{\lambda}+1}\right)}$ Note: This MLE equation has no closed form solution (White *et al.* 2008) and must therefore be solved numerically (see text).
	Random number equations (in all cases *r* represents a uniform random number in the interval [0,1]
Power-law	$x = x_{min}(1 - r)^{-1/(a-1)}$
Exponential	$x = x_{min} - \frac{1}{a} \ln (1 - r)$
Truncated Pareto	$x = x_{min} \left\{ r \left[1 - \left(\frac{x_{max}}{x_{min}}\right)^{1-a} \right] + \left(\frac{x_{max}}{x_{min}}\right)^{1-a} \right\}^{1/(1-a)}$

In some cases data storage tags convert integer pressure readings to real depth measurements by multiplying by 5.379, resulting in depths, and consequently step-lengths, that are multiples of 5.379. Therefore, discrete approximation was used as described by Clauset *et al.* (2009), but using the observed step-length multiple (e.g. 5.379) so that the best fit datasets used in Kolmogorov-Smirnov tests had a similar structure to the observed distribution. However, when generating the rank step-length plots, the best fit distribution parameters were used to generate points from a continuous distribution as the resulting plots are easier to interpret, and doing so provides good confirmation of the accuracy of the approximations.

2.1.2 MLE model selection

The methodology used to estimate the exponents and parameters of the exponential and truncated Pareto distributions frequently results in different x_{min} and x_{max} values, thus resulting in fitting the two distributions to different ranges of the original data. Consequently, it is not possible to compute separately comparable log-likelihoods (LLHs) from the two fitted distributions. Here we dealt with this by splitting the analysis into two sections, whereby LLHs and Akaike weights for both distributions are computed from each fitted dataset. First, we compute an LLH for the fitted TP distribution and using the same dataset (defined by the x_{min} and x_{max} parameters) compute the LLH for the competing exponential distribution using Eqn 2 and Eqn 3:

$$llhE = n\left(\ln \cdot \lambda + \lambda \cdot x_{min}\right) - \left(\lambda \cdot \sum (x)\right)$$

Eqn 2

$$llhTP = n \ln\left(\frac{\mu - 1}{(x_{min}^{1-\mu}) - (x_{max}^{1-\mu})}\right) - \mu \cdot \sum \ln x$$

Eqn 3

From these LLHs we can compute *w*AIC using Eqn 4 and Eqn 5,

$$AIC = -2(loglikelihood) + 2K$$

Eqn 4

(where *K* is the number of parameters in the model)

$$w_i = \frac{\exp(-\Delta_i/2)}{\displaystyle\sum_{r=1}^{R} \exp(-\Delta_r/2)} \; where \; \Delta_i = AIC_i - AIC_{min}$$

<div align="right">**Eqn 5**</div>

which can be compared in the usual way to perform the first step in model selection (Burnham and Anderson 2004). The result of this first step might be that the TP distribution is favoured over the competing exponential distribution *for that range of the data*. The second step tests this more completely by repeating the calculations using the fitted exponential, and then proceeding to fit the competing TP distribution to that data range. This provides a second comparison of *w*AIC that can be used confidently to rule out the exponential distribution if it was not selected during the first or second steps. Using this two-step method therefore, we only consider a dataset to be fitted by the TP distribution if *w*AIC favours the fitted TP over the competing exponential (step 1), and favours the competing TP over the fitted exponential (step 2).

This method suffices when the results of the *w*AIC analysis are unambiguous for steps 1 and 2. However, because the distributions can be fitted to different ranges of the data it is possible for the *w*AIC results to be conflicted, whereby the TP fitting favours the competing exponential and *vice versa* or for one of the distributions to fit a much smaller range of the data (Figure 9). To resolve these conflicts we use the goodness of fit of the two fitted distributions, which in this case is the Kolmogorov-Smirnov *D* statistic which has already been computed as part of the fitting process (Clauset *et al.* 2009). There is a requirement to select the distribution that not only fits the observations closely, but also which fits as much of the data set as possible. For example, a distribution that is a very good fit but to only 10% of the data set (and might as a consequence have a low *D*-statistic) should be rejected in favour of a distribution with a slightly worse *D* statistic (i.e. higher), but which fits significantly more of the dataset (see Figure 9). Therefore, in this study, the GOF was adjusted to account for how much of the original dataset was fitted by the distribution, using the equation:

$$D_{adj} = D \cdot \log(Total\,Steps)/\log(Fitted\,Steps)$$

where D is the KS-D statistic. Taking the log of total and fitted steps serves to reduce the impact of a difference of just a few points. If the fit is to the entire dataset then the result is D; hence, the less of the data fitted by the best fit distribution the poorer (larger) the resulting GOF value becomes. Adjusting the D statistic in this way allows a better comparison between distributions fitted to different ranges of the dataset.
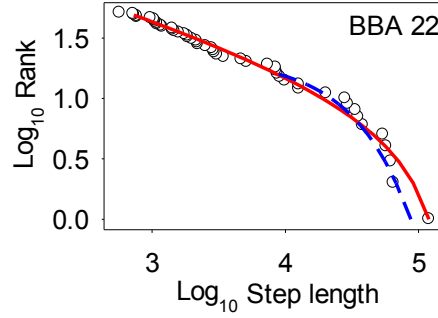
Figure 9: A ranked step-length plot showing a partial exponential fit
Both the TP distribution (red line) and the exponential distribution (blue dashed line) are good fits to the data (black circles) but the exponential fit is to a smaller subset of the data. The adjusted GOF value compensates for this.

The decision process used in this study is summarised in Table 2. For datasets where the wAIC decision is to be classed as a best fit TP, there are the additional requirements that the estimated exponent μ falls within the Lévy range ($1 < \mu \leq 3$), and that the range of data fitted (i.e. $x_{max} - x_{min}$) should span at least 1.5 orders of magnitude. Candidate TP datasets that fail these requirements are assigned to the Mixed-model category since it is assumed that such data may represent more complex behaviour patterns, e.g. a mixture of Lévy and Brownian strategies, or other movement patterns entirely.

Table 2: The simple 'truth-table' used to perform model selection.
TP denotes the truncated Pareto distribution.

	wAIC values			
Fitted TP	Competing exponential	Fitted exponential	Competing TP	Result
1	0	0	1	TP
0	1	1	0	Exponential
1	0	1	0	Resolve using GOF
0	1	0	1	Mixed-model

The decision process used for model selection is given in detail in Figure 10 below, and the decisions are further explained as follows:

A. Does AIC support the fitted TP over the alternate exponential?

B. Does AIC support the fitted exponential over the alternate TP?

C. Does the adjusted GOF support exponential over TP?

D. Does AIC reject the fitted exponential in favour of the alternate TP?

E. Does the adjusted GOF reject exponential in favour of TP?

F. Is the TP exponent in the range 1.0 to 3.0?

G. Does the fitted TP range (i.e. x_{min} to x_{max}) span at least 1.5 orders of magnitude?
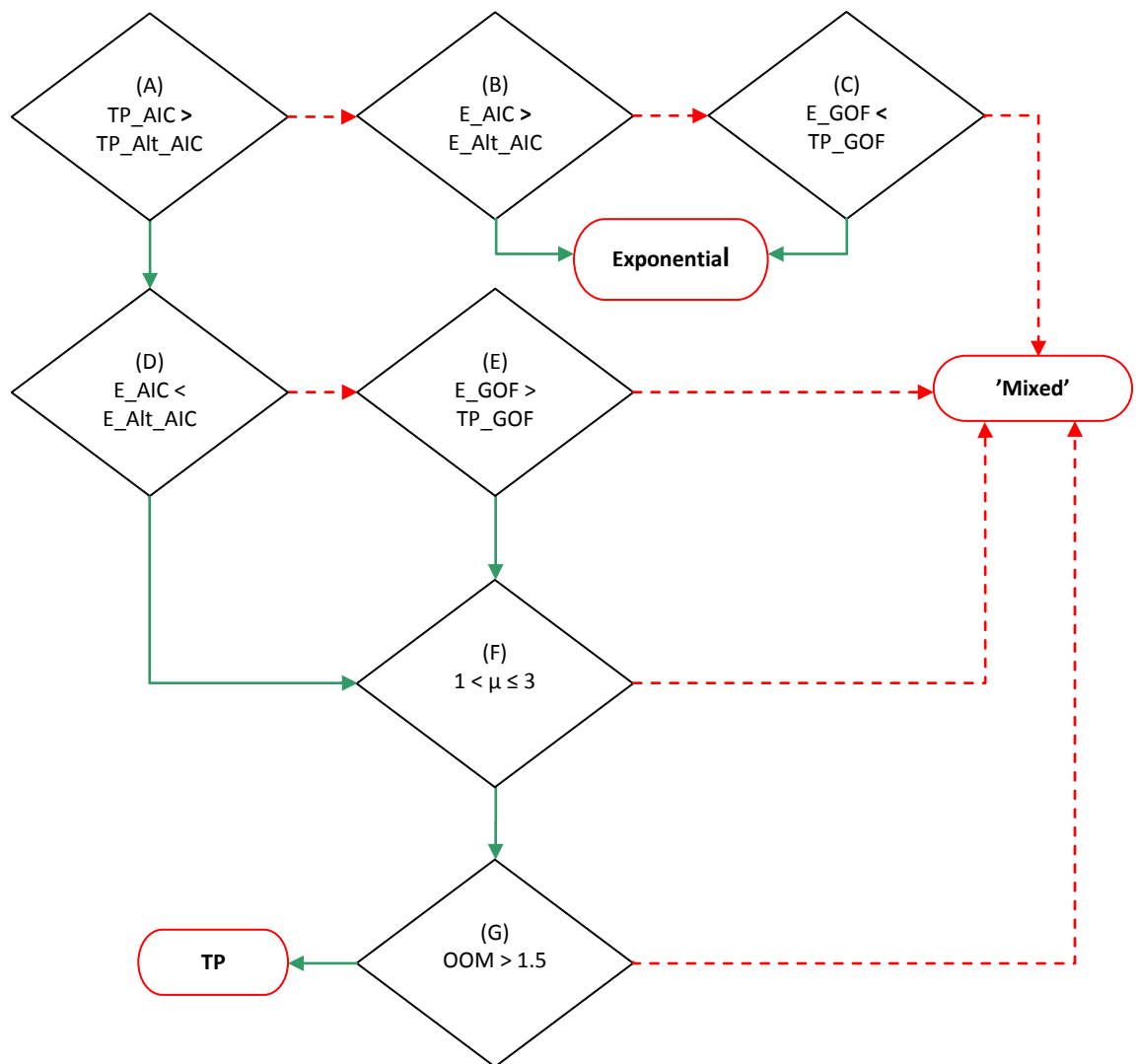
Figure 10: The decision process used for model selection

The process begins at question (A) with green lines being followed for positive responses and red dashed lines for negative responses. A truncated power-law (TP) fit is only concluded when there is considerable certainty that it is the correct conclusion. OOM is orders of magnitude.

An alternative description of the process, perhaps more familiar to a biologist, would be a dichotomous key as follows:

A. Does AIC support TP over the alternate exponential? | Yes → D
No → B

B. Does AIC support exponential over the alternate TP? | Yes → **Exponential**
No → (C)

C. Does the adjusted GOF support exponential over TP? | Yes → **Exponential**
No → **Mixed**

D. Does AIC reject exponential in favour of TP? | Yes → (F)
No → (E)

E. Does the adjusted GOF reject exponential in favour of TP? | Yes → (F)
No → **Mixed**

F. Is the TP exponent in the Lévy range of 1.0 to 3.0? | Yes → (G)
No → **Mixed**

G. Does the fitted TP range cover > 1.5 orders of magnitude? | Yes → **TP**
No → **Mixed**

The outcome from this model selection process was the categorisation of each dataset into one of the three categories (TP, exponential or mixed), based on Akaike weights, a valid Lévy exponent and a sufficient range of fit in terms of the orders of magnitude over which data were fitted. Thus, all the criteria must be met and there must be unequivocal support from AIC weights or GOF for an individual dataset to be placed in the TP category. This methodology is appropriately robust because model selection is strict and entirely objective. Nevertheless, this process did not remove the need to perform a final check by visually scrutinising the model fit to the data on ranked step-length plots (e.g. Figure 11). This final visual check is important because Akaike weights do not confirm the goodness of fit, but merely help decide which of the competing distributions is least bad (Burnham and Anderson 2004). Therefore, it is entirely feasible for both distributions to have very poor fits to the underlying observations but AIC will still select one poor model fit over another equally poor fit. The model fitting and selection methodology described here can be applied to any appropriate data, with any suitably relevant distributions, and could therefore find wide applicability,

particularly in the study of movement data where a conceptual framework already exists in terms of the LFF hypothesis and other movement models (Bartumeus 2007, Viswanathan *et al.* 2008).
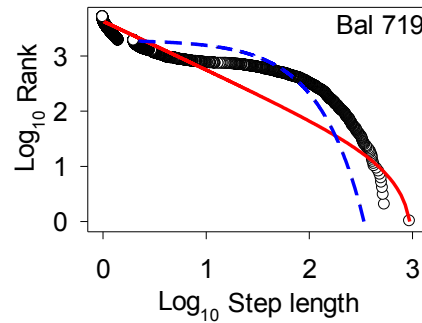
Figure 11: A ranked step-length plot showing a poor fit for both models
This plot (comprising synthetic data) shows observations (black circles), the fitted TP distribution (red line) and the fitted exponential distribution (dashed blue line). It is clear that, although AIC supports the TP distribution, neither distribution can be considered to be a good fit to the data.

2.1.3 Model selection validation

The model selection methodology described above was validated using simulations to determine whether the method was sufficiently accurate in assigning known move step-length distributions to their correct category. Simulated datasets were generated comprising 50 truncated Pareto distribution (TP) move steps, 50 exponential move steps or 100 steps comprising a 50:50 mixture of both, with 100 data sets being generated in each case, giving 300 datasets for analysis. It should be noted that small datasets were used as it is known that reducing the size of the dataset reduces the accuracy of exponent estimation (Sims *et al.* 2007) and will therefore be a stronger test of the methodology. The results of the analysis are shown in Table 3. It is evident from this analysis that none of the pure TP datasets were wrongly assigned as exponential, and none of the pure exponential datasets were wrongly assigned as TP. Although a large percentage of both the TP and exponential datasets were classified as mixed (59% and 65% respectively); we consider it to be more important to reduce the number of misclassifications at the cost of losing some datasets from further analysis. The majority of the mixed datasets were correctly classified as mixed model (81%), as expected, with 18 datasets being classified as TP and only one as exponential. With the mixed data it is probable that in some cases the TP steps will be the predominant feature and in others the exponential. However, the presence of some longer steps in the TP distributions tends to rule out their classification as exponential.

The relatively low number of unambiguous classifications was attributed to the low number of steps in these datasets which is known to reduce the accuracy of the analysis as described above. To confirm whether this was the case the validation was repeated using datasets with 250 steps, the results of which are given in Table 4. It is clear from this analysis that with more steps the percentage of correct assignments increases, hence the accuracy becomes greater. It was confirmed therefore that as before there were no incorrect identifications of either TP or exponential datasets and now 92% of the TP and 80% of the exponential datasets were correctly identified.

Table 3: Results of the model selection validation tests with 50 steps.

| Input Data | Resulting category | | |
	TP	Exponential	Mixed
TP	41%	0%	59%
Exponential	0%	35%	65%
Mixed	18%	1%	81%

Table 4: Results of the model selection validation tests with 250 steps.

| Input Data | Resulting category | | |
	TP	Exponential	Mixed
TP	92%	0%	8%
Exponential	0%	80%	20%
Mixed	14%	0%	86%

2.1.4   Sensitivity of MLE analysis to behavioural complexity

Track sections are sometimes poorly fitted by either power-law, truncated Pareto or exponential distributions. It was hypothesised that some of the poor fits might be caused by behavioural complexities in the movement time-series arising from the inclusion of simple Brownian motion in addition to Lévy motion. Theoretical studies (Viswanathan *et al.* 2002) have shown that when prey is relatively abundant Brownian motion is an optimum search strategy, which would explain the presence of exponentially distributed step-lengths. To test this hypothesis, simulated time series were generated using steps from a truncated Pareto (power-law) distribution with 5, 15 or 25% of steps being drawn from an exponential distribution. The parameters for the exponential distribution were derived by using MLE to fit an exponential distribution to the synthetic truncated Pareto distribution dataset. Fitting in this way ensured that the exponential step-lengths covered a similar range to the truncated

Pareto step-lengths and could in principle, therefore, have been generated by the same animal. As hypothesised, the MLE analysis (Figure 12a-c) reveals that increasing proportions of exponential move steps results in increasingly poorer fits. Interestingly, comparison of the synthetic data and model fits to empirical examples (basking shark, bigeye and yellowfin tunas) (Figure 12d-f) shows distinct similarities in form, supporting the hypothesis that poorer fits to the truncated Pareto distribution in some individuals may well be the result of behavioural switches in response to changes in prey field density. Behavioural complexity such as this could explain why Lévy behaviour can be difficult to detect in longer time-series where the likelihood of recording different movement behaviours is increased (Sims *et al.* 2008a). It seems likely that good fits to power-law or truncated power-law distributions will only be found when Lévy behaviour is adopted by foragers for the majority of the period within a time series section being analysed, even if a statistical technique such as split-moving window is used to identify discontinuities.

Given the effect of complex biological data on the form of rank-frequency plots (e.g. Figure 12) visual inspection of plots can be useful to help assess whether any particular distribution is a good fit when testing for the presence of power-laws or truncated power-laws to infer Lévy behaviour. This may be particularly relevant in the context of testing for the presence of biological Lévy flights because it is the heavy (fat) tail of the move step-length frequency distribution that should be reasonably accounted for by any candidate best fit model for the identification of Lévy behaviour to be reliably detected. The frequency of longer move steps that make up the heavy tail of a distribution (the right-hand side of the distribution) is low compared with the more frequent smaller steps making up the left hand side. Importantly in this context, MLE model fitting to empirical data plotted as a rank-frequency plot gives equal weight to all points even though the vast majority of points are clustered on the left hand side. This may be a potential problem for model selection in some cases because strong support for a model using Akaike weight values (e.g. *w*AIC = 1.0; strongest support) may be based on a good fit to the left hand side of the distribution rather than to the heavy tail also.

Figure 12: Analysis of complex synthetic data.
Black circles represent synthetic or empirical observations; red lines represent MLE best fit truncated Pareto distributions. (a-c) Synthetic truncated Pareto distribution datasets including 5, 15 and 25% move steps derived from an exponential distribution; (d) basking shark *Cetorhinus maximus* 2, section 2; (e) bigeye tuna *Thunnus obesus* 3, section 4; (f) yellowfin tuna *Thunnus albacares* 1, section 5, showing visually similar patterns to synthetic Lévy-Brownian (exponential) datasets. Arrows indicate departures from a good fit to the truncated Pareto distribution.

2.1.5   Problems with testing GOF I: KS-Test and Akaike weights

When determining the best fit values for the x_{min} and x_{max} parameters it is necessary to compare the proposed theoretical distribution with the empirical data using a test that provides some measure of the goodness of fit. Several statistical methods can be employed, such as the Cramér-von-Mises criterion, the Anderson–Darling test, the Wald–Wolfowitz runs test or the Kolmogorov-Smirnov (KS) test. Clauset *et al.* (2009) recommends the KS test as this is the commonest test for non-parametric data and is particularly sensitive to right-skewed data typical of power-law distributions. In some cases, despite reasonable visual fits to empirical data, both the GOF values and the Akaike weights were found to favour the alternative distribution and consequently some of these ambiguous sections were marked as not fitting any distribution well. However, with some other ambiguous sections the model fitting plots often showed strong support such that the statistical results could be considered unreliable or at least biased. These ambiguities in both the KS-*D* statistic and in Akaike weights highlight the importance of inspecting the fits graphically before concluding that any particular distribution is a good fit. This is especially important when testing for the presence of power-laws or truncated power-laws to infer Lévy behaviour because it is

the heavy (fat) tail of the move step-length frequency distribution that must be reasonably accounted for by any candidate best fit model (see previous section). Therefore it is better to rely not solely on the model comparison values but to inspect plots of model fits to the empirical data visually. Figure 13 shows some examples of where visual inspection of model fits to data conflict with the statistical analysis. It is interesting that Akaike weights seem to become unreliable when exponent values for the truncated Pareto distribution approach 3; for example, as with silky sharks 2 and 3 in Figure 13 (a and b) where silky shark 2 has an exponent of 2.99 and silky shark 3 an exponent of 2.03. Despite both being good visual fits to a truncated Pareto (red line), and clearly not being a good fit to the exponential (blue line), silky shark 2 has an Akaike weight that favours the exponential distribution.
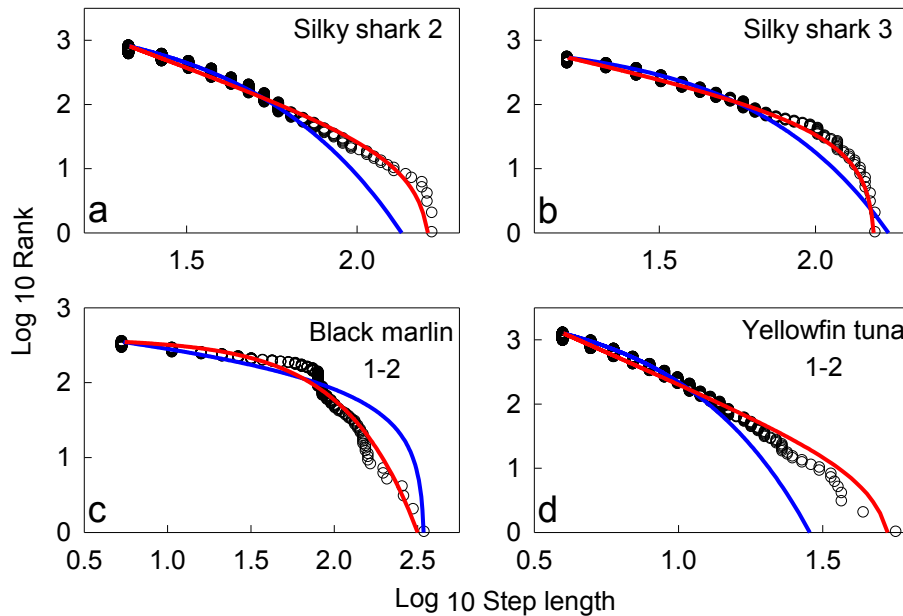
Figure 13: Good visual model fits with conflicting model comparison statistical results.
Black circles represent empirical observations. (a) Silky shark 2 shows a good fit to a truncated Pareto distribution (red line) despite having both GOF values and Akaike weights that favour the exponential (blue line) (TP GOF 0.210, AICw 0.0, exponential GOF 0.146 AICw 1.0). (b) Silky shark 3 shows a good fit to a truncated Pareto (power-law) distribution (red) despite GOF values that favour the exponential (blue) (TP GOF 0.181, exponential GOF 0.102). (c) Black marlin 1 section 2 is a better fit to the exponential (Red) than the truncated Pareto (power-law) model fit (blue), but has both GOF and AICw values that favour the truncated power-law (Exp GOF 0.181, AICw 0.02; TP GOF 0.178, AICw 0.98). (d) Yellowfin tuna 2 section 2 is a better fit to the truncated power-law (red) than exponential (blue) but has Akaike weights in favour of the exponential model fit (TP AICw 0, exponential AICw 1) despite being one of the few sections to have a significant p-value of 0.340 in favour of the truncated Pareto (power-law) distribution.

2.1.6 *Problems with testing GOF II: p-values*

Increasing complexity in the synthetic movement time-series has a marked effect on *p*-values calculated to determine the statistical significance of the fitted relationship. Figure 14a-c shows a sharp decline in the significance of the truncated Pareto best fits to the simulated data with an increase in introduced exponential move steps (note

that, as described above, higher *p*-values represent better fits). The pattern of decreasing *p*-values was also evident in empirical data, where the deviations between data points and the fitted line in each plot were similar. What is evident from this analysis is that time-series of free-ranging animal movements are often naturally complex and consequently non-significant *p*-values found with this method ($p < 0.1$) may not necessarily mean that Lévy behaviour is not exhibited, or indeed, dominant. The inconsistencies arising in *p*-values generated from complex biological data represents clear evidence that numerical methods should not be relied upon solely, but rather that ranked-step-length plots with MLE best fits should be examined visually to determine the goodness of fit (Aban *et al.* 2006).
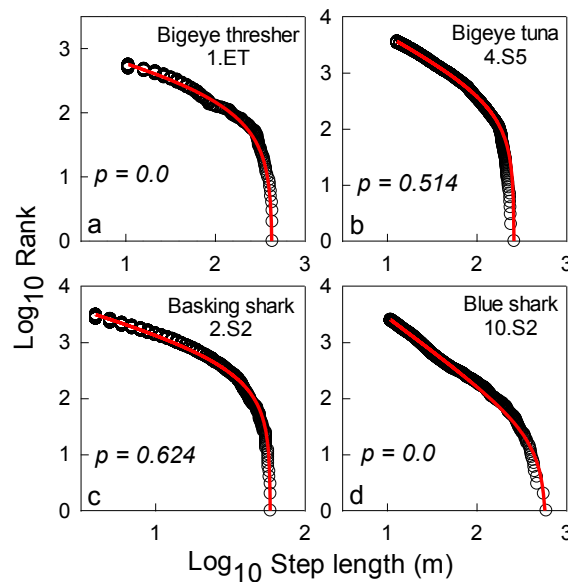
Figure 14: Comparison of *p*-values from MLE calculations.
Track sections showing good visual fits to a truncated Pareto distribution but with anomalous *p*-values and K-S GOF values: (a) bigeye thresher 1 entire track, GOF 0.142, no significant *p*-value; (b) bigeye tuna 4019 section 5, GOF 0.031, significant *p*-value (0.514); (c) basking shark 2 section 2, GOF 0.063, significant *p*-value (0.624); Blue shark 10 section 2, GOF 0.038, no significant *p*-value.

2.2 Movement of virtual foragers & predators

All the simulations written for and used in this study involve virtual organisms (foragers, predators or prey) that require movement patterns based on specified move step-length distributions. All the individual move steps can be generated using the random number generators described above in Table 1, with the computer language's built-in uniform random number generator used for the uniform distribution.

2.2.1 Move steps

The foragers or predators are always located and moved within continuous space with real coordinates and all move steps are therefore continuous rather than discrete values. Each step is computed as a vector (distance), drawn from the specified distribution, and a turn angle which is uniform random on the interval $[0,2\pi]$ radians. Further, all the organisms require each move step to be interpolated, either to check the contents of grid cells over which it is moving, for the foraging lab and predator prey simulations, or to check for contact with land, in the case of the shark simulator.

2.2.2 Interpolation of move steps

To perform a single, interpolated, move step values of ΔX and ΔY, are first computed from the turn angle and move step-length. The move is always interpolated as a move of approximately one unit in either x or y and a fractional move in the other dimension. Therefore, if $\Delta X > \Delta Y$, interpolated steps are computed where $\Delta X' = 1.0$ and $\Delta Y' = \Delta X/\Delta Y$; this is essentially Bresenham's algorithm (Bresenham 1965). The interpolated deltas are added to the X and Y coordinates in continuous space and after each interpolated step the grid cell in which the forager is found is calculated by simply taking the integer value of the continuous X and Y variables. Note that this simple algorithm leads to discontinuities in step-lengths between 1.414 and 2.0 and 2.828 and 3.0 because each move step is performed as an integral number of interpolated move steps. The smallest step that can be performed will have one delta set to 1.0 and the other set to zero, giving a step of 1.0. The largest vector that can be moved as a single step will have both deltas set to 1.0, giving a step-length of 1.414 ($\sqrt{2}$). If the vector is slightly larger, then two moves are required which will result, as a minimum, in one delta being the sum of two 1.0 deltas and the other a value of zero resulting a move step of 2.0 ($\sqrt{4}$). Given that the maximum step-length is generally > 500 this discontinuity is not considered to be important, however it is noticeable (and accentuated) by rank frequency plots that plot the log of the step-length.

3 An exploration of Lévy flight as a foraging strategy

3.1 Introduction

Empirical tests of the Lévy flight foraging hypothesis (LFF) are very difficult to perform for a variety of reasons. Field tests require free-ranging animals to be tagged to record their movements which can result in understandably limited information (i.e. often just a time series of depth and temperature). In addition, there can be no control over prey field densities and no direct evidence concerning the activities the animal is actually engaged in at any point in time. Under controlled conditions in the laboratory there are logistical constraints: enclosures or aquaria are generally not large enough for spatial movements spanning a broad range of scales, hence these restrict the animal's movements to a large degree. Therefore field studies are limited to natural experiments which are inevitably time consuming and expensive (e.g. Priede 1984, Sims and Merrett 1997, Kohler and Turner 2001), while laboratory studies are limited to smaller organisms (e.g. Bartumeus *et al.* 2003, Reynolds and Frye 2007) with necessarily much simpler behaviour. Consequently, as foraging models in more than one dimension are analytically intractable (Hartig *et al.* 2011), computer simulation studies have been used extensively to test many different aspects of the LFF hypothesis (e.g. Viswanathan *et al.* 1999, Viswanathan *et al.* 2000, Bartumeus *et al.* 2002, Reynolds and Bartumeus 2009). In this chapter a computer simulation was developed to explore the consequences of virtual foragers employing different search strategies in differing prey fields, resulting in a thorough and robust independent test of the Lévy flight foraging hypothesis.

There is a distinct need for a thorough test of the theoretical results because most of them have come from experiments undertaken by collaborating researchers (e.g. Viswanathan *et al.* 2011) using what appears to be the same testing framework and simulation code. Other less comprehensive simulations have been undertaken that confirm the results of Viswanathan and co-workers, however, there are other researchers who have not found the same results with a different, albeit less comprehensive simulation, that set out to test the same general ideas. Hence some doubts have been expressed about whether a Lévy flight search does indeed confer the advantages proposed in earlier studies. For example, in a recent paper James *et al*. (2011) replicated the simulation study performed as part of an influential empirical study by Sims *et al.* (2008a) in which it was demonstrated that, for a 'blind' forager in a sparse environment, Lévy movements conferred an advantage over simple, uniform, random movement approximating normal, Brownian, diffusion. The advantage was found to be greatest when the prey field had a Lévy, rather than a uniform distribution. The results obtained by James *et al*. appears to be at odds with those found by Sims *et al.*, concluding instead that foraging efficiency (which they define as the proportion of available biomass consumed per unit area searched) converges to a constant value regardless of the movement pattern employed by the forager. The convergence is described as slow, suggesting it took many simulation runs for the convergence to become evident. However, James *et al.* performed only 10^4 foraging runs, compared to the 10^5 runs performed for each test by Sims *et al*. The results are summarised in their figure 4 (James *et al.* 2011), which presents a running mean for each of the four simulation scenarios studied; nevertheless, no table of results was provided, so actual simulation outcomes cannot be accurately compared. From the prey density figures presented in their Appendix A the total biomass in the simulation is described as being set at 10^6 units, but exactly how this biomass is distributed throughout the simulation arena was not made clear. For example, the paper does not state how many of the 2500x5000 cells have > 0 biomass or what the size or distribution of prey patches was. Consequently, it is not clear whether the prey field experienced by the virtual foragers is sparse and heterogenic, or relatively homogeneous.

Given the apparent controversy over the Lévy flight foraging hypothesis (Buchanan 2008) and the contradictory papers publishing both mathematical analysis and

simulation results as discussed in Chapter 1 (e.g. Raposo *et al.* 2003, Benhamou 2007, Plank and James 2008, Oshanin *et al.* 2009, Plank and Codling 2009, Reynolds and Bartumeus 2009, Reynolds and Rhodes 2009), together with the discrepancy between the results obtained by Sims *et al.* (2008a) and by James *et al*. (2011), it seems appropriate to present a thorough exploration of Lévy flight as a foraging strategy; particularly as many of the previous simulation studies have used a somewhat impoverished set of simulations and scenarios. Therefore, this chapter will present results from a robust and straightforward simulation model that allows different foraging styles (e.g. Lévy, uniform, exponential) in the form of random walks, to be compared for both foraging efficiency and encounter rates under varying scenarios of prey field distribution and foraging strategy. The program is entirely independent from and different to that employed by Viswanathan and co-workers.

From this new simulation program, it will be shown that in the majority of cases Lévy foragers with μ = 2.0 outperform other foragers and that the advantage is robust to prey field densities, prey field distributions and prey depletion. Importantly the simulation presented here is a 2D simulation, in contrast to the biologically unrealistic 1D scenarios that are frequently used, principally because of their analytical tractability (e.g. James *et al.* 2008, Plank and James 2008).

3.2 Methods

3.2.1 *The foraging simulator*

For this study a new computer program was developed which more realistically simulates a 2D forager, a full description of which is given in Appendix F. Briefly, however, the simulation begins with the specification of the study arena (the simulation is designed to allow simulation of laboratory trials) in which virtual foragers will be released. Rectangular arenas can be set up with sizes ranging from a small laboratory aquaria to an ocean basin and comprise a 2D grid of cells into which prey patches can be 'pasted' to generate a prey field. The number, distribution and density of prey patches and the overall available biomass can all be specified; once generated a configuration can be saved for future reuse and therefore multiple simulations can use exactly the same prey field, thereby controlling for prey field variability in the results.

A single foraging run involves the generation of a random walk through the study arena with turn angles being always drawn from a uniform turn angle on the interval [0,2π] radians and a move step (or vector) being draw from a pre-defined distribution as follows: Uniform, with a single parameter of maximum length (note that because at least one interpolated step is always performed the X_{min} parameter is effectively 1); exponential with parameters of exponent and X_{min}; power-law, with parameters of exponent (μ) and X_{min}; truncated power-law (truncated Pareto) with parameters of exponent (μ), X_{min} and X_{max}. Each move step is interpolated across the prey-field grid with any prey encountered being counted and, optionally, consumed (i.e. in the 'destructive' foraging scenarios). If at any point the boundary is encountered the move is reflected, i.e. the forager is contained within the arena (see Figure 15). A foraging run can be limited to a number of steps, a maximum path length, or both (i.e. whichever limit is reached first). Any number of replicate runs can be performed with statistics being collected on biomass consumed and distance travelled.
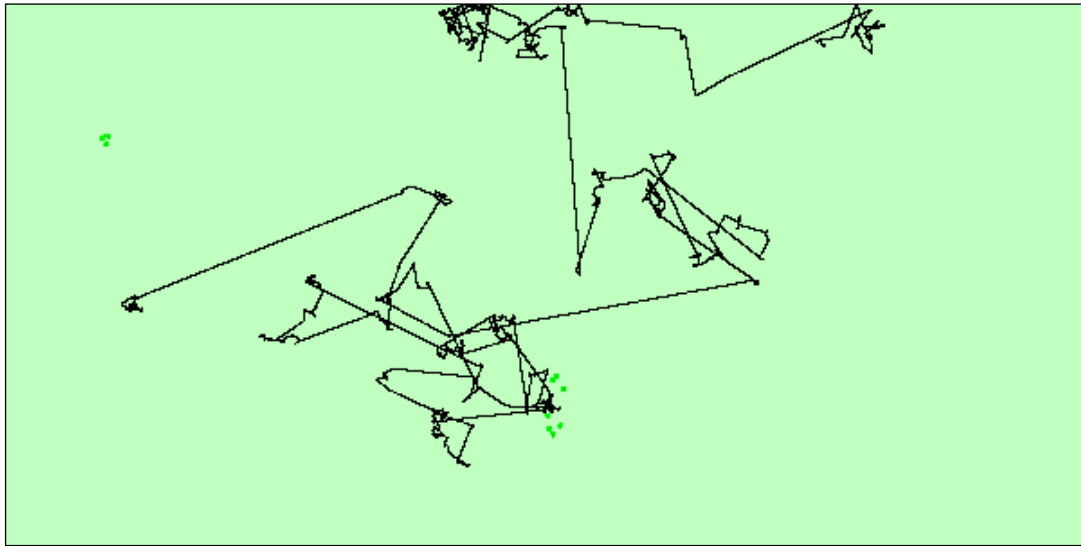
Figure 15: An example foraging run
> A truncated Pareto move step distribution with x_{min} = 5, μ = 2.0 x_{max} = 2500. Steps can be seen to be reflected from the boundary of the tank. Lévy distributed prey patches are shown in green.

3.2.2 General methods

The simple simulations performed by Sims *et al*. (2008a) replicated the simplest foraging model of non-destructive foraging and no prey targeting in the simulations and analysis performed by Viswanathan *et al*. (e.g. 1999, 2000, 2001), which included prey targeting whereby the forager stopped moving when a prey item was encountered and a new move was then performed. This simple scenario was also considered by James *et al*. (2011), however, the Sims *et al*. (2008a) simulation was actually closer to the destructive foraging scenario because no back-tracking occurred;

this is because the forager moved at a constant horizontal rate of one cell per step and with varying vertical step-lengths (to reflect the diving movements analysed empirically). Therefore, prey patches could not be revisited in the Sims *et al*. (2008a) simulation, a subtlety that was perhaps not fully understood at the time. The simulations performed here will cover the four combinations of destructive and targeted foraging. The simulations performed by James *et al.* (2011) were very short, comprising only 10^4 replicates, despite those in Sims *et al.* comprising 10^5 runs (some 6 x 10^5 replicates in total). In this study 10^5 replicates are also used. Unless otherwise specified each forager performs 5000 steps in each simulation, which was also the case in the simulations performed by Sims *et al* (2008a). In order to remove the effect of differing path lengths *Foraging Efficiency* was measured as biomass consumed per unit distance travelled. A further measure of foraging success reported here was the percentage of successful foraging runs, i.e. the number of runs where at least one encounter with prey occurred, expressed as *Encounters per unit distance travelled*.

3.2.3   Prey fields

The prey field environment was set up to match the Sims *et al*. (2008a) simulation, setting the arena to 2500x5000 cells. Unless otherwise specified the simulations use a sparse prey field with a total biomass of 6000 units distributed as 10 patches giving a total of 1876 populated cells with each patch enclosed within a 20x20 area. This gives a mean biomass density of 0.00048 units per cell and a populated cell proportion of 0.015%. Periodic boundary conditions are observed for the placement of patch pixels (i.e. if the edge is reached the patch is wrapped around) and biomass is added to any already present if a patch overlaps a previously placed patch.

3.2.4   Simulation scenarios and foraging strategies

Four simulation scenarios were considered with five different foraging strategies. The scenarios were (1) non-destructive, no targeting; (2) destructive, no targeting; (3) non-destructive, targeted; (4) destructive and targeted. The five foraging strategies (i.e. move step-length distributions) used were (1) uniform, maximum step 16; (2) truncated Pareto (TP) X_{min} 1.0, μ 1.5, X_{max} 2500; (3) TP as 2 but with μ 2.0 (the hypothetically optimal strategy); (4) TP as 3 but with μ 2.5; (5) Exponential with X_{min} 1.0, exponent 0.148. The uniform and exponential foraging strategies were configured to give a mean step-length of ~8, roughly equivalent to the TP with μ 2.0 (this is not

particularly important because results are expressed as per unit distance travelled but might affect encounter rates). Note that in all these simulations a truncated Pareto, rather than a pure power-law was used for the Lévy foragers. The reasons for this are twofold; firstly pure power-laws are rare in empirical data (Humphries *et al.* 2010) and therefore using truncated power-law distributions of move step-lengths here makes this work more relevant to empirical field studies; secondly the simulation environment is bounded to dimensions of 2500x5000 and pure power-laws would cause excessively long steps that would frequently exceed these boundaries.

3.3 Comparison of Lévy, uniform and exponential foragers

The principal question asked by many studies is simply whether a Lévy foraging style is more efficient than other foraging styles (e.g. Viswanathan *et al.* 1999, Viswanathan *et al.* 2000), with efficiency typically being measured as the quantity of biomass consumed per unit distance travelled. Here, in the first simulation scenario, that question was addressed by comparing the three Lévy foragers with the two simple foragers (i.e. uniform and exponential), that have movement patterns similar to Brownian motion. The initial comparison therefore comprised five different foragers in a sparse prey field and foraging was non-destructive (i.e. prey patches were not depleted and were therefore revisitable).

The results are given in Figure 16, Figure 17, Table A1 and Table A2. It can be seen that the Lévy forager with μ = 2.0 performed slightly, though significantly, better than the other foragers in terms of efficiency; 2.95% better than the exponential forager (Kruskal-Wallis One Way Analysis of Variance on Ranks; $p < 0.001$). Differences between all foragers were significant at $p < 0.05$ (Tukey Test). This result is as predicted by the Lévy flight foraging hypothesis except that Viswanathan (1999) employed prey targeting, whereas here μ = 2.0 was found to be marginally more efficient in even the simplest case. However, the most obvious discriminator in this scenario is the number of simulation runs that encounter prey, presented as successful (i.e. non-zero runs) / mean path length. Clearly it is important to correct for differences in mean path length which ranged from 14541 to 249938. Here the Lévy forager with μ = 2.0 outperformed all other foraging strategies and outperformed the worst, the uniform forager, by ~2.6 times (Mann-Whitney Rank Sum Test; $p < 0.001$, Figure 17).
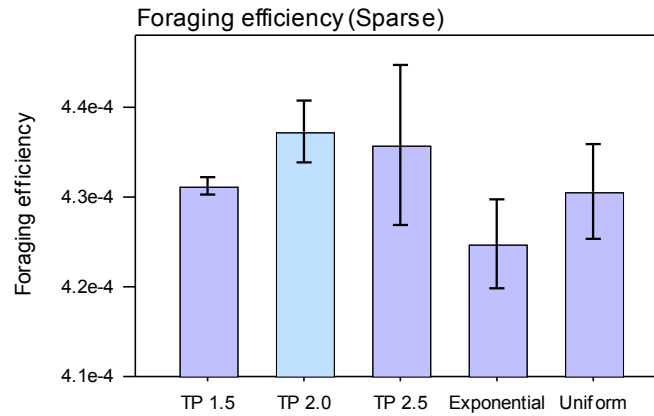
Figure 16: Comparison of Lévy with exponential and uniform foragers
The Lévy (TP) forager with μ=2.0 marginally outperformed the other foragers in terms of foraging efficiency (i.e. biomass consumed per unit distance travelled). The difference was small (e.g. ~3% > exponential) but significant ($p < 0.001$, Kruskal-Wallis One Way Analysis of Variance on Ranks); all pairwise comparisons were significantly different at $p < 0.05$ (Tukey test), see text and Table A2. The error bars show ±S.E.
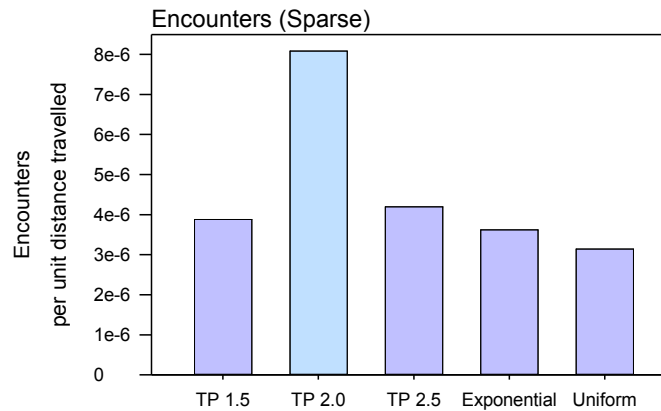
Figure 17: Encounter rates (measured as successful foraging runs) per mean unit distance travelled
In the simplest foraging scenario it is the encounter rate of the Lévy forager with μ=2.0 that was the most obvious discriminator of performance. The TP2.0 forager was twice as successful as the other foragers.

3.4   Destructive vs. non-destructive foraging

Previous studies have suggested that Lévy foraging is only advantageous when a prey patch is revisitable (Viswanathan *et al.* 1999, Viswanathan *et al.* 2001, James *et al.* 2011), i.e. when prey is not depleted, as might be the case with pelagic predators preying on large schools of fish or on patches of zooplankton. Other work focusing on encounter rates has found that the encounter rate for Lévy foragers was higher even if prey was consumed (Bartumeus *et al.* 2002). To investigate the hypothesis that Lévy foragers lose the advantage when foraging is destructive the simulations from the first scenario were repeated but with prey being consumed. In this scenario prey is depleted, i.e. prey was not replaced somewhere within the arena when consumed (which would be complex to achieve while maintaining the prey distribution), so the overall level of prey availability fell as the simulation proceeds.

The results are given in Figure 18, Figure 19 and Table A1. Here the TP 1.5 forager (approaching ballistic movement) outperformed other search patterns (~30% better than uniform and ~16% better than exponential, Mann-Whitney Rank Sum Test $p <$ 0.001) with TP 2.0 being a little less successful (~20% better than uniform and ~8% better than exponential, Kruskal-Wallis One Way Analysis of Variance on Ranks $p <$ 0.001). The overall foraging efficiency was reduced from a maximum rate of 4.37E-04 for non-destructive foraging to 4.21E-04 (3.66% less) as would be expected with prey being depleted. With destructive foraging there now seems to be an advantage in leaving a patch and exploring further afield; the TP 1.5 forager had more frequent long relocations than the other foragers and spent less time in any given patch. The poor performance of the TP 2.5 forager adds weight to this suggestion as this forager had less frequent long relocations and therefore tended to remain in a more localised area. The difference between the TP 2.0 and the uniform forager was ~11% (Kruskal-Wallis One Way Analysis of Variance on Ranks; $p < 0.001$), similar to the difference found by Sims *et al.* (2008a), supporting the contention that the 2008 simulation is consistent with the destructive foraging scenario. It should be noted that both the mean path length and the number of encounters was consistent throughout the simulations depending only on the foraging strategy, as can be seen in Figure 19 and Table A1.
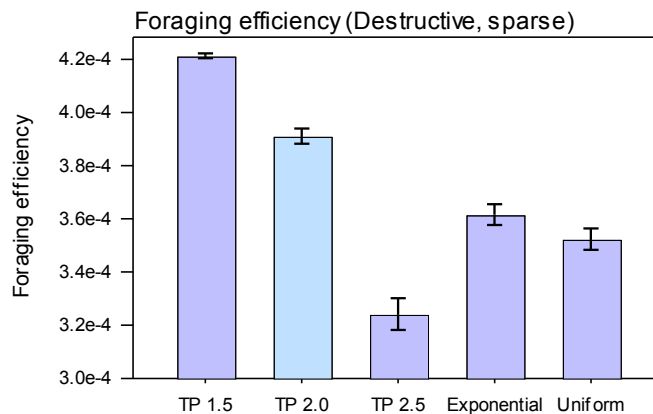
Figure 18: Destructive foraging in a sparse prey field

In this scenario the TP 1.5 forager was clearly more efficient in terms of biomass consumed per unit distance travelled; however the TP 2.0 forager still outperformed the others. Error bars show ± S.E. Variance was considerably less than with the non-destructive scenario.
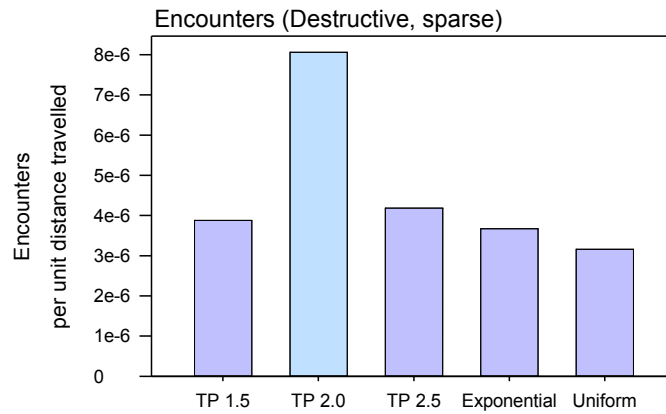
Figure 19: Encounter rates with destructive foraging
The encounter rates were unchanged from the first scenario with non-destructive foraging, despite the depletion of the prey field.

3.5 The effect of prey targeting

In the simulation model of Viswanathan *et al.* (1999, 2000) the forager continually scans the surroundings, within a radius of detection, and halts a move step if prey is encountered, then proceeding directly to the prey. In the preceding simulations a simpler model was employed, where the forager does not alter the path and therefore those simulations were simply an investigation into the effect of the movement pattern. However, the model used by Viswanathan *et al*. is biologically realistic, and it is with this model that the optimality of μ = 2.0 was originally determined. To investigate the effect of prey targeting, a set of simulations was performed with prey targeting by halting a move step when a grid cell containing biomass was encountered and then selecting another move step; the forager was not randomly relocated. The radius of detection for the forager was just one unit, being the most conservative case. These simulations covered scenarios (3) and (4) as described above, i.e. non-destructive and destructive foraging with prey targeting and employed the same five foragers.

The results are given in Figure 20, Figure 21 and Table A1. As with the first scenario the TP 2.0 forager clearly outperformed the others, although here it was by a greater margin, 18% greater than the next best forager (TP 2.5), 2.17 times greater than the exponential forager and 2.5 times greater than the worst performing uniform forager (Kruskal-Wallis One Way Analysis of Variance on Ranks, *p* < 0.001 in all cases). In the destructive foraging scenario the results differ from the previous destructive foraging simulations but were very similar to the non-destructive, targeted scenario with the TP 2.0 again being the most successful. Apart from the expected reduction in the overall

level of prey consumption there was little difference between the destructive and non-destructive results when prey targeting was employed.

The success of the TP2.0 forager was in fact much greater than expected, given that the advantage conferred by prey targeting (in terms of the exploitation of a patch once encountered) was the same regardless of the movement pattern of the forager. Once a patch was encountered, and a step halted, subsequent steps often led immediately to another cell containing biomass, causing a further halt and new step. Because prey lies within only one or two cells of the present location it made no difference what distribution the move step was drawn from and therefore all foragers gained the same advantage once a prey patch was encountered. Once within a patch, therefore, all foragers proceeded by simple Brownian diffusion until they left the patch. A simplified example of such a path is shown in Figure 22. The most likely explanation of the much greater success of the TP2.0 forager, therefore, was that the forager encountered more new prey patches than the other foragers and consequently was able to exploit more patches. The results from all four foraging scenarios are summarised in Figure 23 where the significant difference conferred by prey targeting is clear.

It is also worth noting that the relative efficiencies were the same under the destructive foraging scenario. However, in these simulations prey patches were used, not single prey items and therefore although encountered prey was consumed there remained further prey in the immediate vicinity that was exploited. Consequently, the destructive foraging scenario explored here differs from that used by Viswanathan *et al*.

The most consistent result from these simulations was the success of the TP 2.0 forager in terms of the percentage of successful foraging runs (i.e. runs where some, rather than no, prey was encountered), when adjusted for the distance travelled. There was, as expected, a clear relationship between the chance of a foraging run being successful and the mean path length, as shown in Figure 24. The TP1.5 forager experienced an unsuccessful run < 3% of the time. The TP2.0 forager however, was almost twice as successful as the exponential and uniform foragers, both of which were designed to have almost identical path lengths. Ultimately, it was this increased encounter rate that led to the overall success of the TP2.0 forager. A further interesting observation was that the percentage of successful foraging runs was

completely independent of the foraging scenario being tested, as shown in Figure 25, where it is clear that only the movement pattern affects the encounter success.
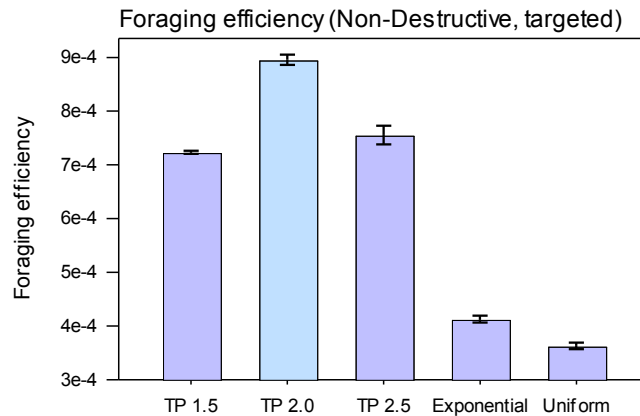
Figure 20: Non-destructive, targeted foraging
The results are similar to the first, non-destructive, scenario where the TP 2.0 forager was the most efficient, although here the advantage of the TP 2.0 forager was even greater (~1.47 times > uniform). The uniform forager however performed very poorly and was in last place rather than fourth. The overall prey consumption was much higher, as would be expected given the improved prey patch exploitation in this scenario. Again error bars are ± S.E.
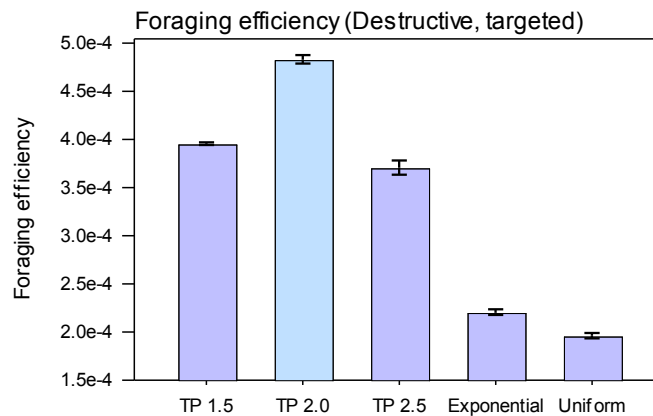
Figure 21: Destructive targeted foraging
Contrary to the previous simulations with destructive foraging (Figure 18) these results are almost identical to the non-destructive, targeted simulations. The principal difference was an expected reduction in the overall prey consumption. Error bars are ± S.E.
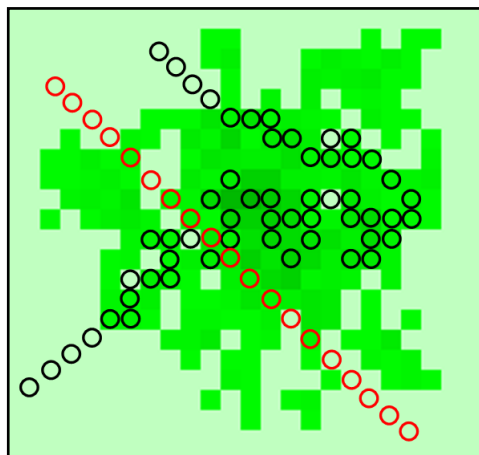
Figure 22: Prey targeting allows greater prey-patch exploitation
A forager with prey targeting (black circles) performs a complex, diffusive random walk throughout the prey patch, halted at every move that encounters prey. Consequently significantly more of the prey patch is exploited than is the case with the simple forager (red circles) that moves blindly through the patch, as a virtual forager would in this simulation without prey targeting.
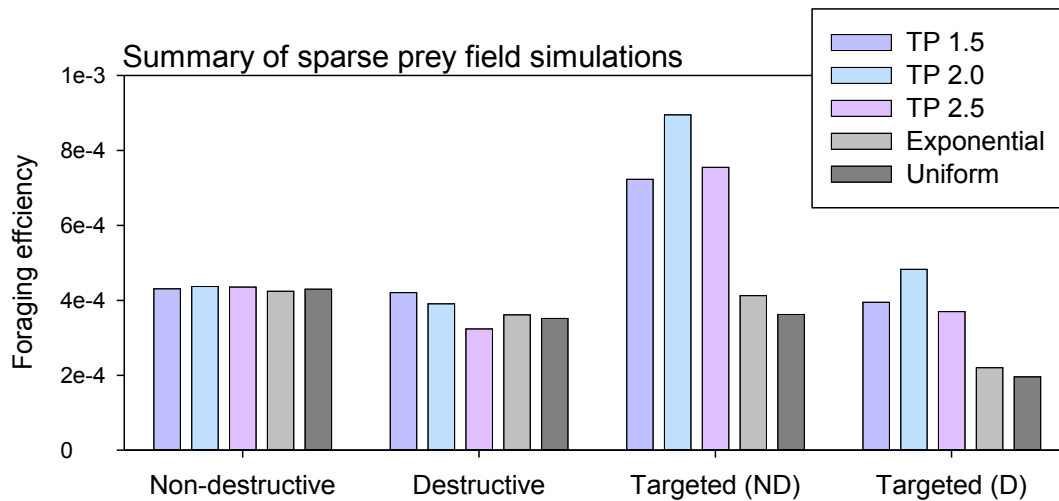
Figure 23: Summary of sparse prey field simulations

Differences between the foragers can be seen to be relatively minimal in the simplest non-destructive non-targeted case but are quite pronounced in the targeted scenarios. (D) Destructive, (ND) non-destructive.
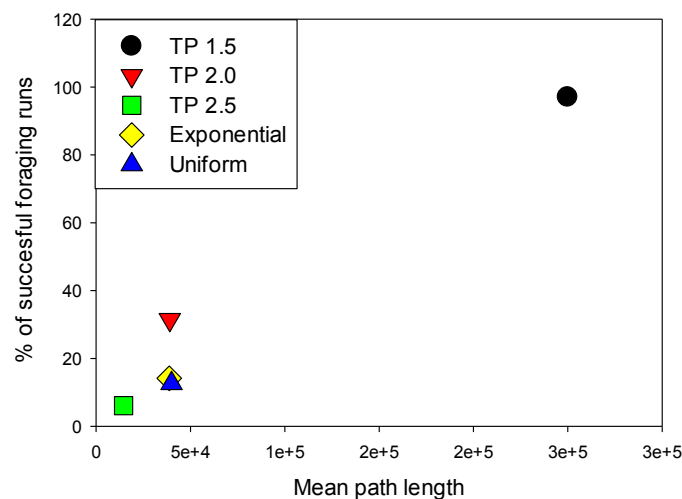
Figure 24: Percentage of successful foraging runs *vs* mean path length

With increasing mean path length there is an expected increase in the percentage of foraging runs that encounter prey and it was therefore not surprising that the TP1.5 forager, with a mean path length 17 times greater than the uniform forager, has about 97% of successful runs. What was most interesting here was the performance of the TP2.0 forager compared to the exponential and uniform foragers which were designed to have the same mean path length. The TP2.0 forager yielded 31% success compared to 14 and 12% for the exponential and uniform foragers respectively; more than twice as successful.
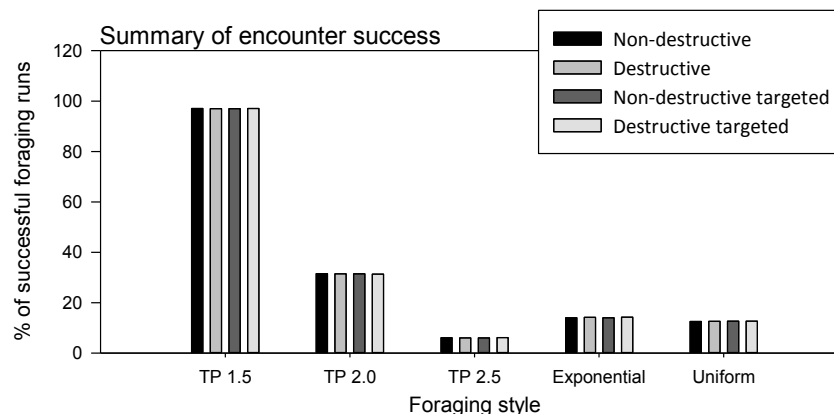
Figure 25: Summary of encounter success

Remarkably, regardless of the scenario being tested, the percentage of successful encounters for each of the foragers is unchanged. There is clearly a superficial correlation with the mean path length as shown in Figure 24, but the TP2.0 forager easily outperforms all but the TP.15 forager, despite having a similar

mean path length to the exponential and uniform foragers.

3.6 Investigation of stabilisation/convergence of foragers after many runs

James *et al.* (2011) suggest that after 10^4 simulation runs the results from all four foraging strategies studied (Lévy or uniform foragers in Lévy or uniform prey fields) converge to the same foraging efficiency. This was not the outcome found by Sims *et al.* (2008a) after 10^5 runs and it is clear that different foragers do not converge in the simulations performed here except perhaps the simplest case of scenario 1 (non-destructive, non-targeted foraging). With scenario 1 the differences between the foragers are small and there is therefore a possibility that they do indeed converge after sufficient simulations have been performed. Therefore, to explore this, the results from the simulations performed here were analysed further by calculating a running mean from the individual simulation results over all 10^5 simulation runs. The mean was calculated as the sum of biomass consumed per unit travelled for runs 1 to *n*, divided by *n*, for all simulations in the sparse, uniform prey-field set.

The results are given in Figures 26-29. For scenario one it was clear that the simulations were very far from convergence at 10^4 runs, contrary to the findings of James *et al*. (2011) and have not properly stabilised after 10^5 runs. There was an indication that the TP2.0 forager will remain marginally better, and that the exponential forager will remain the poorest performer, as reported in the results from these simulations. However, the outcome was quite unclear and in fact it is possible that the stochastic variations might always exceed the intrinsic differences in performance, leading the outcome never to settle on any one forager as being the most efficient. Taking the TP2.5 forager as an example, the mean biomass consumption is 6.33 and the standard deviation is 40.61 (*n* = 10^5). With such a large variance in individual simulations and with small differences in performance (~3%) it seems likely that the foragers will never converge on distinct outcomes. The exception being the TP1.5 forager which seemed to have stabilised by about the 40,000[th] run and had a mean biomass consumption of 107.78 (76.61 s.d.), confirming the lower stochastic variation.

In scenarios 2 to 4 the results were different, with all five foragers quickly settling to clearly defined and different efficiencies. There was still considerable stochastic

variation (mean 5.38, s.d. 33.5, $n = 10^5$ for the TP 2.5 forager, scenario 4), but in scenarios 2 to 4 the variation was well below the level of difference in efficiency. We can therefore be confident that the reported results for these simulations are robust and correct.

To explore further the lack of convergence or stabilisation in scenario 1, 10^6 simulations were performed and again the running mean was calculated. The results are shown in Figure 30 where it is evident that even after 10^6 runs the foraging efficiencies have still not either converged or stabilised. Furthermore, it is also clear that the ranking of the five foragers was different from the previous simulations and that the apparent superiority of the TP2.0 forager was simply a stochastic variation. Examining the standard deviations of foraging efficiency for the five foragers (Table 5) it can be seen that the TP2.5 forager has the most variation and the TP1.5 the least, as expected from the plot in Figure 30.

There is an interesting difference between the Lévy foragers with an apparent inverse correlation between the variance and the exponent; the TP1.5 forager settled relatively quickly to a steady result, whereas the TP2.5 forager was far from settling after 10^6 runs, with the TP2.0 forager being intermediate. It is possible that this result was a consequence of the marked difference in path lengths between the three Lévy foragers; the TP1.5 forager has a mean path length of 249,928 compared to 39,016 for the TP2.0 and 14,543 for the TP2.5 foragers. To test whether this is the case the convergence simulations were repeated using a limited path instead of limited steps; the path length was set to 40,000 units, to match the TP2.0 forager. The results are given in Figure 31 and Table 5 and show that even with limited path length there was still a difference in the standard deviation of foraging efficiency between the five foragers. The standard deviation of the uniform, exponential and TP2.0 foragers was similar between step-limited and path-limited simulations; however, the TP1.5 forager had increased variance (3.07E-04 for step-limited and 7.62E-04 for path-limited) while the TP2.5 forager had reduced variance (2.80E-03 for step-limited and 1.72E-03 for path-limited). Given that the TP1.5 forager had the longest mean path length under the step-limited simulations and therefore was subject to the greatest reduction in path length, the increase in variance was in line with the prediction; albeit less than expected. Similarly with the TP2.25 forager, which had the shortest path length under

the step-limited simulations and therefore was subject to the greatest increase in path length the reduction in variance is again in line with predictions. The uniform, exponential and TP2.0 forager's path lengths were unchanged, as was the variance in foraging efficiency. It can therefore be concluded that while path length is an important factor in the variance in foraging efficiency it is only part of the explanation and some of the differences in variance must be due to differences in the movement patterns. Limited path simulations are investigated in more detail below in Section 3.9.

Given the lack of stabilisation in scenario 1 the remaining investigations here used only scenarios 2, 3 and 4; namely destructive, targeted non-destructive and targeted destructive foraging.
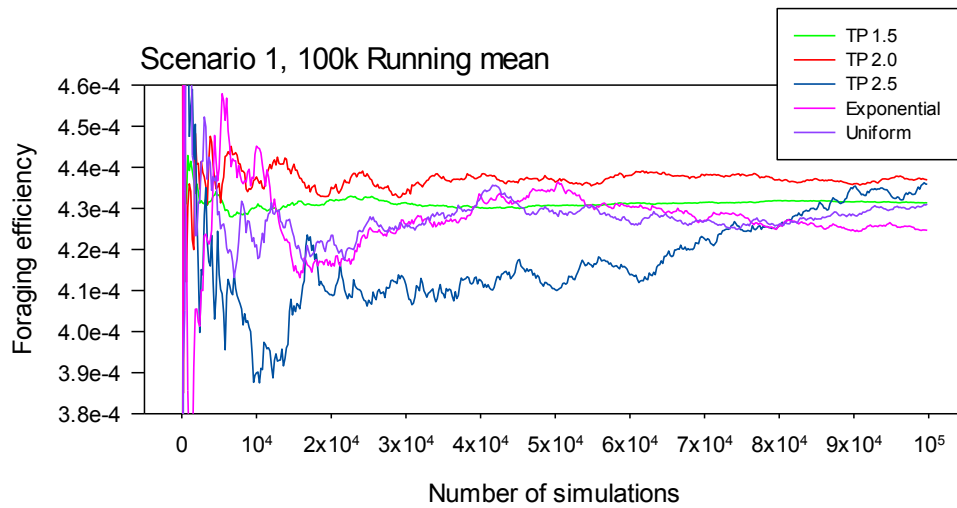
Figure 26: Stabilisation of scenario one simulations after 10^5 runs

Large stochastic variations can still be seen to cause the outcome to meander after 10^5 runs, suggesting either that further runs are required before the simulations settle on a final value or that stochastic variations might always exceed the intrinsic differences between the foragers, leading to a constantly varying outcome. At around 10,000 runs it is clear that the situation is still very dynamic. The stability of the TP1.5 forager is in marked contrast to the other foragers.
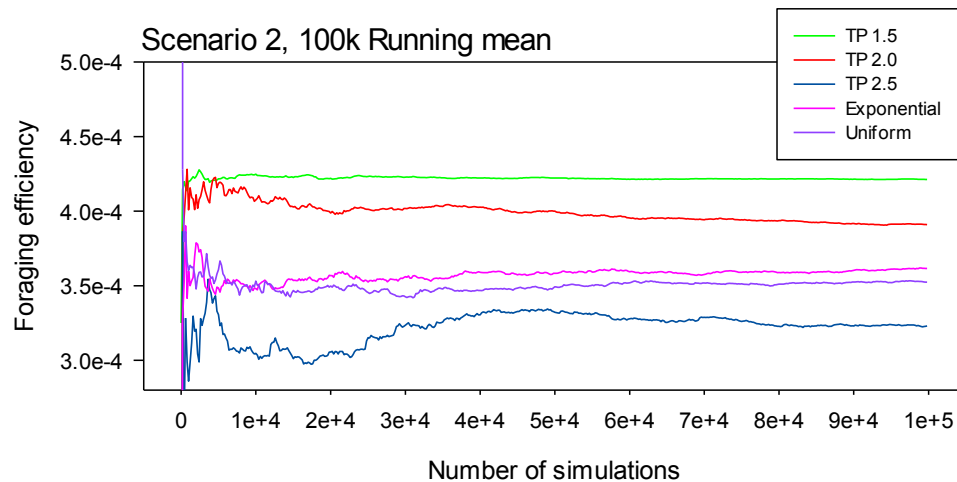
Figure 27: Stabilisation of scenario two simulations after 10^5 runs

With destructive foraging the results are quite different from scenario 1 (Figure 26 and Figure 30) with all five foragers settling to distinct outcomes by the 40,000[th] run. The ranking of the foragers is unchanged

after about run 15,000, but large stochastic variations make the final outcome unclear prior to that point.
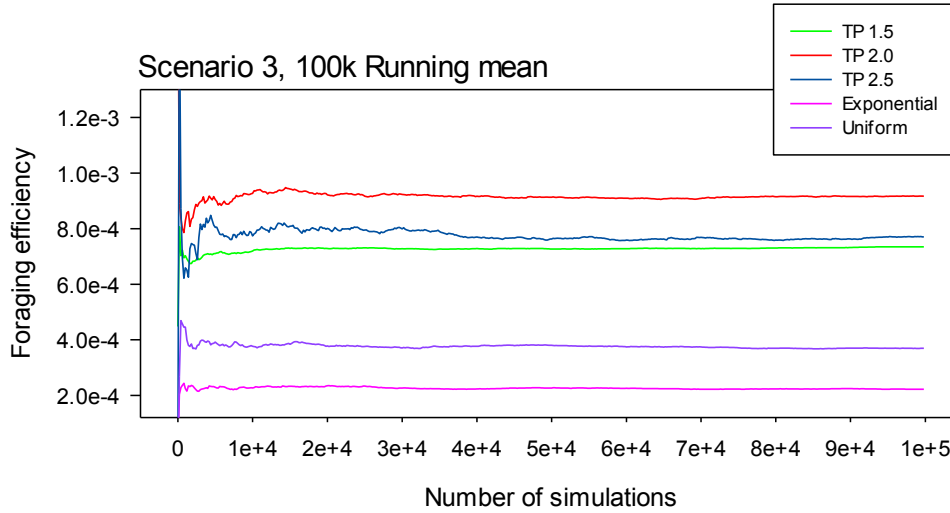
Figure 28: Stabilisation of scenario three simulations after 10^5 runs
With prey targeting and non-destructive foraging the foragers stabilise much more quickly, with the ranking unchanging after less than 5000 runs.
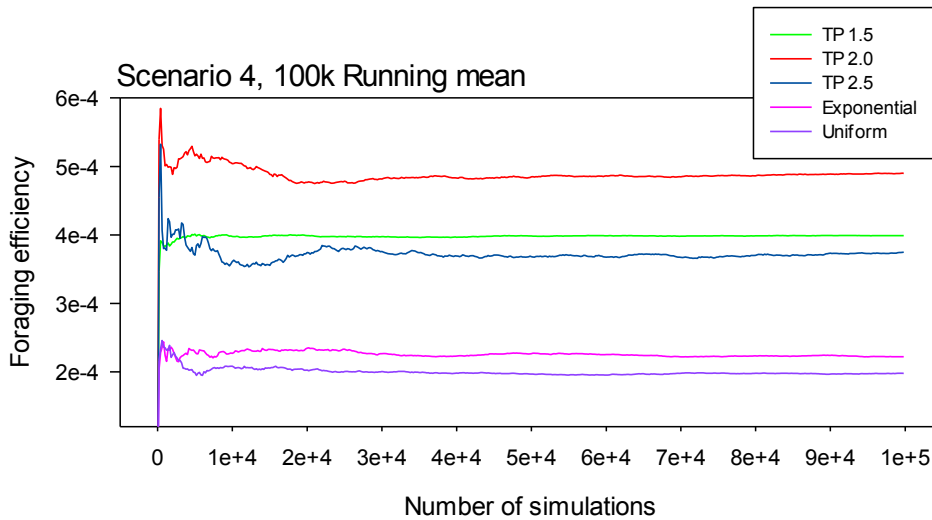
Figure 29: Stabilisation of scenario four simulations after 10^5 runs
With destructive, targeted foraging the simulation outcomes settle to clear and distinctly different results after 10,000 runs, with little change in relative values after 50,000 runs. 10^5 runs, as used in all simulations in this study, is therefore a sufficient number for confidence in the results.
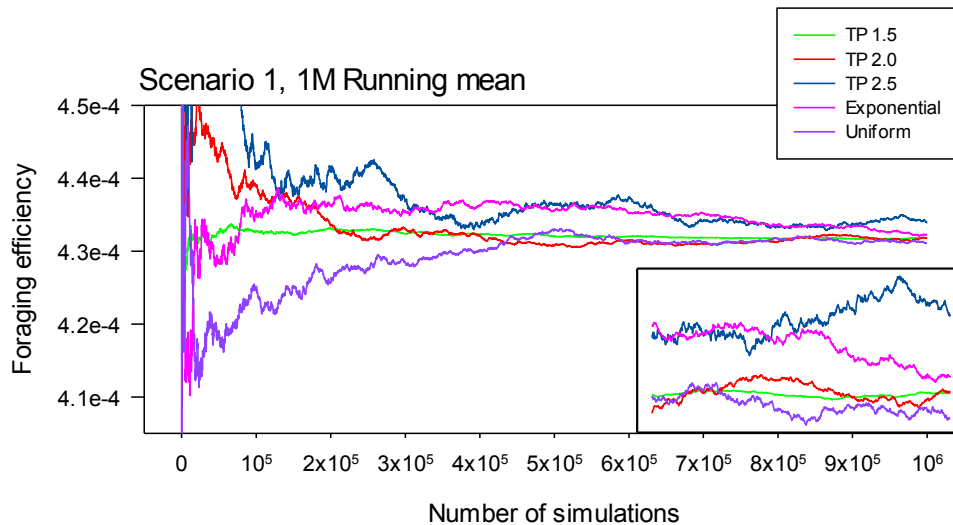
Figure 30: Stabilisation of scenario one after 10^6 simulation runs
Even after 10^6 simulations stochastic variation exceeds the difference between the foragers. The inset

78

shows the last 20000 simulations, confirming the continuing variability and uncertainty.

Figure 31: Stabilisation of scenario one after 10^6 limited path simulation runs
Even after 10^6 simulations stochastic variation exceeds the difference in efficiency between the foragers. The inset shows the last 20000 simulations, confirming the continuing variability and uncertainty. Limiting the path length does seem to reduce the variability slightly, but the differing paths lengths are clearly not the whole story.

Table 5: Variation in foraging efficiency after 10^6 simulations
The table below gives the mean foraging efficiencies for the limited step and limited path simulations. Difference is calculated as the absolute value of the difference between the mean of the foraging efficiency and the average value of all means. In all cases the standard deviation significantly exceeds the differences in the means, indicating that with the non-destructive, non-targeted scenario the simulations will not stabilise to a final result.

	Limited step			Limited path		
Forager	Mean	Difference	S.D.	Mean	Difference	S.D.
Uniform	4.3110E-04	1.0954E-06	1.6943E-03	4.3218E-04	6.1717E-07	1.6972E-03
Exponential	4.3227E-04	7.4259E-08	1.5868E-03	4.3377E-04	9.6977E-07	1.5639E-03
TP 1.5	4.3180E-04	3.8961E-07	3.0717E-04	4.3192E-04	8.7928E-07	7.6294E-04
TP 2.0	4.3185E-04	3.3779E-07	1.0763E-03	4.3319E-04	3.9262E-07	1.0561E-03
TP 2.5	4.3394E-04	1.7485E-06	2.8045E-03	4.3293E-04	1.3406E-07	1.7221E-03

3.7 Comparison of sparse and abundant prey fields

A further contention that has been discussed in many studies is that Lévy foraging is only significantly advantageous when prey are scarce (Viswanathan *et al.* 1999, Bartumeus *et al.* 2002, Bartumeus *et al.* 2005, Reynolds and Bartumeus 2009, James *et al.* 2011). Therefore, to investigate differences in foraging efficiency of Lévy flight search patterns caused by prey field density, all the simulations reported above in Sections 3 to 5 were repeated with an abundant prey field with 10^6 biomass units distributed as 166 patches with a total of 61144 populated cells. This gave a mean biomass density of 0.00489 units per cell and a populated cell proportion of 0.489% (as discussed later a biologically realistic value, based on plankton densities might be much lower at 0.26% (Sims 1999)). This prey field was specified so as to have the same

density as that used by James *et al* (2011). For comparison both prey field distributions are given in Figure 37 and example sparse and abundant prey patches are shown in Figure 38. The expectation for these simulations is that the exponential and uniform strategies would perform as well as the Lévy search (TP) strategies, as suggested by Viswanathan *et al.* (2002).

The results for all simulations are given in Figure 32 and in Table A3, and contrary to expectations the relative performance of the five foragers in the abundant prey field was similar to that of the sparse prey field (Figure 23). The only noticeable difference was in the quantity of prey consumed. In the destructive non-targeted scenario the TP1.5 forager was still the best by about the same margin as that found in the sparse prey field (28.79%, Mann-Whitney Rank Sum Test $p < 0.001$). With prey targeting the TP 2.0 forager was clearly the most efficient, performing 2.4 times better than the worst forager (uniform), 2.15 times better than exponential when foraging was non-destructive, and 2.75 and 2.35 times better than uniform and exponential, respectively, when foraging was destructive (Kruskal-Wallis One Way Analysis of Variance on Ranks $p < 0.001$ in all cases).

Encounter rates in the abundant prey field (Figure 33) were not only very different to those obtained with the sparse prey field but seem at odds with the efficiency results; the TP 2.5 forager, which was the poorest performing in terms of biomass consumed, was the most successful in terms of the number of foraging runs where prey were found, when corrected for mean path length. The encounter rates were also robust to the foraging scenario, as with the sparse prey field. However, the problem in this case was that there were a very small number of unsuccessful foraging runs, so the number of encounters was more a reflection of differences in mean path length, a likelihood confirmed in Figure 34 where mean path lengths showed a correlation with the encounter rates. The effect of mean path length will be explored further in a set of limited path length simulations described below (section 3.9).

To investigate the possibility that the prey field being used was simply not abundant enough to provide sufficient difference with the sparse prey field to separate the foraging efficiencies, as expected, a second, more abundant prey field was used (i.e. 30×10^6 biomass units were distributed as 5000 patches with a total of 1,716,802 populated cells with each patch enclosed within a 20x20 area). This gave a mean

biomass density of 2.4 units per cell and a populated cell proportion of 13.73%. The results are given in Figure 35 and Table A4 and in the destructive non-targeted scenario the results are unchanged, with the TP1.5 forager performing 26% better than uniform and 10% better than exponential (Kruskal-Wallis One Way Analysis of Variance on Ranks; $p < 0.001$). In the non-destructive targeted scenario the differences between the foragers was now, as expected, less than in either the sparse or abundant prey fields, with the TP2.0 forager now only 78% better that the uniform forager in the non-destructive targeted scenario, compared to 2.4 and 2.75 times the sparse and abundant prey fields, respectively (Kruskal-Wallis One Way Analysis of Variance on Ranks; $p < 0.001$). The pattern was similar in the destructive targeted scenario with the TP2.0 forager being 89% better than uniform and 65% better than exponential (Kruskal-Wallis One Way Analysis of Variance on Ranks; $p < 0.001$).

As the expected parity between the foragers had still not been achieved the simulations were repeated with an even denser prey field (i.e. 120×10^6 biomass units, distributed as 2×10^4 patches with a total of 5,568,712 populated cells; 9.6 biomass units per cell, 44.55% populated cells). The results are given in Figure 36 and Table A5 and here the advantage of the Lévy foragers was much reduced, although in the destructive targeted scenario the TP2.0 forager still outperforms the rest (47% better than uniform, 33% better than exponential) (Kruskal-Wallis One Way Analysis of Variance on Ranks; $p < 0.001$). Again in the non-targeted destructive scenario the results are unchanged, with the TP1.5 forager still performing 29% better than the worst performer. All differences are significant at $p < 0.001$ (Kruskal-Wallis One Way Analysis of Variance on Ranks).
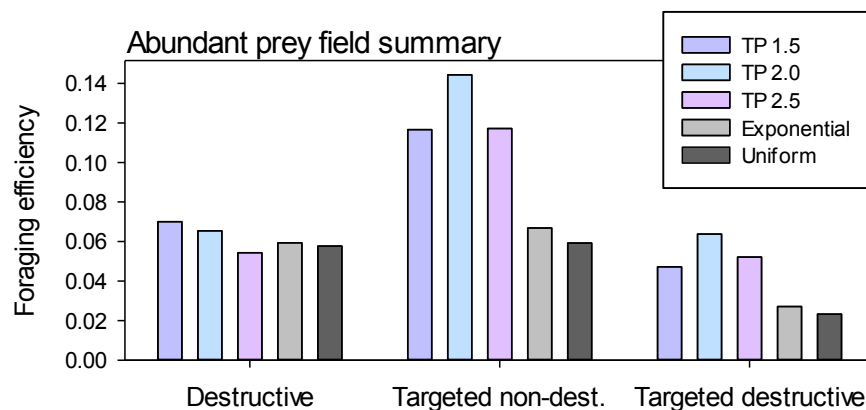
Figure 32: Summary of abundant prey field simulations
The results are almost identical to the results with the sparse prey field, contrary to expectations and suggesting that the prey field used was not abundant enough to fulfil theoretical expectations.
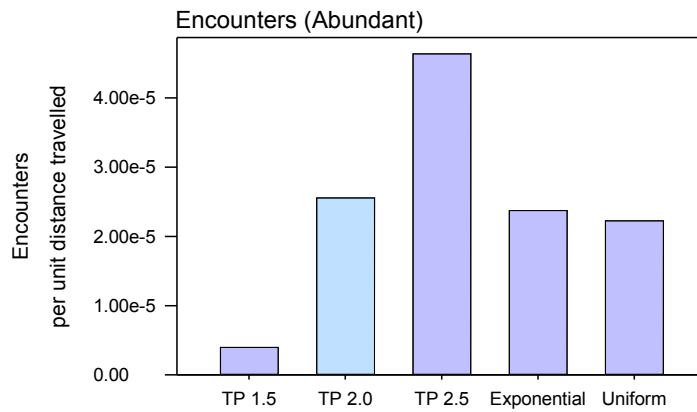
Figure 33: Encounter rates with abundant prey

Results here are quite different from the sparse prey field. Note that this shows the number of successful foraging runs, rather than the number of prey items encountered. Therefore while more of the TP2.5 forager runs find some prey, less prey per unit distance travelled is found than with the TP2.0 forager.
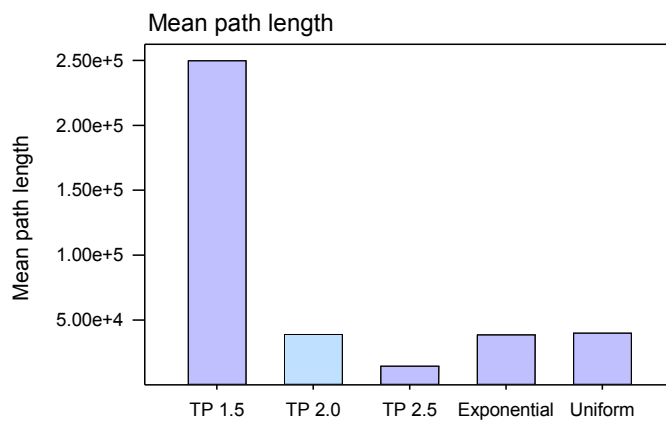
Figure 34: Mean path length

There is a clear inverse correlation between the mean path length and the encounter rate per unit distance travelled as shown in Figure 33.
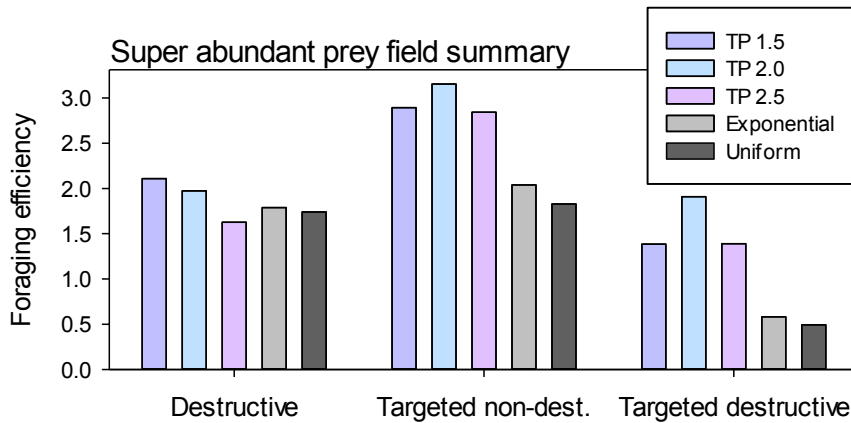
Figure 35: Summary of simulations in a super-abundant prey field

The difference between foragers is now less than with the sparse prey field, as expected.
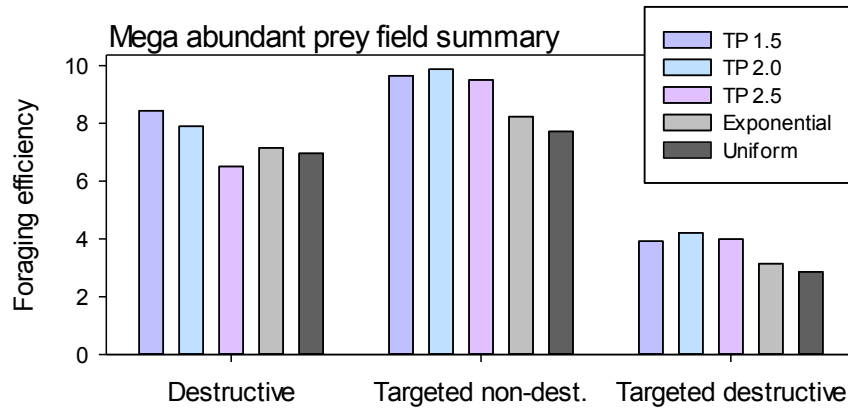
Figure 36: Destructive, targeted foraging in a mega-abundant prey field
The difference between the foragers is now considerably reduced, although in the targeted destructive scenario the TP2.0 forager was still 47% better than the uniform forager and all the Lévy foragers still have the advantage, despite the abundance of prey covering 44% of populated cells.
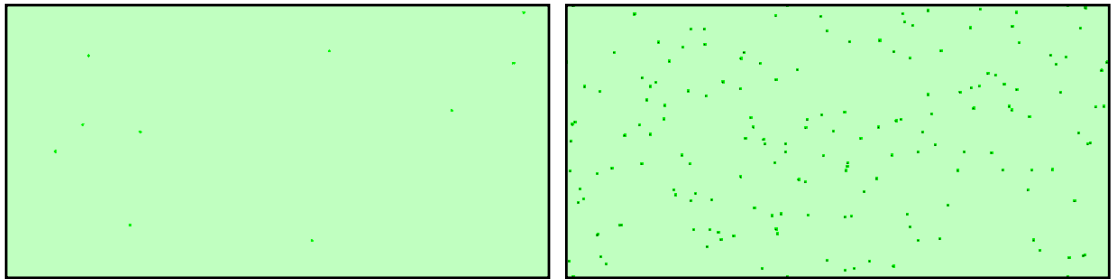
Figure 37: Sparse and abundant uniform random prey fields
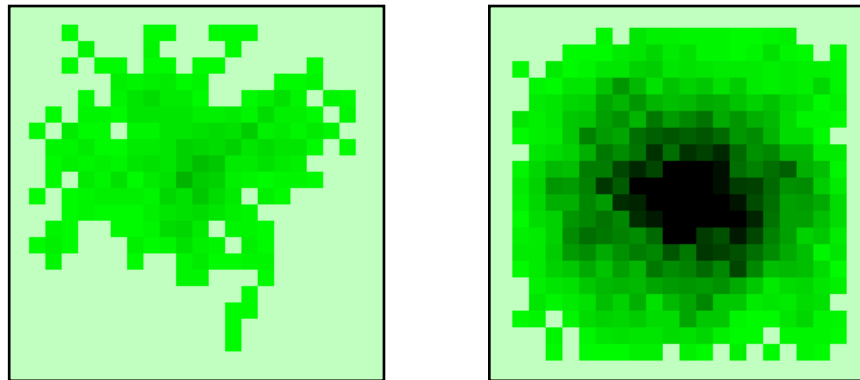
Figure 38: Sparse and abundant prey patches
Darker pixels indicate higher values of biomass in that grid cell. Prey patches are generated by overlaying multiple random walks with the origin at the centre of the patch with each walk adding one unit to the biomass of each visited cell.

3.8 Comparison of Lévy and uniformly distributed prey patches

In the simulations performed by Sims *et al.* (2008a) the Lévy forager was found to perform even better than the uniform forager when the prey patches were distributed with inter-patch distances being drawn from a Lévy distribution. The simulations were therefore repeated using both sparse and abundant Lévy-distributed prey fields, with a truncated Pareto distribution being used with X_{min} = 10.0, μ = 2.0 and X_{max} = 2500, to provide the inter-patch prey field distances. The prey field was constructed in the same

way as with Sims *et al.* (2008a), with the first patch being located using uniform random numbers for the *x* and *y* coordinates. Subsequent patches are then located relative to the first patch by calculating a vector (from the TP distribution) and a uniform turning angle; periodic boundary conditions were observed. The resulting pattern has been referred to as a Lévy 'dust' (Miramontes *et al.* 2012).

Results with the sparse Lévy prey field are given in Figure 39 and Table A6. With the destructive non-targeting foraging scenario the overall pattern was the same as with the uniform prey field (Figure 23 and Table A1) where the TP 1.5 forager was best having a 25.07% advantage over the worst (TP2.5) forager, and the TP2.0 forager being second best with a 16.52% advantage. Compared to the uniform forager, the TP2.0 forager was 13.18% better, a value that corresponds very well with the 14% advantage found by Sims *et al.* (2008a). In addition the TP2.0 forager was 9.42% better than the exponential forager. All differences were significant at $p < 0.001$ (Kruskal-Wallis One Way Analysis of Variance on Ranks).

With prey targeting the pattern was almost identical to the other simulations. However, the advantage of the TP2.0 forager was even greater at 2.90 times better than the uniform forager for both the non-destructive and destructive scenarios, compared to 2.4 times greater for the uniform prey field, and 2.63 and 2.50 greater than the exponential forager in the non-destructive and destructive scenarios respectively. All differences were significant at $p < 0.001$ (Kruskal-Wallis One Way Analysis of Variance on Ranks).

With the abundant Lévy prey field (Figure 40 and Table A7) the results of the destructive, non-targeted scenario were almost identical to the uniform prey field results, with the TP1.5 forager being the most successful with a 28.79% advantage over the TP2.5 forager. In the targeted scenarios the results were, again, almost identical to all the other targeted simulations although the advantage of TP2.0 forager was now even greater, being 3.2 times greater in the non-destructive, and 3.44 times in the destructive targeted scenarios than the uniform forager, and 2.75 and 2.90 better than exponential, respectively.

As a final test the simulations were repeated using the super-abundant Lévy prey field. The results are given in Figure 41 and Table A8. The overall relative performance of all foragers was unchanged in all three scenarios, however the advantage of the TP2.0

forager was reduced, being greater by 2.55 times in the targeted non-destructive scenario and by 2.56 times in the targeted destructive scenario. Again all differences are significant at *p* < 0.001 (Kruskal-Wallis One Way Analysis of Variance on Ranks). This result differs from the super-abundant uniform prey results where the TP2.0 performance advantage was more noticeably reduced with increasing prey abundance. Because the Lévy prey field has greater heterogeneity prey abundance can increase without a concomitant increase in the number of encounters, consequently it was likely that the abundance level at which TP2.0 performance began to decline was higher in a Lévy prey field.
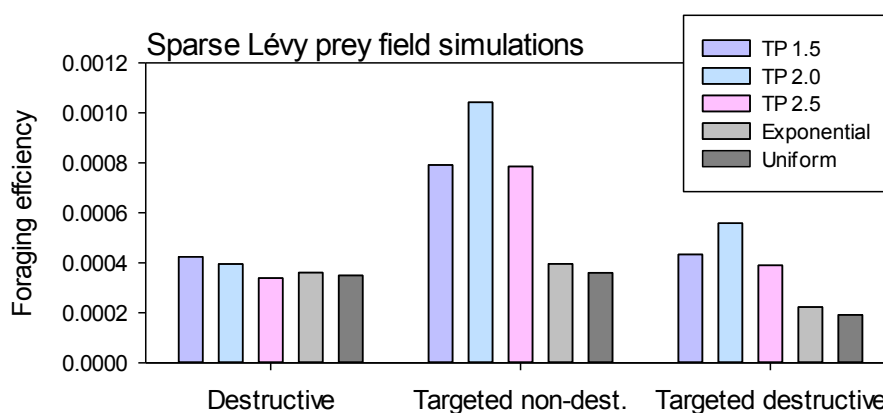
Figure 39: Simulation results with the sparse Lévy prey field
Results with all scenarios are almost identical to the results obtained with the sparse uniform prey field.
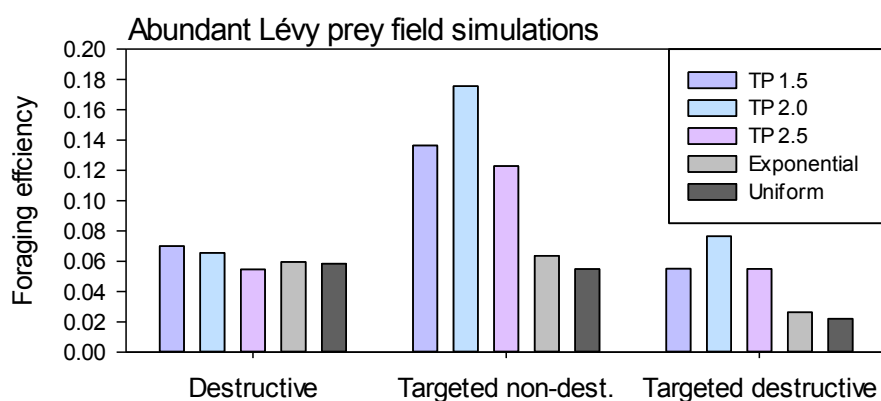
Figure 40: Simulation results with the abundant Lévy prey field
Again, the results are almost identical to all other scenarios.
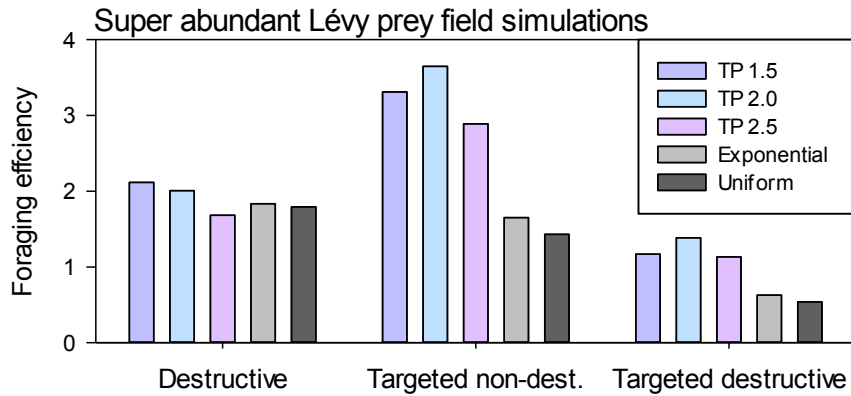
Figure 41 Simulation results with the super-abundant Lévy prey field
Other than the expected increase in biomass consumed there is no significant difference in the relative performance of the foragers.

3.9 Comparison of limited path length rather than step-limited number

In the previous simulations each foraging run was limited by the number of steps made. Given the wide range of mean step-lengths resulting from the different Lévy distributions used there was a similar wide range of overall path lengths (e.g. the TP1.5 forager had a mean path length of around 250,000 compared to 14,500 for the TP 2.5 forager). While the simulation results, in terms of both biomass consumed and encounters, were corrected for this difference it was possible that the large discrepancy affected results in some cases. In particular it is possible that the greater mean path length unduly increased the number of prey patch encounters and greatly increased the likelihood that a foraging run will be successful (i.e. will find and consume some prey). The simulations were therefore repeated, using the uniform sparse and abundant prey fields but with the foraging runs limited to a maximum path length of 40,000 units, rather than 5,000 steps. The value of 40,000 was selected as this approximates the mean path length for the TP2.0, exponential and uniform foragers used previously in the limited step simulations. Foraging runs were halted, following completion of a step, once the path length limit had been reached; consequently the final path lengths are slightly greater than 40,000 by the remainder of the last step taken. However the differences average only 0.3%.

The results obtained with the sparse prey field are given in Figure 42 and Table A9. Again there is no difference in the overall pattern, with TP1.5 being the most efficient in the destructive scenario (a 31.95% advantage) and TP2.0 being second (22.36% advantage); these values are very close to the step-limited simulations (29.98% and

20.66% advantages respectively). In the targeted scenarios TP2.0 is once again much more efficient, having an advantage over the worst performer (uniform) of ~2.5 times in both the non- and destructive scenarios and of ~2.26 and ~2.23 times over the exponential forager in the non- and destructive scenarios respectively. All differences are significant at $p < 0.001$ (Kruskal-Wallis One Way Analysis of Variance on Ranks).

The results obtained with the abundant prey field are given in Figure 43 and Table A10. With all scenarios the pattern is the same as with previous simulations; TP1.5 performs best with destructive, non-targeted (32% greater) and TP2.0 is the best in both targeted scenarios performing 2.46 times better in the non-destructive and 2.75 times better in the destructive scenario. All differences are significant at $p < 0.001$ (Kruskal-Wallis One Way Analysis of Variance on Ranks).

The most obvious difference between the step-limited and path-limited simulations was the number of successful foraging runs (Figure 44 and Figure 45). In the sparse prey field the step-limited TP2.0 forager had the greater number of successful foraging runs, while with the path-limited simulations it was the TP1.5 forager, which performed ~3.4 times better than the worst performer (uniform). The TP2.0 forager still clearly outperformed the remaining foragers by a very similar margin to the step-limited simulations of ~2.13 times. In the abundant prey field the outcome is different again; here it is now the TP2.0 forager that has most successful foraging runs, closely followed by the TP.15 forager. In the path-limited scenario it was the TP2.5 forager that had the most successful foraging runs, by a considerable margin. All differences are significant at $p < 0.001$ (Kruskal-Wallis One Way Analysis of Variance on Ranks).

Therefore, limiting the mean path length rather than the number of steps had very little effect on the relative foraging efficiency of the 5 foragers. The principal difference was found to be in the number of foraging runs that found some, rather than no prey, and with this simple measure it was the TP1.5 forager that performed best, rather than the TP2.0.
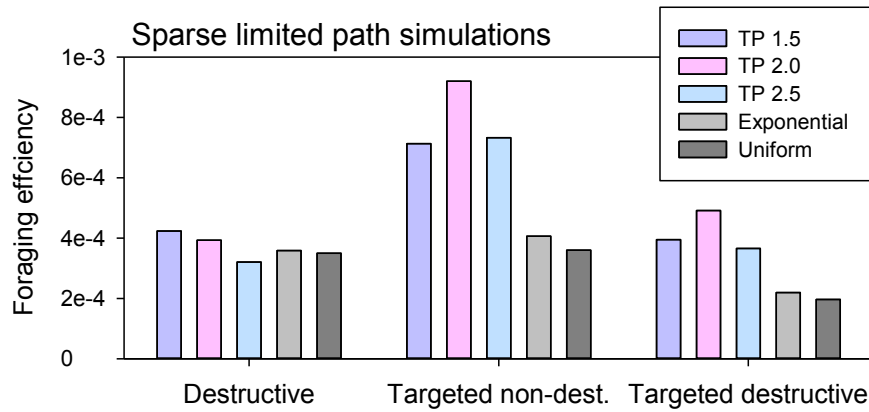
Figure 42: Sparse limited path simulations

Apart from very minor differences in the non-destructive, non-targeted scenario these results are almost identical to the step-limited simulations.
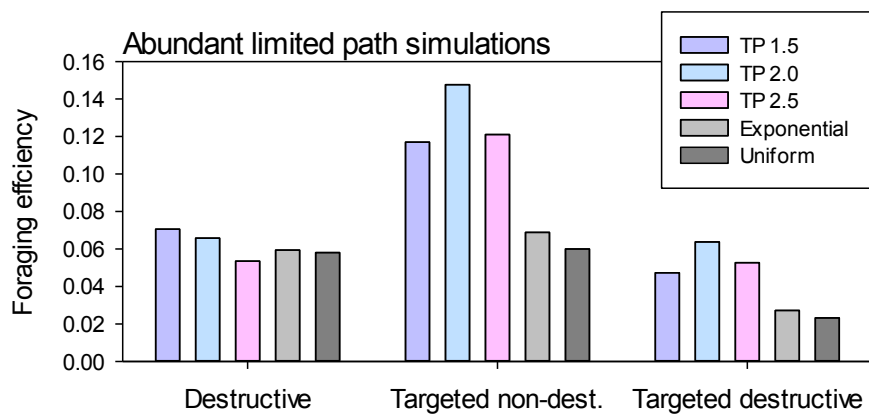
Figure 43: Abundant limited path simulations

The results in the abundant prey field match those in the sparse prey field.
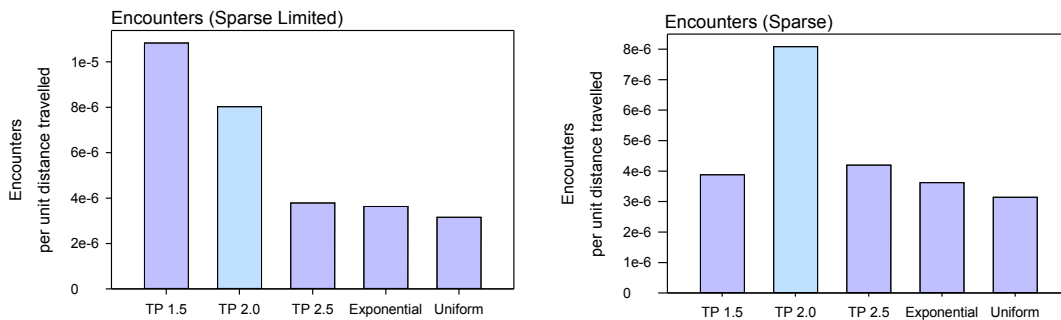
Figure 44: Limited path encounters in a sparse prey field

These results are different from the step-limited simulations (right) where the TP2.0 forager is clearly the most successful. While the advantage of the TP2.0 forager is maintained over the TP2.5, exponential and uniform foragers it is the TP1.5 forager that has the most successful foraging runs. The encounter rates are not significantly affected by the foraging scenario, with the same pattern emerging in each case.
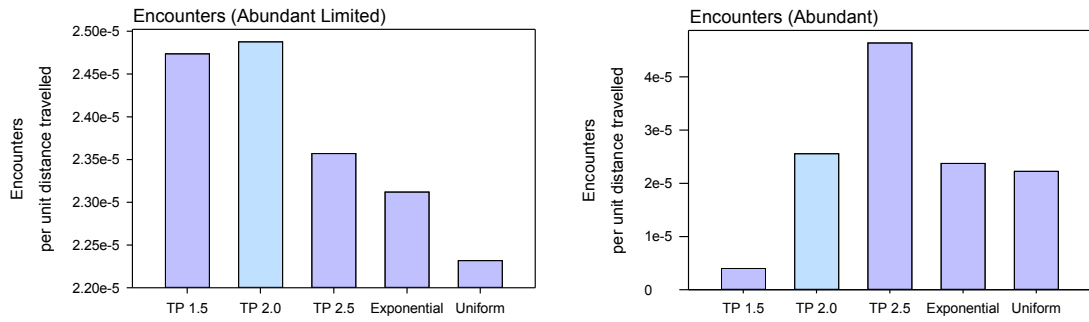
Figure 45: Limited path encounters, abundant prey

With the abundant prey field the encounter rates are again different from the step-limited simulations (right).
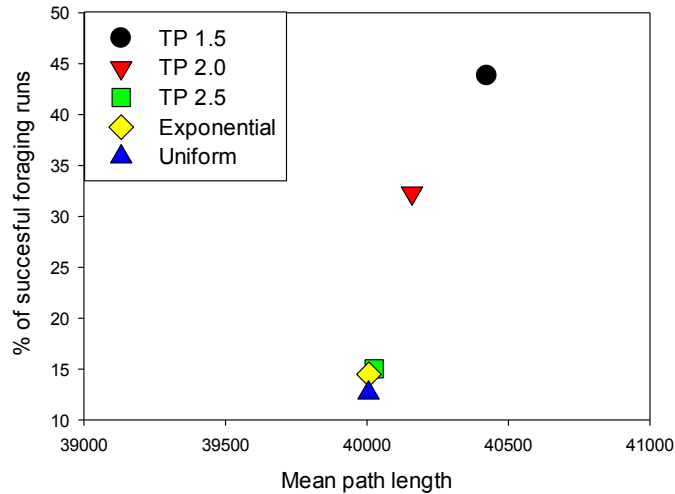
Figure 46: Successful encounter rates with limited path length

With the limited mean path scenario there is still some variation in mean path length caused by the completion of the final step, however the range of path lengths is now reduced to only ~1%. The results here differ from the limited step scenario in that the TP2.5 forager now performs worse than the exponential and uniform foragers; however the advantage of the TP2.0 forager was still twice that of all but the TP1.5 forager. Although the TP1.5 forager was still the best the advantage was considerably reduced compared with the step limited scenario (Figure 24).

3.10 Robustness of results to differing prey fields

All the simulations performed so far used fixed prey fields for each of the four environments (sparse or abundant uniformly distributed, and sparse or abundant Lévy distributed) which removed prey field variability from the results. Given that the results have been shown to be robust to all these environments it seemed unlikely that different prey fields of a given environment (e.g. sparse Lévy) would be likely to affect the outcome significantly. However it was necessary to confirm this, therefore the TP2.0 forager was used with the scenario 4 simulation (i.e. destructive, targeted foraging) to test the effect of using different prey fields. Two sets of simulations were performed; 1000 simulations were repeated 400 times using either a fixed sparse Lévy prey field or a different sparse Lévy prey field for each set of simulations. The intention

being simply to confirm that the results previously obtained were not due in any part to the particular prey field configuration being used.

Figure 47 shows the results from 50 simulations from each set and it can be seen that, while variability between simulations is, as expected, very high, there are no clear differences between the fixed and varying scenarios.

Table 6: Results of fixed and varying prey field simulations
Mann-Whitney U Statistic= 74189, T = 154389, n(small)= 400, n(big)= 400, *p* = 0.075. We can therefore conclude that the results are robust to differing prey fields.

Group	N	Median	25%	75%
Varying prey field	400	0.000544	0.000507	0.000584
Fixed prey field	400	0.000550	0.000509	0.000595
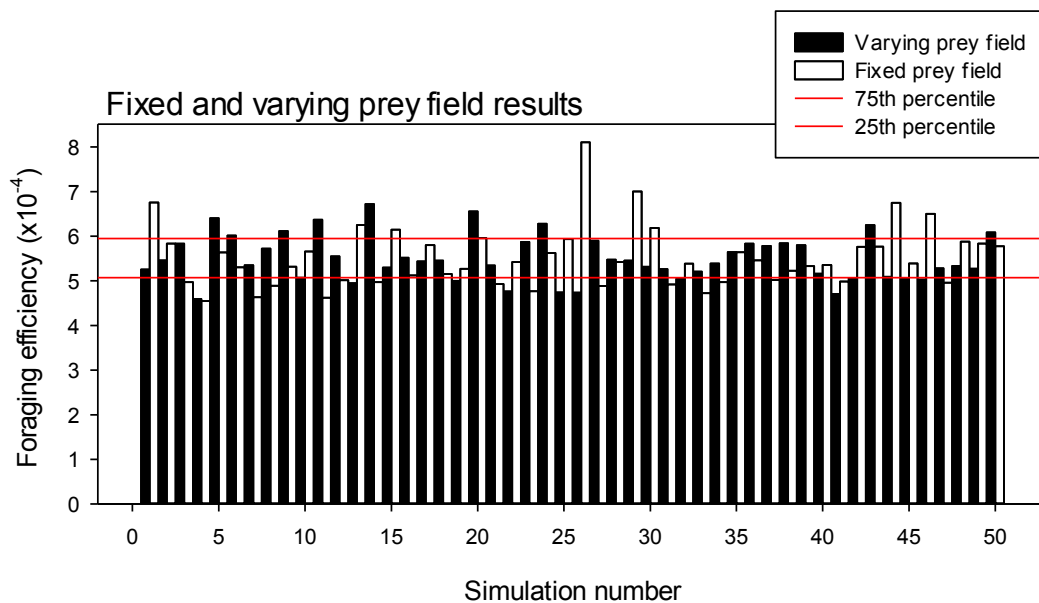
Figure 47: Foraging efficiency in fixed and varying prey fields
50 simulation results are shown from each scenario, with the 25th and 75th percentiles shown as red horizontal lines. It can be seen that variation between individual simulations is greater than between the two groups as a whole.

3.11 Innate or emergent behaviour

A subject that has received much discussion in the literature is whether the observed movement patterns from tagged animals result from innate movement processes or are simply an artefact of the animal's interaction with the environment (Viswanathan *et al.* 2002, Bartumeus *et al.* 2005, Boyer *et al.* 2006, Bartumeus 2007, Benhamou 2007, Bartumeus and Levin 2008, Plank and James 2008, Boyer *et al.* 2009, Reynolds 2009, Reynolds and Rhodes 2009, Reynolds *et al.* 2009, de Jager *et al.* 2011). It is conceivable that an animal moving with a pattern based on a simple correlated random walk, but changing direction on encountering prey, would generate a

movement pattern that simply reflected the prey field distribution. Therefore, in a Lévy-distributed prey field a Lévy pattern might arise, while in a uniformly (or exponentially) distributed prey field an exponential pattern might be found. This question is difficult to settle empirically as only in a few studies is anything known about the actual prey field density or structure through which tagged animals are moving (Sims and Quayle 1998, Sims *et al.* 2006b). General prey field characteristics can be inferred from proxies such as chlorophyll 'a' concentration (for primary productivity), or water column stratification, and can be correlated with observed movement patterns (Sims *et al.* 2008a, Humphries *et al.* 2010), but this does not help to determine how the observed pattern arose.

In a simulation environment however it is possible to control both the prey field density and structure and to specify directly the innate movement behaviour of the forager. It is therefore possible to test the hypothesis that observed movement patterns are the result of a simple diffusive, or ballistic, forager interacting with prey patches. To do so the five original foragers and a ballistic forager were used in the most biologically realistic scenario of prey targeting with destructive foraging and either uniformly or Lévy-distributed prey patches. The prey fields differed from previous prey fields in that the prey patches were not the complex high biomass patches used in previous simulations but instead were single grid cells; simple patches were used here to remove the complexities caused by the large number of very small move steps that result from intra-patch rather than inter-patch movements. Also both prey fields were considerably more abundant than previous prey fields employed, to ensure sufficient encounters to affect the resultant path significantly. Here the prey fields comprised 6×10^5 populated grid cells (4.8% occupation, Figure 54). For each simulation the movement paths resulting from the interaction of the forager with the prey fields from 1000 runs were recorded and analysed using maximum likelihood estimation and model selection as described in Chapter 2 (Clauset *et al.* 2009, Humphries *et al.* 2012) to determine whether the resulting path was best fit by a truncated power-law, an exponential distribution or neither. To remove the boundary effects caused by reflection off the edges of the arena a separate set of coordinates was maintained using un-reflected deltas in X and Y (see Appendix F). The recorded paths therefore represent a forager moving in an unbounded area with the prey field effectively reflected in a tessellated pattern (see Appendix F).

It was expected that by interacting with a uniformly distributed prey field the resulting path from any forager would be best fit by an exponential distribution; while with the Lévy prey field a truncated power-law might result. A further expectation was that while Lévy foragers might produce exponential paths as a result of the step truncation resulting from prey field interactions the converse would not be true, as an exponential forager can never produce the long relocations necessary for a power-law (or truncated power-law) distribution. Additionally, with the TP foragers, interaction with the prey field, which will lead to truncation of move steps, was also expected to raise the value of μ, and reduce the value of x_{max}, consistent with more, shorter step-lengths.

3.11.1 Analysis of resulting paths – Lévy prey fields

Results from both prey fields are given in Table 7. All the TP1.5 and the majority of the TP2.0 and TP2.5 paths were correctly classified as TP, however the classification by AIC was not unequivocal, with only 6 of the TP2.5 paths having full support from AIC. In all cases the fitted TP was favoured over the competing exponential, but the fitted exponential was favoured over the competing TP, the conflict being resolved by the adjusted goodness of fit (GOF) value which favoured the TP distribution in all cases. An examination of the plots in Figure 48, which show the fitted TP and the fitted exponential, reveal that the exponential, despite the support from AIC, was a poor fit to the data in comparison to the TP distribution. It seems that the exponential fit to the very small steps (< 1.0 units) was responsible for the AIC result; this emphasises the importance of visual inspection to confirm the statistical results.

There were 22 TP2.0 and 292 TP2.5 paths that were unclassified as a result of the fitted TP spanning less than 1.5 orders of magnitude; if this constraint were relaxed then all paths would be classified correctly. From the plots shown in Figure 48 it can be seen that the TP1.5 forager, as expected, suffered the greatest level of step-length truncation as the lower exponent results in a greater proportion of long step-lengths. Interaction with the prey field and the resulting truncation of step-lengths resulted in elevated values for the exponent and reduced values for X_{max}, as given in Table 8. The change in the exponent is at most only ~5% however the reduction in X_{max} is considerable as was expected given the density of the prey field and that the original value was 2500. It is the TP1.5 paths, which begin with the longest step-lengths, which

were subject to the greatest level of truncation and consequently the largest changes in μ and $X_{max.}$

All the exponential paths were classified as exponential with all but 3 being fully supported by AIC and the plots shown in Figure 49 confirm the very good fit.

Of the ballistic paths 998 were classed as TP but none had full support from AIC with again the fitted TP being favoured over the exponential and the fitted exponential over the TP; the conflict being resolved by the GOF. Plots for the ballistic paths are given in Figure 50 where both the fitted TP and the fitted exponential distributions are illustrated. It is clear that despite the evidence from AIC neither distribution fitted well to the entire dataset. The mean fitted TP parameters are given in Table 9. The value for μ (1.12) was significantly lower than the value used in the construction of the prey field (2.0). Lower exponents result in more ballistic paths so this finding was not surprising, however it was clear that the resultant path does not simply reflect the prey field characteristics, despite being modified by it.

3.11.2 Analysis of resulting paths – uniform prey fields

While the majority of TP paths were still classified as TP in the uniform prey field, fewer attained full support from AIC and more paths were unclassified again because the fit spanned less than 1.5 orders of magnitude. However the plots in Figure 51 show that the fit to the TP distribution was better than to the exponential and again it would seem that it was the fitting of the exponential to small step-lengths that biases AIC in favour of the exponential. The effect of truncation on the values of μ and X_{max} are similar to those found in the Lévy prey field.

All the exponential paths were classified as exponential with all but 16 being fully supported by AIC and the plots shown in Figure 52 confirm the very good fit.

The expectation with the ballistic paths was that the resultant paths would reflect the prey field distribution and this is confirmed with the uniform prey field results where all of the ballistic paths are categorised as exponential with only 10 not having full support from AIC. The plots shown in Figure 53 illustrate the good fit.

Given the patchier distribution of the Lévy prey field, and the larger voids that result, it is not surprising that the uniform prey field has a greater effect on the emergent paths; interactions are far more frequent.

Note that in some of the ranked step-length plots shown below there is a noticeable break in the observed values (shown as black circles); this break occurs between step-length values of 1.414 and 2.0 and was a result of the way that moves were interpolated. This issue is discussed further in section 2.2.2 and Appendix F.

In summary these results show that interaction with the environment is not sufficient to produce Lévy patterns from paths that are intrinsically exponential or *vice versa*. All the exponential paths were correctly identified as such, as were the Lévy paths, if the constraint regarding the number of orders of magnitude spanned by the data is relaxed. Only the ballistic paths produced patterns that reflected the prey field distribution. The Lévy paths were affected (i.e. interaction with the prey field did occur) but only in terms of a truncation of X_{max} and an increase in the value of μ.
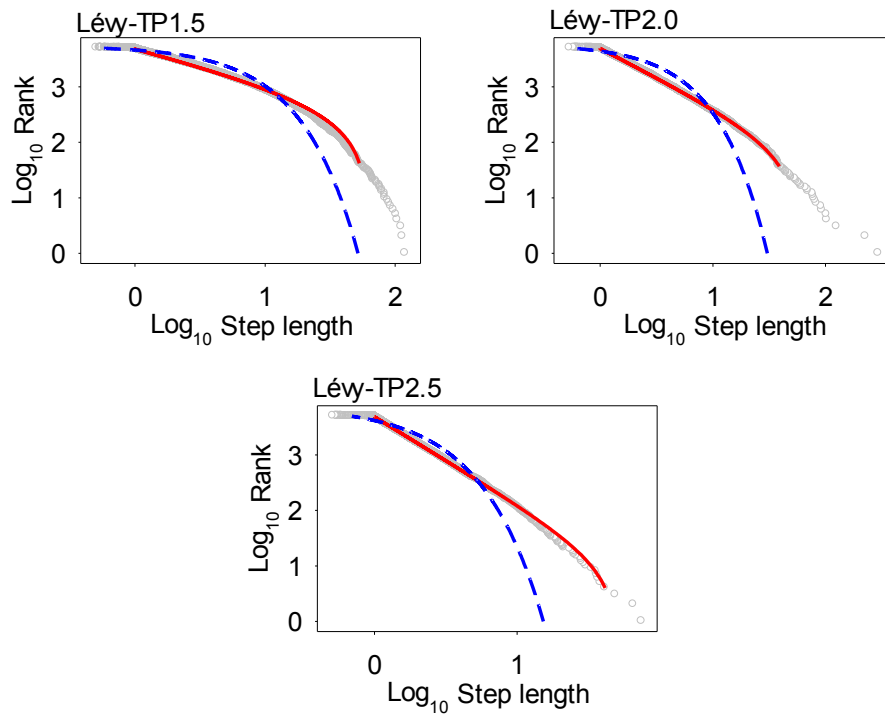
Figure 48: Rank step-length plots of Lévy paths in the Lévy prey field
Red lines show fitted truncated Pareto; blue dashed lines show fitted exponential; grey circles are simulated path data. Despite the very good fit of the TP distribution, which is favoured over the competing exponential, AIC favours the fitted exponential over the competing TP and therefore the AIC results are conflicted. The reason for this would appear to be the large number of points around X_{min} that bias the log-likelihood values used in the AIC calculations (see text, section 3.11.1).
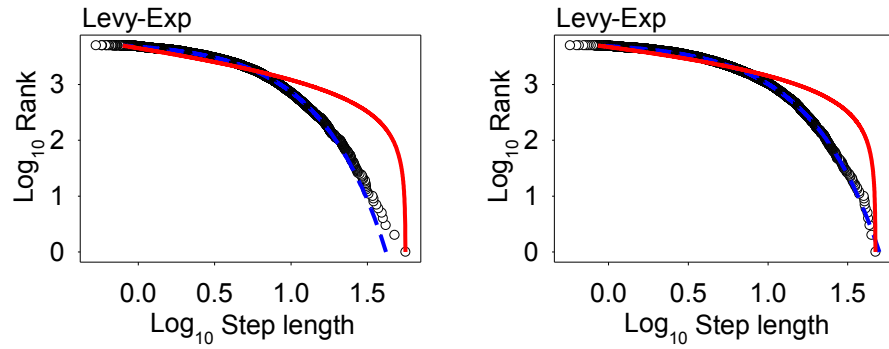
Figure 49: Rank step-length plots of exponential paths in the Lévy prey field

Two examples of exponential foragers in a Lévy prey field. Blue dashed lines show fitted exponential; red lines show competing truncated Pareto; black circles are simulated path data. The exponential forager is unaffected by interaction with the Lévy prey field.
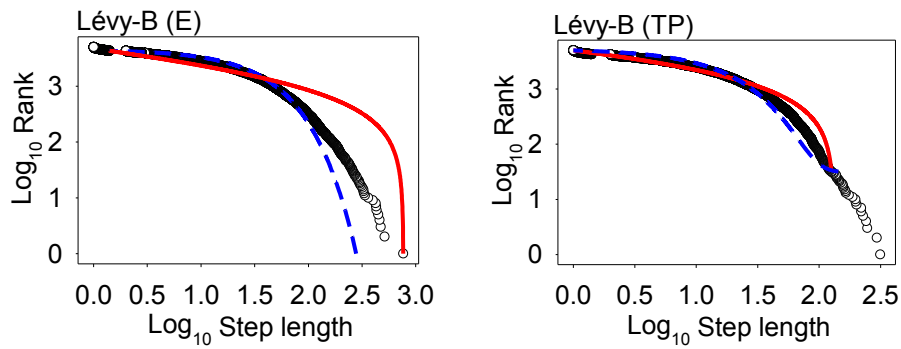
Figure 50: Rank step-length plots of ballistic paths in the Lévy prey field

In Lévy-B (E) blue dashed lines show fitted exponential; red lines show the competing truncated Pareto. In Lévy-B (TP) red lines show fitted truncated Pareto; blue dashed lines show the competing exponential. Black circles are simulated path data. Neither distribution fits well to all the data.
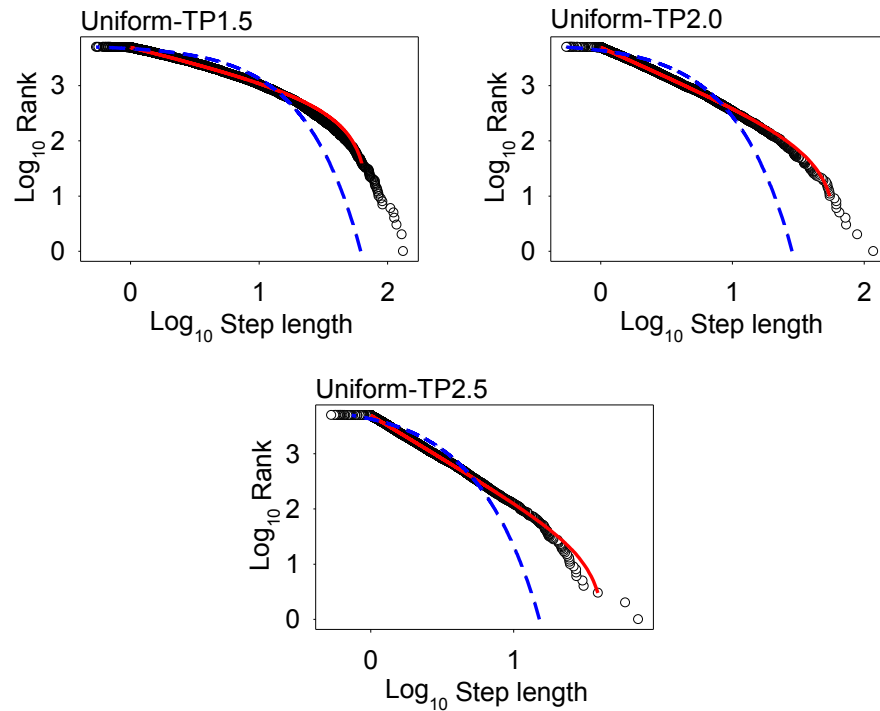
Figure 51: Rank step-length plots of Lévy paths in the uniform prey field

Red lines show fitted truncated Pareto; blue dashed lines show fitted exponential; black circles are simulated path data. Despite the conflicting evidence from AIC it is clear that the fitted TP is a better fit than the exponential in all cases.
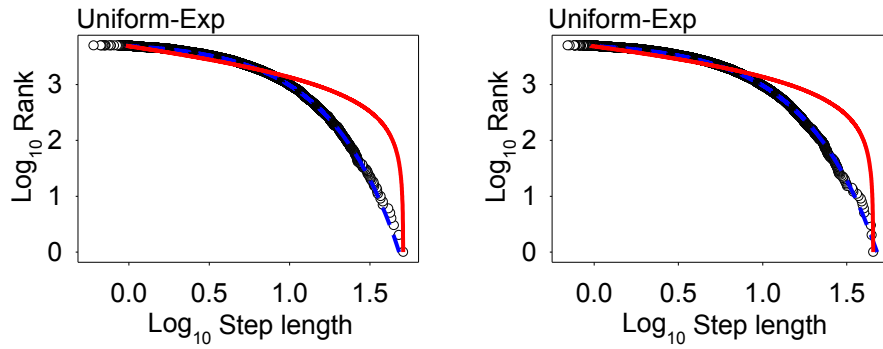
Figure 52: Rank step-length plots of exponential paths in the uniform prey field
Red lines show fitted exponential; blue dashed lines show competing truncated Pareto; black circles are simulated path data. The exponential forager is unaffected by interaction with the prey field.
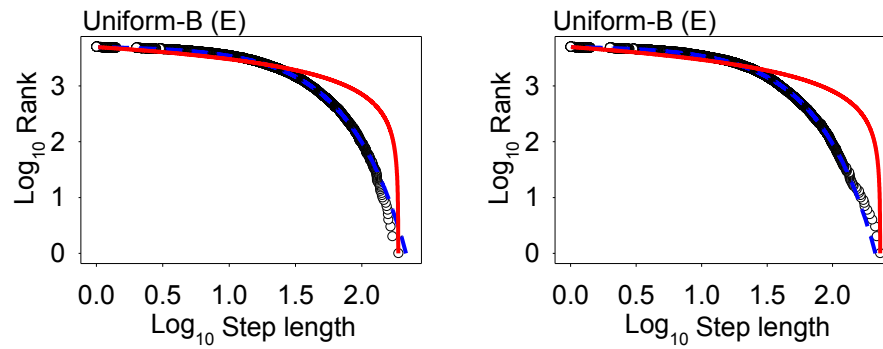
Figure 53: Rank step-length plots of ballistic paths in the uniform prey field
Two examples of ballistic foragers in a uniform prey field. Blue dashed lines show fitted exponential; red lines show competing truncated Pareto; black circles are simulated path data. The majority of ballistic paths result in good fits to the exponential distribution when interacting with a uniform prey field.

Table 7: Emergent path MLE analysis results
The emergent movement paths of Lévy, exponential and ballistic foragers (rows), resulting from interactions with either Lévy or uniform prey fields were analysed and classified as either TP, Exponential or unclassified (columns). Figures in parentheses show the number of unequivocal AIC fits

Forager	Prey field	TP	Exponential	Unclassified	Notes on unclassified
TP1.5	Levy	1000 (897)			
TP1.5	Uniform	1000 (275)			
TP2.0	Levy	977 (261)	1 (0)	22	< 1.5 orders of magnitude
TP2.0	Uniform	981 (0)		19	< 1.5 orders of magnitude
TP2.5	Levy	708 (6)		292	< 1.5 orders of magnitude
TP2.5	Uniform	535 (2)		465	< 1.5 orders of magnitude
Ballistic	Levy	998 (0)	2 (0)		
Ballistic	Uniform		1000 (990)		
Exponential	Levy		1000 (997)		
Exponential	Uniform		1000 (984)		

Table 8: Mean exponent and X_{max} shift for Lévy paths

Prey field	μ	Resulting μ	Increase	Resulting Xmax	Decrease
Levy	1.5	1.58	5.3%	95	96.2%
Levy	2.0	2.06	3.0%	69	97.2%
Levy	2.5	2.54	1.6%	63	97.5%
Uniform	1.5	1.52	1.3%	66	97.4%
Uniform	2.0	2.04	2.0%	49	98.0%
Uniform	2.5	2.54	1.6%	45	98.2%

Table 9: Mean parameters values for ballistic paths in the Lévy prey field

Parameter	Mean value	S.D.
X_{min}	1	0
μ	1.12	0.024
X_{max}	195.22	52.16
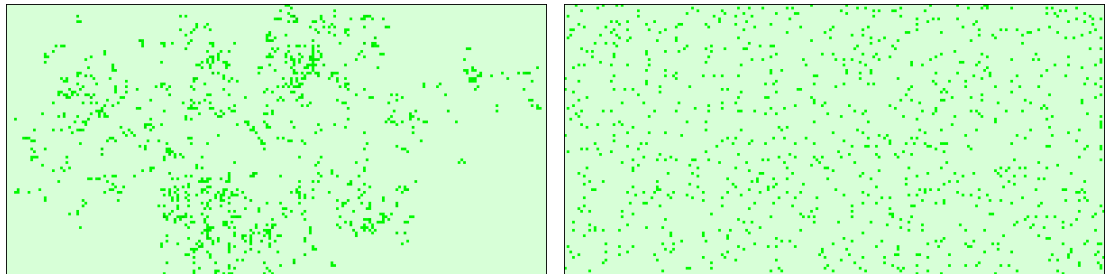
Figure 54: Simple prey fields for emergent path analysis
Left, a Lévy distributed field, right a uniform distributed field. For clarity both figures show a 200x100 cell section of the prey field. Approximately 4.8% of cells are occupied.

3.12 Feast or famine

Foraging efficiency, in terms of resources obtained for effort expended, is clearly an important biological quantity and has been the focus of the simulation studies presented here. There is however a further consideration that is of great importance to individual animals, namely the experienced heterogeneity of resource availability. Regardless of the actual abundance of available resources the foraging behaviour of an individual animal has not only to allow the animal to locate sufficient mean resources in a given time, but must do so in a way that avoids long periods without food which increase the likelihood of starvation.

In the simulation environment used here it was possible to study resource heterogeneity directly for individual foragers. The sum of interpolated move steps performed between each encounter with food (i.e. the actual distance travelled) was considered to represent the length of a single famine period. At the end of each foraging run the number of famine periods (i.e. the number of intervals between prey

encounters) and the mean duration of the periods were recorded. The number of famine periods is directly related to the number of feeding events and therefore, possibly counter-intuitively, a higher number of famine periods represents higher resource homogeneity; similarly it follows that where the number of famine periods is higher the mean duration will be lower, for a given path length. Given that the TP2.0 forager has been shown in previous simulations to have higher encounter rates it was expected that the number of famine periods would be higher and the mean famine duration lower.

Simulations recording famine periods were run for the five foragers in both abundant uniform and abundant Lévy-distributed prey fields. Abundant prey fields were used to ensure sufficient encounters for reliable statistics. The simulations were run 10^5 times using the most biologically realistic scenarios of destructive foraging, with and without prey targeting and with limited path length rather than step-limited number to remove that factor of variability.

The results from the prey-targeted simulations are summarised in Figure 55, Figure 56, Table A11 and Table A12 and confirm that the TP2.0 forager experiences greater resource homogeneity. In the uniform prey field the TP2.0 forager experiences 3.2 times more famine periods than the uniform forager (the worst performer) which experienced a median famine duration 3.2 times greater than the TP2.0 forager. All the Lévy foragers outperformed the uniform and exponential foragers in this respect. Results in the Lévy prey field were very similar, but were more pronounced with the TP2.0 forager having experienced 96 times more famine periods with a correspondingly shorter duration. Again, it was the uniform forager that performed worst. Statistical results from Kruskal-Wallis One Way Analysis of Variance on Ranks tests are shown in Table A11; all results are significant at $p < 0.001$ and all pair wise comparisons are significant at $p < 0.01$.

Interestingly, despite the significant differences in prey heterogeneity, the overall proportion of time spent in famine (calculated as the product of the number of periods and mean duration) was similar between all foragers (Figure 57 and Table A12). In the uniform prey field the TP2.5 forager was marginally better than the TP2.0 forager and both are significantly better than the rest. In the Lévy prey field the TP2.0 forager performed best which conformed to expectations, as the TP2.5 forager has a more

Brownian-like movement pattern that is predicted to perform sufficiently well in uniform abundant prey fields. The very small differences in total famine time reflect the very small proportion of time any of the foragers spent feeding, even in the abundant prey fields.

Results from the non-targeted destructive scenario are given in Figure 58, Figure 59, Table A13 and Table A14. The results here reflect the outcome of nearly all the other simulations performed using the destructive non-targeting scenario, where the TP1.5 forager performed best, followed closely by the TP2.0 forager with the same relative performance for the other foragers. Total famine time for the non-targeted scenario showed even less difference than with the targeted scenario, with a maximum difference of only 0.077% in the uniform prey field.

The replication of the pattern of relative performance between all foragers in the two scenarios was confirmed (Figure 60).
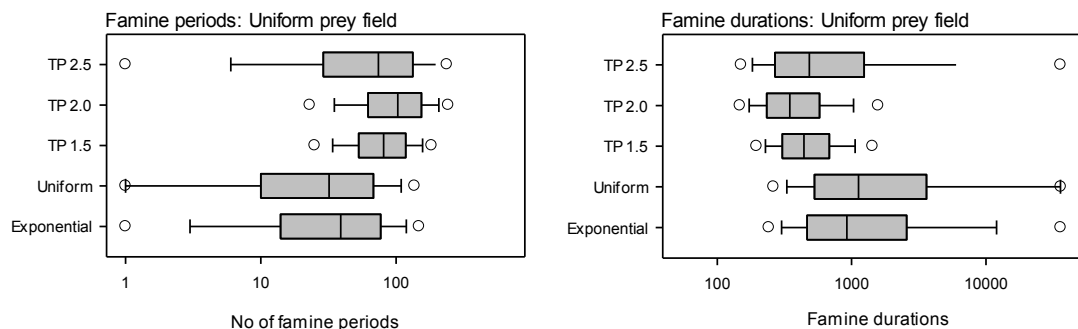
Figure 55: Feast and famine results – uniform prey field
> The number of famine periods is directly linked to the number of feeding events therefore a large number of famine periods indicates more feeding events and more homogenous resource availability. The TP2.0 forager experiences more famine periods of shorter overall duration. As expected there is an inverse correlation between the number of famine periods and the famine duration.
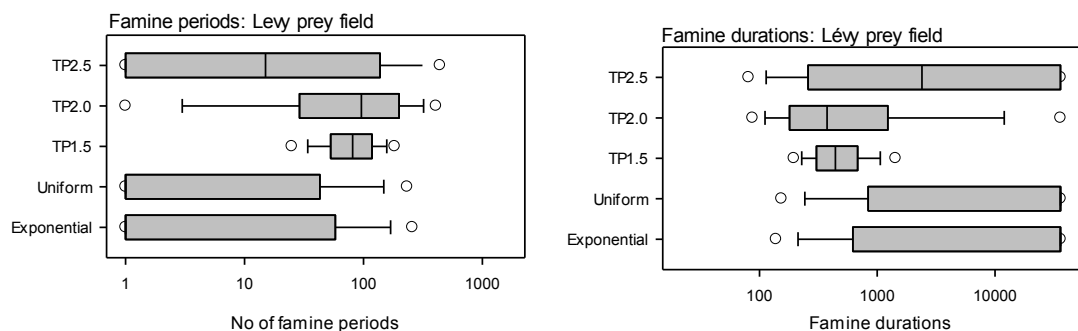
Figure 56: Feast and famine results – Lévy prey field
> There is considerably more variability in the results from the Lévy prey field, which is expected given the more heterogenic distribution of prey. However the overall results are very similar to those from the uniform prey field.
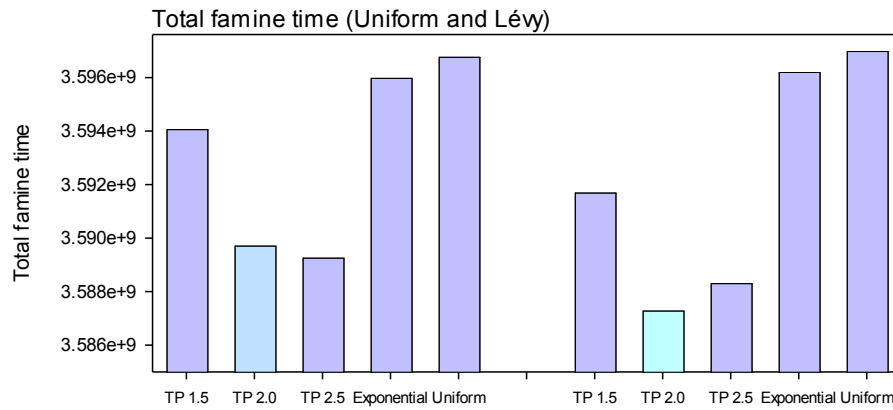
Figure 57: Total famine time calculated from number of periods and mean duration

Results from the uniform prey field are shown on the left, from the Lévy prey field on the right. In the uniform prey field the TP2.5 forager is marginally better than the TP2.0 forager; in the Lévy prey field the TP2.0 forager is clearly the better. However, differences between all foragers are very small (0.25% max.), reflecting the very small amount of time spent feeding by any of the foragers.
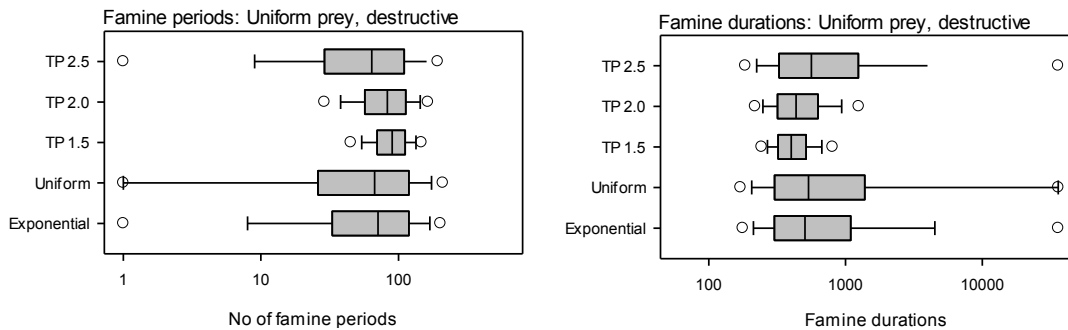
Figure 58: Non-targeted feast and famine results – uniform prey field

The results here are consistent with the other results with the non-targeted, destructive foraging scenario in that the TP1.5 forager is the best, having more famine periods of shorter duration (and therefore more frequent feeding events).
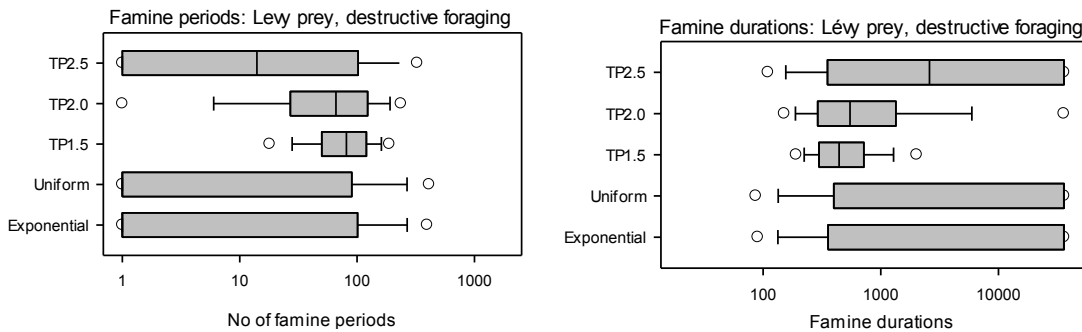
Figure 59: Non-targeted feast and famine results – Lévy prey field

There is considerably more variability in the results from the Lévy prey field, which is expected given the more heterogenic distribution of prey. However the overall results are very similar to those from the uniform prey field.
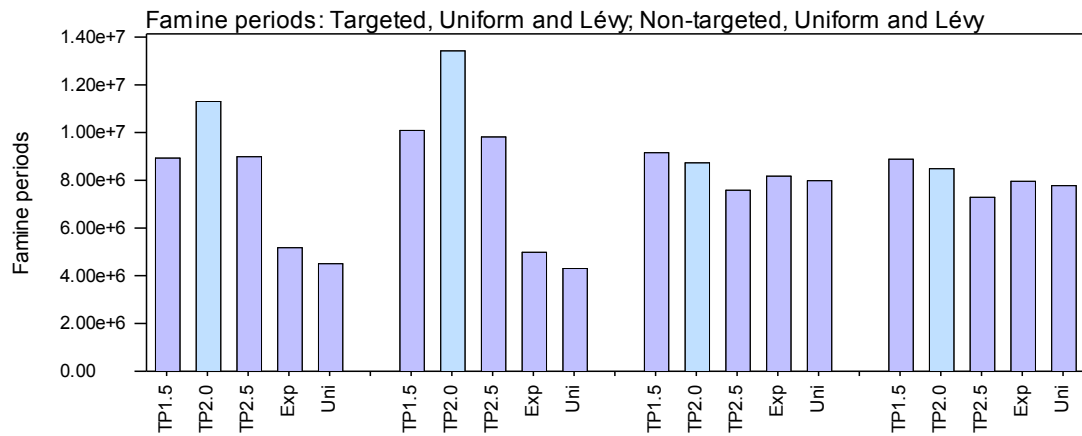
Figure 60: Summary of famine period results
From left to right the figure shows targeted uniform, targeted Lévy, non-targeted uniform, non-targeted Lévy. The relative performances of the five foragers are remarkably similar to the results obtained in the other simulations, with the TP2.0 forager performing best under prey-targeting conditions and the TP1.5 forager performing best with destructive foraging but no targeting.

3.13 The optimality of $\mu = 2.0$

The original simulation and mathematical analysis work performed by Viswanathan *et al.* (2000) demonstrated that Lévy searches are optimal when $\mu = 2.0$ and showed (in their figure 4d, reproduced below as Figure 61) how foraging efficiency changes with values of μ from 1.0 to 3.0. Having explored many of the questions regarding the Lévy flight foraging hypothesis it seems appropriate to end this chapter by confirming whether the pattern found by Viswanathan *et al.* can be replicated using a very different simulation environment. Therefore, simulations were performed to determine foraging efficiencies for Lévy foragers with values of μ from 1.5 to 2.5. The destructive targeted scenario was used with a path limited to 40000 units and the abundant Lévy prey field which conforms closely to the prey densities used by Viswanathan *et al.* (2000).

The results are given in Figure 62 and confirm a close congruence between the original analysis and the foraging simulations developed here: a search pattern approaching $\mu = 2.0$ conferred the highest foraging efficiency. The result was robust to prey field density and structure and, interestingly, it can be seen that the Lévy foragers were even more efficient in locating prey in a Lévy rather than a uniform prey field. This confirms the finding by Sims *et al.* (2008a). The results obtained with the sparse prey fields are subject to greater variability as the total number of encounters was very low; consequently the plots appear less smooth.
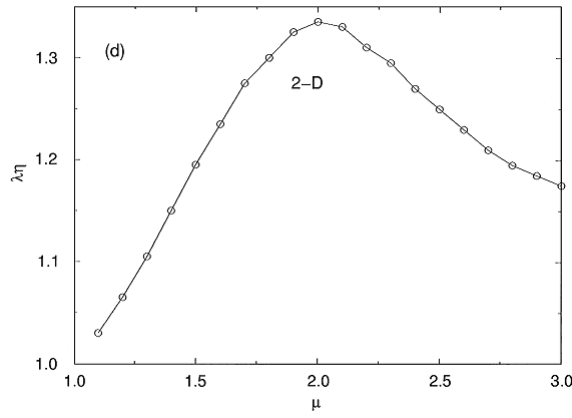
Figure 61: Optimality of _μ_ = 2.0 taken from Viswanathan _et al_. 2000.
    Reproduced from the original figure 4d. The optimality of _μ_ = 2.0 is shown for the case of non-destructive foraging in a 2-D environment.
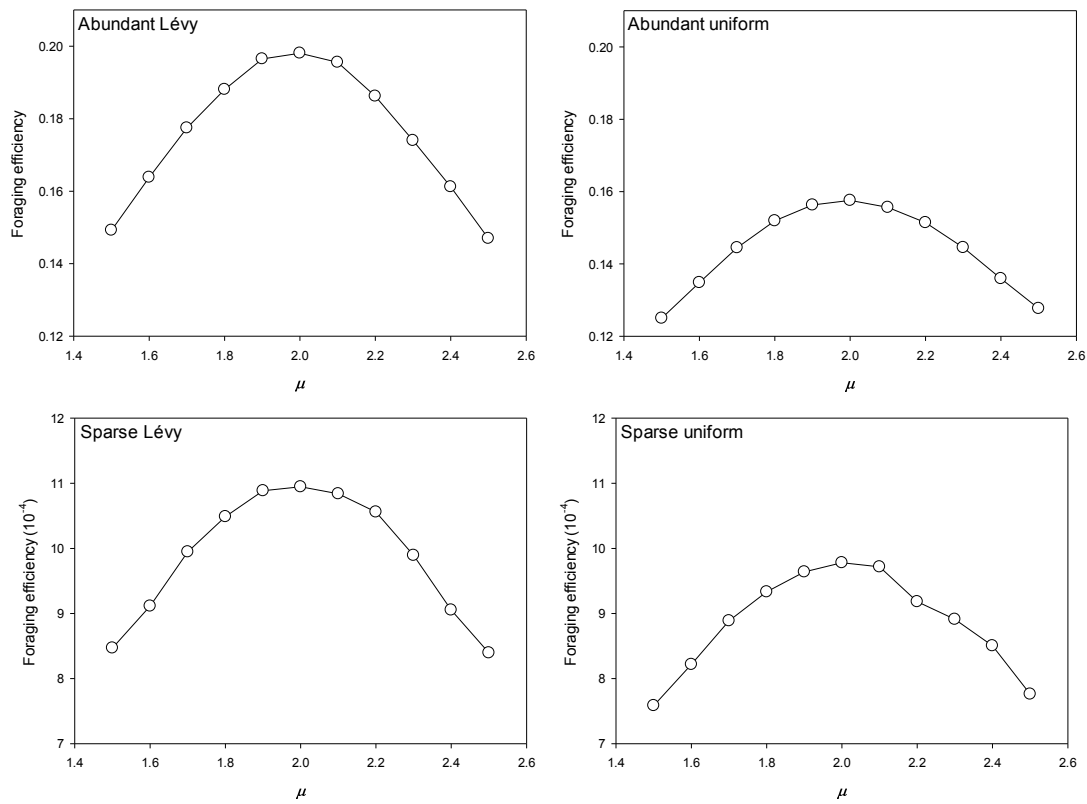
Figure 62: Optimality of _μ_ = 2.0 from the foraging simulations in this study.
    In the abundant Lévy prey field the results are almost identical to those obtained by Viswanathan et al. In the sparse prey fields the results are less clear, as the very low number of prey encounters leads to an under-sampling of the true values.

3.14 Discussion

It is clear from these investigations that the simplest foraging simulation scenario, with non-destructive prey consumption and no prey targeting was, for all foragers, overwhelmed by stochastic variability and consequently produced unreliable results, regardless of how many simulations were run. The results essentially converged to within around 3% as found by James _et al_. (2011). The failure of any of the foraging

strategies to stabilise under this simple scenario, however, makes it useless for foraging investigations and casts doubt on the reliability of some aspects of the study by James *et al.* (2011). The implication of the simulation results presented here is that in actual foraging scenarios, where prey is not specifically targeted and where prey is not effectively depleted, the movement strategy of the forager will play little part in the efficiency of foraging; under such a foraging scenario it appears that anything will do. Such a scenario might be found with filter-feeding macro-predators such as whales or basking sharks on occasions where very large patches of plankton are encountered; while within the patch the animal does not need to halt and handle prey and the patch to some extent 'recovers' from the passage of the animal by the re-distribution of prey through turbulent mixing. On these occasions, while the prey patch lasts, the fine scale movements of the animals within the prey patch can take any form and be equally efficient. On the whole though, it seems likely that such occasions may occur relatively rarely in the natural environment.

3.14.1 The stability of destructive or targeted foraging

One of the most striking results from these investigations is the robust stability of the remaining three foraging scenarios. In the destructive non-targeted scenario the TP1.5 forager is always the most efficient, as predicted by the more rapid patch leaving behaviour this forager will exhibit. The advantage varied from 25 to 32% which was highly significant. Destructive foraging is likely to be more biologically realistic than non-destructive as even macro-scale plankton patches, as discussed above, will become depleted eventually. This result therefore confirms one of the Lévy-flight foraging hypothesis' predictions: that with destructive foraging Lévy foragers with low exponents win out (Bartumeus *et al.* 2005). It is interesting to note that in this scenario the TP2.5 forager was always the least efficient; it might seem that this is related simply to the mean path length, which at 14,500 units was less than half that of the other foragers. However, the TP2.5 forager also performs worst in the limited path scenario, where path lengths are equal. Comparing a typical TP2.5 path (which is more Brownian-like than the other Lévy foragers) with uniform and exponential paths reveals the TP2.5 to have significantly more long relocations, but, nonetheless, to cover considerably less of the prey field than the uniform and exponential foragers (as shown in Figure 63). Using ImageJ (Rasband 1997-2012) to compute a histogram from

each image gives a value that represents the proportion of the image covered (i.e. the proportion of black pixels, see Figure 63). The results show that the TP2.5 forager covers 2.0%, while the uniform and exponential foragers cover 6.2 and 6.0% respectively, confirming that the TP2.5 forager would encounter less biomass and have a lower foraging efficiency.

It is interesting that incorporating destructive foraging reduces stochastic variability sufficiently for the performance of the foragers to settle reasonably quickly (i.e. within 3.5×10^4 simulations). As some studies have performed only 10^4 simulations it is possible that previously reported results (e.g. James *et al.* 2011) show foragers that have not reached efficiency stability. As a final comment on the destructive non-targeted scenario it is interesting that in all simulations the TP2.0 forager outperforms the uniform forager by between 8.35 to 13.78%, a figure that is in close agreement with the result found by Sims *et al*. (2008a), confirming that the simulations performed for that paper were closer to a destructive foraging scenario than was realised at the time.
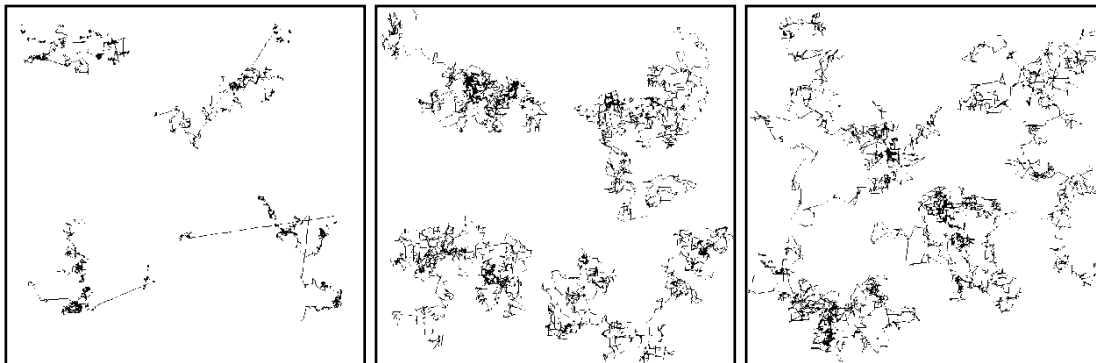
Figure 63: Example foraging paths for TP2.5, uniform and exponential foragers
Four sample paths from each of a TP2.5 (left), uniform (middle) and exponential forager (right), arranged so as not to overlap. It is clear, simply from the overall darkness of each image, that the TP2.5 forager searches a smaller proportion of the prey field.

3.14.2 The importance of prey targeting

In the original studies by Viswanathan (Viswanathan *et al.* 1999, Viswanathan *et al.* 2000) the foraging model included prey targeting. The results presented here make it abundantly clear, firstly, that with prey targeting the TP2.0 forager consistently emerges as the most efficient searcher and, secondly, that the relative performance of the other foragers is also strongly conserved. Overall the foraging efficiencies shown by the TP2.0 forager and the relative performances of the other foragers were robust to prey field abundance, prey field distribution, prey field variability and prey patch revisitability. It is worth reiterating that the destructive scenario used here differs from

that of Viswanathan, where individual prey items were used. Here, much of a patch of prey remained when a single item (grid cell) was destructively consumed, which is perhaps more comparable to natural prey patches. As mentioned in the results it is somewhat surprising that prey targeting should produce such a stable outcome, given that the advantage gained when a patch is encountered is the same for all foragers (Figure 22). The most likely explanation is that the TP2.0 forager, as predicted, encounters more new prey patches per unit distance travelled and consequently has more prey to exploit. This is supported by the encounter rates measured here simply as the number of simulation runs that encounter biomass, which have been shown to be remarkably robust to the foraging scenario (as shown in Figure 24 and Figure 25). This is not the only or perhaps not the best measure of encounter rates, particularly in abundant prey fields where few foragers find zero biomass regardless of movement pattern. The results from the feast and famine simulations are likely a more accurate reflection of actual prey encounter rates and these confirm the TP2.0 forager as having more encounters. Prey targeting adds further biological realism to the simulations; predators are not blind to prey and simply halting a move step probably represents a very conservative interaction.

Prey targeting adds a further dimension to the simulation in that it represents a behavioural switch; on encountering prey a move step is terminated. With a power-law distribution of move-steps subsequent steps are likely to be small, representing a slowing of movement, or increased tortuosity. The virtual foragers in this study cannot alter their move-step distribution in order to respond to prey-fields with changing densities, a behaviour that would be expected in real foragers, with switching to area-restricted search being commonly observed when prey-field densities are greater (Pinaud and Weimerskirch 2005, Hamer *et al.* 2009). It is all the more interesting, therefore, that prey targeting is so important in differentiating between the different foragers.

3.14.3 Prey abundance is less important than first thought

As prey field abundance was increased the difference between the five foragers was reduced as predicted. However the level of abundance required for parity was much higher than expected so it is interesting that previous studies have concluded Lévy foraging is only more efficient when prey is sparse (Viswanathan *et al.* 1999,

Viswanathan *et al.* 2000, Bartumeus *et al.* 2002, Viswanathan *et al.* 2002). It is possible that the use of simplified 1D simulations caused this result, although it is clear that this conclusion might also be reached if the simulation scenario used did not include prey-targeting. In the mathematical analysis by Viswanathan *et al.* (2000) the conclusion regarding prey abundance, i.e. that Brownian movement emerges though interaction with the prey field, is made when the abundance is such that the distance to the next prey item is less than or equal to the radius of detection (described in the paper as $\lambda \leq r_v$). The radius of detection used in this simulation is set to 1 unit, the most conservative value, and clearly it is not possible to have prey abundance set to such a density without all cells being populated. It is worth noting that even the level of prey abundance in these simulations cannot be considered biologically realistic as it represents far too dense a concentration. For example, if the scale of the simulation represented a 1cm grid and the biomass represented plankton, such as copepods, with each unit of biomass comprising a single copepod, then the prey density in the mega-abundant prey field (44.55% populated cells) would be equivalent to 445,500 copepods m^{-3}. Even at this density parity between the foragers had not been achieved. One field measurement of plankton density, recorded by Sims (1999; based on total zooplankters) was found to be around 2600 m^{-3}, which would represent a populated cell density of 0.26%; corresponding well with the first abundant prey field used in this section. This density was the highest reported in that study and agrees well with other studies that put maximum regional concentrations at around 10^3 individuals m^{-3} (Pendleton *et al.* 2009), yet is much lower than the density at which a significant difference between the foragers was found here. While much higher plankton densities have been recorded on scales of < 1m, associated with the sea surface boundary (Gallager *et al.* 1996) these represent micro-scale aggregations and are not representative of the patch as a whole. At a larger scale such densities could represent fish within a shoal as opposed to the distribution of shoals within the ocean. In general it was clear that within the scale of biologically realistic prey patch abundances the Lévy foragers will consistently outperform the exponential and uniform foragers by a substantial margin.

3.14.4 Innate or emergent?

Several studies have argued that observed Lévy patterns are not likely to be the result of an innate process the output of which is a scale-invariant movement pattern, but instead are the result of simple movements interacting with the environment (e.g. Boyer *et al.* 2006, Brown *et al.* 2007, Reynolds and Frye 2007, Guy *et al.* 2008, Reynolds 2008). There is growing support however, for the presence of power-laws in neuronal systems (Klaus *et al.* 2011) and in simple organisms under controlled conditions (Cole 1995, Ohkubo *et al.* 2010, Bendesky *et al.* 2011) suggesting a neurophysiological basis for observed fractal movement patterns. In this chapter it has been shown that interaction with the modelled environment does not change a Lévy pattern into an exponential pattern nor *vice versa* and therefore, if an animal's movement is intrinsically either Lévy or exponential, then it is most likely to be recognised as such, regardless of the prey field distribution.

Only the ballistic paths show a switching of outcome dependent on the prey field distribution. The outcome of the ballistic foragers was as expected with paths being recognised as exponential in the uniform prey field and as Lévy through interaction with the Lévy prey field, albeit with low exponents. However, in the natural environment, animals do not move with intrinsically ballistic patterns until they find an object, rather it is evident that animals show spontaneous changes of direction independent of objects (Bartumeus and Levin 2008, Proekt *et al.* 2012). Therefore, on balance, it seems unlikely that this provides a sufficient explanation of the observed fits to power-law or exponential distributions.

Given that exponential paths have few long relocations it was not expected that exponential paths would produce Lévy patterns, where such long relocations are characteristic. There were however two expectations regarding Lévy paths that were not met. Firstly there was an expectation that TP 1.5 paths, which include relatively many long relocations, would interact with the prey field in much the same way as the ballistic paths, producing exponential patterns. Secondly, given the more Brownian nature of the TP2.5 paths, it was expected that these might give rise to exponential paths. Instead the Lévy patterns of both were preserved with, in the case of TP1.5, higher exponents and truncated x_{max} values. That neither of these expectations was met adds support to the contention that the patterns observed in nature are the result

of intrinsic behaviour and are therefore the result of an adapted innate behaviour and not an emergent property of environment structure.

Finally, it is worth noting that the conflicting support for TP fits by AIC serves as a reminder of the importance of plotting the results for visual confirmation. Regardless of the findings of MLE and AIC all the TP paths are in fact a good visual fit to the TP distribution.

3.14.5 Feast and famine

Heterogeneity in prey availability requires energetically expensive adaptations to deal with the resulting periods of feast or famine, such as excess digestive capacity (Armstrong and Schindler 2011) and lipid storage (Arrington *et al.* 2006). Piscivores in particular have been found to have empty stomachs more often than other feeding guilds (Arrington *et al.* 2002) and, while difficult to observe in the wild (although stomach loggers are becoming available for sharks: Papastamatiou *et al.* 2007), a feast and famine feeding pattern has been observed in captive seven-gill sharks (*Notorynchus cepedianus*) (Vandykhuizen and Mollet 1992). In this context the TP2.0 forager delivers a double benefit; increasing the number of new prey-patch encounters not only increases the quantity of prey available but reduces the mean time between feeding events. Theoretically Lévy foragers are therefore less likely to starve, or suffer from malnutrition, than uniform or exponential foragers, which clearly confers many physiological benefits. Thus, Lévy foraging results in more predictable resources in unpredictable environments. These findings make it increasingly likely that movement patterns approximating a Lévy flight would have been naturally selected since the advantages to trophic status appear so strong. In support of this, the fundamental result from Viswanathan *et al*. (2000) demonstrating the optimality of μ = 2.0 was reproduced here using a very different simulation program and environment with different parameterisation. This adds considerable independent support to the central hypothesis concerning the Lévy flight foraging hypothesis. As such, search patterns similar to an idealised Lévy flight will clearly be a very efficient foraging strategy under a much broader range of conditions than previously thought.

Even the most biologically realistic scenario presented here falls far short of the behavioural complexity exhibited by an apex predator such as a shark. No account is taken of refined sensory input, memory effects or the sophisticated hunting and

foraging behaviour that is ubiquitous among higher organisms. The foragers presented here are therefore very much a null model of foraging; all that is being studied is the effect that simple, basal movement patterns have on the efficiency of an uninformed random search. It is likely that even nematodes, such as *Caenorhabditis elegans*, by sensing chemical gradients (Ohkubo *et al.* 2010), have at least some knowledge of their wider resource environment. Nevertheless, it is clear that differences in these simple patterns produce significant differences in foraging efficiency which are robust to differences in prey abundance or distribution. The differences are not small; in the sparse, Lévy-distributed prey field the TP2.0 forager has a foraging efficiency 2.6 times that of the exponential forager. Given that all that is required for an organism to produce a Lévy movement pattern is a time-fractal activity pattern (Bartumeus and Levin 2008), which has been observed in even simple animals such as *Drosophila* (Cole 1995), it seems very likely that such behaviour would have been selected for during evolution.

When studying complex organisms, such as marine vertebrates, these simple movement patterns are only going to be observed on those occasions when the animal is actively engaged in foraging, when information of the location of prey is absent and when other behaviours, such as prey avoidance, migration or response to environmental cues are not dominating the animal's movement. It is therefore to be expected that empirical evidence for these patterns will be relatively rare. There is at the present time some limited empirical support for Lévy movement patterns in a range of taxa, including insects (Cole 1995, Reynolds and Frye 2007, Reynolds *et al.* 2007), dinoflagellates (Bartumeus *et al.* 2003), marine gastropods (Seuront *et al.* 2007), some marine predators (Sims *et al.* 2008a) and primates (Ramos-Fernandez et al. 2004) including humans (Brown *et al.* 2007, Gonzalez *et al.* 2008, Rhee *et al.* 2008). However, there has not been a thorough and robust empirical test of the Lévy-flight foraging hypothesis in free-ranging animals.

Perhaps it is expected that Lévy patterns would not be common in terrestrial animals as stable environmental structures (i.e. topology, trees etc.) provide very persistent clues as to the location of prey or other resources. Nor are they likely to be common among higher vertebrates such as bears, *Ursus arctos*, where the animals rely on good spatio-temporal mental maps of resource availability and rarely perform large-scale

random searches (Bojarska and Selva 2012). Therefore, it seems likely that Lévy search patterns should be most common in an environment such as the open sea because resources are often highly sparse, have complex dynamic distributions and are transported by currents over widely different spatio-temporal scales. As such, submerged predators are only likely to have an incomplete knowledge of resource location and the detection of such resources at distance (e.g. vision, olfaction) will be limited by the seawater medium compared to terrestrial or aerial environments. Hence, for a robust test of the Lévy flight foraging hypothesis the study of pelagic open ocean predators may provide particularly interesting and long-lasting insights.

4 Environmental context explains Lévy and Brownian movement patterns of marine predators

This chapter was published in **Nature** as: Humphries, N. E., Queiroz, N., Dyer, J. R. M., Pade, N. G., Musyl, M. K., Schaefer, K. M., Fuller, D. W., Brunnschweiler, J. M., Doyle, T. K., Houghton, J. D. R., Hays, G. C., Jones, C. S., Noble, L. R., Wearmouth, V. J., Southall, E. J. & Sims, D. W. (2010) Environmental context explains Lévy and Brownian movement patterns of marine predators. *Nature,* **465,** 1066-1069.

4.1 Introduction

An optimal search theory, the so-called Lévy flight foraging hypothesis (Viswanathan *et al.* 2008), predicts predators should adopt search strategies known as Lévy flights where prey is sparse and distributed unpredictably, whereas Brownian movement is sufficiently efficient for locating abundant prey (Viswanathan *et al.* 1999, Bartumeus *et al.* 2002, Bartumeus *et al.* 2005). Empirical studies have generated controversy because less accurate statistical methods have been used to identify Lévy behaviour (Edwards *et al.* 2007, Sims *et al.* 2007). Consequently whether foragers exhibit Lévy flights in the wild remains unclear. Crucially, moreover, it has not been tested whether observed movement patterns across natural landscapes having different expected resource distributions conform to the theory's central predictions. Here we use maximum likelihood methods to test for Lévy patterns in relation to environmental gradients in the largest animal movement dataset assembled for this purpose. Strong support was found for Lévy search patterns across 14 species of open-ocean fish predator (sharks, tuna, billfish, ocean sunfish), with some individuals switching between Lévy and Brownian movement as they traversed different habitat types. We tested the spatial occurrence of these two principal patterns and found Lévy behaviour

associated with less productive waters (sparser prey) and Brownian movements associated with productive shelf or convergence-front habitats (abundant prey). These results are consistent with the Lévy flight foraging hypothesis (Bartumeus 2007, Viswanathan *et al.* 2008), supporting the contention (Travis 2007, Buchanan 2008) that animal search strategies evolved to exploit optimal Lévy patterns.

4.1.1 The Lévy flight foraging hypothesis

Lévy flights are a special class of random walk with movement displacements (steps) drawn from a probability distribution with a power-law tail (the so-called Pareto-Lévy distribution) (Shlesinger and Klafter 1986, Viswanathan *et al.* 2008), giving rise to stochastic processes closely linked to fractal geometry and anomalous diffusion phenomena (Shlesinger *et al.* 1993, Bartumeus 2007). Lévy flights describe a movement pattern characterised by many small steps connected by longer relocations, with this pattern having scale invariance under projection, such that $P(l) \sim l^{-\mu}$, with $1 < \mu \leq 3$ where l is the flight length (move step-length), and μ the power-law exponent. Lévy flights comprise instantaneous flight lengths, hence involve infinite velocities, whereas a Lévy walk (Shlesinger and Klafter 1986) refers to a finite velocity walk such that displacement is determined after a time t, reflecting a dynamical process such as movement (Shlesinger and Klafter 1986, Shlesinger *et al.* 1993, Viswanathan *et al.* 2008). Lévy flights and walks are theorised to be the most efficient movement pattern for locating patchy prey in low concentrations at spatial scales beyond a searcher's sensory range, with an optimal search having a power-law exponent of $\mu \approx 2$ (Bartumeus *et al.* 2005, Sims *et al.* 2008a). It is hypothesised that organisms have, therefore, evolved to exploit optimal Lévy search patterns (Bartumeus 2007, Sims *et al.* 2008a, Viswanathan *et al.* 2008).

4.1.2 Controversy over empirical evidence

Burgeoning empirical support for this hypothesis recently foundered however following studies suggesting methodological shortcomings in both the estimation of power-law exponents and in determining the goodness of fit of the distribution to the data (Edwards *et al.* 2007, Sims *et al.* 2007, Edwards 2008, White *et al.* 2008, Clauset *et al.* 2009), thus casting doubt on some, if not all, of the empirical studies to use such methods (Travis 2007, Buchanan 2008). Hence, controversy remains over whether Lévy behaviour occurs in nature (Benhamou 2007, Edwards *et al.* 2007, Buchanan

2008), despite many empirical studies (Viswanathan *et al.* 2008, Bartumeus and Catalan 2009). Furthermore, long time series of movements (weeks to months) derived from animal-attached electronic tags will very likely capture complex movement data resulting from different types of behaviour (e.g. searching, travelling, resting) as animals respond to various biotic and abiotic factors over time. Previous studies analysing free-ranging animal movement data (Viswanathan *et al.* 1996, Edwards *et al.* 2007, Sims *et al.* 2008a) for Lévy motion used data across long time periods and different habitat types, without sufficient consideration given to the issue of different types of behaviour interspersed within the time series. The lack of analysis of separate behaviour pattern types may be at least one reason why evidence for Lévy flights in animal behaviour has proved challenging to detect unequivocally (Benhamou 2007, Buchanan 2008).

4.2 Methods

Here we present an analysis of the largest dataset of recorded movements (n = 12,294,347 steps) assembled to test the Lévy flight foraging (LFF) hypothesis (Viswanathan *et al.* 2008) using statistical methods (Maximum Likelihood Estimation, MLE, and Akaike's Information Criteria weights, wAIC, for model comparisons) that are considered robust and accurate (Edwards *et al.* 2007, Edwards 2008, White *et al.* 2008, Clauset *et al.* 2009). To test the predictions of the LFF hypothesis we focused analysis on vertical movement data recorded over 5,700 days by electronic tags attached to open-ocean fish predators (sharks, tunas, billfish, ocean sunfish; Table B1). These species may be among those most likely to exhibit Lévy behaviour because they occupy unpredictable and depauperate environments with highly patchy prey distributions (Sims *et al.* 2008a), where Lévy motion is hypothesised to increase new-patch encounter probability (Viswanathan *et al.* 2000).

4.2.1 *Study animals*

In total, 129 track sections from 55 individuals collected over more than 5,700 days were analysed, representing 14 species: bigeye thresher shark (*Alopias superciliosus*, Lowe 1841) n = 2 individuals; blue shark (*Prionace glauca*, Linnaeus 1758) n = 12; shortfin mako shark (*Isurus oxyrinchus*, Rafinesque 1810) n = 1; porbeagle shark (*Lamna nasus*, Bonnaterre 1788) n = 1; silky shark (*Carcharhinus falciformis*, Müller &

Henle 1839) *n* = 3; oceanic whitetip shark (*Carcharhinus longimanus*, Poey 1861) *n* = 1; basking shark (*Cetorhinus maximus*, Gunnerus 1765) *n* = 6; whale shark (*Rhincodon typus*, Smith 1828) *n* = 1; bigeye tuna (*Thunnus obesus*, Lowe, 1839) *n* = 5; yellowfin tuna (*Thunnus albacares,* Bonnaterre, 1788) *n* = 6; black marlin (*Makaira indica,* Cuvier 1832) *n* = 1; blue marlin (*Makaira nigricans*, Lacepède 1802) *n* = 11; swordfish (*Xiphias gladius*, L. 1758) *n* = 1; ocean sunfish (*Mola mola*, L. 1758) *n* = 1. These comprise 5 taxonomic or functional groups (macropredatory sharks, planktivorous sharks, tunas, billfish, ocean sunfish) with 12.2 million individual movement steps analysed. Table B1 gives tag types used and technical details, together with tagging locations. Long-term high resolution depth datasets from fish are difficult to obtain given the very limited bandwidth of the Argos data-relay satellite system (Hays *et al.* 2007). We made serendipitous use of an extensive number of satellite and archival tags that had been recovered after long deployments and contained complete high resolution datasets. Only the basking shark dive data (*n* = 6 individuals; 10.9% of total individuals) have been analysed previously in the context of Lévy flights (Sims *et al.* 2008a), although, importantly, this did not include division of tracks into sections that were then geo-referenced and compared with environmental habitat type, the prime objective in the current paper.

4.2.2   *Division of recorded time series into behaviourally consistent sections*

It is hypothesised that long and complex dive time series (vertical tracks) recorded by animal-attached electronic tags are likely to have captured a series of different movement behaviours. This is due, at least in part, to animals encountering differing environmental conditions such as sea temperature, depth or prey densities, for example. If analysed as a whole, these time series may result in more complex move step-length frequency distributions which may not be readily or accurately interpreted by the proposed statistical analysis for exploring underlying model fits to empirical data (i.e. Maximum Likelihood Estimation, MLE). It is therefore desirable to divide such tracks into sections which are behaviourally more consistent. Furthermore, it is an aim of this study to explore different movement patterns in relation to environmental gradients. Hence, there is an additional requirement that the track divisions should be made, where possible, at or at least temporally close to encountered environmental boundaries (e.g. between water masses with different characteristics). An examination

of the dive time series often reveals clear changes in patterns of vertical space use which can in turn, when spatial data is available, be linked to environmental changes such as water temperature gradients and sea depth (Queiroz *et al.* 2012).

Although for some tracks discontinuities are clearly identified by changes in patterns of vertical space use in a time depth plot in other cases changes are less clear and therefore an objective method is needed to identify discontinuities.

Therefore, to enable a more robust test of the LFF hypothesis, long and complex time series of vertical diving movements (hereinafter tracks, or sections) undertaken as fish moved horizontally across their ranges, were divided into shorter sections using a split-moving window analysis (Cornelius and Reynolds 1991) to identify discontinuities in the pattern of vertical space use which represent transitions from one pattern of space use to another (see Chapter 5 for details). In total, tracks from 55 individuals across 14 species (shark, 8 species; tuna, 2; billfish, 3; ocean sunfish, 1) were divided into 129 sections. MLE methods (Clauset *et al.* 2009) were used to fit three models (power-law, truncated power-law (truncated Pareto) or exponential) to the observed move step-length frequency distributions. Sections that from visual inspection of MLE model fits to empirical data were a poor fit to all candidate distributions were excluded from further analysis (n = 35) since our objective was to test the spatial occurrence of good fits to step-length distributions. MLE methods with AIC weights (Edwards *et al.* 2007, Edwards 2008) (wAIC) were then used to determine model best fits for the remaining 94 sections. Since movements can only take place in finite space (e.g. moves are limited by the sea surface, seabed or range edge) leading to upper cut-offs in the move step-length frequency distribution, only truncated Lévy walks are biologically plausible (Viswanathan *et al.* 2008). Therefore, our principal intention was not to find which kinds of all possible probability distributions best fit the data, rather, it was to test between truncated Lévy (truncated power-law model) and Brownian-type (exponential model) movement patterns.

To perform the analysis a two dimensional (2D) time-at-depth matrix, with 6 hour time bins (as columns) and 10 m depth bins (as rows), is first constructed from the raw dive time-series data by calculating the proportion of time spent at each depth within each time period (Figure 64a). A virtual window with a width of 6 time bins is placed at the start of the time-at-depth matrix and a measure of dissimilarity between the two

window halves is calculated and assigned to the centre position of the window. The dissimilarity measure used here was the multivariate measure of Euclidean distance between averaged time at each depth. The window position is then advanced by one time bin and the calculation is repeated until the window reaches the end of the time series. Statistical significance of each dissimilarity value is calculated using a Monte-Carlo technique whereby the calculation is repeated 1000 times with a shuffled time-at-depth matrix. The number of times the dissimilarity value exceeds that calculated using the real data is counted and converted to a percentage which represents the *p*-value. Significant discontinuities in the time series will have higher dissimilarity values than most of those calculated using a random re-arrangement of the data, resulting in very few randomisations yielding higher dissimilarity values. The width of the window is then incremented by two and the process is repeated up to a width of 32, giving 14 window sizes. The *p*-values calculated from each window size and position are stored and finally plotted by stacking them vertically, with significant values (in this case $p < 0.001$) being plotted in black, as shown in Figure 65. Discontinuities in the dive time series are revealed by the presence of inverted triangles which 'point' to the discontinuity and indicate the position at which the time series can be divided as a quantitative estimate of where different movement patterns are located in the time series.

The vertical movement tracks of large marine fish analysed in this study are complex and therefore the results of the split-moving window analysis can appear 'noisy', in some cases, with many discontinuities being identified. Referring to Figure 65a below it can be seen that the discontinuities labelled i, iii, iv and vi extend over many window sizes and have a general trend of increasing width at smaller window sizes. These discontinuities represent shifts between prolonged behavioural bouts and are therefore the points at which this track was divided. The smaller discontinuities labelled ii, v, vii and viii, although statistically significant, are of shorter duration or extend over only a few window sizes and are therefore ignored since they do not capture persistent pattern changes. Accurate detection of power-laws in biological data can be affected by small dataset size (Sims *et al.* 2007, White *et al.* 2008) so there is a further consideration not to divide the tracks into sections with too few data points. Therefore in the current study only the clearest discontinuities arising from the SMW analysis were used to divide the tracks.

Patterns of vertical space use of marine fish can be analysed using simple binning techniques to generate a time-at-depth matrix with temporal and depth resolution set to the required level of detail (Figure 64). Therefore, vertical space use is a good candidate measure for the identification of movement pattern discontinuities that would encompass both responses to changes in environment (e.g. sea depth or thermocline depth) as well as other behavioural shifts (Queiroz *et al.* 2010). An alternative measure that could be used is the move step-length distribution. It is a central hypothesis of the current study that long, complex tracks will comprise different move step-length frequency distributions and that changes in these could be related to environmental gradients and other variables. Move step-length frequency distributions are, however, relatively poorly analysed using simple binning techniques and the equivalent time/step-length frequency matrix (Figure 64b) reveals considerably less detail than that generated from depth usage (Figure 64a). One reason for the lack of detail could be the very small sample sizes that result from the 6-hour time divisions used to generate the matrix; using longer time windows, however, results in a much coarser analysis and missed discontinuities (Figure 65).
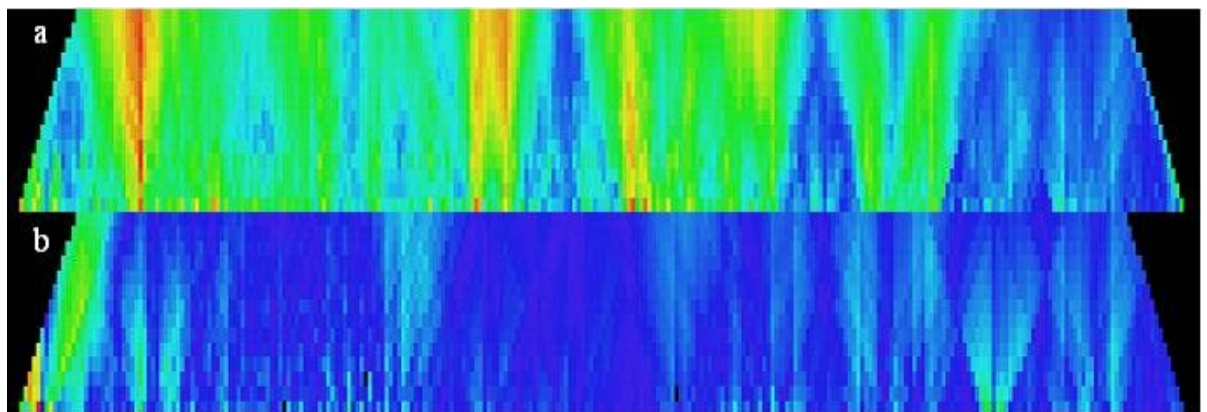
Figure 64: Identification of movement pattern discontinuities.
Time at depth (a) and time step-length (b) dissimilarity matrices generated from depth data of blue shark 10. Red colour shows areas of high dissimilarity and blue low dissimilarity. The step-length matrix lacks contrast in comparison to the time-at-depth matrix and is therefore likely to miss some significant discontinuities.
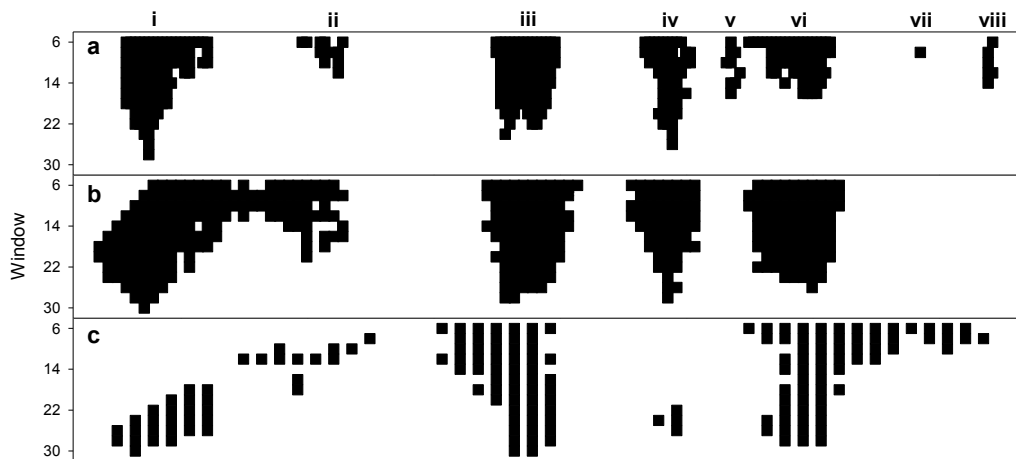
Figure 65: Split-moving window analysis plots at differing time resolutions.
For blue shark 10 with time divisions set to (a) 6 hours, (b) 12 hours and (c) 24 hours. Increasing the time division results in decreasing resolution of the discontinuities.

4.2.3 Preliminary data analysis

Prior to performing the MLE analysis all sections, which comprised time-stamped depth measurements, were converted into move step-lengths by calculating vertical movement deltas between successive pairs of data points. As part of the process, three causes of potential calculation error were addressed. Firstly, some datasets were recorded at very high temporal resolution (e.g. 1s) which can in some cases be insufficient time to record movement deltas greater than the depth resolution of the tag, resulting in considerable step-wise alternating values, i.e. long series of alternating move steps with lengths close to the vertical resolution of the tag (Figure 66). High temporal resolution datasets were therefore under-sampled at 1 in 10 to give a sampling interval of 10 seconds, which was found to be sufficient time for the animal to make moves significantly greater than the tag depth resolution (Figure 67). Where the data was recorded with high vertical (i.e. depth) resolution then the accuracy of the tag is sufficient to prevent the effects of jitter (Figure 68). Secondly, in all datasets, sampling artefacts were introduced when the animal made long movements with a temporal interval that exceeded the sampling interval (Figure 69). Even with a sampling interval of 1 hour it was found that some long movements had been artificially divided into a series of shorter steps. Correction of this second sampling artefact involved coalescing steps that were part of a single movement (i.e. where the trend of consecutive steps was either a continuously increasing or decreasing depth) into a single step rather than many smaller steps. It should be noted that this method of path integration maintains move step-lengths consistent with that of a Lévy walk since displacements have finite velocity and are dependent on a time *t* (Shlesinger and

Klafter 1986, Viswanathan *et al.* 2008). Finally, some of the datasets obtained via Argos satellite telemetry inevitably contained gaps where data was not retrieved, or was recovered corrupted and so was discarded (Hays *et al.* 2007). If uncorrected, a spurious step would have been calculated between points either side of a gap; therefore, any step occurring immediately following a gap was ignored, ensuring that only genuine movement steps for which both the start and end depth had been recorded were included. Previous work has shown that small datasets can be prone to large statistical fluctuations and may result in poor fits to a candidate distribution or inaccurate estimates of the exponent (Sims *et al.* 2007). Therefore, datasets with fewer than 500 data points prior to pre-processing were excluded from the analysis.
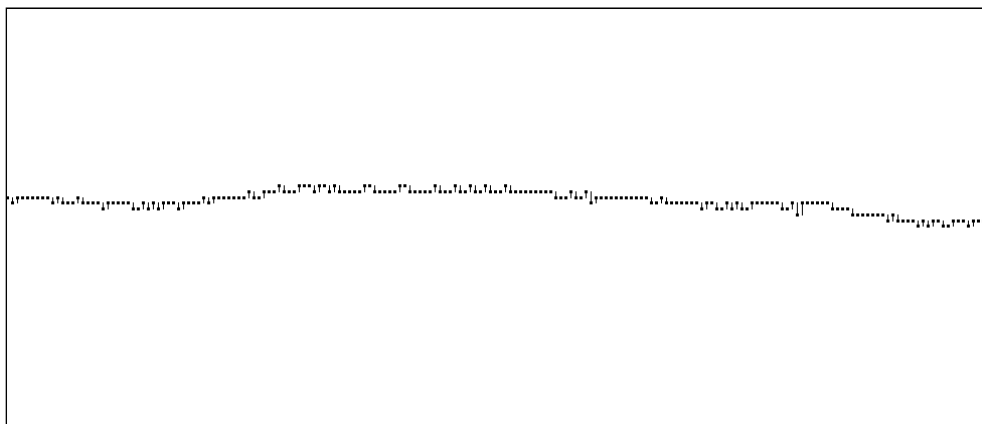
Figure 66: An example of high temporal resolution data exhibiting jitter
In this case the data was recorded at 1 s intervals from a porbeagle shark (*Lamna nasus*). Jitter can be seen as small alternating vertical displacements.
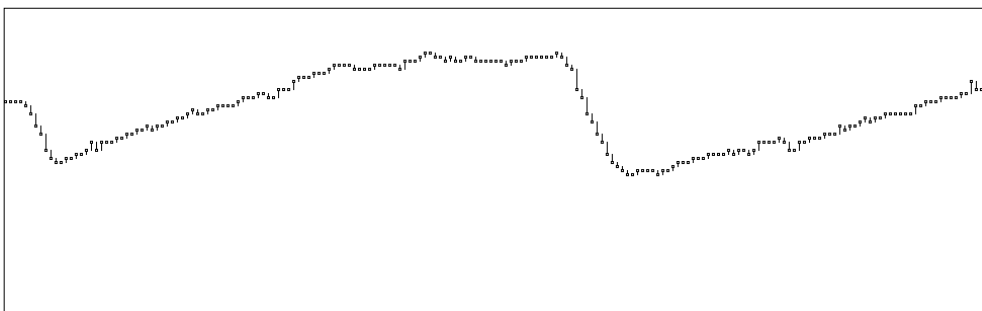
Figure 67: Under sampled depth data
Under-sampling the data at 1 in 10 to give a 10 s resolution reduces the jitter.
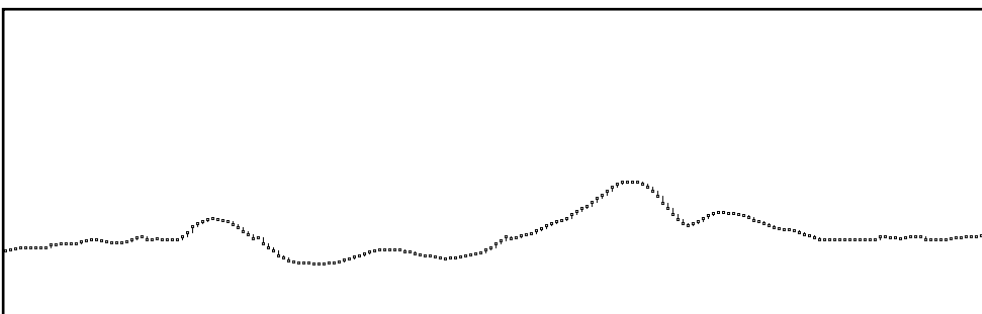
Figure 68: High resolution dive data
If data is recorded at a high spatial resolution then there is little or no jitter, even when recorded at a high temporal resolution. Here the depth resolution is 4cm and the temporal resolution is 1 s.
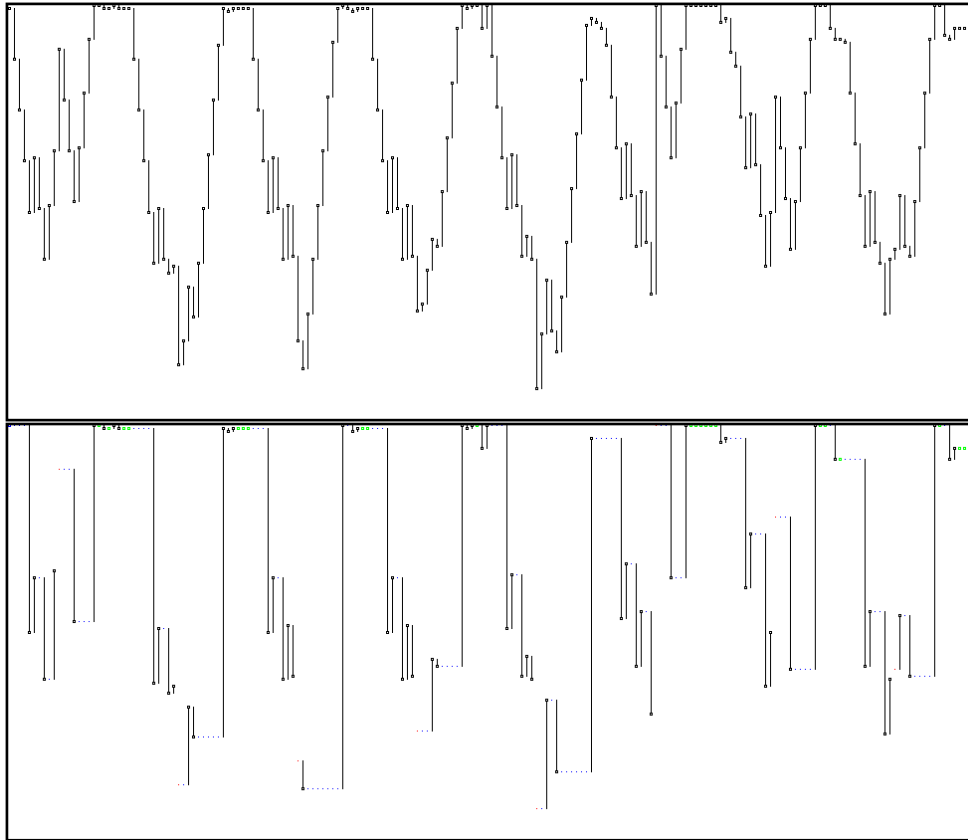
Figure 69: Sampling artefacts producing short step-lengths
When the animal makes moves with a duration that greatly exceeds the sampling interval of the tag long steps are truncated. In this case the data was recorded at 1 hour intervals from a swordfish (*Xiphius gladius*). Lower panel shows corrected data.

4.3 Results

We found clear and persistent signals of Lévy and Brownian motion; of the 94 sections analysed statistically (MLE with *w*AIC), one section was best fit by a pure power-law (Figure 70b) and 60 sections were found to best fit a truncated Pareto-Lévy distribution (e.g. Figure 70d,e;Table B2), with exponents (μ) in the Lévy range $1 < \mu \leq 3$ and so were consistent with Lévy behaviour. The mean μ value for the Lévy sections was 1.94 (S.D. 0.43, $n = 61$) which is close to the proposed optimum ($\mu_{opt} = 2$) (Viswanathan *et al.* 1999, Bartumeus *et al.* 2005, Viswanathan *et al.* 2008). Six sections best fit by a truncated power-law yielded exponents outside the Lévy range.

Lévy searching in open ocean predators therefore appears not only present, but prevalent, however, it does not appear to be a universal pattern to explain all movements nor does it occur in all individuals at all times (occurring in only 47% of sections). A logical extension therefore supports the hypothesis that other movement behaviour types intersperse Lévy patterns. In support of this we found 27 sections (21%) were best fitted by an exponential model describing normal random processes

(Brownian motion) (Table B2) that under the LFF hypothesis are consistent with optimal searches where prey are abundant (Viswanathan *et al.* 2008). The 35 sections (27%) that were poorly fit by any of the distributions was, perhaps because the sections comprised many different movement patterns making them too complex for the statistical methods employed here.
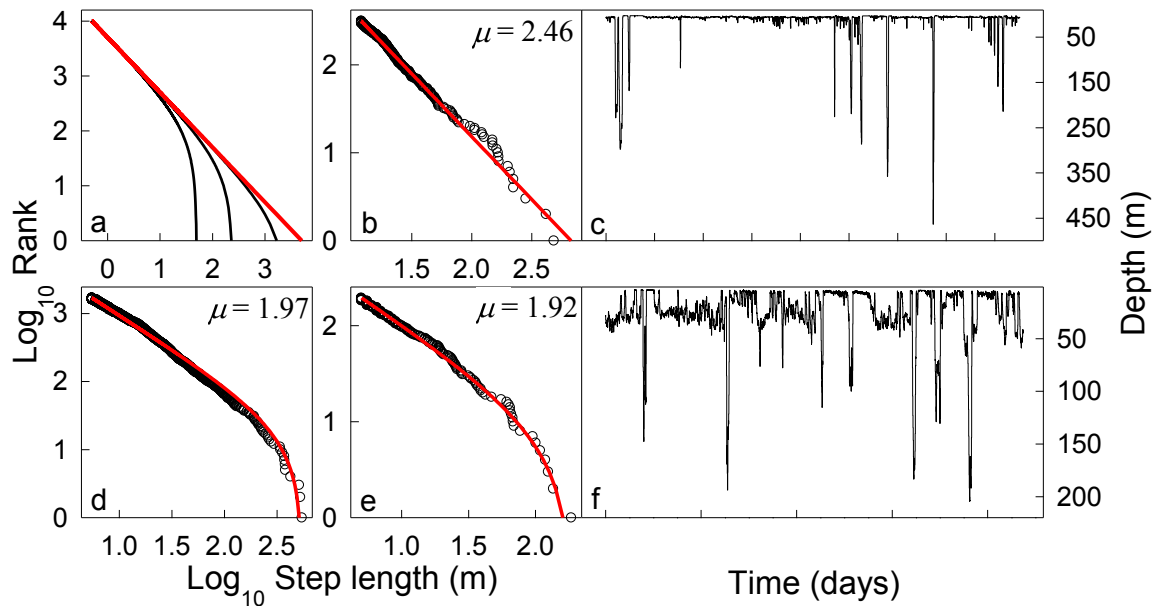
Figure 70: Examples of good fits to power-law and truncated power-law distributions.
(a) Synthetic power-law and truncated power-law (Pareto) distributions with upper truncations set to 50, 250, 5000, compared with empirical power-law and truncated power-law fits to dive data from (b, d) individual blue sharks (*Prionace glauca*), together with (c) the diving time series for the individual in b (over ≈ 8 days), and (e) an ocean sunfish (*Mola mola*) with (f) dive time series (≈ 4 days). Tick marks in c and f are 24 h. Red line in (a) shows synthetic power-law, (b) a power-law and (d, e) truncated power-law MLE model fits to empirical data.

4.3.1 Maximum Likelihood Estimation (MLE) results

MLE best fit parameters, log-likelihoods and Akaike weights for all track sections are given in Table B2. Details for the best fitting sections (i.e. those used in the spatial analysis, or shown in figures) are given in Table B3. Figure 71 shows plots for those sections best fitted by a power-law or truncated Pareto models that do not appear elsewhere in the paper showing two competing model fits.

Truncated power-laws provided the majority of best fits to empirical movement data of tracked fish predators. It is perhaps unsurprising that natural phenomena such as animal movement data should be better fitted by truncated Pareto-Lévy distributions rather than pure power-laws: where the animal is restricted by the depth of the water column or other factors (e.g. thermal or oxygen tolerances, predator physiological

capacity to withstand increased depths, prey absence) the truncation of the best fit distribution is increased (see Figure 70).

For the best fitting truncated Pareto-Lévy (power-law) sections, MLE and the R Gamma functions (R Development Core Team 2009) were used to attempt to fit a (shifted) Gamma distribution to ensure that this model was not a better alternative. GOF values calculated using the Kolmogorov-Smirnov test are given in Table B3 and ranked step-length plots of the fits are shown in Figure 72. Overall, it was found that gamma distributions were not better fits to the move step-length frequency distributions best fitted by a truncated power-law.
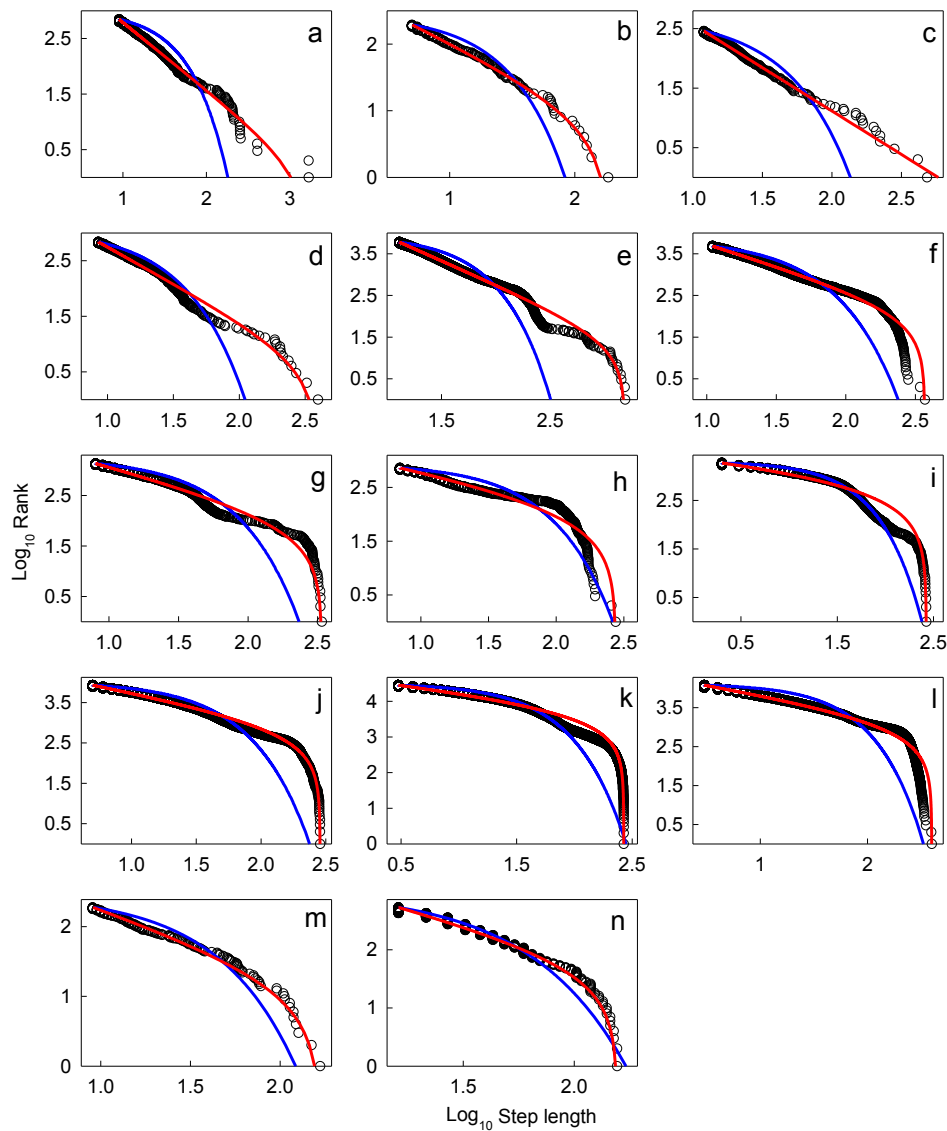
Figure 71: Ranked step-length plots for sections well fitted by a truncated Pareto-Lévy distribution.
Best fit truncated Pareto (power-law) (red line) and exponential (blue) models to observed data (black circles) for those figures not shown elsewhere. (a) bigeye tuna 1 section 4; (b) ocean sunfish 1 s2; (c) blue shark 9 s3 (note that this fit is to a power-law, not a truncated power-law); (d) blue shark 12 s2; (e) bigeye tuna 5 s4; (f) yellowfin tuna 2 s1; (g) yellowfin tuna 4 s4; (h) yellowfin tuna 5 s1; (i) yellowfin tuna 5 s3; (j) yellowfin tuna 1 s3; (k) yellowfin tuna 3 s3; (l) yellowfin tuna 3 s4; (m) blue shark 9 s2; (n) silky shark 3 s1.
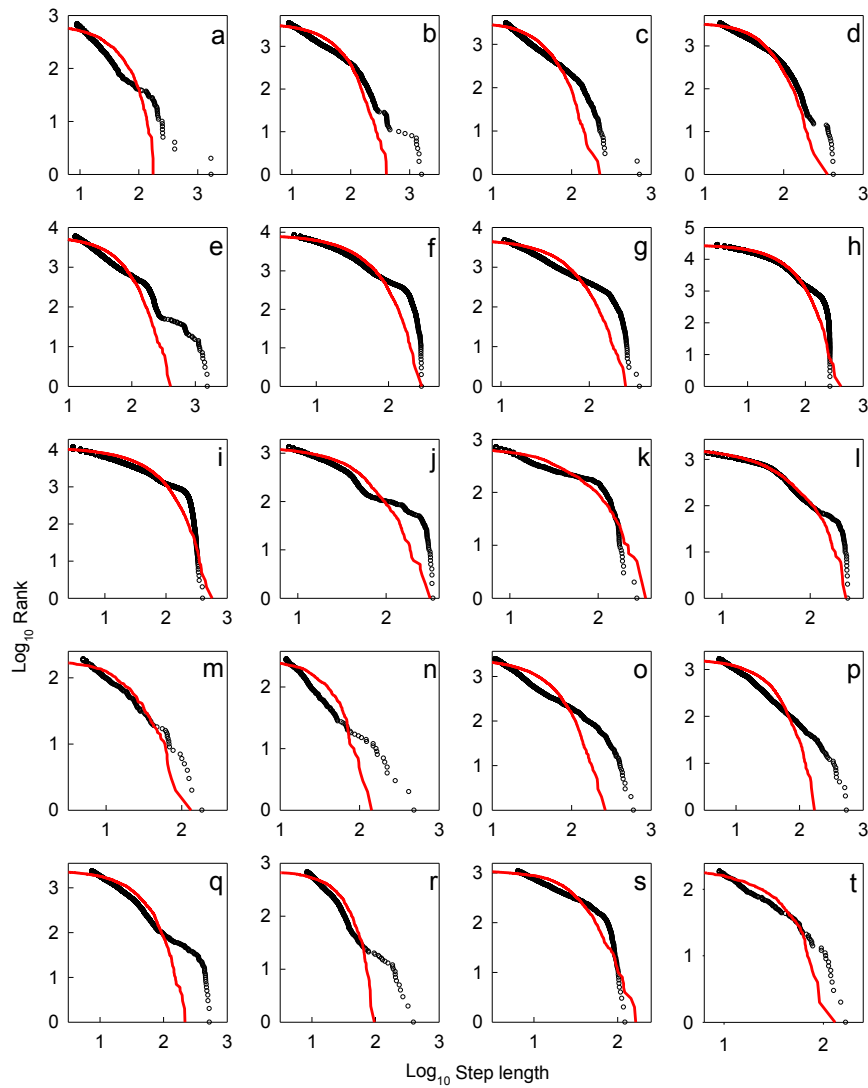
Figure 72: Gamma distribution fits to empirical data best fitted by the truncated Pareto distribution.
Best fit Gamma (red) and observed data (black circles). (a) bigeye tuna 1 section 4; (b) bigeye tuna 2 s3; (c) bigeye tuna 2 s6; (d) bigeye tuna 2 s8; (e) bigeye tuna 5 s4; (f) yellowfin tuna 1 s3; (g) yellowfin tuna 2 s1; (h) yellowfin tuna 3 s3; (i) yellowfin tuna 3 s4; (j) yellowfin tuna 4 s4; (k) yellowfin tuna 5 s1; (l) yellowfin tuna 5 s3; (m) ocean sunfish 1 s2; (n) blue shark 9 s3; (o) blue shark 10 s2; (p), blue shark 10 s4; (q) blue shark 10 s5; (r) blue shark 12 s2; (s) silky shark 3; (t) blue shark 10 s1. See Supplementary Table S4 for model comparison values.

4.3.2   *Environmental context: Behavioural switching*

To investigate the environmental context of different behaviour patterns we mapped the horizontal tracks of individual predators in the Atlantic or Pacific Oceans to determine in which types of habitat the sections showing Lévy and Brownian vertical movement patterns occurred. For example, in the Central North Pacific in productive waters of the Equatorial Convergence Front, the entire track of a silky shark *Carcharhinus falciformis* was best fit by an exponential model, whereas for another silky shark tracked further north in oligotrophic waters the best fit was a truncated power-law with an exponent of 2.02, close to the theoretical optimum for Lévy

movement (μ_{opt} = 2). We also found for 8 individuals of 5 species of fish predator (bigeye tuna *Thunnus obesus*, yellowfin tuna *Thunnus albacares*, blue *Prionace glauca*, basking *Cetorhinus maximus* and whale sharks *Rhincodon typus*) where different model fits occurred between different habitat types within an individual. For example, a blue shark tracked in the Northeast Atlantic moving from highly productive, shelf habitat of the western English Channel south to the less productive, deep water of the Bay of Biscay, showed switches in the pattern of vertical movement (Figure 73a-e). The shark showed diving behaviour in tidal front waters on the shelf (0 – 200 m depth) well fitted by an exponential model (Figure 73a,f,k; Table B3). Moving off-shelf into less productive waters (with well-developed thermal stratification) (Figure 73m,q), vertical movements down to 700 m conformed well to a truncated power-law with an exponent of μ = 2.19 (Figure 73b,g,l), before diving movements shifted to a pattern better approximated by an exponential fit when in colder, shelf-edge habitat in the southern Bay of Biscay (Figure 73c,h,m). Returning to warmer, well stratified but less productive open ocean habitat (Figure 73d,e,n,o,q), this shark once again exhibited vertical movements best fit by truncated power-laws with μ = 1.97 and 1.99 (Figure 73i,j). A bigeye tuna in the Central Eastern Pacific near the Galapagos Islands switched several times between diving movements best fit by a truncated power-law when in warmer, stratified waters, to movements approximated by an exponential model in colder waters of the Equatorial Convergence Front.
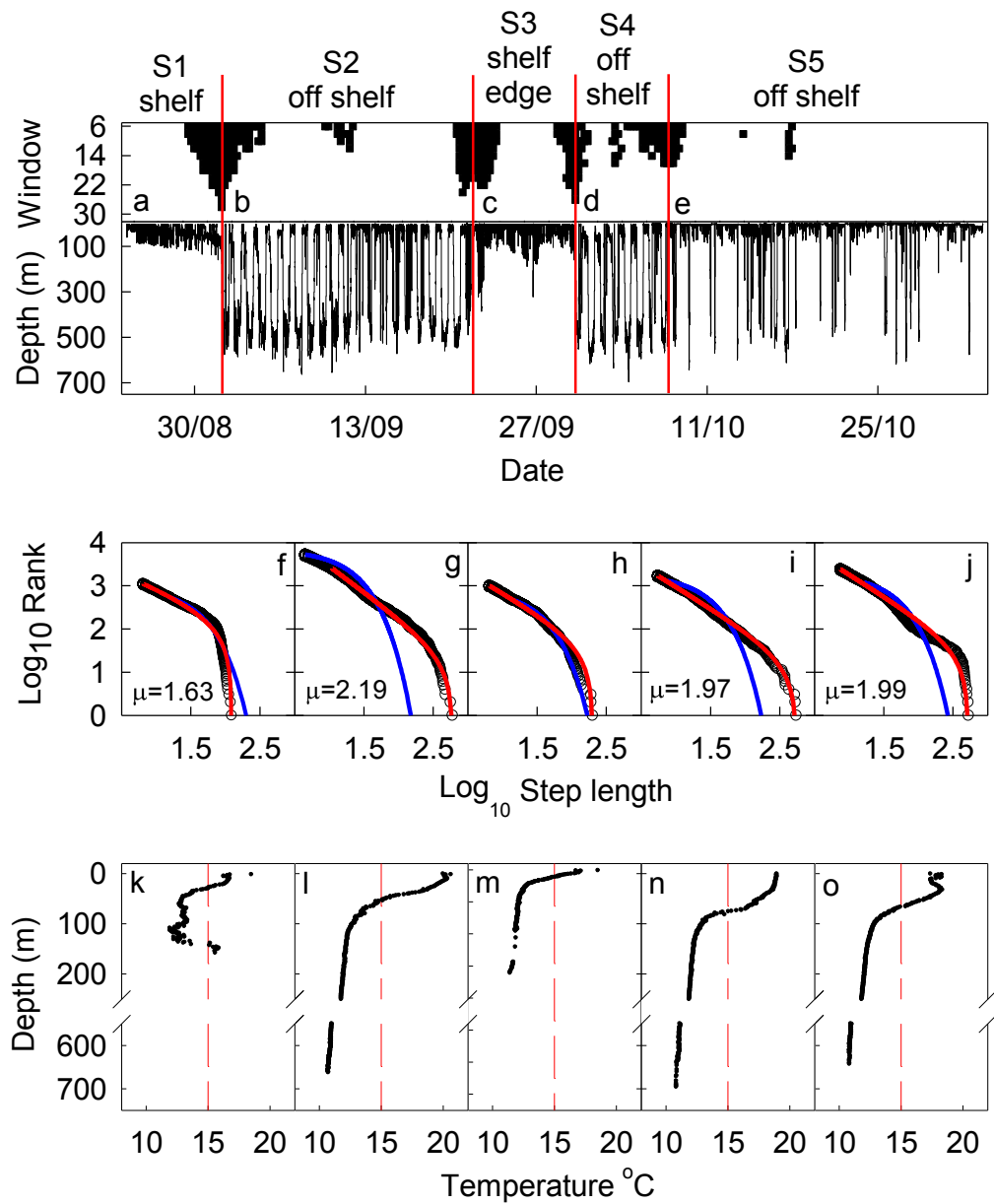
Figure 73: Behavioural switching between Lévy and Brownian motion in relation to habitat type.
(a-e) Split-moving window analysis showing significant discontinuities in the dive time series of blue shark 10. Red lines indicate points where the time series was divided into sections (S). (f-j) MLE analysis with μ values for sections best fitting a truncated power-law distribution; black circles, observed step-lengths; red lines, best fit truncated power-law; blue lines, best fit exponential distribution. (k-o) Electronic tag recorded depth profiles of sea temperature. (Continued below...)
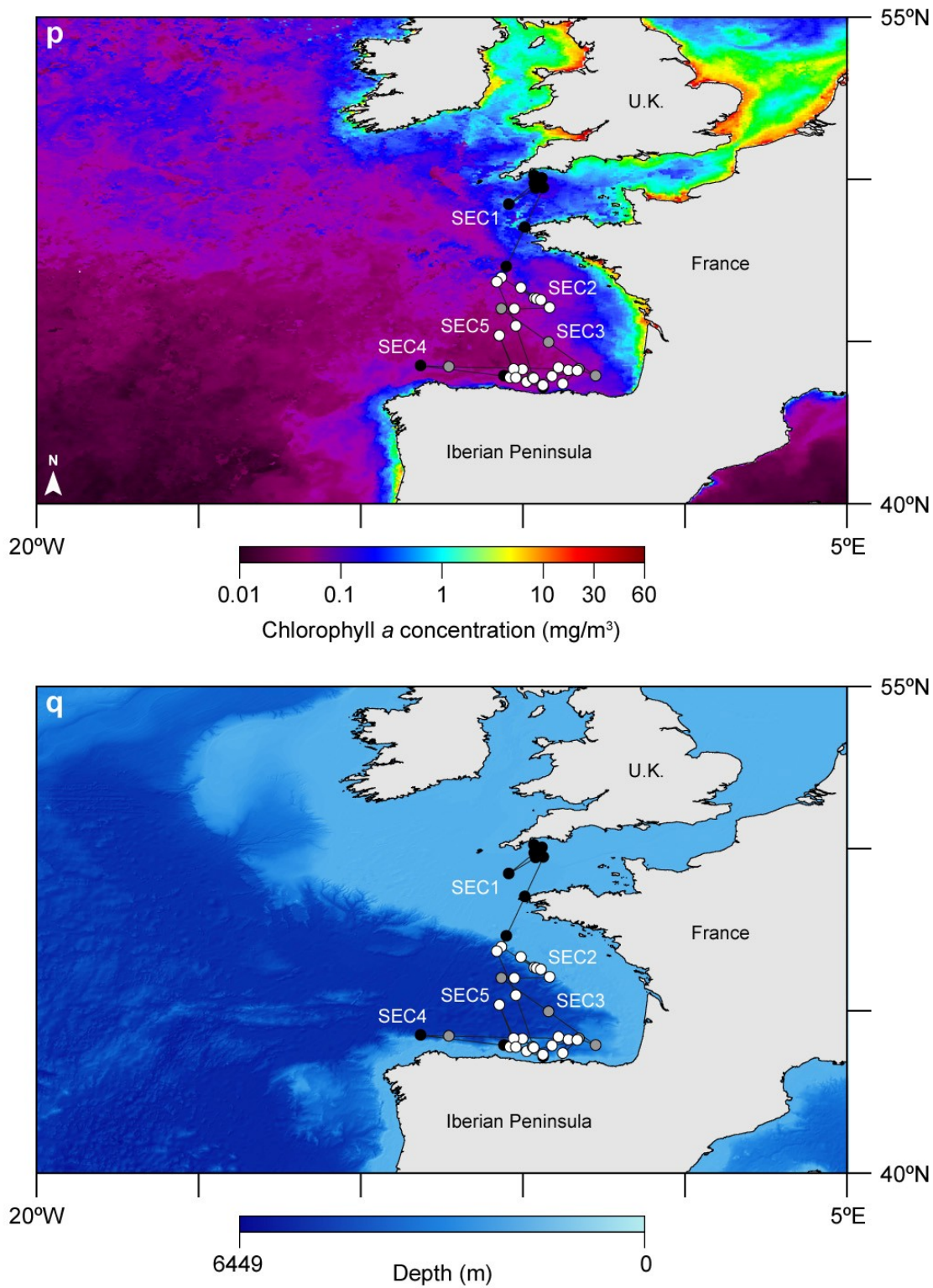
Figure 73 (Continued):
(p) Geo-referenced track sections of blue shark 10 overlaid on bathymetry and (q) chlorophyll 'a' concentrations. Section (SEC) numbers correspond to those in a-e.

4.3.3   *Statistical significance*

These results conform to the LFF hypothesis prediction that Lévy behaviour should occur in environments where prey is sparsely distributed whereas Brownian motion is theoretically optimal where prey is abundant (Bartumeus *et al.* 2002). To test the significance of this with our habitat-mapped data we compared the frequency of

sections that conformed to this broad prediction. It was assumed prey were likely to be more sparsely distributed in open ocean habitats having lower primary (Behrenfeld and Falkowski 1997) and secondary production (Sims *et al.* 2006b), compared with more productive shelf, frontal and convergence zone habitats where prey of the predators we tracked is known to be more highly abundant (Clarke and Stevens 1974, Moteki *et al.* 2001, Sims *et al.* 2006b, Zainuddin *et al.* 2006). We used only geo-referenced sections yielding best fits where the step-length data spanned at least 1.5 orders of magnitude (range, 1.53 – 2.27).

For 4 species of fish predator (3 sharks and ocean sunfish) in the Northeast Atlantic that moved between continental shelf areas with high surface zooplankton abundance and open ocean areas with lower abundance (Sims *et al.* 2006b), that provide a proxy for prey-abundant and prey-sparse environments, respectively, 14 mapped sections were available. Movement patterns in 12 sections performed as hypothesised (sparse prey, Lévy behaviour; abundant prey, Brownian motion) (chi-squared with Yates correction for continuity: χ^2 = 5.78, $\chi^2_{0.05,2} = 3.84$, *P* < 0.025) (Figure 74a). This indicates that the frequency of observed movement patterns approximated by a Lévy distribution in less productive areas and by an exponential distribution (Brownian) in more productive waters, did not deviate significantly from theoretical predictions of the LFF hypothesis (Bartumeus *et al.* 2005, Viswanathan *et al.* 2008). For bigeye and yellowfin tuna in the Central Eastern Pacific moving between warm stratified waters and cooler, more productive convergence front waters there were 21 sections for analysis. A higher number of sections best fit by an exponential distribution occurred in convergence front waters than in stratified waters (chi-squared with Yates correction for continuity: χ^2 = 4.00, $\chi^2_{0.05,2} = 3.84$, *P* < 0.05) (Figure 74b). Therefore, the occurrence of Brownian-type behaviour of tuna in the Pacific agrees with predictions of the LFF hypothesis. Interestingly, the number of sections where diving movements conformed to a truncated power-law was equal between convergence front and stratified waters. We speculate that one reason for tuna in the productive convergence zone exhibiting Lévy diving movements characterised by longer vertical steps is that fish prey may become spatially constrained within mesoscale eddy features (Zainuddin *et al.* 2006) that are common in the region and have diameters between about 50 and 200 km. Thus, even in this productive environment, tuna movement may be optimised by

longer vertical re-orientations (searching) between eddies since prey hot-spots may be patchily distributed across a wide range of scales linked to turbulent eddy formation, size and persistence (Powell *et al.* 1975).
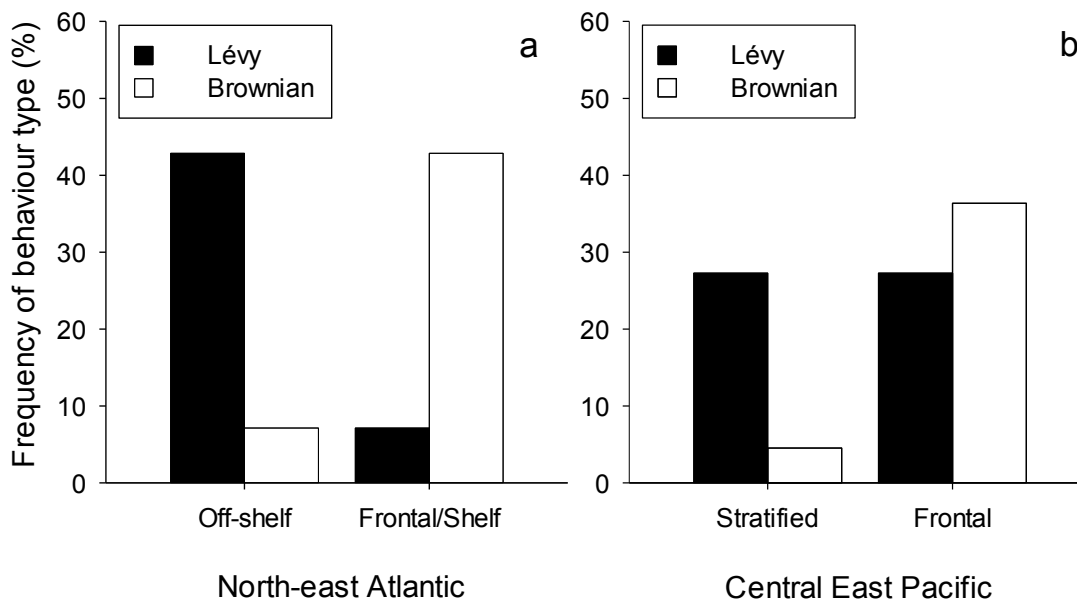
Figure 74: Spatial occurrence of Lévy and Brownian behaviour types.

Frequencies of behaviour types in (a) productive (frontal/shelf) and less productive (off-shelf) habitats in the Northeast Atlantic and in (b) productive (frontal) and less productive (stratified) habitats in the Central Eastern Pacific. Tests of two theoretical assumptions of the Lévy flight foraging hypothesis (sparse prey predicts Lévy behaviour; abundant prey predicts Brownian movement) were performed on frequency data (not percent frequency data). See main text for statistical test details.

4.3.4   Environmental context and Lévy behaviour of silky sharks

In further support of the prediction that when prey is abundant Brownian motion is an optimum search strategy, whereas when prey is sparse Lévy is optimum, Figure 75 shows geo-referenced tracks from two silky sharks (*Carcharhinus falciformis*) in relation to chlorophyll 'a' concentrations, a proxy for productivity. Silky shark 2 was located in comparatively productive waters with a move (dive) step-length distribution best fitted by an exponential distribution representing Brownian motion. In contrast, silky shark 3 remained in very low productivity (oligotrophic) waters with diving behaviour approximated by a truncated power-law with an exponent of $\mu = 2.02$, close to the theoretical optimum for Lévy behaviour in an environment with sparse target sites.
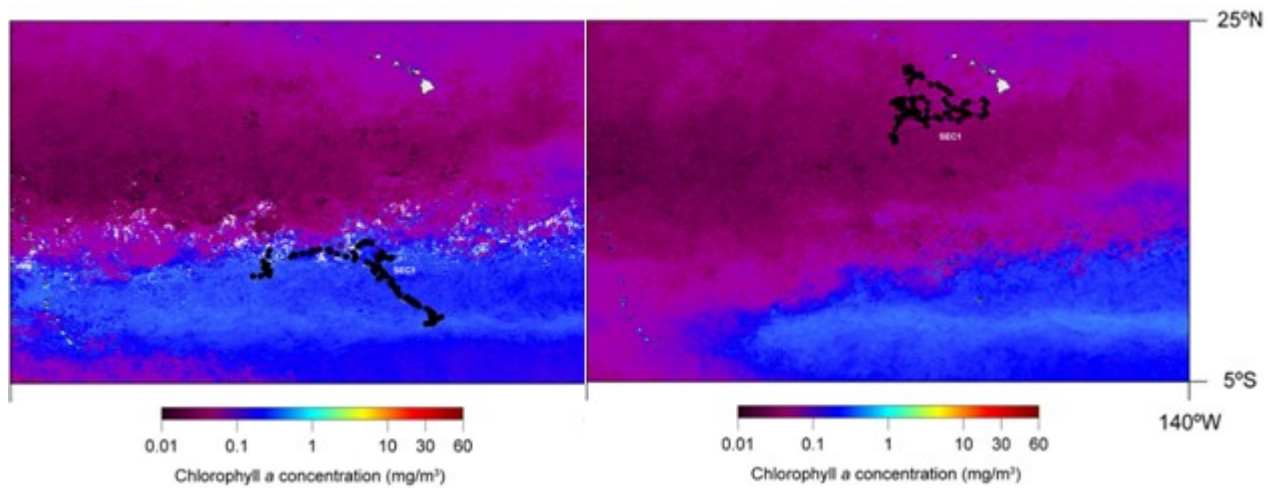
Figure 75: Horizontal movements of silky sharks in different productivity zones.
Left panel, silky shark (*Carcharhinus falciformis*) 2 in productive waters (Equatorial Convergence Zone) with vertical movements following an exponential distribution; right panel, silky shark 3 in less productive, oligotrophic waters (south of the Hawaiian Islands) with vertical movements approximated by a truncated power-law exponent of 2.02.

4.3.5 Behavioural pattern switching of a bigeye tuna in relation to habitat type

Under the adaptive (optimal) behaviour conceptual framework of the Lévy flight foraging hypothesis, changes in searching behaviour are expected as an animal moves between areas of differing productivity and hence prey density. In the Northeast Atlantic, continental shelf waters with abundant, seasonally persistent tidal and shelf-break fronts have generally higher primary and secondary productivity than open ocean waters where the water column is less well mixed and characterised by strong and stable vertical thermal stratification (Le Fèvre 1986, Sims *et al.* 2003). Here we defined two principal habitats for the purposes of simple analysis of behaviour types in relation to environmental gradients: productive shelf waters with strong tidal front presence (Frontal/Shelf) and less productive off-shelf areas typified by thermally stratified water with a deep thermocline at around 50 – 100 m depth (Off-shelf). In the Central Eastern Pacific, near the Galapagos Islands, the northerly flowing Peru Current meets the southward turning Equatorial Counter Current which form zones of upwelling and convergence along the westward flowing Equatorial Current. At these boundaries cold, nutrient rich water is up-welled and mixed with warmer surface waters creating a highly productive habitat characterised by plankton blooms (Le Fèvre 1986). Adjacent to these areas, to the north and south, the ocean is relatively oligotrophic and vertically thermally stratified with a thermocline depth of about 100 m. Here we defined two principal habitats to examine tuna behaviour: highly productive upwelling/convergence zone fronts (Frontal) and oligotrophic stratified water with a strong and stable thermocline (Stratified).

Although in this study switching behaviour was observed in only 8 individuals (from 55 individuals for which we had data), this is largely due to the difficulty of obtaining high-temporal resolution tracking data over long time periods where different large-scale habitat types were encountered. Longer tracks traversing different oceanographic regimes provided a greater chance of recording changes in patterns of search behaviour.

Switching between behaviour types – identified by split-moving window analysis, MLE model fits and Akaike weights (wAIC) model comparison values, and as a function of ocean productivity – was found for bigeye tuna (*Thunnus obesus*) (n = 2) and yellowfin tuna (*T. albacares*) (n = 2) in addition to blue shark (n = 1), basking shark (n = 2) and whale shark (n = 1) Table B2 & Table B3). As a representative example, Figure 76 shows the vertical movements of bigeye tuna 2, together with the MLE model fits to move-step frequency distributions of the different sections, water temperature-at-depth profiles and the horizontal movements corresponding to the analysed sections. The split-moving window analysis identified eight adjacent sections as having different features (Figure 76a,b). Horizontal movements were characterised by traversing east-west movements mostly along the boundary between the Equatorial Convergence Front spreading west of the Galapagos Islands and lower productivity, stratified waters further south (Figure 76c,d,e). The analysed sections show changes in vertical movement pattern, with Lévy behaviour occurring predominantly in the west and Brownian-type movement in the east. The switch from Lévy to Brownian patterns of movement (Figure 76c sections 3 to 4) and back again (Figure 76c sections 5 to 6, and sections 6 and 7) was also coincident with a change in water mass type, from warm well-stratified water to cooler surface-layer water with a weaker thermocline that is characteristic of zones of upwelling and convergence (Figure 76d sections 3 to 4).

The behaviour of the bigeye tuna shows changes in relation to the environment and we speculate that prey may have been more abundant in the eastern region nearer the Galapagos since Brownian motion was identified there. The physical complexity of the Equatorial Convergence Zone characterised by upwelling, meso-scale fronts and eddies (Zainuddin *et al.* 2006) is likely to entrain complex distributions of prey, including aggregation of individuals (Fiedler and Bernard 1987), and will likely

contribute to the observed complexity in tuna behaviour such as switching between different optimal strategies as resource conditions change.
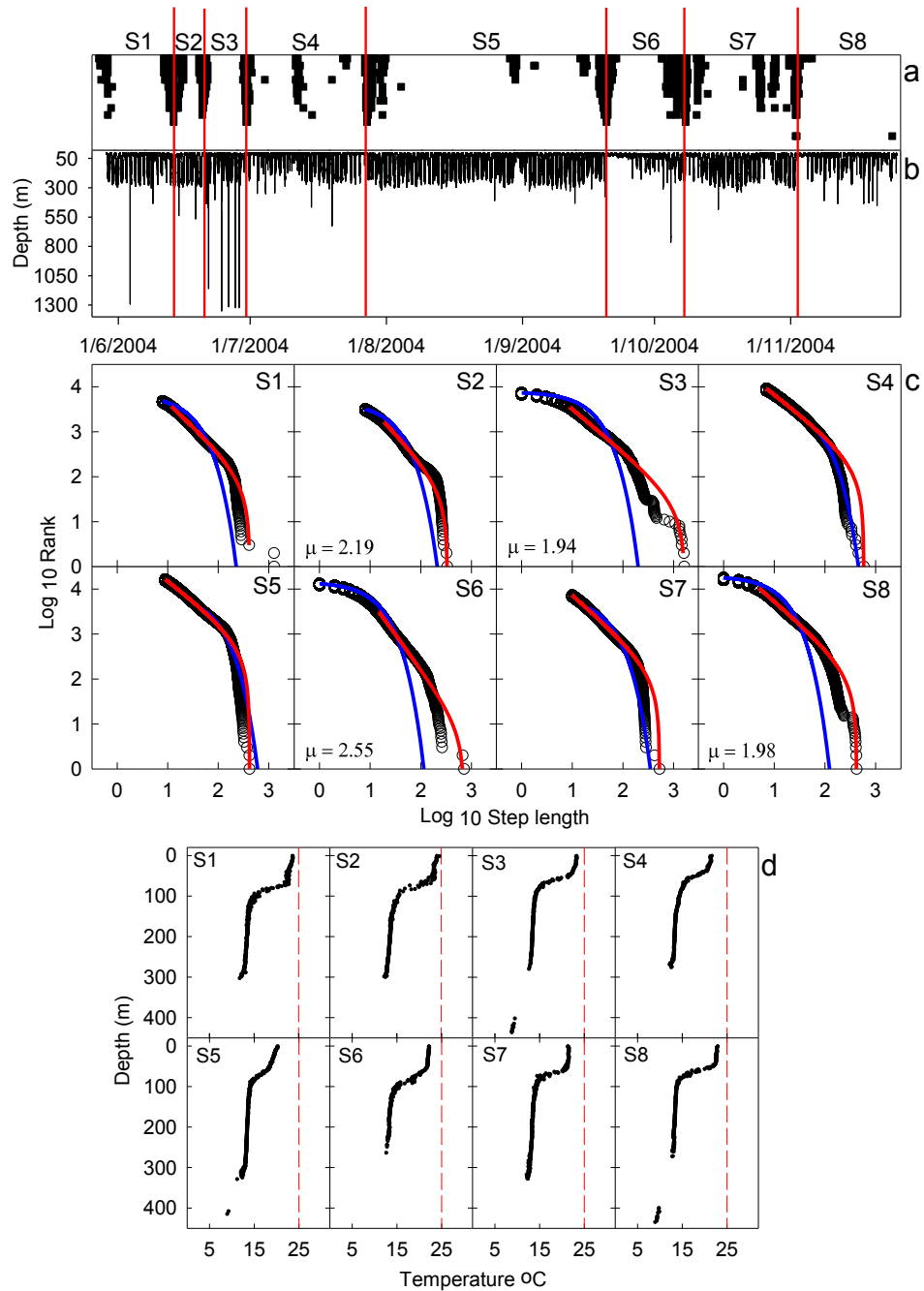
Figure 76: A bigeye tuna switching diving behaviour in relation to environmental gradients.

(a) Split-moving window analysis and (b) time depth profile for bigeye tuna 2 showing the seven points of most significant discontinuity at which the track was divided. (c) MLE analysis of the eight sections showing μ values for those sections best fitted by a truncated Pareto (power-law) distribution. Maximum Likelihood Estimation (MLE) model parameters and Akaike's Information Criteria (AIC) weights model comparisons for c given in Supplementary Tables S3 and S4. (d) Profiles of temperature at depth recorded by fish-attached electronic tags. These show the thermal profile of the water column and thermocline depth being similar from S3 to S5 followed by a decrease in upper layer temperatures and weaker thermocline (S4 and S5) and re-establishment of a stronger thermocline and higher temperatures from S6-S8. The weaker thermocline is associated with a better fit of vertical move step-lengths within a section to an exponential distribution (S5) while vertical move steps within well stratified waters are better fit by a truncated power-law distribution (S1, S8).

Figure 76 (Continued)

(e) Horizontal movements of bigeye tuna 2 west of the Galapagos Islands along the southern boundary of the Equatorial Convergence Front. Sections are numbered as for a-c and arrows in the lower panel indicate directions of movement paths.

4.3.6 *Lévy flight behaviour in a productive convergence zone*

As expected from the Lévy flight foraging hypothesis (LFF) bigeye (*Thunnus obesus*) and yellowfin tuna (*T. albacares*) displayed a higher frequency of Brownian-type diving movements than Lévy movements in the Equatorial Convergence Zone. However, both species were found to exhibit Lévy movements in a productive zone at least as frequently (in terms of frequency of time series sections) as in a lower productivity region, which is more often than might be expected according to the LFF hypothesis. This contrasts with the occurrence of Lévy behaviour in the Northeast Atlantic where clearer spatial difference between productive and less productive large-scale habitats was evident (productive shelf/frontal habitat versus lower productivity off-shelf habitat) and where Lévy movement patterns were associated with off-shelf regions.

That tuna exhibited both Lévy and Brownian movement types in the Equatorial Convergence Zone west of the Galapagos Islands suggests a requirement for a flexible approach to searching that may be linked to complexity in prey distributions (as mentioned above). One possible explanation for this flexibility in tuna movement pattern is that although prey resources are generally higher in frontal zones compared

to adjacent regions (Le Fèvre 1986), physical processes act to influence distributions of prey in complex ways. For example, the heterogeneity in distribution and abundance of zooplankton species in the Northwest Atlantic has been shown to be related to their associations with specific water masses of different origin and associated temperature/density discontinuities such as pycnoclines and fronts (Gallager *et al.* 1996, Zimmerman and Biggs 1999). Indeed, along mesoscale frontal features in the Eastern North Pacific albacore (*Thunnus alalunga*) and skipjack tuna (*Katsowonus pelamis*) were found to be aggregated in high productivity areas where prey such as anchovy, pelagic red crab and euphausids were enhanced (Fiedler and Bernard 1987). However, even along frontal features prey distributions were highly patchy across a broad range of mesoscales (Fiedler and Bernard 1987).

In the present study it is possible that the adoption of Lévy and Brownian movements by tuna are responses to changes in patchy prey distributions that are entrained by frontal features such as eddies. It has been observed that in Pacific inter-tropical convergence zones albacore tuna are associated with meso-scale fronts and eddies (Zainuddin *et al.* 2006). These oceanographic features create local aggregations of prey organisms and patchier distributions of prey than might otherwise be expected at the meso-scale (Zimmerman and Biggs 1999). Therefore, very rich prey areas are expected within or near eddies, whereas relatively lower concentrations of prey may be available between such systems. This could account for the change between an optimal strategy for sparse prey environments and a strategy for where prey is more abundant occurring in the Equatorial Convergence Zone near the Galapagos Islands.

The tuna tracked in this study covered very large distances (1502 to 7867 km) and areas (87,399 to 1,111,654 km^2) (Figure 77, Figure 78) which greatly exceed the scale of eddies in this region (*ca.* 50 – 200 km diameter). It is therefore possible that at the scales over which the tuna ranged prey is not always highly abundant but patchy over a wide range of scales, and therefore Lévy diving movements may be a more efficient strategy for large interpatch distances than the expected Brownian diving movements.
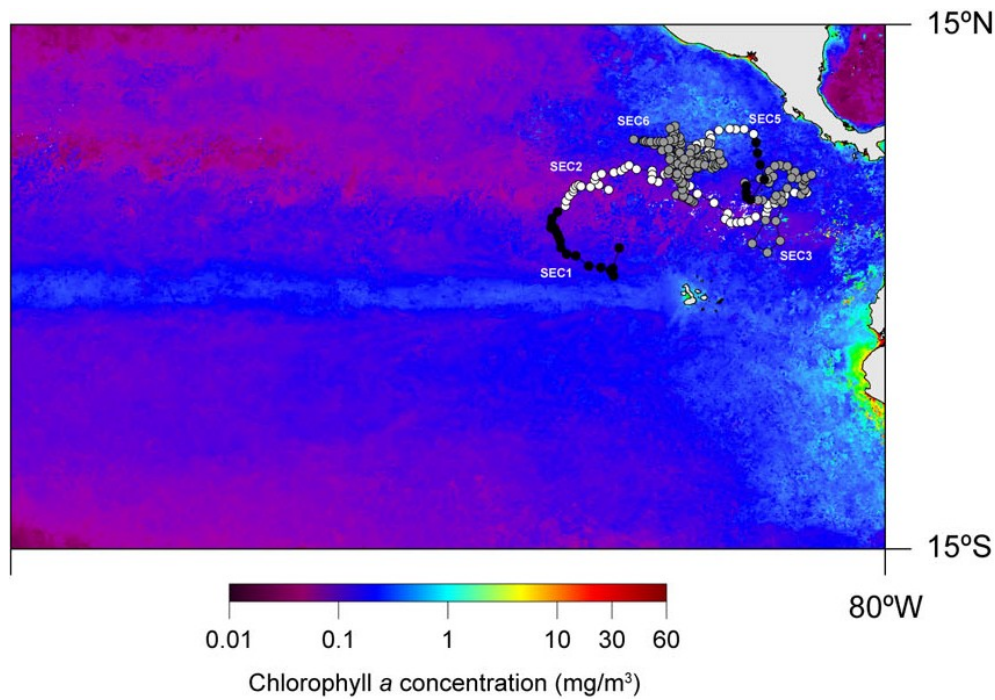
Figure 77: Yellowfin tuna horizontal movements across different productivity zones.
Yellowfin tuna 2 (*Thunnus albacares*) covered a distance of 7,867km and an approximate area of 249,751km^2 while traversing habitats with differing productivity.
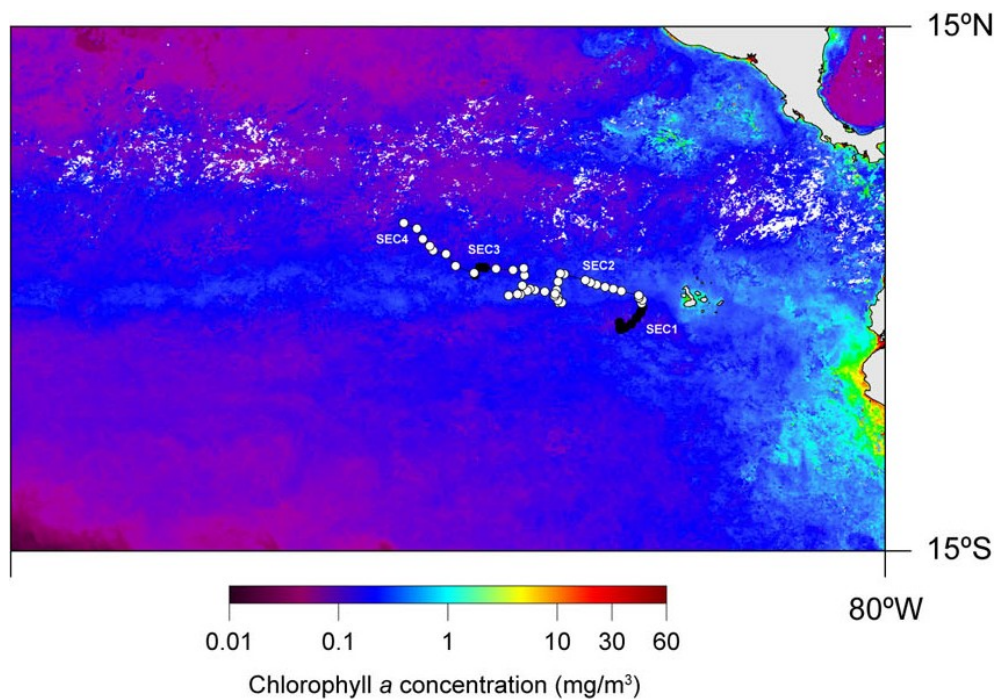
Figure 78: Bigeye tuna horizontal movements across different productivity zones.
Bigeye tuna 3 (*Thunnus obesus*) crossed the equatorial convergence zone from near the Galapagos Islands northwest into warmer oligotrophic waters, covering a distance of 2,609km.

4.4 Discussion

In summary, our analysis provides the strongest evidence yet for Lévy behaviour in diverse animals ranging across natural landscapes. Furthermore, movement patterns of some individuals approximated theoretically optimal Lévy searches. It was also evident, however, that Lévy behaviour is not a universal pattern; rather, some

individuals utilise other patterns approximated by normal random processes, sometimes interspersed with Lévy movements. We found that mapping the locations of where Lévy and Brownian movements occurred enabled a preliminary field test of the Lévy flight foraging hypothesis, confirming theoretical predictions. Therefore, our results not only lend strong support to the contention that Lévy flights do occur in free-ranging animals, but our observations of pattern switching between Lévy to Brownian type motion suggest searching animals adjust adaptively their optimal pattern of movements to different environmental resource distributions.. We recognise however, that our analysis could not detect how the movement patterns arose, that is, whether the patterns identified were an adaptive behaviour or whether observed patterns were an emergent property of the spatial distributions of prey (Boyer *et al.* 2006, Benhamou 2007, Sims *et al.* 2008a). To resolve this issue, controlled experiments (Bartumeus *et al.* 2003) rather than natural experiments, as here, will be needed. Such tests will be important to progress from asking whether Lévy flights (walks) occur in animals (Travis 2007, Buchanan 2008) to explore why they occur and whether animals evolved to exploit Lévy flights as an optimal search strategy for living in complex, highly changeable natural landscapes. Simulations of biological evolution indicate varying environments posing complex goals can speed up natural selection (Kashtan *et al.* 2007), which also raises the question that if animals have evolved Lévy flight behaviour, when did such a strategy first appear among organisms?

5 Foraging success of biological Lévy flights recorded *in situ*

5.1 Introduction

Recent, statistically robust, empirical studies, such as described in Chapter 4, have now identified Lévy flights in individual insects (Cole 1995; Maye *et al*. 2007), jellyfish (Hays *et al.* 2012), sharks, tuna, billfish, turtles and penguins (Sims *et al.* 2008a, Humphries *et al.* 2010, Sims *et al.* 2011), and in the population movement patterns of shearwaters (Bartumeus *et al.* 2010). Interestingly, Lévy patterns did not occur at all times in marine predators (Bartumeus *et al.* 2010, Humphries *et al.* 2010, Sims *et al.* 2011, Hays *et al.* 2012), rather their occurrence was dependent on environmental context – such as prey-sparse distributions – as predicted by theory (Viswanathan *et al.* 1999). However, in none of the studies was the foraging success measured; such a measure represents the ultimate test of whether Lévy flight might represent an advantage to the forager. Given that albatrosses often forage in highly heterogeneous habitats on squid and fish prey they catch at the surface (Weimerskirch 2007) it is reasonable to assume that a search strategy aimed at increasing the chance of encountering sparse prey, such as Lévy flight, may be present. Furthermore, given that the albatross studied here were brooding chicks, the foraging trips had to provide sufficient food

with sufficient regularity for the chick to thrive and not starve. It has been estimated that a pair of *D. exulans* require 1.7 kg bird^{-1} day^{-1} of food (an estimated total of 2733 MJ for both birds for the 365 days of the breeding season, giving 3800 kJ per bird per day) in order to raise a chick (Shaffer 2004) with chicks requiring 60-65 kg of food in total (Berrow and Croxall 2001) and with foraging trips lasting from 12h to 6 days (Weimerskirch and Lys 2000). From the Feast and Famine simulations in Chapter 3 it is clear that Lévy flight foraging, with the increased encounter rate it confers, could be an advantageous strategy to improve chick survival. In particular, when the chick is young food is required more frequently (Weimerskirch and Lys 2000) and therefore longer intervals between feeding events could result in starvation, even if the total food returned by the parent was sufficient. Shorter less productive foraging trips might be favoured at this time over longer more productive trips. The virtual Lévy foragers studied in Chapter 2 experienced more frequent prey encounters and would be expected therefore to be more successful in rearing young that are vulnerable to starvation. Therefore, using appropriate datasets and robust statistical methods we (1) tested whether Lévy flight search patterns were present in albatrosses, and (2) using prey capture events, determined whether Lévy flights do result in successful foraging trips compared with another strategy, such as a Brownian walk, as predicted by the LFF hypothesis.

5.2 Methods

Animal-attached GPS tags provided time-stamped location datasets for 61 black browed albatrosses (*Thalassarche melanophrys*) brooding chicks on Kerguelen Island (49.35°S 70.22°E) and 27 wandering albatrosses (*Diomedea exulans*) incubating or brooding chicks on Possession Island (46.40°S 51.76°E) in the Crozet Islands archipelago. Between 2002 and 2010, birds were equipped just before taking off for the sea with GPS loggers attached with adhesive tape on the back feathers; the total mass of devices (between 20 and 45 g according to the season and species) was far below the recommended 3% threshold. A summary of the original GPS datasets is given in Table C1. Eleven of these birds were also fitted with a stomach temperature logger for determining the timing of prey capture and estimating prey mass ingested. Details of deployment procedures for GPS tags and stomach temperature loggers are given in Weimerskirch *et al*. (1994, 2002a, 2007).

For the prey capture study we also analysed 17 individual location time series of wandering albatross tagged in 1998, 1999 and 2001 that were each fitted with an Argos satellite transmitter, a wet/dry logger on one leg and were induced to swallow a stomach temperature logger. A summary of these datasets is given in Table C2. Full details of procedures and studies are given in Weimerskirch *et al*. (2005). Landing times of these birds were known from the wet/dry logger data and therefore no flight profile analysis was required. For consistency flight times were analysed using the same MLE and model selection methodology used for the 88 other birds in this study where no wet/dry logger data was available.

5.2.1 *Processing of GPS time series data*

The data obtained from the GPS tags are a time series of geographic locations at intervals of between a few seconds to several minutes, depending on both tag configuration and the time taken for the tag to acquire sufficient satellites to compute a location. This high resolution data captures the complex swooping flight path performed by the bird as it soars over the wave crests (Richardson 2011). Our intention was to test whether the bird flight steps that link periods of rest on the water or possible feeding events follow either a Lévy or exponential distribution. An exponential distribution might be expected if the movement pattern was essentially Brownian, resulting from a Poisson process; a Lévy pattern could suggest an optimal foraging search pattern such as a Lévy flight (Bartumeus *et al.* 2005), which would emerge from a bird conducting a Lévy walk since the turning points (landings for resting or feeding) in a Lévy walk are a Lévy flight (Shlesinger *et al.* 1993). Alternatively, a Lévy (heavy-tailed) pattern could arise by random movements across a fractal distribution of prey patches (Fritz *et al.* 2003, Nams 2005, Pinaud and Weimerskirch 2005). Because the majority of tags did not include a salt water switch (wet/dry logger) we determined whether the bird was in flight or at rest from variations in flight speed and for consistency used this method for all tags. Periods of time spent resting on the sea surface and drifting with the current would have low speeds, whereas flight speeds would be necessarily higher. We used a speed threshold of 10 km h^{-1} (Wakefield *et al.* 2009) above which the bird was most probably in flight and below which the bird was most likely at rest (or feeding) on the water. The first processing step converted the time series of locations into a series of movement steps using the Haversine equation

to calculate great circle distances, which together with the time intervals, average speeds were calculated. The undulating form of the flight path results in sudden changes in speed and would produce a complex flight profile if each move step below the threshold were taken to be a rest step, and each step above the threshold as a flight step (Figure 79, upper grey plot). Therefore, the second processing step converted the movement steps into a flight profile, where unrealistically short periods of time, either at rest or in flight, were ignored. The time series was divided into one minute intervals and an average speed was computed for each interval (Figure 79, upper blue plot). If the speed was below the 10 km h^{-1} threshold then the interval was considered to be a rest interval. However, if more than 90% of the steps included in the interval had a speed above the threshold then the decision was reversed and the interval was set to be a flight interval. In the same way, intervals originally considered to be in flight because the average speed was above the threshold would be reversed and become rest intervals if 90% of the steps in the interval had speeds below the threshold. This reduces the bias associated with steps with unusually high or low speeds. Finally, to remove short-term transient changes in speed from the flight profile, any single rest or flight intervals were also ignored, as indicated by arrows in Figure 79. The resulting flight profile accurately captures the clear bimodal pattern of activity and rest indicated by the raw tag data (Figure 79, grey line) while removing the noise inherent in the bird's complex flight. From each flight profile (Figure 79, lower plot) the flight step-lengths were calculated as the great circle distance from the start and end locations of flight steps using the Haversine equation. Additionally, for comparison, the total distance travelled (summed from individual step-lengths) and the flight times were calculated. The data processing of GPS locations therefore generated three separate sets of data for each bird, representing three different aspects of the calculated flight profile, all of which are suitable for analysis using Maximum Likelihood Estimation (MLE): (1) move step-lengths between consecutive landings, (2) total distance travelled between consecutive landings, and (3) time between consecutive landings. After this flight profile analysis, three flight profiles comprised only two flight steps and were therefore discarded (BBA28, BBA36 and BBA56), leaving 85 flight profiles available for further analysis.

Figure 79: Flight speed profile of black-browed albatross 29

Upper plot: Grey line shows flight speeds computed from the raw GPS tag data; blue line shows average speeds for one minute intervals; red reference line indicates the 10 km h^{-1} speed threshold. Lower plot shows the resulting flight profile comprising periods of flight (grey) or rest (white). Green arrows indicate intervals where the speed threshold decision has been overridden.

5.2.2 Maximum Likelihood Estimation (MLE) Analysis

The Maximum Likelihood Estimation (MLE) methodology employed was that described in Chapter 2 (General methods) resulting in each dataset being categorised as either fitting a truncated Pareto or exponential model or being categorised as mixed model. While the focus of this study was the analysis of step-lengths the distance and time datasets produced by the flight profile analysis were also analysed to provide a comparison.

5.3 Results

The general pattern of foraging movements of the two species was different, with *T. melanophrys* concentrating searches closer to the shelf edge (Figure 80), whereas trips of *D. exulans* were either mostly in neritic (shelf < 2000m depth) or oceanic waters (> 2000m) (Figure 81). Individual foraging tracks showed a similar complex pattern at increasing scales that were reminiscent of the scale-invariant (fractal) patterns of Lévy flights (e.g. Figure 80a).

5.3.1 MLE Analysis of flight step-lengths

From the Maximum Likelihood Estimation (MLE) analysis we found strong support for individual bird movements approximating truncated Lévy flight (power-law) and Brownian (exponential) search patterns in both black-browed and wandering albatrosses (see Figure 82 for TP plots and Appendix C for exponential and mixed model plots and tables of results). Lévy flights occurred in 22 (38%) individual *T. melanophrys* and 4 (15%) *D. exulans* (Figure 82), whereas exponential (Brownian type) movements were exhibited by 11 (18%) and 7 (26%) birds, respectively (Figure 80c,

Figure C1 and Table C4). A significant proportion of trajectories (41% *T. melanophrys*; 59% *D. exulans*) were not fitted by either distribution and were of more complex form, which may represent tracks having both Lévy and Brownian features, as might be expected if similar time is spent by a bird in both shelf and oceanic habitats (see Figure C2 and Table C5). The lower proportion of Lévy best fits in the *D. exulans* data was likely due to the much lower number of landings per km (and therefore flight steps) for individual birds of this species compared to *T. melanophrys*, as more data points are required to identify power-law distributions clearly (Sims *et al.* 2007) (see *MLE Fitting correlations* below for a detailed analysis). The μ values of truncated power-law fits were within the range of values consistent with the LFF hypothesis ($1 < \mu \leq 3$), but were lower than the theoretical optimum for non-destructive search ($\mu \approx 2$) where prey is distributed in revisitable patches and is only temporarily depleted (Viswanathan *et al.* 2011). Instead, we calculated mean exponent values of 1.27 for black-browed and 1.19 for wandering albatrosses. These lower exponents are consistent with optimal Lévy flight search patterns ($\mu \to 1$) expected under the LFF hypothesis when encountered prey are consumed (destructive search) and not available to subsequent searches (non-revisitable patches) (Santos *et al.* 2004, Sims *et al.* 2011, Viswanathan *et al.* 2011); this predicts optimal searches when fewer prey are sparsely distributed (e.g. single prey; see prey capture results below; Table 10).
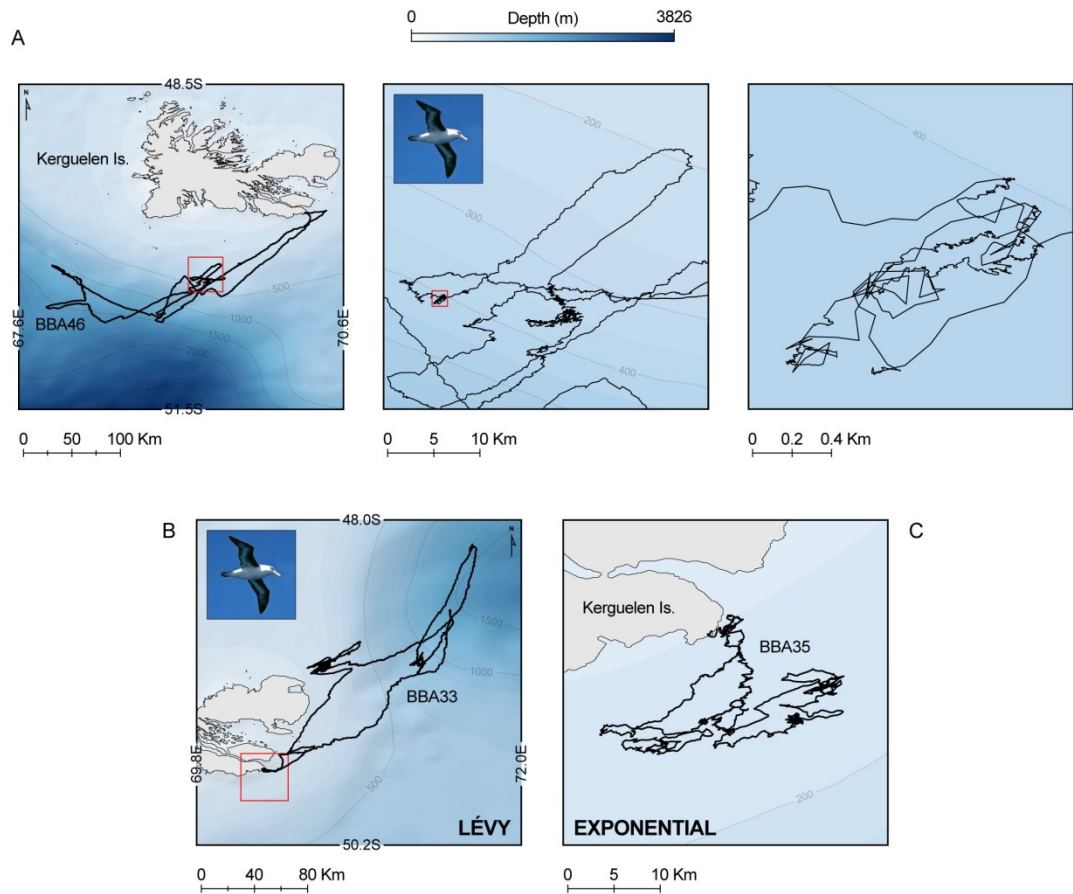
Figure 80: GPS tracks of albatross foraging indicate scale-invariant patterns.
 (*A*) GPS foraging track of a black-browed albatross (BBA46) off the Kerguelen Islands, Southern Indian Ocean, viewed across large (100s km; left panel) to small (10s m; right panel) scales showing similar patterns of trajectory complexity at all scales. Background colour denotes bathymetry in m. Each red square denotes area covered by panel adjacent right. (*B*) Foraging track of a black-browed albatross (BBA33) with flight steps between landings best approximated by a truncated Lévy distribution (μ = 1.28), with movements principally in deep shelf and oceanic habitats. (*C*) Foraging track of BBA35, best approximated by an exponential distribution, was more spatially intensive in shelf and shelf edge habitats. Colour denotes water depth, with bathymetric contours identifying neritic shelf waters < 2000 m and oceanic waters > 2000 m. Red square denotes area shown in (*B*).
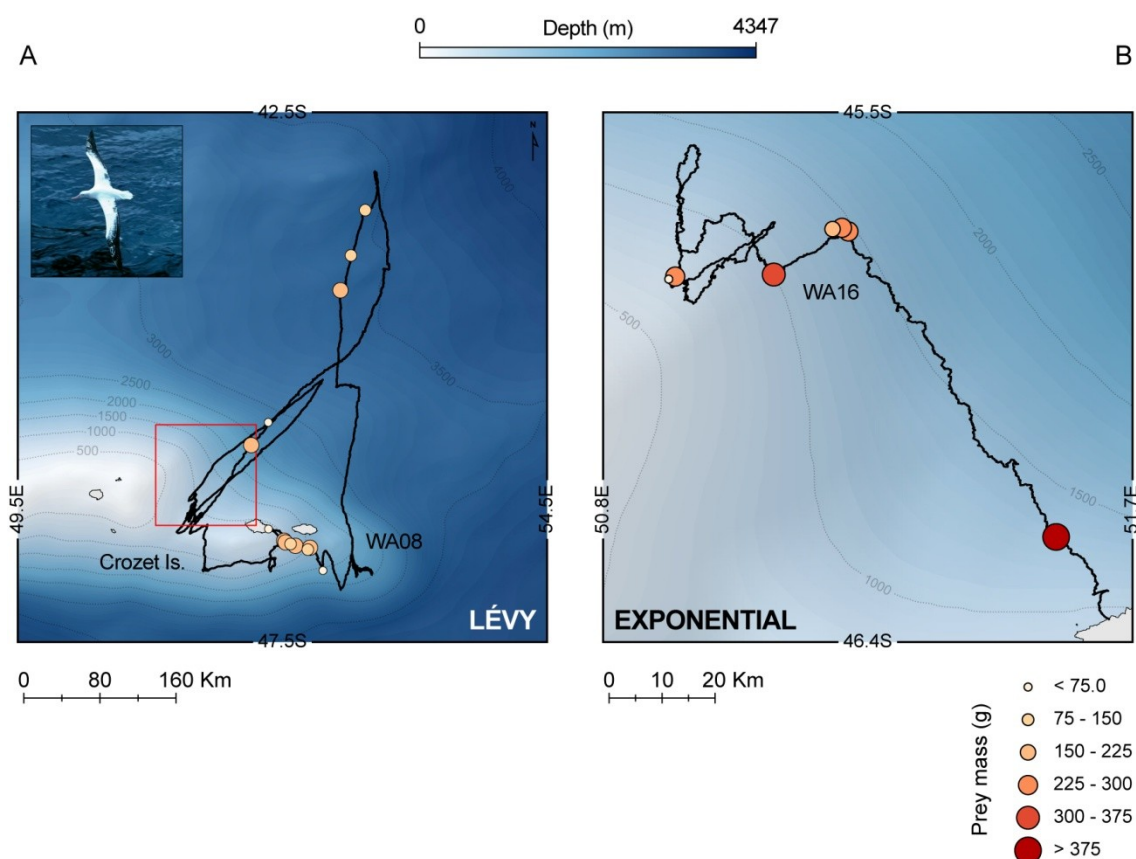
Figure 81: GPS tracks and prey capture contrasts between Lévy and exponential patterns

(*A*) Foraging track, prey capture locations and prey masses of wandering albatross WA08 during an 89 h foraging trip approximated by a Lévy pattern ($\mu = 1.25$) occurring principally over deep shelf edge (1000-2000 m) and oceanic waters (> 2000 m). Captures totalled 3.5 kg, but prey were generally solitary and taken further apart indicating prey sparse habitats. Red square denotes area shown in (*B*). (*B*) Foraging movements by wandering albatross WA16 during which it captured 1.8 kg of prey in 21.5 h when over shallow shelf (500 – 1000 m) and shelf edge habitats during landings best described by an exponential distribution (Brownian pattern). Numerous prey items were often taken in a single landing, indicating a greater abundance of prey.

Figure 82: Ranked step-length plots for best fits to TP distributions for albatross flight steps
Black circles are step-lengths; red line is the best fit TP distribution; blue dashed line is the competing exponential distribution. Plots are shown in descending sequence of number of points.
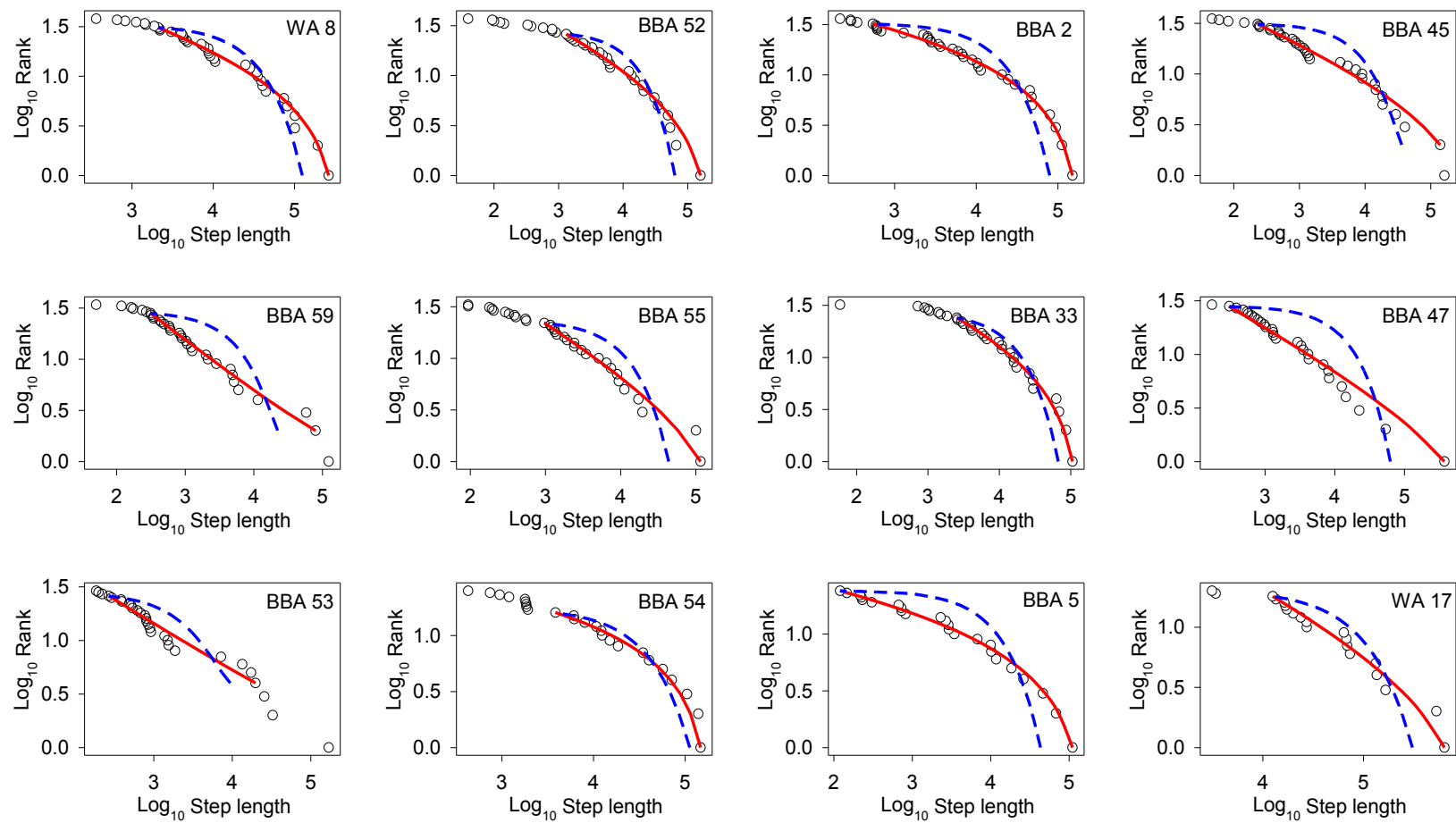
Figure 82: Continued...
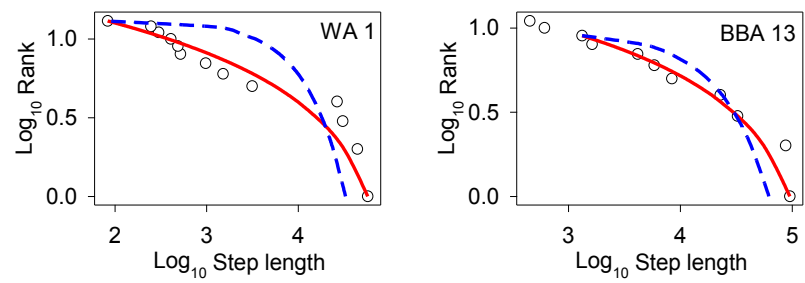
Figure 82: Continued...

5.3.2 Species differences between black-browed and wandering albatross datasets

The MLE analysis revealed clear species differences. Four of the 27 (15%) wandering albatross datasets were found to be best fitted by a TP distribution whereas 22 out of 61 black browed albatross datasets were fitted by the distribution (38%). Ten of the 24 exponential best fits were to wandering albatross movement datasets (42%), in addition to 14 of the 35 mixed model tracks (40%). One possibility for the species difference was that fewer TP best fits were found because the wandering albatross datasets comprised on average only about half the number of flight steps than black-browed albatross individual datasets (Mann-Whitney Rank Sum Test: BBA median = 24, n = 58; WA median = 15, n = 27, p = 0.005). This difference in the number of landings estimated for wandering albatross GPS tracks has been shown to affect the likelihood of finding a good fit to a TP distribution. However, the difference in the number of flight steps suggests that the two species behave differently because the duration that wandering albatrosses were tracked for was similar to those of black-browed albatross tracks (Mann-Whitney Rank sum test: BBA median = 37.9 h, n = 58; WA median = 43.4 h, n = 27, p = 0.137). If their foraging behaviour or feeding event frequencies were similar it may be expected that both species might land with similar frequency if tracks were of similar duration. This interpretation is consistent with previous observations on the foraging behaviour of the two species (Weimerskirch and Guionnet 2002, Phalan *et al.* 2007, Mackley *et al.* 2010).

From the flight profiles calculated here we find a mean landing rate of 0.75 h^{-1} for the black-browed and 0.34 h^{-1} for wandering albatrosses. While these figures are lower than those found by Waugh and Weimerskirch (2003), where a figure of 1.35 flight steps h^{-1} was found for wandering albatross, it is still in general agreement with the observation that wandering albatrosses make fewer flight steps and spend more time on the water than other, smaller species. Clearly, the landing frequency will be dependent on the foraging environment and the availability of prey, with richer areas resulting in more frequent landings. This might indicate that the birds in this study were foraging in areas (or at times) of sparser prey availability than those studied by Waugh and Weimerskirch (2003).

5.3.3   *Habitat dependence of Lévy and Brownian movements*

Having identified the presence of Lévy and Brownian patterns in the landing distributions of both black-browed and wandering albatrosses, we next tested whether search patterns were associated with particular habitats. The Lévy flight foraging (LFF) hypothesis (Viswanathan *et al.* 2008, Viswanathan *et al.* 2011) predicts that Lévy patterns should occur where resource distributions are sparse and Brownian patterns where resources are more abundant. To test this for albatrosses we calculated the water depths at each landing location as a proxy for habitat type and compared these between birds showing Lévy and Brownian patterns. The Kerguelen and Crozet Islands in the southern Indian Ocean are remote islands with three principal bathymetric domains: namely, shelf waters (depth < 200 m), slope waters (200 to 2000 m; including deep shelf-edge waters, 1500 to 2000 m), and oceanic waters (> 2000 m) (Weimerskirch *et al.* 2005). Shelf and slope waters are together termed neritic waters (< 2000 m). Therefore, water depth indicates habitat types that have different productivities and resource distributions; for example, primary productivity at the Kerguelen Islands has higher concentrations in neritic waters (Fig. S7A,B) and the squid prey of albatrosses at Crozet are found closer together in neritic than in oceanic waters (Weimerskirch *et al.* 2005).

Analysis shows that black-browed albatrosses exhibiting a Lévy pattern landed on average over deeper water (mean 520.3 m, S.D. 522.5, random data reduction from *n* = 958 to *n* = 165) than those individuals exhibiting a Brownian pattern (mean 396.8 m, S.D. 561.9, *n* = 165) (*t* test: t = -2.07, *P* < 0.05). Comparing the 25 deepest habitat depths over which surface landings occurred, confirmed that birds showing Lévy patterns occupied deeper slope waters than Brownian birds (Mann-Whitney test: *W* = 524, *P* < 0.05).

 The landing locations of wandering albatrosses exhibiting a Lévy pattern and for which prey capture data were available, were associated with significantly deeper water habitats than those showing Brownian patterns (Lévy, mean habitat depth 1587.4 m, S.D. 934.3, *n* = 23, random data reduction to match Brownian, with mean 958.3 m, S.D. 601.9, *n* = 23; *t* test, *t* = -2.71, *P* < 0.01). This is consistent with Lévy search patterns occurring more frequently in deep shelf edge and oceanic habitats than Brownian patterns which occurred mainly in shallow shelf and shelf edge habitats. There were

several exceptions to this general pattern. For example, the pattern of landings of albatross WA18 was best described by an exponential distribution, although the prey capture data showed that some 24 of the 25 capture events recorded occurred in oceanic habitat. Mapping the prey capture locations along the track showed that 22 prey capture events took place during 7 landings within a comparatively localised area (45 x 20 km). This shows that WA18 encountered a very abundant patch or patches of prey in oceanic habitat and because short distances occurred between landings as a result, the dominant pattern found for this bird was best described by Brownian motion. This demonstrates that although Lévy patterns of wandering albatrosses were generally dependent on deep shelf edge and oceanic habitats, a Brownian pattern may dominate when particularly high concentrations of prey are found regardless of habitat. This finding is consistent with predictions of the LFF hypothesis.

5.3.4 *Prey capture and foraging efficiency*

A significant gap in our knowledge is whether Lévy flights actually confer the advantages to foragers that have been theorised (Viswanathan *et al.* 2011). We were able to test whether Lévy flights yield sufficient prey gain compared with Brownian behaviour – as expected under the LFF hypothesis – by using 11 GPS and 18 satellite-tracked wandering albatrosses fitted with stomach temperature loggers that recorded timing and estimated the mass of prey captured (Weimerskirch *et al.* 1994, Weimerskirch *et al.* 2005, Weimerskirch *et al.* 2007). In contrast to GPS tracked individuals where time spent on water is measured from flight speed, landing locations of satellite tracked birds were detected by a wet/dry logger attached to one of the bird's legs; the time between consecutive landings is shown to approximate the distance flown. MLE analysis of this data found 4 datasets with a good fit to a truncated Pareto distribution, 1 to an exponential with the remaining 12 being classified as mixed model (see Figure 83 for plots of TP fits and Appendix C for plots of the exponential and mixed model fits and the MLE results).

Analysis showed that *D. exulans* with Lévy patterns landed a greater number of times during a foraging trip than Brownian foragers, although the number of prey captures per km flown was similar between Lévy and Brownian foragers, as was the total mass of prey consumed per trip (Table 10). Wandering albatrosses that showed statistically reliable approximations to a Lévy flight achieved net energy gains despite longer

foraging trips further from the nest. We calculated that *D. exulans* showing Lévy behaviour ingested on average 1.46 kg of prey per day, which is sufficient to exceed daily energy requirements of the bird (Weimerskirch *et al.* 2002b) by nearly four-fold (Table 10). A pair of birds could in theory, therefore, collect 2.92 Kg of food, well in excess of the 1.7 Kg required to raise a chick (Shaffer 2004). Hence, Lévy flight search patterns by albatrosses represent a viable alternative strategy, compared with Brownian movements, for attaining net energy gain.

The apparent success of Lévy flights in albatrosses is consistent with expectations under the LFF hypothesis. Furthermore, an assumption of the hypothesis is that Lévy flight search is optimal where prey are sparsely and randomly distributed. Hence, we tested the corollary that greater heterogeneity is expected where birds exhibit Lévy flight patterns, whereas more homogeneous resources are expected where Brownian patterns are identified (Humphries *et al.* 2010, Sims *et al.* 2011). We tested for biological heterogeneity in black-browed albatross described as having Lévy (*n* = 22) or Brownian movement patterns (*n* = 11) by extracting time-referenced chlorophyll 'a' concentrations at landing locations as a proxy for resource availability in areas visited (Figure 84 a&b). During individual trips by *T. melanophrys*, concentrations were significantly more variable for the Lévy pattern than for individuals exhibiting Brownian patterns, confirming the theoretical prediction of longer distances between abundant resources where Lévy behaviour is observed (Figure 84 c&d). In addition, the sea-surface areas where *T. melanophrys* exhibited movements modelled by Lévy flights were over significantly deeper water depths than those having Brownian patterns, which supports the prediction that Lévy flights may be more advantageous in oceanic waters (> 2000m) or deep shelf edge (1500–2000 m) where albatross prey are sparse compared to shallower shelf edge where resources are more abundant (Weimerskirch *et al.* 2005). Supporting this, we found for *D. exulans* that Lévy patterns comprised landing locations in both neritic and oceanic zones, but that prey captures occurred mainly in shelf edge or oceanic habitats (72% of capture events; Figure 81). Prey distribution in habitats visited appears sparse because prey capture during Lévy movements was typified by consumption of solitary, larger prey items that were further apart (lower intake per landing, with more unsuccessful landings), compared to Brownian patterns where numerous smaller items were ingested within a single

landing in prey abundant areas (higher intake per landing) (Table 10; Figure 81b). For the majority of tracks where Brownian patterns described landings of *D. exulans*, prey captures were in more productive neritic waters (76%), although on occasion a high density prey patch was encountered in oceanic habitat, where multiple prey capture events occurred within a highly localised area, a finding predicted by the LFF hypothesis. Taken together, these results suggest Lévy patterns of both species occurred in prey-sparse and thus less predictable habitats.
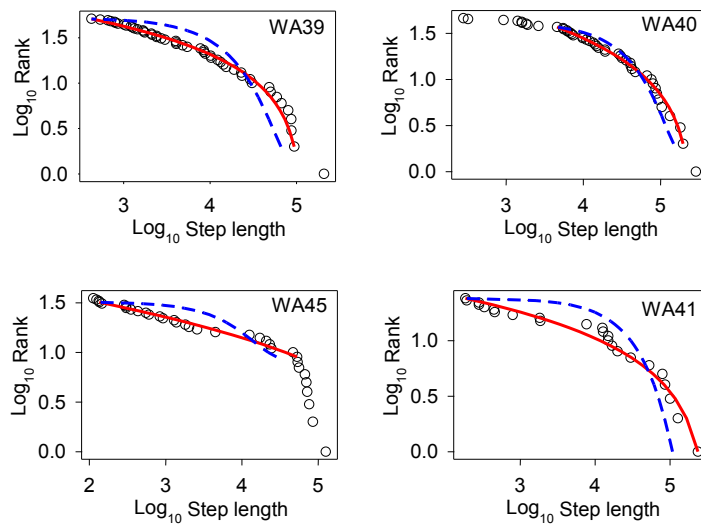
Figure 83: Truncated Pareto fits for flight step distributions from wet dry logger data
Red line represents the fitted TP distribution; black circles are observations; blue dashed line is the competing exponential.

Table 10: Foraging performance from prey capture results

Means (± 1 s.d.) for 13 birds

	No. landings	Distance flown (km)	Total prey mass captured (kg)*	Mass captured per landing (g)	Mass per capture (g)	Total mass per day (kg d-1)	Energy ingested per day (kJ kg-1 d-1)†	Factorial increase of ingested energy per day over daily energy requirements‡
Truncated Lévy (n=7)	34.6 (13.8)	1151.9 (660.9)	3.74 (1.53)	97.9 (37.7)	346.4 (170.9)	1.46 (0.86)	734.8 (390.5)	3.68 (2.49)
Exponential (Brownian) (n=6)	15.5 (7.5)	699.1 (556.5)	4.18 (2.37)	352.6 (304.9)	296.1 (126.8)	2.53 (0.56)	1364.8 (491.0)	7.69 (3.12)

Means in bold indicate significant difference between pattern types (truncated Lévy vs exponential): number of landings (t-test), t = 3.01, $p < 0.02$. All other comparisons not significant at p = 0.05.

*Prey capture data from stomach temperature loggers was available for 6 Lévy and 4 Brownian birds. Of the 10 birds, landing patterns for 5 of them (4 Levy, 1 Brownian) were calculated from times between landings recorded by wet/dry loggers (Weimerskirch *et al.* 2005) rather than distances from GPS-derived landing locations (*Supporting Results 2.5*).

†*D. exulans* feed mainly on squid. An energy value of Antarctic squid of 4.64 kJ g^{-1} wet weight was used (Clarke and Prince 1980).

‡Daily energy requirement of 157 kJ kg^{-1} d^{-1} was an average determined from heart rate telemetry during the brooding period and validated with indirect calorimetry of oxygen consumption (Weimerskirch *et al.* 2002b).
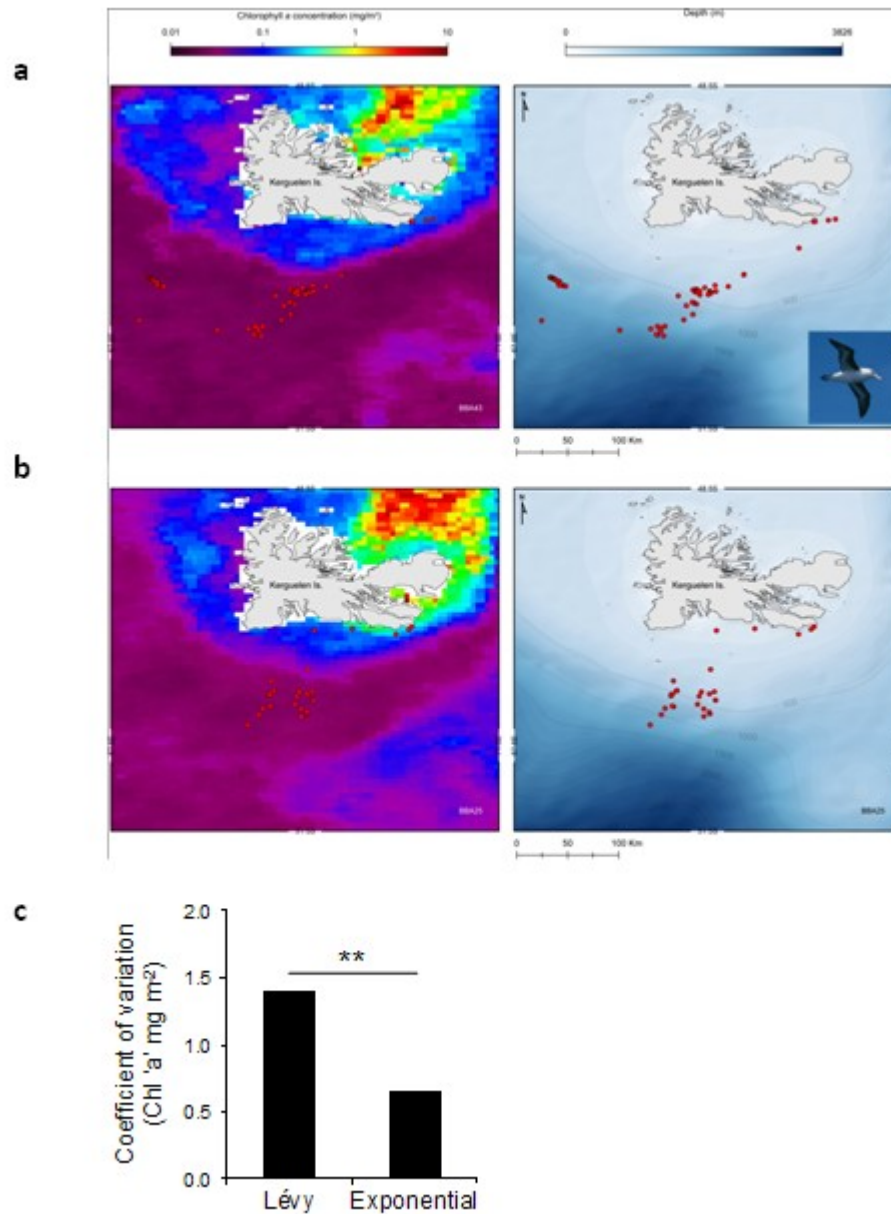
Figure 84. Lévy flight patterns encounter greater environmental heterogeneity.
Examples of (a) truncated Lévy and (b) exponential distributions of distances between landing locations (red circles) for two different black-browed albatrosses off Kerguelen Island and in relation to the distribution of chlorophyll 'a' concentrations, where warm colours represent higher concentrations of primary productivity. c, Abundance of environmental resources was nearly twice as variable during truncated Lévy search patterns of *T. melanophrys* than for exponential (Brownian) foraging patterns. ** denotes *P* < 0.001.

5.3.5 Reanalysis of 2004 Albatross data

Our analysis of albatross movements from high-resolution GPS tracking of birds foraging in the southern Indian Ocean indicate the presence of movement patterns approximated by Lévy flights. However, a previous study by Edwards *et al*. (2007), having corrected an error in the analysis of wandering albatross data recorded in 1992 in the Southern Ocean (Bird Island, South Georgia) (Viswanathan *et al.* 1996), found no

evidence for Lévy flight. Analysis of new data from foraging wandering albatrosses collected in 2004 also contributed to the conclusion that wandering albatrosses do not conduct Lévy flights and, as a consequence therefore, the evidence for biological Lévy flights was weaker, at that time, than previously thought. Nevertheless, the paper by Edwards *et al*. (2007) did not test the LFF hypothesis explicitly on individual albatross tracks. Even though 20 individual wandering albatross wet/dry logger-recorded flight times collected in 2004 were analysed (Edwards *et al.* 2007) MLE fits of the truncated power-law distribution to these data were not estimated. Hence, the conclusion that wandering albatross do not exhibit movement patterns consistent with Lévy flights can be considered premature in the absence of statistically robust fitting of an alternative model (e.g. truncated power-law distribution) to the ones fitted by Edwards *et al*. (2007) (i.e. exponential and shifted gamma distributions). Therefore, we tested the LFF hypothesis by fitting truncated power-law distributions to the data given in Edwards *et al*. (2007).

 The 20 datasets in Edwards *et al*. (2007) comprising time steps in seconds of wandering albatrosses tracked with wet/dry loggers in 2004 were kindly provided for reanalysis here by A. M. Edwards and R. A. Phillips. The data required no pre-processing by us and was subject to identical analysis to the albatross data we described previously, with the one difference being that the correction for discrete data was used as described in Clauset *et al*. (2009). In the original paper (Edwards *et al.* 2007), the data was pooled and was fitted to a gamma distribution without fitting the x_{min} parameter. Therefore in our study, as well as analysing the datasets separately for individual birds, the datasets were again pooled and were analysed both with and without fitting the x_{min} and x_{max} parameters to provide a direct comparison with Figures S3, S4 and S5 in the original Supplementary Information (Edwards *et al.* 2007); the pooled results are shown with the reference 2004_P (pooled) and 2004_PNF (pooled no fitting), respectively.

For 20 individual datasets, we found 11 best fits to the truncated power-law (TP) distribution and 3 best fits to the exponential distribution with 8 datasets being classified as mixed (see Figure 85 below for plots of TP fits and Appendix C for the exponential and mixed model fits). Hence, we find good support for the truncated

power-law (Pareto-Lévy) distribution approximating the movement pattern of wandering albatrosses. Although we also find support for the exponential distribution it was less prevalent than the truncated power-law fit. These results are consistent with other studies analysing the complex behavioural data of marine predators (Sims *et al.* 2008a, Humphries *et al.* 2010), where some individual animal datasets provide good support for Lévy movement while others are best supported by an exponential (i.e. Brownian) movement pattern. It is proposed that the observation of both Lévy and Brownian patterns reflects the complex range of behaviours exhibited by different animals at different times.

Our results of this reanalysis of published data are at odds with the conclusions drawn in the paper by Edwards *et al*. (2007), where no support was found for power-law distributed move steps (flight times). It should be noted that in the latter paper no attempt was made to fit a power or truncated power-law to either the pooled or individual datasets so no comparison similar to that reported here was possible. As an example, wandering albatross 2004_5 was found here to be best fit by a TP distribution; indeed from visual inspection it seems clear from the plot of this data in Figure 85 in Edwards *et al*. (2007) that the TP best fit we found better describes the empirical data than the shifted gamma or exponential fits shown in the original Supplementary Figure S3. Individual bird 2004_3 (Figure 85)(Edwards *et al.* 2007) provides another example: in our analysis a best fit to the TP distribution was found for this dataset comprising only 29 data points. With the limited size of individual datasets in terms of data points for MLE analysis available here compared to previous studies (e.g. Sims *et al.* 2008a, Humphries *et al.* 2010), it is also relevant to note that although the MLE methodology finds best fit values for x_{min} and x_{max}, in nearly all the datasets we analysed the x_{max} fitted value was also the maximum value in the data. Therefore, the best fits presented here are fits to most of the dataset in each case since very few data were not included in the best fit model using the method of Clauset *et al*. (2009).
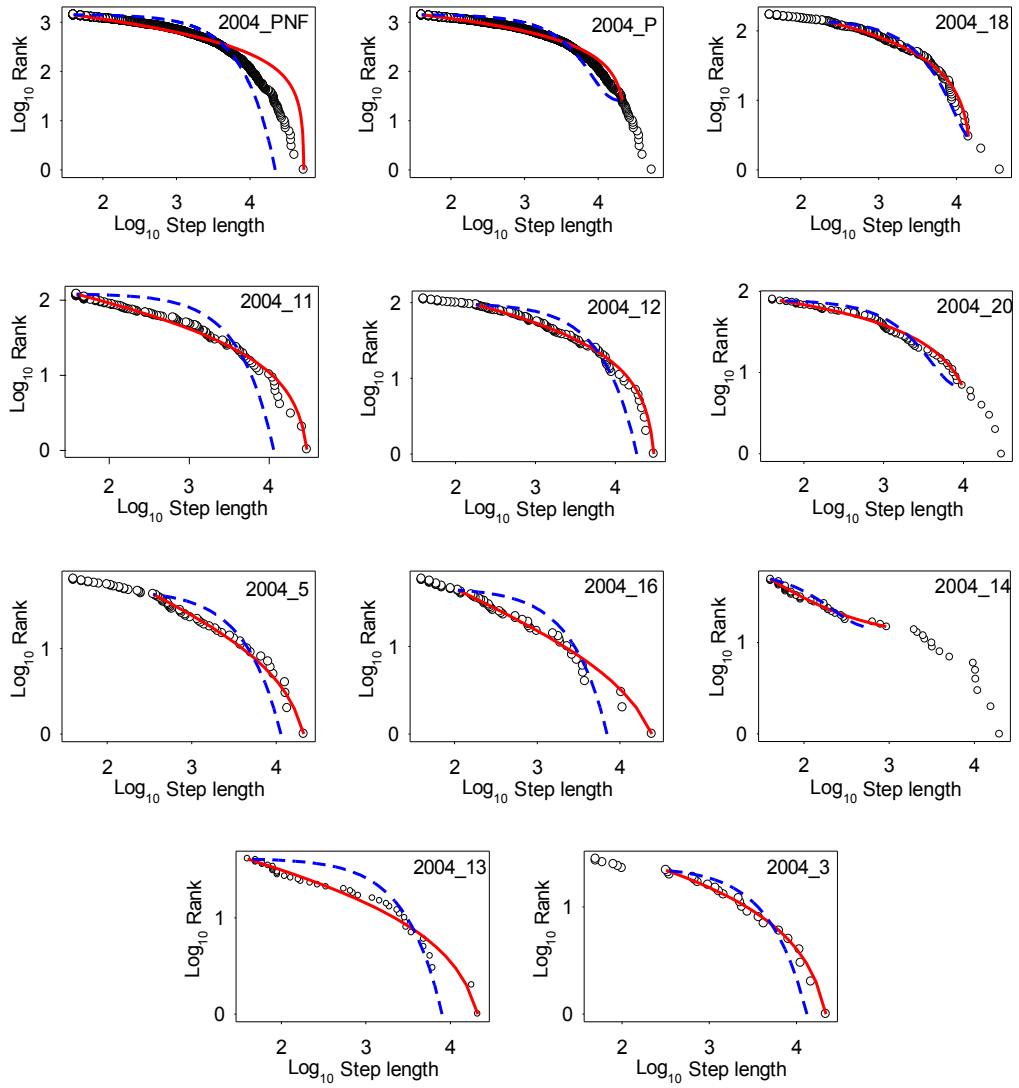
Figure 85: Truncated Pareto fits from the 2004 reanalysed albatross data
Here the blue dashed line represents the alternate exponential distribution.

5.3.6 MLE Fitting correlations

There was a significant correlation between the number of steps (lengths between landings) in an individual bird dataset and the likelihood that the dataset will be fitted by either truncated power-law (Pareto-Lévy) or exponential distributions (Mann-Whitney Rank Sum Test; $p < 0.001$). Generally, smaller datasets were more likely to yield best model fits to the exponential distribution. This is illustrated by the box plot in Figure 86. It seems likely therefore that the low numbers of steps in the wandering albatross datasets may well explain why these gave principally exponential best fits since larger datasets will have a greater chance of containing longer step-lengths, if they were exhibited by the albatrosses. Although this bias affects the results in terms of the number of individuals exhibiting movements approximated by TP and

exponential distributions, it does not affect the test of the LFF conducted here, which is to determine whether albatrosses do indeed show movement patterns best approximated by a Lévy flight pattern.

The average number of points comprising datasets best fitted by the TP distribution was ~41 (n = 26; median = 38.5), yet all of the exponential fits were to datasets with fewer than 42 steps (maximum 29, mean ~15, median = 12.5, n = 18). While the numbers of steps available for this analysis are lower than has been considered ideal from simulation studies (see Sims *et al.* 2007), we analysed individual albatross trajectories rather than pooling multiple individuals' step-lengths, which occurs usually in an attempt to increase n number (for an example of pooling albatross step lengths see Edwards *et al.* 2007). The problem with pooling data from several individuals is that different patterns of movement by different individuals may emerge as a Lévy flight without any one individual displaying such a pattern (Petrovskii *et al.* 2011). Although the datasets used here were of relatively low n number, they each described the movement pattern of an individual albatross and provided appropriate ranges of move step data spanning several orders of magnitude in some cases, which can counteract the effect of a lower number of steps. Hence, we found there were clear and reliable best fits of the TP distribution to the albatross movement data. For example, BBA2 in Figure 86 provided 37 steps for analysis yet yielded a robust best fit to the TP distribution over 2.45 orders of magnitude in move step-length.
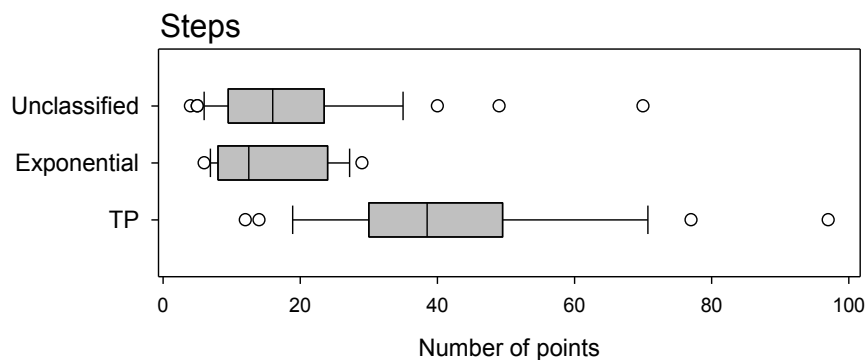
Figure 86. MLE Fitting correlations in flight step-length data.
Boxes show 25th to 75th percentiles; whiskers show the 10th and 90th percentiles. There is a statistically significant difference ($P < 0.001$) between the exponential and the TP groups.

5.3.7   Comparison of MLE results using steps, distances and times

The main focus of our analysis was on the step-lengths calculated as great circle distances between the start and end of flights (straight line distances between

consecutive landings), where the landings between flights are considered to be the turning points in a Lévy walk. Two other measures were calculated from the flight profile; cumulative distances were calculated as the sum of the individual steps comprising a flight, and times were calculated from the start and end times of each flight. For a direct comparison these datasets for each individual bird were analysed in the same way as the move steps. It was hypothesised that neither of these measures would provide as many best fits to a truncated power-law (Pareto-Lévy) distribution because the distances include many complex movements associated with the bird's soaring flight, while the times do not take account of the variations in the bird's speed and so do not properly reflect the distance travelled. Table 11 shows a summary of the best fitting results for the three different data sets. As expected the distance and time measures produce slightly fewer TP best fits (25 and 23 respectively, compared to 26 for the step-lengths). There were 39 datasets where the analysis results are the same for all data types (12 TP, 8 exponential and 19 mixed model fits). Overall, therefore, it seems that distances and times between consecutive landings can be considered to be reasonable proxies for step-length measurements used to test the LFF hypothesis, although it should be noted that not all Lévy patterns will be detected by these proxies.

Table 11: Summary of fitted distributions to the three different sets of data

Fitted distribution	Steps	Distances	Times
TP	26	25	23
Exponential	18	17	25
Mixed model	41	43	37

5.4   Discussion

Our analyses of albatross foraging tracks indicate a significant proportion (29%) of Lévy flight patterns among 126 individuals from two species, overturning a principal conclusion of the study by Edwards *et al*. (2007). An important result in this study was that foraging albatrosses undertaking Lévy flight-modelled search patterns have comparatively high energy gains despite foraging in more heterogenic environments. Although several modelling studies demonstrate Lévy searches confer foraging advantages in certain types of environment (for review see Viswanathan *et al.* 2011)

ours is the first study to quantify empirically the foraging success of biological Lévy flights in a free-ranging organism. We also found evidence that Lévy-flight modelled movements for both species were theoretically optimal and occurred in more prey-sparse habitat; such habitat dependence is predicted by the LFF hypothesis. It is possible that albatrosses exhibit movement patterns approximated by Lévy flights as a response to unpredictable habitat such as the oceanic environment, where prey are larger but also highly patchy in their distribution (Weimerskirch *et al.* 2005, Weimerskirch *et al.* 2007). Similarly, albatross movements may emerge as Brownian motion when foraging in more predictable environments, such as shelf edges where prey availability is more likely to be concentrated. Thus, our results may explain the field observation that albatrosses show high site fidelity to more predictable shelf waters, but in unpredictable oceanic habitat rarely return to the same coarse scale sites (Weimerskirch *et al.* 2007). The foraging advantage conferred by Lévy flight search patterns is further strengthened for the birds studied here by the reduction in the duration of famine periods experienced by the chicks. The chick survival rate is clearly a significant factor in the success of the population and will be subject to strong selective pressure. It would be expected that a search strategy that reduced chick mortality would have evolved naturally in albatross populations. In addition to Lévy and Brownian patterns, we found evidence of more complex movements that were perhaps a result of switching between behaviours during single trips by individual birds. Recent analyses of predatory marine fish (Humphries *et al.* 2010, Sims *et al.* 2011) have found similar links between Lévy patterns and habitats with sparsely distributed resource fields, including switching behaviour by individuals, indicating that Lévy flight patterns may be a solution to the search problem for diverse animals occupying unpredictable environments.

5.4.1 Reanalysis of 2004 Albatross data

Our results with the pooled data of 20 wandering albatrosses from 2004 are also interesting and contrast with those of Edwards *et al*. (2007). With both analysis methods (i.e. fitting of x_{min} and x_{max} and no fitting) the pooled data was best fit by a TP distribution. However, when best fitting is performed there is a conflict between the wAIC values for the exponential and TP best fits, which was here resolved by the GOF

value which favoured the TP distribution. However, there is a serious problem with pooling datasets comprising complex movement data, as Edwards *et al* (2007) have done. While pooling homogenous data can result in more powerful statistical testing (Zar 1999), this is not the case with complex heterogeneous data. The datasets analysed in this study describe movements from individual animals, each of which are likely to be behaving and moving in different ways. Pooling such data confuses these individual movements and can have unpredictable results, such as concluding the presence of Lévy flight when it is not exhibited by any one individual, and concluding Brownian motion even though an individual in the pool may have a very different behaviour pattern (e.g. Codling and Plank 2011, Petrovskii *et al.* 2011). This difference can be seen in the comparison of the MLE results obtained with the pooled data and an individual dataset such as 2004_11, both shown in Figure 85, where it is clear that not only does the individual data fit a TP distribution but the difference in the observed step-lengths is quite noticeable. Therefore, for an unbiased test of whether albatrosses exhibit movements approximated by Lévy flights it was preferable to analyse individual movement trajectories by fitting both truncated power-law and exponential distributions. In summary, we find no support for the conclusion of Edwards *et al*. (2007) questioning the strength of the evidence for biological Lévy flights, and find that this was both incorrect and premature.

6 The ambush predator: Encounter rates and waiting times

6.1   Introduction

The foraging simulations explored in Chapter 3 investigated the consequences of differing search patterns with a cruise predator and stationary prey patches, concluding that Lévy movement confers a significant advantage in terms of the number of prey items located for the effort expended. In this chapter the scenario of moving prey targets is considered. Viswanathan *et al.* (2002) showed that with moving targets Lévy flight would only be advantageous if the predator moves faster than the target and that with fast moving targets Brownian search strategies or stationary predators are optimal.

This chapter will explore some of the consequences of the ambush predation strategy. Many marine animals, such as barnacles, have adopted a sedentary life style, benefiting from the energetic advantage conferred by simply waiting for the prey to move, or be moved, to them. However, entirely sedentary animals require other adaptations that tend to balance the energetic cost saving. For example, adaptations such as broadcast-spawning, with the concomitant production of abundant gametes, are required when adults cannot move to find mates and are found in diverse taxa such as corals (Graham *et al.* 2008, Gleason and Hofmann 2011), sea anemones (Scott and Harrison 2007) and holothurians (Mercier *et al.* 2007). Further, as with many marine organisms, dispersal requires a planktonic larval stage which itself involves considerable energetic costs, such as the costs of metamorphosis, and risks such as predation, dispersal away from suitable settling locations and increased susceptibility to environmental stress (Pechenik 1999). Sedentary predators can be seen as one end

of an activity continuum which ends with fast cruise predators such as mako sharks (*Isurus oxyrinchus*) or Atlantic bluefin tuna (*Thunnus thynnus*). Mobile foraging strategies that increase encounter rates with prey are also likely to increase the encounter rate with predators, and there is, therefore, a balance to be made between foraging success and predation risk (Visser 2007, Ferrari *et al.* 2010, Alos *et al.* 2012). These factors are likely to have played a role in the evolution of the broad continuum of observed foraging strategies from sessile through sit-and-wait, saltatory movement across different spatial scales and continuous activity characteristic of pelagic cruise swimming.

The ambush predator is faced with many decisions that affect foraging success, principally the selection of a suitable location, how long to wait before giving up and how far to move to find a new patch (Nishimura 1991, Beachly *et al.* 1995, Visser 2007). In real world scenarios learning and sensory input play an important role (Gall and Fernandez-Juricic 2010, Nilsson *et al.* 2010) however such complexities can make understanding the underlying principles problematic. In this chapter a simulation will be used where the focus will be on the effect of predator and prey movement strategies and predator waiting times. The aim will be to gain a better understanding of predator-prey encounter rates when prey are mobile and of the optimal strategies employed by ambush predators.

The initial investigations validated the simulation program and confirmed simple predictions about the factors which are expected to affect encounter rates. Encounter rates with stationary prey were then considered and were expected to be in close agreement with the results from Chapter 3. Moving prey was then investigated and the advantage gained by the ambush predator strategy was considered with a test of the prediction by Viswanathan *et al.* (2002) regarding the emergence of the ambush predator. The final investigations focused on the optimum waiting times for ambush predators in differing prey fields.

6.2   The simulation model

The Predator-Prey simulation model is described in detail in Appendix G but, briefly, a 2D arena of 500x250 grid cells is populated with a number of predators (sharks) and

prey (fish). Within the simulation both predators and prey are moved in turn through interpolated steps and encounters are recorded. Each individual is placed at a random location in the arena and, as with the foraging simulations in Chapter 3, performs a random walk with uniform random turn angles and step-lengths drawn from the specified distribution (e.g. exponential, truncated Pareto). The simulation proceeds by giving each individual a turn in which it moves one interpolated move step and checks the surrounding grid cells to a radius r for the presence of other individuals, each of which will represent an encounter. Interpolated steps are computed in the same way as with the foraging simulations, where moves are in continuous space and each interpolated step is ≈1 grid cell unit (see Chapter 2, General Methods). When a shark encounters a fish the encounter can be either non-destructive or, optionally, destructive i.e. the fish is relocated to a new random start location, removing it from further immediate encounters with the shark. Statistics are gathered on the number and type of encounters e.g. Fish-Fish, Sharks-Fish etc. For both fish and sharks the familiar movement styles are employed with move step-lengths being drawn from either truncated Pareto, exponential or uniform distributions with a further option of *still* whereby the fish do not move. Sharks can be set to be in *ambush* mode, whereby the shark does not move but encounters are checked at each turn. Following an encounter with a fish the shark can either continue waiting or can relocate. For ambushing sharks a statistical distribution of waiting times can be set after which, if no encounter has occurred, the shark relocates using the defined movement style. During the relocation move all encounters are ignored.

It is important to note that as each individual within the simulation moves a single interpolated step at each turn, and as each interpolated step is ≈1 unit of distance (i.e. one grid cell), all individuals move at a similar speed and consequently cover a similar distance during the course of a simulation run. What differs between different move step-length distributions is the rate of diffusion and therefore the net displacement. Individuals with super-diffusive movement paths will appear to move faster than those with normally diffusive or sub-diffusive movements. Because there are small differences in the total distance travelled all statistics are expressed as encounters per unit distance travelled.

Note that, for brevity, where the movement style is described as TP this refers to a distribution of move steps drawn from a truncated Pareto distribution with, unless otherwise stated, x_{min} = 1 and x_{max} = 500; TP2.0 signifies an exponent of 2.0 etc. Exponential in all cases refers to an exponential distribution of move steps with x_{min} = 1 and, unless otherwise stated, an exponent of 0.19; these parameters are chosen to give the same mean step-length as the TP2.0 predator. Uniform refers to a uniform distribution of move steps on the interval [1, 12], unless otherwise stated, again to result in a mean step-length equivalent to the TP2.0 predator.

6.3 Validation of the simulation program

In a real world 3D scenario, encounter rates for an individual predator with immobile prey can be described by $Z = \pi r^2 fv$, where Z is the encounter rate, r the detection radius, f the prey (fish) concentration and v the swimming speed (after Visser 2007). In the 2D world of the simulation used here the swept volume of πr^2 now becomes the swept area $2r$ giving $Z_{2D} = 2rfv$. Because, as will be described below, all individuals move at the same speed ($\approx$1 interpolated grid cell per turn) there is no proper concept of speed in the simulation. Changes in movement style (e.g. in Lévy exponent) result in changes in diffusivity and consequently the relation to velocity must be dropped to give the simpler relation $Z_{2D} = 2rf$. To consider encounters from all predators in the simulation the predator concentration must also be included giving $Z_{2D} = 2rfs$, where s is the predator (shark) concentration. Finally, as this is a turn based simulation, the number of encounters will also be proportional to the number of turns (t) giving a final equation of $Z_{2D} = 2rfst$. This equation is essentially the two dimensional analogue of the "ideal gas model" of animal encounters described by Hutchinson and Waser (2007) and represents a useful null model of animal encounter rates.

This equation was used to make some general predictions about encounter rates in the predator-prey simulation and allow some tests to be performed to validate the simulation program's performance. We should in fact find that encounter rates are linearly proportional to the detection radius, prey concentration, predator concentration and the run time. In the validation tests, unless otherwise specified, the simulations used in program validation had 10 still fish, 10 TP2.0 sharks, destructive

predation without prey targeting and comprised 1000 repeats of 100,000 turns to enable robust statistical analysis.

6.3.1 Detection radius

With constant speed the encounter rate is simply proportional to the detection radius r and the prey concentration f. This corresponds to the encounter rate to detection radius relationship found by Cole (1995) where increasing the detection radius resulted in an approximately linear increase in detection rate for a Lévy predator with $\mu = 1.37$. Clearly from $Z_{2D} = 2rfst$ this program should also give a linear increase in encounter rate with increasing radius. However there is a complication in that after each interpolated step it is the area around the individual that is scanned to a radius r for encounters; for $r = 2$ this represents a 5x5 square (see Appendix G). Consequently it might be expected that the encounter rate might increase as a function of area (i.e. a power-law) rather than simply a swept area which would be linear. To test this assertion a series of simulations were performed with the radius of detection set to 1...5 units, with 10 still fish and 10 TP2.0 sharks. The results are shown in Figure 87 and Table D1 where it is clear that the relation is linear ($r^2 = 1$, $p < 0.0001$, SigmaPlot linear regression) and therefore it is the swept area, rather than the area scanned at each interpolated step, that is important.

6.3.2 Prey concentration

With the detection radius fixed at a default value of 2 units and the 'speed' being constant at one unit per turn the encounter rate should be directly proportional to the prey concentration. To check this relationship a series of simulations were run with 10 sharks and increasing numbers of fish, from 2 to 20 in steps of 2. The results are shown in Figure 88 and Table D2 and as expected there is a clear linear relationship ($r^2 = 0.998$, $p < 0.0001$, SigmaPlot linear regression).

6.3.3 Predator-Prey numbers and effective prey field density

From $Z_{2D} = 2rfst$ it is clear that the effective prey field density is dependent on both the number of fish and the number of sharks, and should scale with the square of the sum of the fish and sharks. A further series of simulations was performed to test this, with equal numbers of fish and sharks increasing in total number from 4 to 40. The

results are shown in Figure 89 and Table D3 and confirm the power-law relationship with exponent 2.012 (r^2 = 1, p < 0.0001, SigmaPlot non-linear regression).

6.3.4   Number of turns

From Z_{2D} = 2$rfst$ it follows that the number of encounters in any given simulation will depend on the number of turns. Therefore the number of encounters is expected to scale linearly with the number of turns and this is confirmed by the results shown in Figure 90 and Table D4 (r^2 = 1, p < 0.0001, SigmaPlot linear regression).

6.3.5   Optimum predator and prey ratios

From the investigation into predator:prey ratios above it was clear that the same effective prey field will result from using 10 fish and 1 shark or 1 fish and 10 sharks. Both scenarios involve 11 individuals and therefore have the same computational effort. However, given that the effective prey field scales with the product of total number of sharks and fish, we should find that equal numbers of both generates the highest effective prey field density and, therefore, the highest number of encounters for the same computational effort. To test this assertion a series of simulations were performed using a total of 20 individuals but in ratios varying from 1 fish to 19 sharks to 19 fish to 1 shark. The results are shown in Figure 91, where it is clear that the optimum encounter rate does occur with equal numbers of sharks and fish.

6.3.6   Faster moving sharks

All the fish or sharks move at the same 'speed' and will cover the same distance over the course of a simulation. The different movement patterns result in changes in diffusivity and therefore in net displacement which cannot simply be substituted for v in the original equation $Z = \pi r^2 fv$. To prove this, a series of simulations were performed using 10 still fish but with sharks moving with a simple uniform distribution with maximum step-lengths ranging from 5 to 65. The results are shown in Figure 92 and Table D6, and it is clear that changes in the encounter rate are not linear, but are found to rise with an exponential growth function. This reflects the fact that a uniform distribution of step-lengths confers Brownian motion and, therefore, there is an exponential relationship between the step-length x and the area covered. In this example parameters were fitted to the function

$$f = a \cdot (1 - \exp(-b \cdot x))$$

such that a = 464.9819 and b = 0.0522 (r^2 = 0.9996, $p < 0.0001$; SigmaPlot non-linear regression). There was therefore no linear relationship with the mean step-length and, as expected, no simple analogue for velocity. Lévy predators will exhibit super-diffusive movements with, again, no simple relationship expected between the exponent and the area explored. While this relationship is investigated in more detail in a later section it is worth repeating the previous simulations using changes in Lévy exponent rather than mean step-length. The results are shown in Figure 93 and Table D7, and it can be seen that over the range 1.2 to 2.8 the relationship is very closely sigmoidal with parameters for the equation

$$f = a / (1 + \exp(-(x - x_0) / b))$$

being a = 567.98, b = -0.46 and $x0$ = 2.219 (r^2 = 0.999, $p < 0.0001$, SigmaPlot non-linear regression). Over a more restricted range of 1.6 to 2.4, however, the relationship is seen to be approximately linear, which is confirmed through linear regression which gives r^2 = 0.9987, $p < 0.0001$, SigmaPlot linear regression. The overall distance travelled is almost the same with differing values of μ as can be seen in Table D7; the slightly lower distances for higher exponents are caused by minor interpolation errors with very small steps, the number of which is greater with higher exponents.

6.3.7 Summary

The accuracy of the scaling of the encounter rates with detection radius, prey concentration, predator prey population ratios, total individuals and number of turns demonstrates that the simulation program is performing precisely as expected and allows further simulations to be performed in confidence. It should be noted that many of the datasets generated in the preceding simulations were not normally distributed (see Table D4) and therefore for all the following investigations, unless otherwise stated, it will be the median number of encounters that will be reported and non-parametric statistical tests (i.e. Mann-Whitney rank sum test or ANOVAR on ranks) that will be used. Median values will be written either with the 1st and 3rd quartiles (Q1, Q3) or the inter-quartile range (IQR) as a measure of variance.
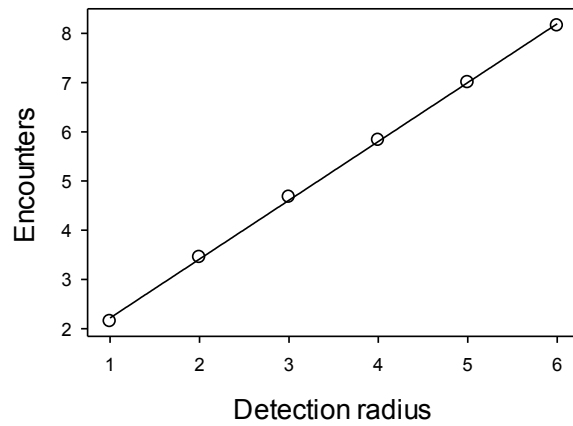
Figure 87: Detection radius and encounter rates

There is a clear linear relationship between the detection radius and the number of encounters.
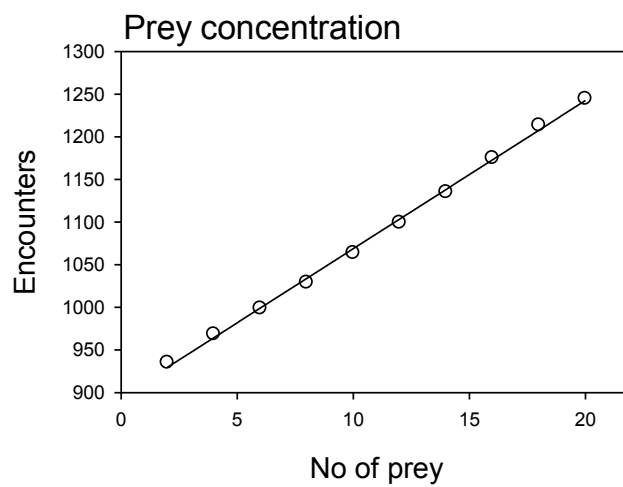
Figure 88: Encounter rates with increasing prey concentration

With 10 sharks increasing the prey concentration (i.e. the number of fish) produces a linear increase in the number of encounters.
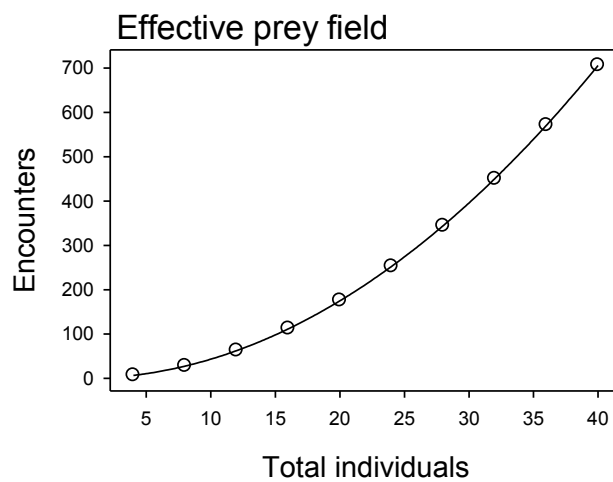
Figure 89: Encounter rates with increasing numbers of fish and sharks

As the total number of fish and sharks increases there is a power-law increase in the number of encounters. In each simulation equal numbers of sharks and fish are used with total numbers of 4-40 individuals.
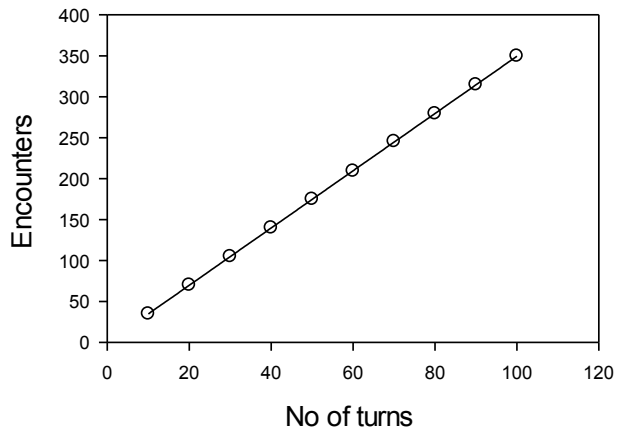
Figure 90: Encounter rates with increasing turns

As the number of turns increases there is a linear increase in the number of recorded encounters between sharks and fish.
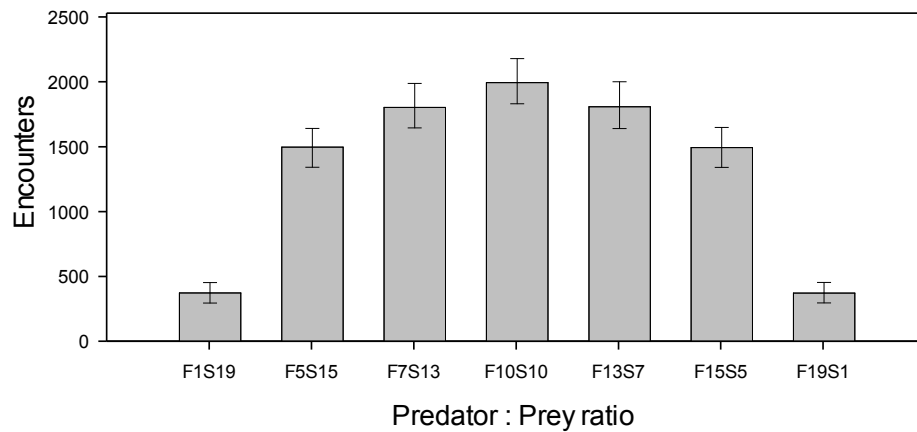
Figure 91: Encounter rates with different ratios of fish and sharks

Maintaining the total number of individuals but varying the ratio of fish to sharks shows that a maximum number of shark-fish encounters is achieved with equal numbers of both. F1S19 represents 1 fish and 19 sharks. Values are medians and error bars represent 10th and 90th percentiles.
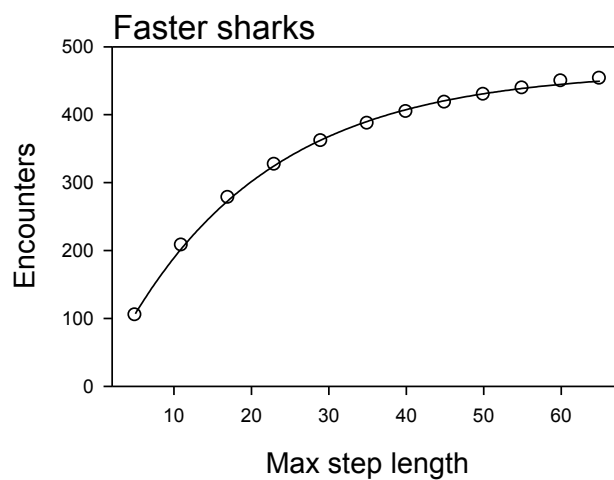
Figure 92: Increasing encounter rate with increasing diffusivity

With steps drawn from a uniform distribution with increasing maximum step-length the encounter rate increases following an exponential function.
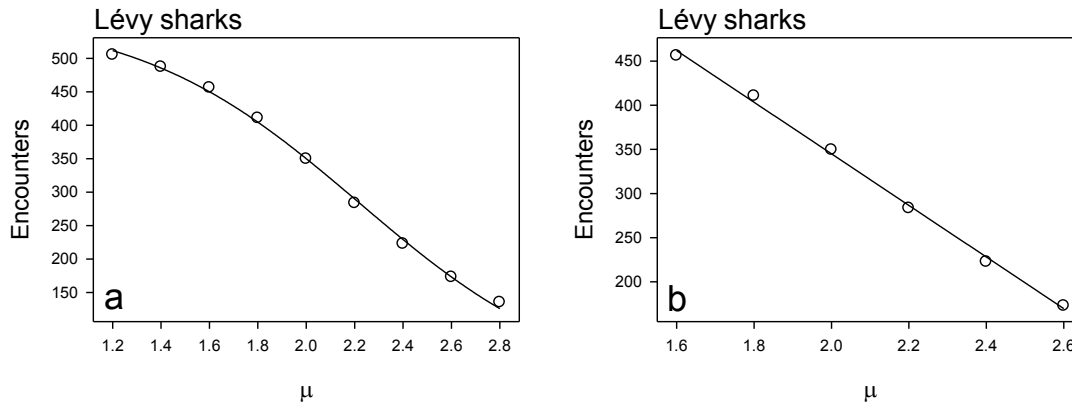
Figure 93: Encounter rate with changing Lévy exponent

With increasing values for μ the movement becomes less super-diffusive and more Brownian, leading to a reduce area explored and lower encounter rates. Over the range 1.2 to 2.8 (a) the relationship is sigmoidal, however over the narrower range 1.6 to 2.6 (b) the relationship is very close to linear.

6.4   Encounters with stationary prey

Foraging efficiency with stationary prey patches has been covered previously in Chapter 3, with the foraging simulation experiments, and clearly an ambush predator will fare poorly with stationary prey. However, the foraging simulations did not count encounters directly, in the way that the Predator-Prey simulation does, and therefore it is useful to begin these investigations with a verification of this aspect of the Predator-Prey simulation. With the foraging model described by Viswanathan *et al.* (1999) two scenarios were considered; destructive, where prey were relocated on encounter, and non-destructive where encountered prey were not relocated. In the destructive scenario low μ values (≈1) were found to be most efficient while in the non-destructive case μ = 2.0 was the most efficient. Two sets of simulations were performed to confirm these predictions, one with destructive and one with non-destructive predation. Both used 10 still fish and 10 moving sharks with prey targeting (where the predator halts a move on encountering prey, truncating the step) to simulate more natural encounters. In each case sharks were set up to be either Lévy predators, with move steps drawn from a truncated Pareto distribution with a range of exponents from 1.2 to 2.8 (TP1.2 to TP2.8), or from exponential or uniform distributions, as described above.

The results using destructive foraging are shown in Figure 94 (see also Table D7 and Table D8), and confirm the predictions. Differences are significant (one-way ANOVA on ranks, *p* < 0.001) as are most pairwise comparisons except TP1.2 and TP1.4, and Exp

and TP2.4. Prey once encountered is consumed (relocated) and therefore there is no benefit in staying in the area. Consequently, it is the Lévy predators with lower exponents that perform better as these have higher diffusivity and faster patch-leaving behaviour. Nonetheless, the TP2.0 predator outperforms the exponential predator by 38.6%. Therefore, while μ = 2.0 may not be optimal, it is still a much better strategy than exponential. The results of the non-destructive scenario are shown in Figure 95 (and Table D9), and now the optimality of μ = 2.0 is recovered. The performance of the TP2.0 predator is slightly, but significantly, better than all but the TP2.2 predator (one-way ANOVA on ranks, $p < 0.001$) and is considerably better than the exponential and uniform foragers (55% and 62% respectively). These tests confirm that the predator-prey simulation performs as expected from the models employed by Viswanathan *et al*. (1999, 2000, 2001).

We can see that in all the non-destructive scenarios the encounters measured here would be the same if seen from the perspective of the ambush predator with moving prey i.e. the encounter rates will be symmetrical. There is, therefore, no requirement for further simulations to determine encounter rates between a still (i.e. sessile) ambush predator and prey moving in different ways; Lévy prey with low exponents will generate more encounters.
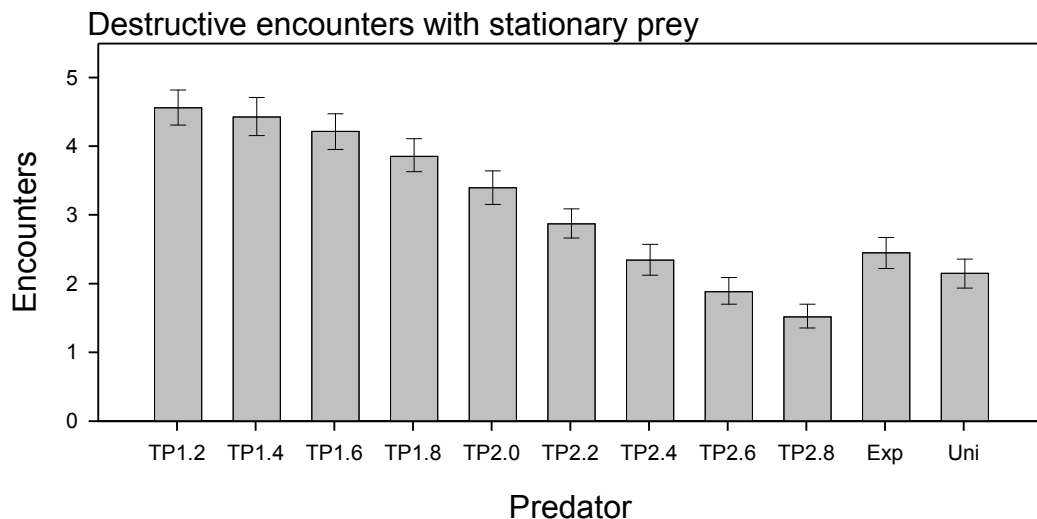
Figure 94: Destructive encounters with stationary prey
    With destructive foraging the situation is similar to the foraging lab simulations without prey targeting, with Lévy predators with lower exponents performing better. While not optimal the TP2.0 predator still performs better than the exponential or uniform predators. Values are medians and error bars represent 10th and 90th percentiles.
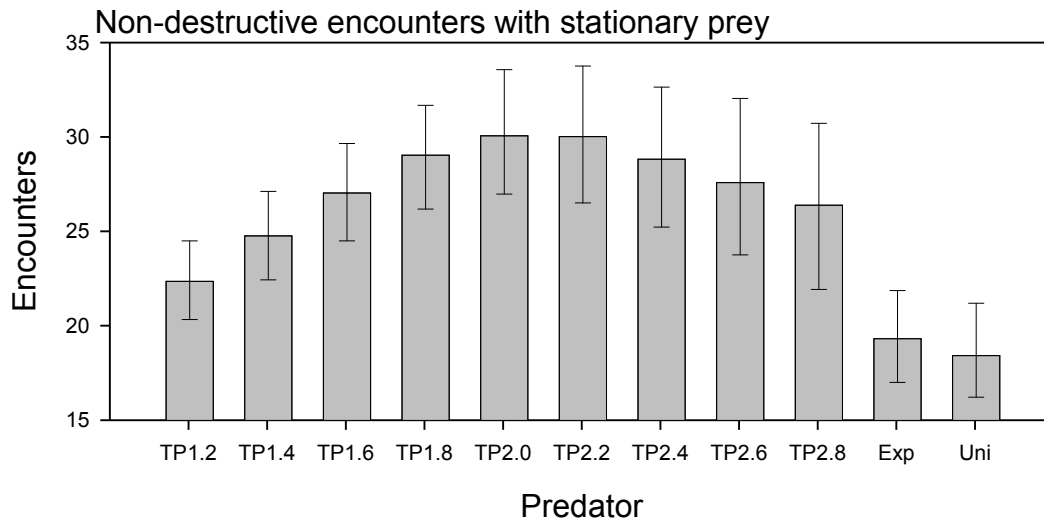
Figure 95: Non-destructive encounters with stationary prey
This scenario closely matches the results from Chapter 3, with the TP2.0 predator being the most efficient performer. However, the optimality is less pronounced as there is no significant prey patch to exploit. All the Lévy predators outperform the exponential and uniform foragers by a considerable margin. Values are medians and error bars represent 10th and 90th percentiles.

6.5 Encounters with moving prey

The optimality of a Lévy search is predicted to be reduced if the prey move fast in relation to the predator, with Brownian or ambush predators then being the most efficient (Viswanathan *et al.* 2002). To explore the consequences of moving prey with moving predators, two sets of simulations were performed using either slow moving prey (uniform with max step of 5) or fast moving prey (uniform with max step of 60, 5x the mean TP2.0 move step). In these simulations six predators were tested, three Lévy predators (TP with μ = 1.5, 2.0 and 2.5), exponential with exponent = 0.19, uniform with x_{max} = 12 and a still, ambush predator. Again these simulations used 10 fish and 10 sharks with destructive predation and prey targeting.

Results of the slow fish simulations are shown in Figure 96 and Table D10. As expected these results are similar to those obtained using stationary prey and although the ambush predator performed worst in terms of the total number of encounters these results cannot be simply adjusted for distance travelled (as the distance travelled by the still predators is zero) and therefore do not reflect any measure of efficiency. Consequently, comparisons based on encounters alone may well be misleading. In order to compare more accurately the benefits of active pursuit with ambush predation, it is necessary to introduce some measure of energetic cost, which will differ between the more and less active predators. For the purpose of this comparison

the values can be arbitrary, as long as the difference between the active and waiting costs is realistic (i.e. is comparable to differences recorded in marine fish). Taking as an example a pelagic shark, the scalloped hammerhead (*Sphyrna lewini*), estimates of standard (Rs) and maximum (Rm) metabolic rates ranged from 161 to 501 mg O_2 kg^{-1} h^{-1} (Lowe 2001). Standardising these values, for simplicity, by setting Rs to 1, gives a value for Rm of ≈3. These values can, therefore, be used as energetic costs by using Rs as the standard metabolic cost incurred for each 10^4 turns, whether moving or not, and Rm as the active metabolic cost incurred for each 10^4 units of movement. Clearly, this is a gross simplification and does not take into account any physiological differences which exist between pursuit and ambush predators. For example, some ambush predators, such as anglerfish (*LophiusI* sp.) are sluggish swimmers (Grove and Sidell 2002) and probably incur a greater energetic cost of movement than well adapted pelagic predators such as sharks. Nonetheless, these energetic cost values are sufficient to provide a more robust comparison of encounter efficiency.

Using these simple assumptions a value of encounters per unit energy expended was calculated, the results of which are shown in Figure 97 and Table D11, where it is clear that the ambush predator was easily the most efficient, being 6.3 times more efficient than the TP1.5 predator.

Results with the fast moving fish are shown in Figure 98 and Table D12 and here, as predicted, the Lévy optimality is greatly reduced, although the TP1.5 predator did perform marginally better than the other moving predators. However, the ambush predator performed almost as well as the rest. If the encounter rates are adjusted, as described above for the slow fish, then it is again the TP1.5 predator that performed marginally better out of the moving predators; however the still predator performed 24 times better (Figure 99 and Table D13).

Repeating these simulations with non-destructive predation and slow moving fish the optimality of the TP2.0 predator was recovered, albeit with less advantage than with the still fish simulations, being 22% better (Figure 100; one way ANOVA on ranks, *p* < 0.001). With fast moving fish (Figure 101) the TP2.0 predator was only slightly better than the other moving predators (3% better than the TP2.5 predator) but was outperformed by the still predator by 1.6% (one-way ANOVA on ranks, *p* < 0.001). If

results are adjusted to take the simple energetic costs into account then the ambush predator outperforms the next best (TP2.5 in both cases) by 24.7 and 29.3 times for the slow and fast fish, respectively.

These results therefore confirm those of Viswanathan et al. (2002) and demonstrate the, considerable, estimated energetic advantage of ambush predation when the prey are fast moving, or super-diffusive.
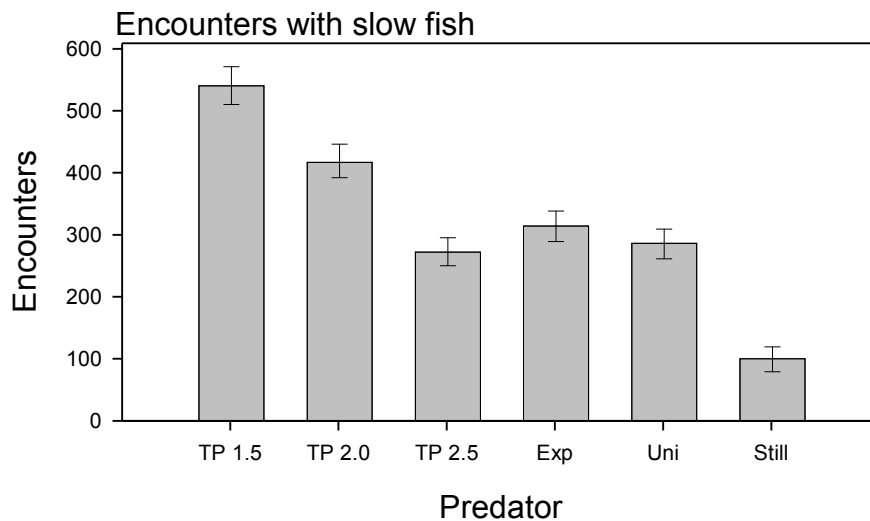
Figure 96: Encounters with slow moving fish
As expected with slow moving fish destructive encounter rates are similar to those obtained using still fish. The ambush predator performs worst in terms of encounters but this result does not take account of the energy conserved by not moving. Error bars are 10th and 90th percentiles.
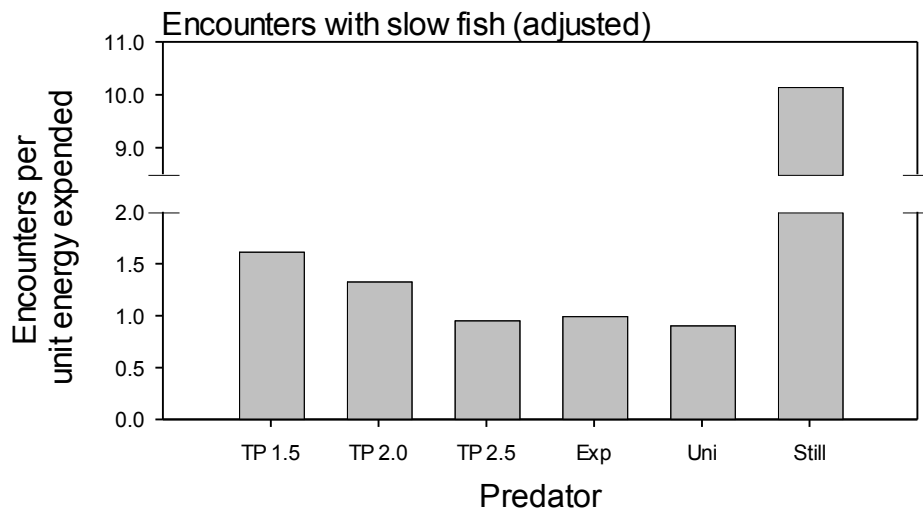
Figure 97: Adjusted encounters with slow fish
If all predators are assumed to have the same standard metabolic cost and the results are adjusted to allow for an assumed energetic cost of movement then the ambush predator is easily the most efficient, about 2.2 times better than the TP1.5 predator.
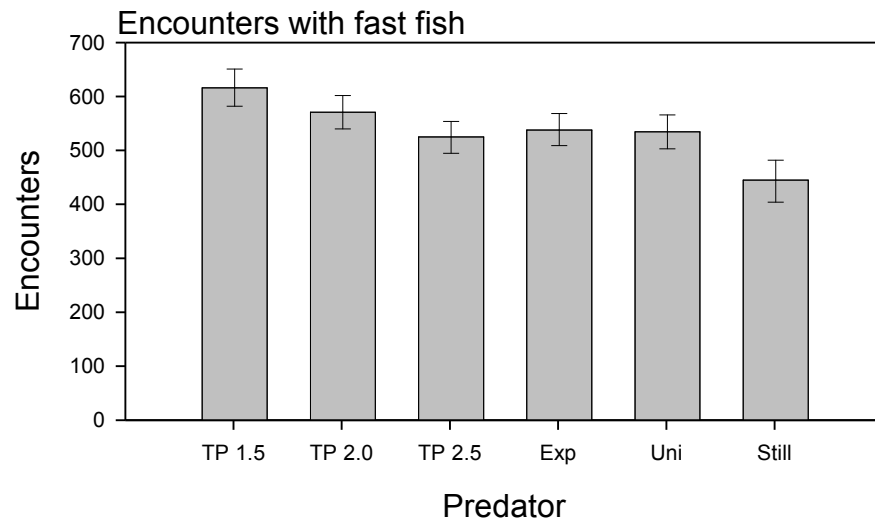
Figure 98: Encounters with fast fish

With fast moving fish the advantage of the Lévy predators is greatly reduced and the ambush predator performed nearly as well as the rest. Error bars are 10th and 90th percentiles.
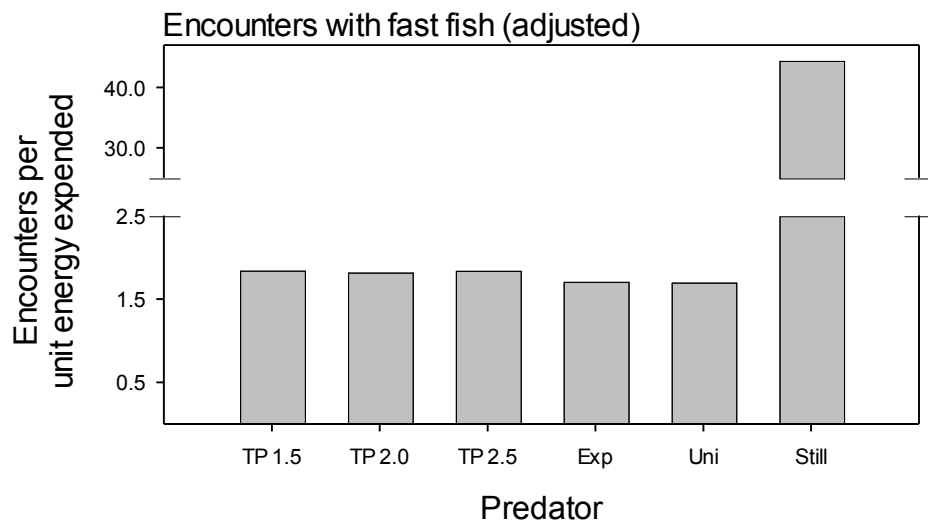
Figure 99: Adjusted encounters with fast fish

When the encounter rate is adjusted for distance travelled the differences between the moving predators are small. The best mobile predator (TP1.5) was 8.5 times less efficient than the still predator.
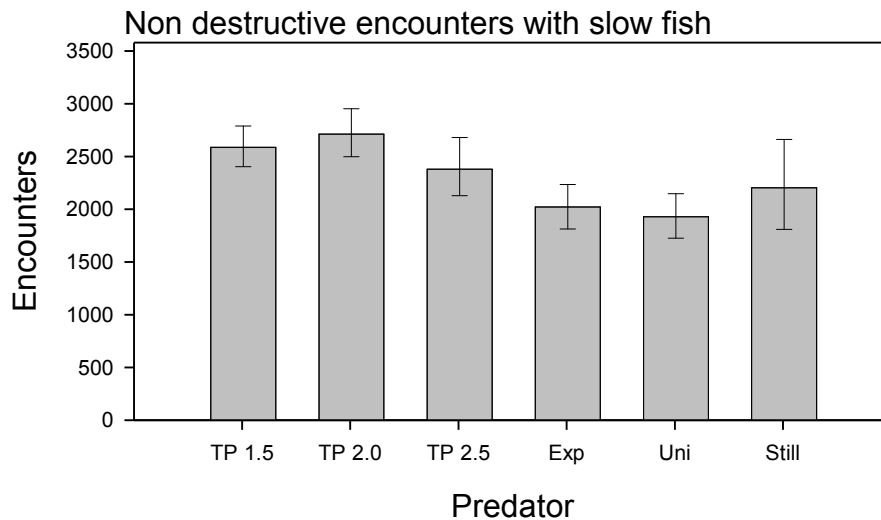
Figure 100: Non-destructive encounters with slow moving fish
With non-destructive encounters, as with the still fish, the optimality of the TP2.0 predator is recovered. However the advantage gained with moving prey is less than with still prey and the still (ambush) predator performs almost as well.
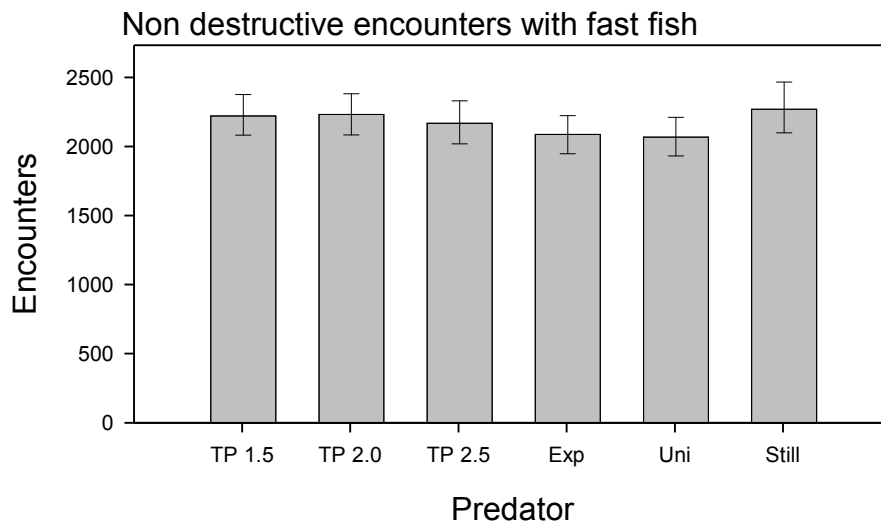
Figure 101: Non-destructive encounters with fast moving fish
With fast moving fish the optimality of the TP2.0 predator is much reduced and the still (ambush) predator performs best.

6.6   Homogenous and heterogeneous prey fields

If prey is distributed homogenously, as it has been for the preceding simulations and as illustrated in Figure 102, then the location of an ambush predator is of little consequence, one place being as likely as another to afford encounters with prey. Consequently, there is no benefit in moving and a sessile predator will be the most efficient. However, if the prey field is heterogeneous, as will be the case in the majority of natural settings, moving can be beneficial if the predator is located in an area of low prey abundance. Therefore to investigate aspects of the ambush predator strategy

such as waiting times a heterogeneous prey field is required. In this section a prey field grid will be introduced, as a mechanism for generating a heterogeneous prey field, and simulation results will be presented that show that a certain minimum prey field density is required for the heterogeneity to become evident.

The heterogeneous prey field illustrated in Figure 103 was generated by specifying a 2x2 prey field grid and populating the area with 4000 fish. Each cell of the grid is randomly marked as either sparse or abundant with an equal number of each. The prey field grid operates by increasing the diffusivity of fish that are located within a prey field grid cell marked as sparse i.e. the speed at which a fish leaves the grid cell is increased (as described in full in Appendix G). To determine the density of fish required to achieve a significant difference in encounter rates between the prey abundant and prey sparse grid cells a series of simulations was performed using 25, 50, 100, 200 or 500 slow moving fish with uniformly distributed move steps on the interval [1, 5] and a single still shark in ambush mode. With this configuration the shark, which will not move throughout each repeat of the simulation, will be either in a prey abundant or prey sparse grid cell (or at the boundary between the two) and it would be expected that a bimodal distribution of encounter rates would result from many repeats of the simulation. Each simulation comprised 10^3 repeats of 10^5 turns. The results are shown in Figure 104 and a clear bimodal pattern can be seen to develop as the prey field density increases. With 25 fish there is no clear pattern; with 50 fish there is a clear spike at around 15 encounters and with 200 or 500 fish the expected bimodal pattern is very clear. To perform a statistical test the results from each simulation (i.e. the number of shark-fish encounters from each run) were sorted and divided so that the lowest 500 values were grouped as 'sparse' and the highest 500 as 'abundant'; this is a reasonable approach given that there is a 50:50 chance of the shark being located in either a sparse or abundant area. Differences between all simulations were significant (Mann-Whitney rank sum test; $p < 0.001$). The results are given in Table 12 and it can be seen that there is a linear increase in the values for the sparse and abundant prey fields, as expected from the prey field investigations performed previously. A further observation is that the number of encounters in the abundant areas is between 2.44

and 2.66 times greater than the median value in sparse areas, indicating that the heterogeneity of the prey field is consistent with increasing prey field density.

It should be noted that this mechanism of producing sparse and abundant areas only works well with relatively slow moving fish, such as the fish used here. With fast, or rather, super-diffusive fish, this simple mechanism of increasing diffusivity is insufficient to maintain the disparity between areas; simply put, the fast fish quickly diffuse throughout the simulation arena as can be seen in Figure 105.

Table 12: Encounter rates for the sparse and abundant prey field areas

Number of Fish	Sparse median (IQR)	Abundant median (IQR)	% difference
25	9 (4)	22 (9)	244
50	18 (6)	47 (12)	261
100	36 (9)	95 (22)	263
200	72 (16)	189.5 (44)	263
500	183.5 (29)	489.5 (71)	266
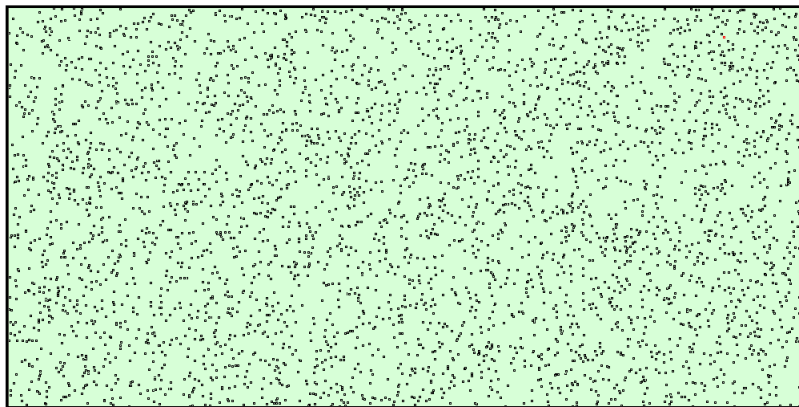
Figure 102: A densely populated homogenous prey field
Without a prey field grid the 4000 fish are distributed homogenously.
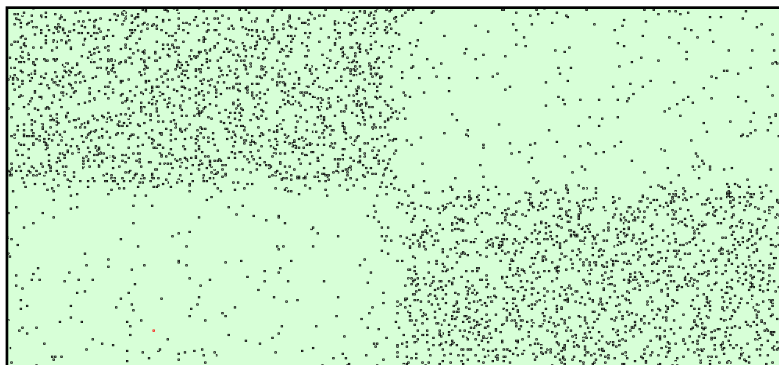
Figure 103: A densely populated heterogeneous prey field
With 4000 fish the heterogeneity of the 2x2 prey field grid is clear.
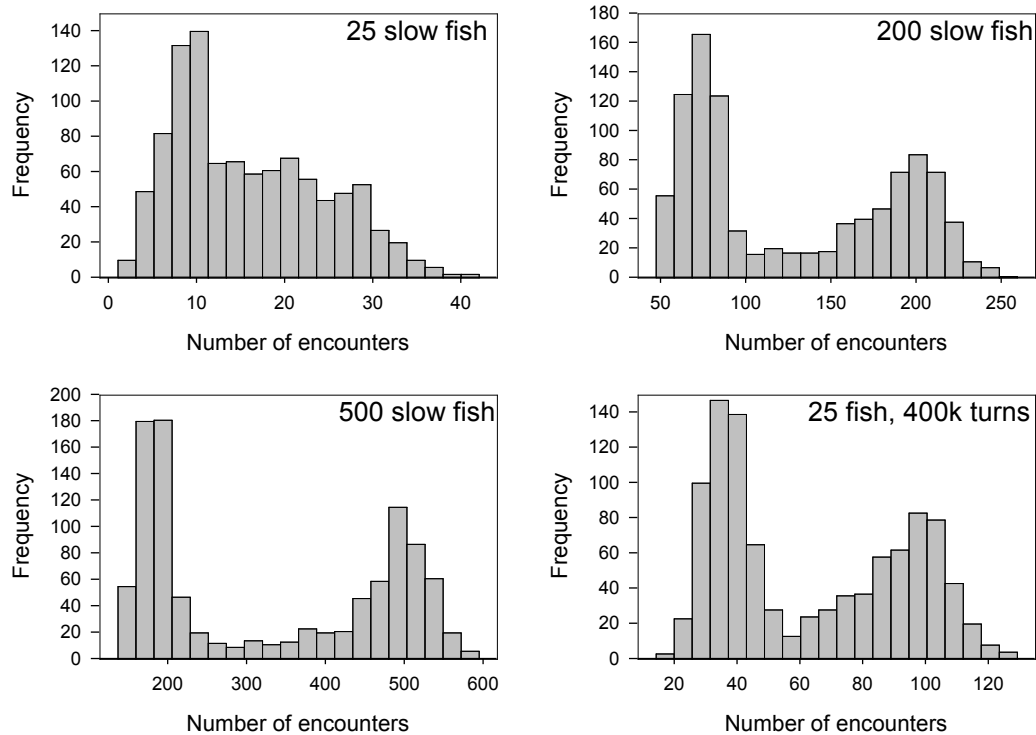
Figure 104: Encounter rates in a heterogeneous prey field
The bimodal pattern of encounter rates only becomes evident with a sufficiently dense prey field of slow moving fish. With 50k turns and a sparse prey field of 25 fish there is no clear effect, but the expected bimodal pattern becomes clearer as the prey density increases. The pattern also becomes clearer if the number of turns is increased as can be seen in the final figure with 25 fish and 400k turns.
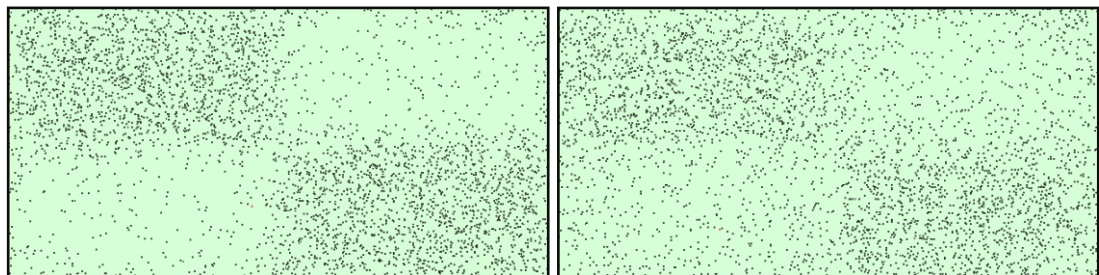
Figure 105: Loss of prey field heterogeneity with super-diffusive fish
With super-diffusive TP.20 fish the prey field quickly loses its integrity. The image on the left shows the prey field near the start of a run, the image on the right is after less than 1000 turns and already the prey field is becoming homogenous. This method of generating heterogeneity only works with slow (normally diffusing) fish.

6.7 Waiting times

In a heterogeneous prey field the ambush predator could be located in either a prey rich or prey sparse area. The predator may not be aware of the status of the current location except through prey encounters and therefore, if encounters are infrequent, there might well be a benefit in giving up the wait and moving to a new area. The question becomes one of how long the predator should wait; giving up too soon in a prey rich area will miss opportunities while waiting too long in a sparse area could lead

to starvation (Nishimura 1991). Ideally, if following an encounter the predator extends the waiting time (i.e. responds to a successful encounter by waiting longer in that place), the wait time should be set to be just longer than the mean time between encounters in a prey rich area; this would ensure that the predator remained in prey rich areas but moved from prey sparse areas. The prediction therefore would be that waiting strategies with very long or very short waiting times, relative to the encounter rate, would result in fewer encounters than intermediate strategies. To test this prediction a series of simulations was performed using a 2x2 prey field grid and slow moving fish having a uniform distribution of move steps on the interval [1, 5] as used previously. Each simulation used 40 sharks in ambush mode with a truncated Pareto movement strategy (x_{min} = 1, μ = 2.0, x_{max} = 500). Simulations were repeated with 50, 100, 200, 500, 1000 and 2000 fish and with uniform waiting times set on the intervals of 1 to 10, 50, 100, 200, 500, 1k and 10k turns and also a still ambush predator as a control. In the program, move on encounter was set to 'false' and destructive foraging to 'true'. These parameters result in sharks that wait for encounters until the waiting time is up and then move super-diffusively to a new location. If prey is encountered then the prey is relocated (i.e. predation is destructive) but the shark stays where it is and the waiting time is extended by a new increment drawn from the distribution. Several predictions can be made for this scenario: firstly an optimum waiting time should be found which maximises the number of encounters and performs significantly better than the still predator; secondly, as waiting times increase, the scenario becomes increasingly similar to the still ambush predator which should result in the emergence of the bimodal pattern of encounter frequencies and consequently increased variance in the number of encounters; finally, as the number of fish increases and consequently the mean time between encounters decreases, the optimum waiting time should also decrease. In these simulations more fish are used than in the program validation simulations performed earlier and therefore, as encounters scale linearly with turns, fewer repeats are required to produce robust statistics; 100 repeats are therefore employed. Further, to produce results which are easier to compare between simulations the number of turns was adjusted in line with the number of fish to generate similar encounter rates; with 50 fish 400k turns were

performed, with 2000 fish only 10k turns are required to generate the same number of encounters as 100k turns with 200 fish.

 The results are shown in Figure 106 and with 50 fish a clear optimum value of around 1000 turns was found. As predicted, as the number of fish increased the optimum value decreased, as summarised in Table 13, with a value of 50 for 2000 fish. There was also a clear increase in variance as the waiting time increases, resulting from predators spending more time in either prey sparse or prey abundant areas. The advantage, in terms of percentage increase in encounters over a still predator was in all cases around 50%. The average encounter rate for still predators will be the mean rate for both sparse and abundant areas. Taking the simulation with 500 fish and a single shark described above as an example, the sparse areas have an encounter rate of 183, the abundant areas of 489 (Table 12), an average rate for this simulation should be about 336.5 encounters for one shark and 50,000 turns. With the simulations performed here with 500 fish, 40 sharks and 40000 turns, the expected rate is therefore 4/5 * 40 * 336 = 10768; reasonably close to the 11635 recorded for still predators with 500 fish (8% difference). The fish with a maximum waiting time of 200 turns spent 1,585,235 of 1,600,000 turns waiting, the rest was spent moving and therefore about 1% of the available waiting time was lost. If this predator spent all of the waiting time in an abundant area the expected encounter rate would be 0.99 * 4/5 * 40 * 489 = 15491; the recorded rate was 17831 (Q1=17055; Q3=18507.5), 14% better which is greater than the inter-quartile range of about 8%, suggesting that the predator might be optimising encounters within the fine scale distribution of prey in the abundant patches, rather than simply matching the encounter rate recorded by a still predator. However it is also possible that the measured improvement was simply down to stochastic variability between simulations. To test this the scenario was re-run a further 3 times with 1000 repeats (rather than 100) which gave values of 18080 (Q1=16669.25,Q3=19317.75), 17273 (Q1=15800.5,Q3=18613.75), and 17033 (Q1=15511, Q3=18367.75). While found to be significantly different (ANOVAR on Ranks; $p < 0.001$), runs 2 and 3 were not different at $p < 0.05$ (Tukey test) and the differences are small, averaging only 4%. Therefore, it seems that encounter rates were indeed better than would be expected than with a still predator located at some

fixed point within an abundant patch. The moving predator does appear to be able to respond to the fine scale prey distributions within the abundant patches; further maximising the encounter rate to a value greater than the average abundant patch value.

Table 13: Optimum waiting times

No of fish	Optimum waiting time (turns)	Peak waiting time (turns)	Peak median encounter rate (IQR)	Median still encounter rate (IQR)	% Advantage over still
50	1k	1k	16644 (1679)	11707 (2653)	42
100	~750	1k	180751 (1795)	11485 (2366)	57
200	500	500	17662 (2237)	11872 (2451)	49
500	~300	200	17831 (1452)	11635 (2595)	53
1000	~75	100	17623 (2316)	11961 (3090)	47
2000	50	50	17964 (1637)	11635 (2233)	54
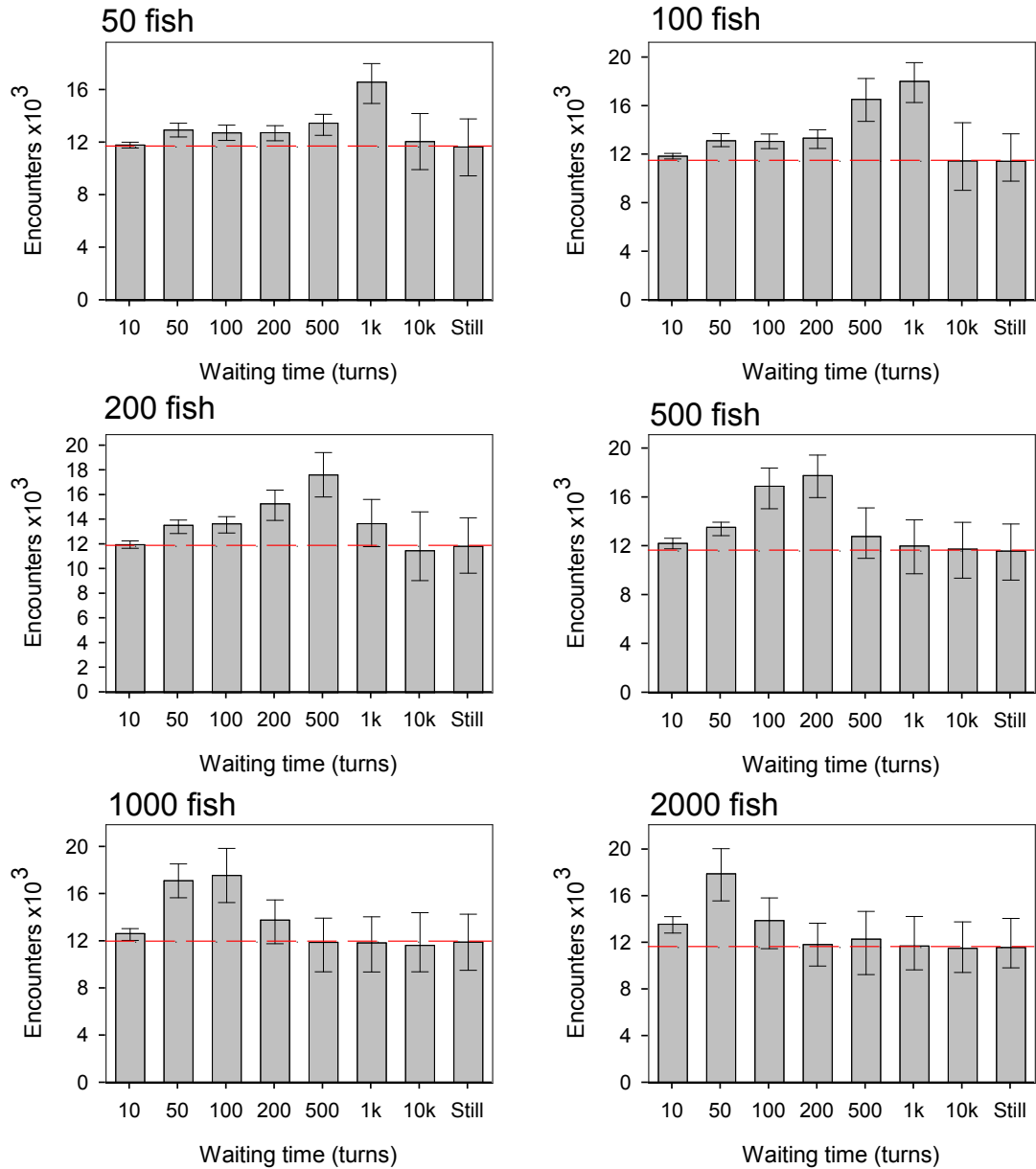
Figure 106: Optimum waiting times with increasing prey field density

With increasing waiting times the encounter rate also increases up to an optimum value, above which the penalty of waiting too long in a sparse environment leads to a reduction in encounters. As the prey field density increases the mean time between encounters decreases and so the optimum waiting time also decreases. Values are medians and error bars are 10th and 90th percentiles. The red dashed reference line represents the encounter rate for the still predator.

6.7.1 Optimising the minimum waiting time

In the preceding simulations a simple uniform distribution was specified with a lower bound of 1, i.e. a maximum value of 500 generated values uniform on the interval [1, 500]. As described above, the mean for such a distribution is just the mean of the minimum and maximum values; so 250 for the example just given. The simulations performed above demonstrated that the optimum maximum value for the waiting time reduced with increasing prey density but did not investigate optimum minimum

waiting times. There is, presumably, a range of values (x_{min} to x_{max}) which will be optimal for a given combination of prey field density and prey swimming speeds and it would be possible, through a systematic search of all the options to determine this combination of values. There is a more elegant solution to the problem however, which is to employ an evolutionary algorithm to fine tune the x_{min} and x_{max} values.

To implement this a few changes were required to the Predator-Prey simulation program. The principal change was that after a certain number of turns, sufficient for predator performance to be evaluated, the bottom 30% of sharks (in terms of encounters) 'die', to be replaced by reproduction of the upper 30%. During the reproduction process (which simply 'clones' individual sharks) mutations will occur that alter either the x_{min} or x_{max} values by either increasing or decreasing the value by a mutation factor. To achieve this, rather than all sharks sharing the same waiting time parameters, each shark requires its own parameter set (i.e. the μ, x_{min} and x_{max} values) for the waiting time distribution, however all sharks share the same movement style (e.g. uniform).

Simulations were performed using 200 fish, as used previously, and with 100 sharks in ambush mode, in order to provide a reasonable population for the evolution process. As before the sharks did not move on encounter but on cessation of waiting moved using a move step drawn from a truncated Pareto distribution with x_{min} = 1, μ = 2.0 and x_{max} = 500. Initial values for the uniform waiting time x_{min} and x_{max} values were set to 400 and 600 respectively; these values were deliberately set higher than the expected optimum value of around 250 (from the previous simulation using 200 fish) in order to investigate the manner in which the values change. The simulation performed 100k turns (one generation) after which an evolution step occurred as described above, with the chance of a mutation occurring during each reproduction (the mutation rate) being set to 50%; this rate results in 50% of the reproducing 30% being subject to a mutation, therefore 15% of the population is changing with each generation. If a mutation occurred it was implemented by changing either the x_{min} or x_{max} value by a mutation factor of ±10%. This process was repeated for 1000 generations and the results are shown in Figure 107. It can be seen that encounter rates rapidly increase in a linear fashion until an optimum value is reached at about

300 generations, at which point the encounter rate settles to a steady value, albeit with considerable variability. If the results from the last 100 generations are compared with the results obtained above (having corrected for using 100 rather than 40 fish) the number of encounters is 23770 [uncorrected 59425 (Q1=54895.25,Q3=62874.5)] which is significantly greater than the previous result (17662) by more than 32% (Mann-Whitney Rank Sum Test; $p < 0.001$).

Figure 107 also illustrates the changes to the x_{min} and x_{max} values from the best performing 30% of the population as the simulation proceeded and it can be seen that as expected the changes mirror the changes in encounter rate. It is interesting that the changes were both rapid and roughly linear, which might be expected given the fixed mutation rate (50%) and mutation factor (±10%) being used. For the last 100 generations the optimised median values for x_{min} and x_{max} are 99 (Q1=90, Q3=111) and 239 (Q1=221, Q3=247) respectively with an overall mean waiting time of 169. This figure is somewhat lower than the rough estimate of 250 from the previous simulations, but the significantly higher encounter rate demonstrates the importance of raising the minimum waiting time (x_{min}) from 1 to 99.

If the prey field density is increased by increasing the number of fish then it would be expected that the optimised x_{min} and x_{max} values would be reduced. To check this hypothesis the simulation was repeated with 400 fish and, as encounter rates will be doubled, 50k rather than 100k turns to provide comparable results in terms of the total number of encounters. The results are shown in Figure 108 and as predicted, for the last 100 generations, the median x_{min} and x_{max} values are reduced to 48 and 119 respectively, almost exactly half the value found with 200 fish. The median encounter rate for the last 100 generations was 57455 (Q1=52999.75, Q3=61595.25) which was not significantly different from the value of 59425 obtained with 200 fish (Mann-Whitney Rank Sum Test; $p = 0.088$). This result demonstrates that the optimum values for x_{min} and x_{max} and the optimal encounter rate are dependent primarily on the prey field density.

The variability in encounter rates attributable to the variability in the x_{min} and x_{max} values could perhaps be lowered by reducing both the mutation rate and the mutation factor. Both measures will increase the proportion of the population that matches the

most successful individuals and while the optimisation will take longer to reach a stable point, the variability at that point should be reduced, and the mean encounter rate should be increased. To test this hypothesis a further simulation was performed as above, with 200 fish, but with the mutation rate reduced from 0.5 to 0.2 (20% of the reproducing 30% are subject to mutation, therefore 6% of the population changes with each generation). The mutation factor is also reduced from 0.1 to 0.05 (±5%) which will slow the rate of change of the parameters. To investigate the long term stability of the encounter rate, and the optimised values, the simulation was allowed to run for 5000 generations. The results are shown in Figure 109 and as expected encounter rates take much longer to reach an optimum value, about 1000 generations rather than about 300 with higher mutation rates. The encounter rate obtained for the last 100 generations is the same as with faster mutations rates, 59847 (Q1=56472.25, Q3=63181) compared to 59425 (Mann-Whitney Rank Sum Test; p = 0.265). This result was unexpected as it seemed probable that if the x_{min} and x_{max} values had less variability within the population then more members of the population would have optimal values for x_{min} and x_{max}, leading to an overall increase in mean encounter rate. However, there was no expected reduction in the variability of the encounter rate or of the optimised values of x_{min} and x_{max}.

To investigate the cause of the variance, the difference in encounter rates between the best and worst performing 30% of the population was calculated from the original 200 fish simulation results. The plot in Figure 110 illustrates the results and shows clearly that the variability of encounter rates is not reduced as the population evolves. Initially the difference is lower, reflecting the fact that all individuals begin the simulation with identical parameters. As the simulation proceeded the range of parameter values increased and this is shown in the higher variability. However, in the final 100 generations, it might be expected that parameter values would have converged on more optimal values and that variation within the population would be reduced as suggested by the plot of x_{min} and x_{max} values in Figure 107. The remaining variability must therefore be intrinsic to the simulation. The inter-quartile range of the first 100 and last 100 generations is almost unchanged at 7173 and 7979 respectively adding

support to the hypothesis that the variance seen is essentially intrinsic to the simulation.
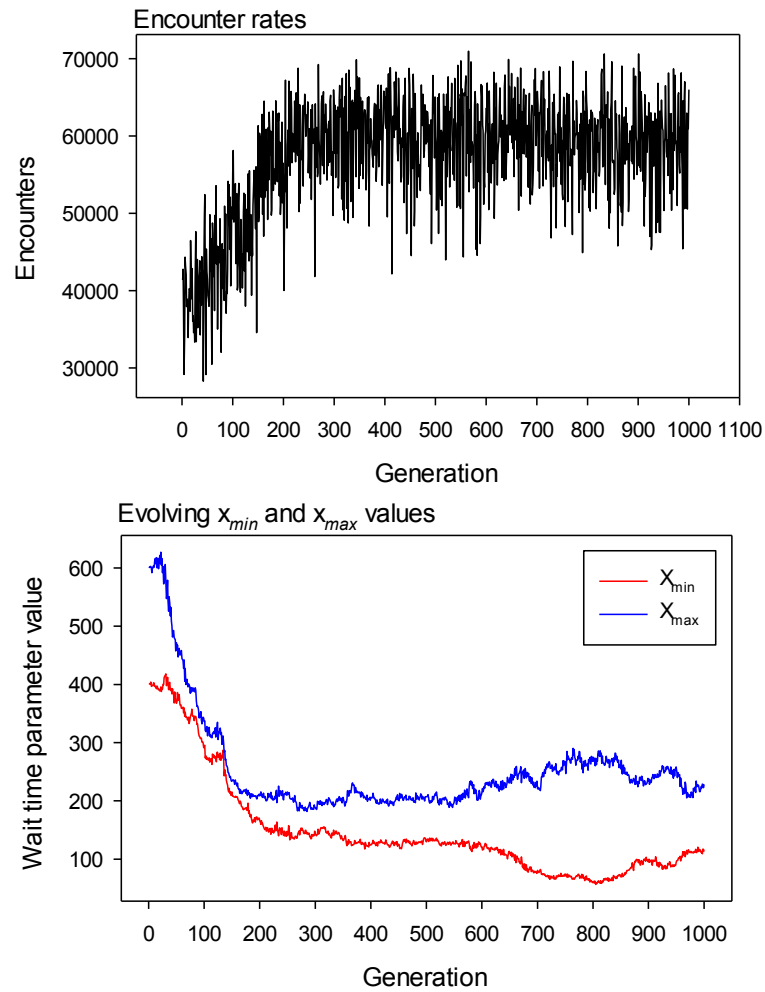
Figure 107: Encounter rates increase as x$_{min}$ and x$_{max}$ values are optimised
There is a rapid increase in the number of encounters until an optimum value is reached at around 300 generations. The lower plot shows mean values for x$_{min}$ and x$_{max}$ calculated from the top performing 30% of the population. The initial rate of change is rapid and approximately linear. There is considerable stochastic variation in the final values.
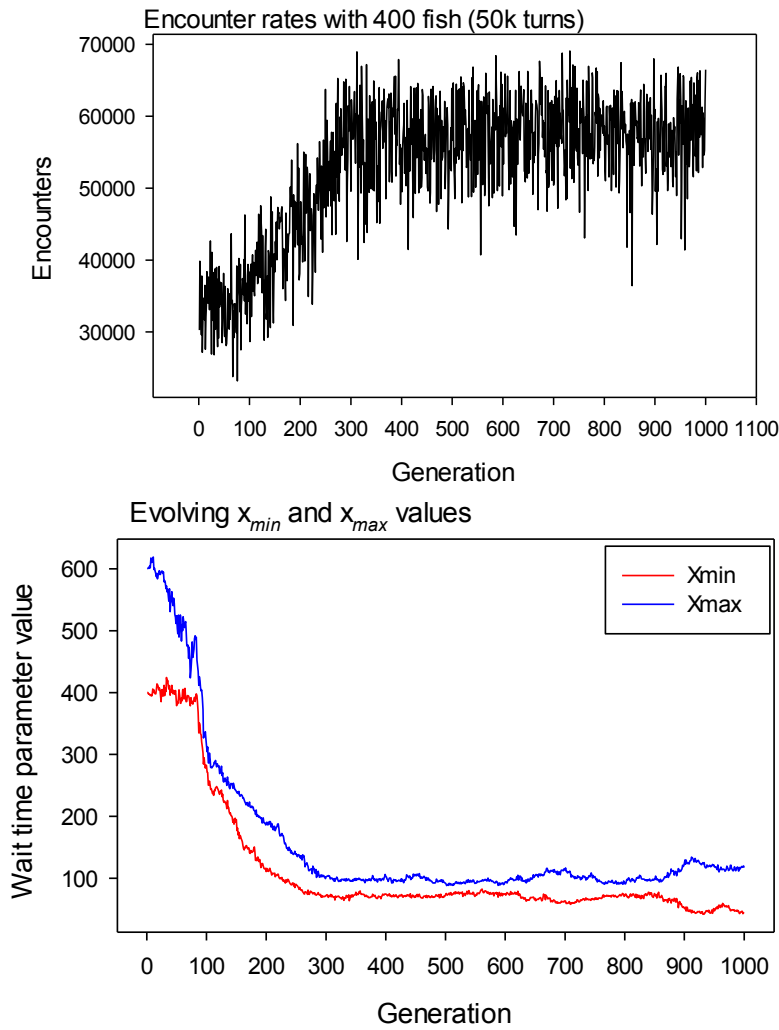
Figure 108: Evolution of encounter rates with 400 fish

With 400 fish and 50k turns encounter rates reach a similar optimum value to that found with 200 fish and 100k turns as expected. With the higher prey field density of 400 fish the optimum values for x_{min} and x_{max} are approximately half of those obtained with 200 fish. There is a noticeable delay before the population begins to evolve but optimum values are still achieved at around generation 300.
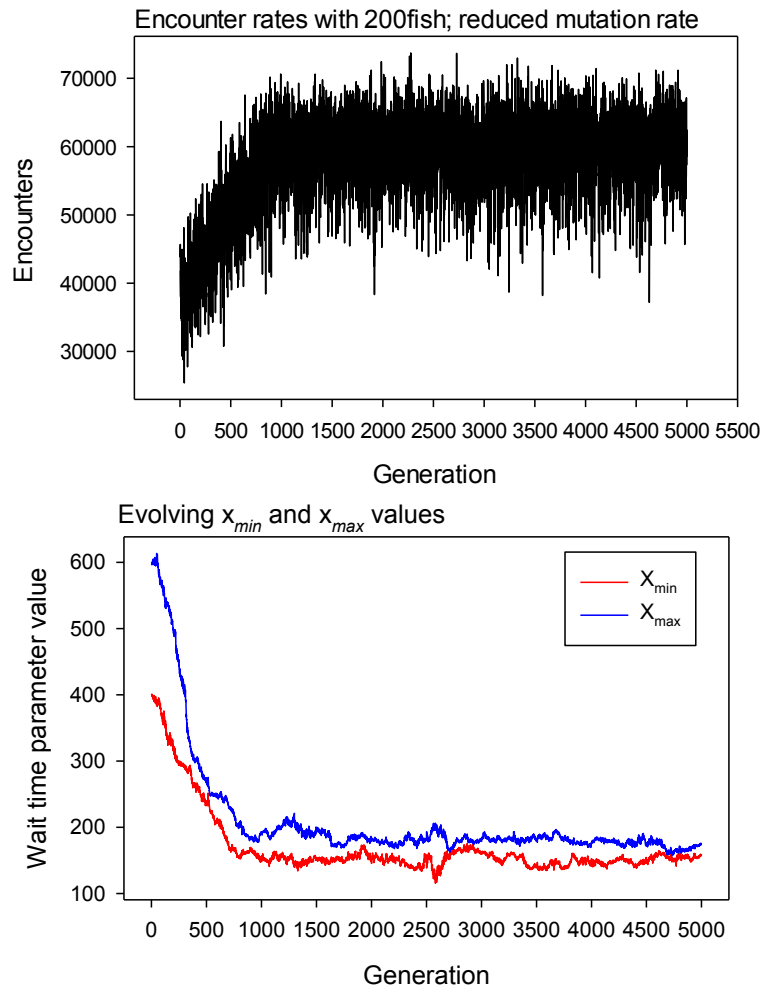
Figure 109: Evolution of encounter rates with reduced mutation rates

With the mutation rate reduced to 0.2 and the mutation factor to 0.05 the rate of change is, as expected, considerably slower, taking over 1000 generations to achieve optimal values. Optimum values are reached at over 1000, rather than around 300, generations. However the values do not settle to more stable values as predicted, rather there is still considerable variability even in the long term.
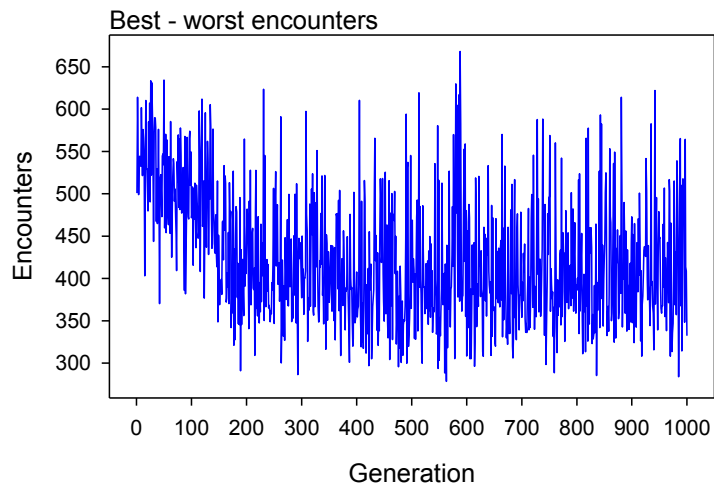
Figure 110: Difference in encounter rate between best and worst performers

The plot shows the difference in mean encounters between the best and worst performing 30% of the population from the simulation with 200 fish. It is clear that there is significant intrinsic variability which does not reduce as the population evolves.

6.7.2　Optimised values with faster moving prey

With faster moving prey, encounter rates should be higher and therefore waiting times should be lower just as with increasing prey field densities. Encounter rates have an exponential relation to the maximum step-length of a uniform distribution as demonstrated previously, so the final encounter rate with faster moving prey is difficult to calculate. The present method of maintaining prey field heterogeneity places upper limits on how fast the fish can be, however it is possible to increase the x_{max} value from 5 to 10, which will be sufficient for a noticeable increase in encounter rates. The results are shown in Figure 111 and it can be seen that the encounter rate and parameters reach optimum values somewhat later than with the slower moving fish, at around 400 generations. The median encounter rate for the last 100 generations was 95125 (Q1=90026.75, Q3=98803) which was significantly higher than with slow fish (59425) by 60% (Mann-Whitney Rank Sum Test; $p < 0.001$). Interestingly the value for x_{min} for the last 100 generations was not significantly different from that obtained with the slow fish at 98.78 compared to 98.66 (Mann-Whitney Rank Sum Test; $p = 0.478$). The value for x_{max} however was half the value of that with the slower fish at 121 and 239 respectively and was significantly different (Mann-Whitney Rank Sum Test; $p < 0.001$). It is interesting that with increased prey field density both the x_{min} and x_{max} values were halved, as expected, but with increased prey diffusivity only the x_{max} value was affected.
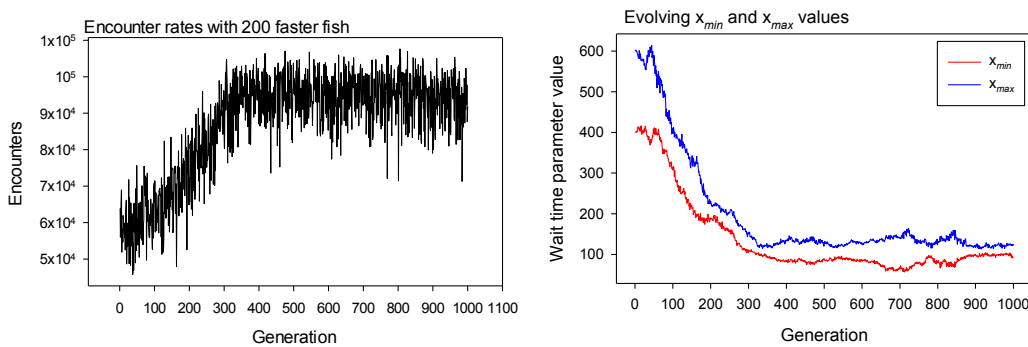
Figure 111: Optimisation of encounter rates with faster moving fish
With fish moving (diffusing) approximately twice as fast the encounter rates quickly reach an optimum value which is not quite twice as high as with the slower moving fish. The optimised x_{min} and x_{max} values however are lower than those obtained with the slower fish as expected.

6.7.3　Non-uniform waiting times

The previous investigations used uniformly distributed waiting times as a simple way to illustrate the underlying principles. Here we investigate the performance of both

exponential and power-law distributed waiting times by using the evolution algorithm to determine optimised values for x_{min}, x_{max} and the exponent as appropriate. Initial values for x_{min} and x_{max} were set to 400 and 600, as with the uniform distribution and, for power and truncated Pareto distributions, μ was set to the Lévy optimum value of 2.0. For the exponential distribution an exponent of 0.02 was used which gives a similar mean value of 164 which is sufficient as a starting value. While the value of μ was adjusted through mutation in the same way as the x_{min} and x_{max} values it was not allowed to become < 1 or > 3; i.e. it was kept within the Lévy range. There were several questions regarding these simulations: would the x_{min} and x_{max} values differ significantly from those obtained with a uniform distribution; what value would the exponent take and would the mean encounter rate be greater for the TP or exponential predator than the uniform predator?

The results from the exponential distribution are shown in Figure 112 with statistical results for this and the other distributions given in Table D14 and Table D15. The evolution of encounter rates showed a similar rapid change as for the uniform distribution. The rate for the last 100 generations is 60654 (Q1=58020.25, Q3=64123) which while significantly different from that obtained with the uniform distribution (Mann-Whitney Rank Sum Test; $p = 0.03$) was greater by only 2.06%. The value for x_{min} rapidly settles to a reasonably constant value of 157 by 300 generations. The exponent (λ) ranges from 0.0389 to 0.127 (median 0.105) which, from simulated data with x_{min} set to 157, gives mean waiting times of 182 ($n = 50000$, s.d. 25.98) and 164 ($n = 50000$, s.d 7.8) respectively, and an overall mean waiting time of around 173. These values are close to the optimum mean of 167 for the uniform distribution. The x_{min} value for the last 100 generations was kept with about 15% of the median, however the exponent was only kept within about 37% of the median, suggesting that selection pressure on this parameter was less than for the x_{min} value and that the exponent was therefore less critical in determining the optimum waiting time.

The results from the power-law simulation are shown in Figure 113. The evolution of encounter rates was very similar to that obtained with the uniform distribution but the rate for the last 100 generations was not significantly different at 59119 (Q1=55169, Q3=61705.25) compared to 59425 (Mann-Whitney Rank Sum Test; $p = 0.647$). The

value for x_{min} from the last 100 generations was 81 and for μ was 2.84. From simulated data these parameters generate a mean waiting time of 177 (n = 50,000, s.d. 310), which was close to the mean value obtained with the uniform distribution of 167. The x_{min} and exponent reach their optimum values at about the same time as the exponential distribution, after about 200 generations. The exponent (μ) was kept with about 7% of the final value and x_{min} was kept within about 14%.

The results from the truncated Pareto distribution are shown in Figure 114. The optimisation of encounters proceeds more slowly than with the uniform or power-law distributions which was expected given that there are now three parameters being mutated; not only does each parameter change more slowly as a result (as only one parameter was changed with each mutation), but the parameter trade space (i.e. the number of possible combinations of all parameters) was now much larger. Each parameter effectively adds a dimension to the parameter trade space, considerably increasing the time required to find optimal values in the 'fitness landscape' (Sole *et al.* 1999). The encounter rate for the last 100 generations was 60573 (Q1=56458.25, Q3=62357.5) which was not significantly different from the value of 59425 obtained with the uniform simulation (Mann-Whitney Rank Sum Test; p = 0.317). The value for x_{min} for the last 100 generations was 90, which is comparable to the power-law value (81). For x_{max} the value was 353, which was much higher than that obtained for the uniform distribution (174). The value for μ does not seem to settle to an optimised value, instead meandering with stochastic variation between 1.4 and 1.9 (median = 1.7). This represents an overall variation of about 30%. From simulated data generated using these parameters it can be seen that with μ = 1.4 the mean waiting time was 178 (n = 50000, s.d. 70) and with μ = 1.9 the mean waiting time was 165 (n = 50000, s.d. 66), so it is interesting to note that the overall mean waiting time of 171.5 was again very close to that obtained with the uniform distribution (169). Variation in x_{min} was about 18% and in x_{max} was 41%.
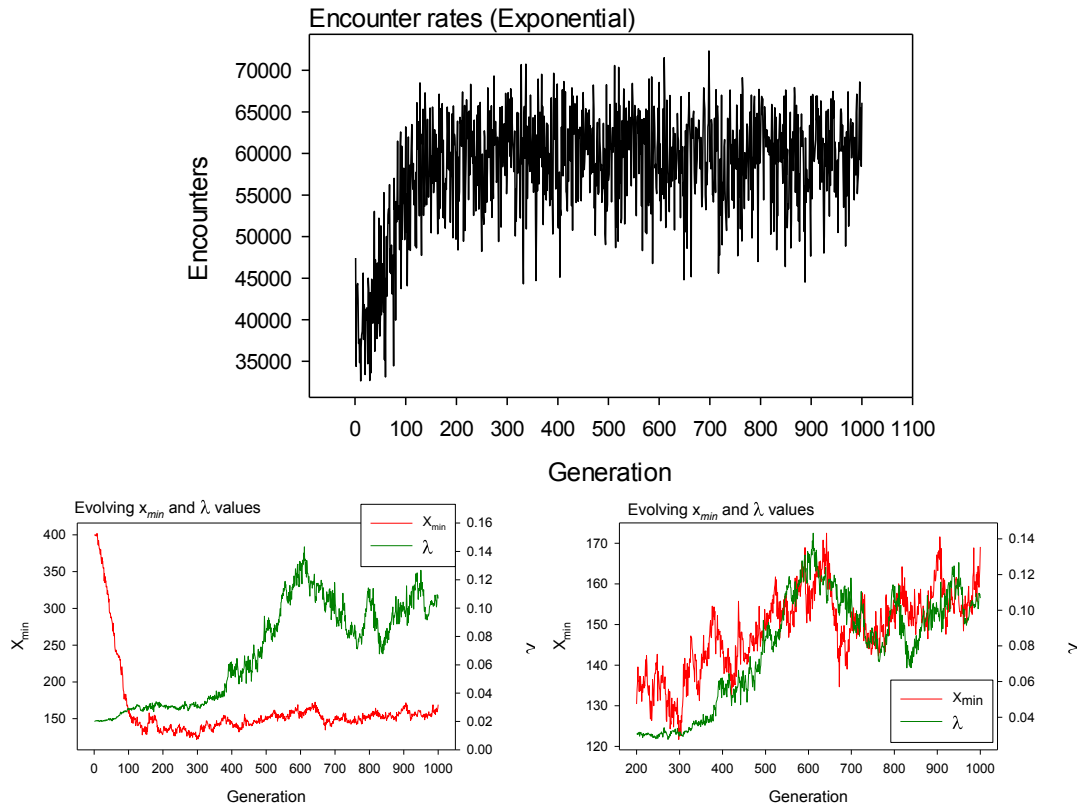
Figure 112: Evolving encounter rates with exponentially distributed waiting times

This result is very similar to that obtained with the uniform distribution. While the x_{min} value quickly settles to an optimum value the exponent seems to meander with stochastic variation, suggesting lower selection pressure on this parameter. The bottom right plot shows the values from generation 200, allowing a more revealing scale. From this plot it can be seen that both parameters vary considerably and that there seems to be some correlation between the two.
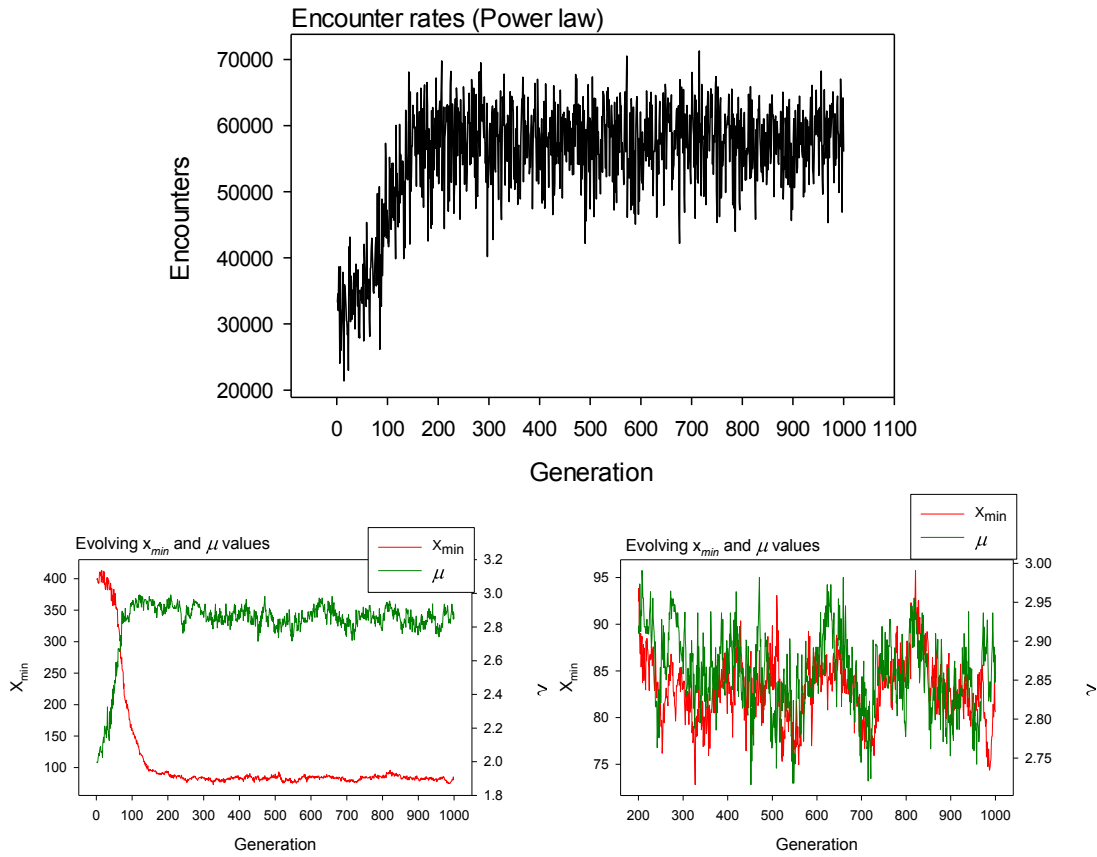
Figure 113: Evolving encounter rates with power-law distributed waiting times

This figure is very similar to the results obtained with the uniform distribution except that the final encounter rate is somewhat lower. Both values quickly evolved to optimum values with x_{min} settling at a mean of 68 and μ at 2.83. The bottom right plot shows the values from generation 200, allowing a more revealing scale. From this plot it can be seen that both parameters varied considerably and that there seems to be some correlation between the two.
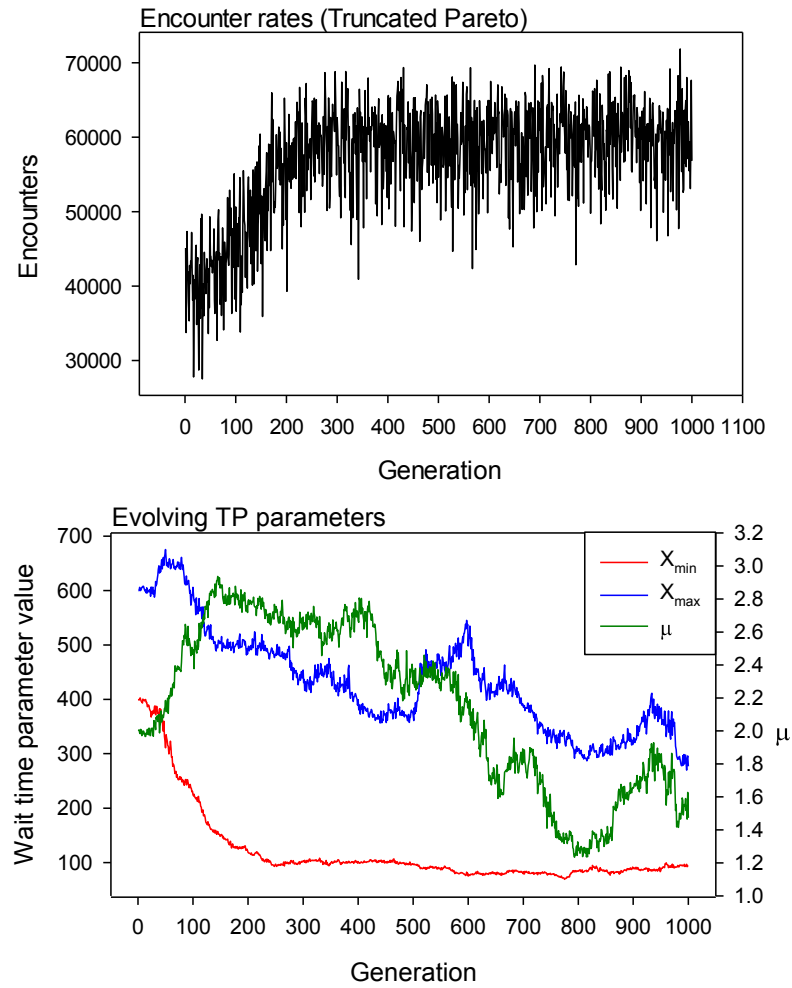
Figure 114: Encounter rates with truncated Pareto waiting times
While the x_{min} and x_{max} values reach optimum values after about 300 generations the exponent value meanders through stochastic variation implying that selection pressure on this parameter was low or non-existent.

6.8 Discussion

From the simple equation derived to describe encounter rates ($Z_{2D} = 2rfst$) it is clear that the relationship between most parameters and the encounter rate is linear for the range of values used. Such a simple relationship has made validation of this simulation program relatively straightforward and, therefore, it is possible to be confident in the more complex results obtained in some scenarios. The only aspect that proved to be more complicated was relating increased diffusivity to the encounter rate as an analogue for velocity. Increased diffusivity results in increased net displacement, but the relationship is too complex to allow straightforward investigations into encounter rates between predators and prey moving at different speeds. Instead, the investigations were couched in more general terms of more or less diffusive

individuals, however this was sufficient to identify the predicted differences in encounter rates between predators and still or moving prey. Similar simulations have been used before and have run into problems in the way that velocity was dealt with (e.g. see Scharf *et al.* 2006, Avgar *et al.* 2008, Scharf *et al.* 2008). Future work could better consider the implications of velocity by modifying the simulation to allow multiple interpolated steps to be performed per turn, although this would only deal with integer velocities. Another problem with dealing with differing velocities lies in correctly modelling the simultaneous movements of individuals. In a turn-based framework two close individuals could perform moves separately on paths that cross; in reality the two should meet but by taking turns they will miss. This problem was raised by Avgar *et al.*(2008) and has, as yet, no clear solution in a simple grid based simulation such as the one employed here. To properly deal with different velocities the simple regular grid approach would have to be discarded and accurate collision detection algorithms would have to be employed, as is the case with modern 3D games (Jimenez *et al.* 2001). However, dealing with large numbers of objects can become computationally intensive and many complex but efficient algorithms have been developed to speed up the process (e.g. Leszczynski and Ciesielski 2004, Liu *et al.* 2010).

An important outcome in this study was confirming the optimality of low exponents (μ = 1.5) for Lévy predators in destructive foraging scenarios, and the optimality of μ = 2.0 in non-destructive scenarios, providing a useful independent verification of the predictions made by Viswanathan *et al.* (1999, 2000, 2001). The simulation presented in this chapter differs significantly from both the mathematical model presented by Viswanathan *et al.* and from the simulation presented in Chapter 3, and therefore to obtain such similar results provides very strong support for the theoretical basis of the Lévy flight foraging hypothesis.

The simulations have also upheld those predictions concerning ambush predators, namely that with faster moving prey the movement pattern of the predator becomes less important and that the ambush predator can be the most efficient in terms of the number of encounters (Viswanathan *et al.* 1999, Scharf *et al.* 2006). This advantage

was not just in terms of encounter efficiency (i.e. encounters per unit energy expended) but in absolute terms of the number of encounters occurring.

The natural environment is heterogeneous and this will result in problems for sedentary predators. Sessile organisms, which include non-relocating ambush predators such as ant-lions (Scharf and Ovadia 2006), will only thrive where conditions are suitable and cannot usually relocate in an attempt to improve encounter rates; sessile organisms that settle in adverse conditions simply die. More mobile ambush predators such as angel sharks (*Squatina squatina*) or anglerfish (*Lophius piscatorius*) are able to give up waiting in less favourable conditions and relocate to new areas. From the results presented here it is clear that for given levels of prey field density and heterogeneity there are consistent values for the minimum and maximum waiting times that significantly optimise the overall encounter rate. Of particular interest is that there is a mean value for the waiting time independent of the waiting time distribution. In all cases examined here the mean waiting time was around 172.6 (uniform 169, exponential 173, power-law 177 and TP 171.5). Previous studies have also suggested that in heterogeneous environments an optimal waiting time is expected (Nishimura 1991), however, to date, the link between optimum waiting time and prey field density has only been shown in one dimension (Benichou *et al.* 2011). In this study, it has been demonstrated clearly that there is an inverse relationship between prey field density and the optimum waiting time. While, in itself, this is not an unexpected finding the evidence that the actual distribution (i.e. uniform, exponential or power-law) plays no significant role is interesting. In the foraging simulations performed in Chapter 3, it was found that the distribution was a very significant factor, with a truncated Pareto distribution with μ = 2.0 outperforming the other distributions, even when the mean step-length was comparable. Consequently, it was not expected that the distribution would have so little effect in these simulations. This suggests that the foraging scenarios of Chapter 3 are less analogous to the scenarios presented here than was first expected.

In all cases there was also a range of values, between x_{min} and x_{max}, rather than a single value, suggesting an advantage in having some variability in the waiting time. It could be that having a broad range of values helps in dealing with the intrinsic stochastic

variability of the simulation environment as well as the heterogeneity of the prey field. In the evolutionary simulations the x_{min} and x_{max} values changed rapidly from the starting values to more optimised values, yet failed to converge on a single value. It seems likely, therefore, that the range of values was important in optimising encounters in the simulation environment, where there was strong, random, prey field heterogeneity. Consequently, the waiting time of an individual predator had to deal with both sparse and abundant prey patch densities. Further work could test this idea using homogenous prey fields. A further factor that would have affected the optimised x_{min} and x_{max} values, in this study, is that the predators could not choose to 'give up' waiting in response to environmental cues. Previous studies have considered the problem of predator choice in waiting times (Nishimura 1991), concluding that the optimum strategy is to initially decide on a long waiting time, and then adjust this time, in subsequent trials, in response to prey capture. Again, however, in the simulations performed by Nishimura (1991), the predator could not 'change its mind' and give up early. It seems likely that natural ambush predators base waiting decisions on perceived prey availability, rather than actual prey capture, as the majority of ambush predators have a sensory range that exceeds the prey capture range; e.g. parasitic wasps (White and Andow 2007) or anglerfish (Laurenson *et al.* 2004). Consequently, more informed decisions regarding patch quality can be made by natural predators than by the simulated predators in these studies.

Decisions about patch quality, and how long to wait for a prey encounter, require memory. Memory windows, where behaviour is learned, retained and then forgotten, have been demonstrated in a range of lower vertebrates; e.g. fish (Mackney and Hughes 1995) and tadpoles (Ferrari *et al.* 2010) where prey handling and predator avoidance were shown respectively. Therefore, it is likely that ambush predators can learn to adjust their waiting time (i.e. be more patient) if environmental cues suggest the patch to be profitable, rather than unprofitable, and *vice versa*. Furthermore, it has been shown that limited memory capacity, as would be expected in lower vertebrates, can actually improve the identification of correlations in a heterogeneous environment. Kareev (1995) showed that small sample sizes tend to overstate correlations, i.e. if a correlation exists then it is more likely to be found in a small

sample than a large sample; suggesting that it is quite possible to make quick decision about patch quality. Further, in dynamic heterogeneous environments, long term memories could be maladaptive as they become out of date, therefore shorter memory windows are expected to be advantageous in changing environments (Mackney and Hughes 1995, Fortin 2002). Therefore, it is possible that the optimised x_{min} and x_{max} values found in these simulations could represent some aspect of an animal's memory window.

The use of an evolutionary algorithm provided a relatively straightforward way to investigate the optimisation of waiting time parameters that would have been time consuming and difficult to achieve with other methods (such as performing factorial simulation experiments). Genetic algorithms (of which this was a very simple implementation) have been used extensively in many fields including ecology and optimal foraging (Strand *et al.* 2002, Scharf *et al.* 2009). However a full investigation of either the algorithmic details, such as optimum population sizes and mutation parameters, while very interesting, is beyond the scope of this chapter. It is, perhaps, of more importance to recognise that if artificial selection processes work so effectively to optimise attributes which have quite subtle effects, then it is very likely that the same has occurred in nature.

Consequently, it is reasonable to conclude that observed behavioural patterns, such as waiting times, will also very likely represent optimised values; although the full suite of factors for which these values are optimised are more difficult to elucidate. Clearly, in the natural environment, predators must respond to a range of factors, such as light intensity, temperature, salinity and depth, as well as the likely profitability of the current prey patch. How these environmental factors are integrated with other factors, such as predation risk or hunger, in the optimisation of waiting strategies of marine ambush predators such as anglerfish (*Lophius* sp.), will prove challenging to determine.

7 Assessing the potential impact of long-line fisheries on a wide-ranging pelagic predator: a simulation study

This chapter was presented at the symposium 'Marine Protected Areas on the High Seas' as

Humphries, N. E., N. Queiroz, G. R. Mucientes, L. L. Sousa, and D. W. Sims. 2011. Assessing capture risk of pelagic fish by satellite-tracked long-line vessels and the effectiveness of Marine Protected Areas. Marine Protected Areas on the High Seas, February 2011, Institute of Zoology, Regents Park, London, NW1 4RY, UK.

The analysis methodology presented in this chapter has been used in Queiroz, N., N. E. Humphries, L. R. Noble, A. M. Santos, and D. W. Sims. 2012. Spatial Dynamics and Expanded Vertical Niche of Blue Sharks in Oceanographic Fronts Reveal Habitat Targets for Conservation. *PLoS ONE* **7** (2), e32374.

7.1 Introduction

It has long been known that the rise of industrialised fishing has resulted in largely unsustainable increases in catches of the target species (Garstang 1900, Thurstan *et al.* 2010). Another consequence of larger, more powerful fishing vessels entering the industry since the 1940s is a significant impact on large open-ocean species, such as pelagic sharks (Megalofonou *et al.* 2005b, Zeeberg *et al.* 2006, Dulvy *et al.* 2008, Campana *et al.* 2009), by more technologically sophisticated long-liners. Up until the

1950s, open-ocean pelagic sharks were largely beyond the range of most of the fishing fleet. Significant changes in the pelagic fish community and in the size structure of populations have been observed since the 1950s (Ward and Myers 2005) and other more complex ecosystem effects on shark populations have been predicted using ecosystem models (Kitchell *et al.* 2002). Industrialised fishing fleets not only affect the target species however, but can have a significant impact on non-target by-catch species, which in the case of the long-line fishing fleet can be turtles, seabirds or fish (Marin *et al.* 1998, Baez *et al.* 2007, Jimenez *et al.* 2010, Casale 2011, Tuck *et al.* 2011), and especially sharks such as blue (*Prionace glauca*), mako (*Isurus oxyrinchus*) or silky (*Carcharius falciformis*) which have suffered major declines (Buencuerpo *et al.* 1998, Campana *et al.* 2006, Aires-da-Silva *et al.* 2008, Cortes *et al.* 2010).

Other than increasing regulation regarding the practice of 'finning', there are currently few catch limits on pelagic sharks and no size restrictions in place. In Canadian waters there is a recognised directed fishery for porbeagle sharks (*Lamna nasus*), despite recommendations for the fish to be listed as endangered by the Committee on the Status of Endangered Wildlife in Canada (COSEWIC). The Canadian Atlantic Pelagic Shark Integrated Fisheries Management Plan also places restrictions on the total allowable catch (TAC) of blue and mako sharks, totalling < 100 tons per year. In the USA, NOAA Fisheries management set the commercial quotas at 273mt for blue sharks, 1.7mt for porbeagle and at 488mt for all other pelagic sharks, up to December 2012. European regulations, however, are less strict. There are zero TAC limits for porbeagle, spiny dogfish (*Squalas acanthius*) and deepwater sharks and prohibitions on handling and landing of skates, rays and angelsharks (*Squatina squatina*). However, the EU currently places no restrictions on pelagic sharks. Given the slow population recovery potential, resulting from the low fecundity and late age of maturity of many pelagic sharks (Cheung *et al.* 2007), the likelihood of further declines appears probable (Cortes *et al.* 2010), unless management measures are implemented. A potential mitigation of over-exploitation of pelagic sharks is spatial management, which imposes large areas where fishing for pelagic sharks is prohibited. Recent developments in this approach have seen the establishment of vast marine protected areas (MPAs). For example, the Chagos Islands Marine Reserve, established in April 2010, covers more

than 600,000 km^2 of the Indian Ocean and was implemented primarily to protect coral reef habitat (Sheppard *et al.* 2012). In September 2011 a 1M km^2 protected marine reserve was announced for the Cook Islands in the Pacific Ocean. In the NE Atlantic, somewhat to the north of the study area in this chapter, a network of six MPAs was established in 2010 by the OSPAR convention, which totals 286,200 km^2 (O'Leary *et al.* 2012). Nevertheless, how well such areas or other potential methods for catch reduction by the long-line fishing fleet will protect highly migratory species, such as pelagic sharks, is only poorly understood.

Pelagic sharks such as blue, or shortfin makos (*Isurus oxyrinchus*) are the most commonly caught shark on pelagic long-lines, but catches are currently unregulated and are under pressure from both targeted fishing effort (for fins or meat) or as by-catch from other fisheries, especially long-liners targeting tuna or billfish (Megalofonou *et al.* 2005a, Megalofonou *et al.* 2005b). For many species of pelagic shark the intrinsic low productivity resulting from late maturity and low fecundity make them vulnerable to over-fishing, resulting in significant declines in wild populations in recent years (Cortes *et al.* 2010). Many studies into the impact of fishing fleets on by-catch species have relied on data from landings (e.g. Buencuerpo *et al.* 1998) or from observers (Rogan and Mackey 2007, Sims and Cox et al.2008b) however, both these methods have some shortcomings. Data from landings does not include detailed information about where or when the by-catch was caught, and does not document discards made at sea, which can be significant (Stevens *et al.* 2000, Campana *et al.* 2009). Observer programs are more accurate but suffer from poor coverage as only a small percentage of vessels will have observers aboard. Consequently, the full extent of the risk posed by long-line and other fisheries to pelagic shark populations is not fully understood. If pelagic sharks are to be managed sustainably then clearly some form of regulation is required whereby-catches are limited and numbers caught, whether landed or discarded, are accurately recorded. For such protection measures to be economically viable and enforceable they must be focussed on the locations and times at which the sharks are most at risk, for example mating or pupping aggregations. Therefore, a detailed understanding of the movements and migrations of these widely distributed sharks is essential. However, it is equally important to understand the spatio-temporal

distribution of fishing effort that is posing the risk to the sharks. Mitigation measures such as Marine Protected Areas (MPAs), seasonal closures or fleet restrictions will not result in a reduction of risk unless they target those areas and times during which the sharks are at risk.

Accurate distributions of fishing effort are now available for some fleets, in the form of Vessel Monitoring System (VMS) data which record the location, speed and heading of each vessel every two hours (or more frequently in some cases). It is therefore possible to determine seasonal and spatial hotspots of fishing activity. The missing piece, however, is similar data concerning the movements of sharks. Technological advances in the design of electronic tags and in global positioning systems has led to an acceleration in tagging studies seeking to fill this gap in our knowledge (e.g. Block *et al.* 2011). Such studies are time consuming and expensive and to date the information regarding the movement and migration of pelagic sharks is scant (however, see Pade *et al.* 2009, Queiroz *et al.* 2010), and as yet, insufficient for a detailed analysis of the interactions between the Atlantic fishing fleet and the shark populations.

This study will investigate the effect of several by-catch mitigation measures using fleet movement data provided by the vessel monitoring system (VMS) for the Spanish and Portuguese long-lining fleets in a shared grid occupancy analysis. Ideally, the prey field for the analysis would be populated using tracks recorded from the by-catch species of interest (i.e. blue, mako or silky sharks) resident in the N.E. Atlantic where the fleet are fishing; however, the number and extent of tagged animals is currently insufficient for a comprehensive analysis (Queiroz *et al.* 2010). Consequently, this study uses a simulated prey field representing a wide-ranging pelagic predator, such as a blue shark (*Prionace glauca*), constructed using tracks generated by a shark simulator program, described in full in Appendix H.

As will be shown in this study, fishing effort by Spanish and Portuguese long-liners has an extensive but patchy distribution in the NE Atlantic, with 'hotspots' occurring in different locations at different times of the year. The overall fishing effort also varies throughout the year. These differences are driven primarily by the movements and migrations of the principal target species which, for the Spanish and Portuguese long-liners, is generally swordfish (*Xiphias gladius*). However, the fishery has an impact on

non-target or targeted by-catch species, such as blue sharks (Buencuerpo *et al.* 1998, Marin *et al.* 1998, Vega and Licandeo 2009) which have overlapping feeding niches with those of swordfish (Pusineri *et al.* 2008, Queiroz *et al.* 2012). Fisheries controls, such as closed seasons or no take zones, created to maintain the sustainability of the target species may have different and even detrimental consequences for non-target or targeted by-catch species with differing temporal and spatial distributions (Hyrenbach *et al.* 2000, Blyth-Skyrme *et al.* 2006, Cadiou *et al.* 2009, Jennings 2009).

By using vessel monitoring data from long-line fleets it is possible to determine both the spatial and temporal distribution of fishing effort. If detailed information were available on the movements and distribution of a non-target or targeted by-catch species, such as blue, mako (*Isurus oxyrinchus*) or silky sharks (*Carchirhinus falciformis*), then it would be possible to investigate spatial and temporal 'hotspots' of interaction between the fleet and the sharks under different fisheries management scenarios. Unfortunately, detailed information on the individual movements of sharks in the form of tracks recorded by animal-attached electronic tags, is available for only a few individuals (around 50 at the current time) and only for short durations (i.e. months rather than years). It is therefore difficult to determine what the impact of different fisheries control measures might be on by-catch species. Ultimately, this could result in marine protected areas (MPAs) being established in locations where interactions between fishers and the protected species are already low, causing unnecessary and unhelpful reductions in fishing activity without commensurate reductions in fishing pressure to the focal species of concern. To investigate the effect mitigation measures might have on by-catch it is possible instead to use a modelled prey population. Several modelling studies have been used to investigate the design of MPAs, either for particular species such as sand eels (*Ammodytes marinus*) (Christensen *et al.* 2009) or Mediterranean hake (*Merluccius merluccius*) (Apostolaki *et al.* 2002), where population dynamics models are combined with fisheries models to determine the effect reduced fishing pressure would have on the populations. Other studies have used models to consider the effect of fishing effort displacement (Greenstreet *et al.* 2009). In this chapter a simulation model was used to generate a modelled prey field which was combined with VMS-derived fishing vessel movements in a grid occupancy analysis to

investigate the effects that various by-catch mitigation measures could have on the risk posed to the by-catch species by a long-line fishing fleet.

Using movement patterns of blue sharks determined from recent electronic tagging studies in the North Atlantic, together with some general thermal tolerance characteristics of blue shark (Queiroz *et al.* 2012), it was possible to simulate the annual movements of a generalised free-ranging pelagic predator and to generate from these movements a simulated 'prey' field available to the fishing fleet. This prey field was then used to investigate the spatio-temporal interactions between the prey and the fishing fleet. While these modelled predators do not reflect all the details of the complex large-scale movements and migrations of real blue sharks, they do provide a useful probe with which to explore the distribution of fishing effort and allow general conclusions about interactions between the fleet and the prey to be drawn. The prey field for this study was created by simulating individual, generic, open-ocean predators which moved in response to a daily map of sea surface temperature (SST) based on a thermal preference of 16 to 23°C. The simulation program used to generate the tracks is described in full in Appendix H. For each analysis 1000 simulated shark tracks were randomly selected from a pool of 20,000 tracks.

The impact of a fishing fleet, or of a vessel within the fleet, could have been estimated from the number of days spent fishing each year. However, this simple metric does not take into account the spatial distribution of the fishing effort nor, importantly, how that effort is distributed in relation to highly mobile, free-ranging prey species. The Spanish and Portuguese long-line fishing fleets primarily target swordfish, so it would be expected that the spatial distribution of the fishing effort should closely match that of the migratory patterns of the swordfish. However, given the differing thermal preferences of blue sharks, and the resulting differences in distribution, it is expected that the impact of the fishery, and of changes to the fleet, will be different for this by-catch species.

7.2   Methods

7.2.1   Simulated sharks

The shark simulation program is described in full in Appendix H, but, briefly, an individual shark movement path, comprising one location per day, is constructed as a random walk throughout the study area. Move step-lengths are drawn from a distribution derived from the movements of satellite tracked blue sharks (Queiroz *et al.* 2012). Turn angles are drawn from a uniform distribution, but are modified in order to constrain the shark to sea surface temperatures within a tolerance of 16 to 23°C. The simple method used to implement this constraint was for the shark to have an increased tendency to head south when surface waters were too cold and north when too warm, based on daily interpolated SST maps. Move–steps were halted if land was encountered. Each shark path therefore comprised 366 locations with an overall north south seasonal migration being evident.

7.2.2   The 3D grid occupancy analysis program

The 3D Grid Occupancy analysis quantifies the shared space use of a fishing fleet (e.g. long-liners) and pelagic fish (e.g. blue sharks) over time in the north east Atlantic. Shared space use is determined by calculating occupancy of cells within a 2D grid covering the study area, with grid cell dimensions equating to approximately 1 degree, for each day analysed. Two separate levels of analysis can be performed, referred to as 2D or 3D. The 2D grid occupancy analysis focuses on shared space use averaged over the specified time period while the 3D grid occupancy analysis generates measures for each day within the time period. The study area is situated in the north east Atlantic from 20 - 55°N and 0 - 35°W, encompassing the Azores islands, Canary Islands, Madeira and the coasts of north west Africa, the Iberian peninsula, southern Ireland and south west England. The grid cell dimensions of one degree in the Plate Carrée projection used (111.319km) results in a 2D grid of 35x35 cells.

Boat VMS data is imported into the analysis program from time series of locations that were previously converted from latitude and longitude to X, Y coordinates in metres using a simple Plate Carrée projection. After the conversion two filters were applied: (i) a maximum fishing speed, set to 5ms^{-1} and (ii) a maximum time interval between points, set to 12h, so that travel between fishing locations could be ignored.

Consequently, the converted track comprises a series of points where each point represents a day when fishing occurred, that is when a baited long-line of hooks was deployed and actively fished.

Shark tracks were imported in the same way as boat tracks but no filters were applied as the sharks were always considered to be present, whereas boats might be present, but not be fishing.

7.2.3   2D Analysis

The 2D analysis output comprises occupancy values for each grid cell for combined (boats plus sharks), boats only, sharks only or shared (simultaneous boats and sharks). The 2D analysis can be run over a specified date range, which defaults to the earliest start date of any imported track to the latest end date. Taking the boat-only analysis as an example, the analysis proceeds by mapping all points for every boat track onto the 2D grid and maintaining counts of the number of boats in each grid cell. The same process is used for the shark-only analysis and the combined analysis simply sums the boat and shark values together. The shared occupancy analysis processes all boat and shark tracks then calculates a metric of shared occupancy for each grid cell which is simply Number of Boats * Number of Sharks.

7.2.4   3D Analysis

The output of the 3D analysis comprises a measure of shared space use (an overlap coefficient) for each day and, for each grid cell, a sum of the number of days for which shared occupancy (i.e. the presence of both boats and sharks) was recorded. The analysis also calculates, for each day, the numbers of shared cells, boat-only cells and shark-only cells; the maximum number of boats or sharks in a single grid cell (maximum occupancy), the number of boats fishing, and a fisheries impact factor calculated from the overlap coefficient divided by the number of boats fishing on that day. For each boat the number of days fishing is calculated, together with the number of days where the boat shares a cell with a shark (termed *days of threat*), although this figure is not currently used. For each shark the number of days where the shark shares a cell with a boat is calculated (termed *days at risk*). It should be noted that as the

measure of days at risk is based on the interactions with individual sharks, this figure can exceed the number of days fishing.

For the 3D analysis, as with the 2D analysis, a date range can be specified which defaults to the earliest start date of any imported track to the latest end date. For each day of the analysis, each boat track is examined to determine whether a point exists for that date. If so, then the grid coordinates are calculated from the X, Y coordinated and the grid-cell boat count is updated. Given the scale of the long lining operation, with 100km lines, it is only reasonable to consider one grid cell per day's fishing. Once all boat tracks have been processed the shark tracks are then processed in the same way with interpolated grid cells updated with occupancy and counts made of cells containing both boats and sharks (days at risk). Once all boats and shark tracks have been processed the 2D array of grid cells is analysed to derive the measures of days of threat, maximum occupancy and boats fishing etc. From the shared occupancy statistics for all grid cells a coefficient of overlap (*O*) is then calculated for that day using the equation derived by Horn (1966) and modified by Rijnsdorp *et al.* (1998):

$$O = 2 \sum_{j} \left(P_{bj} P_{sj} \right) \bigg/ \left(\sum_{j} P_{bj}^2 + \sum_{j} P_{sj}^2 \right)$$

where P_{bj} = Proportion of boats in grid cell j, P_{sj} = Proportion of sharks in grid cell j.

The analysis was repeated for each day in the specified period and daily overlap coefficients were accumulated for each grid cell to generate a 2D summary.

A fisheries impact factor was calculated from the two metrics of boats fishing per day and the overlap coefficient. The impact factor is a positive value when the overlap coefficient is higher than would be expected for a given number of boats fishing and is negative when the overlap coefficient is lower than expected. To calculate the factor an adjusted overlap coefficient (O_a) was first calculated to match the same range as the boats fishing values (by multiplying *O* by Max(boats fishing) / Max(*O*)). The factor is then calculated as O_a − Boats fishing, for each day. In the graphs shown below the fisheries impact factor is shown as a 7-day running mean in order to smooth the line

To provide some baseline and control data the 2D and 3D analysis was first performed for the full fleets for the full year, and then a seasonal analysis was performed for each quarter Q1 to Q4 representing the months 1-3, 4-6, 7-9 and 10-12.

7.2.5 Fleet composition analysis

To investigate the impact of changes to the fleet composition, boats were ordered by the number of days fishing and divided into 10 percentiles such that each of the ten groups represented approximately the same number of days fishing (as accurately as possible given that exact percentiles cannot be achieved given the discrete nature of the boats involved). The upper percentiles therefore had fewer, busier boats while the lower percentiles comprised many less busy boats. The advantage of dividing the fleet in this way is that for each analysis the fishing pressure, in terms of days fishing, is approximately equal; results are in any case presented as a metric of fishing pressure per day fishing. Dividing the fleet in this way places the larger, more commercial vessels in the upper percentiles and smaller, artisanal boats, in the lower percentiles, allowing some investigation into fleet structure and the impact of different sectors despite having no information about the actual vessels. A summary of the composition of the ten groups for each fleet is shown below in Figure 115 and Figure 116; full details can be seen in Tables E1-4. It can be seen that while each group had approximately 10% of the total days fishing for the fleet, the number of boats in the lower groups was much higher than in the upper groups. The smaller number of boats in the Portuguese fleet makes the division into groups more difficult than with the Spanish fleet. However, as the analysis metric was risk per day fishing, the results were not unduly affected. The 2D and 3D Grid occupancy analysis was repeated having imported just the boats from one of the ten groups at a time. The results from the full fleet analysis were used as a control.
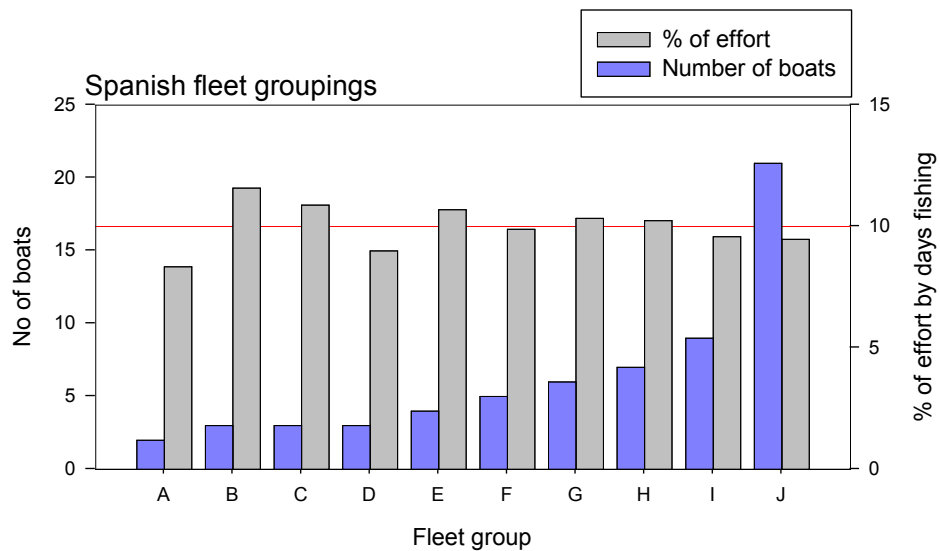
Figure 115: Spanish fleet groupings
Each group represents about 10% of the overall fishing effort, in terms of days fishing. Group A comprises the busiest boats (based on the number of days fishing per year), group H the least busy (see text). Grey bars show percentage effort in terms of number of days fishing for each of the groups; blue bars show the number of boats in each group. The red line indicates the target effort of 10%. All groups represent a similar fishing effort.
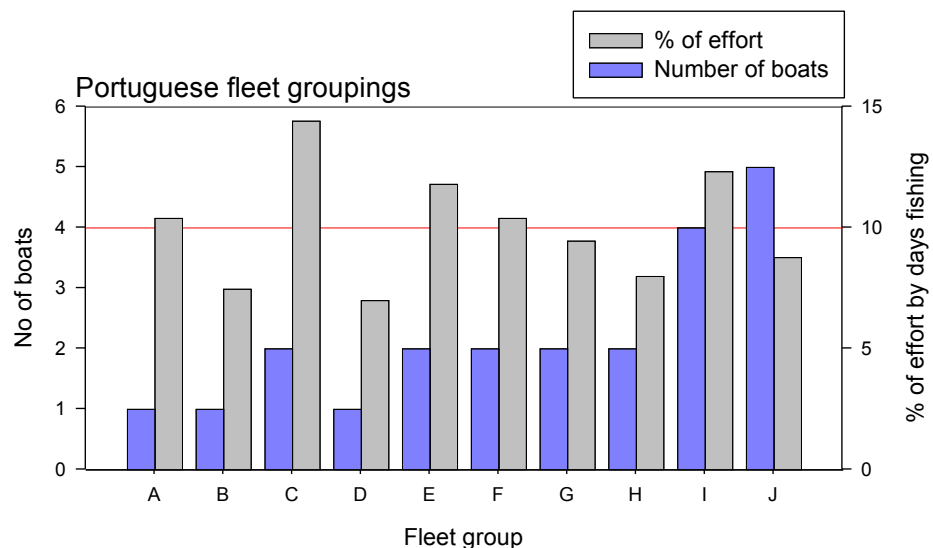
Figure 116: Portuguese fleet groupings
Grey bars show percentage effort in terms of number of days fishing for each of the groups; blue bars show the number of boats in each group. The red line indicates the target effort of 10%. With fewer boats overall the Portuguese fleet cannot be divided into such equal groupings as the Spanish fleet.

7.2.6   Marine protected areas

To investigate the effect that high seas marine protected areas (MPAs) would have on the threat posed to the by-catch species, MPAs were implemented in this study as no-take zones for only the by-catch species. Doing so allowed the VMS boat tracks to be used without alteration, as the boats would simply continue along the recorded track but with no days fishing and no interactions recorded while the vessel was within the bounds of an MPA. The restriction on retaining sharks in the catch from within the

MPAs is therefore in force for the by-catch rather than the target species and it can be considered that only the target species are retained, all others being released. Implementing MPAs in this way also removes the complications involved with the relocation of fishing effort which has been found to occur around MPAs where all fishing is banned with fishing activity concentrated on the borders of the MPA (Murawski *et al.* 2005, Forcada *et al.* 2010). Relocation of effort is clearly difficult to predict as skippers might opt to travel further afield to other grounds or to change to a different target species. Furthermore, in this study it was more important that the VMS tracks be followed accurately.

For this initial study three MPAs were defined and were placed in areas according to the hotspots of fishing pressure identified for the two fleets. The areas were West Africa, Iberian Peninsula and Goban Spur; W. Africa and the Goban Spur were selected for the Spanish fleet and the Iberian Peninsula for the Portuguese fleet. The details of all areas are given in Table E5 and are illustrated below in Figure 117 where the overlap with the fishing hotspots can be seen.

The values calculated for days of risk, days fishing and risk per day fishing refer to the entire study area, with whatever MPA is in force effectively removed and are therefore a measure of the effect the MPA has on the overall fleet fishing pressure and potential risk.
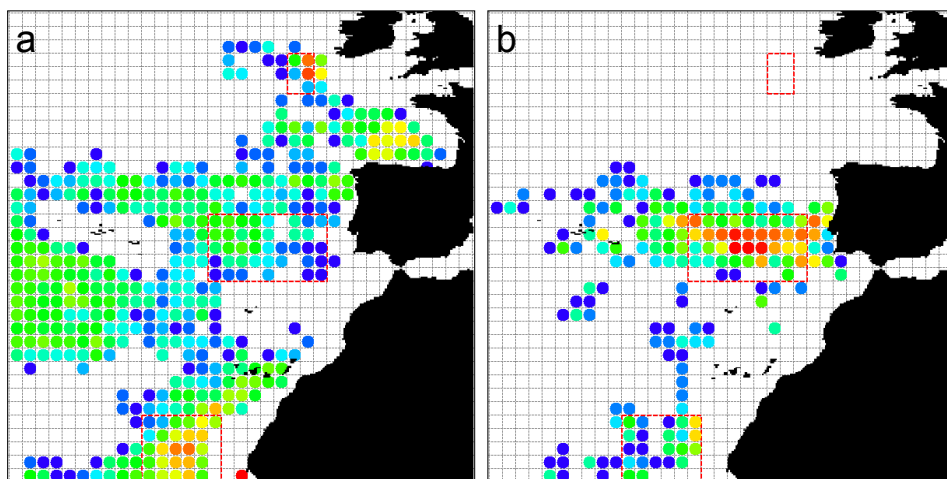
Figure 117: MPAs overlaid on the spatial distribution of fishing effort
a Spanish fleet; b Portuguese fleet. Warmer colours represent greater fishing effort. The MPAs (red line boxes) are, from top to bottom, Goban Spur, Iberian Peninsula and W. Africa.

7.2.7 Closed seasons

A further modification to fishing practices investigated here was the seasonal closure of the entire fleet. Such closures have been used, usually in restricted areas, to protect spawning populations (e.g. Moltschaniwskyj *et al.* 2002, Kraus *et al.* 2009). Here, the effect of closing the entire fishery on a seasonal basis was investigated by ignoring interactions occurring during a closed season. As with the spatial MPAs the protection was implemented as a no-take for the by-catch species, with the fishing vessels continuing along the recorded paths. As before, seasons were defined simply as Q1 to Q4 representing the months 1-3, 4-6, 7-9 and 10-12.

1.1.1.1 Null sharks

For the fleet manipulation investigations the entire fleet acts as a suitable control with which to compare the fleet group results. For the MPA analysis one control was provided by having no MPA, however, a further control was provided by using null sharks. Null sharks are modelled virtual sharks as described above in section 7.2.1, but with no thermal preference and therefore no seasonal migration of habitat preference. These sharks were used to generate a prey field in the same way as the other modelled sharks by selecting 1000 at random from a pool of 20,000 for each simulation run.

7.3 Results

7.3.1 Spanish fleet

1.1.1.2 Spatial distribution of fishing effort

The fishing effort was distributed across a large area of the N.E. Atlantic (Figure 118a & b) reaching north to the British Isles and South to the West coast of Africa. Coastal regions of Africa are avoided as are the Azores and the area around Madeira where Portugal operates an exclusive economic zone (EEZ). There was a clear difference in the spatial concentration of long-line vessel (hereafter boat) occupancy compared to the shared occupancy shown in Figure 118a,b & c. Fishing effort was concentrated off the coast of West Africa and in the Bay of Biscay, whereas shared occupancy was concentrated around the Canary Islands and between the West coast of Portugal and north of the Azores. Shared occupancy is a measure of the spatial overlap between the

fleet and the prey field but has no temporal component. There was also a difference between the distribution of fishing effort and the distribution of interactions as shown in the 3D analysis in Figure 118d. The 3D analysis represents a map of the spatio-temporal hotspots of interaction between the fleet and the by-catch prey field where hotter colours represent a greater number of daily occurrences of both boats and sharks within that grid cell. Figure 118d is effectively a map of the threat posed to the by-catch species by the fleet.

Figure 119 shows the results of the 3D grid occupancy analysis with plots of boats fishing per day, the overlap coefficient and the fisheries impact factor. The simple measure of boats fishing per day reveals clear peaks of activity in January, July and August with reduced activity in the remaining months especially in late May and June when there was a virtual cessation of fishing activity. The overlap coefficient shows peaks in the spring and winter months but during May through August shows very low values, indicating little interaction. Consequently, the fisheries impact factor was strongly negative during July, August and September, when interactions were low but days fishing was high, and only showed peaks around March and April. What is clear is that neither the overlap coefficient, nor the fisheries impact values, were simply correlated with the number of boats fishing.
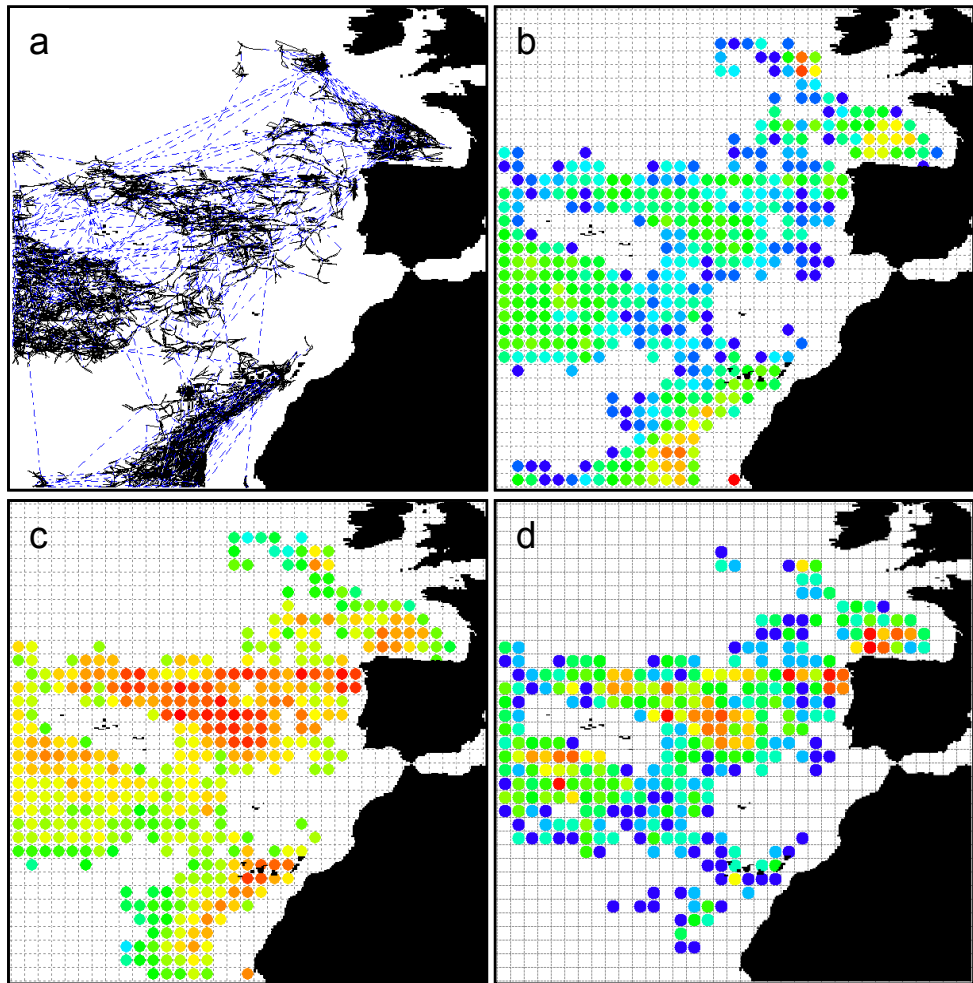
Figure 118: Spatial distribution of Spanish fishing effort.

a) Vessel tracks with fishing locations shown in black and relocations in blue; b) annual density of boats fishing by grid square (blue is low density, red is high); c) 2D grid occupancy analysis showing shared occupancy between the fleet and a simulated prey-field of 1k sharks; d) 3D grid occupancy analysis showing spatio-temporal hotspots of interaction between the fleet and a simulated prey field of 1k sharks.
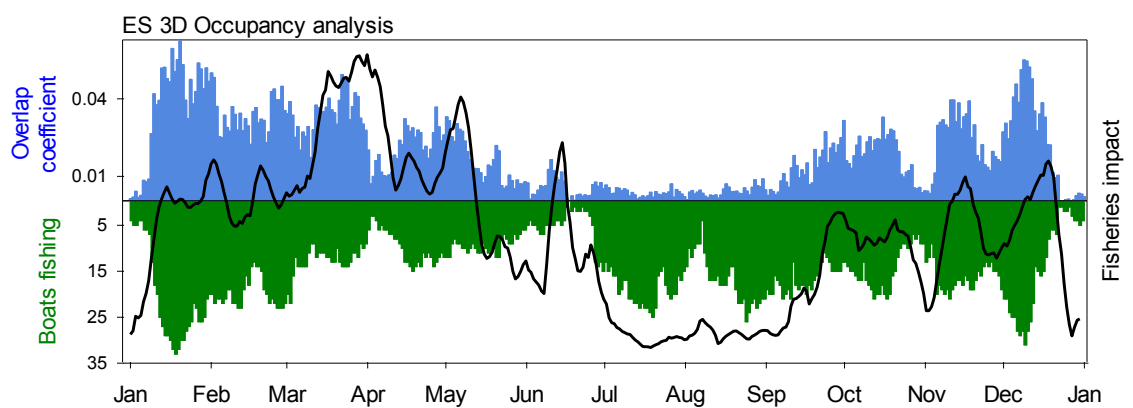
Figure 119: 3D Grid occupancy results for the Spanish fleet.

Upper blue bars are overlap coefficient; lower green bars, number of boats fishing; black line is fisheries impact factor (see Methods).

1.1.1.3 Seasonal spatial distribution of fishing effort

By restricting the grid occupancy analysis to three month intervals it was possible to reveal seasonal changes in the spatial distribution of fishing effort as shown in Figure 120. There were marked differences between the seasons; during Spring and Winter the fleet was generally fishing closer to the mainland, dispersing throughout Summer and Autumn to areas further afield. This dispersal resulted in lower overall fishing intensity, in the study area, during these months, as confirmed by the occupancy analysis shown in Figure 119.
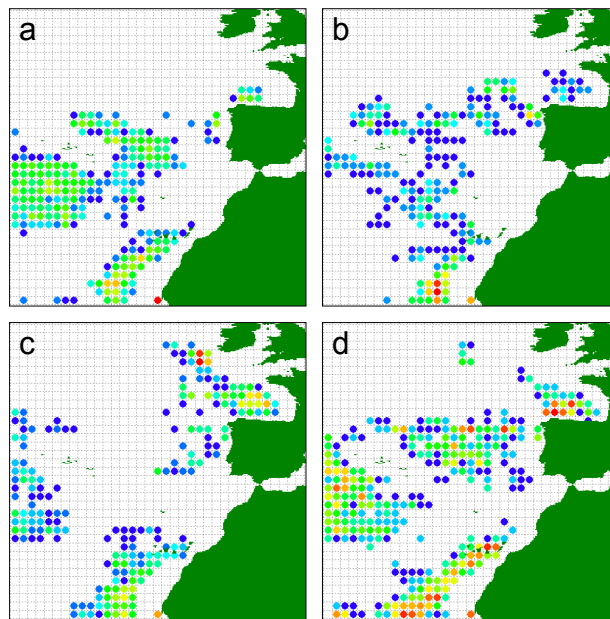
Figure 120: Seasonal spatial distribution of Spanish fishing effort
    2D analysis of boat occupancy for the four quarters Q1 to Q4 (where Q1 represents months 1 to 3 etc.) in figures a-d respectively. There were significant changes in the spatial distribution of fishing effort throughout the year with boats more dispersed in Q3.

1.1.1.4 Fleet manipulations

A 3D grid occupancy analysis was performed with each of the ten fleet groups and the total days at risk for all sharks was calculated for each analysis run as a measure of the potential impact on the by-catch species. The analysis was repeated 1000 times with a new set of 1000 randomly selected modelled sharks from the pool of 20k sharks. A summary of the results is shown in Figure 121 and Figure 122. There were clear differences in days at risk between some groups with three sub-groups being apparent; Groups A, H and J had the lowest impact, followed by all other groups except D which had an impact factor of 2.03, almost twice that of the next largest group, I (Figure 121). The box plot shown in Figure 122 reveals clear separation

between the fleet groups. The results failed a Shapiro-Wilk normality test (Table E6), therefore a one-way ANOVA on ranks was performed (Kruskal-Wallis). Differences between the groups were significant at $p < 0.001$ (Table E7) and most pair wise differences were also significant at $p < 0.001$ (Tukey Test; Table E8). Only the pairs I-F, and G-C were not significantly different. It is interesting that the vessels representing group A, the busiest boats in the fleet in terms of days fishing per year, had the lowest days at risk. Figure 123, below, shows the vessel track for the group A vessels superimposed on a mean annual occupancy chart for the simulated prey-field. It can be seen that the vessels spent most time towards the southern limit of the range of the simulated sharks where encounters were less frequent. The same is true for the vessels in group H (Figure 124), the group with the next lowest impact. In comparison the vessels in group D, which had by far the greatest impact, shown in Figure 125, spent most time in areas where prey-field density was high so it is understandable that the 2D (i.e. boat) occupancy and the 3D (i.e. shared) occupancy distributions were very similar. Figure 126 shows the 3D grid occupancy analysis results for the vessels comprising group H, the group with the second lowest mean days at risk. Fishing activity for this group was limited to January, July through August and December and at all times the overlap coefficient was very low and consequently the fisheries impact factor was strongly negative, confirming the spatial mismatch between fleet group H and the prey field found above.
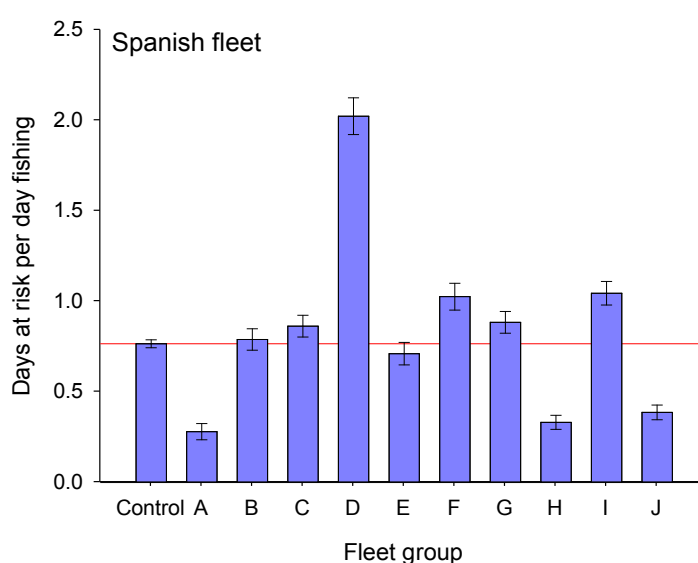
Figure 121: Mean days at risk per day fishing – Spanish Fleet

Red line shows control. The group with the busiest boats was, unexpectedly, the group with the lowest number of days of risk to the by-catch sharks. Error bars are 10th and 90th percentiles.
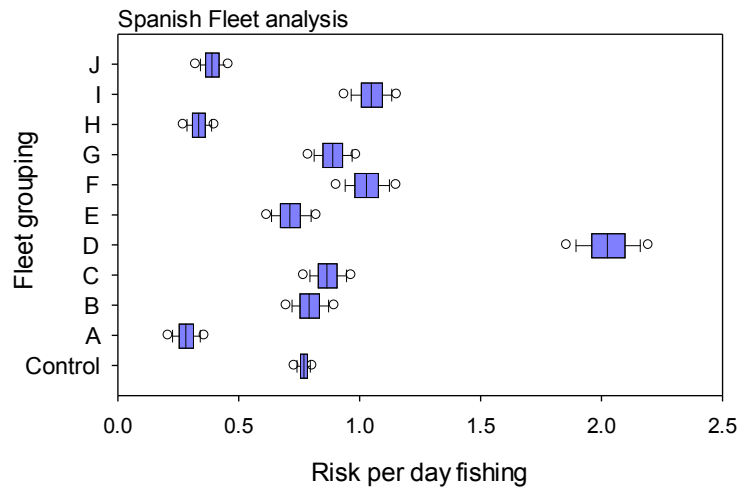
Figure 122: Spanish fleet group analysis

The box plot reveals a clear separation between the fleet groups. Three groupings are evident, with group D being significantly different from the rest.
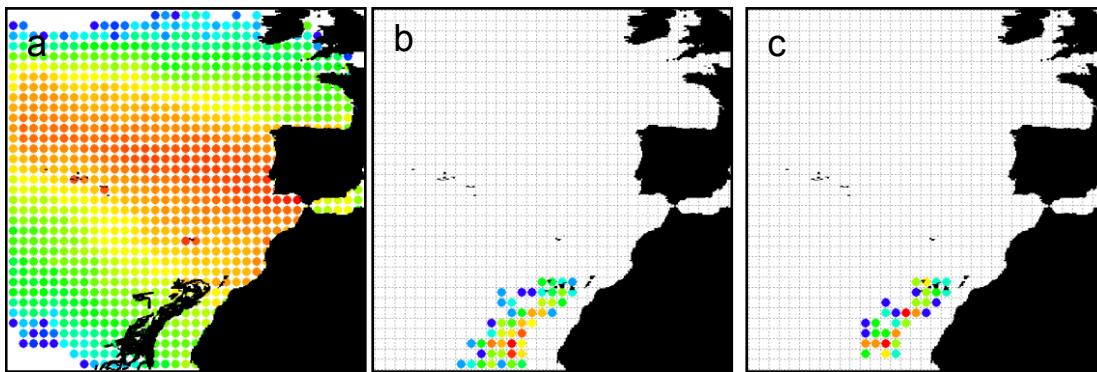
Figure 123: Occupancy for the Spanish vessels representing group A.

a) Mean annual occupancy of the simulated prey-field with superimposed vessel track; b) 2D (boat) occupancy and c) 3D (shared) occupancy. This vessel spent most time towards the southern limit of the range of the simulated prey-field where encounters are less frequent.
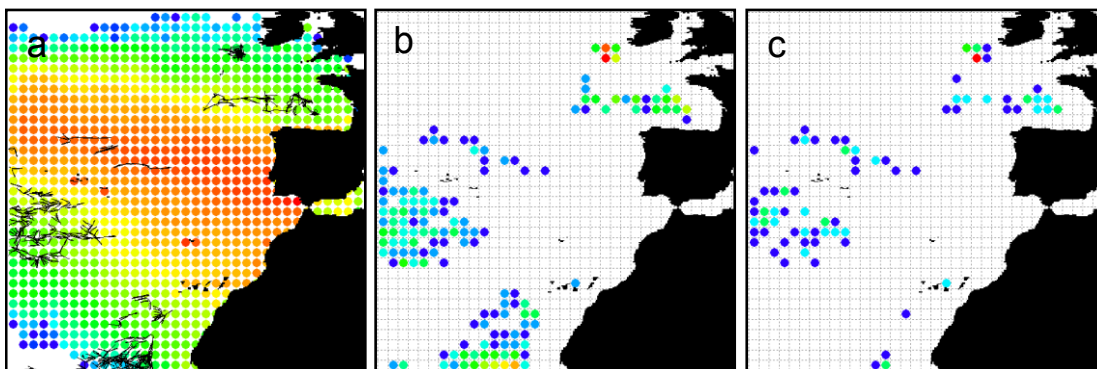
Figure 124: Occupancy for the Spanish vessels in group H.

a) Mean annual occupancy of the simulated prey-field with superimposed vessel tracks; b) 2D (boat) occupancy and c) 3D (shared) occupancy. These vessels spent most time towards the limits of the range of the simulated prey-field where encounters were less frequent; resulting in differences between the 2D and 3D occupancy patterns.

220
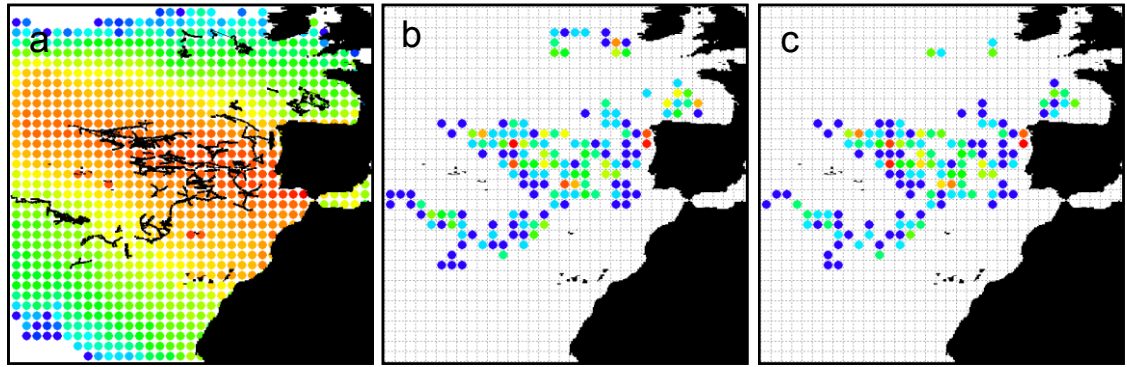
Figure 125: Occupancy for the Spanish vessels in group D.
a) Mean annual occupancy of the simulated prey-field with superimposed vessel tracks; b) 2D (boat) occupancy and c) 3D (shared) occupancy. These vessels spent most time towards the centre of the range of the simulated prey-field where encounters were more frequent and consequently the 2D and 3D occupancy distributions are almost identical.
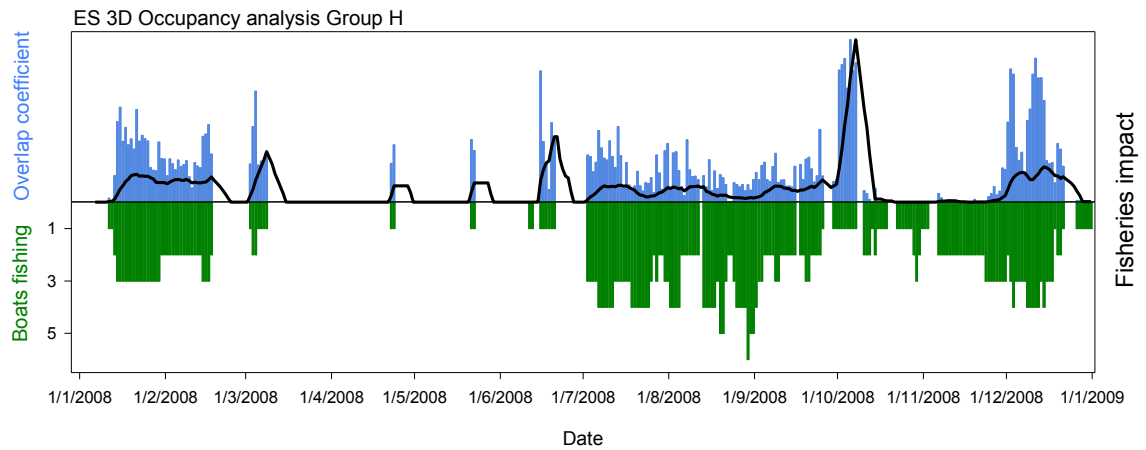
Figure 126: 3D Occupancy results for the Spanish vessels in Group H.
Upper blue bars are overlap coefficient; lower green bars, number of boats fishing; black line is fisheries impact factor (see Methods).

7.3.2   Portuguese fleet

1.1.1.5   Spatial distribution of fishing effort

The Portuguese fishing effort was concentrated in the area between the west coast of Portugal and the Azores, with some activity off the west coast of Africa but none as far north as the Bay of Biscay (Figure 127). As with the Spanish fleet the coastal regions directly off Africa were avoided. Unlike the Spanish fleet however, the 2D analysis revealed a strong coincidence of occupancy between the fleet and the simulated prey-field as shown in Figure 127b & c. The 3D analysis shown in Figure 127d is very similar to the 2D results, with the exception of the areas off the West coast of Africa where interactions were virtually absent.

Figure 128 shows the results of the 3D grid occupancy analysis with plots of boats fishing per day, the overlap coefficient and the fisheries impact factor. In the Portuguese fleet there was a clear monthly periodicity to the number of boats fishing with peaks mid-month for every month with activity. Activity was greatest during January to March and from mid-September to December, but during the summer months fishing activity was very low and the number of boats fishing was frequently zero. The overlap coefficient followed this trend more closely than with the Spanish fleet, suggesting a greater coincidence between the Portuguese fleet and the by-catch prey field. However, there were interesting differences in the fisheries impact that would not otherwise be revealed. Firstly, there was a marked dip in fisheries impact in mid-January and unexpected peaks in late July and late August. Clearly, as with the Spanish fleet, the dynamics of the interactions are more complex than suggested by the simple measures of the number of boats fishing and the overlap coefficient.
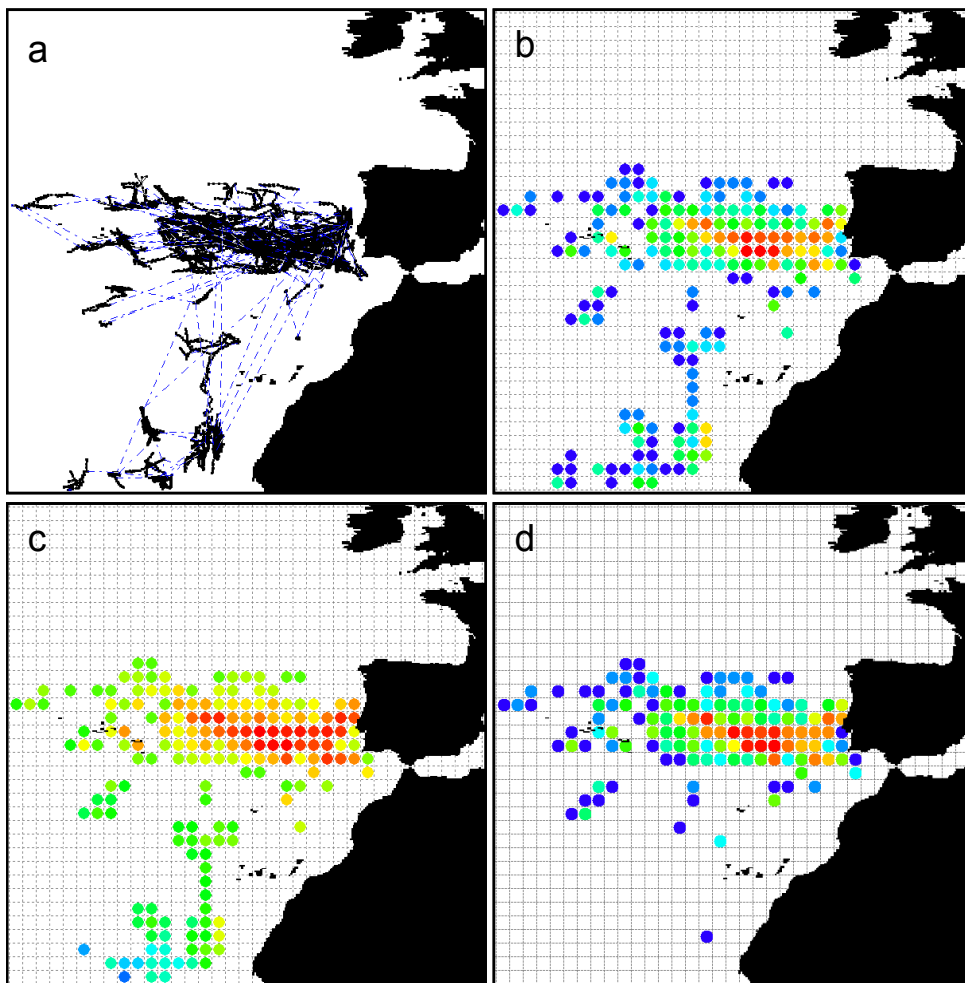
Figure 127: Spatial distribution of Portuguese fishing effort.
a) Vessel tracks with fishing locations shown in black and relocations in blue; b) annual density of boats fishing by grid square (blue is low density, red is high); c) 2D grid occupancy analysis showing shared

occupancy between the fleet and a simulated prey-field of 1k sharks; d) 3D grid occupancy analysis showing spatio-temporal hotspots of interaction between the fleet and a simulated prey field of 1k sharks
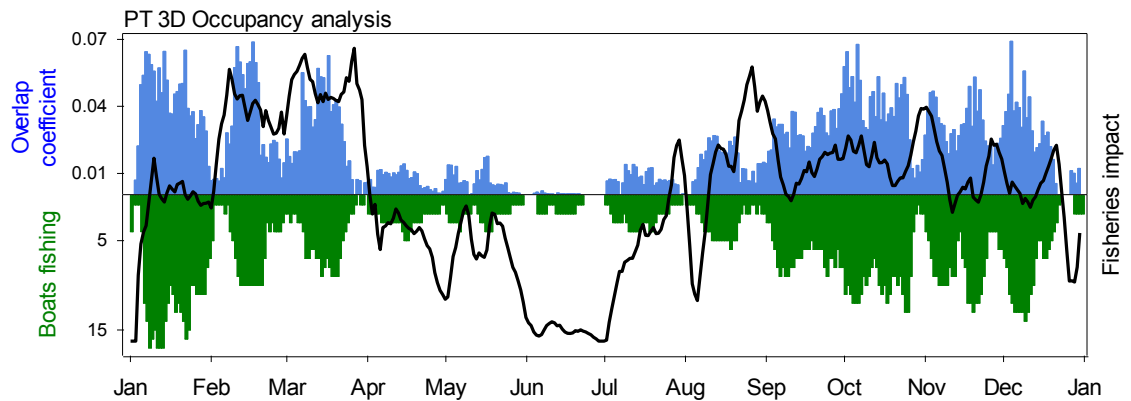
Figure 128: 3D Occupancy results for the Portuguese fleet.
Upper blue bars are overlap coefficient; lower green bars, number of boats fishing; black line is fisheries impact factor (see Methods).

1.1.1.6 Seasonal distribution of fishing effort

Seasonal changes in the spatial distribution of fishing effort for the Portuguese fleet are shown in Figure 129 and Figure 120. The differences between the seasons were similar to those found with the Spanish fleet; during Spring and Winter the fleet was generally fishing closer to the mainland, dispersing throughout Summer and Autumn to areas further afield resulting in lower overall fishing intensity in the study area during these months, in agreement with the occupancy analysis shown previously in Figure 128.
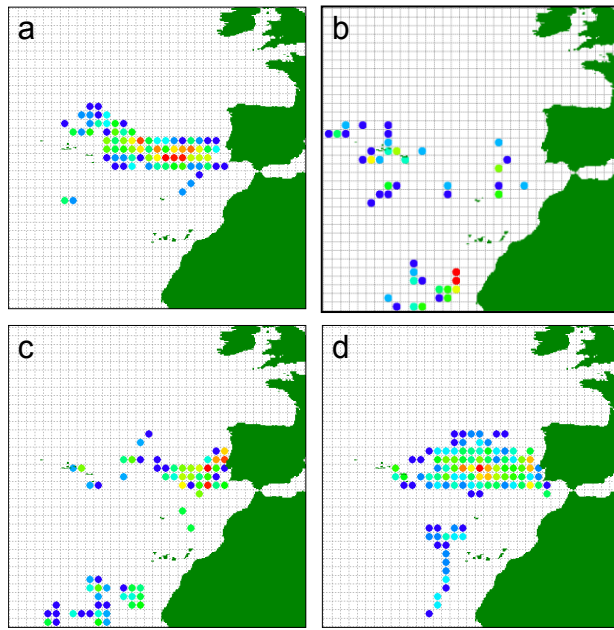
Figure 129: Seasonal spatial distribution of Portuguese fishing effort

2D analysis of boat occupancy for the four quarters Q1 to Q4 in figures a-d respectively. As with the Spanish fleet there are significant changes in the spatial distribution of fishing effort throughout the year.

1.1.1.7 Fleet manipulations

As with the Spanish fleet a 3D grid occupancy analysis was performed with each of the ten fleet groups and the total days at risk for all sharks was calculated for each analysis run as a measure of the potential impact on the by-catch species. A summary of the results is shown in Figure 130 and Figure 131. Differences between groups are less obvious than with the Spanish fleet but, interestingly, the busiest group (A) again had the lowest impact on the by-catch prey field. The box plot in Figure 131 shows less separation between the groups than was found with the Spanish fleet (Figure 122). Groups E to H are similar and had the highest impact with groups A and I having the lowest. In general the impact of the Portuguese fleet on the simulated shark population was much greater than that of the Spanish fleet (Portuguese mean 2.09, S.D. 0.01; Spanish mean 0.767, S.D. 0.022). Figure 132 shows vessel tracks from group A superimposed on the mean annual prey-field; there was considerable spatial overlap between the two which was unexpected given that group A has the lowest impact factor. In Figure 133 the overlap between vessels in group E (highest impact factor) and the prey-field is as expected for a high impact factor group with little discernable difference between the 2D and 3D occupancy. As with the Spanish fleet groups the results failed normality in some cases (Table E9) and therefore one-way ANOVA on ranks was performed (Kruskal-Wallis). Differences between the groups were significant

at $p < 0.001$ (Table E10) and nearly all pair wise differences were also significant at $p < 0.001$ (Tukey Test; Table E11). Only the pairs D-B, E-G and Control-I were not significantly different at $p < 0.001$.
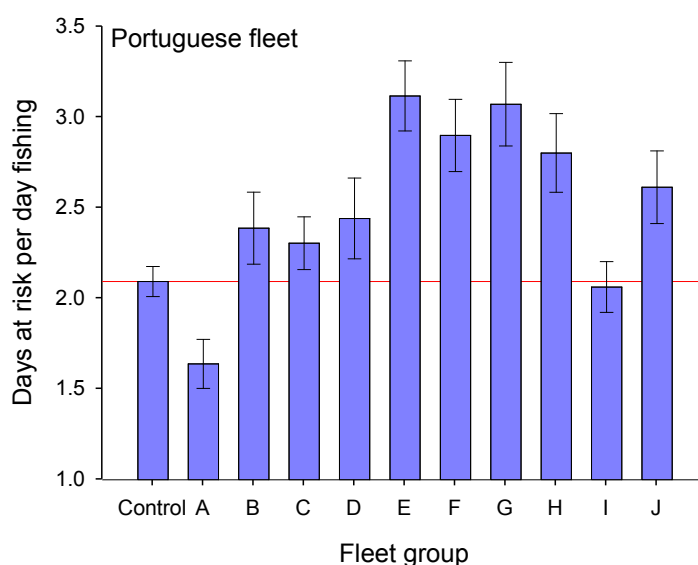
Figure 130: Mean days at risk per day fishing – Portuguese fleet.
Red line shows control. As with the Spanish fleet it was the group with the busiest boats that has the lowest impact. Error bars are 10th and 90th percentiles.
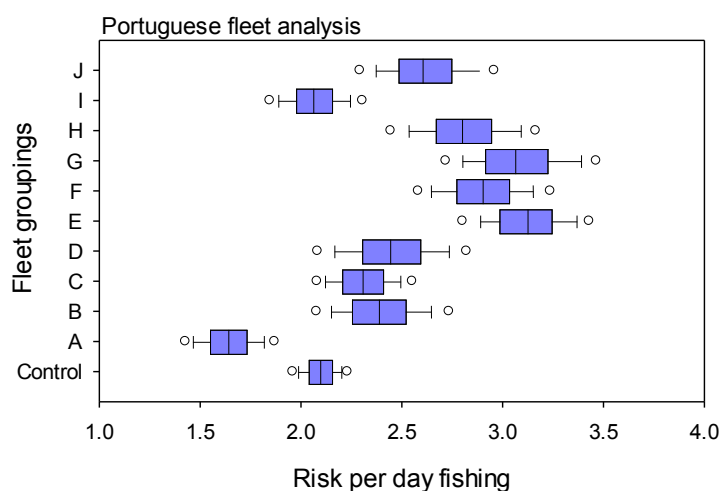
Figure 131: Portuguese fleet group analysis
There is more overlap between the groups with the Portuguese fleet than the Spanish fleet. Other than groups A and I all groups presented a greater threat than the control (all groups).
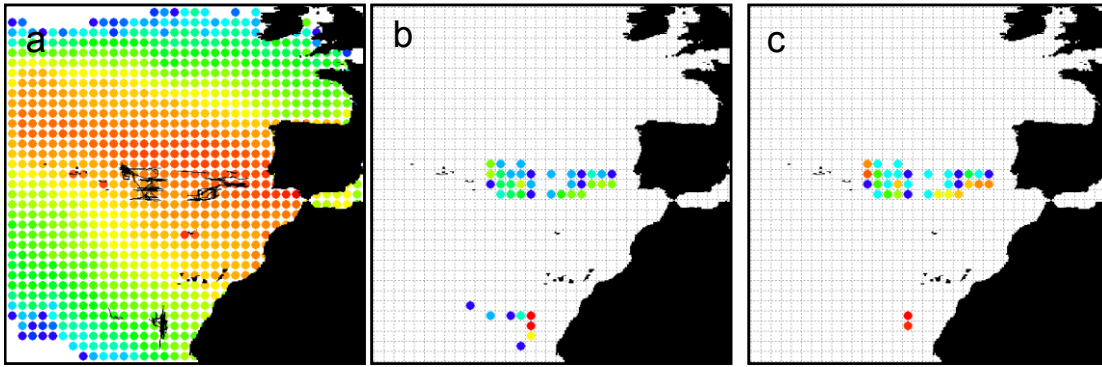
Figure 132: Occupancy for the Portuguese vessel representing group A.
a) Mean annual occupancy of the simulated prey-field with superimposed vessel track; b) 2D (boat) occupancy and c) 3D (shared) occupancy. The considerable overlap was unexpected given that group A has the lowest impact.
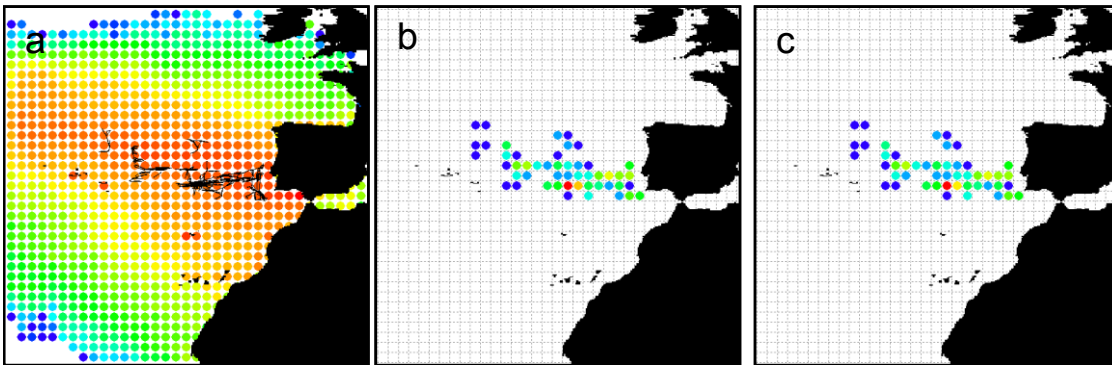
Figure 133: Occupancy for the Portuguese vessels in group E.
a) Mean annual occupancy of the simulated prey-field with superimposed vessel tracks; b) 2D (boat) occupancy and c) 3D (shared) occupancy. These vessels are spending most time towards the centre of the range of the simulated prey-field where encounters are more frequent and the 2D and 3D occupancy distributions are almost identical. Here the considerable overlap is as expected.
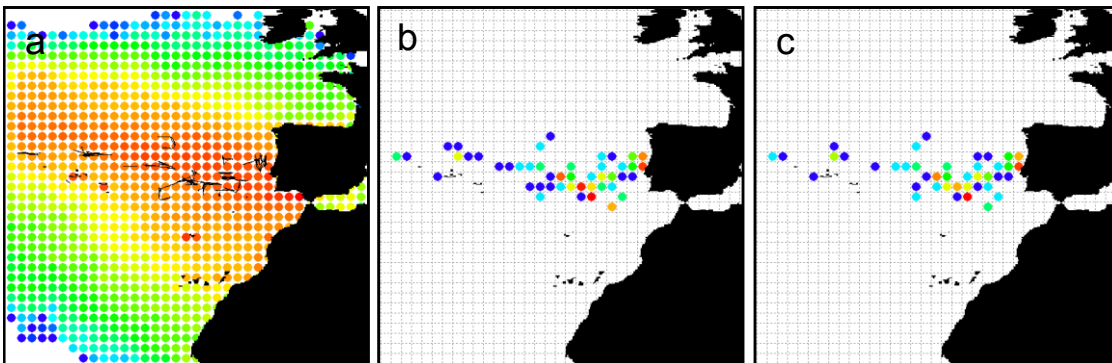
Figure 134: Occupancy for the Portuguese vessels in group J.
a) Mean annual occupancy of the simulated prey-field with superimposed vessel tracks; b) 2D (boat) occupancy and c) 3D (shared) occupancy. These vessels spent most time towards the centre of the range of the simulated prey-field where encounters were more frequent and the 2D and 3D occupancy distributions were very similar. Here the considerable overlap was as expected.

226
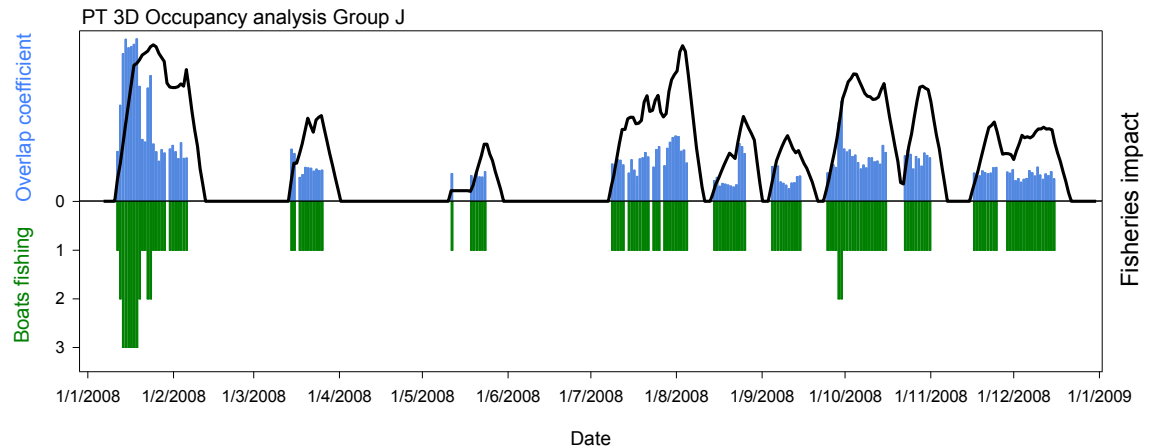
Figure 135: 3D Occupancy results for the Portuguese vessels in Group J.
Upper blue bars are overlap coefficient; lower green bars, number of boats fishing; black line is fisheries impact factor (see Methods). Group J comprises the boats with the fewest days fishing buts ranks 5th in terms of risk per day fishing

7.3.3   MPA analysis

1.1.1.8   Spanish fleet

The results of the MPA analysis with the Spanish fleet are shown in Figure 136 which shows days fishing, total days of risk and risk per day fishing for the control (i.e. no MPA in force), for each MPA and for the Iberian MPA with closed seasons in Q1 to Q4. The Iberian MPA considerably reduced risk per day (-16.68%) and days at risk (-20.93%) while having very little effect on days fishing, imposing a reduction of only -5.1%. Conversely, the West African MPA reduced days fishing from 5312 to 4237 (-20.23%) but produced only a small reduction in days at risk (-1.91%), thereby causing an increase in risk per day of 22.98%. These two results confirm that the area of greatest fishing pressure, where the W. African MPA was located, did not correspond to the area of maximum interaction between the boats and the sharks, which coincided instead with the Iberian MPA. Differences between all groups were significant at $p < 0.001$ (Kruskal-Wallis one-way ANOVA on Ranks; Table E12 and Table E13) except for Control vs Q2.

Figure 137 shows a box plot of the MPA results where the separation between the groups is clear. This figure also presents the results from the MPA analysis using the null shark population. Given that the null sharks have an even, non-seasonal distribution it was expected that fishing pressure would be equally evenly distributed

and that closure of any area would therefore make no difference to the risk per days fishing; each days fishing should carry the same risk and therefore removal of any days will not affect the average value. This is found to be true for all MPAs except for the Goban Spur where a slight increase in risk results.

1.1.1.9   Seasonal MPA closure

The Q1 closure of the Iberian MPA reduced days at risk by 11.14% and risk per day by 8.74%, almost as much as closure for the full year (reductions of 20.93% and 16.68% respectively). The Q2 closure had very little impact on the fleet, reducing days fishing from 5312 to 5304 (- 0.15%) and consequently had little impact on overall risk to the sharks, a reduction of only 0.52%, so the similarity to the control was as expected.

1.1.1.10 Within-MPA activity

To determine the activity that would normally have occurred within the MPA the 3D occupancy analysis was re-run with interactions within the MPA, rather than outside, being counted resulting in the plots shown in Figure 138. It can be seen that activity within some of the MPAs was distinctly seasonal. Fishing activity in the W. African MPA can be seen to have occurred throughout the year; however, significant overlap with the by-catch prey field only occurred during the first half of the year when there was a positive fisheries impact factor. During the rest of the year, although the number of boats fishing was similar, there is very little overlap and a low impact factor. Closing this MPA for the first half of the year was expected to reduce overall risk, as both the fishing effort and interactions would be reduced; however in the second half of the year only the fishing effort would be reduced with no concomitant reduction in interactions, leading to an increased overall risk per day fishing. This, therefore, confirms the results shown in Figure 136, where overall closure of the W. African MPA did increase risk. In the Iberian MPA, fishing activity was seasonal only occurring during January and December; however, whenever boats were fishing there was considerable overlap with the by-catch prey field producing a very high impact factor at those times (few boats fishing but many interactions). Activity in the Goban Spur MPA was restricted to just the months of August and September with interactions peaking in mid September. Interestingly however, during August and early September the

number of boats fishing was relatively high but the overlap was quite low; overlap peaked during late September when the number of boats fishing had dwindled to only two or three. Activity patterns in this small area over a short time frame were more complex than were expected.
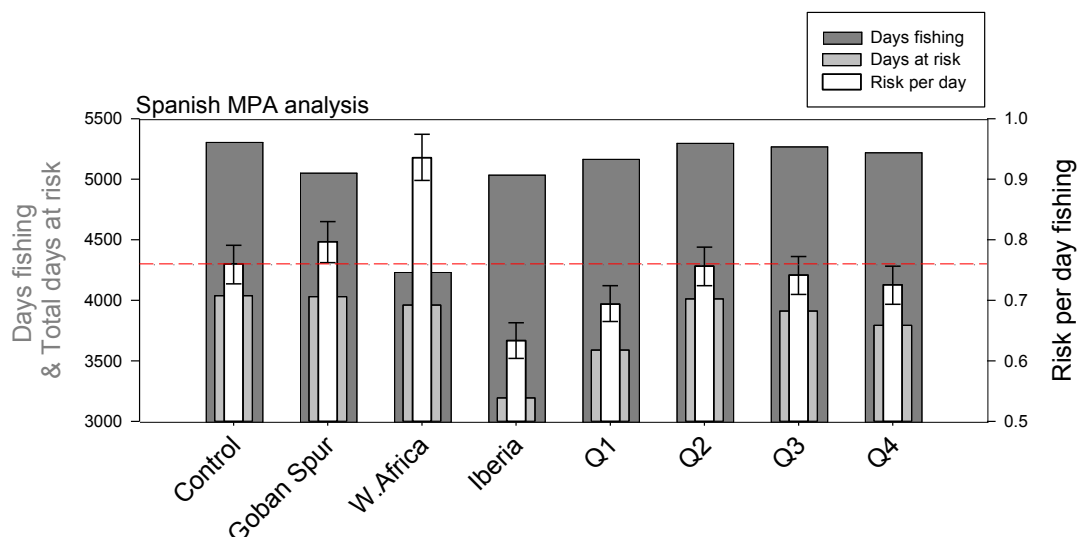
Figure 136: Spanish MPA results

The red dashed line indicates the risk per day for the control. Only the Iberian MPA significantly reduced risk per day. Q1 to Q4 show the effect of closing the Iberian MPA for each quarter of the year.
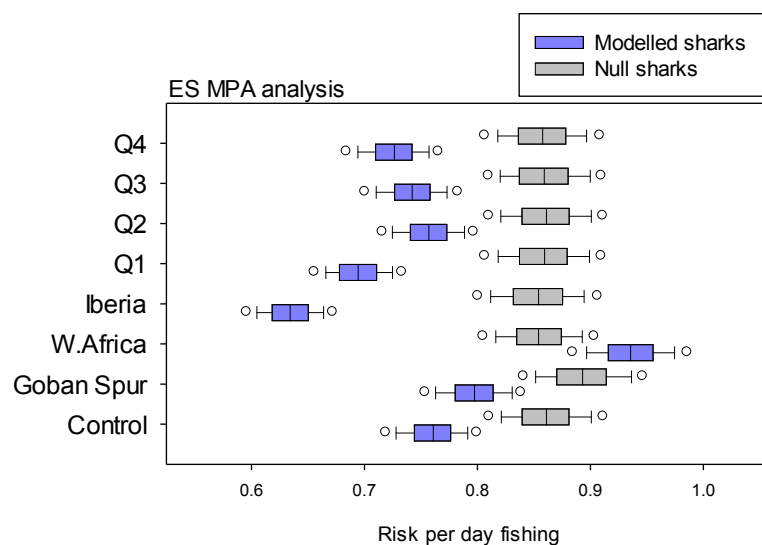
Figure 137: Box plot of Spanish MPA results

The plot shows risk per day fishing for the three MPAs and for the seasonal closure of the Iberian MPA. Boxes show median, 25th and 75th percentiles. Whiskers are 5th and 95th percentiles, outliers shown as circles. As expected the MPAs had no effect with the null sharks, except for the Goban Spur where the high concentration of boats within a few grid cells skews the results.
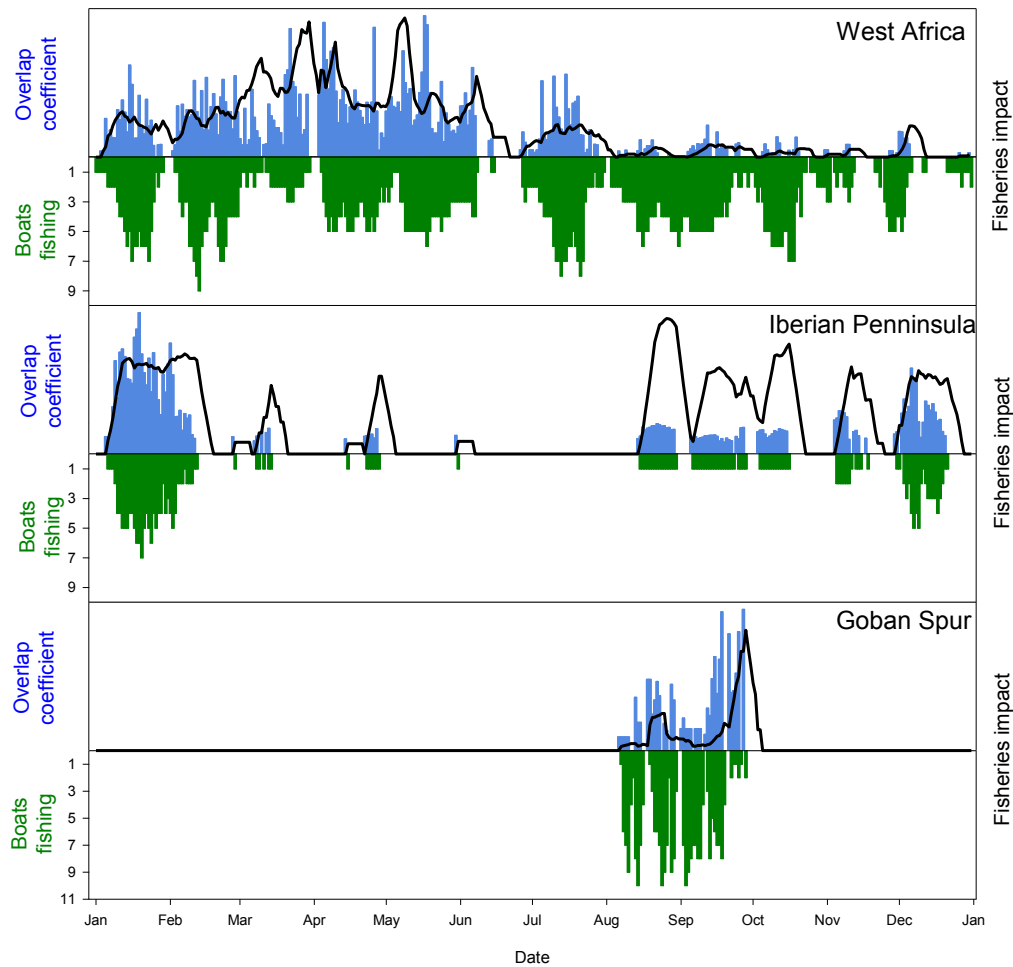
Figure 138: Spanish 3D MPA occupancy results
Results of the 3D grid occupancy analysis for the areas enclosed by the MPAs described above. The seasonality of the fishing effort is clear. Blue bars overlap coefficient; green bars boats fishing; black line fisheries impact factor. Plots are top W. Africa; middle Iberian Peninsula; bottom Goban Spur.

1.1.1.11 Portuguese fleet

Results of the MPA analysis with the Portuguese fleet are shown in Figure 139. As expected the Goban Spur MPA had no effect on days fishing or days of risk and only the Iberian MPA had any significant effect. As with the Spanish fleet, closure of the W. African MPA reduced boats fishing, but being somewhat south of the range of the modelled sharks in the latter half of the year, did not similarly reduce interactions, leading to an overall increase in risk per day fishing. The Iberian MPA, as expected given the spatial coincidence with the Portuguese fishing hotspots, reduced both days fishing (by 56%) and days of risk (by 60%), giving a small but significant reduction in risk per day of 7.8% (differences significant at p < 0.001 Kruskal-Wallis One-way ANOVA on Ranks and all differences with the control significant at p < 0.05 except for Q2 and the

Goban Spur, Tukey Test; Table E14 and Table E15). The box plot in Figure 140 highlights the difference between the modelled and null sharks with the Portuguese fleet. Interactions were much less frequent with the null sharks showing that the spatiotemporal dynamics of the modelled sharks more closely matches those of the fleet.

1.1.1.12 Seasonal MPA closure

The Q1 closure of the Iberian MPA did not have the same effect as with the Spanish fleet, resulting in only a very small reduction in overall risk (1.44%), despite the Iberian MPA having a significant effect when closed for the year.

1.1.1.13 Within-MPA activity

Repeating the analysis with the focus inside rather than outside the MPA reveals interesting seasonal dynamics as shown in Figure 141. Activity in the West African MPA was concentrated from April to August and during most of that time there was significant overlap with the modelled sharks, resulting in a positive impact factor. Within the Iberian MPA the pattern was almost exactly opposite to the West African MPA with activity from January to March and from August to December. There was almost no activity during Q2 as confirmed by the results shown in Figure 139. This explains why the Q1 closure had little effect, as activity was fairly evenly spread through Q1, Q3 and Q4.
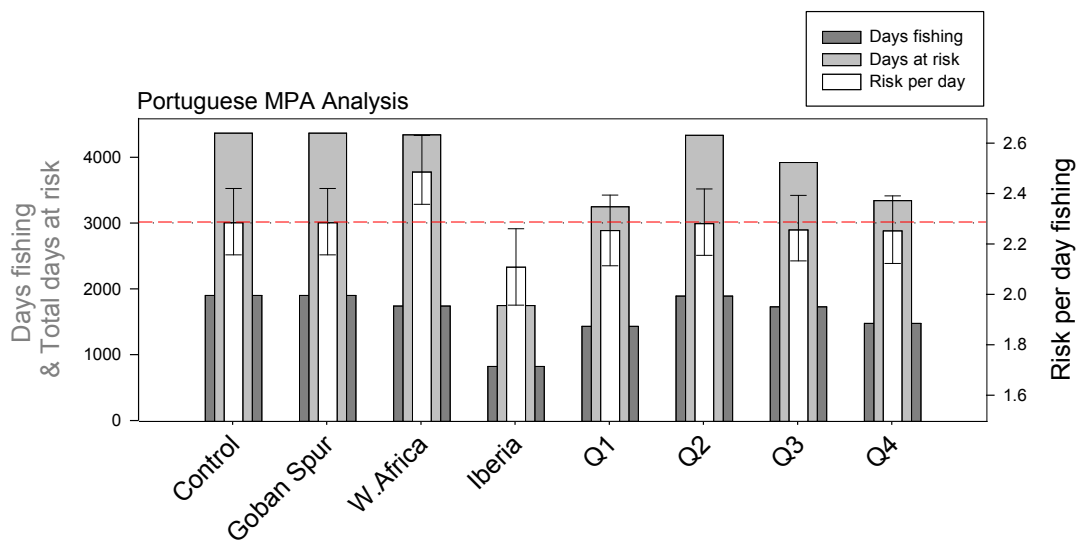
Figure 139: Portuguese MPA analysis
The red line indicates the risk per day for the control. Only the Iberian MPA significantly reduced risk per day.
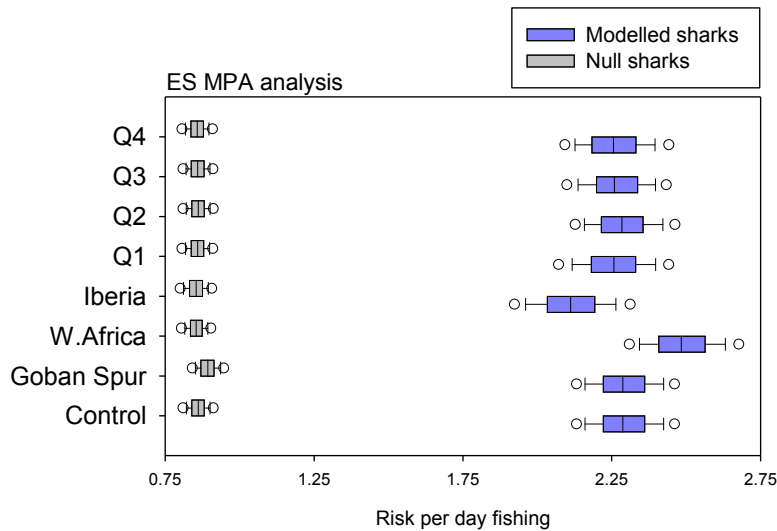
Figure 140: Box plot of Portuguese MPA results

The plot shows risk per day fishing for the three MPAs and for the seasonal closure of the Iberian MPA. Boxes show median, 25th and 75th percentiles. Whiskers are 5th and 95th percentiles, outliers shown as circles. There is a marked difference between the null shark and modelled shark results, emphasising the coincidence of occupancy between the Portuguese fleet and the modelled sharks.
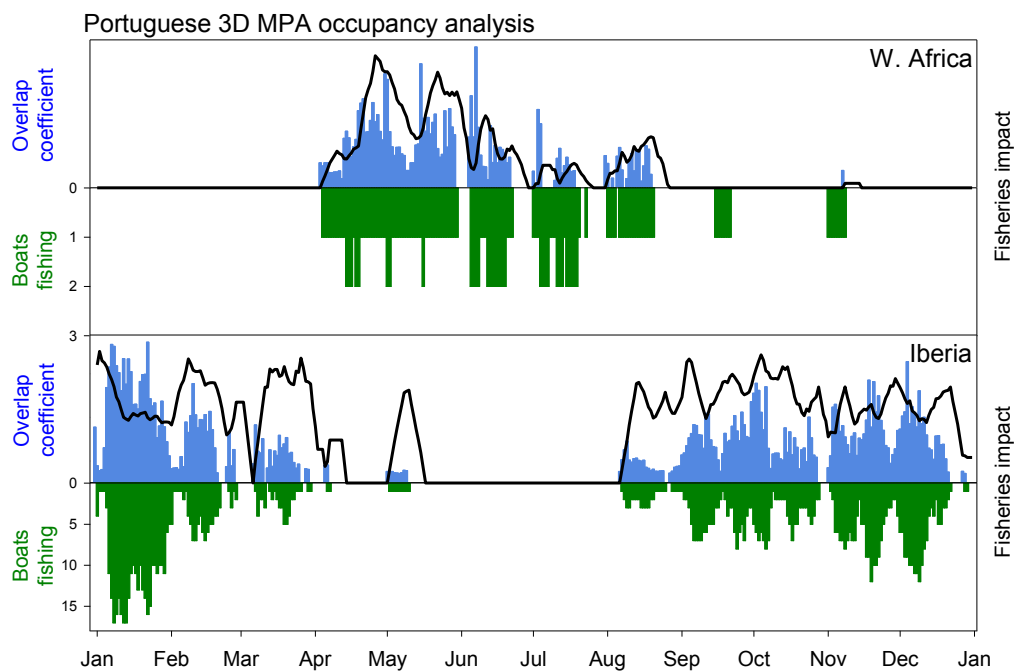
Figure 141: Portuguese 3D MPA occupancy analysis

Results of the 3D grid occupancy analysis for the areas enclosed by the MPAs described above. The seasonality of the fishing effort is clear. Blue bars overlap coefficient; green bars boats fishing; black lines fisheries impact factor. Plots are top W. Africa; bottom Iberian Peninsula. There is no activity in the Goban Spur MPA from the Portuguese fleet.

7.3.4 Closed season analysis

1.1.1.14 Spanish fleet

The results from the seasonal analysis are illustrated in Figure 142. All seasonal closures resulted in significant differences ($p < 0.001$, Kruskal-Wallis one-way ANOVA on Ranks, Table E16) and all pair wise comparisons were significant at $p < 0.05$ (Tukey test, Table E17). Q3 produced the greatest increase in risk (26%) and Q1 the greatest decrease (19%). Both closures produced a similar reduction in days fishing (34%), but as can be seen from the full fleet occupancy analysis (Figure 119), there was a greater degree of overlap in months January to March than in July to September where the fisheries impact factor was very low. Consequently, the Q3 closure reduced days fishing without reducing interactions, hence the increased risk per day fishing. In Q4 the reduction in days at risk was in line with the reduction in days fishing, hence the risk per day was almost the same as the control, suggesting that activity in Q4 was similar to the year as a whole.
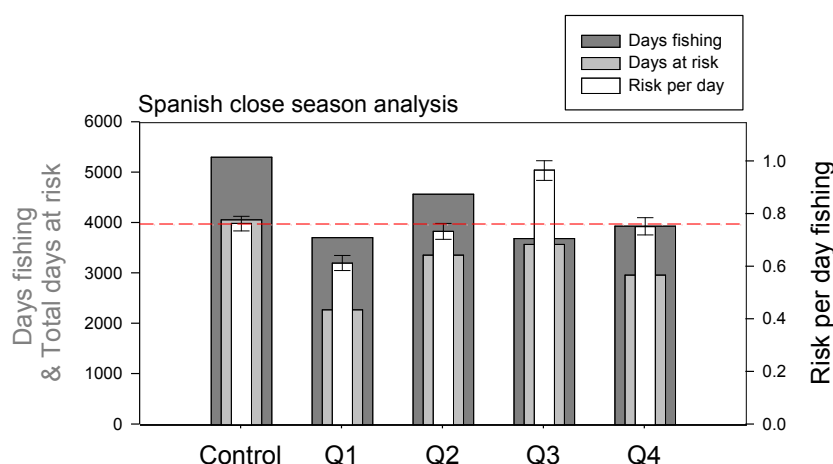
Figure 142: Spanish closed season results
> The red line indicates risk per day for the control. All seasonal closures result in significant changes to fishing effort and days of risk.

1.1.1.15 Portuguese fleet

The results from the seasonal analysis are illustrated in Figure 143. All seasonal closures resulted in significant differences ($p < 0.001$, Kruskal-Wallis one-way ANOVA on Ranks, Table E18) and all pair-wise comparisons were significant at $p < 0.05$ (Tukey test, Table E19). Q1 produced the greatest reduction in days at risk (43%), but as this was at the cost of a reduction of 34% in days fishing, the reduction in risk per day is relatively small (13%). Q4 produced the greatest decrease in days fishing (37%) but did

not reduce days at risk by the same amount (only 32%) so increases risk per day, as does Q2.
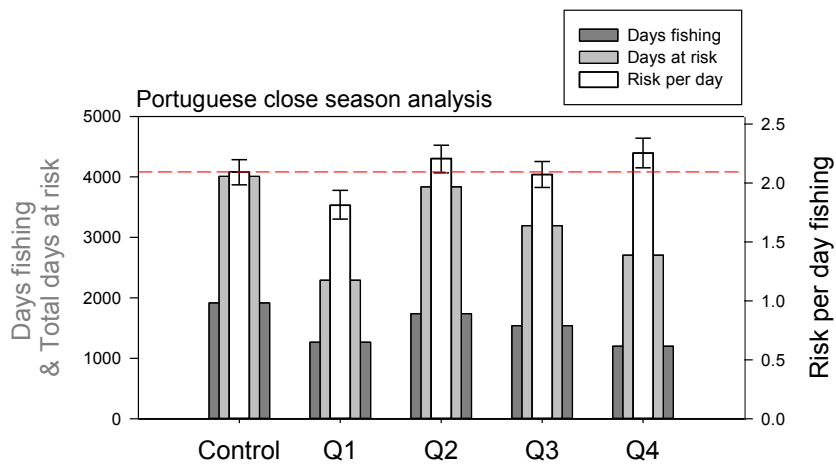
Figure 143: Portuguese closed season results

The red line indicates risk per day for the control. All seasonal closures result in significant changes to fishing effort and days of risk, however it is only Q1 that reduces risk per day.

7.4 Discussion

In this study a new approach to the analysis of the dynamics of interaction is presented which is able to take full advantage of both VMS and tagged shark data as it becomes available. To illustrate the methodology, and explore the consequences of some mitigation methods, a simulated prey-field is used, based on a generalised pelagic predator with thermal preferences similar to those recorded from blue sharks for which data is available from recent studies (Queiroz *et al.* 2012). Clearly, a simulated prey field such as this does not reflect the true distribution of sharks in the N.E Atlantic and in particular includes no knowledge of associations which are known to occur between sharks and either bathymetric features (e.g. seamounts), oceanic fronts or upwellings (Worm *et al.* 2003, Priede and Miller 2009, Lucifora *et al.* 2012, Queiroz *et al.* 2012) nor of behavioural patterns such as sex, size or life stage segregation (Mucientes *et al.* 2009, Vogler *et al.* 2011). The prey field does, however, exhibit seasonal dynamics, allowing the investigation of a more complex interaction between the fleet and the sharks.

The focus here has been to investigate how useful the grid occupancy analysis can be for determining the effectiveness of by-catch mitigation measures, considering specifically those of fleet reductions, marine protected areas (MPAs) and seasonal

closures. For the latter two scenarios it is only the by-catch that is prohibited, with the fishing vessels continuing to follow the VMS track, generally targeting swordfish.

7.4.1 Fleet reduction analysis

The analysis performed here to investigate the effect of changing the size or composition of the fishing fleet is hampered somewhat by the anonymity of the fishing vessels which made it impossible to determine the risk posed by specific classes of vessel. Instead, the simple measure of days fishing was used to classify the vessels into groups such that each group comprised vessels with progressively lower fishing extent. The results were unexpected: the busiest vessels from both fleets posed the lowest capture risk to the simulated shark population. It seems likely that these vessels were larger as they were travelling for longer and further afield, beyond the limits of the distribution of the simulated sharks. With both fleets there is no clear trend for the remaining vessel groups with the impact on the by-catch prey field being somewhat unpredictable. Without more information being made available regarding the vessel type, it is clear that it would be very difficult to design effective, economic, fleet reduction measures to protect the by-catch species.

7.4.2 Marine protected areas

Because the vessel tracks were determined from the VMS data it was not possible to study effects such as the displacement of fishing effort, which can lead to overfishing in other areas (Dinmore *et al.* 2003). Nor was it possible to investigate what effect the MPA might have on the protected populations within the area, or more complex effects such as spill-over of thriving populations to adjacent areas (Murawski *et al.* 2005).

The areas in this study used to investigate the potential effectiveness of high seas MPAs were selected simply on the basis of fishing intensity. The results emphasise that such a simple approach is likely to be unsuccessful for by-catch species, showing instead that it is the areas where interactions occur between the fleet and the by-caught fish that should be targeted for mitigation. Furthermore, it is shown that the timing of closures is also important; clearly there is little point closing an area to fishing at a time when either the fleet or the fish are absent. The results argue persuasively

for the need for adaptive management of any high seas MPAs that may be instituted in the area studied. What is important in this context is that the grid occupancy analysis is able to determine the effectiveness of a proposed MPA, allowing fishing interactions both inside and outside the MPA to be measured.

7.4.3   Seasonal closures

Seasonal closures could offer potential benefits in that they could be simpler to regulate and allow the fishing fleet to target other areas or species during the closure. The closure can be specifically targeted to protect pupping or mating aggregations, maximising the benefit. However, closure of the entire fishing fleet is too blunt an instrument because, although the Q1 closures do reduce risk per day to the by-catch species, there is also a significant reduction in days fishing and therefore likely to be a significant economic impact. The analysis performed here highlights the importance of timing closures to target times of maximum interaction and suggests that combining seasonal, or temporary, closures with MPAs could improve the performance of both protection measures. Temporary closure of Mexico's Economic Exclusion Zone (EEZ) to long-lining for striped marlin (*Kajikia audax*) was found to increase abundance by up to 22% (Jensen *et al.* 2010). However, this was a long term (4 year) closure of a large area (a 200 nautical mile EEZ); a subsequent, shorter closure of 2 years produced likely increases in abundance of around 12%. Further, striped marlin, while highly mobile, tend to have more restricted movements than other billfish species (Domeier 2006) which might have increased the efficacy of the MPA.

Overall, it is possible that an analysis such as presented here would lead to a better understanding of the dynamics of interaction between the fishing fleet and the by-catch species, helping to inform the placement and timing of high seas MPAs for highly migratory species such as pelagic sharks. Other studies have considered interactions in other ways, for example Tuck *et al*. (2011) combined data from The International Commission for the Conservation of Atlantic Tunas (ICCAT) on the number of hooks set in 5° grid squares with distribution data on 60 populations of seabirds, known to be at risk as long-line by-catch, (e.g. wandering (*Diomedes exulans*), black-browed (*Thalassarche melanophris*) and Atlantic yellow-nosed (*T. chlororhynchos*) albatrosses. Interactions were assessed as the product of fishing effort (i.e. hooks set) and

percentage distribution of the bird population within each grid square for each month of the study, concluding that the fishery had significant conservation implications for the birds. However, the VMS data used in the present study provides a much finer spatial and temporal resolution and therefore offers the potential for more accurate estimates of overlap. VMS data, from UK trawlers and scallop dredgers, was used by Stelzenmüller *et al.* (2008) to assess the distribution of fishing pressure on the marine landscape off the English and Welsh coasts. The study considered correlations between fishing effort and substrate or tide state, rather than with species distributions; however this information would help inform the siting of MPAs, in that areas of high fishing pressure could be targeted. Fishing pressure is very likely to be highest in areas of higher fish density, so this represents an indirect measure of the distribution of the target fish species.

There is some doubt as to the efficacy of MPAs with highly migratory species (Kaiser 2005), especially in high latitudes where there is greater larval dispersal (Laurel and Bradbury 2006). However, MPAs can be effective if placed to protect sensitive phases of the life cycle, such as spawning. The Mediterranean hake (*Merluccius merluccius*) performs seasonal migrations but was found, in a modelling study, to benefit from an MPA sited to protect spawning aggregations (Apostolaki *et al.* 2002). By contrast, however, a study into the consequences of MPAs for the South African deep-water hake (*Merluccius paradoxus*) found a negligible benefit (Edwards *et al.* 2009), although the authors acknowledge that this might be due to deficiencies in the model. Tagging experiments with north Atlantic cod (*Gadus morhua)* within two MPAs found benefits for small (immature) individuals, but not for larger cod, which exhibited less site fidelity (Schopka *et al.* 2010).

Timing of closures is also important, as was found by Loher (2011) in a study on the closure of the Pacific halibut (*Hippoglossus stenolepis*) fishery. Opening and closing dates were based on economics, as well as biology, to protect spawning migrations. The closure was found to be consistently too short to protect the entirety of the migration season. Detailed information regarding the movements and migrations of the species to be protected and, in particular, assessing issues such as source-sink population dynamics (Crowder *et al.* 2000), density-dependant movements, ontogenic

dispersal, and behavioural polymorphism are therefore very important to the success of an MPA (West *et al.* 2009, Grüss *et al.* 2011). However, such information is clearly of little use if overridden by economic demands. Conversely, it is possible to select sites for pelagic, high-seas MPAs based on the location of relatively static oceanographic features, such as frontal systems, ocean ridges or sea-mounts (Game *et al.* 2009). Locations such as these often represent 'hot-spots' of abundance for many highly mobile or migratory species, especially sharks (Priede *et al.* 2006) and could offer significant protection while simplifying spatial planning. Worm *et al.* (2003) suggest that when such features occur at between 20-30°N or S they represent biodiversity hotspots, and protection of such areas could outperform other closures. While more recent studies cast some doubt on seamounts having very high biodiversity (Howell *et al.* 2010), or aggregating animals as extensively as first thought (Morato *et al.* 2008) they do represent significant aggregations and high abundances of many species.

Empirical studies into the efficacy of MPAs have found a number of benefits. For example La Mesa *et al*. (2011) found evidence of spill-over in three species of sea breams (*Diplodus puntazzo, D. sargus and D. vulgaris*) across the boundaries of the Portofino MPA (NW Mediterranean). A sharp decline in abundance was found 100m from the MPA boundary, suggesting that the MPA was successful in increasing abundance (density and biomass) within and just beyond the MPA. It was suggested that the spill-over effect was, however, only moderately pronounced due to increased fishing pressure at the MPA boundary. Increased abundance and biomass, and greater average size, have been reported in several studies (Gell and Roberts 2003, Rodríguez-Cabello *et al.* 2008, Yemane *et al.* 2009), with no take zones being, unsurprisingly, more effective than partially protected sites (Lester and Halpern 2008).

One of the most significant, potential, problems with MPAs that has received much attention is the displacement of fishing activity to other areas. Dinmore *et al.* (2003) used the observed response of the north sea beam trawl fleet to the closure of the 'cod box', together with a size-based model of the impact of beam trawling to predict the effect of seasonal closures. They concluded that repeated seasonal closures would lead to a slightly more homogenous distribution of fishing effort that would have greater impacts on benthic invertebrates, particularly if the displacement was to

previously un-fished areas. Greenstreet *et al.* (2009) also found that the displacement of fishing effort greatly reduced the efficacy of MPAs in the north sea, unless the MPA was combined with restrictions on total allowable catch (TAC). Without TAC restrictions the modelling study found only a 1.7 to 3.8% reduction in fish mortality through the closure of 7.7% of the North Sea. However when combined with a TAC restriction the mortality was reduced by around 17%.

The grid occupancy analysis presented here has the additional advantage of being able to determine accurately the impact on the fishing fleet, as well as the fish, which can be an important factor in assessing the economic, or political, viability of a scheme. An important factor missing from the analysis is the vertical coincidence of the long-line hooks and the sharks. The simplifying assumption here is that sharks will always be at risk if they share a grid cell with an active fishing vessel, i.e. that there is always a vertical overlap between the sharks and the long-line hooks. While this has been shown to very often be the case (Queiroz *et al.* 2012), this analysis does not currently allow other scenarios to be investigated. It is possible, for example, that while there might be a geographic coincidence between the target species and the by-catch there might not always be a vertical coincidence. The two species might have differing dial vertical migration behaviour, or might be constrained to different depths, especially at geographic range margins, through thermoregulatory requirements. Walsh *et al*. (2009) found that using deep-set hooks in the Hawaii-based pelagic long-line fishery, targeting bigeye tuna (*Thunnus obesus*) rather than shallow set hooks, targeting swordfish, significantly reduced the by-catch of blue and shortfin mako sharks. Other measures, such as reducing soak times (Carruthers *et al.* 2011) or using circle rather than J-hooks (Kerstetter and Graves 2006, Yokota *et al.* 2006, Gilman *et al.* 2007) should also be considered alongside MPAs to reduce by-catch of species such as sharks, turtles or seabirds. The analysis methodology presented here will only be successful in real world situations if there is sufficient, detailed information about the movements and migrations of the species in question, including site fidelity to static features in the marine landscape. While the simulated prey field is sufficient to demonstrate the principal, it does not capture sufficient reality to investigate actual interactions, or inform the placement of real MPAs.

Marine protected areas do, therefore, have the potential to significantly reduce by-catch as well as providing protection from over-fishing. However, there are problems associated with appropriately locating MPAs for highly mobile species that would benefit from the high spatial and temporal resolution analysis of interactions presented here.

8 General discussion

The work presented in this thesis has investigated several aspects of the movement patterns, behavioural functions and population redistributions of marine predators in relation to environmental heterogeneity, including anthropogenic impacts (e.g. long-line fishing). In this General Discussion the main results from each chapter will be discussed and drawn together to contribute to a broader understanding of how and why predators move in the ways they do.

8.1 The Lévy flight foraging hypothesis

The foraging simulation results presented in Chapters 3 and 6 confirm the findings of Viswanathan *et al.* (1999, 2000, 2002) and others (Bartumeus *et al.* 2002, Raposo *et al.* 2003, Bartumeus *et al.* 2005, Raposo *et al.* 2009), that Lévy flight movement patterns optimise random searches, further strengthening the theoretical underpinning of the Lévy flight foraging (LFF) hypothesis. Importantly, the simulations presented here show Lévy foraging to be advantageous under a broader range of conditions than previously reported. For example, the prey does not need to be sparse (Viswanathan *et al.* 1999, Bartumeus *et al.* 2002), nor does the prey need to be revisitable for a Lévy forager with μ=2.0 to outperform a Brownian (exponential) forager (Viswanathan *et al.* 2001), although as predicted, lower Lévy exponents perform better when prey is non-

revisitable; i.e. it is confirmed that μ=2.0 is not optimal under all conditions. However, it is also clear that simple pattern matching (i.e. fractal movements in a fractal environment) cannot alone explain this optimality because the simplest scenario that tested this was shown to offer no significant advantage to any of the foragers, whether Lévy, Brownian or other type. The inclusion of prey targeting, which simply adds some biological realism in the form of prey detection, a pause to process or ingest encountered prey, makes the μ_{opt}=2 forager significantly more successful in all scenarios and is perhaps one of the most important findings from the simulation studies presented here. As the overwhelming majority of predator-prey encounters involve a prey-handling pause, the implication is that Lévy μ_{opt}=2 foraging presents an almost universal advantage in random searches performed by 'blind' hunters; that is, where there is no prior knowledge of the location of prey that would allow a more direct path to it to be taken. Finally, a further constraint on the LFF was confirmed in that Lévy foraging is only energetically more efficient for cruise predators that move significantly faster than their prey (Viswanathan *et al.* 2002).

8.2   Empirical evidence: the case for biological Lévy flight

Despite mounting empirical evidence for Lévy movement patterns in diverse species there has been some debate about whether the observed patterns are likely to be real and not simply an artefact of the analysis method. Furthermore, it is contested whether such movements are intrinsic processes resulting from adaptive behaviour, or whether they simply result from a normal random path interacting with a heterogeneous (e.g. fractal) environment. The work presented here has attempted to approach some answers to these questions: for example, I have demonstrated using simulations that Lévy patterns of movement can only arise through interaction with a fractal environment if the animal moves with perfect ballistic motion. As animals do not move in pure, ballistic straight lines between encounters with targets (e.g. food, shelter, mates), this finding strengthens the proposition that Lévy flights approximate naturally evolved stochastic movement patterns.

Much of the uncertainty in the interpretation of recorded movement patterns stems from the need to consider a movement path as a series of move steps and turns in

order to perform the analysis of move step-lengths. Animals very rarely move in such a structured way and therefore the analysis imposes a set of external rules, such as maximum turning angles or path deviations, to derive step-lengths between turns and hence 'discretise' what is essentially an analogue path (Turchin 1998). The process is very sensitive to both the sampling rate with which the original path was recorded (or re-sampled) and to the methods and parameters used in turn identification. These problems were highlighted by Codling and Plank (2011) who point out that the lack of a rigorous and objective method for determining turn points can result in paths that were not generated from a power law distribution of step-lengths being incorrectly identified as Lévy, and *vice versa*. This same problem was encountered in Chapter 5 where high-resolution GPS data of albatross movements was available for analysis. Several different methods of turn identification were attempted and it was realised that the resulting analysis output was strongly dependent on the input parameters used. Without an objective method for determining what turn angle, or path deviation, represented a turn it was not possible to robustly defend either the parameter decision or the results. For example, with some parameters the calculated step-lengths would be best fitted by an exponential distribution, whilst with other parameters a Lévy distribution would be the best fit. The solution in the case of albatross GPS data was to identify landings on the sea from a flight profile analysis and use these as robust and unambiguous turning points in the path. The identification of Lévy patterns in horizontal movement data is therefore fraught with problems and this issue seems to underlie much of the controversy surrounding biological Lévy flights. It is perhaps unsurprising therefore that the most robust evidence for Lévy flights has been found in data where the identification of turning points is unambiguous, as in the analysis of animal diving time-series data, where the turning points are simply where the animal changes from diving (descending) to ascending, or *vice versa*, as shown in Chapter 4 (see also Sims *et al.* 2008a, Hays *et al.* 2012, Sims *et al.* 2012). Even with this data however, care must be taken in the analysis to remove sampling artefacts (as described in Chapter 2). A further example of relatively unambiguous turning points is in the movements of fruit flies (*Drosophila melanogaster*). These movements, referred to as saccades (Fry *et al.* 2003), are well approximated by a sequence of straight steps and turns. From the results shown in Chapter 4 and other published work (Sims *et al.*

2008a, Hays *et al.* 2012, Sims *et al.* 2012) it seems likely that where the recorded path can be analysed unambiguously Lévy flight movement patterns will be found; with the now familiar caveat that these patterns are only to be expected when the animal is searching.

A question that is yet to be resolved is whether, when Lévy movement patterns are observed in pelagic predators, the animals are in fact foraging. While Lévy patterns have been observed in animals that spend time in deep scattering layers (Humphries *et al.* 2010, Queiroz *et al.* 2012) where fish and squid prey are known to reside, suggests it is highly probable that the primary activity is often foraging, however such patterns have not been linked directly to feeding events. The analysis of albatross movements in Chapter 5 addressed this knowledge gap directly by using stomach-temperature logger data to identify prey capture events and was therefore able to compare prey capture statistics between Lévy and non-Lévy foragers. It is a realistic assumption that albatrosses rearing chicks will indeed spend most of their time at sea foraging, however the analysis was of the distribution of landing locations, rather than specifically of the searching movements leading to prey capture. Nonetheless, the results presented in Chapter 5 provide the first empirical results showing that the foraging success of Lévy-type movements by albatrosses in the open ocean, where prey is sparser, is similar to prey capture success recorded for non-Lévy foragers where prey is abundant. That the estimated energy gain of Lévy foraging albatrosses was four times greater than the costs of searching, provides further support for adaptations having evolved that approximate optimal Lévy random movements.

A similar analysis has not yet been performed for the large pelagic fish predators considered in Chapter 4, leaving some uncertainty as to whether the patterns observed always correspond to actual searching and foraging. However, satellite relay transmission of ectotherm stomach temperature and acoustic transponding stomach loggers that record pH in sharks, allowing prey capture events to be recorded, have both now been developed (Papastamatiou *et al.* 2007) suggesting that this question could be addressed in the near future. Lévy flight optimises random searches, not foraging specifically, therefore these patterns could be expected when animals are searching for resources other than food, such as mates or, in the case of honey bees, a

nest site (Reynolds *et al.* 2007). The Lévy flight foraging hypothesis has perhaps focussed too much on the search for a single, admittedly important, resource (i.e. food) when there is in fact a much broader application of it in the analysis of animal movement to identify bouts of searching behaviour in general.

Finally, the movement patterns of the pelagic predators analysed in Chapter 4 were vertical displacements representing searching of the water column. Clearly the animals do not just move vertically, rather what has been measured by the tag is the vertical component of a three dimensional movement. The development of tags with tri-axial accelerometers (e.g. Fossette *et al.* 2010, Shamoun-Baranes *et al.* 2012) means that it might now be possible to record the movements of pelagic predators in three dimensions, allowing a much more detailed analysis of the movements to be performed.

8.3   Pattern generation

There is now ample theoretical evidence that Lévy movements optimise random searches and burgeoning empirical evidence that these movement patterns occur and are widespread in nature. Given these recent advances, it is reasonable for attention to turn to consider how these patterns are generated and how they may have evolved. One popular comment, made in connection with the results of Chapter 4, that must be immediately dismissed is that "sharks do math" (Witze 2010); clearly, the animals neither consciously draw their movements from a Lévy distribution, nor are likely to make conscious decisions about what search strategies to use. At present, the motivations that drive predators to adopt particular movement patterns at different times are too complex to elucidate, however research is beginning to reveal the mechanisms that might underlie the generation of step-lengths. Intermittency in locomotion, whereby a movement is interrupted by power law distributed (i.e. fractal) reorientations, has been shown theoretically to generate Lévy movement patterns (Bartumeus and Levin 2008). The principle is straightforward: if the animal moves at a roughly constant speed and the times between reorientations follow a Lévy distribution then the resulting step-lengths will also be Lévy distributed. The fractal reorientations themselves are a result of what has been referred to as 'bursty'

behaviour which is characterised by a heavy tailed distribution of intervals between events (Barabasi 2005). Maye *et al.* (2007) also found temporal power-law patterns in the spontaneous flight manoeuvres of tethered *D. melanogaster* and suggested that a general neural mechanism is responsible for the observed patterns. Recent work by Sorribes *et al.* (2011) has sought to identify such mechanisms in *D. melanogaster* and has found links with the dopaminergic system and the brain's mushroom body, both of which are involved in decision making processes. For example, mutant flies with disrupted dopaminergic function showed different levels of burstiness in their behaviour. The bursty behaviour giving rise to Lévy movement patterns may be based, therefore, on neural control and with the behaviour being intrinsic rather than extrinsic.

Given the significant advantage that Lévy search patterns confer it seems highly likely that adaptations leading to intrinsic pattern generation of Lévy movement will have naturally evolved. Recent work has demonstrated bursty behavioural patterns in mice (Proekt *et al.* 2012), desert locusts (*Schistocerca gregaria*) (Bazazi *et al.* 2012) and in human activities (Barabasi 2005), suggesting that this type of behavioural pattern generation may be widespread in organisms. Indeed, heavy tailed distributions in move step-lengths have even been observed in the movement patterns of the nematode *Caenorhabditis elegans* (Ohkubo *et al.* 2010). It is worth noting, however, that in evolutionary terms the underlying mechanism is largely irrelevant; it does not matter whether it is neurological, chemical or even mechanical, natural selection operates on the resulting behaviour of the animal. This observation only serves to strengthen the argument that optimised searching behaviour could have evolved very early in life's history as a fundamental characteristic of predatory animals. Some extinct animals have left fossil tracks which could provide clues as to when Lévy-type foraging may have evolved (ichnofossils) (Plotnick 2012, D.W. Sims, V.J. Wearmouth, R.J. Twitchett, unpublished data). Such tracks are relatively rare, however, and most commonly belong to animals which burrow or graze in marine sediments; pelagic cruise predators leave no trace. With the meandering tortuous traces that have been found (such as Cosmorhaphe e.g. Crimes and Crossley 1991) it is possible that the patterns of area restricted search, which can appear similar to a Lévy walk, result from

the animal grazing in areas of higher resource availability rather than forming part of a random search, as shown in several invertebrate species, such as snails, worms and crabs (Koy and Plotnick 2010). The shift to area restricted search in response to increased resource availability requires a different behavioural process to the intrinsic search movements of a Lévy flight. Given the significant advantage conferred by Lévy foraging it seems likely that it would have evolved at the same time as fast prey-targeting predators. Some evidence suggests that these taxa might have arisen first in the Early Cambrian when there was a dramatic diversification in ichnotaxa and evidence of vertical bioturbation, that is, the signs of more active predators (Seilacher *et al.* 2005). Further study into the movements of diverse and more primitive taxa than the higher vertebrates considered here might provide further clues as to when Lévy-type search patterns first evolved. Recent work has suggested an alternative possibility to fast predators as the driving mechanism behind the evolution of Lévy movement patterns. In the formation of cooperative aggregations, de Jager *et. al.* (2011), found that young mussels (*Mytilus edulis*) move in a Lévy walk when forming spatially patterned beds which enhance individual fitness, in terms of the local availability of algae and reduced predation risk. A Lévy walk, with μ = 2.0, was found to maximise the rate of pattern formation. Identification of Lévy processes in pattern formation in taxa such as mussels suggests that the intrinsic timing mechanisms responsible for Lévy behaviour might have evolved very early.

8.4 Balancing hunting with predation risk

The animals that formed the focus of the work in Chapter 4 were all large apex predators such as sharks, tunas and billfish, and for all these species Lévy movements were found to be prevalent. However, are such movements also prevalent in smaller-bodied predators? While such movements clearly optimise the search for prey, the super-diffusive nature of Lévy walks also results in more encounters with predators (Visser 2007). Therefore, it might be expected that Lévy foraging bouts in smaller, more vulnerable predators, might be restricted to times and locations where the risk of predation was reduced. This is a difficult question to answer in a pelagic fish tagging study, as smaller animals are currently more difficult to tag given the size ratio of the tag to the fish (which by rule of thumb should not exceed 2%), and small tags are less

likely to be spotted and returned from a purse seiner catching mackerel (*Scomber scombrus)* than a long-liner catching blue sharks (*Prionace glauca*) with large, externally attached tags. Smaller predators such as mackerel would be interesting to study given the necessary compromises that must be made between finding food and avoiding predation. Further, as a behavioural defence against predation, many small fish form schools and consequently individual movements are strongly influenced by those of nearby fish and by the school as a whole (Romey 1996, Hubbard *et al.* 2004). Whether Lévy foraging occurs in these fish, and whether it occurs at the individual or school level, is therefore a very interesting but difficult question to approach, and which will need to wait for the development of smaller and cheaper tags. Nevertheless, another species which has been successfully tagged in the past and might help with this question is the ocean sunfish (*Mola mola*). These fish are known to form aggregations and schools (Pope *et al.* 2010, Abe *et al.* 2012). In a preliminary investigation the current author was involved with (N. Queiroz, L. Sousa, N. Humphries, D.W. Sims, unpublished data), four small *M. mola* (~1m) were tagged with archival data storage tags (DSTs) and were kept for two days in the holding pen of a large tuna set-net. Under these semi-natural conditions the four fish showed correlated vertical movements consistent with schooling behaviour (as shown in Figure 144). All possible pairings of individual sunfish show correlations and in Figure 145 the similarities in the depth-at-time plots are clear. Smaller *M. mola* are also known to exhibit Lévy searching, as shown in Chapter 4, however, the predation risk to these young sunfish is difficult to ascertain so it is not possible to determine how it may affect the occurrence of Lévy behaviour. A further problem with pelagic tagging studies is the inability to link the observed movement patterns accurately with specific activities such as feeding or prey avoidance. Despite this, these preliminary results indicate that young predators may mitigate the increased encounters expected with other (possibly larger) organisms when they exhibit Lévy-type movements, by forming aggregations or schools.

Alternatively, the general question of how best to optimise the conflicting goals of finding prey and avoiding predators could be explored using a simulation. By combining the Foraging Lab and Predator-Prey simulations it would be possible to assess both the foraging success and survival rates of the virtual animals occupying the

middle trophic level under a range of predation risks from cruise or ambush predators. It might be expected that the Lévy exponent might increase, resulting in a more Brownian like movement pattern as the risk of predation increases. The incorporation of an evolutionary algorithm could again be used to explore the trade space of movement behaviours. Animals do not perform a single behaviour however, so it is most likely that in real, small predators what would be observed is a switch between foraging and hiding in response to predator presence. While possible to simulate such a scenario it is difficult to do so without introducing arbitrary movement patterns or controlling parameters. However, future simulation work could explore some of these possibilities to test predictions.

An extreme case of balancing hunting and hiding is, of course, the ambush predator, which in many cases manages to combine the two goals very effectively (cf. camouflage in cuttlefish). Ambush predators can have a significant energetic advantage, as shown in the simulations presented in Chapter 6, and this is in itself probably sufficient for this predatory lifestyle to have evolved. While some ambush predators, such as angler fish (*Lophias spp.*) or angel sharks (*Squatina spp.*) will have reduced predation risk as adults through their larger body size, young individuals and smaller species will not and will therefore gain an additional advantage. Young fish hide from predators in a variety of ways, by occupying shallower water in lagoons, as with lemon sharks (*Negaprion brevirostris*) (Feldheim *et al.* 2002) or by sheltering amongst mangrove roots (Mumby 2006). Selection pressure on successful hiding could therefore have been an additional driver in the evolution of ambush predation. The advantage of reduced predation risk was not considered in the simulations in Chapter 6 which focussed on one simple aspect of ambush predation, the optimum waiting time in a strongly heterogeneous prey field. Under the perhaps rather artificial conditions of those simulations it was interesting that the optimum waiting (or giving up) time was dependent only on the prey field density (i.e. the encounter rate) and not on the distribution used to derive waiting times. On giving up waiting, the simulated ambush predator moved super-diffusively with a TP2.0 movement pattern; however, it was not investigated whether this was in fact the best movement style to adopt between waiting periods. Given the sedentary habits of ambush predators such as

angler fish (although see Rountree *et al.* 2008 for evidence of more energetic behaviour) it is possible that movements following prey capture or on cessation of waiting are less extensive. It would be interesting to pursue this further in a simulation with a fixed waiting time and a range of different movement patterns; it may be that super-diffusive movements between waits confer no particular advantage in this case.

The findings in Chapter 6 regarding mobile (cruise) predators again confirmed the predictions of Viswanathan *et al.* (2002) showing that Lévy foraging is only advantageous when the predator moves significantly faster than the prey. This adds further weight to the suggestion that large pelagic predators are the most promising candidates for studying the nature of biological Lévy flights.
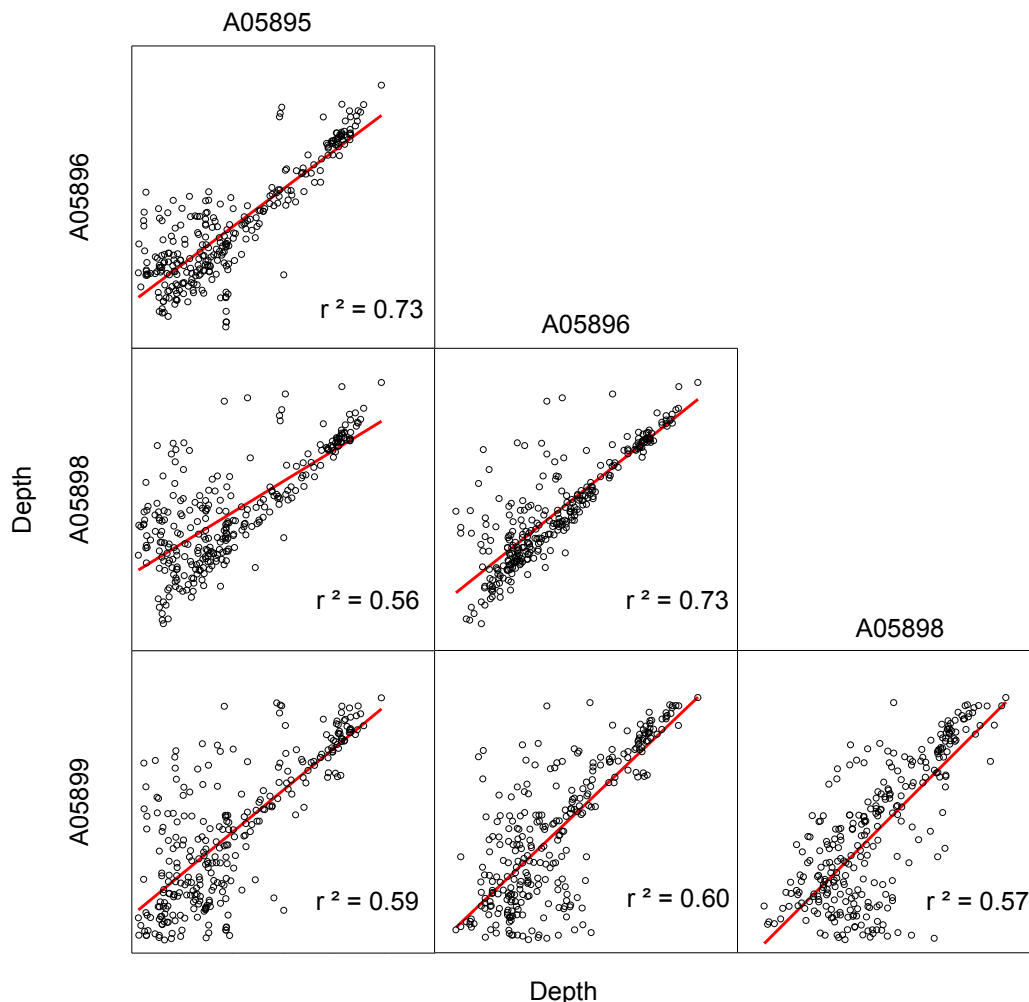
Figure 144: Schooling behaviour in four ocean sunfish (*Mola mola*)

    The six scatter plots show correlations between time at depth for four ocean sunfish tagged with archival DSTs and moving within the confines of a set net.
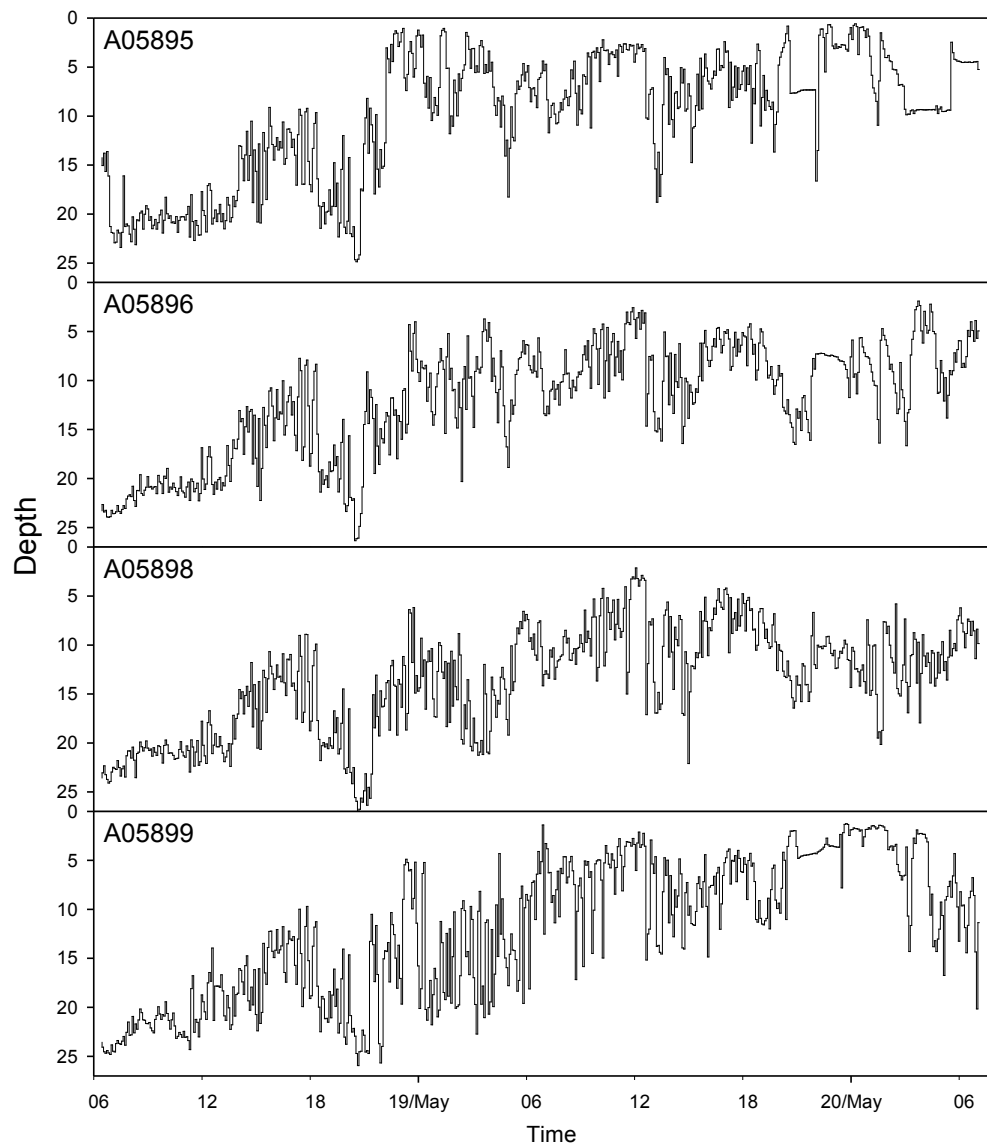
Figure 145: Time depth plots of four ocean sunfish

The plots show the depths recorded by archival DSTs for the four sunfish shown in Figure 145. The overall pattern of coordinated vertical movements is clear.

8.5 Using the LFF hypothesis to analyse movement data

The statistical tools to identify biologically meaningful step-length distributions in animal movement data are now mature and robust in the form of maximum likelihood estimation, fitting algorithms and Akaike weights for model selection. The necessary equations are available for power-law and exponential distributions as well as truncated versions of these. (The truncated exponential was not used in the current work although it is perhaps a less contentious alternative model to the truncated Pareto than the exponential.) The possibility therefore exists to use this statistical analysis as a probe to locate bouts of search behaviour in a tag-recorded time series of

displacements, providing a deeper insight into not just where an animal is located, but in what activity it might have been engaged. Work presented here identifies several caveats, however, that limit the usefulness of the technique. Firstly, there is the problem of 'noisy' biological data; tag recorded data encompasses a suite of behaviours, of which searching may not be the most dominant. Consequently, the searching signal can be weak or lost altogether. Much of the analysis in Chapter 4 focussed on identifying consistent bouts of movement that offered a sufficiently good fit to one of the competing distributions. In this case a split-moving window matrix analysis was employed that provided an objective method for dividing the time series. However, it is clear that divisions of a week or more still include many behaviours other than searching, such as diel vertical migration, that significantly affect the outcome of the MLE analysis. The boxplot shown in Figure 146 shows the range of μ values obtained for seven of the species analysed in Chapter 4, all of which are known to perform regular diel vertical migrations (DVM, see Figure 147). Of these, the billfish all have low μ values, close to or below 1.0, which might suggest foraging in sparse environments for prey in non-revisitable patches. It is equally possible however, that the low μ values result from the large number of long step-lengths associated with DVM, as shown in the time depth profiles in Figure 147 where these large vertical displacements can be seen to dominate the movements. Despite this possibility, there is no clear correlation between the presence of DVM in the time series and low μ values; both blue sharks (*Prionace glauca*) and bigeye tuna (*Thunnus obesus*) show strong DVM yet have optimised μ values of around 2.0. These inconsistencies mean that some predictions about the underlying behaviour may be less robust, which without reference to the species or individual-specific movement patterns may reduce the generality of the LFF hypothesis between some species. However, given that the scale-free movements associated with a $\mu=2$ forager must be the dominant pattern for it to be recognised, and the extent to which the pattern optimises random searches, it is most likely that power-law distributed step-lengths indicate a period of searching behaviour. The LFF hypothesis is therefore likely to be most useful in the general recognition of search patterns, but perhaps less so in attempts to use particular μ values to predict particular environmental contexts. One example where this has been successful, however, was in the study of the vertical movements of great white sharks

(*Carcharodon carcharias*) (Sims *et al.* 2012). In this case the association of different prey items with different geographic locations was known *apriori* and, consequently, accurate predictions of the movement pattern were achieved. For example Brownian movement was predicted when resident at a seal colony, ballistic movements when in shallow seas hunting for shoaling fish and optimal Lévy movements when in deep water, where the likely prey were dolphins; both predictions were confirmed.
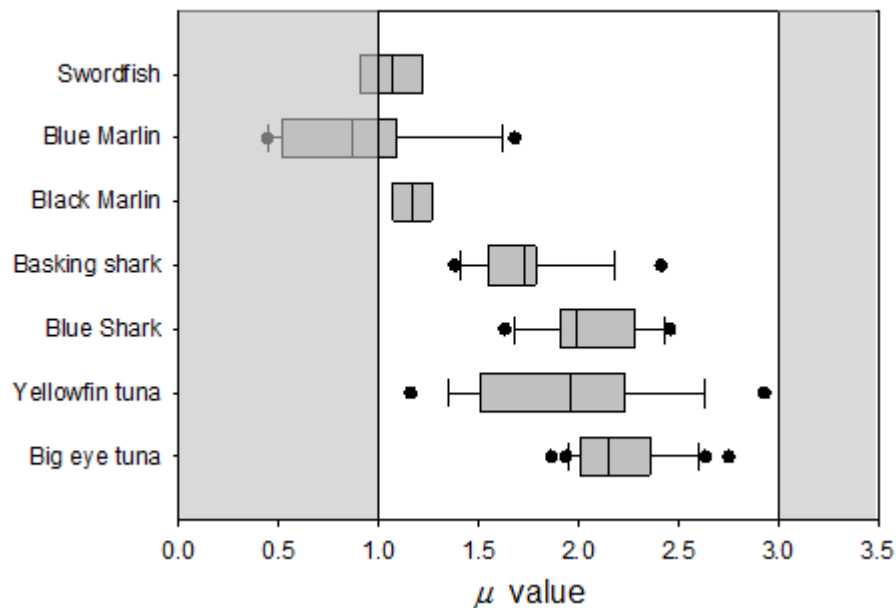
Figure 146: Diversity in μ values from Chapter 4
The long step-lengths resulting from diel vertical migrations significantly reduce the μ value calculated for the billfish in the study in Chapter 4. However, other predators, also known to perform diel vertical migration, such as blue sharks or big eye tunas, are less affected. Shaded areas on the plot indicate regions where the value of μ is outside the range of Lévy exponents.
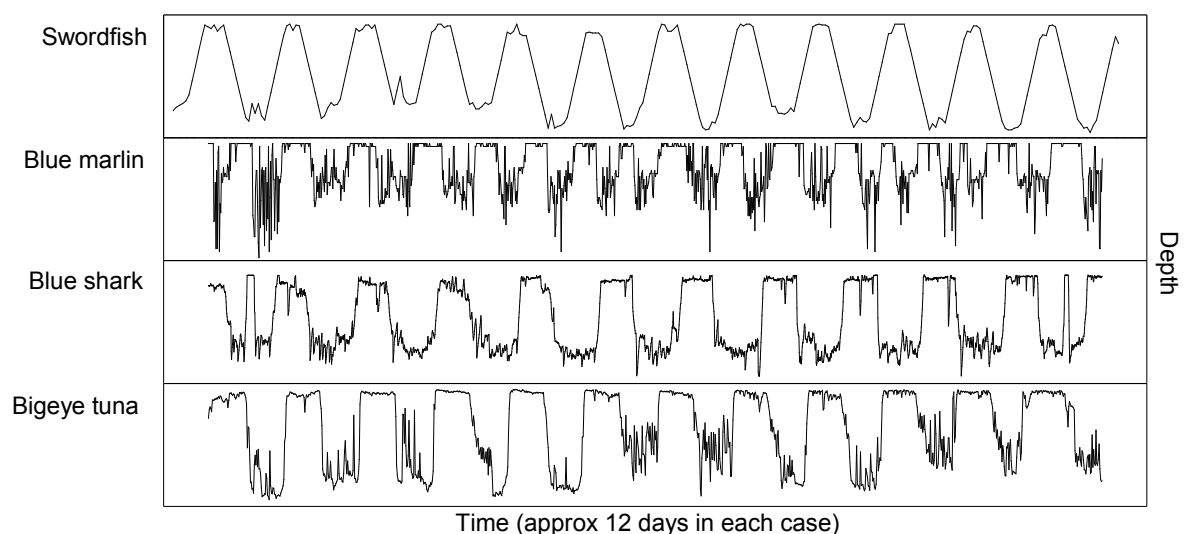
Figure 147: Time depth profiles of species with low μ values
All these species exhibit strong diel vertical migrations which result in many long step-lengths, however only the swordfish (*Xiphius gladius*) and blue marlin (*Makaira nigricans*) have low μ values (Figure 146).

8.6 The assessment of fisheries controls

The grid occupancy analysis presented in Chapter 7 demonstrates an application of behavioural movement analysis which combines recorded and simulated data. The underlying analysis can however be used with any track-based movement data to study the spatio-temporal dynamics of interaction between, in principle, any number of participants. Therefore, while this application considered fishing vessels and simulated sharks, it could just as easily be applied to the movements of blue and mako sharks, or male and female blue sharks, when sufficient data becomes available. The metric used here was 'days at risk' but this is, of course, equivalent to days of co-occurrence, and the coefficient of overlap (Rijnsdorp *et al.* 1998) can be extended to deal with more than two entities, by adding additional terms P_{xj} as required to the equation:

$$O = 2 \sum_{j} \left(P_{bj} P_{sj} \right) \Bigg/ \left(\sum_{j} P_{bj}^2 + \sum_{j} P_{sj}^2 \right)$$

The focus of the study here was to explore the effectiveness of by-catch mitigation measures with long-line fishing fleets with fleet composition, marine protected areas (MPAs) and seasonal closures being considered. While a simulated prey field was used here the analysis was able to highlight problems which would be expected if real shark data were used. The key point is that the mitigation measures used here are all reliant on the accurate targeting of times and locations where interactions between the fleet and the sharks are maximised. This finding emphasises the importance of having accurate movement data from the species to be protected if any of these measures are to be successful and economically viable.

There are potential benefits associated with MPAs that cannot be assessed using the grid occupancy analysis. For example spillover is an expected consequence of an MPA, whereby the enhanced population levels within the MPA result in migration of individuals to outside the MPA. Spillover can provide more productive fishing at the borders of the MPA. For example Murawski *et al.* (2005) found that trawling revenue was twice as high within 4km of the MPA boundary, although catch variability was greater. Nor is it possible to determine the effect of the displacement of fishing effort to other areas which might result in increased fishing intensity in those areas outside

the MPA that fishers consider to be viable alternative targets (Dinmore *et al.* 2003). The placement of MPAs and timing of seasonal closures can be targeted in ways that do not require the kind of analysis presented here. For instance, short-term closures can protect spawning aggregations leading to improved reproductive success, a result of reduced disruption and disturbance, which was found to be the case with spawning southern calamari (*Sepioteuthis australis*) (Moltschaniwskyj *et al.* 2002). There can also be a direct effect of protecting vulnerable spawning aggregations that could otherwise be targeted and fished to the point of extinction such as the red hind (*Epinephelus guttatus*) aggregations studied by (Beets and Friedlander 1999)

Considerably more information is needed about the movement and migration of highly mobile widely ranging marine predators such as pelagic sharks if high seas MPAs are to be effectively located. There is some evidence that mating or pupping aggregations (which are vulnerable to disturbance) might be found associated with bathymetric features such as sea mounts (Worm *et al.* 2003) which would simplify the location of MPAs. However modern technology, such as the GPS-based vessel monitoring system would allow more complex, mobile MPAs to be defined and monitored, through the real-time tracking of vessels, which might be the only way high seas MPAs will work with wide ranging predators such as pelagic sharks.

8.7 Summary

The work presented here has attempted to take a step beyond the descriptive nature of the 'where' and 'when' in animal movement analyses to elucidate what activity the animal might have exhibited, i.e. whether it was searching, and to explore 'why' certain behaviour patterns occur. A theoretical framework for the analysis of the fine structure of animal movements, in the form of the Lévy flight foraging hypothesis, has been confirmed as an optimal search strategy under a broad range of conditions and this movement pattern has been found to be prevalent in the vertical displacements of pelagic fish predators and in the foraging patterns of albatrosses. The implication therefore is that much of the time these predators are searching, which is a reasonable conclusion given the sparse and patchy distribution of prey in the open ocean where these animals were tagged and tracked (Sims and Merrett 1997, Sims 1999). There are

some limitations however with this statistical approach. The principal difficulty perhaps is the application to horizontal movement data. As well as the issue of determining turning points, as described previously, there is a further problem with the large error fields that accompany location data derived from light-level geolocation and Argos satellite tracking. These errors have been shown in simulations to lead potentially to incorrect conclusions in the estimation of the Lévy exponent (μ) and in the accurate identification of a track as a Lévy walk (Bradshaw *et al.* 2007). While methods such as state-space models have been developed in an attempt to interpolate smoothly the animals movement while accounting for these error fields (Jonsen *et al.* 2006, Tremblay *et al.* 2009), the resulting paths are difficult to validate and are not suitable for a statistical analysis. The advent of GPS transmitters solves, to a large extent, the problem of determining an accurate location, but has the significant disadvantage for pelagic predators that these devices will only work when at the surface and are able to obtain a fix of the GPS satellite constellation. For animals that do surface regularly, however, such as ocean sunfish (*Mola mola*) these tags have proved to very useful (Sims *et al.* 2009b) but still do not solve the problem of identifying turning points objectively along paths, as discussed in Chapter 5. While these problems do not, in general, exist with vertical (dive time series) data there is the problem that it has not yet been confirmed empirically that animals moving in a Lévy pattern are indeed searching for food. This missing link between the pattern and the activity weakens to some extent the conclusions that can be drawn about what the animal is doing. The identification of feeding events through the use of stomach temperature loggers would be a useful goal for future research.

Several studies have sought to extend Lévy dynamics to human activities (Bertrand *et al.* 2005, Brown *et al.* 2007, Gonzalez *et al.* 2008). In the case of activity patterns explored by Barabasi (2005), where the time taken to answer emails was found to follow a power law, the underlying process is found to be the way in which queued items are prioritised and dealt with; a very human activity resulting in a 'bursty' behavioural pattern very similar to that potentially underlying the Lévy patterns explored here. However, while the patterns are similar the processes are not, which is especially true in the case of movement patterns where the extension of the Lévy

model to human activities is less appropriate. If we consider the movements of a person over a period of time we would expect to find a large number of small steps, as the individual moves around the house, garden or office for example, and with larger steps associated with trips to local shops, and perhaps a few much longer steps derived from travelling further afield. The resulting distribution of many short and a few long step-lengths might well be very well fitted by a power law distribution. However, it would not be an appropriate model, because the Lévy flight foraging hypothesis pertains to random searches, whereas the individual's movements are usually largely deterministic (i.e. mostly directed). Similar caution is required in testing the Lévy flight foraging hypothesis when considering other predators where movements are more likely to be directed than random. For example, while one might be able to fit a power-law distribution to the movements of a bear (*Ursus* spp.) these animals have a very good knowledge of the spatio-temporal distribution of resources, having spent several years as a cub learning from their mother (e.g. Mattson 2004, Smith and Partridge 2004, Coop *et al.* 2005, Mattson *et al.* 2005) and consequently spend far less time performing random searches and more time in directed movements between known resource locations. This argues for the need for researchers to apply the Lévy flight paradigm where they have reasonable evidence that the movements results from a random, rather than a directed, search.

The animals that have been the focus of this study form part of one of the largest ecosystems on the planet, the marine pelagic realm. Difficult to study and poorly understood, this ecosystem is threatened by climate change, both from increased temperature and acidification, as well as over–exploitation, pollution and habitat degradation. The impacts of these processes have already resulted in declines for some species and populations, such as Atlantic Cod (*Gadus morhua*) (Hutchings 2000), sooty shearwaters (*Puffinus griseus*) (Veit *et al.* 1997) and many pelagic sharks (Baum *et al.* 2003). The long term consequences, while far from clear, are likely to be difficult to reverse. Continued research into this ecosystem through quantitative studies and the modelling of the movements and migrations of the apex pelagic predators that have such an important trophic role is vital, not just for our own social well-being and economy, but for that of marine ecosystems more generally.

9 Appendix A: Chapter 3 tables of results

In the following tables:
* The value shown here is the number of successful forage runs / mean path length.
** % Difference is calculated relative to the worst performer in the group.

Table A1: Simulation results from the sparse uniform prey field scenarios

Scenario	Forager	Mean path length	Mean biomass consumed	Biomass per unit travelled	Encounters per unit travelled*	% Difference**
Non-Destructive	TP 1.5	249938	1.08E+02	4.31E-04	3.88E-06	1.52%
	TP 2.0	39006	1.71E+01	4.37E-04	8.09E-06	2.95%
	TP 2.5	14541	6.34E+00	4.36E-04	4.20E-06	2.59%
	Exp.	38755	1.65E+01	4.25E-04	3.62E-06	0.00%
	Uniform	39985	1.72E+01	4.31E-04	3.14E-06	1.37%
Destructive	TP 1.5	249974	1.05E+02	4.21E-04	3.88E-06	29.98%
	TP 2.0	39032	1.53E+01	3.91E-04	8.06E-06	20.66%
	TP 2.5	14543	4.71E+00	3.24E-04	4.19E-06	0.00%
	Exp.	38757	1.40E+01	3.62E-04	3.67E-06	11.56%
	Uniform	39986	1.41E+01	3.52E-04	3.16E-06	8.71%
Non-Destructive, targeted	TP 1.5	245536	1.78E+02	7.23E-04	3.95E-06	99.30%
	TP 2.0	38831	3.48E+01	8.96E-04	8.04E-06	146.84%
	TP 2.5	14532	1.10E+01	7.56E-04	4.27E-06	108.18%
	Exp.	38724	1.60E+01	4.13E-04	3.68E-06	13.78%
	Uniform	39952	1.45E+01	3.63E-04	3.15E-06	0.00%
Destructive, targeted	TP 1.5	246535	9.75E+01	3.96E-04	3.94E-06	101.61%
	TP 2.0	38872	1.88E+01	4.83E-04	8.09E-06	146.29%
	TP 2.5	14534	5.39E+00	3.71E-04	4.25E-06	88.97%
	Exp.	38736	8.55E+00	2.21E-04	3.64E-06	12.45%
	Uniform	39966	7.84E+00	1.96E-04	3.15E-06	0.00%

Table A2: Statistical results from the sparse uniform prey field scenarios

Comparison	Diff of Ranks	q	P<0.05
TP1.5 vs TP2.5	20673162408	452.926	Yes
TP1.5 vs Uniform	18861317428	413.23	Yes
TP1.5 vs Exponential	18466109287	404.572	Yes
TP1.5 vs TP2.0	14161121247	310.254	Yes
TP2.0 vs TP2.5	6512041161	142.672	Yes
TP2.0 vs Uniform	4700196181	102.976	Yes
TP2.0 vs Exponential	4304988040	94.317	Yes
Exponential vs TP2.5	2207053121	48.354	Yes
Uniform vs TP2.5	1811844980	39.695	Yes
Exponential vs Uniform	395208141	8.659	Yes

Table A3: Simulation results from the abundant uniform prey field scenarios

Scenario	Forager	Mean path length	Mean biomass consumed	Biomass per unit travelled	Encounters per unit travelled*	% Difference**
Destructive	TP 1.5	249868	17492	7.00E-02	4.00E-06	28.79%
	TP 2.0	39020	2553	6.54E-02	2.56E-05	20.38%
	TP 2.5	14542	790	5.44E-02	4.66E-05	0.00%
	Exp.	38756	2301	5.94E-02	2.38E-05	9.23%
	Uniform	39986	2309	5.77E-02	2.24E-05	6.23%
Non-Destructive, targeted	TP 1.5	169412	19757	1.17E-01	5.90E-06	96.72%
	TP 2.0	35241	5088	1.44E-01	2.83E-05	143.54%
	TP 2.5	14259	1672	1.17E-01	4.76E-05	97.75%
	Exp.	37728	2524	6.69E-02	2.44E-05	12.84%
	Uniform	38991	2311	5.93E-02	2.29E-05	0.00%
Destructive, targeted	TP 1.5	190458	8995	4.72E-02	5.25E-06	103.54%
	TP 2.0	36049	2300	6.38E-02	2.77E-05	174.99%
	TP 2.5	14335	747	5.21E-02	4.73E-05	124.49%
	Exp.	38253	1036	2.71E-02	2.41E-05	16.70%
	Uniform	39529	917	2.32E-02	2.26E-05	0.00%

Table A4: Super-abundant uniform prey field results

Scenario	Forager	Mean path length	Mean biomass consumed	Biomass per unit travelled	Encounters per unit travelled*	% Difference**
Destructive	TP 1.5	249938	528758	2.12E+00	4.00E-06	26.27%
	TP 2.0	39137	78341	2.00E+00	2.56E-05	19.47%
	TP 2.5	14699	24627	1.68E+00	6.80E-05	0.00%
	Exp.	38783	70838	1.83E+00	2.58E-05	9.02%
	Uniform	39999	70955	1.77E+00	2.50E-05	5.88%
Non-Destructive, targeted	TP 1.5	22508	68858	3.06E+00	4.44E-05	61.14%
	TP 2.0	14315	48388	3.38E+00	6.99E-05	78.05%
	TP 2.5	10413	31639	3.04E+00	9.60E-05	60.05%
	Exp.	21372	45436	2.13E+00	4.68E-05	11.98%
	Uniform	22658	43015	1.90E+00	4.41E-05	0.00%
Destructive, targeted	TP 1.5	35801	41452	1.16E+00	2.79E-05	65.34%
	TP 2.0	18476	24454	1.32E+00	5.41E-05	88.99%
	TP 2.5	11916	14105	1.18E+00	8.39E-05	69.03%
	Exp.	28454	22715	7.98E-01	3.51E-05	14.00%
	Uniform	30165	21124	7.00E-01	3.32E-05	0.00%

Table A5: Mega-abundant uniform prey field results

Scenario	Forager	Mean path length	Mean biomass consumed	Biomass per unit travelled	Encounters per unit travelled*	% Difference**
Destructive	TP 1.5	249960	2108485	8.44E+00	4.00E-06	29.56%
	TP 2.0	39018	308245	7.90E+00	2.56E-05	21.33%
	TP 2.5	14541	94675	6.51E+00	6.88E-05	0.00%
	Exp.	38755	277300	7.16E+00	2.58E-05	9.89%
	Uniform	39984	278306	6.96E+00	2.50E-05	6.90%
Non-Destructive, targeted	TP 1.5	10082	97295	9.65E+00	9.92E-05	24.99%
	TP 2.0	8674	85656	9.88E+00	1.15E-04	27.91%
	TP 2.5	7764	73787	9.50E+00	1.29E-04	23.10%
	Exp.	10940	90056	8.23E+00	9.14E-05	6.62%
	Uniform	11282	87100	7.72E+00	8.86E-05	0.00%
Destructive, targeted	TP 1.5	17640	69194	3.92E+00	5.67E-05	37.28%
	TP 2.0	12452	52390	4.21E+00	8.03E-05	47.25%
	TP 2.5	9780	39021	3.99E+00	1.02E-04	39.63%
	Exp.	18938	59524	3.14E+00	5.28E-05	10.00%
	Uniform	20198	57711	2.86E+00	4.95E-05	0.00%

Table A6: Simulation results from the sparse Lévy prey field scenarios

Scenario	Forager	Mean path length	Mean biomass consumed	Biomass per unit travelled	Encounters per unit travelled*	% Difference**
Destructive	TP 1.5	249945	106.04	4.24E-04	3.70E-06	25.07%
	TP 2.0	39037	15.40	3.95E-04	5.55E-06	16.52%
	TP 2.5	14535	4.92	3.39E-04	2.48E-06	0.00%
	Exp.	38756	13.98	3.61E-04	1.57E-06	6.49%
	Uniform	39984	13.94	3.49E-04	1.34E-06	2.95%
Non-Destructive, targeted	TP 1.5	245166	194.01	7.91E-04	3.78E-06	119.72%
	TP 2.0	38845	40.47	1.04E-03	5.62E-06	189.39%
	TP 2.5	14529	11.41	7.85E-04	2.44E-06	118.06%
	Exp.	38722	15.35	3.96E-04	1.59E-06	10.00%
	Uniform	39954	14.37	3.60E-04	1.34E-06	0.00%
Destructive, targeted	TP 1.5	246322	106.67	4.33E-04	3.75E-06	125.52%
	TP 2.0	38859	21.67	5.58E-04	5.64E-06	190.63%
	TP 2.5	14531	5.67	3.90E-04	2.44E-06	103.13%
	Exp.	38738	8.63	2.23E-04	1.60E-06	16.15%
	Uniform	39968	7.69	1.92E-04	1.36E-06	0.00%

Table A7: Simulation results from the abundant Lévy prey field scenarios

Scenario	Forager	Mean path length	Mean biomass consumed	Biomass per unit travelled	Encounters per unit travelled*	% Difference**
Destructive	TP 1.5	249910	17514	7.01E-02	4.00E-06	28.05%
	TP 2.0	39007	2558	6.56E-02	2.33E-05	19.82%
	TP 2.5	14543	796	5.47E-02	2.33E-05	0.00%
	Exp.	38754	2310	5.96E-02	1.18E-05	8.93%
	Uniform	39983	2340	5.85E-02	1.06E-05	6.95%
Non-Destructive, targeted	TP 1.5	166598	22721	1.36E-01	6.00E-06	148.23%
	TP 2.0	35227	6184	1.76E-01	2.58E-05	219.49%
	TP 2.5	14284	1755	1.23E-01	2.37E-05	123.60%
	Exp.	37807	2409	6.37E-02	1.22E-05	15.95%
	Uniform	39086	2148	5.49E-02	1.08E-05	0.00%
Destructive, targeted	TP 1.5	189982	10478	5.52E-02	5.26E-06	148.31%
	TP 2.0	36185	2769	7.65E-02	2.51E-05	244.55%
	TP 2.5	14359	791	5.51E-02	2.35E-05	148.05%
	Exp.	38289	1009	2.64E-02	1.20E-05	18.66%
	Uniform	39563	879	2.22E-02	1.06E-05	0.00%

Table A8: Super-abundant Lévy prey field results

Scenario	Forager	Mean path length	Mean biomass consumed	Biomass per unit travelled	Encounters per unit travelled*	% Difference**
Destructive	TP 1.5	250106	529749	2.12E+00	4.00E-06	25.82%
	TP 2.0	39139	78563	2.01E+00	2.55E-05	19.24%
	TP 2.5	14702	24749	1.68E+00	6.38E-05	0.00%
	Exp.	38786	71197	1.84E+00	2.53E-05	9.04%
	Uniform	40000	71796	1.79E+00	2.43E-05	6.62%
Non-Destructive, targeted	TP 1.5	29122	96409	3.31E+00	3.43E-05	131.26%
	TP 2.0	17144	62559	3.65E+00	5.83E-05	154.91%
	TP 2.5	11515	33259	2.89E+00	8.14E-05	101.77%
	Exp.	26422	43672	1.65E+00	3.71E-05	15.46%
	Uniform	27971	40040	1.43E+00	3.48E-05	0.00%
Destructive, targeted	TP 1.5	48644	56894	1.17E+00	2.06E-05	116.31%
	TP 2.0	21882	30327	1.39E+00	4.57E-05	156.33%
	TP 2.5	12736	14439	1.13E+00	7.37E-05	109.68%
	Exp.	32094	20213	6.30E-01	3.06E-05	16.48%
	Uniform	33774	18261	5.41E-01	2.88E-05	0.00%

Table A9: Limited path simulation results with a sparse uniform prey field

Scenario	Forager	Mean path length	Mean biomass consumed	Biomass per unit travelled	Encounters per unit travelled*	% Difference**
Destructive	TP 1.5	40426	17.13	4.24E-04	1.08E-05	31.95%
	TP 2.0	40159	15.78	3.93E-04	8.05E-06	22.36%
	TP 2.5	40025	12.86	3.21E-04	3.77E-06	0.00%
	Exp.	40007	14.35	3.59E-04	3.61E-06	11.69%
	Uniform	40005	14.00	3.50E-04	3.18E-06	8.93%
Non-Destructive, targeted	TP 1.5	40423	28.84	7.14E-04	1.08E-05	98.03%
	TP 2.0	40159	36.95	9.20E-04	8.02E-06	155.38%
	TP 2.5	40025	29.34	7.33E-04	3.72E-06	103.44%
	Exp.	40007	16.28	4.07E-04	3.63E-06	12.93%
	Uniform	40005	14.41	3.60E-04	3.12E-06	0.00%
Destructive, targeted	TP 1.5	40421	15.99	3.96E-04	1.09E-05	100.51%
	TP 2.0	40159	19.76	4.92E-04	8.07E-06	149.42%
	TP 2.5	40024	14.66	3.66E-04	3.74E-06	85.68%
	Exp.	40007	8.79	2.20E-04	3.61E-06	11.38%
	Uniform	40005	7.89	1.97E-04	3.19E-06	0.00%

Table A10: Limited path simulation results with an abundant uniform prey field

Scenario	Forager	Mean path length	Mean biomass consumed	Biomass per unit travelled	Encounters per unit travelled*	% Difference**
Destructive	TP 1.5	40426	2853	7.06E-02	2.47E-05	32.01%
	TP 2.0	40161	2642	6.58E-02	2.49E-05	23.04%
	TP 2.5	40025	2140	5.35E-02	2.36E-05	0.00%
	Exp.	40007	2374	5.93E-02	2.32E-05	11.01%
	Uniform	40005	2322	5.80E-02	2.23E-05	8.56%
Non-Destructive, targeted	TP 1.5	40353	4722	1.17E-01	2.48E-05	94.90%
	TP 2.0	40129	5924	1.48E-01	2.49E-05	145.90%
	TP 2.5	40022	4844	1.21E-01	2.35E-05	101.61%
	Exp.	40007	2754	6.88E-02	2.32E-05	14.67%
	Uniform	40005	2402	6.00E-02	2.23E-05	0.00%
Destructive, targeted	TP 1.5	40355	1910	4.73E-02	2.48E-05	103.94%
	TP 2.0	40130	2559	6.38E-02	2.49E-05	174.80%
	TP 2.5	40022	2109	5.27E-02	2.35E-05	127.12%
	Exp.	40007	1088	2.72E-02	2.31E-05	17.25%
	Uniform	40005	928	2.32E-02	2.23E-05	0.00%

Table A11: Statistical results from the feast and famine simulations

Prey field	Forager	Periods			Durations		
		Median	25%	75%	Median	25%	75%
Uniform	TP1.5	81	53	118	441.96	304.51	682.88
	TP2.0	103	62	154	347.16	233.57	577.81
	TP2.5	74	29	133	484.18	269.01	1241.86
	Exp.	39	14	77	921.77	466.23	2572.14
	Uniform	32	10	68	1125.19	528.93	3606.30
Lévy	TP1.5	81	53	118	441.96	304.51	682.88
	TP2.0	96	29	199	374.82	180.13	1231.10
	TP2.5	15	1	138	2400.77	259.13	35963.75
	Exp.	1	1	58	35913.00	621.43	36018.00
	Uniform	1	1	43	35950.00	837.09	36023.00

Table A12: Summary results of the feast & famine analysis

Prey field	Forager	Famine periods	Mean duration	Period difference	Duration difference	Total famine time	Time difference
Uniform	TP 1.5	8978151	400.32	97.41%	49.38%	3.5941E+09	0.134%
	TP 2.0	11399034	314.92	150.64%	60.18%	3.5897E+09	0.012%
	TP 2.5	9019545	397.95	98.32%	49.68%	3.5893E+09	0.000%
	Exp.	5220879	688.77	14.80%	12.91%	3.5960E+09	0.187%
	Uniform	4547908	790.87	0.00%	0.00%	3.5968E+09	0.209%
Lévy	TP 1.5	10129451	354.58	133.18%	57.18%	3.5917E+09	0.123%
	TP 2.0	13468623	266.35	210.04%	67.83%	3.5873E+09	0.000%
	TP 2.5	9858815	363.97	126.95%	56.04%	3.5883E+09	0.028%
	Exp.	5027762	715.27	15.74%	13.62%	3.5962E+09	0.248%
	Uniform	4344092	828.02	0.00%	0.00%	3.5970E+09	0.270%

Table A13: Statistical results from the destructive, non-targeted feast & famine analysis

Prey field	Forager	Periods			Durations		
		Median	25%	75%	Median	25%	75%
Uniform	TP1.5	90	70	112	400.56	321.12	514.92
	TP2.0	83	57	113	434.49	317.94	629.50
	TP2.5	64	29	110	561.97	326.26	1241.93
	Exp.	71	33	119	505.69	301.87	1090.82
	Uniform	67	26	119	536.31	302.36	1382.69
Lévy	TP1.5	81	50	120	441.94	298.12	717.56
	TP2.0	66	27	123	548.05	290.69	1343.82
	TP2.5	14	1	102	2590.18	352.14	35966.00
	Exp.	1	1	101	35912.00	355.81	36018.00
	Uniform	1	1	90	35950.00	398.97	36024.00

Table A14: Summary results of the destructive, non-targeted feast & famine analysis

Prey field	Forager	Famine periods	Mean duration	Period difference	Duration difference	Total famine time	Time difference
Uniform	TP 1.5	9199040	390.49	20.66%	17.09%	3.5921E+09	0.039%
	TP 2.0	8777389	409.21	15.13%	13.12%	3.5918E+09	0.030%
	TP 2.5	7623772	470.99	0.00%	0.00%	3.5907E+09	0.000%
	Exp.	8214469	437.42	7.75%	7.13%	3.5931E+09	0.067%
	Uniform	8024755	447.80	5.26%	4.92%	3.5935E+09	0.077%
Lévy	TP 1.5	8928444	402.33	21.79%	17.87%	3.5921E+09	0.032%
	TP 2.0	8530378	421.10	16.36%	14.03%	3.5922E+09	0.033%
	TP 2.5	7330875	489.84	0.00%	0.00%	3.5910E+09	0.000%
	Exp.	8001127	449.10	9.14%	8.32%	3.5933E+09	0.065%
	Uniform	7814031	459.90	6.59%	6.11%	3.5937E+09	0.075%

10 Appendix B: Chapter 4 tables of results

Table B1 Summary information of electronic tags deployed.

Species (approx. body size cm)[1] or weight (kg)	Tagging location	Tag type[2]	Recording interval (min / sec)	Depth resolution (m)	n datasets[3]	Reference
Bigeye thresher shark (~220cm FL)	N.Pacific	MT PTT-100	60 min	5.4	2	Musyl et al. unpubl. data, (Musyl *et al.* 2004)
Blue shark (120-215cm FL)	NE. Atlantic	WC PAT Mk10	1.0 s	< 0.5	3	(Queiroz *et al.* 2010)
	N.Pacific	MT PTT-100	60 min	5.4	16	Musyl et al. unpubl. data, (Musyl *et al.* 2004)
Shortfin mako shark (210 cm FL)	N.Pacific	MT PTT-100	60 min	5.4	1	Musyl et al. unpubl. data
Porbeagle shark (180 cm FL)	NE.Atlantic	WC PAT Mk10	1.0 s	< 0.5	1	(Pade *et al.* 2009)
Silky shark (120 – 213cm FL)	N.Pacific	MT PTT-100	15-60 min	5.4	10	Musyl et al. unpubl. data,(Musyl *et al.* 2004)
Oceanic whitetip shark (115-215cm FL)	N.Pacific	MT PTT-100	15-60 min	5.4	13	Musyl et al. unpubl. data,(Musyl *et al.* 2004)
Basking shark (400 – 700cm TL)	NE.Atlantic	WC PAT 3 & 4	1 min	< 0.5	6	(Sims *et al.* 2003)
Whale shark (600 – 700cm TL)	W.Indian Ocean	MT PTT-100	15 min	5.4	1	(Brunnschweiler *et al.* 2009)
Bigeye tuna (65-99cm FL)	Eq. Eastern Pacific	LW LTD 2310	1 min	1.0	5	(Schaefer *et al.* 2009)
Yellowfin tuna (51-60cm FL)	Central N.Pacific	MT PTT-100	60 min	5.4	1	(Musyl *et al.* 2004)
	Eq. Eastern Pacific	LW LTD 2310	1 min	1.0	5	(Schaefer *et al.* 2009)

Species (approx. body size cm)[1] or weight (kg)	Tagging location	Tag type[2]	Recording interval (min / sec)	Depth resolution (m)	n datasets[3]	Reference
Black marlin (453kg)	N.Pacific	MT PTT-100	60 min	5.4	1	Musyl et al. unpubl. data,(Musyl *et al.* 2004)
Blue marlin (45-204kg)	N.Pacific	MT PTT-100	15-60 min	5.4	14	Musyl et al. unpubl. data,(Musyl *et al.* 2004)
Swordfish (215-240cm)	N.Pacific	MT PTT-100	15-60 min	5.4	10	Musyl et al. unpubl. data,(Musyl *et al.* 2004)
Ocean sunfish (60cm TL)	NE.Atlantic	WC PAT Mk10	1.0 s	< 0.5	1	(Sims *et al.* 2009a)

1. Body size: TL, total length, FL Fork length.

2. Tag Manufacturers: LW, Lotek Wireless; MT, Microwave Telemetry; WC, Wildlife Computers. Tag type: PAT, pop-up archival transmitting tag; PTT, platform terminal transmitter, LTD, archival tag (light, temperature, depth).

3. Some of the datasets were too short or had too many gaps to be included in the analysis.

Table B2. Summary of the data used and results of the MLE best fit parameters and model comparison analysis.

[log-likelihoods (LLH) and Akaike weights (wAIC)]. P, TP and E denote power-law, truncated Pareto (power-law) and exponential models respectively; -- indicates that none of the proposed models were considered to be a good fit. Exp denotes the exponential model in the model comparison results. For a few sections where the estimated exponent for the truncated Pareto distribution was < 1 it was not possible to calculate the log-likelihood. When this occurred (in 8 sections), then the Akaike weights could not be calculated.

Species	ID	Section	Total points	Max step-length (m)	Best fit distribution	Best fit exponent	Best fit Xmin	Best fit Xmax	TP / P GOF	Exp GOF	TP / P LLH	Exp LLH	TP / P wAIC	Exp wAIC
Big eye tuna	1	Section 1	48881	719	--									
Big eye tuna	1	Section 2	52801	1531	TP	2.062	15.000	466.000	0.022	0.186	-34989	-36223	1.000	0.000
Big eye tuna	1	Section 3	6001	259	TP	2.012	15.000	259.000	0.036	0.167	-4818	-4946	1.000	0.000
Big eye tuna	1	Section 4	5281	1683	TP	2.213	9.000	1683.000	0.037	0.258	-2657	-2954	1.000	0.000
Big eye tuna	1	Section 5	67321	627	--									
Big eye tuna	1	Section 6	18721	336	TP	2.022	10.000	297.000	0.027	0.172	-12937	-13505	1.000	0.000
Big eye tuna	1	Section 7	7899	336	--									
Big eye tuna	2	Section 1	19801	1281	--									
Big eye tuna	2	Section 2	11521	334	TP	2.189	19.000	334.000	0.032	0.166	-7097	-7332	1.000	0.000
Big eye tuna	2	Section 3	14401	1635	TP	1.938	9.000	1601.000	0.029	0.262	-14885	-15925	1.000	0.000
Big eye tuna	2	Section 4	38881	586	E	0.018	53.000		0.069	0.040	-7217	-7120	0.000	1.000
Big eye tuna	2	Section 5	79201	415	E	0.015	42.000		0.069	0.072	-20058	-19945	0.000	1.000
Big eye tuna	2	Section 6	25921	715	TP	2.548	15.000	715.000	0.027	0.189	-12029	-12425	1.000	0.000
Big eye tuna	2	Section 7	36001	529	TP	1.988	10.000	529.000	0.028	0.185	-30064	-31204	1.000	0.000
Big eye tuna	2	Section 8	33481	422	TP	1.975	5.000	422.000	0.026	0.217	-36913	-39232	1.000	0.000
Big eye tuna	3	Section 1	13072	249	TP	2.752	8.000	249.000	0.041	0.135	-8269	-8325	1.000	0.000
Big eye tuna	3	Section 2	49081	1526	TP	2.129	23.000	677.000	0.026	0.171	-28517	-29182	1.000	0.000
Big eye tuna	3	Section 3	4741	212	E	0.102	2.000		0.158	0.022	-7228	-6801	0.000	1.000
Big eye tuna	3	Section 4	11581	317	TP	2.072	13.000	317.000	0.058	0.095	-9459	-9520	1.000	0.000
Big eye tuna	4	Section 1	7200	302	--									
Big eye tuna	4	Section 2	33120	301	TP	2.525	18.000	301.000	0.022	0.159	-15726	-16065	1.000	0.000

Species	ID	Section	Total points	Max step-length (m)	Best fit distribution	Best fit exponent	Best fit Xmin	Best fit Xmax	TP / P GOF	Exp GOF	TP / P LLH	Exp LLH	TP / P wAIC	Exp wAIC
Big eye tuna	4	Section 3	7200	539	--									
Big eye tuna	4	Section 4	27360	409	--									
Big eye tuna	4	Section 5	15841	648	TP	1.863	13.000	262.000	0.031	0.140	-15605	-15892	1.000	0.000
Big eye tuna	5	Section 1	20067	271	TP	2.369	9.000	271.000	0.034	0.208	-11380	-12077	1.000	0.000
Big eye tuna	5	Section 2	15841	281	TP	2.213	9.000	281.000	0.029	0.208	-14620	-15496	1.000	0.000
Big eye tuna	5	Section 3	15426	412	--									
Big eye tuna	5	Section 4	30241	1541	TP	2.155	13.000	1541.000	0.025	0.238	-25494	-27279	1.000	0.000
Big eye tuna	5	Section 5	5761	271	--									
Big eye tuna	5	Section 6	15841	695	--									
Big eye tuna	5	Section 7	12961	363	TP	2.323	18.000	363.000	0.02	0.160	-5819	-5960	1.000	0.000
Big eye tuna	5	Section 8	50761	735	TP	2.636	33.000	395.000	0.02	0.124	-18969	-19080	1.000	0.000
Yellowfin tuna	1	Section 1	6121	316	E	0.037	4.000		0.109	0.073	-11286	-11136	0.000	1.000
Yellowfin tuna	1	Section 2	4321	57	E	0.262	1.000		0.148	0.036	-5587	-5928	0.000	1.000
Yellowfin tuna	1	Section 3	28801	324	TP	1.610	5.000	286.000	0.043	0.175	-34348	-35298	1.000	0.000
Yellowfin tuna	1	Section 4	17281	315	E	0.033	15.000		0.101	0.027	-16697	-16330	0.000	1.000
Yellowfin tuna	1	Section 5	37081	339	--									
Yellowfin tuna	2	Section 1	23711	370	TP	2.059	11.000	370.000	0.026	0.184	-19744	-20596	1.000	0.000
Yellowfin tuna	2	Section 2	68401	133	E	0.044	4.000		0.123	0.051	-110071	-107593	0.000	1.000
Yellowfin tuna	2	Section 3	50401	1018	E	0.037	8.000		0.107	0.045	-59448	-57663	0.000	1.000
Yellowfin tuna	2	Section 4	10801	370	--									
Yellowfin tuna	2	Section 5	23041	133	E	0.027	4.000		0.143	0.022	-47195	-45065	0.000	1.000
Yellowfin tuna	2	Section 6	154080	1018	--									
Yellowfin tuna	3	Section 1	3948	202	TP	2.187	12.000	202.000	0.065	0.212	-2871	-3007	1.000	0.000
Yellowfin tuna	3	Section 2	12961	350	TP	2.071	12.000	333.000	0.047	0.230	-9477	-9946	1.000	0.000

270

Species	ID	Section	Total points	Max step-length (m)	Best fit distribution	Best fit exponent	Best fit Xmin	Best fit Xmax	TP / P GOF	Exp GOF	TP / P LLH	Exp LLH	TP / P wAIC	Exp wAIC
Yellowfin tuna	3	Section 3	86041	414	TP	1.364	3.000	267.000	0.063	0.159	-118329	-121948	1.000	0.000
Yellowfin tuna	3	Section 4	38881	414	TP	1.464	3.000	397.000	0.058	0.291	-48854	-54359	1.000	0.000
Yellowfin tuna	4	Section 1	2521	200	TP	2.235	13.000	200.000	0.052	0.179	-2101	-2175	1.000	0.000
Yellowfin tuna	4	Section 2	36001	327	TP	2.600	18.000	291.000	0.051	0.124	-20834	-21144	1.000	0.000
Yellowfin tuna	4	Section 3	8641	539	TP	2.584	23.000	539.000	0.023	0.181	-5806	-5947	1.000	0.000
Yellowfin tuna	4	Section 4	5761	339	TP	1.743	8.000	339.000	0.07	0.173	-5729	-5995	1.000	0.000
Yellowfin tuna	4	Section 5	10441	331	TP	1.859	11.000	331.000	0.077	0.125	-8706	-8844	1.000	0.000
Yellowfin tuna	5	Section 1	2521	275	TP	1.505	7.000	275.000	0.088	0.268	-3208	-3377	1.000	0.000
Yellowfin tuna	5	Section 2	34081	293	TP	2.931	25.000	231.000	0.029	0.104	-13483	-13546	1.000	0.000
Yellowfin tuna	5	Section 3	4801	334	TP	1.160	2.000	266.000	0.102	0.133	-8162	-8274	1.000	0.000
Yellowfin tuna	5	Section 4	9001	318	--									
Yellowfin tuna	6	Entire	1058	177	E	0.022	5.380		0.215	0.085	-2825	-2720	0.000	1.000
Black Marlin	1	Section 1	590	204	TP	1.071	5.380	91.450	0.143	0.165	-1661	-1744	1.000	0.000
Black Marlin	1	Section 2	863	349	TP	1.266	5.380	349.670	0.185	0.193	-1808	-1849	1.000	0.000
Blue Marlin	1	Entire	1519	177.522	TP	0.519	5.379	145.000	0.123	0.196	0			
Blue Marlin	2	Entire	1110	177.522	--									
Blue Marlin	3	Entire	1903	290.491	--									
Blue Marlin	4	Entire	1302	215.179	--									
Blue Marlin	5	Entire	1688	107.589	TP	0.442	5.379	80.700	0.145	0.224	0			
Blue Marlin	6	Entire	2174	156.004	TP	0.971	5.379	123.700	0.145	0.152	0			
Blue Marlin	7	Entire	2534	172.143	TP	0.768	5.379	86.100	0.142	0.176	0			
Blue Marlin	8	Entire	2985	209.799	TP	1.092	5.379	166.800	0.122	0.169	-4315	-4484	1.000	0.000
Blue Marlin	9	Entire	2468	129.107	--									
Blue Marlin	10	Entire	2117	172.143	TP	1.680	21.500	150.000	0.107	0.082	-1404	-1425	1.000	0.000

Species	ID	Section	Total points	Max step-length (m)	Best fit distribution	Best fit exponent	Best fit Xmin	Best fit Xmax	TP / P GOF	Exp GOF	TP / P LLH	Exp LLH	TP / P wAIC	Exp wAIC
Blue Marlin	11	Entire	4128	204.42	E	0.027	5.380		0.17	0.133	-7166	-7052	0.000	1.000
Swordfish	1	Entire	1191	597	TP	0.908	5.379	597.100	0.107	0.178	0			
Swordfish	2	Entire	2035	962	--									
Swordfish	3	Entire	1429	624	--									
Swordfish	4	Entire	2650	1285	TP	1.223	5.379	1285.600	0.108	0.307	-7385	-8097	1.000	0.000
Ocean sunfish	1	Section 1	305100	145	TP	2.052	7.000	145.000	0.063	0.151	-891	-913	1.000	0.000
Ocean sunfish	1	Section 2	378000	185	TP	1.924	5.000	185.000	0.077	0.232	-675	-714	1.000	0.000
Big Eye Thresher	1	Entire	1440	473	TP	1.329	10.758	435.700	0.118	0.147	-2903	-3003	1.000	0.000
Big Eye Thresher	2	Entire	1492	457	TP	1.195	32.276	457.200	0.116	0.168	-2285	-2350	1.000	0.000
Blue Shark	1	Entire	819	381	E	0.013	5.380		0.126	0.102	-2207	-2201	0.000	1.000
Blue Shark	2	Entire	1211	387	E	0.017	5.380		0.166	0.180	-3488	-3417	0.000	1.000
Blue Shark	3	Entire	1541	387	--									
Blue Shark	4	Entire	2621	177	TP	0.458	5.379	161.300	0.14	0.205	0			
Blue Shark	5	Entire	2256	532	E	0.012	5.380		0.171	0.151	0			
Blue Shark	6	Entire	4133	430	--									
Blue Shark	7	Entire	846	333	--									
Blue Shark	8	Entire	1924	371	--									
Blue Shark	9	Section 1	29160	121	--									
Blue Shark	9	Section 2	25920	482	TP	1.886	9.000	167.000	0.063	0.217	-741	-765	1.000	0.000
Blue Shark	9	Section 3	70435	482	P	2.458	12.000		0.066	0.237	-1089	-1162	1.000	0.000
Blue Shark	10	Section 1	653040	122	TP	1.630	6.500	122.000	0.062	0.187	-4254	-4405	1.000	0.000
Blue Shark	10	Section 2	1900800	599	TP	2.190	11.000	599.000	0.038	0.242	-9949	-10696	1.000	0.000
Blue Shark	10	Section 3	864000	200	E	0.040	15.000		0.075	0.062	-1916	-1904	0.000	1.000
Blue Shark	10	Section 4	777600	545	TP	1.972	5.500	545.000	0.056	0.234	-6143	-6642	1.000	0.000

Species	ID	Section	Total points	Max step-length (m)	Best fit distribution	Best fit exponent	Best fit Xmin	Best fit Xmax	TP / P GOF	Exp GOF	TP / P LLH	Exp LLH	TP / P wAIC	Exp wAIC
Blue Shark	10	Section 5	2125260	523	TP	1.993	7.500	523.000	0.049	0.206	-9326	-9949	1.000	0.000
Blue Shark	11	Entire	38090	87	--									
Blue Shark	12	Section 1	121403	132	E	0.047	12.500		0.069	0.055	-2645	-2630	0.000	1.000
Blue Shark	12	Section 2	98699	396	TP	2.316	8.500	396.000	0.054	0.173	-2455	-2563	1.000	0.000
Mako shark	1	Section 1	145	376	E	0.017	16.140		0.121	0.106	-333	-333	0.275	0.725
Mako shark	1	Section 2	1273	398	E	0.018	5.380		0.15	0.108	-4031	-3916	0.000	1.000
Mako shark	1	Section 3	865	338	E	0.021	5.380		0.176	0.129	-2319	-2257	0.000	1.000
Mako shark	1	Section 4	532	355	E	0.016	5.380		0.153	0.078	-1530	-1504	0.000	1.000
Porbeagle	1	Entire	2571721	38.5	E	0.172	7.500		0.079	0.080	-2012	-1951	0.000	1.000
Silky shark	1	Entire	2667	231	E	0.027	5.380		0.187	0.079	-7201	-7101	0.000	1.000
Silky shark	2	Entire	4272	193	E	0.055	21.520		0.229	0.137	-2975	-2839	0.000	1.000
Silky shark	3	Entire	1584	166.7	TP	2.030	16.138	156.000	0.181	0.102	-2217	-2256	1.000	0.000
White tip shark	1	Entire	3405	166	TP	1.839	21.520	129.110	0.12	0.114	-4480	-4546	1.000	0.000
Basking shark	1	Section 1	4784	62	TP	1.463	3.000	62.000	0.102	0.166	-935	-972	1.000	0.000
Basking shark	1	Section 2	4705	72	--									
Basking shark	2	Section 1	5715	66	TP	1.576	4.000	66.000	0.073	0.182	-3325	-3464	1.000	0.000
Basking shark	2	Section 2	25439	59	TP	1.750	4.000	59.000	0.063	0.137	-9715	-9832	1.000	0.000
Basking shark	2	Section 3	2880	80	--									
Basking shark	2	Section 4	11521	73	TP	1.379	7.000	73.000	0.134	0.178	-3224	-3338	1.000	0.000
Basking shark	3	Section 1	26770	160.5	TP	1.596	5.500	159.000	0.064	0.214	-7597	-8007	1.000	0.000
Basking shark	3	Section 2	27360	138.5	--									
Basking shark	3	Section 3	42120	161	TP	1.776	7.500	146.000	0.081	0.233	-9741	-10331	1.000	0.000
Basking shark	4	Section 1	51385	100	--									
Basking shark	4	Section 2	12960	182	E	0.030	14.000		0.121	0.104	-2933	-2891	0.000	1.000

Species	ID	Section	Total points	Max step-length (m)	Best fit distribution	Best fit exponent	Best fit Xmin	Best fit Xmax	TP / P GOF	Exp GOF	TP / P LLH	Exp LLH	TP / P wAIC	Exp wAIC
Basking shark	4	Section 3	213892	168	TP	2.414	18.000	168.000	0.058	0.127	-12712	-12735	1.000	0.000
Basking shark	5	Section 1	43437	186	--									
Basking shark	5	Section 2	236425	72	E	0.107	32.000		0.244	0.244	-275	-206	0.000	1.000
Basking shark	6	Section 1	24258	112	TP	1.820	12.000	112.000	0.121	0.180	-4836	-4874	1.000	0.000
Basking shark	6	Section 2	17281	120	E	0.039	16.000		0.085	0.105	-2340	-2304	0.000	1.000
Basking shark	6	Section 3	5761	140	--									
Basking shark	6	Section 4	5761	132	--									
Basking shark	6	Section 5	11521	116	--									
Basking shark	6	Section 6	5224	156	TP	1.732	14.000	156.000	0.137	0.179	-405	-413	0.999	0.001
Whale shark	1	Section 1	1753	80	TP	2.023	5.379	59.200	0.368	0.264	-2529	-2610	1.000	0.000
Whale shark	1	Section 2	721	1285	E	0.012	5.380		0.135	0.012	0			
Whale shark	1	Section 3	4828	1285	--									

Table B3. Kolmogorov-Smirnov goodness of fit values, log-likelihoods and Akaike weights
for key sections analysed and shown in figures or in the spatial analysis.

Species	ID	Section	Best fit distribution	Best fit exponent	Best fit Xmin	Best fit Xmax	TP / P GOF	Exp GOF	TP / P LLH	Exp LLH	TP / P wAIC	Exp wAIC	Gamma GOF
Big eye tuna	1	Section 4	TP	2.213	9.0	1683.0	0.037	0.258	-2657	-2954	1.000	0.000	0.242
Big eye tuna	2	Section 2	TP	2.189	19.0	334.0	0.032	0.166	-7097	-7332	1.000	0.000	0.105
Big eye tuna	2	Section 3	TP	1.938	9.0	1601.0	0.029	0.262	-14885	-15925	1.000	0.000	0.196
Big eye tuna	2	Section 4	E	0.018	53.0		0.069	0.040	-7217	-7120	0.000	1.000	
Big eye tuna	2	Section 5	E	0.015	42.0		0.069	0.072	-20058	-19945	0.000	1.000	
Big eye tuna	2	Section 6	TP	2.548	15.0	715.0	0.027	0.189	-12029	-12425	1.000	0.000	0.185
Big eye tuna	2	Section 7	TP	1.988	10.0	529.0	0.028	0.185	-30064	-31204	1.000	0.000	0.136

Species	ID	Section	Best fit distribution	Best fit exponent	Best fit Xmin	Best fit Xmax	TP / P GOF	Exp GOF	TP / P LLH	Exp LLH	TP / P wAIC	Exp wAIC	Gamma GOF
Big eye tuna	2	Section 8	TP	1.975	5.0	422.0	0.026	0.217	-36913	-39232	1.000	0.000	0.148
Big eye tuna	3	Section 3	E	0.102	2.0		0.158	0.022	-7228	-6801	0.000	1.000	
Big eye tuna	5	Section 4	TP	2.155	13.0	1541.0	0.025	0.238	-25494	-27279	1.000	0.000	0.233
Yellowfin tuna	1	Section 1	E	0.037	4.0		0.109	0.073	-11286	-11136	0.000	1.000	
Yellowfin tuna	1	Section 3	TP	1.610	5.0	286.0	0.043	0.175	-34348	-35298	1.000	0.000	0.144
Yellowfin tuna	1	Section 4	E	0.033	15.0		0.101	0.027	-16697	-16330	0.000	1.000	
Yellowfin tuna	2	Section 1	TP	2.059	11.0	370.0	0.026	0.184	-19744	-20596	1.000	0.000	0.175
Yellowfin tuna	2	Section 2	E	0.044	4.0		0.123	0.051	-110071	-107593	0.000	1.000	
Yellowfin tuna	2	Section 3	E	0.037	8.0		0.107	0.045	-59448	-57663	0.000	1.000	
Yellowfin tuna	2	Section 5	E	0.027	4.0		0.143	0.022	-47195	-45065	0.000	1.000	
Yellowfin tuna	3	Section 3	TP	1.364	3.0	267.0	0.063	0.159	-118329	-121948	1.000	0.000	0.112
Yellowfin tuna	3	Section 4	TP	1.464	3.0	397.0	0.058	0.291	-48854	-54359	1.000	0.000	0.160
Yellowfin tuna	4	Section 4	TP	1.743	8.0	339.0	0.07	0.173	-5729	-5995	1.000	0.000	0.154
Yellowfin tuna	4	Section 5	TP	1.859	11.0	331.0	0.077	0.125	-8706	-8844	1.000	0.000	
Yellowfin tuna	5	Section 1	TP	1.505	7.0	275.0	0.088	0.268	-3208	-3377	1.000	0.000	0.203
Yellowfin tuna	5	Section 3	TP	1.160	2.0	266.0	0.102	0.133	-8162	-8274	1.000	0.000	0.081
Yellowfin tuna	6	Entire	E	0.022	5.4		0.215	0.085	-2825	-2720	0.000	1.000	
Mola mola	1	Section 2	TP	1.924	5.0	185.0	0.077	0.232	-675	-714	1.000	0.000	0.173
Blue Shark	9	Section 2	TP	1.886	9.0	167.0	0.063	0.217	-741	-765	1.000	0.000	0.185
Blue Shark	9	Section 3	P	2.458	12.0		0.066	0.237	-1089	-1162	1.000	0.000	0.214
Blue Shark	10	Section 1	TP	1.630	6.5	122.0	0.062	0.187	-4254	-4405	1.000	0.000	0.157
Blue Shark	10	Section 2	TP	2.190	11.0	599.0	0.038	0.242	-9949	-10696	1.000	0.000	0.215
Blue Shark	10	Section 3	E	0.040	15.0		0.075	0.062	-1916	-1904	0.000	1.000	

Species	ID	Section	Best fit distribution	Best fit exponent	Best fit Xmin	Best fit Xmax	TP / P GOF	Exp GOF	TP / P LLH	Exp LLH	TP / P wAIC	Exp wAIC	Gamma GOF
Blue Shark	10	Section 4	TP	1.972	5.5	545.0	0.056	0.234	-6143	-6642	1.000	0.000	0.182
Blue Shark	10	Section 5	TP	1.993	7.5	523.0	0.049	0.206	-9326	-9949	1.000	0.000	0.179
Blue Shark	12	Section 2	TP	2.316	8.5	396.0	0.054	0.173	-2455	-2563	1.000	0.000	0.180
Silky shark	2	Entire	E	0.055	21.520		0.229	0.137	-2975	-2839	0.000	1.000	
Silky shark	3	Entire	TP	2.030	16.138	156.000	0.181	0.102	-2217	-2256	1.000	0.000	0.160

11 Appendix C: Chapter 5 additional tables and figures

Table C1: Summary of the original GPS location data used to calculate the flight profiles.
BBA is black-browed and WA is wandering albatross.

Reference	Points	Elapsed Time (hours)	Length (m)	Min Step (m)	Max Step (m)	No of flight steps
BBA01	2638	47.83	640345	0.58	2677.48	41
BBA02	2528	46.25	935469	1.08	1992.37	37
BBA03	2432	46.64	752561	0.45	2354.88	41
BBA04	732	37.69	306117	3.72	10847.04	24
BBA05	1424	24.78	449560	0.89	1339.30	25
BBA06	1516	26.78	727512	1.40	2504.82	18
BBA07	4792	83.93	1425396	0.45	308381.90	70
BBA08	853	15.60	404979	0.45	2680.43	12
BBA09	2503	44.80	652106	0.50	1771.48	46
BBA10	2117	36.98	777877	1.77	2270.50	24
BBA11	3170	59.25	1167475	0.73	3911.72	77
BBA12	1392	24.98	534236	2.08	1884.21	49
BBA13	703	18.11	513686	4.80	12499.82	12
BBA14	2294	41.94	741684	0.45	2668.50	51
BBA15	3433	60.87	861308	0.45	2066.58	46
BBA16	3457	67.88	1407061	1.32	3516.70	97
BBA17	1311	24.00	434634	3.43	5656.79	15
BBA18	2512	46.49	810655	0.45	2889.89	54
BBA19	240	12.16	111097	0.89	2456.46	13
BBA20	565	33.19	543329	3.06	8530.54	16
BBA21	655	33.69	736786	1.32	5419.73	23
BBA22	1806	96.95	1477311	0.33	8464.50	52
BBA23	1663	87.35	1309014	0.33	11372.01	22
BBA24	1521	27.58	579787	0.78	2425.25	35
BBA25	14774	48.62	1566633	0.18	2451.97	29
BBA26	8690	28.53	1214995	0.36	3529.26	9
BBA27	15059	47.99	1245957	0.13	1037.72	19
BBA28	160	2.61	38018	0.63	21267.48	2
BBA29	16852	49.38	1508445	0.29	1060.35	32
BBA30	17106	50.81	1866018	0.11	7154.09	20
BBA31	9612	38.87	1000653	0.18	5467.32	20
BBA32	8567	30.28	835572	0.29	2754.65	11
BBA33	15535	48.01	1355576	0.22	1663.76	33
BBA34	11377	36.17	1237470	0.29	8207.48	17
BBA35	2744	8.76	235204	0.23	1122.48	7
BBA36	5680	22.64	917187	1.71	3974.96	2
BBA37	22450	69.68	2240907	0.18	2702.88	49
BBA38	8708	42.86	363093	0.13	715.15	33
BBA39	4904	19.99	527722	0.29	1705.60	7

Reference	Points	Elapsed Time (hours)	Length (m)	Min Step (m)	Max Step (m)	No of flight steps
BBA40	9471	34.55	823298	0.22	4456.25	9
BBA41	5224	21.98	511339	0.31	3483.31	14
BBA42	7496	27.63	810469	0.13	3090.90	18
BBA43	21833	66.11	2197770	0.13	22959.36	35
BBA44	12259	38.18	988215	0.18	14807.79	27
BBA45	14917	49.63	1305995	0.22	12442.33	36
BBA46	24158	79.80	1287188	0.07	3244.49	68
BBA47	13285	43.89	1867030	0.13	379082.90	30
BBA48	6440	21.44	301416	0.13	7796.18	8
BBA49	10485	35.43	1082602	0.11	11769.75	9
BBA50	1918	5.37	175063	0.53	601.17	6
BBA51	15706	56.66	791716	0.13	2355.02	16
BBA52	19543	69.02	1694744	0.13	7467.27	38
BBA53	7075	21.56	719796	0.18	2177.53	30
BBA54	12727	44.97	1293197	0.22	3698.27	26
BBA55	13599	44.68	1121769	0.07	3167.87	34
BBA56	570	2.14	90557	0.66	1696.93	2
BBA57	3550	10.25	402538	0.23	514.57	6
BBA58	10384	33.21	1242367	0.23	3031.86	17
BBA59	6056	22.60	547045	0.30	1832.12	35
BBA60	10451	32.40	1040653	0.31	1279.98	14
BBA61	3257	11.46	404602	0.49	1986.44	9
WA01	8609	18.70	427702	0.22	12839.40	14
WA02	6993	18.38	514517	0.08	32056.53	10
WA03	27734	37.48	1371064	0.11	11292.90	16
WA04	27423	43.38	1046134	0.23	105668.40	15
WA05	9887	30.74	1449278	0.34	906.95	9
WA06	22488	78.56	2531244	0.19	12147.15	34
WA07	7399	32.52	631939	0.19	1029.00	5
WA08	28672	89.26	2426064	0.14	17363.29	39
WA09	9629	29.19	967481	0.27	2033.50	9
WA10	13985	44.43	1395147	0.19	13507.16	15
WA11	7572	24.95	311985	0.14	1026.84	5
WA12	23566	72.77	2951930	0.08	29393.30	27
WA13	16350	48.79	1424881	0.15	1961.04	20
WA14	7212	31.40	897982	0.30	4382.00	7
WA15	7284	30.38	332189	0.19	3195.47	12
WA16	4602	21.53	350554	0.27	914.56	11
WA17	27696	90.39	3398509	0.11	3540.00	21
WA18	13777	52.35	1358927	0.11	1901.25	8
WA19	12224	41.97	1503415	0.27	1646.33	6
WA20	12881	41.31	757913	0.14	5110.63	14
WA21	31197	90.42	3994637	0.11	1206.78	40
WA22	23064	71.10	2046603	0.24	1800.14	42

Reference	Points	Elapsed Time (hours)	Length (m)	Min Step (m)	Max Step (m)	No of flight steps
WA23	29659	88.48	4718301	0.20	26374.45	27
WA24	30209	86.92	3287408	0.08	2666.38	18
WA25	23086	73.83	2476751	0.14	9196.77	23
WA26	24906	76.24	2212841	0.11	5116.33	17
WA27	2864	8.15	319635	0.30	1118.82	4

Table C2: Summary of the wet/dry logger data

Reference	No of Steps	Elapsed Time (hours)	Length (m)	Min Step (m)	Max Step (m)
WA30	22	21.52	140946	177	80717
WA31	30	59.88	1192241	11	191640
WA32	19	45.57	718688	258	176911
WA33	8	4.97	142697	2134	81093
WA34	35	64.37	1475209	125	190528
WA35	10	23.45	150878	239	42776
WA36	4	2.05	93014	1075	69558
WA37	30	38.38	708676	57	173671
WA38	21	46.63	411277	437	69387
WA39	54	74.43	1076748	657	207885
WA40	47	72.90	1938794	281	287843
WA41	28	39.43	827186	194	237290
WA42	13	41.65	138905	696	38840
WA43	30	141.38	2651628	114	272700
WA44	21	39.97	1187369	710	267044
WA45	36	53.38	782257	113	126758
WA46	14	24.45	311699	67	110136

In the following tables Comp AICw refers to the competing distribution; OoM refers to Orders of Magnitude. In some cases (unusually high or low TP exponents) it is not possible to calculate log-likelihoods and in other cases (fewer than 5 fitted steps) it is not possible to calculate Akaike weights, values are therefore shown as --.

Table C3. Truncated Pareto (TP) fits for flight step distributions

Reference	Steps	Min Step	Max Step	Xmin	Exponent	Xmax	Exp AICw	Exp Comp AICw	TP AICw	TP Comp AICw	Exp Fit	TP Fit	Fitted steps	OoM
BBA16	97	103	90018	344	1.35	65495	0.00	1.00	1.00	0.00	0.335	0.052	80	2.28
BBA11	77	61	75555	244	1.33	58867	0.09	0.91	1.00	0.00	0.171	0.062	67	2.38
BBA46	68	21	85913	323	1.30	47717	0.20	0.80	1.00	0.00	0.162	0.123	52	2.17
BBA18	54	30	87001	732	1.28	31986	0.18	0.82	1.00	0.00	0.171	0.051	42	1.64
BBA22	52	569	119532	728	1.34	119532	0.66	0.34	1.00	0.00	0.178	0.083	49	2.22
BBA14	51	19	131879	137	1.13	52015	0.01	0.99	1.00	0.00	0.309	0.067	46	2.58
BBA37	49	70	107824	129	1.26	33017	0.01	0.99	1.00	0.00	0.204	0.084	38	2.41
BBA09	46	178	73229	1938	1.44	70914	0.08	0.92	1.00	0.00	0.274	0.100	24	1.56
BBA15	46	56	75897	95	1.07	68676	0.07	0.93	1.00	0.00	0.159	0.122	42	2.86
WA22	42	119	94364	983	1.04	37622	0.04	0.96	0.96	0.04	0.246	0.097	33	1.58
BBA03	41	110	60098	469	1.29	15664	0.00	1.00	0.99	0.01	0.345	0.076	29	1.52
BBA01	41	25	126983	313	1.30	126983	0.69	0.31	1.00	0.00	0.161	0.129	33	2.61
WA08	39	364	265214	2104	1.25	265214	0.55	0.45	1.00	0.00	0.165	0.103	31	2.10
BBA52	38	40	158908	1321	1.31	158908	0.82	0.18	1.00	0.00	0.122	0.086	26	2.08
BBA02	37	216	151350	543	1.11	151350	0.00	1.00	1.00	0.00	0.298	0.130	32	2.45
BBA45	36	47	162559	233	1.28	140678	0.00	1.00	1.00	0.00	0.298	0.105	30	2.78
BBA59	35	51	123722	315	1.52	79569	0.00	1.00	1.00	0.00	0.534	0.080	27	2.40
BBA55	34	94	116256	972	1.46	116256	0.00	1.00	1.00	0.00	0.339	0.104	22	2.08
BBA33	33	59	106320	2539	1.28	106320	0.15	0.85	0.99	0.01	0.187	0.092	24	1.62
BBA47	30	174	376409	309	1.37	376409	0.00	1.00	1.00	0.00	0.552	0.109	28	3.09

Reference	Steps	Min Step	Max Step	Xmin	Exponent	Xmax	Exp AICw	Exp Comp AICw	TP AICw	TP Comp AICw	Exp Fit	TP Fit	Fitted steps	OoM
BBA53	30	185	169608	267	1.46	19799	0.11	0.89	1.00	0.00	0.295	0.141	23	1.87
BBA54	26	430	147638	3853	1.03	147638	0.41	0.59	0.89	0.11	0.247	0.147	16	1.58
BBA05	25	121	110475	121	1.10	110475	0.91	0.09	1.00	0.00	0.236	0.084	24	2.96
WA17	21	3128	640030	12547	1.45	640030	0.66	0.34	1.00	0.00	0.264	0.117	18	1.71
WA01	14	83	57494	83	1.03	57494	0.00	0.00	1.00	0.00	0.476	0.158	13	2.84
BBA13	12	453	95362	1328	1.00	95362	0.17	0.83	0.83	0.17	0.251	0.126	9	1.86

Table C4. Exponential fits for flight step distributions

Reference	Steps	Min Step	Max Step	Xmin	Exponent	Exp AICw	Exp Comp AICw	TP AICw	TP Comp AICw	Exp Fit	TP Fit	Fitted steps	OoM
BBA25	29	217	82855	606	6.46E-05	0.87	0.13	0.46	0.54	0.088	0.105	24	2.14
WA23	27	416	657713	7205	7.44E-06	0.78	0.22	1.00	0.00	0.110	0.123	20	1.96
WA12	27	545	442310	13758	1.08E-05	0.79	0.21	0.99	0.01	0.089	0.091	14	1.51
BBA44	27	139	70814	19547	6.79E-05	0.96	0.04	0.43	0.57	0.198	0.089	8	0.56
BBA21	23	838	79991	1447	4.73E-05	0.54	0.46	0.98	0.02	0.121	0.138	18	1.74
BBA30	20	706	227013	45408	2.57E-05	0.88	0.12	0.03	0.97	0.090	0.151	13	0.70
WA24	18	774	354412	42323	8.96E-06	0.64	0.36	0.02	0.98	0.173	0.174	13	0.92
BBA51	16	91	105091	91	5.13E-05	0.54	0.46	0.14	0.86	0.137	0.167	15	3.06
BBA19	13	348	21110	2299	2.04E-04	1.00	0.00	0.26	0.74	0.319	0.111	5	0.96
WA15	12	2707	52412	2707	7.66E-05	0.83	0.17	0.22	0.78	0.188	0.251	11	1.29
WA16	11	104	67625	104	6.65E-05	0.67	0.33	0.00	1.00	0.104	0.298	10	2.81
WA05	9	2471	402166	90015	9.81E-06	1.00	0.00	0.00	1.00	0.273	0.273	5	0.65
BBA49	9	666	191927	7010	1.81E-05	1.00	0.00	0.09	0.91	0.273	0.204	5	1.44
BBA48	8	765	43379	765	4.68E-05	0.76	0.24	0.02	0.98	0.305	0.193	7	1.75
WA18	8	387	441150	387	8.43E-06	0.76	0.24	0.03	0.97	0.153	0.193	7	3.06

Reference	Steps	Min Step	Max Step	Xmin	Exponent	Exp AICw	Exp Comp AICw	TP AICw	TP Comp AICw	Exp Fit	TP Fit	Fitted steps	OoM
BBA39	7	1379	43882	1379	5.07E-05	0.94	0.06	0.00	1.00	0.362	0.242	6	1.50
BBA35	7	756	9727	756	3.09E-04	0.99	0.01	0.01	0.99	0.181	0.181	6	1.11
BBA50	6	105	21844	105	1.34E-04	1.00	0.00	--	--	0.223	0.323	5	2.32

Table C5. Mixed model flight step distributions

Reference	Steps	Min Step	Max Step	Exp Xmin	Exp Exponent	TP Xmin	TP Exponent	TP Xmax	Exp AICw	Exp Comp AICw	TP AICw	TP Comp AICw	Exp Fit	TP Fit	TP OoM	Exp OoM
BBA07	70	92	43848	229	1.41E-04	225	0.91	21728	0.00	1.00	1.00	0.00	0.138	0.066	1.99	2.28
BBA12	49	52	70669	52	1.64E-04	237	1.87	3340	0.00	1.00	0.44	0.56	0.586	0.097	1.15	3.13
WA21	40	2386	348474	2386	1.78E-05	16910	1.73	348474	1.00	0.00	0.96	0.04	0.155	0.123	1.31	2.16
BBA43	35	35	91744	237	4.59E-05	35	0.78	91744	0.17	0.83	1.00	0.00	0.109	0.119	3.42	2.59
BBA24	35	136	52189	1058	6.33E-05	136	0.96	32329	0.10	0.90	1.00	0.00	0.148	0.070	2.38	1.69
WA06	34	144	242265	2331	2.01E-05	11679	1.05	146353	0.84	0.16	0.72	0.28	0.079	0.055	1.10	2.02
BBA38	33	92	35748	577	1.88E-04	420	1.16	11042	0.02	0.98	0.85	0.15	0.183	0.083	1.42	1.79
BBA29	32	125	60158	680	5.26E-05	281	0.89	60158	0.04	0.96	1.00	0.00	0.136	0.102	2.33	1.95
BBA04	24	586	56878	586	1.30E-04	1350	1.15	13797	0.36	0.64	0.55	0.45	0.220	0.114	1.01	1.99
BBA10	24	260	119171	651	5.45E-05	260	0.80	12612	0.00	1.00	0.97	0.03	0.284	0.114	1.69	2.26
WA25	23	633	384623	22188	8.52E-06	10365	1.25	170763	0.49	0.51	0.48	0.52	0.210	0.105	1.22	1.24
BBA23	22	803	90633	803	3.51E-05	7288	1.28	86467	0.12	0.88	0.80	0.20	0.145	0.128	1.07	2.05
WA13	20	320	140636	320	2.19E-05	45090	0.77	140636	0.17	0.83	0.11	0.89	0.107	0.180	0.49	2.64
BBA31	20	49	95834	6537	2.33E-05	1661	0.93	95834	0.47	0.53	0.97	0.03	0.303	0.147	1.76	1.17
BBA27	19	544	60266	5073	4.59E-05	4339	4.00	8149	0.33	0.67	0.00	1.00	0.223	0.274	0.27	1.07
BBA42	18	488	62765	548	6.04E-05	1123	0.89	62765	0.21	0.79	0.73	0.27	0.130	0.142	1.75	2.06
BBA06	18	315	92777	5664	2.87E-05	3066	1.31	92131	0.44	0.56	0.89	0.11	0.292	0.194	1.48	1.21
BBA58	17	126	143584	21770	2.76E-05	126	0.92	143584	0.96	0.04	1.00	0.00	0.208	0.128	3.06	0.82

Reference	Steps	Min Step	Max Step	Exp Xmin	Exp Exponent	TP Xmin	TP Exponent	TP Xmax	Exp AICw	Exp Comp AICw	TP AICw	TP Comp AICw	Exp Fit	TP Fit	TP OoM	Exp OoM
WA26	17	1174	417106	64834	1.15E-05	1174	0.75	97896	0.93	0.07	0.64	0.36	0.143	0.123	1.92	0.81
BBA34	17	252	130486	1572	3.19E-05	12155	1.75	123557	0.16	0.84	0.18	0.82	0.153	0.170	1.01	1.92
BBA20	16	1756	69325	1756	5.43E-05	9025	-0.18	17064	0.33	0.67	0.09	0.91	0.205	0.167	0.28	1.60
WA03	16	53	174220	180	1.35E-05	53	-0.34	205	0.00	1.00	0.25	0.75	0.361	0.204	0.59	2.99
WA10	15	1074	68428	1396	4.50E-05	1074	0.86	68428	0.22	0.78	0.90	0.10	0.162	0.073	1.80	1.69
BBA17	15	222	60606	222	6.39E-05	11773	3.29	33758	0.02	0.98	0.01	0.99	0.220	0.199	0.46	2.44
WA04	15	21	135047	135	2.30E-05	21	0.90	135047	0.01	0.99	1.00	0.00	0.205	0.147	3.81	3.00
WA20	14	477	71643	477	3.54E-05	12878	0.87	71643	0.27	0.73	0.30	0.70	0.158	0.115	0.75	2.18
BBA41	14	502	50948	502	8.82E-05	4922	1.39	50948	0.23	0.77	0.17	0.83	0.158	0.159	1.01	2.01
BBA60	14	1930	65805	1930	4.94E-05	8264	1.12	65805	0.41	0.59	0.26	0.74	0.158	0.229	0.90	1.53
BBA08	12	308	87517	3501	4.47E-05	308	0.90	87517	0.80	0.20	0.79	0.21	0.149	0.094	2.45	1.40
BBA32	11	957	104025	957	5.12E-05	957	0.81	31411	0.38	0.62	0.35	0.65	0.208	0.121	1.52	2.04
WA02	10	78	119567	78	3.13E-05	36728	2.61	119567	0.17	0.83	--	--	0.233	0.415	0.51	3.18
BBA61	9	646	65872	646	4.28E-05	646	0.87	49975	0.35	0.65	0.42	0.58	0.264	0.161	1.89	2.01
BBA40	9	406	85597	406	3.54E-05	47717	2.83	85597	0.37	0.63	--	--	0.264	0.667	0.25	2.32
BBA26	9	770	192692	770	1.32E-05	141268	4.15	192692	0.13	0.87	--	--	0.264	0.667	0.13	2.40
WA09	9	4739	158782	121526	7.75E-05	121526	718.22	121865	--	--	--	--	0.396	0.000	0.00	0.12
WA14	7	43280	106342	77463	8.97E-05	77463	108.67	78915	--	--	--	--	0.351	0.000	0.01	0.14
BBA57	6	3670	21990	3670	8.50E-05	11716	-2.45	21990	1.00	0.00	--	--	0.445	0.323	0.27	0.78
WA19	6	2795	343588	151222	1.34E-05	151222	2.34	343588	--	--	--	--	0.544	0.544	0.36	0.36
WA11	5	233	31330	233	1.00E-04	4444	1.98	31330	--	--	--	--	0.290	0.488	0.85	2.13
WA07	5	1336	147270	1336	1.38E-05	1336	0.76	147270	--	--	--	--	0.580	0.290	2.04	2.04
WA27	4	17908	35046	28545	3.08E-04	28545	1.00	35046	--	--	--	--	1.000	1.000	0.09	0.09
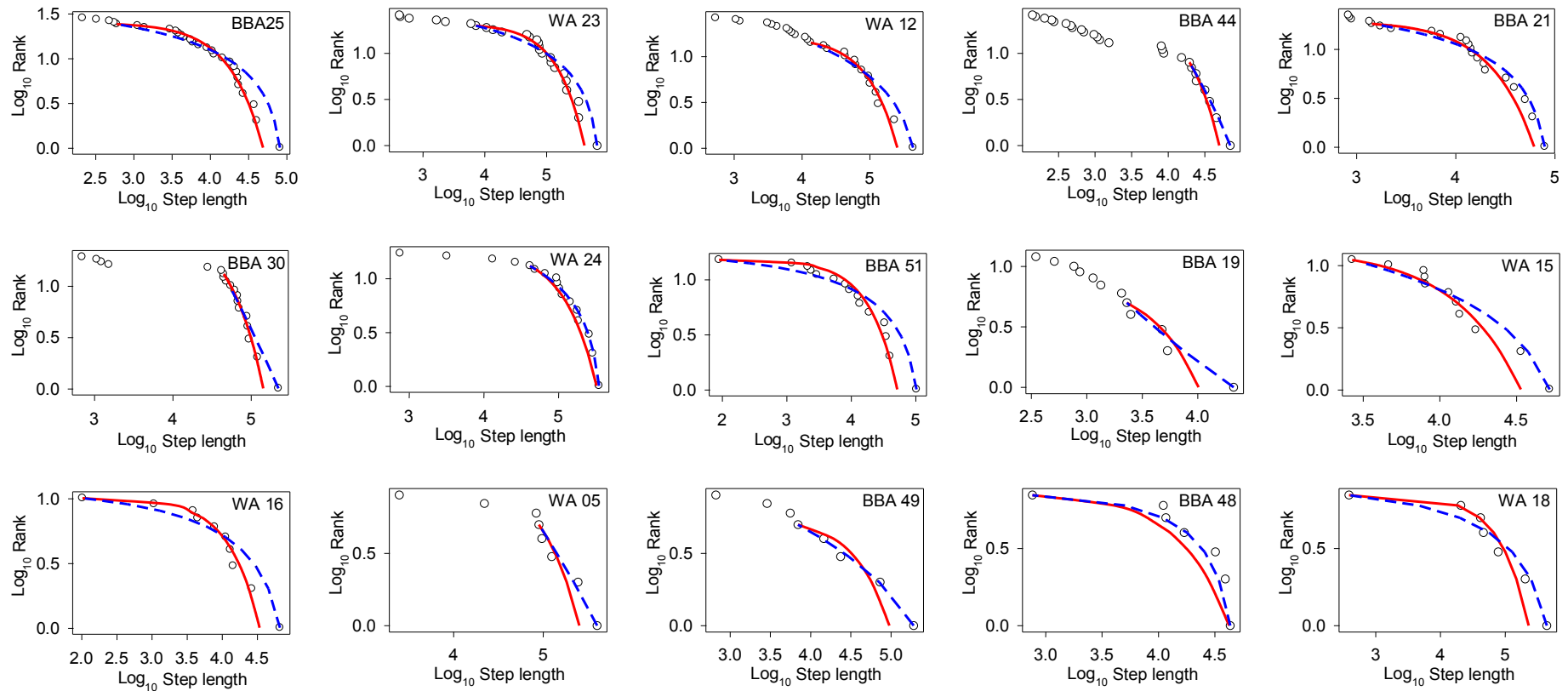
Figure C1. Ranked step-length plots for best fit exponential distributions for albatross flight steps
Black circles are step-lengths; red line is the competing exponential distribution; blue dashed line is the alternate TP distribution.
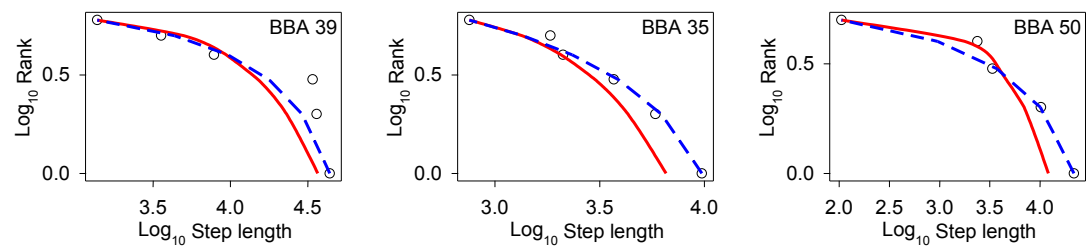
Figure C1 (Continued...)
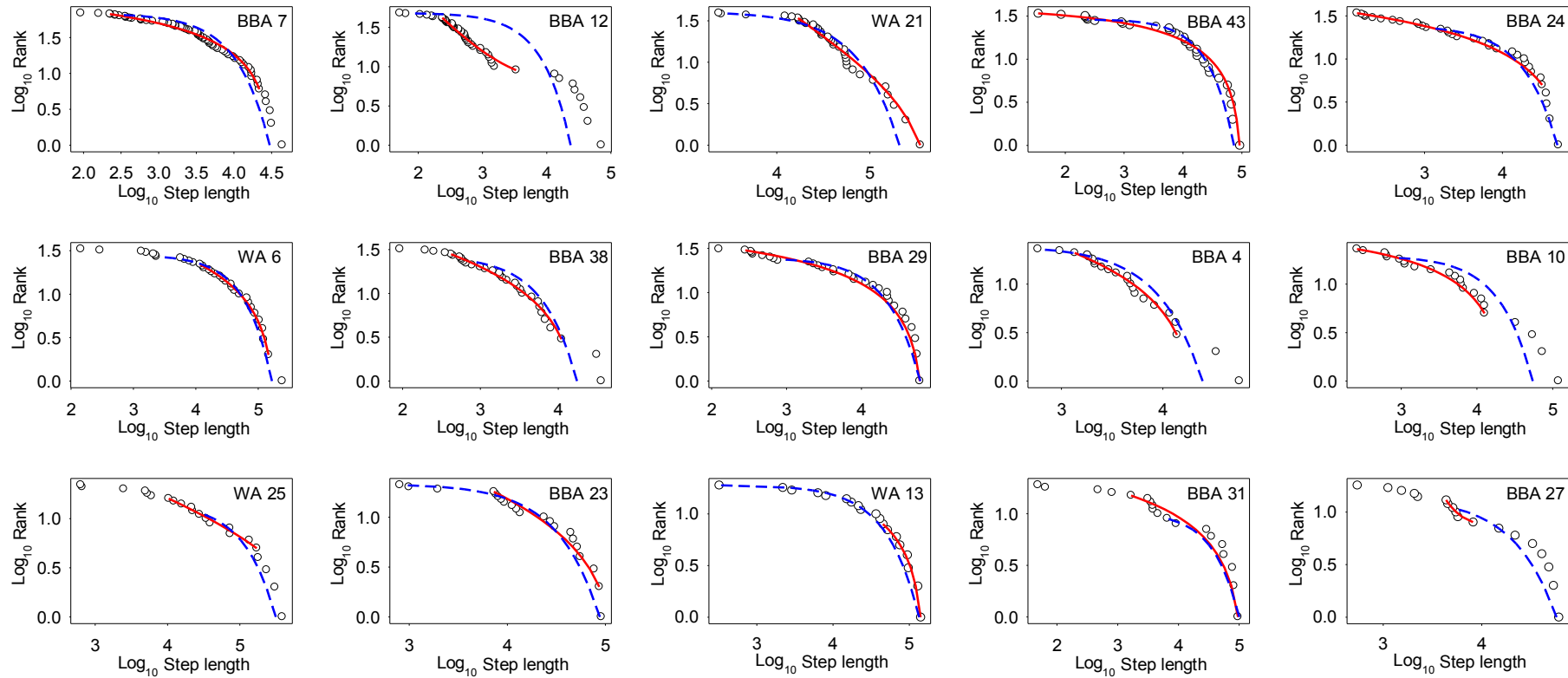
Figure C2. Ranked step-length plots for mixed model fits for flight steps
Black circles are step-lengths; red line is the best fit TP distribution; blue dashed lines are the best fit exponential distribution. Plots with fewer than 15 points are not shown.
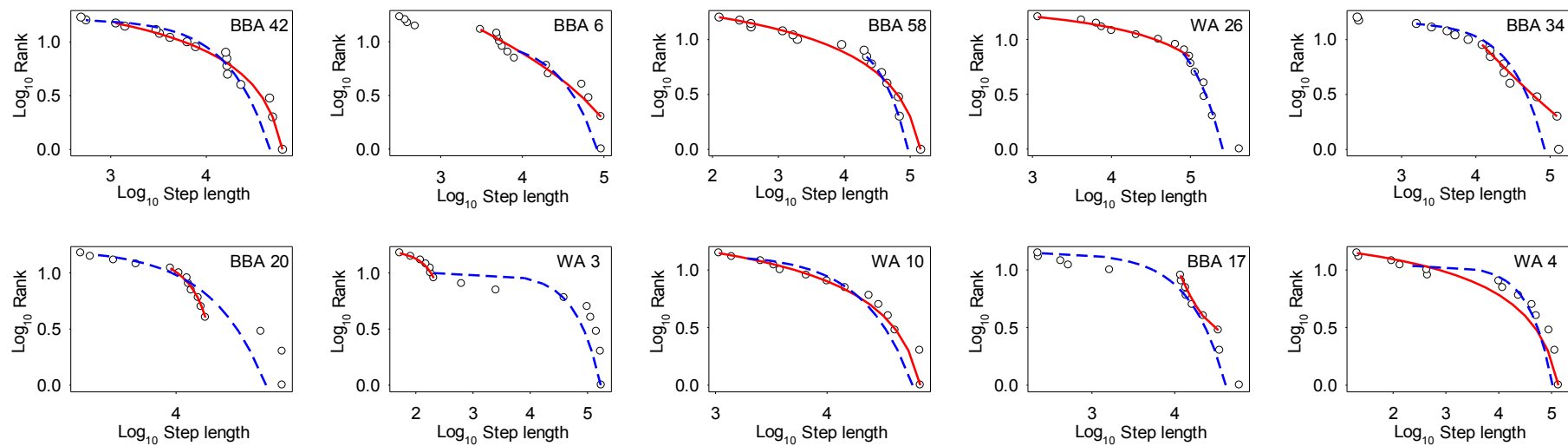
Figure C2 (Continued...)

11.1 MLE Results of wet/dry logger analysis

Table C6: Truncated Pareto (TP) fits for flight step distributions

Reference	Steps	Min Step	Max Step	Xmin	Exponent	Xmax	Exp AICw	Exp Comp AICw	TP AICw	TP Comp AICw	Exp Fit	TP Fit	Fitted steps	OoM
WA39	53	424	207885	424	1.05	94120	0.60	0.40	1.00	0.00	0.142	0.061	50	2.35
WA40	47	281	287843	4597	1.16	196604	0.64	0.36	0.99	0.01	0.107	0.060	36	1.63
WA45	36	113	126514	135	1.11	53049	0.03	0.97	1.00	0.00	0.224	0.094	24	2.59
WA41	28	187	236327	187	1.03	236327	0.71	0.29	1.00	0.00	0.289	0.175	24	3.10

Table C7: Exponential fits for flight step distributions

Reference	Steps	Min Step	Max Step	Xmin	Exponent	Exp AICw	Exp Comp AICw	TP AICw	TP Comp AICw	Exp Fit	TP Fit	Fitted steps	OoM
WA38	21	312	69387	312	5.13E-05	0.65	0.35	0.63	0.37	0.152	0.225	20	2.35

Table C8: Mixed model flight step distributions

Reference	Steps	Min Step	Max Step	Exp Xmin	Exp Exponent	TP Xmin	TP Exponent	TP Xmax	Exp AICw	Exp Comp AICw	TP AICw	TP Comp AICw	Exp Fit	TP Fit	TP OoM	Exp OoM
WA34	35	115	190528	125	2.27E-05	115	0.78	190528	0.00	1.00	1.00	0.00	0.134	0.128	3.22	3.18
WA43	30	76	262529	114	1.21E-05	43832	1.44	229857	0.40	0.60	0.44	0.56	0.109	0.167	0.72	3.36
WA31	30	10	191508	68	2.50E-05	2197	0.71	113910	0.03	0.97	0.90	0.10	0.146	0.134	1.71	3.45
WA37	30	57	173184	2946	2.64E-05	115	0.95	173184	0.33	0.67	1.00	0.00	0.141	0.080	3.18	1.77
WA30	22	177	80188	883	3.34E-05	177	1.34	1060	--	--	0.24	0.76	0.557	0.251	0.78	1.96
WA44	21	358	267037	2366	1.23E-05	358	0.92	267037	0.25	0.75	1.00	0.00	0.165	0.102	2.87	2.05
WA32	19	775	176911	6821	1.82E-05	6821	1.16	160244	0.24	0.76	0.59	0.41	0.223	0.128	1.37	1.41
WA46	14	108	108715	542	3.23E-05	108	0.91	35160	0.26	0.74	0.63	0.37	0.229	0.194	2.51	2.30
WA42	13	555	38827	13164	1.34E-04	555	0.93	38827	1.00	0.00	0.81	0.19	0.239	0.172	1.85	0.47
WA35	10	159	132601	159	3.77E-05	20546	4.79	23909	0.31	0.69	--	--	0.233	0.699	0.07	2.92
WA33	8	1235	81093	4610	4.36E-05	1235	1.27	81093	--	--	0.40	0.60	0.375	0.153	1.82	1.25
WA36	4	910	69134	910	3.34E-05	22381	1.00	69134	--	--	--	--	0.421	1.000	0.49	1.88

Figure C3: Exponential fit for flight step distributions from wet dry logger data
For TP fits see Chapter 5
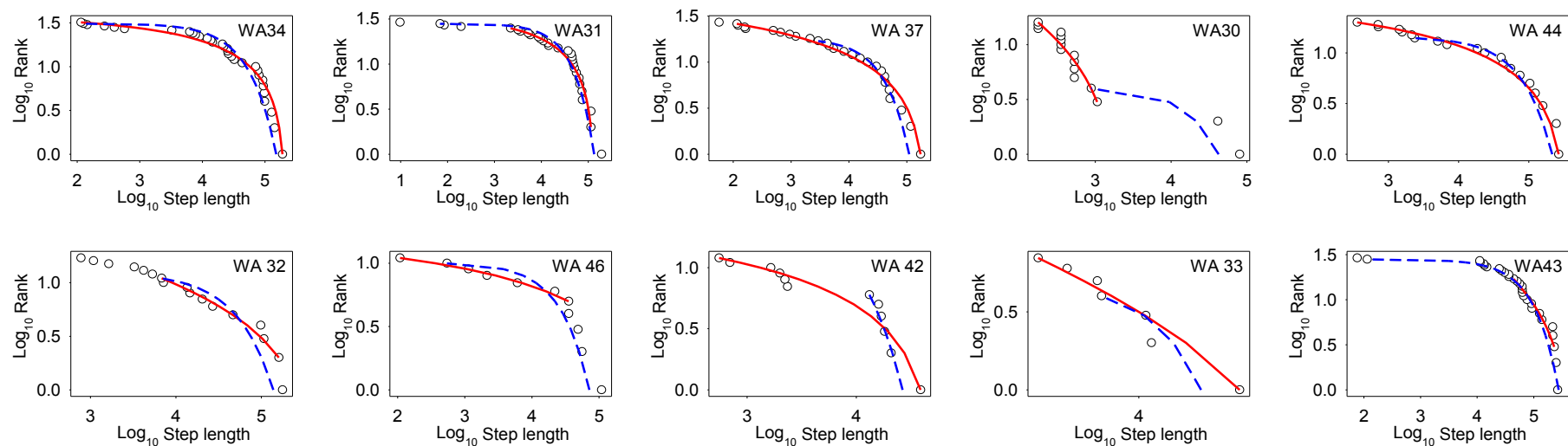
Figure C4: Mixed model fits for flight step distributions from wet/dry logger data.
Two shortest plots not show.

11.2 Reanalysis of 2004 Albatross data

In the following tables, Comp AIC refers to the competing distribution and OoM refers to Orders of Magnitude.

Table C9. Data reanalysis showing TP fits

Reference	Steps	Min Step	Max Step	Xmin	Exponent	Xmax	Exp AICw	Exp Comp AICw	TP AICw	TP Comp AICw	Exp Fit	TP Fit	Fitted steps	OoM
2004_P	1416	40	53590	40	1.05	23430	1.00	0.00	1.00	0.00	0.105	0.052	1396	2.77
2004_PNF	1416	40	53590	40	1.12	53590	0.00	1.00	1.00	0.00	0.257	0.085	1415	3.12
2004_18	171	40	36130	230	1.10	14280	0.96	0.04	1.00	0.00	0.170	0.047	133	1.79
2004_11	119	40	30190	40	1.22	30190	0.00	1.00	1.00	0.00	0.248	0.102	118	2.88
2004_12	113	40	30410	180	1.16	30410	0.00	1.00	1.00	0.00	0.239	0.055	94	2.23
2004_20	82	40	29490	40	1.01	12430	0.00	1.00	1.00	0.00	0.251	0.092	77	2.49
2004_05	66	40	21210	350	1.44	21210	0.50	0.50	1.00	0.00	0.140	0.104	43	1.78
2004_16	60	40	24380	110	1.42	24380	0.05	0.95	1.00	0.00	0.273	0.074	44	2.35
2004_14	51	40	19430	40	1.59	2590	0.22	0.78	1.00	0.00	0.211	0.187	40	1.81
2004_13	42	40	21070	40	1.21	21070	0.19	0.81	1.00	0.00	0.147	0.123	41	2.72
2004_03	29	50	21760	320	1.13	21760	0.39	0.61	0.97	0.03	0.166	0.099	22	1.83

Table C10. Data reanalysis showing exponential fits

Reference	Steps	Min Step	Max Step	Xmin	Exponent	Exp AICw	Exp Comp AICw	TP AICw	TP Comp AICw	Exp GOF	TP GOF	Fitted steps	OoM
2004_08	64	40	53590	70	1.78E-04	1.00	0.00	1.00	0.00	0.097	0.114	54	2.88
2004_07	64	40	35940	320	1.67E-04	0.99	0.01	1.00	0.00	0.062	0.098	37	2.05
2004_17	24	40	20600	230	2.90E-04	0.90	0.10	0.97	0.03	0.122	0.176	18	1.95

Table C11. Data reanalysis showing mixed model fits

Reference	Steps	Min Step	Max Step	Exp Xmin	Exp Exponent	TP Xmin	TP Exponent	TP Xmax	Exp AICw	Exp Comp AICw	TP AICw	TP Comp AICw	Exp Fit	TP Fit	TP OoM	Exp OoM
2004_15	133	50	40020	720	1.94E-04	110	0.97	14960	0.99	0.01	1.00	0.00	0.080	0.050	2.13	1.74
2004_01	117	40	22660	690	2.47E-04	50	0.96	13980	0.93	0.07	1.00	0.00	0.121	0.045	2.45	1.52
2004_10	73	100	12950	100	4.40E-04	350	1.04	6650	0.99	0.01	0.99	0.01	0.125	0.120	1.28	2.11
2004_06	62	50	10900	180	3.45E-04	50	0.84	10900	0.06	0.94	1.00	0.00	0.127	0.082	2.34	1.78
2004_02	50	40	30500	180	2.25E-04	40	0.74	12230	0.93	0.07	1.00	0.00	0.150	0.084	2.49	2.23
2004_09	40	50	34230	1250	1.06E-04	50	0.90	34230	0.48	0.52	1.00	0.00	0.102	0.077	2.84	1.44
2004_04	34	70	36680	120	2.40E-04	110	0.77	6480	0.02	0.98	0.89	0.11	0.173	0.076	1.77	2.49
2004_19	22	60	15980	330	2.02E-04	60	0.98	15980	0.27	0.73	1.00	0.00	0.167	0.097	2.43	1.69

Figure C5. Exponential fits from the 2004 reanalysed data.
Red line is the best fit exponential distribution; dashed blue line is the alternate TP. For TP fits see Chapter 5
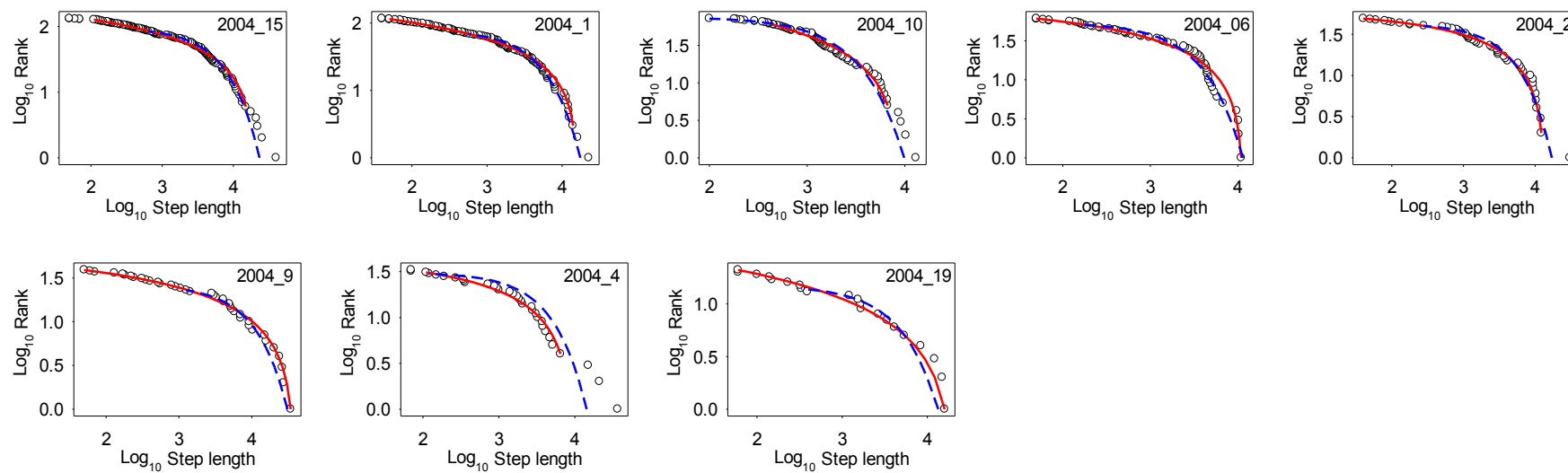
Figure C6. Mixed model fits from the 2004 reanalysed data.
The plots show the best fitting TP (red) and best fitting exponential (blue dashed) distributions.

12 Appendix D: Chapter 6 tables of results

Encounter rates shown are adjusted for distance travelled using (No of encounters * 10^4) / total distance travelled, unless otherwise specified.

Table D1: Encounter rate with increasing detection radius

Detection radius	Shark-Fish encounters
1	0.2224
2	0.3590
3	0.4866
4	0.6056
5	0.7227

Table D2: Encounter rate with increasing prey field concentration

No of fish	Shark-Fish encounters
20	0.0708
40	0.1433
60	0.2171
80	0.2882
100	0.3593
120	0.4312
140	0.5047
160	0.5733
180	0.6496
200	0.7187

Table D3: Encounter rates with increasing numbers of fish and sharks

Total number of fish and sharks	Shark-Fish encounters
20	0.0707
40	0.1435
60	0.2150
80	0.2886
100	0.3584
120	0.4308
140	0.5012
160	0.5757
180	0.6487
200	0.7203

Table D4: Encounter rates with increasing numbers of turns

Number of turns	Encounters	Adjusted encounters
20	677.00	3.2627
40	1356.50	3.2729
60	2029.50	3.2858
80	2689.00	3.2876
100	3368.00	3.2904

Table D5: Results from the prey field analysis

Ratio of fish to sharks	Median	Mean	Std Dev	K-S Prob.
F10 : S190	640	645.437	120.918	0.092
F50 : S150	2545.5	2549.292	241.736	0.133
F70 : S130	3053	3069.078	252.559	0.004
F100 : S100	3379	3386.221	265.67	0.516
F130 : S70	3073	3084.514	245.479	0.304
F150 : S50	2541	2545.489	235.86	0.282
F190 : S10	634	636.795	118.751	0.008

Table D6: Encounter rate and distance travelled (Uniform sharks)

Maximum step-length	Mean number of encounters	Distance travelled
5	104.39	1008040
11	207.33	1045834
17	277.47	1063398
23	326.1	1073295
29	361.06	1079700
35	386.73	1084226
40	403.98	1087046
45	417.56	1089327
50	429.29	1091208
55	438.74	1092779
60	449.03	1094096
65	453.02	1095275

Table D7: Encounter rate and distance travelled (Lévy sharks)

μ	Mean number of encounters	Distance travelled
1.2	504.98	1098363
1.4	486.91	1089642
1.6	455.96	1074021
1.8	410.49	1049143
2	349.46	1014932
2.2	283.33	975375
2.4	222.56	936595
2.6	172.85	902586
2.8	135.03	874615

Table D8: Destructive Lévy optimality results

Predator	Median	Mean	Std Dev
TP 1.2	0.467	0.468	0.0194
TP 1.4	0.462	0.462	0.02
TP 1.6	0.444	0.445	0.02
TP 1.8	0.411	0.412	0.0203
TP 2.0	0.357	0.357	0.0188
TP 2.2	0.292	0.292	0.0174
TP 2.4	0.226	0.226	0.016
TP 2.6	0.172	0.173	0.0135
TP 2.8	0.133	0.133	0.0128
Exponential	0.227	0.227	0.0157
Uniform	0.203	0.203	0.0153

Table D9: Non-destructive Lévy optimality results

Predator	Median	Mean	Std Dev
TP 1.2	2.236	2.24	0.15
TP 1.4	2.531	2.535	0.179
TP 1.6	2.862	2.868	0.206
TP 1.8	3.126	3.13	0.228
TP 2.0	3.266	3.27	0.261
TP 2.2	3.225	3.231	0.292
TP 2.4	3.052	3.057	0.327
TP 2.6	2.85	2.851	0.346
TP 2.8	2.66	2.673	0.374
Exponential	1.912	1.92	0.194
Uniform	1.832	1.836	0.195

Table D10: Encounters with slow fish

Predator	Median	25%	75%
TP 1.5	0.519	0.505	0.534
TP 2.0	0.423	0.409	0.438
TP 2.5	0.269	0.258	0.281
Exponential	0.274	0.263	0.285
Uniform	0.251	0.238	0.262

Table D11: Encounters with slow fish adjusted for energetic costs

Predator	No of encounters	Distance travelled	Energetic cost of movement	Standard metabolic cost	Total energetic cost	Encounters per unit energy expended
TP 1.5	542.65	1081956.22	324.59	10.00	334.59	1.621851
TP 2.0	419.69	1013347.57	304.00	10.00	314.00	1.336574
TP 2.5	274.52	918175.02	275.45	10.00	285.45	0.961701
Exponential	316.11	1018865.16	305.66	10.00	315.66	1.001427
Uniform	287.03	1015369.58	304.61	10.00	314.61	0.912333
Still	101.6	0	--	10.00	10.00	10.160000

Table D12: Encounters with fast fish

Predator	Median	25%	75%
TP 1.5	0.582	0.568	0.597
TP 2.0	0.591	0.573	0.607
TP 2.5	0.620	0.603	0.638
Exponential	0.570	0.554	0.584
Uniform	0.568	0.553	0.585

Table D13: Encounters with fast fish adjusted for energetic costs

Predator	No of encounters	Distance travelled	Energetic cost of movement	Standard metabolic cost	Total energetic cost	Encounters per unit energy expended
TP 1.5	618.34	1082029.55	324.61	10.00	334.61	1.847949
TP 2.0	572.95	1013201.49	303.96	10.00	313.96	1.824911
TP 2.5	526.45	918036.01	275.41	10.00	285.41	1.844534
Exponential	540.77	1018835.85	305.65	10.00	315.65	1.713191
Uniform	536.21	1015387.1	304.62	10.00	314.62	1.704331
Still	445.05	0	--	10.00	10.00	44.505000

Table D14: Encounter rates with evolved parameters

Distribution	Xmin	Exponent	Xmax	Mean waiting time	Encounter rate	% Difference from non-evolved Uniform
Uniform (non-evolved)	1		500	250	44155	
Uniform	119		174	147 s.d. 29	58148	31.69%
Exponential	122	0.068		152 s.d. 52	58890	33.37%
Power	68	2.83		149 s.d. 349	56403	27.74%
TP	70	1.4 to 2.6	343	141 s.d. 65	57946	31.23%

Table D15: Pair wise comparisons for encounter rates with evolved parameters

Comparison	Diff of Ranks	q	P<0.05
Exponential vs Power	120001	9.293	Yes
Uniform vs Power	96193.5	7.449	Yes
TP vs Power	86477.5	6.697	Yes
Exponential vs TP	33523.5	2.596	No
Exponential vs Uniform	23807.5	1.844	Do Not Test
Uniform vs TP	9716	0.752	Do Not Test

13 Appendix E: Chapter 7 tables of results

Table E1: Spanish fleet percentile groups

Group	Days fishing	Group %	No of boats
A	443	8.34%	2
B	615	11.58%	3
C	578	10.88%	3
D	478	9.00%	3
E	568	10.69%	4
F	525	9.88%	5
G	549	10.34%	6
I	509	9.58%	9
J	503	9.47%	21

Table E2: Detail of the Spanish fleet groupings

Vessel	Days fishing	Group	Days fishing	Group % of total	No of boats	Vessel	Days fishing	Group	Day fishing	Group % of total	No of boats
3743091_2008	232	A	443	8.34%	2	3716365_2008	63	I	509	9.58%	9
3969296_2008	211	A				3841462_2008	61	I			
3647457_2008	210	B	615	11.58%	3	3640373_2008	59	I			
3778672_2008	207	B				4165394_2008	59	I			
3646330_2008	198	B				3775935_2008	58	I			
3751624_2008	193	C	578	10.88%	3	3730855_2008	57	I			
4242996_2008	193	C				3723610_2008	53	I			
3841623_2008	192	C				3908921_2008	51	I			
102720_2008	167	D	478	9.00%	3	2540099_2008	48	I			
1693078_2008	156	D				3709925_2008	47	J	503	9.47%	21
4057202_2008	155	D				3834217_2008	45	J			
3730372_2008	152	E	568	10.69%	4	3721517_2008	43	J			
3504328_2008	145	E				2492604_2008	41	J			
2570689_2008	141	E				3525580_2008	39	J			
3268463_2008	130	E				3761284_2008	34	J			
96602_2008	119	F	525	9.88%	5	3948205_2008	32	J			
3786722_2008	113	F				3607046_2008	31	J			
3797348_2008	101	F				3770944_2008	31	J			
4203873_2008	97	F				4085860_2008	27	J			
3860299_2008	95	F				3468103_2008	25	J			
4192925_2008	94	G	549	10.34%	6	4167004_2008	24	J			
3834056_2008	92	G				3507709_2008	19	J			
4241547_2008	92	G				2407596_2008	14	J			
3640695_2008	91	G				3934842_2008	14	J			

Vessel	Days fishing	Group	Days fishing	Group % of total	No of boats		Vessel	Days fishing	Group	Day fishing	Group % of total	No of boats
4178113_2008	91	G					3933393_2008	9	J			
4090207_2008	89	G					3751463_2008	8	J			
3944180_2008	85	H	544	10.24%	7		3724898_2008	6	J			
3589497_2008	83	H					3793162_2008	5	J			
3952069_2008	79	H					3856274_2008	5	J			
3738744_2008	78	H					3889601_2008	4	J			
4234302_2008	75	H										
4027417_2008	73	H										
3808135_2008	71	H										

Table E3: Portuguese fleet percentile groups

Group	Days fishing	Group %	No Of Boats
A	199	10.39%	1
B	143	7.47%	1
C	276	14.41%	2
D	134	7.00%	1
E	226	11.80%	2
F	199	10.39%	2
G	181	9.45%	2
H	153	7.99%	2
I	236	12.32%	4
J	168	8.77%	5

Table E4: Detail of the Portuguese fleet groupings

Boat name	Days fishing	Group	Group %	No Of Boats
56007-2008	199	A	10.39%	1
56463-2008	143	B	7.47%	1
51655-2008	138	C	14.41%	2
57678-2008	138	C		
51532-2008	134	D	7.00%	1
58761-2008	115	E	11.80%	2
56066-2008	111	E		
55765-2008	101	F	10.39%	2
57262-2008	98	F		
53443-2008	92	G	9.45%	2
55976-2008	89	G		
50998-2008	81	H	7.99%	2
58511-2008	72	H		
51728-2008	66	I	12.32%	4
30527-2008	62	I		
53141-2008	56	I		
56683-2008	52	I		
57578-2008	52	J	8.77%	5
56452-2008	36	J		
58603-2008	36	J		
53798-2008	25	J		
50352-2008	19	J		

Table E5: Coordinates of the three Marine Protected Areas

| | Top left | | Bottom right | |
| | Longitude | Latitude | Longitude | Latitude |
MPA				
W. Africa	-25	25	-19	20
Iberian Peninsula	-20	35	-11	40
Goban Spur	-14	49	-12	52

Table E6: Shapiro-Wilk normailty test results for the Spanish fleet groupings

Group	W-Statistic	p value	Result
Control	0.997	0.07	Passed
A	0.996	0.01	Failed
B	0.994	< 0.001	Failed
C	0.998	0.53	Passed
D	0.998	0.23	Passed
E	0.996	0.01	Failed
F	0.996	0.02	Failed
G	0.999	0.58	Passed
H	0.997	0.10	Passed
I	0.999	0.60	Passed
J	0.963	< 0.001	Failed

Table E7: ANOVA results for Spanish fleet groupings

Kruskal-Wallis One-way ANOVA on Ranks

Group	N	Median	25%	75%
Control	1000	0.766	0.752	0.781
A	1000	0.278	0.251	0.309
B	1000	0.788	0.75	0.83
C	1000	0.862	0.825	0.903
D	1000	2.021	1.956	2.094
E	1000	0.708	0.669	0.752
F	1000	1.025	0.977	1.074
G	1000	0.885	0.845	0.927
H	1000	0.331	0.305	0.358
I	1000	1.045	1.004	1.09
J	1000	0.386	0.36	0.416

Table E8: Tukey test results for Spanish fleet groupings

Results are ordered by descending difference of ranks.

Comparison	Diff of Ranks	q	P<0.01	Comparison	Diff of Ranks	q	P<0.01
D vs A	9770088	97.29	Yes	D vs G	3485628	34.71	Yes
D vs H	9024464	89.87	Yes	Control vs H	3283005	32.69	Yes
I vs A	8293796	82.59	Yes	E vs A	3220319	32.07	Yes
D vs J	8205448	81.71	Yes	G vs E	3064142	30.51	Yes
F vs A	8074655	80.41	Yes	B vs J	2985191	29.73	Yes
I vs H	7548172	75.17	Yes	C vs E	2718608	27.07	Yes
F vs H	7329031	72.98	Yes	E vs H	2474695	24.64	Yes
I vs J	6729156	67.01	Yes	Control vs J	2463989	24.54	Yes
D vs E	6549769	65.22	Yes	I vs C	2354869	23.45	Yes
F vs J	6510015	64.83	Yes	G vs Control	2255832	22.46	Yes
G vs A	6284461	62.58	Yes	F vs C	2135728	21.27	Yes
C vs A	5938927	59.14	Yes	I vs G	2009335	20.01	Yes
D vs Control	5741459	57.17	Yes	C vs Control	1910298	19.02	Yes
G vs H	5538837	55.16	Yes	F vs G	1790194	17.83	Yes
D vs B	5220258	51.98	Yes	G vs B	1734630	17.27	Yes
C vs H	5193303	51.72	Yes	D vs F	1695434	16.88	Yes
I vs E	5073477	50.52	Yes	E vs J	1655679	16.49	Yes
F vs E	4854336	48.34	Yes	J vs A	1564640	15.58	Yes
G vs J	4719821	47.00	Yes	D vs I	1476293	14.70	Yes
B vs A	4549831	45.31	Yes	C vs B	1389097	13.83	Yes
C vs J	4374287	43.56	Yes	B vs E	1329512	13.24	Yes
I vs Control	4265167	42.47	Yes	J vs H	819016	8.16	Yes
F vs Control	4046026	40.29	Yes	Control vs E	808310	8.05	Yes
Control vs A	4028629	40.12	Yes	H vs A	745624	7.43	Yes
D vs C	3831161	38.15	Yes	B vs Control	521201.5	5.19	Yes
B vs H	3804207	37.88	Yes	G vs C	345533.5	3.44	No
I vs B	3743965	37.28	Yes	I vs F	219141	2.18	No
F vs B	3524824	35.10	Yes				

Table E9: Shapiro Wilk normaility test results for the Portuguese fleet groups

Group	W-Statistic	p value	Result
Control	0.999	0.82	Passed
A	0.998	0.27	Passed
B	0.997	0.10	Passed
C	0.997	0.11	Passed
D	0.997	0.12	Passed
E	0.997	0.04	Failed
F	0.998	0.30	Passed
G	0.995	0.01	Failed
H	0.998	0.22	Passed
I	0.996	0.02	Failed
J	0.997	0.10	Passed

Table E10: ANOVA results for Portuguese fleet groupings

Group	N	Median	25%	75%
Control	1000	2.093	2.037	2.153
A	1000	1.638	1.548	1.729
B	1000	2.385	2.252	2.517
C	1000	2.304	2.203	2.406
D	1000	2.44	2.3	2.59
E	1000	3.122	2.982	3.242
F	1000	2.899	2.769	3.03
G	1000	3.061	2.912	3.221
H	1000	2.797	2.667	2.941
I	1000	2.059	1.975	2.153
J	1000	2.601	2.482	2.744

Table E11: Tukey test results for Portuguese fleet groupings
Results are ordered by descending difference of ranks.

Comparison	Diff of Ranks	q	P<0.01	Comparison	Diff of Ranks	q	P<0.01
E vs A	9143706	91.05	Yes	F vs D	3245584	32.32	Yes
G vs A	8827049	87.9	Yes	H vs B	2982682	29.7	Yes
F vs A	7852358	78.2	Yes	G vs J	2941663	29.29	Yes
E vs I	7468046	74.37	Yes	D vs I	2931115	29.19	Yes
E vs Control	7323897	72.93	Yes	D vs Control	2786966	27.75	Yes
H vs A	7193651	71.64	Yes	H vs D	2586877	25.76	Yes
G vs I	7151389	71.22	Yes	B vs I	2535309	25.25	Yes
G vs Control	7007240	69.78	Yes	B vs Control	2391161	23.81	Yes
F vs I	6176698	61.51	Yes	J vs C	2311077	23.01	Yes
F vs Control	6032550	60.07	Yes	F vs J	1966973	19.59	Yes
J vs A	5885386	58.61	Yes	E vs H	1950055	19.42	Yes
E vs C	5569397	55.46	Yes	C vs I	1898649	18.91	Yes
H vs I	5517991	54.95	Yes	Control vs A	1819809	18.12	Yes
H vs Control	5373843	53.51	Yes	C vs Control	1754500	17.47	Yes
G vs C	5252740	52.31	Yes	I vs A	1675660	16.69	Yes
E vs B	4932737	49.12	Yes	J vs B	1674417	16.67	Yes
G vs B	4616080	45.97	Yes	G vs H	1633398	16.27	Yes
D vs A	4606775	45.88	Yes	H vs J	1308266	13.03	Yes
E vs D	4536931	45.18	Yes	E vs F	1291348	12.86	Yes
F vs C	4278050	42.6	Yes	J vs D	1278611	12.73	Yes
G vs D	4220274	42.03	Yes	D vs C	1032466	10.28	Yes
B vs A	4210969	41.93	Yes	G vs F	974691	9.71	Yes
J vs I	4209726	41.92	Yes	F vs H	658707	6.56	Yes
J vs Control	4065577	40.49	Yes	B vs C	636661	6.34	Yes
F vs B	3641389	36.26	Yes	D vs B	395806	3.94	No
H vs C	3619343	36.04	Yes	E vs G	316657	3.15	No
C vs A	3574309	35.59	Yes	Control vs I	144149	1.44	No
E vs J	3258320	32.45	Yes				

Table E12: Statistical analysis of the Spanish MPA results
Kruskal-Wallis One-way ANOVA on Ranks

Group	N	Median	25%	75%
Control	1000	0.76	0.743	0.776
Goban Spur	1000	0.797	0.78	0.813
W.Africa	1000	0.935	0.915	0.955
Iberia	1000	0.633	0.618	0.649
Q1	1000	0.694	0.677	0.71
Q2	1000	0.756	0.74	0.772
Q3	1000	0.742	0.726	0.757
Q4	1000	0.726	0.709	0.741

Table E13: Pair wise statistical analysis of the Spanish MPA results

All Pairwise Multiple Comparison Procedures (Tukey Test)

Comparison	Diff of Ranks	q	P<0.01
W.Africa vs Iberia	6956674	95.252	Yes
W.Africa vs Q1	5700847	78.057	Yes
Goban Spur vs Iberia	5585613	76.479	Yes
W.Africa vs Q4	4503318	61.66	Yes
Goban Spur vs Q1	4329786	59.284	Yes
Control vs Iberia	4160391	56.965	Yes
Q2 vs Iberia	3998562	54.749	Yes
W.Africa vs Q3	3710729	50.808	Yes
Q3 vs Iberia	3245946	44.444	Yes
Goban Spur vs Q4	3132257	42.888	Yes
W.Africa vs Q2	2958112	40.503	Yes
Control vs Q1	2904564	39.77	Yes
W.Africa vs Control	2796284	38.287	Yes
Q2 vs Q1	2742735	37.554	Yes
Q4 vs Iberia	2453356	33.592	Yes
Goban Spur vs Q3	2339668	32.035	Yes
Q3 vs Q1	1990119	27.249	Yes
Control vs Q4	1707035	23.373	Yes
Goban Spur vs Q2	1587051	21.73	Yes
Q2 vs Q4	1545206	21.157	Yes
Goban Spur vs Control	1425223	19.514	Yes
W.Africa vs Goban Spur	1371061	18.773	Yes
Q1 vs Iberia	1255827	17.195	Yes
Q4 vs Q1	1197529	16.397	Yes
Control vs Q3	914445	12.521	Yes
Q3 vs Q4	792590	10.852	Yes
Q2 vs Q3	752617	10.305	Yes
Control vs Q2	161829	2.216	No

Table E14: Statistical analysis of the Portuguese MPA results

Kruskal-Wallis One-way ANOVA on Ranks

Group	N	Median	25%	75%
Control	1000	2.287	2.221	2.361
Goban Spur	1000	2.287	2.221	2.361
W.Africa	1000	2.484	2.408	2.563
Iberia	1000	2.112	2.034	2.193
Q1	1000	2.257	2.181	2.33
Q2	1000	2.284	2.215	2.355
Q3	1000	2.259	2.198	2.337
Q4	1000	2.255	2.183	2.331

Table E15: Pair wise statistical analysis of the Portuguese MPA results

All Pairwise Multiple Comparison Procedures (Tukey Test)

Comparison	Diff of Ranks	q	P<0.05
W.Africa vs Iberia	5547694	75.96	Yes
W.Africa vs Q4	3357147	45.97	Yes
W.Africa vs Q1	3347605	45.84	Yes
W.Africa vs Q3	3247634	44.47	Yes
W.Africa vs Q2	2816007	38.56	Yes
Goban Spur vs Iberia	2793893	38.26	Yes
Control vs Iberia	2793893	38.26	Yes
W.Africa vs Control	2753801	37.71	Yes
W.Africa vs Goban Spur	2753801	37.71	Yes
Q2 vs Iberia	2731688	37.40	Yes
Q3 vs Iberia	2300060	31.49	Yes
Q1 vs Iberia	2200089	30.12	Yes
Q4 vs Iberia	2190548	29.99	Yes
Goban Spur vs Q4	603346	8.26	Yes
Control vs Q4	603346	8.26	Yes
Goban Spur vs Q1	593804	8.13	Yes
Control vs Q1	593804	8.13	Yes
Q2 vs Q4	541140	7.41	Yes
Q2 vs Q1	531599	7.28	Yes
Goban Spur vs Q3	493833	6.76	Yes
Control vs Q3	493833	6.76	Yes
Q2 vs Q3	431628	5.91	Yes
Q3 vs Q4	109513	1.50	No
Q3 vs Q1	99971	1.37	No
Goban Spur vs Q2	62206	0.85	No
Control vs Q2	62206	0.85	No
Q1 vs Q4	9542	0.13	No
Goban Spur vs Control	0	0.00	No

Table E16: Statistical analysis of the Spanish close season results

Kruskal-Wallis One-way ANOVA on Ranks

Group	N	Median	25%	75%
Control	1000	0.766	0.752	0.781
Q1	1000	0.615	0.600	0.631
Q2	1000	0.736	0.720	0.752
Q3	1000	0.969	0.949	0.989
Q4	1000	0.754	0.738	0.771

Table E17: Pair wise statistical analysis of the Spanish close season results

All Pairwise Multiple Comparison Procedures (Tukey Test)

Comparison	Diff of Ranks	q	P<0.05
Q3 vs Q1	3999668	87.62	Yes
Q3 vs Q2	2530412	55.43	Yes
Control vs Q1	2468608	54.08	Yes
Q4 vs Q1	2060808	45.15	Yes
Q3 vs Q4	1938860	42.47	Yes
Q3 vs Control	1531060	33.54	Yes
Q2 vs Q1	1469256	32.19	Yes
Control vs Q2	999352	21.89	Yes
Q4 vs Q2	591552	12.96	Yes
Control vs Q4	407800	8.93	Yes

Table E18: Statistical analysis of the Portuguese close season results

Kruskal-Wallis One-way ANOVA on Ranks

Group	N	Median	25%	75%
Control	1000	2.093	2.037	2.153
Q1	1000	1.811	1.745	1.877
Q2	1000	2.207	2.147	2.271
Q3	1000	2.072	2.013	2.130
Q4	1000	2.254	2.187	2.324

Table E19: Pair wise statistical analysis of the Portuguese close season results

All Pairwise Multiple Comparison Procedures (Tukey Test)

Comparison	Diff of Ranks	q	P<0.05
Q4 vs Q1	3405632	74.61	Yes
Q2 vs Q1	3006437	65.86	Yes
Control vs Q1	1815801	39.78	Yes
Q4 vs Q3	1808482	39.62	Yes
Q3 vs Q1	1597150	34.99	Yes
Q4 vs Control	1589831	34.83	Yes
Q2 vs Q3	1409287	30.87	Yes
Q2 vs Control	1190636	26.08	Yes
Q4 vs Q2	399195	8.75	Yes
Control vs Q3	218651	4.79	Yes

Table E20: Numerical results from the Spanish fleet analysis

		Risk per day					Total days at risk				
	Days Fishing	Mean	St dev	Median	5th %	95th%	Mean	St dev	Median	5th %	95th %
Control	5312	0.766	0.022	0.766	0.730	0.804	4071	118.060	4069	3878	4271
Close Q1	3716	0.615	0.023	0.615	0.580	0.653	2287	84.546	2285	2155	2428
Close Q2	4577	0.736	0.024	0.736	0.699	0.775	3369	108.541	3368	3198	3549
Close Q3	3699	0.968	0.030	0.969	0.918	1.016	3582	109.730	3583	3395	3759
Close Q4	3944	0.754	0.025	0.754	0.713	0.797	2976	99.772	2973	2811	3143
Group A	443	0.281	0.045	0.278	0.208	0.357	124	19.833	123	92	158
Group B	615	0.790	0.059	0.788	0.696	0.896	486	36.370	484	428	551
Group C	578	0.864	0.060	0.862	0.768	0.965	499	34.733	498	444	558
Group D	478	2.025	0.102	2.021	1.856	2.195	968	48.591	966	887	1049
Group E	568	0.712	0.062	0.708	0.616	0.820	404	35.287	402	350	466
Group F	525	1.027	0.074	1.025	0.903	1.150	539	38.852	538	474	604
Group G	549	0.885	0.060	0.885	0.787	0.985	486	33.044	486	432	541
Group H	544	0.332	0.039	0.331	0.270	0.399	181	21.205	180	147	217
Group I	509	1.046	0.065	1.045	0.935	1.153	532	33.311	532	476	587
Group J	503	0.387	0.040	0.386	0.322	0.457	195	20.354	194	162	230
MPA W. Africa	4237	0.928	0.027	0.927	0.884	0.970	3930	113.423	3928	3747	4112
MPA Iberia	5041	0.655	0.022	0.655	0.621	0.691	3303	108.437	3303	3129	3482
MPA Goban Spur	5058	0.800	0.023	0.800	0.761	0.839	4045	117.381	4045	3851	4242
MPA Iberia & Q1	5172	0.698	0.021	0.698	0.663	0.733	3608	111.073	3609	3430	3791
MPA Iberia & Q2	5304	0.764	0.022	0.764	0.728	0.802	4053	117.816	4052	3861	4252
MPA Iberia & Q3	5274	0.752	0.022	0.751	0.715	0.789	3965	117.671	3960	3771	4160
MPA Iberia & Q4	5227	0.744	0.022	0.744	0.707	0.780	3890	115.799	3889	3698	4078

Table E21: Numerical results from the Portuguese fleet analysis

	Days Fishing	Risk per day fishing					Days at risk				
		Mean	St dev	Median	5th %	95th %	Mean	St dev	Median	5th %	95th %
Control	1915	2.094	0.083	2.093	1.959	2.230	4010	158.971	4009	3752	4270
Close Q1	1265	1.813	0.093	1.811	1.666	1.967	2294	117.665	2291	2108	2488
Close Q2	1738	2.207	0.091	2.207	2.056	2.351	3836	158.216	3835	3574	4086
Close Q3	1541	2.072	0.087	2.072	1.927	2.216	3193	133.665	3193	2970	3415
Close Q4	1201	2.254	0.101	2.254	2.085	2.424	2707	120.702	2706	2504	2911
Group A	199	1.640	0.135	1.638	1.427	1.869	326	26.952	326	284	372
Group B	143	2.389	0.199	2.385	2.077	2.734	342	28.430	341	297	391
Group C	276	2.306	0.145	2.304	2.080	2.551	636	40.128	636	574	704
Group D	134	2.443	0.223	2.440	2.082	2.821	327	29.868	327	279	378
Group E	226	3.119	0.193	3.122	2.801	3.429	705	43.726	705	633	775
Group F	199	2.901	0.199	2.899	2.578	3.236	577	39.650	577	513	644
Group G	181	3.073	0.231	3.061	2.718	3.464	556	41.730	554	492	627
Group H	153	2.804	0.217	2.797	2.444	3.163	429	33.227	428	374	484
Group I	236	2.064	0.140	2.059	1.843	2.305	487	33.105	486	435	544
Group J	168	2.615	0.201	2.601	2.292	2.958	439	33.748	437	385	497
MPA W. Africa	1753	2.275	0.091	2.274	2.126	2.426	3988	159.181	3987	3727	4252
MPA Iberia	834	1.806	0.091	1.806	1.661	1.953	1506	75.580	1506	1385	1629
MPA Goban Spur	1915	2.094	0.083	2.093	1.959	2.230	4010	158.971	4009	3752	4270
MPA Iberia & Q1	1445	1.912	0.085	1.911	1.778	2.058	2763	123.206	2761	2569	2974
MPA Iberia & Q2	1904	2.090	0.083	2.089	1.954	2.224	3979	158.086	3978	3720	4235
MPA Iberia & Q3	1742	2.037	0.082	2.034	1.905	2.175	3548	142.981	3543	3318	3789
MPA Iberia & Q4	1488	2.181	0.090	2.180	2.036	2.326	3246	133.510	3243	3029	3461

14 Appendix F: Foraging lab simulation program

14.1 Introduction

The 'foraging lab' is a 2D lattice based foraging simulation, written in Microsoft C#, where the lattice, or 'tank' (the simulation is designed as a null model for laboratory studies) can be set to any arbitrary size, memory permitting, and where the forager is a random walker with uniform random turning angles and move step-lengths drawn from either a uniform, exponential, power-law or truncated power-law distribution. The lattice is populated with prey patches which are encountered and optionally consumed by the forager.

14.2 Prey patch construction and distribution

A single prey patch has parameters of size (i.e. the length of the side of a square lattice in no of cells) and the biomass. The patch is created by overlaying random walks, starting at the centre which increment the biomass of each cell visited. All steps in this walk are one unit and move to one of the eight neighbours; each walk is performed until the edge of the patch is reached. By this method a 'fuzzy' patch can be built where the maximum concentration of biomass is at the centre of the patch.

Any number of patches can be created in the tank. The distribution of the patches can be simple random, i.e. distributed according to a Poisson process by selecting uniform random values for the X and Y coordinates. Alternatively patches can be distributed according to a specified distribution (i.e. Uniform, Exponential, power-law or truncated Pareto) whereby the first patch is placed at random coordinates and subsequent patches are placed by using a uniform random angle on the interval $[0,2\pi]$ radians and a vector drawn from the specified distribution.

The total biomass is recorded along with the total number of populated cells (i.e. cells with > 0 biomass). The populated tank can be saved for use in later simulations to ensure prey field variability is not a factor in simulation variability.

14.3 Foraging runs

A virtual forager is specified using parameters of number of move steps, maximum path length and move step-length distribution (i.e. Uniform, Exponential, power-law or truncated Pareto). A single foraging run comprises a random walk performed within the tank in continuous space with boundaries being reflecting; each walk begins at a random location. The generation and interpolation of move steps is as described in the general methods chapter. At each interpolated step the cell coincident on the forager's location is checked for biomass. The foraging run ends when the specified number of steps has been performed or when the total distance travelled reaches the specified maximum. When fewer than 20 foraging runs are performed the resulting paths are displayed with the prey field to allow visual confirmation and testing (Figure F1).

14.4 Foraging strategies

Foraging can either be non-destructive, where the cell biomass contents are unchanged by the forager, or destructive with cell biomass values being set to zero when encountered. Note that the consumed biomass is not replaced within the tank as this would disrupt the prey distribution; consequently prey availability steadily decreases under this scenario.

Prey targeting can be switched on, causing the forager to halt a move step whenever a populated cell is encountered. A new move step is then computed.

14.5 Famine periods

The number of interpolated moves performed between encountering biomass are counted and recorded as famine periods. If the forager encounters no prey then there will be a single famine period with a duration equal to the total number of interpolated move steps performed.

14.6 Statistics

The program records total biomass consumed, total distance travelled and the number and duration of all famine periods for each forager. Two levels of statistics are available: detailed, where the outcome of every foraging run is written to an output

file, in CSV format; or simple where only the computed means and standard deviation of distance travelled and biomass consumed is recorded. Any number of multiple repeats can be performed, and a simple macro language allows a set of studies to be automated.

14.7 Recording foraging paths

A further option exists to record foraging runs, by writing the end points of each move step to an output file in CSV format. It should be noted that if the forager's path reflects off the tank boundary then the actual move step will be lost as only the start and end coordinates will have been recorded. Therefore an option is provided to record an 'un-reflected' movement path. This option maintains separate XY coordinates and the original un-reflected deltas. Normally, when the boundary is reached, either the *dx* or *dy* movement delta is negated, reversing movement in that dimension and effecting a reflection from the boundary. When recording an un-reflected path this still occurs however the separate DX and DY deltas are unchanged and therefore the un-reflected coordinates are incremented as if no boundary was encountered. The overall effect is that the foraging path now continues over a boundless plain which is tessellated by repeated tiles of the foraging arena (Figure F2); long steps are therefore no longer truncated.
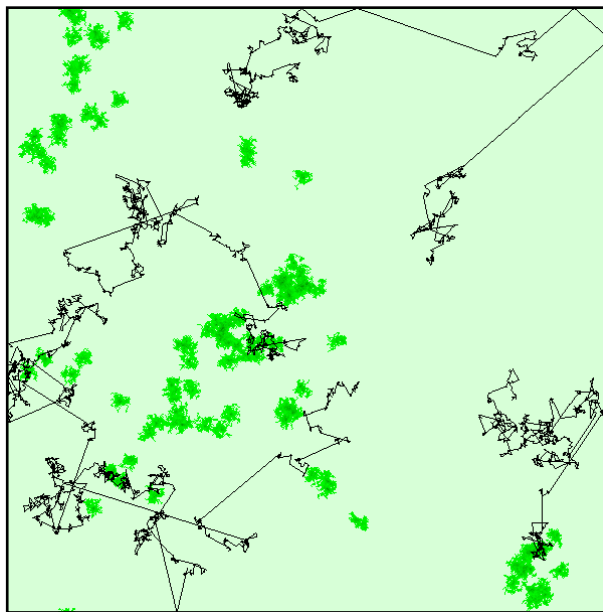
Figure F1: An example screen shot from the 'foraging lab' program
Five TP2.5 foragers in a Lévy distributed prey field. Foraging tracks are only drawn when fewer than 20 runs are performed, for illustrative and testing purposes.
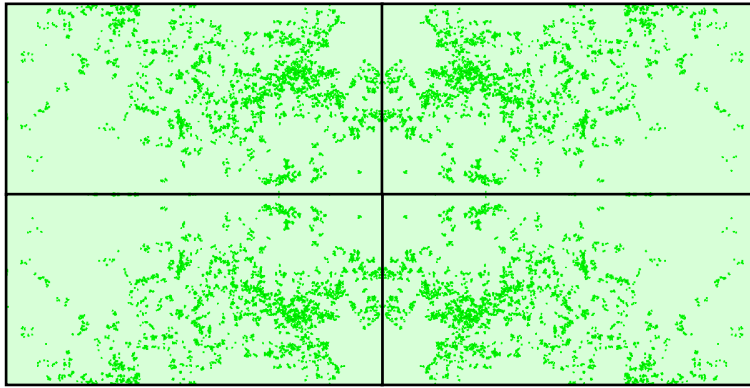
Figure F2: How a reflected prey field appears to an unreflected forager

To an unreflected forager the prey field is effectively tessellated, through either horizontal or vertical reflection, to produce a boundless field with an identical prey distribution. In effect the prey field is reflected rather than the forager.

15 Appendix G: Predator-Prey simulation program

15.1 Introduction

The 'predator-prey' simulation is a 2D lattice based program written in Microsoft C# where the simulation arena comprises 500x250 cells. The purpose of the simulation is to investigate the effect of differing movement patterns on the encounter rates between predators and prey. The program provides a null model of interactions where each interacting individual is unaware of the existence of other individuals outside a narrow sensory range. Two types of predator behaviour can be simulated, cruise predation or ambush predation. In each case foraging can be non-destructive, or destructive with replacement (i.e. relocation). The program records distance travelled and number of encounters for each individual and reports averages over the requested number of runs with standard deviations; the principal metric is therefore encounters per unit distance travelled. For ambush predators the time spent waiting and the time spent active (i.e. moving) are also recorded. Prey behaviour is simpler than predator behaviour, being simply an uncorrelated random walk with step-lengths drawn from one of the standard distributions. However the 'prey-field' can be structured into a grid with cells being allocated randomly as either sparse or abundant allowing simulations in a heterogeneous environment.

15.2 Simulation parameters

Table G1: Predator-Prey simulation parameters
The following parameters control the simulation

Parameter	Type	Description
Number of fish	integer	The number of prey
Fish foraging style	distribution	The distribution and associated parameters to use to control the movement of the prey
Count fish encounters	boolean	Whether to count interactions as 'seen' by the prey
Number of sharks	Integer	The number of predators
Shark foraging style	Integer	The distribution and associated parameters to use to control the movement of the predators
Destructive predation	boolean	Whether prey are 'eaten' (i.e. relocated) when encountered
Prey targeting	boolean	Whether a move step is halted when prey is encountered
Ambush mode	boolean	Whether ambush mode is implemented
Waiting time	distribution	If ambush mode is selected then the waiting time can be set using a probability distribution or can be set to an infinite wait by setting it to Still
Move on encounter	boolean	If ambush mode is selected then the predator can be set to move once a prey is encountered, in which case a move is performed using the shark foraging style
Scan on move	boolean	Whether relocating ambush predators check for encounters during the move
Use prey field grid	boolean	If selected then a heterogeneous prey field will be created using the grid size and Strength parameters
Prey field grid size	integer	One of 3 prey field grid sizes can be specified: 10x10, 5x5, or 2x2 cells.
Prey field strength	integer	The strength of the prey field can be adjusted between 1 and 9, with 1 being the weakest effect and 9 the strongest
Number of turns	integer	The number of k turns that will be performed in a single simulation
Number of repeats	integer	The number of repeats to be performed in order to allow statistical analysis
Evolve sharks	boolean	Whether evolution processing will be performed following each repeat
Evolve move steps	boolean	Whether the move step distribution parameters will be evolved
Evolve waiting times	boolean	Whether the waiting time distribution parameters will be evolved
Mutation rate	decimal	A value between zero and 1.0 that specifies the probability that the parameters of a reproducing shark will undergo a mutation
Mutation factor	decimal	A value between zero and 1.0 that controls the extent to which a parameter changes under mutation; i.e. 0.1 represents a ± 10% change in the value

15.3 Instantiating fish and sharks

At the start of a simulation run (or repeat) the required number of fish and sharks are instantiated and placed at random locations within the 2D array representing the arena. For fish, if the prey field grid is in use, a location within a sparse grid cell can be

rejected with a probability dependant on the prey field grid strength (see below); the location will also be rejected if it is already occupied (which applies to sharks as well); new random locations are selected until a suitable one is found. When an empty cell is found an entry is made at that grid location identifying the fish or shark. Each fish and shark therefore has two sets of location data; coordinates in continuous space and an entry in the 2D array which allows it to be 'seen' by other fish or sharks moving within the simulation.

For fish, or sharks if not in ambush mode, a trajectory is required and is calculated using a vector drawn from the specified distribution and a random angle on the interval [0, 2π] radians. From these values interpolated movement deltas are calculated as described in the General Methods chapter. Note that sharks do not share a single set of movement (and waiting) parameters but have individual values populated from the parameter values at the start, even if evolution processing is not being performed.

For sharks in ambush mode a waiting time is required which is drawn from the specified distribution; all sharks start off waiting when in ambush mode.

15.4 Individual movement

On each turn the interpolated deltas are applied to the current position and from the new position grid cell indices are calculated (simply by taking the integer of the continuous coordinates). If the grid location is unoccupied the shark will be relocated to that position by removing the entry from the old grid cell and making a new entry at the new location. If the location is occupied then the continuous space coordinates are still updated with the new position and the move within the grid is postponed until the next turn at which point the cell is likely to be free.

For ambush predators in waiting mode there is no move to make, instead the waiting time is decremented and on zero a new move trajectory is selected as described above.

Following the move (or wait) the new area is scanned for encounters as described below, unless the entity is a shark in ambush mode that is in the process of relocating.

15.5 Detection area and encounters

The detection area is calculated from the new grid location ± the detection radius as shown below in Figure G1; the number of cells checked for a given radius is given in Table G2. A radius of 2 was used in all simulations except those performed to investigate the effect of changing the value. All the cells in the detection area are checked and if any are occupied the encounter is recorded. For a fish there is no further action taken following the detection of an encounter, it is simply counted (if required). For a shark in cruise predation mode, if prey targeting has been selected, then the shark will halt its current move step and a new step will be calculated as described above. If the encounter is instigated by a shark (being the entity being processed) and the encounter is with a fish and destructive predation is selected then the fish is relocated to a new random location and is given a new trajectory. If the encounter is instigated by a shark in ambush mode and move on encounter is selected then a new trajectory is selected and a move will begin on the next turn. Otherwise the waiting time is extended by a new increment drawn from the specified distribution.

15.6 Prey field grid

To generate a heterogenic prey field a prey field grid (PFG) can be specified which overlays a coarse grid upon the 2d simulation lattice. Two parameters control the PFG, the grid size and the grid strength. The prey field grid size can be specified as 10 x 10, 5 x 5 or 2 x 2; to avoid edge effects in the relatively small arena used in the simulations presented here only the 2x2 grid was used. The strength is an integer on the interval [1, 9] when 1 is weak and 9 is strong; only the value of 9 was used here. The cells of the grid are randomly assigned a value of either sparse (0) or abundant (1) such that 50% of the grid cells are abundant. The grid is used on two occasions within the simulation, firstly when determining a random start location and secondly when computing a new trajectory; the grid is only used when dealing with fish. When determining the start location the PFG cell that corresponds to the proposed start location is checked; if the cell is marked as abundant it is allowed, otherwise it is rejected with a probability dependant on the grid strength. When computing a new trajectory, if the fish is in an abundant PFG cell no changes are made to the move. However if in a sparse PFG cell the number of move steps is increased by a factor based on the PFG strength; with a

strength of 9 this results in 9 x more steps being made. No change is made to the direction of the move. The result of increasing the number of steps is to increase the diffusivity and directionality of the move such that the fish is more likely to quickly leave the grid cell. As discussed previously this method works well when the fish have a movement pattern corresponding to normal (Brownian) diffusion, but breaks down if the fish already have a super-diffusive pattern, such as a Lévy walk. In that situation the fish tend to leave the abundant grid cells too quickly and the heterogeneity disappears.

15.7 Evolution

If evolution is selected then at the end of each repeat (i.e. following the specified number of turns) the shark population is sorted by the number of encounters each has accumulated. The top 30% are then each 'cloned' to replace the bottom 30%. The value of 30% was chosen to provide a reasonably fast rate of change within the population without losing all stability (with a mutation rate of 0.5 one sixth of the population changes at each evolutionary step). During the replication process a movement and/or waiting time parameter can be mutated with a probability set by the mutation rate parameter. If selected for mutation then one of the two or three distribution parameters is selected (with equal probability) and is then adjusted by ± the mutation factor.

Figure G1: Detection area in the Predator-Prey program

The detection area; 0 indicates the location of the shark.

5	5	5	5	5	5	5	5	5	5	5
5	4	4	4	4	4	4	4	4	4	5
5	4	3	3	3	3	3	3	3	4	5
3	4	3	2	2	2	2	2	3	4	5
5	4	3	2	1	1	1	2	3	4	5
5	4	3	2	1	O	1	2	3	4	5
5	4	3	2	1	1	1	2	3	4	5
5	4	3	2	2	2	2	2	3	4	5
5	4	3	3	3	3	3	3	3	4	5
5	4	4	4	4	4	4	4	4	4	5
5	5	5	5	5	5	5	5	5	5	5
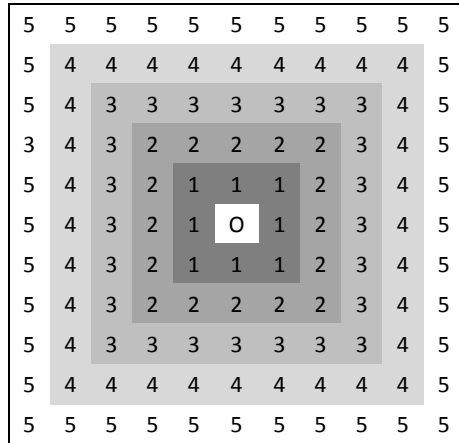
Table G2: Number of cells checked for a specified detection radius

Radius	Cells scanned
1	8
2	24
3	48
4	80
5	120

16 Appendix H: The shark simulation program

16.1 Introduction

Ideally tracks from real sharks, recorded with either SPOT or PAT tags would be used to determine the spatial and temporal interactions between the sharks and the fishing fleets. However, at present, there is simply insufficient data to make the analysis meaningful. Figure H1 illustrates the problem with the tracks of the 20 sharks for which data is currently available; it is clear that the tracks comprise too few locations and are too limited in spatial extent to be useful, with only 5 recorded interactions. In order to investigate how the fleets might interact with a pelagic predator, such as a blue shark, and to gain a better understanding of the spatio-temporal distribution of the risk posed by the fleet, it is possible to use a simulated by-catch prey field. The shark simulation program presented here is designed to build up a prey field through the generation of many individual shark tracks. While it is beyond the scope of this work to attempt to emulate the complex behavioural patterns of migration or site fidelity exhibited by real blue sharks it is never the less possible to simulate the movements of a generic pelagic predator using movement dynamics and thermal preferences based on those recorded from tagged blue sharks.

The program uses a land map to define the coastline (see Figure H1) to constrain simulated sharks geographically and daily sea surface temperature (SST) maps as a thermal constraint. Each generated track comprises 366 move steps with each step representing one day; interactions are to be analysed on a daily basis so finer resolution is not needed. A pool of 20,000 individual tracks was created and the by-catch prey field was built for each analysis run by selection 1000 tracks at random. Further details of how the program worked are given below.

16.2 Program operation

On start up a set of resources are loaded which will be used for all simulation runs; these comprise the coastline bitmap, the temperature maps and the coordinates of the population centre which will be used to help constrain the simulated sharks to the study area and reduce edge effects.

The area matches that used in the Grid Occupancy program and represents the north eastern Atlantic, covering an area of 3896182.18x3896182.18m with the lower left corner positioned at x = -3896182.18; y = 2226389.82.

Unlike with the foraging lab there is no underlying grid representation of the area within which the sharks will move, however there are grid overlays for land & temperature.

Details of the generation of a track are provided below, but in summary each simulated track begins on 2008-01-01 at a location randomly chosen, within the specified maximum distance of the population centre. A step-length is then selected according to the specified movement pattern with a uniform random turn angle on the interval [0, 2π] radians. This turn angle can be modified as described below depending on sea surface temperature or distance from the population centre. The move is performed by interpolating the vector at 20m intervals, prior to each of which a coastline check is made; should land be encountered the move is terminated. Further move steps are generated and executed as described until the specified number of move steps is reached. The end point of each move step is written to a file in comma separated variable (CSV) format for use in the grid occupancy program.

16.2.1 Coastline

On start up a land map is generated from a coastline bitmap which has dimensions of 1200x1200 pixels. The map has dimensions of 604x604 pixels which is sufficient detail for the simulation and reduces memory usage. During shark move processing interactions with land are dealt with by translating shark coordinates (in m) to coastline coordinates to allow checking prior to each interpolated move step, as described below.

16.2.2 Temperature maps

Maps were generated for each month from OSTIA monthly cloud free data sets using ArcGIS with a grid size of 350x350. Factors were calculated to translate shark coordinates (in m) to grid cell coordinates to allow SST to be checked prior to each interpolated move step, as described below. All maps are loaded into an array at start up so that all that is needed to select a new map is to change the current map index.

Once the monthly maps are loaded daily maps are created by interpolation. Having daily maps reduces sudden temperature changes but does not increase processing time, only memory requirements.

16.2.3 Track step-length calculations

Each step of the simulated track will represent the movement from a single day. Step-lengths can be drawn from a statistical distribution, such as exponential, power-law or truncated Pareto, or can be drawn from a sample track (recorded from a tagged shark) which has been pre-loaded for this purpose. Sample tracks used to derive step-lengths are pre-processed to simply interpolate steps to 1 day intervals. If a random number generator is used, especially a power-law, then it is very likely that steps greater than would be possible in one day will be generated. When the step exceeds the daily maximum (86.4km) the step is spread over several days as required. Each step is interpolated at 20m intervals to ensure that the interaction with the coastline is handled accurately.

16.3 Generation of a simulated track

Each track starts within the maximum distance of the population centre (PC) and comprises 366 days of move steps (as the tracks are for 2008) with step-lengths derived as described above. At the start of each move step a direction of movement is computed such that if there are no constrains imposed by either sea surface temperature or distance from the PC then the angle is uniform random on the interval $[0, 2\pi]$ radians. Otherwise the angle of movement is modified as follows.

If the sea surface temperature at the current location is within the specified optimum range (*Trng*; i.e. 16-23°C) then the angle is calculated according to the distance from the PC as described below. Otherwise a base angle ϑ is computed to be π if the temperature is too cold, otherwise is zero. This creates a base angle whereby the shark will head south if too cold or north if too hot which, within the confines of the study area, is sufficient to provide a behavioural response to temperature. The angle is then modified by adding a randomising factor dependant on the extent of the difference between the temperature (*T*) and the average optimum temperature (*Topt*) using:

$$f = \text{Max}[0.1, 1.0 - (|Topt - T| / Trng)]$$

the final angle *a* is found using

$$a = \text{U}[0, 2\pi] + (\vartheta.f).$$

If the SST is within the specified range then temperature will have no effect on the direction of movement which will then only be constrained by the distance from the populations centre. As the distance to the PC (*D*) approaches the maximum specified distance (*Dmax*) then the direction of movement will be controlled so that the Population Centre (PC) will seem to exert a force on the simulated shark: while close to the PC there will be little or no directionality, however as distance from the PC increases movement will become increasingly directed towards the PC. In other words the further the shark is from the PC the more likely it will be to move back towards it. To achieve this two angles are first computed: a) the angle ϑ back from the shark to the PC; b) a random angle on the interval [0, 2π]. The distance from the PC (*D*) is then used to compute a factor *f* ranging from 0.1 to ~ 1.0 using

$$f = \text{Max}[0.1, 1.0 - (D / Dmax)]$$

the final angle *a* is found using

$$a = \text{U}[0, 2\pi] + (\vartheta.f).$$

Therefore when the distance is < the maximum distance the angle is essentially random but as the distance approaches the maximum distance the angle becomes directed back in the general direction of the PC.

16.4 Simulation parameters

Table H1: Shark simulation program parameters
The following parameters control the creation of the simulated track:

Parameter	Description
Number of tracks	The number of tracks to be created.
Number of steps	The number of one day steps in each track. This defaults to the number of days in the specified year which for this study is 2008, so this parameter was set to 366.
Year	The 3D Grid Occupancy program can use tracks from different years to allow analysis of time frames spanning year end. Different years can therefore be specified for the simulated tracks; here all tracks were set to 2008.
Optimum temperature range	The temperature range (°C) that will be used to constrain the track. The range 16-23 was used for these tracks.
Maximum distance from population centre	The population centre acts to prevent simulated sharks moving too far from the centre of the study area thereby reducing edge effects. A value of 120000m was used in this study.
Maximum distance per day	The furthest distance to be travelled in a single day. If a single step exceeds this then it will be split over several days. A value of 86.4km was specified, representing a mean speed of 1ms-1.
Movement style	This specifies either a theoretical distribution (e.g. power-law or exponential) or that step-lengths should be draw from an imported sample track.
Movement distribution parameters	Xmin, μ and Xmax as appropriate.
Population centre coordinates	X = -1948275, Y = 3940710

16.5 Program validation and development

16.5.1 Optimal temperature range

An appropriate temperature range to use to constrain the sharks was determined from records from sharks tagged with pop up archival transmitters (PAT). The returned data provides time at temperature matrices such as that shown Figure H2 and described by Queiroz *et al*. (2010). From this data a histogram was produced to obtain the temperatures experienced by both adult and juvenile sharks (Figure H3) from which a range of 16-23°C was considered to be appropriate as a constraint for the simulated sharks. When remotely sensed SST data sets became available a further analysis was performed, whereby the SST for each location in each of the 20 tagged shark tracks was determined. The results are shown in Figure H4

It is straightforward to add the sea surface temperature (SST) at each point in the simulated track to the output file and therefore to allow a verification of the constraint applied by the SST movement controls. The results of this analysis are shown in Figure H5 and it is clear that at no point does the recorded SST exceed the limits set in the

simulation. Figure H6 shows the sequence of SST changes throughout the year to which the sharks are responding; the rapidly advancing warm front evident in July causes the recorded temperature to rise as shown in Figure H5 and pushes the sharks northward.

16.5.2 *Ensuring an even distribution of modelled sharks*

At the start of each simulation run all sharks start at a position calculated to be one random step away from the coordinates of the population centre. It was found that this tended to concentrate the sharks at this location during the first few months more than was expected as illustrated in Figure H7 which shows the maximum number of sharks recorded in a single grid cell for each day of the year. To reduce this unrealistic concentration each simulation was allowed to run for 360 days before starting to collect location data; i.e. each simulation was started on the 4th of January 2007 with data being collected from the 1st of January 2008. Doing so allows the sharks to disperse sufficiently for no unrealistic clumping to occur, as shown in Figure H8 where shark concentrations fluctuate throughout the year as the sharks respond to changing temperatures. Figure H9 shows the shark simulation program output display with 100 simulated shark tracks.
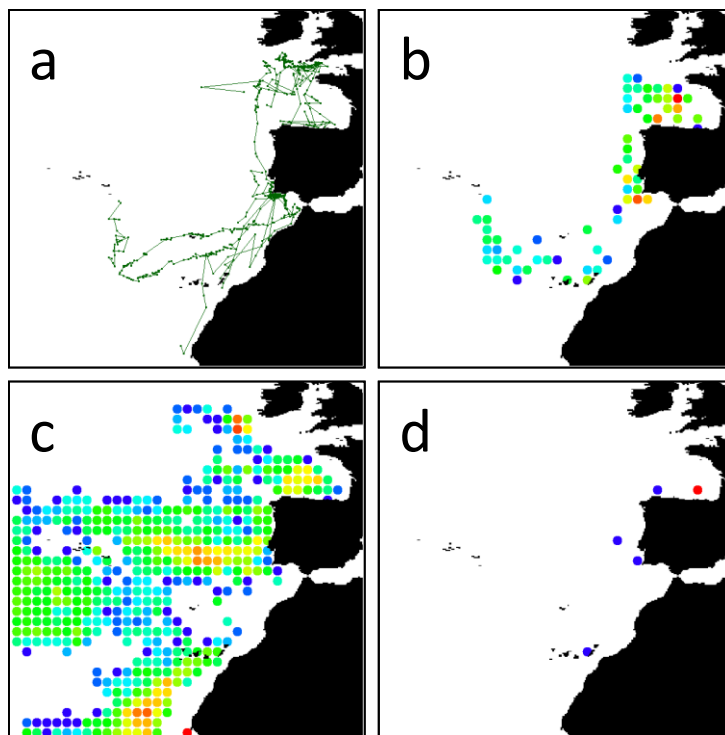
Figure H1: Real shark tracking data
a) Tracks from 20 sharks tagged with either SPOT or PAT tags; b) 2D Grid occupancy summary of space use by the 20 real sharks; c) 2D Grid occupancy summary showing space use for the two fleets; d) 3D Grid

occupancy analysis showing actual interactions between the real sharks and the boats. There are too few interactions to make the analysis useful.
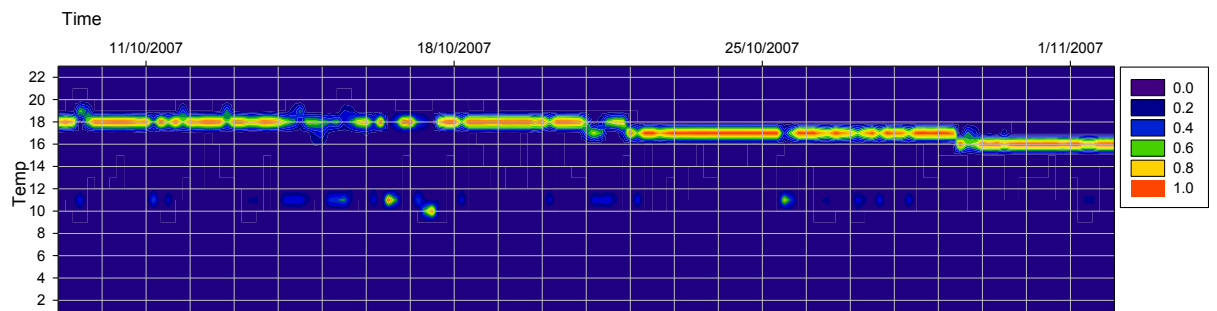
Time at Temperature Matrix - Blue shark 10 S5

Figure H2: Time at temperature matrix for a blue shark
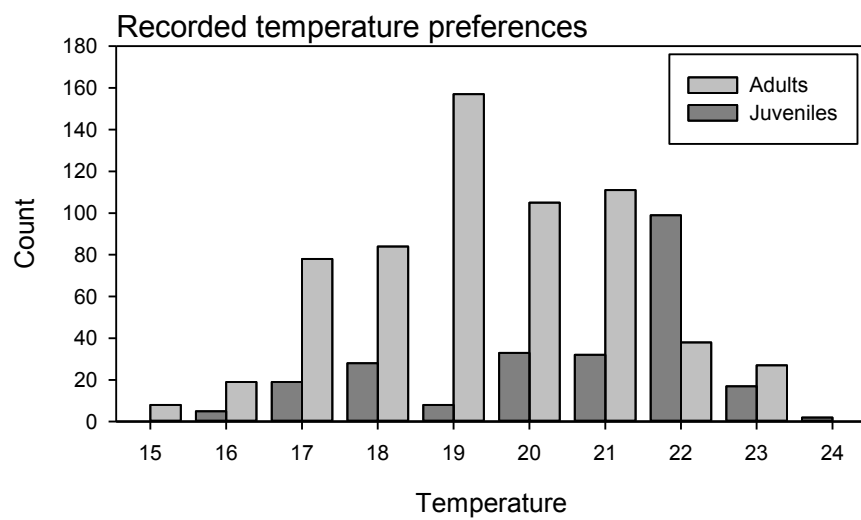
Figure H3: Temperature preferences from tagged sharks

The histogram shows records of temperatures recorded from both adult and juvenile sharks by pop up archival tags (PATs) in the North East Atlantic. A temperature range of 16-23°C is sufficient to encompass most of the recorded values.
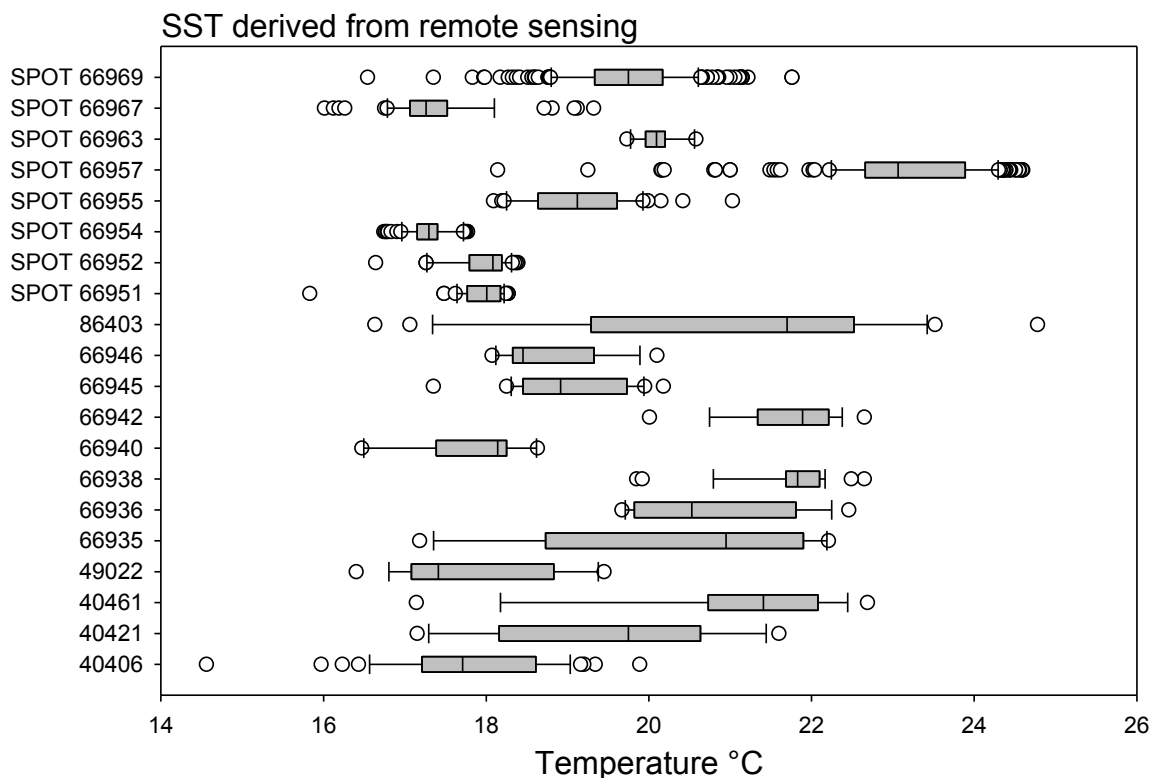
Figure H4: Remotely sensed SST values from tagged blue sharks

Sea surface temperature values derived from remote sensing data for 20 tagged blue sharks. Other than the one shark (SPOT 66957) the selected temperature range of 16-23°C can be seen to encompass the majority of the recorded temperatures. These data compare well with the values obtained from the tag recorded time at temperature histograms, suggesting that, when swimming near the surface, sharks are well above the thermocline.
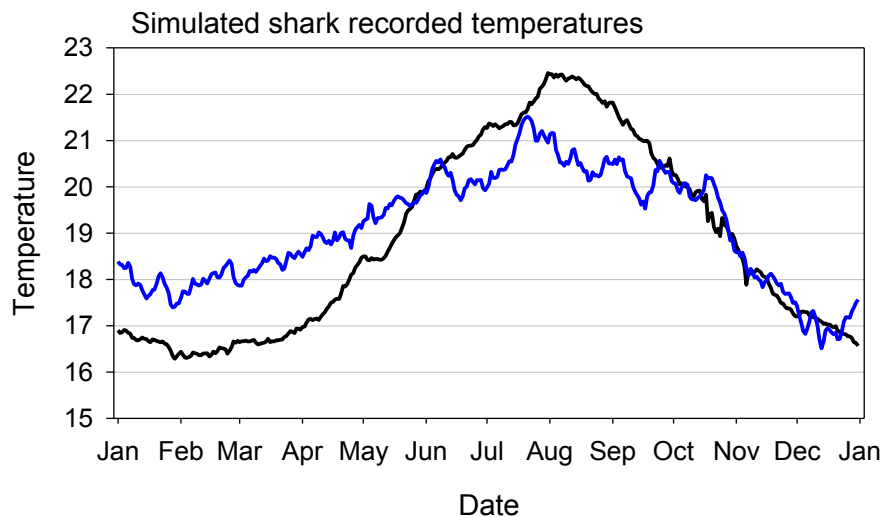
Figure H5: Verification of the temperatures experienced by simulated sharks

Blue line is the temperature record from a single shark; Black line shows the average values from 10 sharks. The recorded temperature stays within the 16-23°C temperature range.

330
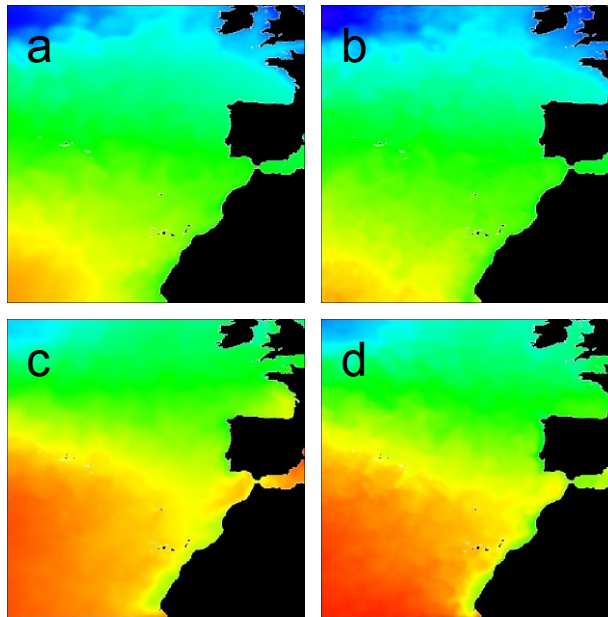
Figure H6: The sequence of SST changes throughout the year
SST maps for the months a) January; b) April; c) July and d) October.
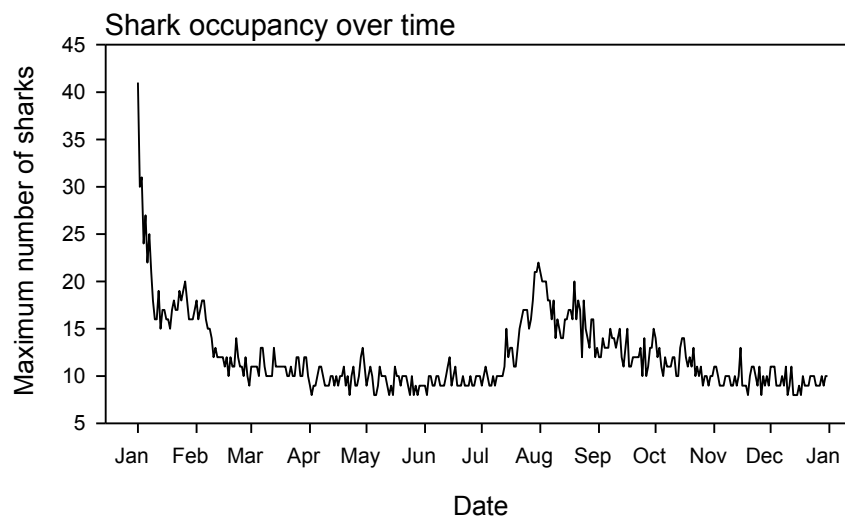
Figure H7: Shark occupancy with no start up delay
When all simulations begin with sharks positioned one move step from the population centre there is an unrealistic clumping of sharks in the first few months, before they disperse throughout the area.
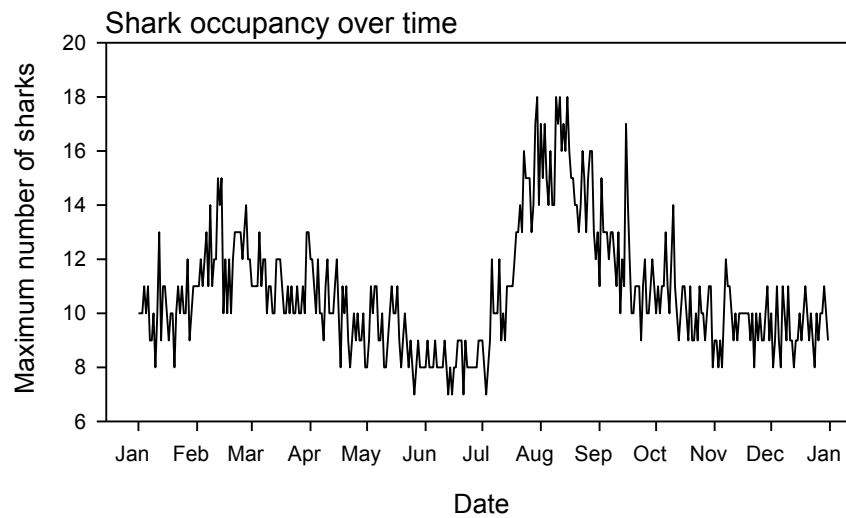
Figure H8: Shark occupancy with a start-up delay

When the simulation is run for 360 days prior to beginning to record the track the sharks have already dispersed before data is collected; there is no longer any clumping in the first few months.
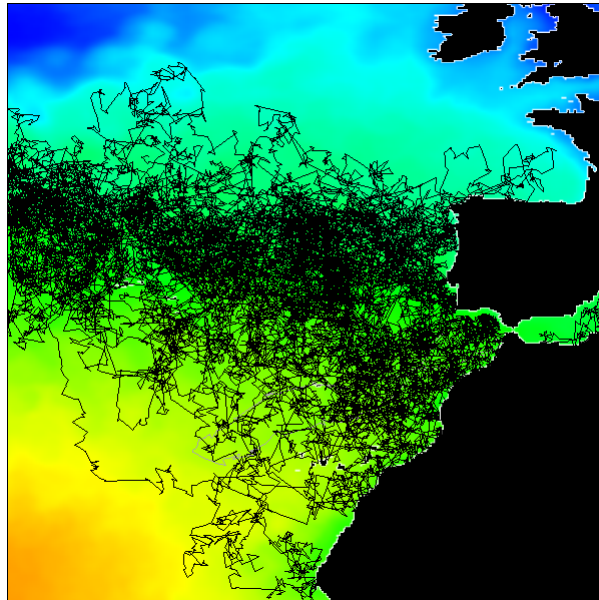
Figure H9: The simulation program display

The figure shows 100 simulated shark tracks overlain on a sea surface temperature map (for January) and the coastline that forms the western boundary of the study area. While most sharks are confined to an area west of the Iberian Peninsula there are many movements which extend well beyond this area, as far south as The Gambia and north into the Bay of Biscay.

17 References

Aban, I. B., M. M. Meerschaert, and A. K. Panorska. 2006. Parameter estimation for the truncated Pareto distribution. Journal of the American Statistical Association **101**:270-277.

Abe, T., K. Sekiguchi, H. Onishi, K. Muramatsu, and T. Kamito. 2012. Observations on a school of ocean sunfish and evidence for a symbiotic cleaning association with albatrosses. Marine Biology **159**:1173-1176.

Aires-da-Silva, A. M., J. J. Hoey, and V. F. Gallucci. 2008. A historical index of abundance for the blue shark (*Prionace glauca*) in the western North Atlantic. Fisheries Research **92**:41-52.

Alos, J., M. Palmer, and R. Arlinghaus. 2012. Consistent Selection towards Low Activity Phenotypes When Catchability Depends on Encounters among Human Predators and Fish. PLoS ONE **7**:9.

Apostolaki, P., E. J. Milner-Gulland, M. K. McAllister, and G. P. Kirkwood. 2002. Modelling the effects of establishing a marine reserve for mobile fish species. Canadian Journal of Fisheries and Aquatic Sciences **59**:405-415.

Armstrong, J. B. and D. E. Schindler. 2011. Excess digestive capacity in predators reflects a life of feast and famine. Nature **476**:84-+.

Arrington, D. A., B. K. Davidson, K. O. Winemiller, and C. A. Layman. 2006. Influence of life history and seasonal hydrology on lipid storage in three neotropical fish species. Journal of Fish Biology **68**:1347-1361.

Arrington, D. A., K. O. Winemiller, W. F. Loftus, and S. Akin. 2002. How often do fishes "run on empty"? Ecology **83**:2145-2151.

Avgar, T., N. Horvitz, L. Broitman, and R. Nathan. 2008. How movement properties affect prey encounter rates of ambush versus active predators: A comment on Scharf et al. American Naturalist **172**:593-595.

Baez, J. C., R. Real, C. Garcia-Soto, J. M. de la Serna, D. Macias, and J. A. Caminas. 2007. Loggerhead turtle by-catch depends on distance to the coast, independent of fishing effort: implications for conservation and fisheries management. Marine Ecology-Progress Series **338**:249-256.

Bailey, K. M. 1997. Structural dynamics and ecology of flatfish populations. Journal of Sea Research **37**:269-280.

Barabasi, A. L. 2005. The origin of bursts and heavy tails in human dynamics. Nature **435**:207-211.

Barnett, C. A., J. Skelhorn, M. Bateson, and C. Rowe. 2012. Educated predators make strategic decisions to eat defended prey according to their toxin content. Behavioral Ecology **23**:418-424.

Bartumeus, F. 2007. Lévy processes in animal movement: An evolutionary hypothesis. Fractals-Complex Geometry Patterns and Scaling in Nature and Society **15**:151-162.

Bartumeus, F. and J. Catalan. 2009. Optimal search behavior and classic foraging theory. Journal of Physics a-Mathematical and Theoretical **42**:12.

Bartumeus, F., J. Catalan, U. L. Fulco, M. L. Lyra, and G. M. Viswanathan. 2002. Optimizing the encounter rate in biological interactions: Lévy versus Brownian strategies. Physical Review Letters **88**:4.

Bartumeus, F., M. G. E. Da Luz, G. M. Viswanathan, and J. Catalan. 2005. Animal search strategies: A quantitative. random-walk analysis. Ecology **86**:3078-3087.

Bartumeus, F., L. Giuggioli, M. Louzao, V. Bretagnolle, D. Oro, and S. A. Levin. 2010. Fishery Discards Impact on Seabird Movement Patterns at Regional Scales. Current Biology **20**:215-222.

Bartumeus, F. and S. A. Levin. 2008. Fractal reorientation clocks: Linking animal behavior to statistical patterns of search. Proceedings of the National Academy of Sciences of the United States of America **105**:19072-19077.

Bartumeus, F., F. Peters, S. Pueyo, C. Marrase, and J. Catalan. 2003. Helical Levy walks: Adjusting searching statistics to resource availability in

microzooplankton. Proceedings of the National Academy of Sciences of the United States of America **100**:12771-12775.

Baum, J. K., R. A. Myers, D. G. Kehler, B. Worm, S. J. Harley, and P. A. Doherty. 2003. Collapse and conservation of shark populations in the Northwest Atlantic. Science **299**:389-392.

Bazazi, S., F. Bartumeus, J. J. Hale, and I. D. Couzin. 2012. Intermittent Motion in Desert Locusts: Behavioural Complexity in Simple Environments. Plos Computational Biology **8**:10.

Beachly, W. M., D. W. Stephens, and K. B. Toyer. 1995. On the economics of sit-and-wait foraging - site selection and assessment. Behavioral Ecology **6**:258-268.

Beets, J. and A. Friedlander. 1999. Evaluation of a conservation strategy: a spawning aggregation closure for red hind, *Epinephelus guttatus*, in the US Virgin Islands. Environmental Biology of Fishes **55**:91-98.

Behrenfeld, M. J. and P. G. Falkowski. 1997. Photosynthetic rates derived from satellite-based chlorophyll concentration. Limnology and Oceanography **42**:1-20.

Bendesky, A., M. Tsunozaki, M. V. Rockman, L. Kruglyak, and C. I. Bargmann. 2011. Catecholamine receptor polymorphisms affect decision-making in C. elegans. Nature **472**:313-U207.

Benhamou, S. 2007. How many animals really do the Lévy walk? Ecology **88**:1962-1969.

Benichou, O., M. Coppey, M. Moreau, P. H. Suet, and R. Voituriez. 2005. Optimal search strategies for hidden targets. Physical Review Letters **94**:4.

Benichou, O., C. Loverdo, M. Moreau, and R. Voituriez. 2011. Intermittent search strategies. Reviews of Modern Physics **83**:49.

Berrow, S. D. and J. P. Croxall. 2001. Provisioning rate and attendance patterns of Wandering Albatrosses at Bird Island, South Georgia. Condor **103**:230-239.

Bertrand, S., J. M. Burgos, F. Gerlotto, and J. Atiquipa. 2005. Levy trajectories of Peruvian purse-seiners as an indicator of the spatial distribution of anchovy (Engraulis ringens). Ices Journal of Marine Science **62**:477-482.

Block, B. A., I. D. Jonsen, S. J. Jorgensen, A. J. Winship, S. A. Shaffer, S. J. Bograd, E. L. Hazen, D. G. Foley, G. A. Breed, A. L. Harrison, J. E. Ganong, A. Swithenbank, M. Castleton, H. Dewar, B. R. Mate, G. L. Shillinger, K. M. Schaefer, S. R. Benson, M. J. Weise, R. W. Henry, and D. P. Costa. 2011. Tracking apex marine predator movements in a dynamic ocean. Nature **475**:86-90.

Blyth-Skyrme, R. E., M. J. Kaiser, J. G. Hiddink, G. Edwards-Jones, and P. J. B. Hart. 2006. Conservation benefits of temperate marine protected areas: Variation among fish species. Conservation Biology **20**:811-820.

Bojarska, K. and N. Selva. 2012. Spatial patterns in brown bear Ursus arctos diet: the role of geographical and environmental factors. Mammal Review **42**:120-143.

Bolle, L. J., E. Hunter, A. D. Rijnsdorp, M. A. Pastoors, J. D. Metcalfe, and J. D. Reynolds. 2005. Do tagging experiments tell the truth? Using electronic tags to evaluate conventional tagging data. Ices Journal of Marine Science **62**:236-246.

Boyer, D., O. Miramontes, and H. Larralde. 2009. Levy-like behaviour in deterministic models of intelligent agents exploring heterogeneous environments. Journal of Physics a-Mathematical and Theoretical **42**.

Boyer, D., G. Ramos-Fernandez, O. Miramontes, J. L. Mateos, G. Cocho, H. Larralde, H. Ramos, and F. Rojas. 2006. Scale-free foraging by primates emerges from their interaction with a complex environment. Proceedings of the Royal Society B-Biological Sciences **273**:1743-1750.

Bradshaw, C. J. A., D. W. Sims, and G. C. Hays. 2007. Measurement error causes scale-dependent threshold erosion of biological signals in animal movement data. Ecological Applications **17**:628-638.

Brander, K. 2010. Impacts of climate change on fisheries. Journal of Marine Systems **79**:389-402.

Bresenham, J. E. 1965. Algorithm for computer control of a digital plotter. IBM Systems Journal **4**:25-30.

Brown, C., L. Liebovitch, and R. Glendon. 2007. Lévy Flights in Dobe Ju/'hoansi Foraging Patterns. Human Ecology: An Interdisciplinary Journal **35**:129-138.

Brunnschweiler, J. M., H. Baensch, S. J. Pierce, and D. W. Sims. 2009. Deep diving behaviour of a whale shark during long-distance movement in the western Indian Ocean. Journal of Fish Biology **74**:706-714.

Buchanan, M. 2008. Ecological modelling: The mathematical mirror to animal nature. Nature **453**:714-716.

Buencuerpo, V., S. Rios, and J. Morón. 1998. Pelagic sharks associated with the swordfish, *Xiphias gladius*, fishery in the eastern North Atlantic Ocean and the Strait of Gibraltar. Fishery Bulletin **96**:667-685.

Burnham, K. P. and D. R. Anderson. 2004. Multimodel inference - understanding AIC and BIC in model selection. Sociological Methods & Research **33**:261-304.

Cadiou, G., C. F. Boudouresque, P. Bonhomme, and L. Le Direac'h. 2009. The management of artisanal fishing within the Marine Protected Area of the Port-Cros National Park (northwest Mediterranean Sea): a success story? ICES Journal of Marine Science: Journal du Conseil **66**:41-49.

Campana, S. E., W. Joyce, and M. J. Manning. 2009. Bycatch and discard mortality in commercially caught blue sharks Prionace glauca assessed using archival satellite pop-up tags. Marine Ecology-Progress Series **387**:241-253.

Campana, S. E., L. Marks, W. Joyce, and N. E. Kohler. 2006. Effects of recreational and commercial fishing on blue sharks (Prionace glauca) in Atlantic Canada, with inferences on the North Atlantic population. Canadian Journal of Fisheries and Aquatic Sciences **63**:670-682.

Carruthers, E. H., J. D. Neilson, and S. C. Smith. 2011. Overlooked bycatch mitigation opportunities in pelagic longline fisheries: Soak time and temperature effects on swordfish (Xiphias gladius) and blue shark (Prionace glauca) catch. Fisheries Research **108**:112-120.

Casale, P. 2011. Sea turtle by-catch in the Mediterranean. Fish and Fisheries **12**:299-316.

Cheung, W. W. L., R. Watson, T. Morato, T. J. Pitcher, and D. Pauly. 2007. Intrinsic vulnerability in the global fish catch. Marine ecology progress series **333**:1-12.

Christensen, A. r., H. Mosegaard, and H. Jensen. 2009. Spatially resolved fish population analysis for designing MPAs: influence on inside and neighbouring habitats. ICES Journal of Marine Science: Journal du Conseil **66**:56-63.

Clarke, A. and P. A. Prince. 1980. Chemical composition and calorific value of food fed to mollymauk chicks Diomedea melanophris and Diomedea chrysostoma at bird-island, South Georgia. Ibis **122**:488-494.

Clarke, M. R. and J. D. Stevens. 1974. Cephalopods, Blue sharks and Migration. Journal of the Marine Biological Association of the United Kingdom **54**:949-957.

Clauset, A., C. R. Shalizi, and M. E. J. Newman. 2009. Power-Law Distributions in Empirical Data. Siam Review **51**:661-703.

Codling, E. A. and M. J. Plank. 2011. Turn designation, sampling rate and the misidentification of power laws in movement path data using maximum likelihood estimates. Theoretical Ecology **4**:397-406.

Cole, B. J. 1995. Fractal time in animal behavior - the movement activity of *Drosophila*. Animal Behaviour **50**:1317-1324.

Coop, J. D., C. D. Hibner, A. J. Miller, and G. H. Clark. 2005. Black bears forage on army cutworm moth aggregations in the Jemez Mountains, New Mexico. Southwestern Naturalist **50**:278-281.

Cornelius, J. M. and J. F. Reynolds. 1991. On determining the significance of discontinuities within ordered ecological data. Ecology **72**:2057-2070.

Cortes, E., F. Arocha, L. Beerkircher, F. Carvalho, A. Domingo, M. Heupel, H. Holtzhausen, M. N. Santos, M. Ribera, and C. Simpfendorfer. 2010. Ecological risk assessment of pelagic sharks caught in Atlantic pelagic longline fisheries. Aquatic Living Resources **23**:25-34.

Coughlin, D. J., J. R. Strickler, and B. Sanderson. 1992. Swimming and search behaviour in clownfish, Amphiprion perideraion, larvae. Animal Behaviour **44, Part 3**:427-440.

Crimes, T. P. and J. D. Crossley. 1991. A diverse ichnofauna from silurian flysch of the aberystwyth grits formation, wales. Geological Journal **26**:27-64.

Crist, T. O., D. S. Guertin, J. A. Wiens, and B. T. Milne. 1992. Animal movement in heterogeneous landscapes - an experiment with Eleodes beetles in shortgrass prairie. Functional Ecology **6**:536-544.

Crowder, L. B., S. J. Lyman, W. F. Figueira, and J. Priddy. 2000. Source-sink population dynamics and the problem of siting marine reserves. Bulletin of Marine Science **66**:799-820.

da Luz, M. G. E., S. V. Buldyrev, S. Havlin, E. P. Raposo, H. E. Stanley, and G. M. Viswanathan. 2001. Improvements in the statistical approach to random Lévy flight searches. Physica a-Statistical Mechanics and Its Applications **295**:89-92.

de Jager, M., F. J. Weissing, P. M. J. Herman, B. A. Nolet, and J. van de Koppel. 2011. Lévy Walks Evolve Through Interaction Between Movement and Environmental Complexity. Science **332**:1551-1553.

Dicke, M. and P. A. Burrough. 1988. Using fractal dimensions for characterizing tortuosity of animal trails. Physiological Entomology **13**:393-398.

Dinmore, T. A., D. E. Duplisea, B. D. Rackham, D. L. Maxwell, and S. Jennings. 2003. Impact of a large-scale area closure on patterns of fishing disturbance

and the consequences for benthic communities. ICES Journal of Marine Science: Journal du Conseil **60**:371-380.

Domeier, M. L. 2006. An analysis of pacific striped marlin (Tetrapturus audax) horizontal movement patterns using pop-up satellite archival tags. Bulletin of Marine Science **79**:811-825.

Dreisig, H. 2012. How long to stay on a plant: the response of bumblebees to encountered nectar levels. Arthropod-Plant Interactions **6**:315-325.

Dulvy, N. K., J. K. Baum, S. Clarke, L. J. V. Compagno, E. Cortés, A. Domingo, S. Fordham, S. Fowler, M. P. Francis, C. Gibson, J. Martínez, J. A. Musick, A. Soldo, J. D. Stevens, and S. Valenti. 2008. You can swim but you can't hide: the global status and conservation of oceanic pelagic sharks and rays. Aquatic Conservation: Marine and Freshwater Ecosystems **18**:459-482.

Edwards, A. M. 2008. Using likelihood to test for Lévy flight search patterns and for general power-law distributions in nature. Journal of Animal Ecology **77**:1212-1222.

Edwards, A. M., R. A. Phillips, N. W. Watkins, M. P. Freeman, E. J. Murphy, V. Afanasyev, S. V. Buldyrev, M. G. E. da Luz, E. P. Raposo, H. E. Stanley, and G. M. Viswanathan. 2007. Revisiting Lévy flight search patterns of wandering albatrosses, bumblebees and deer. Nature **449**:1044-1048.

Edwards, C. T. T., R. b. A. Rademeyer, D. S. Butterworth, and Ã. v. E. PlagÃ¡nyi. 2009. Investigating the consequences of Marine Protected Areas for the South African deep-water hake (Merluccius paradoxus) resource. ICES Journal of Marine Science: Journal du Conseil **66**:72-81.

Fauchald, P. and T. Tveraa. 2003. Using first-passage time in the analysis of area-restricted search and habitat selection. Ecology **84**:282-288.

Feldheim, K. A., S. H. Gruber, and M. V. Ashley. 2002. The breeding biology of lemon sharks at a tropical nursery lagoon. Proceedings of the Royal Society of London Series B-Biological Sciences **269**:1655-1661.

Ferrari, M. C. O., G. E. Brown, G. R. Bortolotti, and D. P. Chivers. 2010. Linking predator risk and uncertainty to adaptive forgetting: a theoretical framework and empirical test using tadpoles. Proceedings of the Royal Society B-Biological Sciences **277**:2205-2210.

Fiedler, P. C. and H. J. Bernard. 1987. Tuna aggregation and feeding near fronts observed in satellite imagery. Continental Shelf Research **7**:871-881.

Forcada, A., C. Valle, J. L. Sá¡nchez-Lizaso, J. T. Bayle-Sempere, and F. Corsi. 2010. Structure and spatio-temporal dynamics of artisanal fisheries around a Mediterranean marine protected area. ICES Journal of Marine Science: Journal du Conseil **67**:191-203.

Fortin, D. 2002. Optimal searching behaviour: the value of sampling information. Ecological Modelling **153**:279-290.

Fossette, S., A. C. Gleiss, A. E. Myers, S. Garner, N. Liebsch, N. M. Whitney, G. C. Hays, R. P. Wilson, and M. E. Lutcavage. 2010. Behaviour and buoyancy regulation in the deepest-diving reptile: the leatherback turtle. Journal of Experimental Biology **213**:4074-4083.

Fritz, H., S. Said, and H. Weimerskirch. 2003. Scale-dependent hierarchical adjustments of movement patterns in a long-range foraging seabird. Proceedings of the Royal Society of London Series B-Biological Sciences **270**:1143-1148.

Fry, S. N., R. Sayaman, and M. H. Dickinson. 2003. The aerodynamics of free-flight maneuvers in Drosophila. Science **300**:495-498.

Gall, M. D. and E. Fernandez-Juricic. 2010. Visual fields, eye movements, and scanning behavior of a sit-and-wait predator, the black phoebe (Sayornis nigricans). Journal of Comparative Physiology a-Neuroethology Sensory Neural and Behavioral Physiology **196**:15-22.

Gallager, S. M., C. S. Davis, A. W. Epstein, A. Solow, and R. C. Beardsley. 1996. High-resolution observations of plankton spatial distributions correlated with hydrography in the Great South Channel, Georges Bank. Deep Sea Research Part II: Topical Studies in Oceanography **43**:1627-1663.

Game, E. T., H. S. Grantham, A. J. Hobday, R. L. Pressey, A. T. Lombard, L. E. Beckley, K. Gjerde, R. Bustamante, H. P. Possingham, and A. J. Richardson. 2009. Pelagic protected areas: the missing dimension in ocean conservation. Trends in Ecology & Evolution **24**:360-369.

Garstang, W. 1900. The Impoverishment of the Sea. A Critical Summary of the Experimental and Statistical Evidence bearing upon the Alleged Depletion of the Trawling Grounds. Journal of the Marine Biological Association of the UK (New Series) **6**:1-69.

Gell, F. R. and C. M. Roberts. 2003. Benefits beyond boundaries: the fishery effects of marine reserves. Trends in Ecology & Evolution **18**:448-455.

Genner, M. J., N. C. Halliday, S. D. Simpson, A. J. Southward, S. J. Hawkins, and D. W. Sims. 2010. Temperature-driven phenological changes within a marine larval fish assemblage. Journal of Plankton Research **32**:699-708.

Gilman, E., D. Kobayashi, T. Swenarton, N. Brothers, P. Dalzell, and I. Kinan-Kelly. 2007. Reducing sea turtle interactions in the Hawaii-based longline swordfish fishery. Biological Conservation **139**:19-28.

Gleason, D. F. and D. K. Hofmann. 2011. Coral larvae: From gametes to recruits. Journal of Experimental Marine Biology and Ecology **408**:42-57.

Gonzalez, M. C., C. A. Hidalgo, and A. L. Barabasi. 2008. Understanding individual human mobility patterns. Nature **453**:779-782.

Graham, E. M., A. H. Baird, and S. R. Connolly. 2008. Survival dynamics of scleractinian coral larvae and implications for dispersal. Coral Reefs **27**:529-539.

Greenstreet, S. P. R., H. M. Fraser, and G. J. Piet. 2009. Using MPAs to address regional-scale ecological objectives in the North Sea: modelling the effects of fishing effort displacement. ICES Journal of Marine Science: Journal du Conseil **66**:90-100.

Grove, T. J. and B. D. Sidell. 2002. Myoglobin deficiency in the hearts of phylogenetically diverse temperate-zone fish species. Canadian Journal of Zoology-Revue Canadienne De Zoologie **80**:893-901.

Grüss, A., D. M. Kaplan, S. Guénette, C. M. Roberts, and L. W. Botsford. 2011. Consequences of adult and juvenile movement for marine protected areas. Biological Conservation **144**:692-702.

Guy, A. G., D. A. Bohan, S. J. Powers, and A. M. Reynolds. 2008. Avoidance of conspecific odour by carabid beetles: a mechanism for the emergence of scale-free searching patterns. Animal Behaviour **76**:585-591.

Hamer, K. C., E. M. Humphreys, M. C. Magalhaes, S. Garthe, J. Hennicke, G. Peters, D. Gremillet, H. Skov, and S. Wanless. 2009. Fine-scale foraging behaviour of a medium-ranging marine predator. Journal of Animal Ecology **78**:880-889.

Hammerschlag, N., A. J. Gallagher, and D. M. Lazarre. 2011. A review of shark satellite tagging studies. Journal of Experimental Marine Biology and Ecology **398**:1-8.

Hartig, F., J. M. Calabrese, B. Reineking, T. Wiegand, and A. Huth. 2011. Statistical inference for stochastic simulation models - theory and application. Ecology Letters **14**:816-827.

Hays, G. C., T. Bastian, T. K. Doyle, S. Fossette, A. C. Gleiss, M. B. Gravenor, V. J. Hobson, N. E. Humphries, M. K. S. Lilley, N. G. Pade, and D. W. Sims. 2012. High activity and Lévy searches: jellyfish can search the water column like fish. Proceedings of the Royal Society B: Biological Sciences.

Hays, G. C., C. J. A. Bradshaw, M. C. James, P. Lovell, and D. W. Sims. 2007. Why do Argos satellite tags deployed on marine animals stop transmitting? Journal of Experimental Marine Biology and Ecology **349**:52-60.

Hazel, J. 2009. Evaluation of fast-acquisition GPS in stationary tests and fine-scale tracking of green turtles. Journal of Experimental Marine Biology and Ecology **374**:58-68.

Horn, H. S. 1966. Measurements of 'overlap' in comparative ecological studies. American Naturalist **100**:419:424.

Howell, K. L., S. L. Mowles, and A. Foggo. 2010. Mounting evidence: near-slope seamounts are faunally indistinct from an adjacent bank. Marine Ecology-an Evolutionary Perspective **31**:52-62.

Hubbard, S., P. Babak, S. T. Sigurdsson, and K. G. Magnusson. 2004. A model of the formation of fish schools and migrations of fish. Ecological Modelling **174**:359-374.

Humphries, N. E., N. Queiroz, J. R. M. Dyer, N. G. Pade, M. K. Musyl, K. M. Schaefer, D. W. Fuller, J. M. Brunnschweiler, T. K. Doyle, J. D. R. Houghton, G. C. Hays, C. S. Jones, L. R. Noble, V. J. Wearmouth, E. J. Southall, and D. W. Sims. 2010. Environmental context explains Lévy and Brownian movement patterns of marine predators. Nature **465**:1066-1069.

Humphries, N. E., H. Weimerskirch, N. Queiroz, E. J. Southall, and D. W. Sims. 2012. Foraging success of biological Lévy flights recorded in situ. Proceedings of the National Academy of Sciences of the United States of America **109**:7169-7174.

Hunter, E., J. N. Aldridge, J. D. Metcalfe, and G. P. Arnold. 2003. Geolocation of free-ranging fish on the European continental shelf as determined from environmental variables - I. Tidal location method. Marine Biology **142**:601-609.

Hunter, E., F. Berry, A. A. Buckley, C. Stewart, and J. D. Metcalfe. 2006. Seasonal migration of thornback rays and implications for closure management. Journal of Applied Ecology **43**:710-720.

Hutchings, J. A. 2000. Collapse and recovery of marine fishes. Nature **406**:882-885.

Hutchinson, J. M. C. and P. M. Waser. 2007. Use, misuse and extensions of "ideal gas" models of animal encounter. Biological Reviews **82**:335-359.

Hyrenbach, K. D., K. A. Forney , and P. K. Dayton. 2000. Marine protected areas and ocean basin management. Aquatic Conservation: Marine and Freshwater Ecosystems **10**:437-458.

Jacoby, D. M. P., D. S. Busawon, and D. W. Sims. 2010. Sex and social networking: the influence of male presence on social structure of female shark groups. Behavioral Ecology **21**:808-818.

James, A., M. J. Plank, and R. Brown. 2008. Optimizing the encounter rate in biological interactions: Ballistic versus Levy versus Brownian strategies. Physical Review E **78**.

James, A., M. J. Plank, and A. M. Edwards. 2011. Assessing Levy walks as models of animal foraging. Journal of the Royal Society Interface **8**:1233-1247.

Jennings, S. 2009. The role of marine protected areas in environmental management. ICES Journal of Marine Science: Journal du Conseil **66**:16-21.

Jennings, S. and K. Brander. 2010. Predicting the effects of climate change on marine communities and the consequences for fisheries. Journal of Marine Systems **79**:418-426.

Jensen, O. P., S. Ortega-Garcia, S. J. D. Martell, R. N. M. Ahrens, M. L. Domeier, C. J. Walters, and J. F. Kitchell. 2010. Local management of a "highly migratory species": The effects of long-line closures and recreational catch-and-release for Baja California striped marlin fisheries. Progress in Oceanography **86**:176-186.

Jimenez, P., F. Thomas, and C. Torras. 2001. 3D collision detection: a survey. Computers & Graphics-Uk **25**:269-285.

Jimenez, S., M. Abreu, M. Pons, M. Ortiz, and A. Domingo. 2010. Assessing the impact of the pelagic longline fishery on albatrosses and petrels in the southwest Atlantic. Aquatic Living Resources **23**:49-64.

Jonsen, I. D., R. A. Myers, and M. C. James. 2006. Robust hierarchical state-space models reveal diel variation in travel rates of migrating leatherback turtles. Journal of Animal Ecology **75**:1046-1057.

Kagan, Y. Y. 2002. Seismic moment distribution revisited: I. Statistical results. Geophysical Journal International **148**:520-541.

Kaiser, M. J. 2005. Are marine protected areas a red herring or fisheries panacea? Canadian Journal of Fisheries and Aquatic Sciences **62**:1194-1199.

Kareev, Y. 1995. Through a narrow window: working memory capacity and the detection of covariation. Cognition **56**:263-269.

Kashtan, N., E. Noor, and U. Alon. 2007. Varying environments can speed up evolution. Proceedings of the National Academy of Sciences of the United States of America **104**:13711-13716.

Kerstetter, D. W. and J. E. Graves. 2006. Effects of circle versus J-style hooks on target and non-target species in a pelagic longline fishery. Fisheries Research **80**:239-250.

Kitchell, J. F., T. E. Essington, C. H. Boggs, D. E. Schindler, and C. J. Walters. 2002. The role of sharks and longline fisheries in a pelagic ecosystem of the Central Pacific. Ecosystems **5**:202-216.

Klafter, J., A. Blumen, G. Zumofen, and M. F. Shlesinger. 1990. Levy walk approach to anomalous diffusion. Physica A **168**:637-645.

Klafter, J., G. Zumofen, and M. F. Shlesinger. 1993. Levy walks in dynamical-systems. Physica A **200**:222-230.

Klaus, A., S. Yu, and D. Plenz. 2011. Statistical Analyses Support Power Law Distributions Found in Neuronal Avalanches. PLoS ONE **6**:12.

Kohler, N. E. and P. A. Turner. 2001. Shark tagging: A review of conventional methods and studies. Environmental Biology of Fishes **60**:191-223.

Koy, K. A. and R. E. Plotnick. 2010. Ichnofossil morphology as a response to resource distribution: Insights from modern invertebrate foraging. Palaeogeography Palaeoclimatology Palaeoecology **292**:272-281.

Kraus, G., D. Pelletier, J. Dubreuil, C. Mollmann, H. H. Hinrichsen, F. Bastardie, Y. Vermard, and S. Mahevas. 2009. A model-based evaluation of Marine Protected Areas: the example of eastern Baltic cod (Gadus morhua callarias L.). Ices Journal of Marine Science **66**:109-121.

La Mesa, G., A. Molinari, S. Bava, M. G. Finoia, R. Cattaneo-Vietti, and L. Tunesi. 2011. Gradients of abundance of sea breams across the boundaries of a Mediterranean marine protected area. Fisheries Research **111**:24-30.

Laurel, B. J. and I. R. Bradbury. 2006. "Big" concerns with high latitude marine protected areas (MPAs): trends in connectivity and MPA size. Canadian Journal of Fisheries and Aquatic Sciences **63**:2603-2607.

Laurenson, C. H., I. R. Hudson, D. O. B. Jones, and I. G. Priede. 2004. Deep water observations of Lophius piscatorius in the north-eastern Atlantic Ocean by means of a remotely operated vehicle. Journal of Fish Biology **65**:947-960.

Le Fèvre, J. 1986. Aspects of the Biology of Frontal Systems. Advances in Marine Biology **23**:163-299.

Lester, S. E. and B. S. Halpern. 2008. Biological responses in marine no-take reserves versus partially protected areas. Marine Ecology-Progress Series **367**:49-56.

Leszczynski, J. S. and M. Ciesielski. 2004. Effective algorithm for detection of a collision between spherical particles. Pages 348-355 *in* M. Bubak, G. D. VanAlbada, P. M. A. Sloot, and J. J. Dongarra, editors. Computational Science - Iccs 2004, Pt 2, Proceedings. Springer-Verlag Berlin, Berlin.

Liu, F., T. Harada, Y. Lee, and Y. J. Kim. 2010. Real-time Collision Culling of a Million Bodies on Graphics Processing Units. Acm Transactions on Graphics **29**:8.

Loher, T. 2011. Analysis of match-mismatch between commercial fishing periods and spawning ecology of Pacific halibut (Hippoglossus stenolepis), based on winter surveys and behavioural data from electronic archival tags. Ices Journal of Marine Science **68**:2240-2251.

Lowe, C. G. 2001. Metabolic rates of juvenile scalloped hammerhead sharks (Sphyrna lewini). Marine Biology **139**:447-453.

Lucifora, L. O., V. B. Garcia, R. C. Menni, and B. Worm. 2012. Spatial patterns in the diversity of sharks, rays, and chimaeras (Chondrichthyes) in the Southwest Atlantic. Biodiversity and Conservation **21**:407-419.

Mackley, E. K., R. A. Phillips, J. R. D. Silk, E. D. Wakefield, V. Afanasyev, J. W. Fox, and R. W. Furness. 2010. Free as a bird? Activity patterns of albatrosses during the nonbreeding period. Marine Ecology-Progress Series **406**:291-303.

Mackney, P. A. and R. N. Hughes. 1995. Foraging behaviour and memory window in sticklebacks. Behaviour **132**:1241-1253.

Marin, Y. H., F. Brum, L. C. Barea, and J. F. Chocca. 1998. Incidental catch associated with swordfish longline fisheries in the south-west Atlantic Ocean. Marine and Freshwater Research **49**:633-639.

Matthaus, F., M. S. Mommer, T. Curk, and J. Dobnikar. 2011. On the Origin and Characteristics of Noise-Induced Levy Walks of E. Coli. PLoS ONE **6**:8.

Mattson, D. J. 2004. Exploitation of pocket gophers and their food caches by grizzly bears. Journal of Mammalogy **85**:731-742.

Mattson, D. J., S. R. Podruzny, and M. A. Haroldson. 2005. Consumption of pondweed rhizomes by Yellowstone grizzly beers. Ursus **16**:41-46.

Maye, A., C. H. Hsieh, G. Sugihara, and B. Brembs. 2007. Order in Spontaneous Behavior. PLoS ONE **2**:14.

Megalofonou, P., D. Damalas, and C. Yannopoulos. 2005a. Composition and abundance of pelagic shark by-catch in the eastern Mediterranean Sea. Cybium **29**:135-140.

Megalofonou, P., C. Yannopoulos, D. Damalas, G. De Metrio, M. Deflorio, and J. M. de la Serna. 2005b. Incidental catch and estimated discards of pelagic sharks from the swordfish and tuna fisheries in the Mediterranean Sea. Fishery Bulletin **103**:620-634.

Mercier, A., R. H. Ycaza, and J. F. Hamel. 2007. Long-term study of gamete release in a broadcast-spawning holothurian: predictable lunar and diel periodicities. Marine ecology progress series **329**:179-189.

Miramontes, O., D. Boyer, and F. Bartumeus. 2012. The Effects of Spatially Heterogeneous Prey Distributions on Detection Patterns in Foraging Seabirds. PLoS ONE **7**:9.

Moltschaniwskyj, N., G. Pecl, and J. Lyle. 2002. An assessment of the use of short-term closures to protect spawning southern calamary aggregations from fishing pressure in Tasmania, Australia. Bulletin of Marine Science **71**:501-514.

Morato, T., D. A. Varkey, C. Damaso, M. Machete, M. Santos, R. Prieto, R. S. Santos, and T. J. Pitcher. 2008. Evidence of a seamount effect on aggregating visitors. Marine ecology progress series **357**:23-32.

Moteki, M., M. Arai, K. Tsuchiya, and H. Okamoto. 2001. Composition of piscine prey in the diet of large pelagic fish in the eastern tropical Pacific Ocean. Fisheries Science **67**:1063-1074.

Mucientes, G. R., N. Queiroz, L. L. Sousa, P. Tarroso, and D. W. Sims. 2009. Sexual segregation of pelagic sharks and the potential threat from fisheries. Biology Letters **5**:156-159.

Mumby, P. J. 2006. Connectivity of reef fish between mangroves and coral reefs: Algorithms for the design of marine reserves at seascape scales. Biological Conservation **128**:215-222.

Murawski, S. A., S. E. Wigley, M. J. Fogarty, P. J. Rago, and D. G. Mountain. 2005. Effort distribution and catch patterns adjacent to temperate MPAs. ICES Journal of Marine Science: Journal du Conseil **62**:1150-1167.

Musyl, M., L. McNaughton, J. Swimmer, and R. Brill. 2004. Convergent evolution of vertical movement behavior in swordfish, bigeye tuna and bigeye thresher sharks. Vertical niche partitioning in the pelagic environment as shown by electronic tagging studies. PFRP Newsletter **9**:1-4.

Nams, V. O. 2005. Using animal movement paths to measure response to spatial scale. Oecologia **143**:179-188.

Nilsson, J., T. S. Kristiansen, J. E. Fosseidengen, L. H. Stien, A. Ferno, and R. van den Bos. 2010. Learning and anticipatory behaviour in a "sit-and-wait" predator: The Atlantic halibut. Behavioural Processes **83**:257-266.

Nishimura, K. 1991. Optimal patch residence time of a sit-and-wait forager. Behavioral Ecology **2**:283-294.

O'Leary, B. C., R. L. Brown, D. E. Johnson, H. von Nordheim, J. Ardron, T. Packeiser, and C. M. Roberts. 2012. The first network of marine protected areas (MPAs) in the high seas: The process, the challenges and where next. Marine Policy **36**:598-605.

Ohkubo, J., K. Yoshida, Y. Iino, and N. Masuda. 2010. Long-tail behavior in locomotion of *Caenorhabditis elegans*. Journal of Theoretical Biology **267**:213-222.

Oshanin, G., K. Lindenberg, H. S. Wio, and S. Burlatsky. 2009. Efficient search by optimized intermittent random walks. Journal of Physics a-Mathematical and Theoretical **42**.

Pade, N. G., N. Queiroz, N. E. Humphries, M. J. Witt, C. S. Jones, L. R. Noble, and D. W. Sims. 2009. First results from satellite-linked archival tagging of porbeagle shark, *Lamna nasus*: Area fidelity, wider-scale movements and plasticity in diel depth changes. Journal of Experimental Marine Biology and Ecology **370**:64-74.

Papastamatiou, Y. P., C. G. Meyer, and K. N. Holland. 2007. A new acoustic pH transmitter for studying the feeding habits of free-ranging sharks. Aquatic Living Resources **20**:287-290.

Pechenik, J. A. 1999. On the advantages and disadvantages of larval stages in benthic marine invertebrate life cycles. Marine Ecology-Progress Series **177**:269-297.

Pendleton, D. E., A. J. Pershing, M. W. Brown, C. A. Mayo, R. D. Kenney, N. R. Record, and T. V. N. Cole. 2009. Regional-scale mean copepod concentration indicates relative abundance of North Atlantic right whales. Marine Ecology-Progress Series **378**:211-225.

Perry, R. I., P. Cury, K. Brander, S. Jennings, C. Mollmann, and B. Planque. 2010. Sensitivity of marine systems to climate and fishing: Concepts, issues and management responses. Journal of Marine Systems **79**:427-435.

Petrovskii, S., A. Mashanova, and V. A. A. Jansen. 2011. Variation in individual walking behavior creates the impression of a Levy flight. Proceedings of the National Academy of Sciences of the United States of America **108**:8704-8707.

Phalan, B., R. A. Phillips, J. R. D. Silk, V. Afanasyev, A. Fukuda, J. Fox, P. Catry, H. Higuchi, and J. P. Croxall. 2007. Foraging behaviour of four albatross species by night and day. Marine Ecology-Progress Series **340**:271-286.

Pinaud, D. and H. Weimerskirch. 2005. Scale-dependent habitat use in a long-ranging central place predator. Journal of Animal Ecology **74**:852-863.

Plank, M. J. and E. A. Codling. 2009. Sampling rate and misidentification of Levy and non-Levy movement paths. Ecology **90**:3546-3553.

Plank, M. J. and A. James. 2008. Optimal foraging: Levy pattern or process? Journal of the Royal Society Interface **5**:1077-1086.

Plotnick, R. E. 2012. Behavioral biology of trace fossils. Paleobiology **38**:459-473.

Pope, E. C., G. C. Hays, T. M. Thys, T. K. Doyle, D. W. Sims, N. Queiroz, V. J. Hobson, L. Kubicek, and J. D. R. Houghton. 2010. The biology and ecology of the ocean sunfish Mola mola: a review of current knowledge and future research perspectives. Reviews in Fish Biology and Fisheries **20**:471-487.

Powell, T. M., P. J. Richerson, T. M. Dillon, B. A. Agee, B. J. Dozier, D. A. Godden, and L. O. Myrup. 1975. Spatial scales of current speed and phytoplankton biomass fluctuations in Lake Tahoe. Science **189**:1088-1090.

Priede, I. G. 1984. A basking shark (*Cetorhinus maximus*) tracked by satellite together with simultaneous remote sensing. Fisheries Research **2**:201-216.

Priede, I. G., R. Froese, D. M. Bailey, O. A. Bergstad, M. A. Collins, J. E. Dyb, C. Henriques, E. G. Jones, and N. King. 2006. The absence of sharks from

abyssal regions of the world's oceans. Proceedings of the Royal Society B-Biological Sciences **273**:1435-1441.

Priede, I. G. and P. I. Miller. 2009. A basking shark (Cetorhinus maximus) tracked by satellite together with simultaneous remote sensing II: New analysis reveals orientation to a thermal front. Fisheries Research **95**:370-372.

Proekt, A., J. R. Banavar, A. Maritan, and D. W. Pfaff. 2012. Scale invariance in the dynamics of spontaneous behavior. Proceedings of the National Academy of Sciences of the United States of America **109**:10564-10569.

Pusineri, C., O. Chancollon, J. Ringelstein, and V. Ridoux. 2008. Feeding niche segregation among the Northeast Atlantic community of oceanic top predators. Marine Ecology-Progress Series **361**:21-34.

Queiroz, N., N. E. Humphries, L. R. Noble, A. M. Santos, and D. W. Sims. 2010. Short-term movements and diving behaviour of satellite-tracked blue sharks Prionace glauca in the northeastern Atlantic Ocean. Marine Ecology-Progress Series **406**:265-279.

Queiroz, N., N. E. Humphries, L. R. Noble, A. n. M. Santos, and D. W. Sims. 2012. Spatial Dynamics and Expanded Vertical Niche of Blue Sharks in Oceanographic Fronts Reveal Habitat Targets for Conservation. PLoS ONE **7**:e32374.

Queiroz, N., F. P. Lima, A. Maia, P. A. Ribeiro, J. P. Correia, and A. A. Santos. 2005. Movement of blue shark, *Prionace glauca*, in the north-east Atlantic based on mark - recapture data. Journal of the Marine Biological Association of the United Kingdom **85**:1107-1112.

R Development Core Team. 2009. R: A Language and Environment for Statistical Computing. R Foundation for Statistical Computing.

Ramos-Fernandez, G., J. L. Mateos, O. Miramontes, G. Cocho, H. Larralde, and B. Ayala-Orozco. 2004. Lévy walk patterns in the foraging movements of spider monkeys (*Ateles geoffroyi*). Behavioral Ecology and Sociobiology **55**:223-230.

Raposo, E. P., S. V. Buldyrev, M. G. E. da Luz, M. C. Santos, H. E. Stanley, and G. M. Viswanathan. 2003. Dynamical robustness of Lévy search strategies. Physical Review Letters **91**.

Raposo, E. P., S. V. Buldyrev, M. G. E. da Luz, G. M. Viswanathan, and H. E. Stanley. 2009. Lévy flights and random searches. Journal of Physics a-Mathematical and Theoretical **42**.

Rasband, W. S. 1997-2012. ImageJ. U. S. National Institutes of Health, Bethesda, Maryland, USA.

Reynolds, A. M. 2008. Deterministic walks with inverse-square power-law scaling are an emergent property of predators that use chemotaxis to locate randomly distributed prey. Phys Rev E Stat Nonlin Soft Matter Phys **78**:011906.

Reynolds, A. M. 2009. Adaptive Levy walks can outperform composite Brownian walks in non-destructive random searching scenarios. Physica a-Statistical Mechanics and Its Applications **388**:561-564.

Reynolds, A. M. and F. Bartumeus. 2009. Optimising the success of random destructive searches: Lévy walks can outperform ballistic motions. Journal of Theoretical Biology **260**:98-103.

Reynolds, A. M. and M. A. Frye. 2007. Free-Flight Odor Tracking in *Drosophila* Is Consistent with an Optimal Intermittent Scale-Free Search. PLoS ONE **2**:e354.

Reynolds, A. M. and C. J. Rhodes. 2009. The Levy flight paradigm: random search patterns and mechanisms. Ecology **90**:877-887.

Reynolds, A. M., A. D. Smith, R. Menzel, U. Greggers, D. R. Reynolds, and J. R. Riley. 2007. Displaced honey bees perform optimal scale-free search flights. Ecology **88**:1955-1961.

Reynolds, A. M., J. L. Swain, A. D. Smith, A. P. Martin, and J. L. Osborne. 2009. Honeybees use a Levy flight search strategy and odour-mediated

anemotaxis to relocate food sources. Behavioral Ecology and Sociobiology **64**:115-123.

Rhee, L., M. Shin, S. Hong, K. Lee, S. Chong, and Ieee. 2008. On the Levy-walk nature of human mobility. Pages 1597-1605 *in* 27th IEEE Conference on Computer Communications (INFOCOM 2008). Ieee, Phoenix, AZ.

Richardson, P. L. 2011. How do albatrosses fly around the world without flapping their wings? Progress in Oceanography **88**:46-58.

Righton, D., V. A. Quayle, S. Hetherington, and G. Burt. 2007. Movements and distribution of cod (Gadus morhua) in the southern North Sea and English Channel: results from conventional and electronic tagging experiments. Journal of the Marine Biological Association of the United Kingdom **87**:599-613.

Rijnsdorp, A. D., A. M. Buys, F. Storbeck, and E. G. Visser. 1998. Micro-scale distribution of beam trawl effort in the southern North Sea between 1993 and 1996 in relation to the trawling frequency of the sea bed and the impact on benthic organisms. Ices Journal of Marine Science **55**:403-419.

Ritchie, M. E. 1998. Scale-dependent foraging and patch choice in fractal environments. Evolutionary Ecology **12**:309-330.

Rodríguez-Cabello, C., F. Sánchez, A. Serrano, and I. Olaso. 2008. Effects of closed trawl fishery areas on some elasmobranch species in the Cantabrian Sea. Journal of Marine Systems **72**:418-428.

Rogan, E. and M. Mackey. 2007. Megafauna bycatch in drift nets for albacore tuna (*Thunnus alalunga*) in the NE Atlantic. Fisheries Research **86**:6-14.

Romey, W. L. 1996. Individual differences make a difference in the trajectories of simulated schools of fish. Ecological Modelling **92**:65-77.

Rountree, R. A., J. P. Groger, and D. Martins. 2008. Large vertical movements by a goosefish, Lophius americanus, suggests the potential of data storage tags for behavioral studies of benthic fishes. Marine and Freshwater Behaviour and Physiology **41**:73-78.

Royer, F., J. M. Fromentin, and P. Gaspar. 2005. A state-space model to derive bluefin tuna movement and habitat from archival tags. Oikos **109**:473-484.

Russell, R. W., G. L. Hunt, K. O. Coyle, and R. T. Cooney. 1992. Foraging in a fractal environment - spatial patterns in a marine predator-prey system. Landscape Ecology **7**:195-209.

Santos, M. C., E. P. Raposo, G. M. Viswanathan, and M. G. E. da Luz. 2004. Optimal random searches of revisitable targets: Crossover from superdiffusive to ballistic random walks. Europhysics Letters **67**:734-740.

Schaefer, K. M., D. W. Fuller, and B. A. Block. 2009. Vertical movements and habitat utilization of skipjack (*Katsuwonus pelamis*), yellowfin (*Thunnus albacares*), and bigeye (*Thunnus obesus*) tunas in the equatorial eastern Pacific Ocean, ascertained through archival tag data.*in* J. L. N. e. al, editor. Tagging and tracking of Marine Animals with electronic devices, Reviews: Methods and Technologies in Fish Biology and Fisheries.

Scharf, I., B. Kotler, and O. Ovadia. 2009. Consequences of food distribution for optimal searching behavior: an evolutionary model. Evolutionary Ecology **23**:245-259.

Scharf, I., E. Nulman, O. Ovadia, and A. Bouskila. 2006. Efficiency evaluation of two competing foraging modes under different conditions. American Naturalist **168**:350-357.

Scharf, I. and O. Ovadia. 2006. Factors influencing site abandonment and site selection in a sit-and-wait predator: A review of pit-building antlion larvae. Journal of Insect Behavior **19**:197-218.

Scharf, I., O. Ovadia, and A. Bouskila. 2008. Prey encounter rate by predators: Discussing the realism of grid-based models and how to model the predator's foraging mode: A reply to Avgar et al. American Naturalist **172**:596-598.

Schopka, S. A., J. Solmundsson, S. A. Ragnarsson, and V. Thorsteinsson. 2010. Using tagging experiments to evaluate the potential of closed areas in

protecting migratory Atlantic cod (Gadus morhua). Ices Journal of Marine Science **67**:1024-1035.

Scott, A. and P. Harrison. 2007. Broadcast spawning of two species of sea anemone, Entacmaea quadricolor and Heteractis crispa, that host anemonefish. Invertebrate Reproduction & Development **50**:163-171.

Seilacher, A., L. A. Buatois, and M. G. Mangano. 2005. Trace fossils in the Ediacaran-Cambrian transition: Behavioral diversification, ecological turnover and environmental shift. Palaeogeography Palaeoclimatology Palaeoecology **227**:323-356.

Seki, M. P., R. R. Bidigare, R. Lumpkin, J. J. Polovina, D. R. Kobayashi, P. Flament, D. G. Foley, M. T. S. M. T. Marine Technology Society, and Society. 2001. Mesoscale cyclonic eddies and pelagic fisheries in Hawaiian waters. Pages 1590-1594 *in* Annual Conference of the Marine-Technology-Society. Marine Technology Soc, Honolulu, Hi.

Seuront, L., A. C. Duponchel, and C. Chapperon. 2007. Heavy-tailed distributions in the intermittent motion behaviour of the intertidal gastropod Littorina littorea. Physica a-Statistical Mechanics and Its Applications **385**:573-582.

Shaffer, S. A. 2004. Annual energy budget and food requirements of breeding wandering albatrosses (Diomedea exulans). Polar Biology **27**:253-256.

Shamoun-Baranes, J., R. Bom, E. E. van Loon, B. J. Ens, K. Oosterbeek, and W. Bouten. 2012. From Sensor Data to Animal Behaviour: An Oystercatcher Example. PLoS ONE **7**:13.

Sheppard, C. R. C., M. Ateweberhan, B. W. Bowen, P. Carr, C. A. Chen, C. Clubbe, M. T. Craig, R. Ebinghaus, J. Eble, N. Fitzsimmons, M. R. Gaither, C. H. Gan, M. Gollock, N. Guzman, N. A. J. Graham, A. Harris, R. Jones, S. Keshavmurthy, H. Koldewey, C. G. Lundin, J. A. Mortimer, D. Obura, M. Pfeiffer, A. R. G. Price, S. Purkis, P. Raines, J. W. Readman, B. Riegl, A. Rogers, M. Schleyer, M. R. D. Seaward, A. L. S. Sheppard, J. Tamelander, J. R. Turner, S. Visram, C. Vogler, S. Vogt, H. Wolschke, J. M. C. Yang, S. Y.

Yang, and C. Yesson. 2012. Reefs and islands of the Chagos Archipelago, Indian Ocean: why it is the world's largest no-take marine protected area. Aquatic Conservation-Marine and Freshwater Ecosystems **22**:232-261.

Shlesinger, M. F. and J. Klafter. 1986. Lévy walks versus Lévy flights. In On Growth and Form. Pages 279-283 *in* H. Stanley and N. Ostrowsky, editors. On Growth and Form. Kluwer.

Shlesinger, M. F., G. M. Zaslavsky, and J. Klafter. 1993. Strange kinetics. Nature **363**:31-37.

Simpfendorfer, C. A., R. E. Hueter, U. Bergman, and S. M. H. Connett. 2002. Results of a fishery-independent survey for pelagic sharks in the western North Atlantic, 1977-1994. Fisheries Research **55**:175-192.

Sims, D. W. 1999. Threshold foraging behaviour of basking sharks on zooplankton: life on an energetic knife-edge? Proceedings of the Royal Society of London Series B-Biological Sciences **266**:1437-1443.

Sims, D. W. 2010. Sharks and Their Relatives II: Biodiversity, Adaptive Physiology, and Conservation. Pages 1-655 *in* J. C. Carrier, J. A. Musick, and M. R. Heithaus, editors. Sharks and Their Relatives Ii: Biodiversity, Adaptive Physiology, and Conservation.

Sims, D. W., N. E. Humphries, R. W. Bradford, and B. D. Bruce. 2012. Levy flight and Brownian search patterns of a free-ranging predator reflect different prey field characteristics. Journal of Animal Ecology **81**:432-442.

Sims, D. W., N. E. Humphries, W. B. Russell, and B. D. Bruce. 2011. Levy flight and Brownian search patterns of a free-ranging predator reflect different prey field characteristics. Journal of Animal Ecology.

Sims, D. W. and D. A. Merrett. 1997. Determination of zooplankton characteristics in the presence of surface feeding basking sharks Cetorhinus maximus. Marine Ecology-Progress Series **158**:297-302.

Sims, D. W., J. P. Nash, and D. Morritt. 2001. Movements and activity of male and female dogfish in a tidal sea lough: alternative behavioural strategies and apparent sexual segregation. Marine Biology **139**:1165-1175.

Sims, D. W. and V. A. Quayle. 1998. Selective foraging behaviour of basking sharks on zooplankton in a small-scale front. Nature **393**:460-464.

Sims, D. W., N. Queiroz, J. I. Doyle, J. D. R. Houghton, and G. C. Hays. 2009a. Satellite tracking the world's largest bony fish, the ocean sunfish *Mola mola* in the North-East Atlantic Ocean. Journal of Experimental Marine Biology and Ecology **370**:127-133.

Sims, D. W., N. Queiroz, N. E. Humphries, F. P. Lima, and G. C. Hays. 2009b. Long-Term GPS Tracking of Ocean Sunfish *Mola mola* Offers a New Direction in Fish Monitoring. PLoS ONE **4**:6.

Sims, D. W., D. Righton, and J. W. Pitchford. 2007. Minimising errors in identifying Lévy flight behaviour of organisms. Journal of Animal Ecology **76**:222-229.

Sims, D. W., E. J. Southall, N. E. Humphries, G. C. Hays, C. J. A. Bradshaw, J. W. Pitchford, A. James, M. Z. Ahmed, A. S. Brierley, M. A. Hindell, D. Morritt, M. K. Musyl, D. Righton, E. L. C. Shepard, V. J. Wearmouth, R. P. Wilson, M. J. Witt, and J. D. Metcalfe. 2008a. Scaling laws of marine predator search behaviour. Nature **451**:1098-1102.

Sims, D. W., E. J. Southall, A. J. Richardson, P. C. Reid, and J. D. Metcalfe. 2003. Seasonal movements and behaviour of basking sharks from archival tagging: no evidence of winter hibernation. Marine Ecology-Progress Series **248**:187-196.

Sims, D. W., V. J. Wearmouth, E. J. Southall, J. M. Hill, P. Moore, K. Rawlinson, N. Hutchinson, G. C. Budd, D. Righton, J. Metcalfe, J. P. Nash, and D. Morritt. 2006a. Hunt warm, rest cool: bioenergetic strategy underlying diel vertical migration of a benthic shark. Journal of Animal Ecology **75**:176-190.

Sims, D. W., M. J. Witt, A. J. Richardson, E. J. Southall, and J. D. Metcalfe. 2006b. Encounter success of free-ranging marine predator movements across a dynamic prey landscape. Proceedings of the Royal Society B-Biological Sciences **273**:1195-1201.

Sims, M., T. Cox, and R. Lewison. 2008b. Modeling spatial patterns in fisheries bycatch: Improving bycatch maps to aid fisheries management. Ecological Applications **18**:649-661.

Smith, T. S. and S. T. Partridge. 2004. Dynamics of intertidal foraging by coastal brown bears in southwestern Alaska. Journal of Wildlife Management **68**:233-240.

Sole, R. V., S. C. Manrubia, M. J. Benton, S. Kauffman, and P. Bak. 1999. Criticality and scaling in evolutionary ecology. Trends in Ecology & Evolution **14**:156-160.

Sorribes, A., B. G. Armendariz, D. Lopez-Pigozzi, C. Murga, and G. G. de Polavieja. 2011. The Origin of Behavioral Bursts in Decision-Making Circuitry. Plos Computational Biology **7**:9.

Spencer, M., S. N. R. Birchenough, N. Mieszkowska, L. A. Robinson, S. D. Simpson, M. T. Burrows, E. Capasso, P. Cleall-Harding, J. Crummy, C. Duck, D. Eloire, M. Frost, A. J. Hall, S. J. Hawkins, D. G. Johns, D. W. Sims, T. J. Smyth, and C. L. J. Frid. 2010. Temporal change in UK marine communities: trends or regime shifts? Marine Ecology:no-no.

Stanley, H. E. 1992. Fractal landscapes in physics and biology. Physica A **186**:1-32.

Stelzenmüller, V., S. I. Rogers, and C. M. Mills. 2008. Spatio-temporal patterns of fishing pressure on UK marine landscapes, and their implications for spatial planning and management. ICES J. Mar. Sci. **65**:1081-1091.

Stephens, D. W. and J. R. Krebs. 1987. Foraging Theory (Monographs in Behavior and Ecology) Princeton University Press.

Stevens, J. D. 1976. 1st results of shark tagging in northeast Atlantic, 1972-1975. Journal of the Marine Biological Association of the United Kingdom **56**:929-937.

Stevens, J. D. 1990. Further results from a tagging study of pelagic sharks in the north-east Atlantic. Journal of the Marine Biological Association of the United Kingdom **70**:707-720.

Stevens, J. D., R. Bonfil, N. K. Dulvy, and P. A. Walker. 2000. The effects of fishing on sharks, rays, and chimaeras (chondrichthyans), and the implications for marine ecosystems. Ices Journal of Marine Science **57**:476-494.

Strand, E., G. Huse, and J. Giske. 2002. Artificial evolution of life history and Behavior. American Naturalist **159**:624-644.

Sumaila, U. R. and L. Huang. 2012. Managing Bluefin Tuna in the Mediterranean Sea. Marine Policy **36**:502-511.

Thurstan, R. H., S. Brockington, and C. M. Roberts. 2010. The effects of 118 years of industrial fishing on UK bottom trawl fisheries. Nature Communications.

Travis, J. 2007. Ecology - Do wandering albatrosses care about math? Science **318**:742-743.

Tremblay, Y., P. W. Robinson, and D. P. Costa. 2009. A Parsimonious Approach to Modeling Animal Movement Data. PLoS ONE **4**:e4711.

Tremblay, Y., S. A. Shaffer, S. L. Fowler, C. E. Kuhn, B. I. McDonald, M. J. Weise, C. A. Bost, H. Weimerskirch, D. E. Crocker, M. E. Goebel, and D. R. Costa. 2006. Interpolation of animal tracking data in a fluid environment. Journal of Experimental Biology **209**:128-140.

Tuck, G. N., R. A. Phillips, C. Small, R. B. Thomson, N. L. Klaer, F. Taylor, R. M. Wanless, and H. Arrizabalaga. 2011. An assessment of seabird-fishery interactions in the Atlantic Ocean. Ices Journal of Marine Science **68**:1628-1637.

Turchin, P. 1998. Quantitative Analysis of Movement: measuring and modeling population redistribution in plants and animals. Sinauer Associates, Sunderland, MA.

Vandykhuizen, G. and H. F. Mollet. 1992. Growth, age estimation and feeding of captive sevengill sharks, Notorynchus cepedianus, at the Monterey Bay aquarium. Australian Journal of Marine and Freshwater Research **43**:297-318.

Vega, R. and R. Licandeo. 2009. The effect of American and Spanish longline systems on target and non-target species in the eastern South Pacific swordfish fishery. Fisheries Research **98**:22-32.

Veit, R. R., J. A. McGowan, D. G. Ainley, T. R. Wahls, and P. Pyle. 1997. Apex marine predator declines ninety percent in association with changing oceanic climate. Global Change Biology **3**:23-28.

Visser, A. W. 2007. Motility of zooplankton: fitness, foraging and predation. Journal of Plankton Research **29**:447-461.

Viswanathan, G. M., V. Afanasyev, S. V. Buldyrev, S. Havlin, M. G. E. da Luz, E. P. Raposo, and H. E. Stanley. 2000. Lévy flights in random searches. Physica A **282**:1-12.

Viswanathan, G. M., V. Afanasyev, S. V. Buldyrev, S. Havlin, M. G. E. da Luz, E. P. Raposo, and H. E. Stanley. 2001. Lévy flights search patterns of biological organisms. Physica A: Statistical Mechanics and its Applications **295**:85-88.

Viswanathan, G. M., V. Afanasyev, S. V. Buldyrev, E. J. Murphy, P. A. Prince, and H. E. Stanley. 1996. Lévy flight search patterns of wandering albatrosses. Nature **381**:413-415.

Viswanathan, G. M., F. Bartumeus, S. V. Buldyrev, J. Catalan, U. L. Fulco, S. Havlin, M. G. E. da Luz, M. L. Lyra, E. P. Raposo, and H. E. Stanley. 2002. Lévy flight random searches in biological phenomena. Physica a-Statistical Mechanics and Its Applications **314**:208-213.

Viswanathan, G. M., S. V. Buldyrev, S. Havlin, M. G. E. da Luz, E. P. Raposo, and H. E. Stanley. 1999. Optimizing the success of random searches. Nature **401**:911-914.

Viswanathan, G. M., M. G. E. da Luz, E. P. Raposo, and H. Stanley. 2011. The Physics of Foraging. Cambridge University Press, New York.

Viswanathan, G. M., E. P. Raposo, and M. G. E. da Luz. 2008. Lévy flights and superdiffusion in the context of biological encounters and random searches. Physics of Life Reviews **5**:133-150.

Vogler, R., E. Beier, S. Ortega-García, H. Santana-Hernáіндеz, and J. J. Valdez-Flores. 2011. Ecological patterns, distribution and population structure of Prionace glauca (Chondrichthyes: Carcharhinidae) in the tropical-subtropical transition zone of the north-eastern Pacific. Marine Environmental Research.

Wakefield, E. D., R. A. Phillips, J. Matthiopoulos, A. Fukuda, H. Higuchi, G. J. Marshall, and P. N. Trathan. 2009. Wind field and sex constrain the flight speeds of central-place foraging albatrosses. Ecological Monographs **79**:663-679.

Walsh, W. A., K. A. Bigelow, and K. L. Sender. 2009. Decreases in Shark Catches and Mortality in the Hawaii-Based Longline Fishery as Documented by Fishery Observers. Marine and Coastal Fisheries **1**:270-282.

Ward, P. and R. A. Myers. 2005. Shifts in open-ocean fish communities coinciding with the commencement of commercial fishing. Ecology **86**:835-847.

Waugh, S. M. and H. Weimerskirch. 2003. Environmental heterogeneity and the evolution of foraging behaviour in long ranging greater albatrosses. Oikos **103**:374-384.

Wearmouth, V. J. and D. W. Sims. 2009. Movement and behaviour patterns of the critically endangered common skate Dipturus batis revealed by electronic tagging. Journal of Experimental Marine Biology and Ecology **380**:77-87.

Weimerskirch, H. 2007. Are seabirds foraging for unpredictable resources? Deep-Sea Research Part Ii-Topical Studies in Oceanography **54**:211-223.

Weimerskirch, H., F. Bonadonna, F. Bailleul, G. Mabille, G. Dell'Omo, and H. P. Lipp. 2002a. GPS tracking of foraging albatrosses. Science **295**:1259-1259.

Weimerskirch, H., C. P. Doncaster, and F. Cuenot-Chaillet. 1994. Pelagic seabirds and the marine-environment - foraging patterns of wandering albatrosses in relation to prey availability and distribution. Proceedings of the Royal Society of London Series B-Biological Sciences **255**:91-97.

Weimerskirch, H., A. Gault, and Y. Cherel. 2005. Prey distribution and patchiness: Factors in foraging success and efficiency of wandering albatrosses. Ecology **86**:2611-2622.

Weimerskirch, H. and T. Guionnet. 2002. Comparative activity pattern during foraging of four albatross species. Ibis **144**:40-50.

Weimerskirch, H. and P. Lys. 2000. Seasonal changes in the provisioning behaviour and mass of male and female wandering albatrosses in relation to the growth of their chick. Polar Biology **23**:733-744.

Weimerskirch, H., D. Pinaud, F. Pawlowski, and C. A. Bost. 2007. Does prey capture induce area-restricted search? A fine-scale study using GPS in a marine predator, the wandering albatross. American Naturalist **170**:734-743.

Weimerskirch, H., S. A. Shaffer, G. Mabille, J. Martin, O. Boutard, and J. L. Rouanet. 2002b. Heart rate and energy expenditure of incubating wandering albatrosses: basal levels, natural variation, and the effects of human disturbance. Journal of Experimental Biology **205**:475-483.

West, C. D., C. Dytham, D. Righton, and J. W. Pitchford. 2009. Preventing overexploitation of migratory fish stocks: the efficacy of marine protected areas in a stochastic environment. Ices Journal of Marine Science **66**:1919-1930.

White, E. P., B. J. Enquist, and J. L. Green. 2008. On estimating the exponent of power-law frequency distributions. Ecology **89**:905-912.

White, J. A. and D. A. Andow. 2007. Foraging for intermittently refuged prey: theory and field observations of a parasitoid. Journal of Animal Ecology **76**:1244-1254.

Witze, A. 2010. Sharks use math to hunt. Science News **178**.

Worm, B., H. K. Lotze, and R. A. Myers. 2003. Predator diversity hotspots in the blue ocean. Proceedings of the National Academy of Sciences of the United States of America **100**:9884-9888.

Yemane, D., Y. J. Shin, and J. G. Field. 2009. Exploring the effect of Marine Protected Areas on the dynamics of fish communities in the southern Benguela: an individual-based modelling approach. Ices Journal of Marine Science **66**:378-387.

Yokota, K., M. Kiyota, and H. Minami. 2006. Shark catch in a pelagic longline fishery: Comparison of circle and tuna hooks. Fisheries Research **81**:337-341.

Zainuddin, M., H. Kiyofuji, K. Saitoh, and S. I. Saitoh. 2006. Using multi-sensor satellite remote sensing and catch data to detect ocean hot spots for albacore (Thunnus alalunga) in the northwestern North Pacific. Deep-Sea Research Part Ii-Topical Studies in Oceanography **53**:419-431.

Zar, J. H. 1999. Biostatistical Analysis 4th edition. Fourth edition. Prentice Hall.

Zeeberg, J., A. Corten, and E. De Graaf. 2006. Bycatch and release of pelagic megafauna in industrial trawler fisheries off Northwest Africa. Fisheries Research **78**:186-195.

Zimmerman, R. A. and D. C. Biggs. 1999. Patterns of distribution of sound-scattering zooplankton in warm- and cold-core eddies in the Gulf of Mexico, from a narrowband acoustic Doppler current profiler survey. Journal of Geophysical Research-Oceans **104**:5251-5262.

Environmental context explains Lévy and Brownian movement patterns of marine predators

Nicolas E. Humphries[1,2], Nuno Queiroz[1,3,4], Jennifer R. M. Dyer[1], Nicolas G. Pade[1,4], Michael K. Musyl[5], Kurt M. Schaefer[6], Daniel W. Fuller[6], Juerg M. Brunnschweiler[7], Thomas K. Doyle[8], Jonathan D. R. Houghton[9], Graeme C. Hays[10], Catherine S. Jones[4], Leslie R. Noble[4], Victoria J. Wearmouth[1], Emily J. Southall[1] & David W. Sims[1,2]

An optimal search theory, the so-called Lévy-flight foraging hypothesis[1], predicts that predators should adopt search strategies known as Lévy flights where prey is sparse and distributed unpredictably, but that Brownian movement is sufficiently efficient for locating abundant prey[2–4]. Empirical studies have generated controversy because the accuracy of statistical methods that have been used to identify Lévy behaviour has recently been questioned[5,6]. Consequently, whether foragers exhibit Lévy flights in the wild remains unclear. Crucially, moreover, it has not been tested whether observed movement patterns across natural landscapes having different expected resource distributions conform to the theory's central predictions. Here we use maximum-likelihood methods to test for Lévy patterns in relation to environmental gradients in the largest animal movement data set assembled for this purpose. Strong support was found for Lévy search patterns across 14 species of open-ocean predatory fish (sharks, tuna, billfish and ocean sunfish), with some individuals switching between Lévy and Brownian movement as they traversed different habitat types. We tested the spatial occurrence of these two principal patterns and found Lévy behaviour to be associated with less productive waters (sparser prey) and Brownian movements to be associated with productive shelf or convergence-front habitats (abundant prey). These results are consistent with the Lévy-flight foraging hypothesis[1,7], supporting the contention[8,9] that organism search strategies naturally evolved in such a way that they exploit optimal Lévy patterns.

Lévy flights are a special class of random walk with movement displacements (steps) drawn from a probability distribution with a power-law tail (the so-called Pareto–Lévy distribution)[1,10], and give rise to stochastic processes closely linked to fractal geometry and anomalous diffusion phenomena[7,11]. Lévy flights describe a movement pattern characterized by many small steps connected by longer relocations, with this pattern having scale invariance under projection, such that the probability density function, $P(l_j)$, has a power-law tail in the long-distance regime: $P(l_j) \approx l_j^{-\mu}$, where l_j is the flight length (step length of move j), and μ, $1 < \mu \leq 3$, is the power-law exponent. Lévy flights comprise instantaneous steps and hence involve infinite velocities, whereas a Lévy walk[10] refers to a finite-velocity walk such that displacement is determined after a time t, reflecting a dynamical process such as movement[1,10,11]. Lévy flights and walks are theorized to be the most efficient movement pattern

for locating patchy prey in low concentrations on spatial scales beyond a searcher's sensory range, with an optimal search having a power-law exponent of $\mu \approx 2$ (refs 4, 13). It is proposed that organisms have therefore naturally evolved search patterns that can be modelled as optimal Lévy flights[1,7,13].

However, burgeoning empirical support for this hypothesis recently foundered following studies suggesting methodological shortcomings in the estimation of power-law exponents and in determining the goodness of fit to the data[5,6,14–16], thus casting doubt on some, if not all, of the empirical studies that used such methods[8,9]. Hence, controversy remains over whether Lévy behaviour occurs in nature[6,9,17], despite many empirical studies[1,18]. Furthermore, long time series of movements (over weeks to months) derived from animal-attached electronic tags will very probably capture complex movement data resulting from different types of behaviour (for example searching, travelling and resting) as animals respond to various biotic and abiotic factors over time. Previous studies analysing movement data[6,12,13] on free-ranging animals for Lévy motion used data collected over long time periods and different habitat types, without giving sufficient consideration to the issue of there being different types of behaviour interspersed within the time series. The lack of analysis of separate behaviour-pattern types may be at least one reason why evidence for Lévy flights in animal behaviour has proved challenging to detect unequivocally[9,17].

Here we present an analysis of the largest data set of recorded movements ($n = 12,294,347$ steps) assembled to test the Lévy-flight foraging (LFF) hypothesis[1] using statistical methods (maximum-likelihood estimation (MLE) and Akaike information criteria (AIC) weights for model comparisons) that are considered robust and accurate[6,14–16]. To test the predictions of the LFF hypothesis, we focused our analysis on vertical movement data recorded over 5,700 days using electronic tags attached to open-ocean predators (sharks, tunas, billfish and ocean sunfish; Methods and Supplementary Table 1). These species may be among those most likely to exhibit Lévy behaviour because they occupy unpredictable and depauperate environments with highly patchy prey distributions[13], where Lévy motion is proposed to increase new-patch encounter probability[19].

To allow for a more robust test of the LFF hypothesis, long and complex time series of vertical diving movements (hereafter tracks, or sections) undertaken as fish moved horizontally across their

[1]Marine Biological Association of the United Kingdom, The Laboratory, Citadel Hill, Plymouth PL1 2PB, UK. [2]Marine Biology and Ecology Research Centre, Marine Institute, School of Marine Sciences and Engineering, University of Plymouth, Drake Circus, Plymouth PL4 8AA, UK. [3]CIBIO – Universidade do Porto, Campus Agrário de Vairão, Rua Padre Armando Quintas, 4485-668 Vairão, Portugal. [4]Institute of Biological and Environmental Sciences, School of Biological Sciences, University of Aberdeen, Tillydrone Avenue, Aberdeen AB24 2TZ, UK. [5]Joint Institute for Marine and Atmospheric Research, University of Hawaii at Manoa, Kewalo Research Facility/NOAA Fisheries, 1125-B Ala Mona Boulevard, Honolulu, Hawaii 96814, USA. [6]Inter-American Tropical Tuna Commission, 8604 La Jolla Shores Drive, La Jolla, California 92037-1508, USA. [7]ETH Zurich, Raemistrasse 101, CH-8092 Zurich, Switzerland. [8]Coastal and Marine Resources Centre, ERI, University College Cork, Glucksman Marine Facility, Naval Base, Haulbowline, Cobh, Cork, Ireland. [9]School of Biological Sciences, Queen's University Belfast, Medical Biology Centre, 97 Lisburn Road, Belfast BT9 7BL, UK. [10]Department of Pure and Applied Ecology, Institute of Environmental Sustainability, Swansea University, Singleton Park, Swansea SA2 8PP, UK.

ranges were divided into shorter sections using a split moving-window analysis[20] (Supplementary Information, sections 1.2 and 1.3) to identify discontinuities in the pattern of vertical space use that represent transitions from one pattern of space use to another. In total, tracks from 55 individuals across 14 species (shark, eight species; tuna, two; billfish, three; ocean sunfish, one) were divided into 129 sections. MLE methods[16] were used to fit three models (power law, truncated power law (truncated Pareto) or exponential) to the observed move step-length frequency distributions (Supplementary Information, section 1.4). Sections that from visual inspection proved to be poor fits to all candidate distributions were excluded from further analysis ($n = 35$), because our objective was to test the spatial occurrence of good fits to step-length distributions. MLE methods with AIC weights[6,15] were then used to determine model best fits for the remaining 94 sections. Because movements can only take place in finite space (moves are limited by, for example, the sea surface, the sea bed or the range edge), which leads to upper cut-offs in the move step-length frequency distribution, only truncated Lévy walks are biologically plausible[1]. Therefore, our principal intention was not to find which kinds of all possible probability distributions best fit the data; rather, it was to test between truncated Lévy (truncated power-law model) and Brownian-type (exponential model) movement patterns.

We found clear and persistent signals of Lévy and Brownian motion; of the 94 sections analysed statistically (MLE with AIC weights), one section was best fitted by a pure power law (Fig. 1a–c) and 60 sections were best fitted by a truncated Pareto–Lévy distribution (see, for example, Fig. 1d–f and Supplementary Table 3) with exponents in the Lévy range, $1 < \mu \leq 3$, and so were consistent with Lévy behaviour. The mean μ value for the Lévy sections was 1.94 (s.d., 0.43; $n = 61$), which is close to the proposed optimum, $\mu_{opt} \approx 2$ (refs 1, 2, 4). Six sections best fitted by a truncated power law yielded exponents outside the Lévy range.

Lévy searching in open-ocean predators therefore seems to be not only present but prevalent; however, it does not seem to be a universal pattern, explaining all movements, nor does it occur in all individuals at all times (it occurs in only 47% of sections). A logical extension of the hypothesis is that other movement behaviour types intersperse Lévy patterns. In support of this, we found that 27 sections (21%) were best fitted by an exponential model describing normal random processes (Brownian motion; Supplementary Table 3) that under the LFF hypothesis are consistent with optimal searches where prey is abundant[1]. We also found that 35 sections (27%) were poorly fitted by all of the distributions; this was perhaps because the sections comprised many different movement patterns, making them too complex for the statistical methods used here (Supplementary Information, section 1.5).

To investigate the environmental context of different behaviour patterns, we mapped the horizontal tracks of individual predators in the Atlantic or the Pacific ocean to determine in which types of habitat the sections showing Lévy and Brownian vertical movement patterns

occurred. For example, in productive waters of the equatorial convergence front of the central North Pacific, the entire track of a silky shark (*Carcharhinus falciformis*) was best fitted by an exponential model, whereas for another silky shark tracked farther north in oligotrophic waters, the best fit was a truncated power law with an exponent of 2.02, close to the theoretical optimum for Lévy movement, $\mu_{opt} \approx 2$ (Supplementary Information, section 2.1, and Supplementary Table 4).

We found that different model fits occurred between different habitat types of the same individual for eight other individuals of five species of predator (bigeye (*Thunnus obesus*) and yellowfin (*Thunnus albacares*) tuna, and blue, basking (*Cetorhinus maximus*) and whale (*Rhincodon typus*) sharks; see Supplementary Table 4 for model comparisons). For example, a blue shark tracked moving south in the northeast Atlantic, from the highly productive shelf habitat of the western English Channel to the less productive, deep water of the Bay of Biscay, showed switches in the pattern of its vertical movement (Fig. 2a–e). The shark showed diving behaviour in tidal front waters on the shelf (0–200-m depth) that was well fitted to the distribution's tail by an exponential model (Fig. 2a, f, k and Supplementary Table 4). Moving off-shelf into less productive waters (with well-developed thermal stratification) (Fig. 2m, p, q), the shark's vertical movements down to 700 m conformed well to a truncated power law with an exponent of $\mu = 2.19$ (Fig. 2b, g, l), before its diving movements shifted to a pattern better approximated by an exponential fit when in colder, shelf-edge habitat in the southern Bay of Biscay (Fig. 2c, h, m). Returning to warmer, well-stratified but less productive open-ocean habitat (Fig. 2d, e, n, o, q), this shark once again exhibited vertical movements best fitted by truncated power laws with $\mu = 1.97$ and 1.99 (Fig. 2i, j).

A bigeye tuna in the central eastern Pacific near the Galapagos Islands switched several times from diving movements best fitted by a truncated power law when in warmer, stratified waters to movements approximated by an exponential model in colder waters of the equatorial convergence front (Supplementary Information, section 2.2).

These results agree with the prediction of the LFF hypothesis that Lévy behaviour should occur in environments where prey is sparsely distributed but that Brownian motion is theoretically optimal where prey is abundant[3]. To test the significance of this with our habitat-mapped data, we compared the frequency of sections that conformed to this broad prediction. We assumed that prey in open-ocean habitats with lower primary[21] and secondary production[22] was likely to be more sparsely distributed than that in more productive shelf, frontal and convergence-zone habitats, where prey of the predators we tracked is known to be more abundant[22–25]. We used only geo-referenced sections yielding best fits where the step-length data spanned at least 1.5 orders of magnitude (range, 1.53–2.27).

For four species of predator (three sharks and ocean sunfish) in the northeast Atlantic that moved between continental-shelf areas with
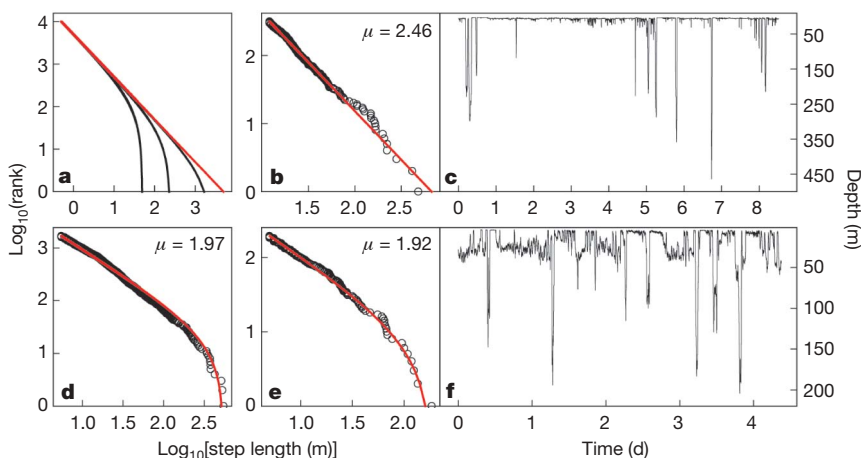
Figure 1 | Examples of good fits to power-law and truncated power-law distributions.
a, Synthetic power-law and truncated power-law (Pareto) distributions with upper truncations set to 50, 250, 5,000. **b–f**, Empirical power-law and truncated power-law fits to dive data from individual blue sharks (*Prionace glauca*; **b**, **d**) and an ocean sunfish (*Mola mola*, **e**), together with the diving time series for the individual in **b** (over ~8 d; **c**) and the individual in **e** (over ~4 d; **f**). The red line indicates a synthetic power law in **a**, a power law in **b** and truncated power-law MLE model fits to empirical data in **d** and **e**.
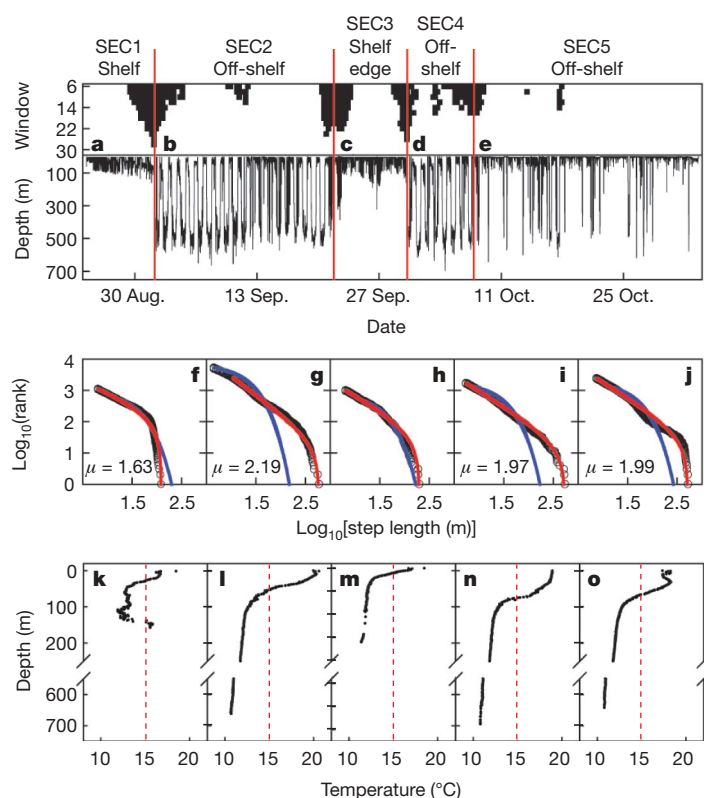
Figure 2 | Behavioural switching between Lévy and Brownian motion in relation to habitat type. a–e, Split moving-window analysis showing significant discontinuities in the dive time series of blue shark 10. Red lines indicate points where the time series was divided into sections (SEC1–SEC5). **f–j,** MLE analysis with μ values for sections best fitting a truncated power-law distribution: black circles, observed step lengths; red lines, best-fit truncated power law; blue lines, best-fit exponential distribution. **k–o,** Depth profiles of sea temperature recorded using electronic tags. **p, q,** Geo-referenced track sections of blue shark 10 overlaid on chlorophyll *a* concentrations (**p**) and bathymetry (**q**). Section numbers correspond to those in **a–e** and different data-point colours correspond to different sections: SEC1, black (higher latitude); SEC2, white (higher latitude); SEC3, grey; SEC4, black (lower latitude); SEC5, white (lower latitude).

high surface zooplankton abundance and open-ocean areas with lower abundance[22], which provide proxies for prey-abundant and prey-sparse environments, respectively, 14 mapped sections were available. Movement patterns in 12 sections performed as proposed (sparse prey, Lévy behaviour; abundant prey, Brownian motion) (chi-squared test with Yates's correction for continuity: $\chi^2 = 5.78$, $\chi^2_{0.05,2} = 3.84$, $P < 0.025$; Fig. 3a). This indicates that the frequency of observed movement patterns approximated by a Lévy distribution in less productive areas and by an exponential (Brownian) distribution in more productive waters did not deviate significantly from
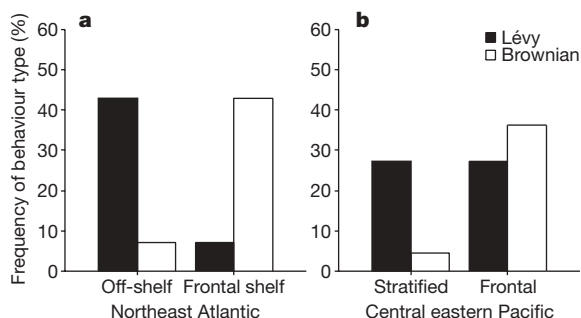
Figure 3 | Spatial occurrence of Lévy and Brownian behaviour types. Frequencies of behaviour types in productive (frontal/shelf) and less productive (off-shelf) habitats in the northeast Atlantic (**a**), and in productive (frontal) and less productive (stratified) habitats in the central eastern Pacific (**b**). Tests of two predictions of the LFF hypothesis (Lévy behaviour where prey is sparse; Brownian movement where prey is abundant and not sparsely distributed) were performed on frequency data (not per cent frequency data). See main text for details of the statistical tests.

theoretical predictions of the LFF hypothesis[1,4]. For bigeye and yellowfin tuna in the central eastern Pacific moving between warm stratified waters and cooler, more productive convergence-front waters (Supplementary Information, sections 2.2 and 2.3) there were 21 sections for analysis. A higher number of sections best fitted by an exponential distribution occurred in convergence-front waters than in stratified waters ($\chi^2 = 4.00$, $\chi^2_{0.05,2} = 3.84$, $P < 0.05$; Fig. 3b). Therefore, the occurrence of Brownian-type behaviour in tuna in the Pacific agrees with predictions of the LFF hypothesis. The number of sections where movements conformed to a truncated power law was the same in convergence-front waters as in stratified waters. We speculate that one reason tuna in the productive convergence zone exhibit Lévy movements characterized by longer vertical steps is that fish prey may become spatially constrained within mesoscale eddy features[25] that are common in the region and have diameters of between about 50 and 200 km. Thus, even in this productive environment, tuna movement may be optimized by longer vertical reorientations (searching) between eddies because prey hot spots may be patchily distributed across a wide range of scales linked to turbulent eddy formation, size and persistence[26] (Supplementary Information, sections 2.2 and 2.3).

Our analysis provides the strongest evidence yet for Lévy behaviour in diverse animals ranging across natural landscapes. Furthermore, the movement patterns of some individuals approximated theoretically optimal Lévy searches. It was also evident, however, that Lévy behaviour is not a universal pattern; rather, some individuals use other patterns approximated by normal random processes, sometimes interspersed with Lévy movements. We found that mapping the locations of where Lévy and Brownian movements occurred allowed a preliminary field test of the LFF hypothesis, confirming theoretical predictions.

Therefore, not only do our results lend strong support to the contention that Lévy flights occur in free-ranging animals, but our observations of pattern switching between Lévy and Brownian-type motion suggest that searching animals adaptively adjust their optimal patterns of movement to different environmental resource distributions. We recognize, however, that our analysis could not detect how the movement patterns arose, that is, whether the patterns identified were an adaptive behaviour or whether observed patterns were an emergent property of the spatial distributions of prey[13,17,27]. Controlled experiments[28], rather than natural experiments as here, will be needed to progress from asking whether Lévy flights (walks) occur in animals[8,9] to exploring why they occur and whether animals evolved such that they exploit Lévy flights as an optimal search strategy for life in complex, highly changeable landscapes. Simulations of biological evolution indicate that varying environments posing complex goals can speed up natural selection[29], which also raises the question of when, if animals have evolved Lévy flight behaviour, did such a strategy first appear among organisms.

METHODS SUMMARY

Study animals. Animal-attached electronic tags provided time-stamped depth records (tracks) for 55 individuals from 14 species: bigeye thresher shark (*Alopias superciliosus*), blue shark, shortfin mako shark (*Isurus oxyrinchus*), porbeagle shark (*Lamna nasus*), silky shark, oceanic whitetip shark (*Carcharhinus longimanus*), basking shark, whale shark, bigeye tuna, yellowfin tuna, black marlin (*Makaira indica*), blue marlin (*Makaira nigricans*), swordfish (*Xiphias gladius*) and ocean sunfish.

Track analysis. We used a split moving-window analysis to identify statistically significant discontinuities in depth use and divided tracks into sections that were considered more behaviourally consistent than the whole. Each of the 129 resulting sections was then corrected for sampling artefacts and converted from depths to a series of vertical displacements (move step lengths).

MLE analysis and model selection. For each track section, parameters for power-law, exponential and truncated Pareto distributions were calculated using MLE[16]. We used plots of ranked move step length, combining empirical and best-fit plots, to reject sections that were a poor fit to all distributions. Log-likelihoods and AIC weights were calculated for the remaining sections and were used to determine which distribution (model) best fitted the data.

1. Viswanathan, G. M., Raposo, E. P. & da Luz, M. G. E. Lévy flights and superdiffusion in the context of biological encounters and random searches. *Phys. Life Rev.* **5**, 133–150 (2008).
2. Viswanathan, G. M. *et al.* Optimizing the success of random searches. *Nature* **401**, 911–914 (1999).
3. Bartumeus, F. *et al.* Optimizing the encounter rate in biological interactions: Lévy versus Brownian strategies. *Phys. Rev. Lett.* **88**, 097901 (2002).
4. Bartumeus, F., Da Luz, M. G. E., Viswanathan, G. M. & Catalan, J. Animal search strategies: a quantitative random-walk analysis. *Ecology* **86**, 3078–3087 (2005).
5. Sims, D. W., Righton, D. & Pitchford, J. W. Minimising errors in identifying Lévy flight behaviour of organisms. *J. Anim. Ecol.* **76**, 222–229 (2007).
6. Edwards, A. M. *et al.* Revisiting Lévy flight search patterns of wandering albatrosses, bumblebees and deer. *Nature* **449**, 1044–1048 (2007).
7. Bartumeus, F. Lévy processes in animal movement: an evolutionary hypothesis. *Fractals* **15**, 151–162 (2007).
8. Travis, J. Ecology: do wandering albatrosses care about math? *Science* **318**, 742–743 (2007).
9. Buchanan, M. Ecological modelling: the mathematical mirror to animal nature. *Nature* **453**, 714–716 (2008).
10. Shlesinger, M. F. & Klafter, J. in *On Growth and Form* (eds Stanley, H. & Ostrowsky, N.) 279–283 (Kluwer, 1986).
11. Shlesinger, M. F., Zaslavsky, G. M. & Klafter, J. Strange kinetics. *Nature* **363**, 31–37 (1993).
12. Viswanathan, G. M. *et al.* Lévy flight search patterns of wandering albatrosses. *Nature* **381**, 413–415 (1996).
13. Sims, D. W. *et al.* Scaling laws of marine predator search behaviour. *Nature* **451**, 1098–1102 (2008).
14. White, E. P., Enquist, B. J. & Green, J. L. On estimating the exponent of power-law frequency distributions. *Ecology* **89**, 905–912 (2008).
15. Edwards, A. M. Using likelihood to test for Lévy flight search patterns and for general power-law distributions in nature. *J. Anim. Ecol.* **77**, 1212–1222 (2008).
16. Clauset, A., Shalizi, C. R. & Newman, M. E. J. Power-law distributions in empirical data. *SIAM Rev.* **51**, 661–703 (2009).
17. Benhamou, S. How many animals really do the Lévy walk? *Ecology* **88**, 1962–1969 (2007).
18. Bartumeus, F. & Catalan, J. Optimal search behavior and classic foraging theory. *J. Phys. A* **42**, 434002 (2009).
19. Viswanathan, G. M. *et al.* Lévy flights in random searches. *Physica A* **282**, 1–12 (2000).
20. Cornelius, J. M. & Reynolds, J. F. On determining the statistical significance of discontinuities within ordered ecological data. *Ecology* **72**, 2057–2070 (1991).
21. Behrenfeld, M. J. & Falkowski, P. G. Photosynthetic rates derived from satellite-based chlorophyll concentration. *Limnol. Oceanogr.* **42**, 1–20 (1997).
22. Sims, D. W. *et al.* Encounter success of free-ranging marine predator movements across a dynamic prey landscape. *Proc. R. Soc. B* **273**, 1195–1201 (2006).
23. Clarke, M. R. & Stevens, J. D. Cephalopods, blue sharks and migration. *J. Mar. Biol. Assoc. UK* **54**, 949–957 (1974).
24. Moteki, M., Arai, M., Tsuchiya, K. & Okamoto, H. Composition of piscine prey in the diet of large pelagic fish in the eastern tropical Pacific Ocean. *Fish. Sci.* **67**, 1063–1074 (2001).
25. Zainuddin, M., Kiyofuji, H., Saitoh, K. & Saitoh, S. I. Using multi-sensor satellite remote sensing and catch data to detect ocean hot spots for albacore (*Thunnus alalunga*) in the northwestern North Pacific. *Deep-Sea Res. II* **53**, 419–431 (2006).
26. Powell, T. M. *et al.* Spatial scales of current speed and phytoplankton biomass fluctuations in Lake Tahoe. *Science* **189**, 1088–1090 (1975).
27. Boyer, D. *et al.* Scale-free foraging by primates emerges from their interaction with a complex environment. *Proc. R. Soc. B* **273**, 1743–1750 (2006).
28. Bartumeus, F. *et al.* Helical Lévy walks: adjusting searching statistics to resource availability in microzooplankton. *Proc. Natl Acad. Sci. USA* **100**, 12771–12775 (2003).
29. Kashtan, N., Noor, E. & Alon, U. Varying environments can speed up evolution. *Proc. Natl Acad. Sci. USA* **104**, 13711–13716 (2007).

Author Contributions D.W.S. designed the study. N.E.H. and D.W.S. completed data analysis with contributions from N.Q. and J.R.M.D. N.E.H. designed and developed the software for MLE and split moving-window analyses. D.W.S. and N.E.H. wrote the paper and all authors contributed to subsequent drafts. Field data were collected by D.W.S., E.J.S., N.Q., N.G.P., M.K.M., K.M.S., D.W.F., J.M.B., T.K.D., J.D.R.H., G.C.H. and V.J.W.

Supplementary Information Contents

1. Methods

    1.1 Study animals

    1.2 Division of recorded time series into behaviourally consistent sections

    1.3 Preliminary data analysis

    1.4 Maximum Likelihood Estimation (MLE) and model comparisons

    1.5 Sensitivity of MLE analysis to behavioural complexity

2. Results

    2.1 Environmental context and Lévy behaviour of silky sharks

    2.2 Behaviour pattern switching of bigeye tuna in relation to habitat type

    2.3 Lévy behaviour of tuna in a productive convergence zone

List of Supplementary Tables

    Table S1. Summary information of electronic tags deployed.

    Table S2. The MLE and RNG equations used in the analysis.

    Table S3. Summary of all the data used and results of the MLE analysis.

    Table S4: Best fit parameters, log-likelihoods and Akaike weights for the best fitting sections used in the statistical spatial analysis and/or shown in figures.

List of Supplementary Figures

1. Supplementary Methods

1.1 Study animals

In total, 129 track sections from 55 individuals collected over more than 5,700 days were analysed, representing 14 species: bigeye thresher shark (*Alopias superciliosus*, Lowe 1841) $n = 2$ individuals; blue shark (*Prionace glauca*, Linnaeus 1758) $n = 12$; shortfin mako shark (*Isurus oxyrinchus*, Rafinesque 1810) $n = 1$; porbeagle shark (*Lamna nasus*, Bonnaterre 1788) $n = 1$; silky shark (*Carcharhinus falciformis*, Müller & Henle 1839) $n = 3$; oceanic whitetip shark (*Carcharhinus longimanus*, Poey 1861) $n = 1$; basking shark (*Cetorhinus maximus*, Gunnerus 1765) $n = 6$; whale shark (*Rhincodon typus*, Smith 1828) $n = 1$; bigeye tuna (*Thunnus obesus*, Lowe, 1839) $n = 5$; yellowfin tuna (*Thunnus albacares,* Bonnaterre, 1788) $n = 6$; black marlin (*Makaira indica,* Cuvier 1832) $n = 1$; blue marlin (*Makaira nigricans*, Lacepède 1802) $n = 11$; swordfish (*Xiphias gladius*, L. 1758) $n = 1$; ocean sunfish (*Mola mola*, L. 1758) $n = 1$. These comprise 5 taxonomic or functional groups (macropredatory sharks, planktivorous sharks, tunas, billfish, ocean sunfish) with 12.2 million individual movement steps analysed. Table S1 gives tag types used and technical details, together with tagging locations. Long-term high resolution depth datasets from fish are difficult to obtain given the very limited bandwidth of the Argos data-relay satellite system[1]. We made serendipitous use of an extensive number of satellite and archival tags that had been recovered after long deployments and contained complete high resolution datasets. Only the basking shark dive data ($n = 6$ individuals; 10.9% of total individuals) have been analysed previously in the context of Lévy flights[2], although, importantly, this did not include division of tracks into sections that were then geo-referenced and compared with environmental habitat type, the prime objective in the current paper.

Table S1. Summary information of electronic tags deployed.

Species (approx. body size cm)[1] or weight (kg)	Tagging location	Tag type[2]	Recording interval (min / sec)	Depth resolution (m)	*n* datasets[3]	Reference
Bigeye thresher shark (~220cm FL)	N.Pacific	MT PTT-100	60 min	5.4	2	Musyl *et al*. unpubl. data, 3
Blue shark (120-215cm FL)	NE. Atlantic	WC PAT Mk10	1.0 s	< 0.5	3	4
	N.Pacific	MT PTT-100	60 min	5.4	16	Musyl *et al*. unpubl. data, 3
Shortfin mako shark (210 cm FL)	N.Pacific	MT PTT-100	60 min	5.4	1	Musyl *et al*. unpubl. data
Porbeagle shark (180 cm FL)	NE.Atlantic	WC PAT Mk10	1.0 s	< 0.5	1	5

Species (approx. body size cm)[1] or weight (kg)	Tagging location	Tag type[2]	Recording interval (min / sec)	Depth resolution (m)	n datasets[3]	Reference
Silky shark (120 – 213cm FL)	N.Pacific	MT PTT-100	15-60 min	5.4	10	Musyl *et al*. unpubl. data, 3
Oceanic whitetip shark (115-215cm FL)	N.Pacific	MT PTT-100	15-60 min	5.4	13	Musyl *et al*. unpubl. data, 3
Basking shark (4000 – 7000cm TL)	NE.Atlantic	WC PAT 3 & 4	1 min	< 0.5	6	6
Whale shark (6000 – 7000cm TL)	W.Indian Ocean	MT PTT-100	15 min	5.4	1	7
Bigeye tuna (65-99cm FL)	Eq. Eastern Pacific	LW LTD 2310	1 min	1.0	5	8

Species (approx. body size cm)[1] or weight (kg)	Tagging location	Tag type[2]	Recording interval (min / sec)	Depth resolution (m)	n datasets[3]	Reference
Yellowfin tuna (51-60cm FL)	Central N.Pacific	MT PTT-100	60 min	5.4	1	3
	Eq. Eastern Pacific	LW LTD 2310	1 min	1.0	5	8
Black marlin (453kg)	N.Pacific	MT PTT-100	60 min	5.4	1	Musyl *et al*. unpubl. data, 3
Blue marlin (45-204kg)	N.Pacific	MT PTT-100	15-60 min	5.4	14	Musyl *et al*. unpubl. data, 3
Swordfish (215-240cm)	N.Pacific	MT PTT-100	15-60 min	5.4	10	Musyl *et al*. unpubl. data, 3

Species (approx. body size cm)[1] or weight (kg)	Tagging location	Tag type[2]	Recording interval (min / sec)	Depth resolution (m)	n datasets[3]	Reference
Ocean sunfish (60cm TL)	NE.Atlantic	WC PAT Mk10	1.0 s	< 0.5	1	9

1. Body size: TL, total length, FL Fork length.

2. Tag Manufacturers: LW, Lotek Wireless; MT, Microwave Telemetry; WC, Wildlife Computers. Tag type: PAT, pop-up archival transmitting tag; PTT, platform terminal transmitter, LTD, archival tag (light, temperature, depth).

3. Some of the datasets were too short or had too many gaps to be included in the analysis.

1.2 Division of recorded time series into behaviourally consistent sections

It is hypothesised that long and complex dive time series (vertical tracks) recorded by animal-attached electronic tags are likely to have captured a series of different movement behaviours. This is due, at least in part, to an animal encountering differing environmental conditions such as sea temperature, depth or prey densities, for example. If analysed as a whole, these time series may result in more complex move step-length frequency distributions which may not be readily or accurately interpreted by the proposed statistical analysis for exploring underlying model fits to empirical data (i.e. Maximum Likelihood Estimation, MLE). It is therefore desirable to divide such tracks into sections which are behaviourally more consistent. Furthermore, it is an aim of this study to explore different movement patterns in relation to environmental gradients. Hence, there is an additional requirement that the track divisions should be made, where possible, at or at least temporally close to encountered environmental boundaries (e.g. between water masses with different characteristics). An examination of the dive time series often reveals clear changes in patterns of vertical space use which can in turn, when spatial data is available, be linked to environmental changes such as water temperature gradients and sea depth[4].

Although for some tracks discontinuities are clearly identified by changes in patterns of vertical space use in a time depth plot, as in Figure 2 (main paper), in other cases changes are less clear and therefore an objective method is needed to identify discontinuities. In this study a split-moving window (SMW) analysis similar to that described by Cornelius and Reynolds[10] was applied to all tracks that were free from temporal gaps in the time series.

To perform the analysis a two dimensional (2D) time-at-depth matrix, with 6 hour time bins (as columns) and 10 m depth bins (as rows), is first constructed from the raw dive time-series data by calculating the proportion of time spent at each depth within each time period (Fig. S1a). A virtual window with a width of 6 time bins is placed at the start of the time-at-depth matrix and a measure of dissimilarity between the two window halves is calculated and assigned to the centre

position of the window. The dissimilarity measure used here was the multivariate measure of Euclidean distance between averaged time at each depth. The window position is then advanced by one time bin and the calculation is repeated until the window reaches the end of the time series. Statistical significance of each dissimilarity value is calculated using a Monte-Carlo technique whereby the calculation is repeated 1000 times with a shuffled time-at-depth matrix. The number of times the dissimilarity value exceeds that calculated using the real data is counted and converted to a percentage which represents the *p*-value. Significant discontinuities in the time series will have higher dissimilarity values than most of those calculated using a random re-arrangement of the data, resulting in very few randomisations yielding higher dissimilarity values. The width of the window is then incremented by two and the process is repeated up to a width of 32, giving 14 window sizes. The *p*-values calculated from each window size and position are stored and finally plotted by stacking them vertically, with significant values (in this case $p < 0.001$) being plotted in black, as shown in Figure S2 (and Fig. 2 main paper). Discontinuities in the dive time series are revealed by the presence of inverted triangles which "point" to the discontinuity and indicate the position at which the time series can be divided as a quantitative estimate of where different movement patterns are located in the time series.

The vertical movement tracks of large marine fish analysed in this study are complex and therefore the results of the split-moving window analysis can appear "noisy", in some cases, with many discontinuities being identified. Referring to Figure S2a below it can be seen that the discontinuities labelled i, iii, iv and vi extend over many window sizes and have a general trend of increasing width at smaller window sizes. These discontinuities represent shifts between prolonged behavioural bouts and are therefore the points at which this track was divided. The smaller discontinuities labelled ii, v, vii and viii, although significant, are of shorter duration or extend over only a few window sizes and are therefore ignored since they do not capture persistent pattern changes. Accurate detection of power laws in biological data can be affected by small dataset size[11,12] so there is a further consideration not to divide the tracks into sections with too few data

points. Therefore in the current study only the clearest discontinuities arising from the SMW analysis were used to divide the tracks.

Patterns of vertical space use of marine fish can be analysed using simple binning techniques to generate a time-at-depth matrix with temporal and depth resolution set to the required level of detail (Fig. S1). Therefore, vertical space use is a good candidate measure for the identification of movement pattern discontinuities that would encompass both responses to changes in environment (e.g. sea depth or thermocline depth) as well as other behavioural shifts[4]. An alternative measure that could be used is the move step-length distribution. It is a central hypothesis of the current study that long, complex tracks will comprise different move step-length frequency distributions and that changes in these could be related to environmental gradients and other variables. Move step-length frequency distributions are, however, relatively poorly analysed using simple binning techniques and the equivalent time/step-length frequency matrix (Fig. S1b) reveals considerably less detail than that generated from depth usage (Fig. S1a). One reason for the lack of detail could be the very small sample sizes that result from the 6-hour time divisions used to generate the matrix; using longer time windows, however, results in a much coarser analysis and missed discontinuities (Fig. S2).
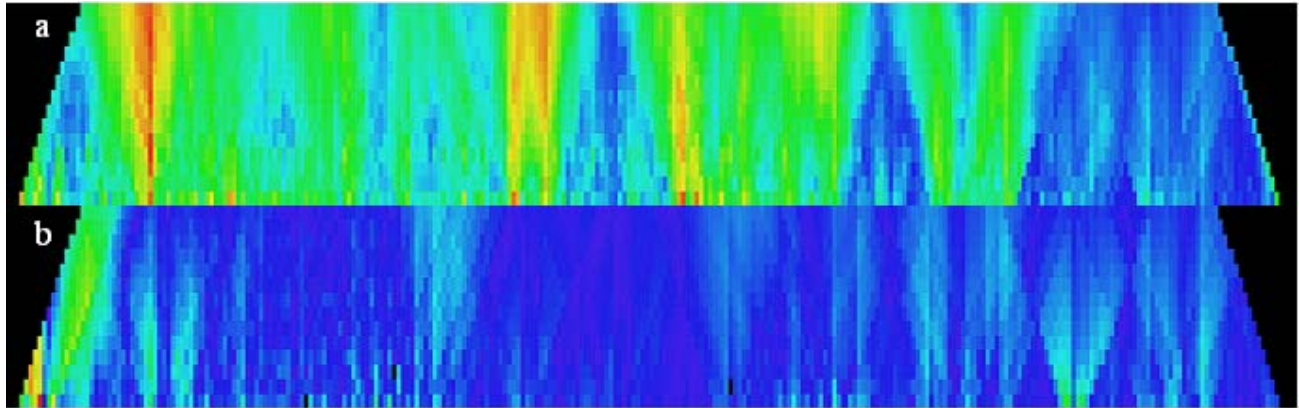
Figure S1. Identification of movement pattern discontinuities. Time at depth (a) and time step-length (b) dissimilarity matrices generated from depth data of blue shark 10. Red colour shows areas of high dissimilarity and blue low dissimilarity. The step-length matrix lacks contrast in comparison to the time-at-depth matrix and is therefore likely to miss some significant discontinuities.
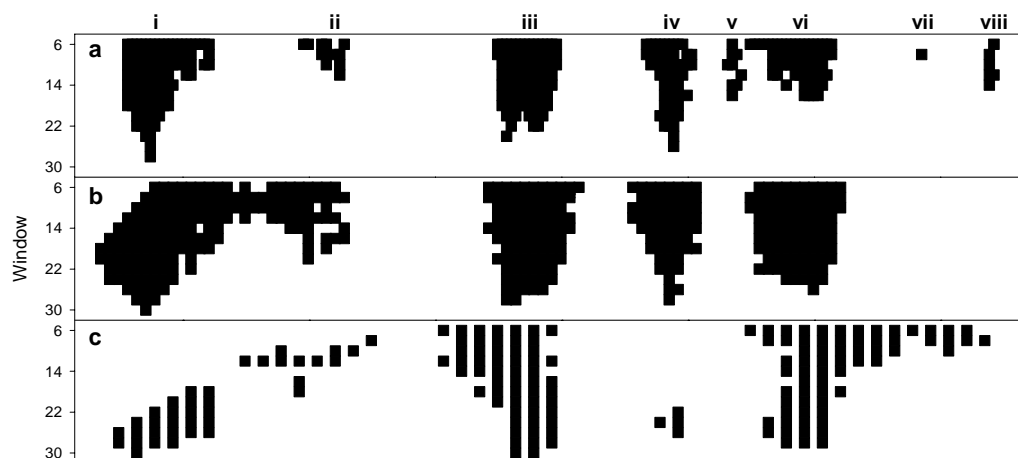
Figure S2. Split-moving window analysis plots at differing time resolutions. For blue shark 10 with time divisions set to (**a**) 6 hours, (**b**) 12 hours and (**c**) 24 hours. Increasing the time division results in decreasing resolution of the discontinuities.

1.3 Preliminary data analysis

Prior to performing the MLE analysis all sections, which comprised time-stamped depth measurements, were converted into move step-lengths by calculating vertical movement deltas between successive pairs of data points. As part of the process, three causes of potential calculation error were addressed. Firstly, some datasets were recorded at very high temporal resolution (e.g. 1s) which can in some cases be insufficient time to record movement deltas greater than the depth resolution of the tag, resulting in considerable step-wise alternating values, i.e. long series of alternating move steps with lengths close to the vertical resolution of the tag. High temporal resolution datasets were therefore under-sampled at 1 in 10 to give a sampling interval of 10 seconds, which was found to be sufficient time for the animal to make moves significantly greater than the tag depth resolution. Secondly, in all datasets, sampling artefacts were introduced when the animal made long movements with a temporal interval that exceeded the sampling interval. Even with a sampling interval of 1 hour it was found that some long movements had been artificially divided into a series of shorter steps. Correction of this second sampling artefact involved coalescing steps that were part of a single movement (i.e. where the trend of consecutive steps was either a continuously increasing or decreasing depth) into a single step rather than many smaller steps. It should be noted that this method of path integration maintains move step lengths consistent with that of a Lévy walk since displacements have finite velocity and are dependent on a time t (Refs.13,14). Finally, some of the datasets obtained via Argos satellite telemetry inevitably contained gaps where data was not retrieved, or was recovered corrupted and so was discarded[1]. If uncorrected, a spurious step would have been calculated between points either side of a gap; therefore, any step occurring immediately following a gap was ignored, ensuring that only genuine movement steps for which both the start and end depth had been recorded were included. Previous work has shown that small datasets can be prone to large statistical fluctuations and may result in poor fits to a candidate distribution or inaccurate estimates of the exponent[11]. Therefore, datasets with fewer than 500 data points prior to pre-processing were excluded from the analysis.

1.4 Maximum Likelihood Estimation (MLE) and model comparisons

The Maximum Likelihood Estimation (MLE) methodology employed was that described by Clauset *et al.*[15] with, in this study, power law, truncated Pareto-Lévy (truncated power law) and exponential distributions being tested. Briefly, the appropriate MLE equation was used to derive an exponent with the initial x_{min} parameter set to the minimum value found in the dataset. A best fit dataset was generated with the estimated parameters and a Kolmogorov-Smirnov (KS) test was used to determine the goodness of fit (the KS D statistic). To determine the best fit value for the x_{min} parameter the calculation was repeated with increasing values for x_{min} taken from the dataset with the value that resulted in the best (lowest) KS-D statistic being retained as the best fit value. When fitting a truncated Pareto distribution the method was repeated to derive a best fit value for the x_{max} parameter, so for the truncated Pareto distribution both the x_{min} and x_{max} parameters were fitted in the same way. There were two departures from the method as implemented in the programming code given in Clauset *et al.*[15]. Firstly, once values for x_{min} and x_{max} had been derived, the dataset was reduced to include only values between those lower and upper bounds. The resulting dataset therefore contained only the step lengths fitting the proposed distribution and it was this that was used to produce plots of $\log_{10}$ rank *vs* $\log_{10}$ step-length that were used to assess the goodness of fit; however, for purposes of clarity, this was plotted against the full set of observations so that the extent of the fit was evident. Secondly, rather than test all values in the dataset as possible candidates for x_{min} or x_{max}, the iterative search routine was halted once five consecutive worse fits had been found to avoid the problem of fitting to a very small sub-set of the data; a problem exacerbated by complex biological data and exponent estimation (see above). The aim of fitting the lower and upper bounds was to find the distribution that best fit most of the data, rather than select a small sub-set of the data that was a very good fit to a particular distribution.

The MLE analysis requires two equations for each distribution to be tested. One is the MLE equation for the distribution and is used to estimate the exponent. The other is a random number

generator (RNG) and is used to generate best-fit datasets. Table S2 gives the equations that were used for each distribution. The power law MLE and the power-law and exponential RNG equations were obtained from Clauset *et al.*[15], the truncated Pareto MLE equation was from White *et al.*[12] and the truncated Pareto RNG was from Kagan[16].

Table S2. The MLE and RNG equations used in the analysis.

	MLE equations	Random number equations (in all cases r represents a uniform random number in the interval $(0,1)$
Power-law	$$\hat{a} = 1 + n \left(\sum_{i=1}^{n} \ln \frac{x_i}{x_{\min}} \right)^{-1}$$	$$x = x_{\min}(1 - r)^{-1/(a-1)}$$
Exponential	$$\hat{a} = n \left(\sum_{i=1}^{n} (x_i - x_{\min}) \right)^{-1}$$	$$x = x_{\min} - \frac{1}{a} \ln(1 - r)$$
Truncated Pareto	$$y = -\frac{\overline{\ln x} - 1}{(-\hat{a} + 1)} + \frac{\left(x_{\max}^{-\hat{a}+1} \ln x_{\max} - x_{\min}^{-\hat{a}+1} \ln x_{\min}\right)}{\left(x_{\max}^{-\hat{a}+1} - x_{\min}^{-\hat{a}+1}\right)}$$	$$x = x_{\min}\left\{ r\left[1 - \left(\frac{x_{\max}}{x_{\min}}\right)^{1-a} \right] + \left(\frac{x_{\max}}{x_{\min}}\right)^{1-a} \right\}^{1/(1-a)}$$

In some cases the tags convert integer pressure readings to real depth measurements by multiplying by 5.379; resulting in depths, and consequently step lengths, that are multiples of 5.379. Therefore, discrete approximation was used as described by Clauset *et al.*[15], but using the observed step-length multiple (e.g. 5.379) so that the best fit datasets used in Kolmogorov-Smirnov tests had a similar structure to the observed distribution. However, when generating the rank/step-length (rank-frequency) plots, the best fit distribution parameters were used to generate points from a continuous distribution as the resulting plots are easier to interpret, and doing so provides good confirmation of the accuracy of the approximations.

The approach to best-fit model selection in this study was to use MLE, log-likelihoods (LL) and Akaike Information Criteria (AIC) weights (*w*AIC) in addition to visual inspection for assessing best fits to rank-frequency plots of observed data. Once MLE best fit parameters for the three candidate distributions [power law, truncated Pareto (power law), exponential] had been derived the observed data and best fits were plotted as $\log_{10}$ rank *vs* $\log_{10}$ step-length (rank-frequency plots) and were assessed visually to determine which, if any, of the three candidate distributions provided a reasonable fit (see Fig. S3 for examples). Of the 129 sections assessed, 35 (27%) rank-frequency plots were found to be of complex form and were not fitted by any of the three distributions we tested; these were excluded from further analysis. The remaining 94 sections were analysed statistically using MLE with *w*AIC to select the best fit model. Log-likelihoods were calculated[17] for the two competing models for each section. Model selection using *w*AIC yielded one power law fit, 60 truncated power law fits within the Lévy range, 6 truncated power law fits outside the Lévy range, and 27 exponential fits to move step-length distributions (*n* = 94). In this study, therefore, model best fits selected for individual sections using log-likelihoods and *w*AIC were used in all analyses to test the Lévy flight foraging hypothesis.

MLE best fit parameters, log-likelihoods and Akaike weights for all track sections are shown in Table S3. Details for the best fitting sections (i.e. those used in the spatial analysis, or shown in figures) are given in Table S4, which also identifies the Figure where the ranked step-length plot for each section is shown [i.e. observed data with truncated Pareto (power law) and exponential model fits]. Figure S3 shows plots for those sections best fitted by a power law or truncated Pareto models that do not appear elsewhere in the paper showing two competing model fits.

Truncated power laws provided the majority of best fits to empirical movement data of tracked fish predators. It is perhaps unsurprising that natural phenomena such as animal movement data should be better fitted by truncated Pareto-Lévy distributions rather than pure power laws: where the animal is restricted by the depth of the water column or other factors (e.g. thermal or oxygen

tolerances, predator physiological capacity to withstand increased depths, prey absence) the truncation of the best fit distribution is increased (see Fig. 1a, b, d, e).

For the best fitting truncated Pareto-Lévy (power law) sections, MLE and the R Gamma functions[18] were used to attempt to fit a (shifted) Gamma distribution to ensure that this model was not a better alternative. GOF values calculated using the Kolmogorov-Smirnov test are given in Table S4 and ranked step-length plots of the fits are shown in Figure S4. Overall, it was found that gamma distributions were not better fits to the move step-length frequency distributions best fitted by a truncated power law.

Figure S3. Ranked step-length plots for sections well fitted by a truncated Pareto-Lévy distribution.

Best fit truncated Pareto (power law) (red line) and exponential (blue) models to observed data (black circles) for those figures not shown elsewhere. (a) bigeye tuna 1 section 4; (b) ocean sunfish 1 s2; (c) blue shark 9 s3 (note that this fit is to a power law, not a truncated power law); (d) blue shark 12 s2; (e) bigeye tuna 5 s4; (f) yellowfin tuna 2 s1; (g) yellowfin tuna 4 s4; (h) yellowfin tuna 5 s1; (i) yellowfin tuna 5 s3; (j) yellowfin tuna 1 s3; (k) yellowfin tuna 3 s3; (l) yellowfin tuna 3 s4; (m) blue shark 9 s2; (n) silky shark 3 s1. For model comparison values see Supplementary Table S3.

tolerances, predator physiological capacity to withstand increased depths, prey absence) the truncation of the best fit distribution is increased (see Fig. 1a, b, d, e).

For the best fitting truncated Pareto-Lévy (power law) sections, MLE and the R Gamma functions[18] were used to attempt to fit a (shifted) Gamma distribution to ensure that this model was not a better alternative. GOF values calculated using the Kolmogorov-Smirnov test are given in Table S4 and ranked step-length plots of the fits are shown in Figure S4. Overall, it was found that gamma distributions were not better fits to the move step-length frequency distributions best fitted by a truncated power law.

1.5 Sensitivity of MLE analysis to behavioural complexity

We found that 35 (27%) of track sections analysed were poorly fitted by either power law, truncated Pareto (power law) or exponential distributions. We hypothesised that some of the poor fits might be caused by behavioural complexities in the movement time-series arising from the inclusion of simple Brownian motion in addition to Lévy motion. Theoretical studies[14] have shown that when prey is relatively abundant Brownian motion is an optimum search strategy, which would explain the presence of exponentially distributed step lengths. To test this hypothesis, simulated time series were generated using steps from a truncated Pareto (power law) distribution with 5, 15 or 25% of steps being drawn from an exponential distribution. The parameters for the exponential distribution were derived by using MLE to fit an exponential distribution to the synthetic truncated Pareto distribution dataset. Fitting in this way ensured that the exponential step lengths covered a similar range to the truncated Pareto step lengths and could in principle, therefore, have been generated by the same animal. As we hypothesised, the MLE analysis (Fig. S5a-c) reveals that increasing proportions of exponential move steps results in increasingly poorer fits. Interestingly, comparison of the synthetic data and model fits to empirical examples (basking shark, bigeye and yellowfin tunas) (Fig. S5d-f) shows distinct similarities in form, supporting the hypothesis that poorer fits to the truncated Pareto distribution in some individuals may well be the result of behavioural switches in response to changes in prey field density.

Analysis using simulated move-step frequency distributions drawn from both Lévy and Brownian distributions to form a single test distribution appeared to account for some of the complex patterns in rank-step length plots that we found, suggesting different search behaviours may be interspersed at finer temporal scales than was possible to detect using our split-moving window technique. Behavioural complexity such as this could explain why Lévy behaviour can be difficult to detect in longer time-series where the likelihood of recording different movement behaviours is increased[2]. It seems likely that good fits to power laws or truncated power law

distributions will only be found when Lévy behaviour is adopted by foragers for the majority of the period within a time series section being analysed, even if a statistical technique such as split-moving window is used to identify discontinuities.

Given the effect of complex biological data on the form of rank-frequency plots (e.g. Fig. S5) visual inspection of plots can be useful to help assess that any particular distribution is a good fit when testing for the presence of power laws or truncated power laws to infer Lévy behaviour. This may be particularly relevant in the context of testing for the presence of biological Lévy flights because it is the heavy (fat) tail of the move step-length frequency distribution that should be reasonably accounted for by any candidate best fit model for the identification of Lévy behaviour to be reliably detected. The frequency of longer move steps that make up the heavy tail of a distribution (the right-hand side of the distribution) is low compared with the more frequent smaller steps making up the left hand side. Importantly in this context, MLE model fitting to empirical data plotted as a rank-frequency plot gives equal weight to all points even though the vast majority of points are clustered on the left hand side. This may be a potential problem for model selection in some cases because strong support for a model using Akaike weight values (e.g. wAIC = 1.0; strongest support) may be based on a good fit to the left hand side of the distribution rather than to the heavy tail also.

Figure S5. Analysis of complex data. Black circles represent synthetic or empirical observations; red lines represent MLE best fit truncated Pareto distributions. (a-c) Synthetic truncated Pareto distribution datasets including 5, 15 and 25% move steps derived from an exponential distribution; (d) basking shark *Cetorhinus maximus* 2, section 2; (e) bigeye tuna *Thunnus obesus* 3, section 4; (f) yellowfin tuna *Thunnus albacares* 1, section 5, showing visually similar patterns to synthetic Lévy-Brownian (exponential) datasets. Arrows indicate departures from a good fit to the truncated Pareto distribution.

2. Supplementary Results

The LFF hypothesis states that Lévy flights (or truncated Lévy flights) optimise random searches, therefore biological organisms must have evolved to exploit Lévy flights[14]. Two predictions have arisen from theoretical analysis: (truncated) Lévy flights (walks) with $\mu \approx 2$ optimise random searches in environments with sparsely distributed random, revisitable target sites, while at higher concentrations of random targets Lévy flight with $\mu > 3$ is optimal, corresponding essentially to Brownian motion[14].

2.1 Environmental context and Lévy behaviour of silky sharks

In further support of the prediction that when prey is abundant Brownian motion is an optimum search strategy, whereas when prey is sparse Lévy is optimum, Figure S6 shows geo-referenced tracks from two silky sharks (*Carcharhinus falciformis*) in relation to chlorophyll 'a' concentrations, a proxy for productivity. Silky shark 2 was located in comparatively productive waters with a move (dive) step-length distribution best fitted by an exponential distribution representing Brownian motion. In contrast, silky shark 3 remained in very low productivity (oligotrophic) waters with diving behaviour approximated by a truncated power law with an exponent of $\mu = 2.02$, close to the theoretical optimum for Lévy behaviour in an environment with sparse target sites.
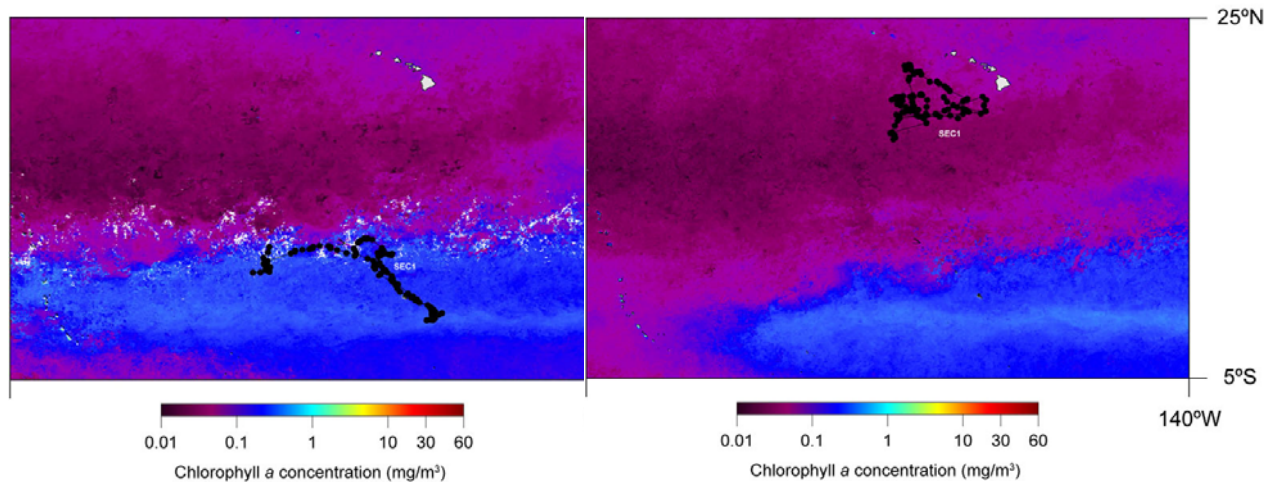
Figure S6. Horizontal movements of silky sharks in different productivity zones. Left panel, silky shark

(*Carcharhinus falciformis*) 2 in productive waters (Equatorial Convergence Zone) with vertical movements

following an exponential distribution; right panel, silky shark 3 in less productive, oligotrophic waters (south of

the Hawaiian Islands) with vertical movements approximated by a truncated power law exponent of 2.02.

2.2 Behaviour pattern switching of a bigeye tuna in relation to habitat type

Under the adaptive (optimal) behaviour conceptual framework of the Lévy flight foraging

hypothesis, changes in searching behaviour are expected as an animal moves between areas of

differing productivity and hence prey density. In the Northeast Atlantic, continental shelf waters

with abundant, seasonally persistent tidal and shelf-break fronts have generally higher primary and

secondary productivity than open ocean waters where the water column is less well mixed and

characterised by strong and stable vertical thermal stratification[6,19]. Here we defined two principal

habitats for the purposes of simple analysis of behaviour types in relation to environmental

gradients: productive shelf waters with strong tidal front presence (Frontal/Shelf) and less

productive off-shelf areas typified by thermally stratified water with a deep thermocline at around 50

– 100 m depth (Off-shelf) (Fig. 3a in the main paper). In the Central Eastern Pacific, near the

Galapagos Islands, the northerly flowing Peru Current meets the southward turning Equatorial Counter Current which form zones of upwelling and convergence along the westward flowing Equatorial Current. At these boundaries cold, nutrient rich water is up-welled and mixed with warmer surface waters creating a highly productive habitat characterised by plankton blooms[19]. Adjacent to these areas, to the north and south, the ocean is relatively oligotrophic and vertically thermally stratified with a thermocline depth of about 100 m. Here we defined two principal habitats to examine tuna behaviour: highly productive upwelling/convergence zone fronts (Frontal) and oligotrophic stratified water with a strong and stable thermocline (Stratified) (Fig. 3b main paper).

Although in this study switching behaviour was observed in only 8 individuals (from 55 individuals for which we had data), this is largely due to the difficulty of obtaining high-temporal resolution tracking data over long time periods where different large-scale habitat types were encountered. Longer tracks traversing different oceanographic regimes provided a greater chance of recording changes in patterns of search behaviour.

Switching between behaviour types – identified by split-moving window analysis, MLE model fits and Akaike weights (wAIC) model comparison values, and as a function of ocean productivity – was found for bigeye tuna (*Thunnus obesus*) ($n = 2$) and yellowfin tuna (*T. albacares*) ($n = 2$) in addition to blue shark ($n = 1$) (e.g. Fig. 2), basking shark ($n = 2$) and whale shark ($n = 1$) (Supplementary Table S3, S4). As a representative example, Figure S7 shows the vertical movements of bigeye tuna 2, together with the MLE model fits to move-step frequency distributions of the different sections, water temperature-at-depth profiles and the horizontal movements corresponding to the analysed sections. The split-moving window analysis identified eight adjacent sections as having different features (Fig. S7a,b). Horizontal movements were characterised by traversing east-west movements mostly along the boundary between the Equatorial Convergence Front spreading west of the Galapagos Islands and lower productivity, stratified waters further south (Fig. S7c,d,e). The analysed sections show changes in vertical movement pattern, with Lévy

behaviour occurring predominantly in the west and Brownian-type movement in the east. The switch from Lévy to Brownian patterns of movement (Fig. S7c sections 3 to 4) and back again (Fig. S7c sections 5 to 6, and sections 6 and 7) was also coincident with a change in water mass type, from warm well-stratified water to cooler surface-layer water with a weaker thermocline that is characteristic of zones of upwelling and convergence (Fig. S7d sections 3 to 4).

The behaviour of the bigeye tuna shows changes in relation to the environment and we speculate that prey may have been more abundant in the eastern region nearer the Galapagos since Brownian motion was identified there. The physical complexity of the Equatorial Convergence Zone characterised by upwelling, meso-scale fronts and eddies[20] is likely to entrain complex distributions of prey, including aggregation of individuals[21], and will likely contribute to the observed complexity in tuna behaviour such as switching between different optimal strategies as resource conditions change.
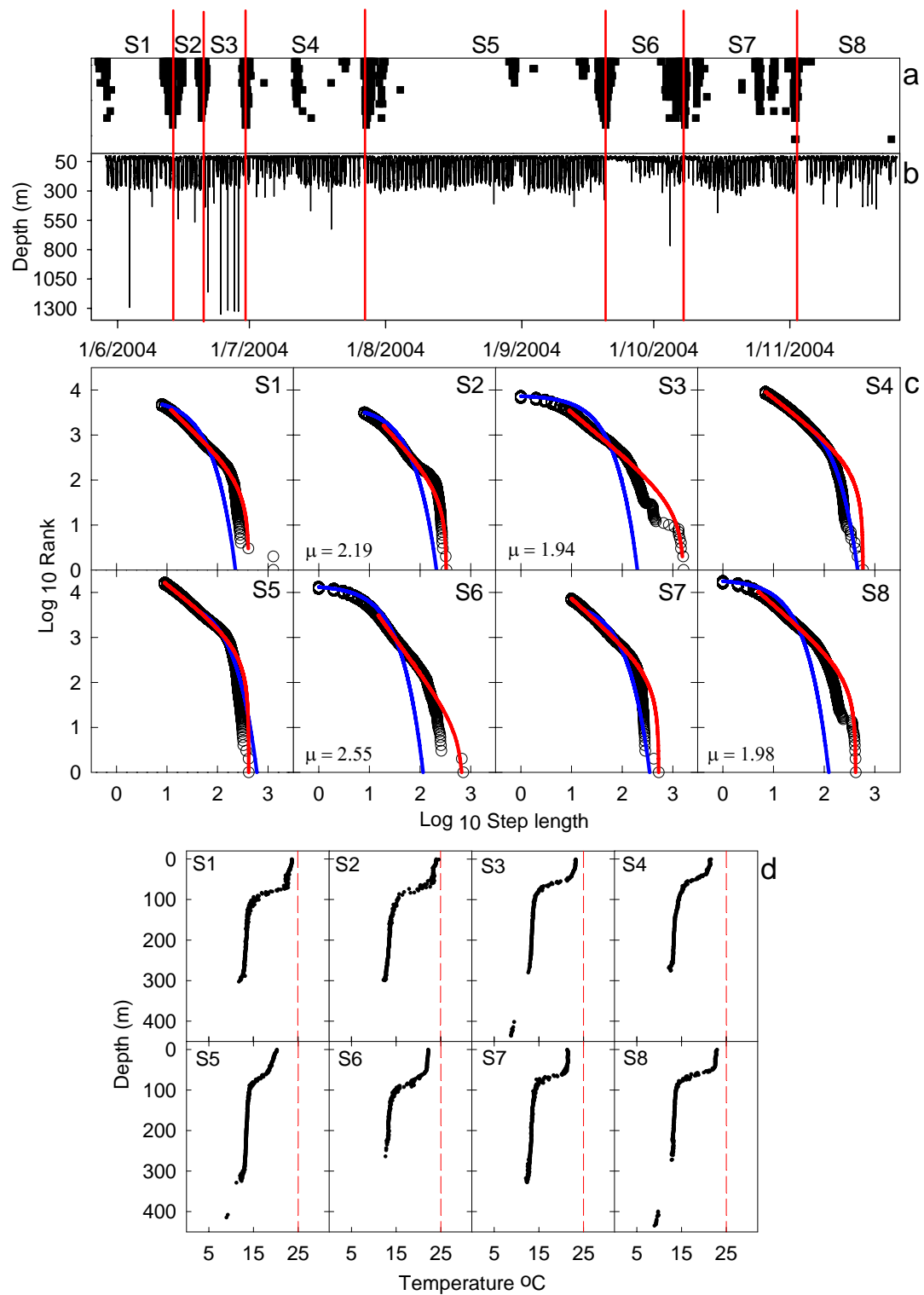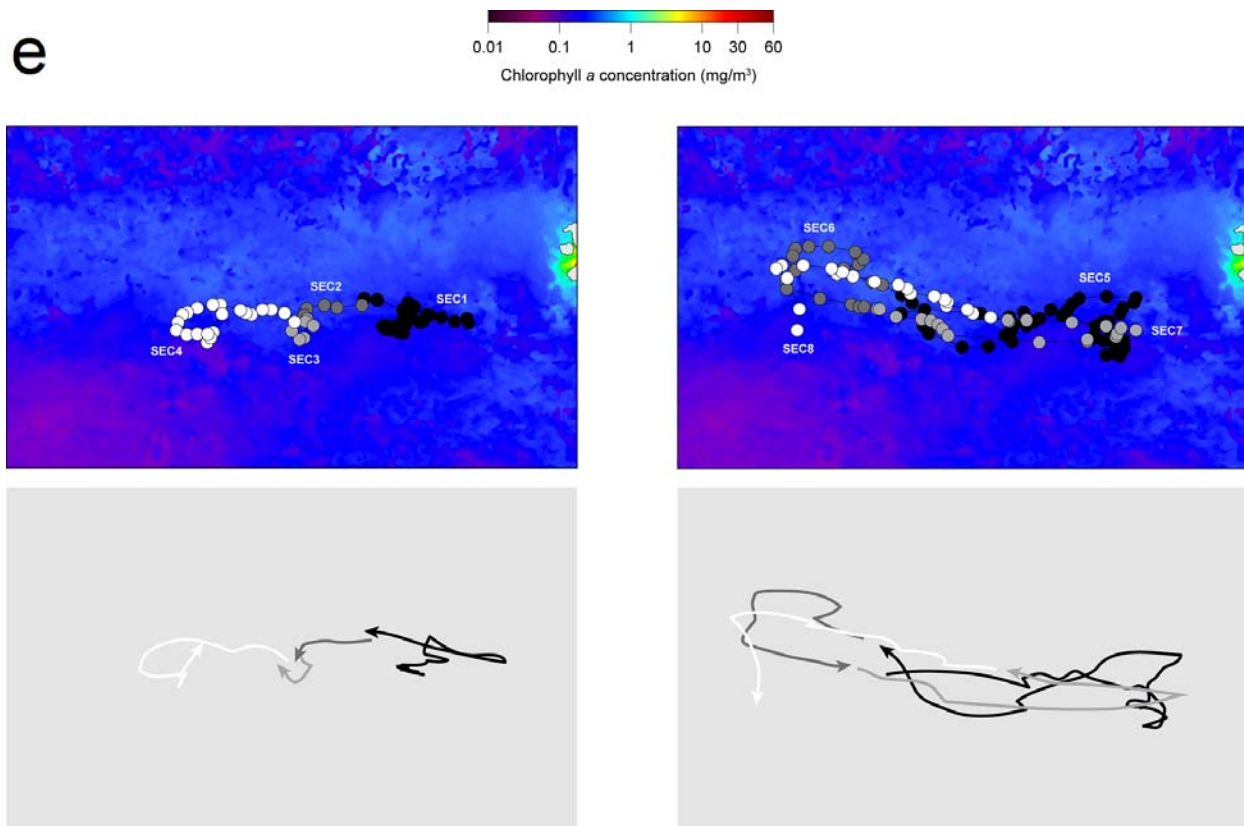
Figure S7. A bigeye tuna switching between diving behaviour types in relation to environmental gradients. (a) Split-moving window analysis and (b) time depth profile for bigeye tuna 2 showing the seven points of most significant discontinuity at which the track was divided. (c) MLE analysis of the eight sections showing μ values for those sections best fitted by a truncated Pareto (power law) distribution. Maximum Likelihood Estimation (MLE) model parameters and Akaike's Information Criteria (AIC) weights model comparisons for c given in Supplementary Tables S3 and S4. (d) Profiles of temperature at depth recorded by fish-attached electronic tags. These show the thermal profile of the water column and thermocline depth being similar from S3 to S5 followed by a decrease in upper layer temperatures and weaker thermocline (S4 and S5) and re-establishment of a stronger thermocline and higher temperatures from S6-S8. The weaker thermocline is associated with a better fit of vertical move step lengths within a section to an exponential distribution (S5) while vertical move steps within well stratified waters are better fit by a truncated power law distribution (S1, S8). (e) Horizontal movements of bigeye tuna 2 west of the Galapagos Islands along the

southern boundary of the Equatorial Convergence Front. Sections are numbered as for a-c and arrows in the lower panel indicate directions of movement paths.

2.3 Lévy flight behaviour in a productive convergence zone

As expected from the Lévy flight foraging hypothesis (LFF) bigeye (*Thunnus obesus*) and yellowfin tuna (*T. albacares*) displayed a higher frequency of Brownian-type diving movements than Lévy movements in the Equatorial Convergence Zone (Fig. 3b main text). However, both species were found to exhibit Lévy movements in a productive zone at least as frequently (in terms of frequency of time series sections) as in a lower productivity region, which is more often than might be expected according to the LFF hypothesis (Fig. 3b). This contrasts with the occurrence of Lévy behaviour in the Northeast Atlantic where clearer spatial difference between productive and less productive large-scale habitats was evident (productive shelf/frontal habitat versus lower productivity off-shelf habitat) and where Lévy movement patterns were associated with off-shelf regions (Figs. 2, 3 in the main paper).

That tuna exhibited both Lévy and Brownian movement types in the Equatorial Convergence Zone west of the Galapagos Islands suggests a requirement for a flexible approach to searching that may be linked to complexity in prey distributions (as mentioned above in Supplementary Results 2.2). One possible explanation for this flexibility in tuna movement pattern is that although prey resources are generally higher in frontal zones compared to adjacent regions[19], physical processes act to influence distributions of prey in complex ways. For example, the heterogeneity in distribution and abundance of zooplankton species in the Northwest Atlantic has been shown to be related to their associations with specific water masses of different origin and associated temperature/density discontinuities such as pycnoclines and fronts[22,23]. Indeed, along mesoscale frontal features in the Eastern North Pacific albacore (*Thunnus alalunga*) and skipjack tuna (*Katsowonus pelamis*) were found to be aggregated in high productivity areas where prey such as anchovy, pelagic red crab and

euphausids were enhanced[21]. However, even along frontal features prey distributions were highly patchy across a broad range of mesoscales[21].

In the present study it is possible that the adoption of Lévy and Brownian movements by tuna are responses to changes in patchy prey distributions that are entrained by frontal features such as eddies. It has been observed that in Pacific inter-tropical convergence zones albacore tuna are associated with meso-scale fronts and eddies[20]. These oceanographic features create local aggregations of prey organisms and patchier distributions of prey than might otherwise be expected at the meso-scale[23]. Therefore, very rich prey areas are expected within or near eddies, whereas relatively lower concentrations of prey may be available between such systems. This could account for the change between an optimal strategy for sparse prey environments and a strategy for where prey is more abundant occurring in the Equatorial Convergence Zone near the Galapagos Islands.

The tuna tracked in this study covered very large distances (1502 to 7867 km) and areas (87,399 to 1,111,654 km^2) (Figs. S8, S9) which greatly exceed the scale of eddies in this region (*ca.* 50 – 200 km diameter). It is therefore possible that at the scales over which the tuna ranged prey is not always highly abundant but patchy over a wide range of scales, and therefore Lévy diving movements may be a more efficient strategy for large interpatch distances than the expected Brownian diving movements.
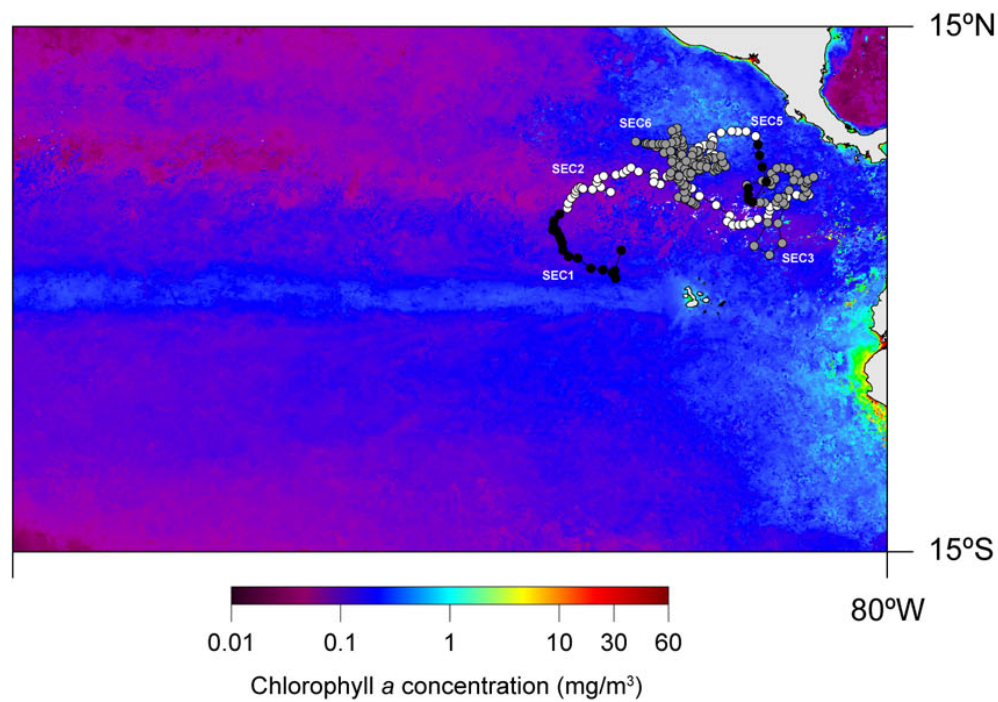
Figure S8. Yellowfin tuna horizontal movements across different productivity zones. Yellowfin tuna 2 (*Thunnus albacares*) covered a distance of 7,867km and an approximate area of 249,751km^2 while traversing habitats with differing productivity.
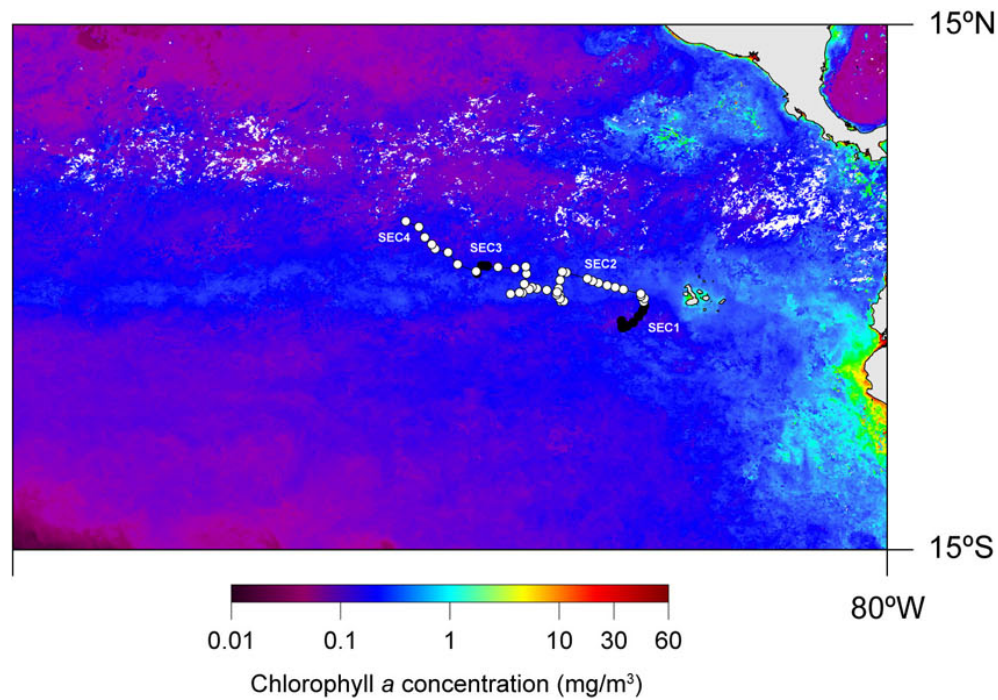
Figure S9. Bigeye tuna horizontal movements across different productivity zones. Bigeye tuna 3 (*Thunnus obesus*) crossed the equatorial convergence zone from near the Galapagos Islands northwest into warmer oligotrophic waters, covering a distance of 2,609km.

References

1.   Hays, G.C. *et al*. Why do Argos satellite tags deployed on marine animals stop transmitting? *J. Exp. Mar. Biol. Ecol.* **349**, 52-60 (2007).

2.   Sims, D.W. *et al*. Scaling laws of marine predator search behaviour. *Nature* **451**, 1098-1102 (2008).

3.   Musyl, M.K., McNaughton, L.M., Swimmer, J.Y., and Brill, R.W., Convergent evolution of vertical movement behavior in swordfish, bigeye tuna and bigeye thresher sharks. Vertical niche partitioning in the pelagic environment as shown by electronic tagging studies. *PFRP Newsletter* **9**, 1-4 (2004).

4.   Queiroz, N. *et al*. Short-term movements and diving behaviour of satellite-tracked blue sharks (*Prionace glauca*) in the North-eastern Atlantic Ocean. *Mar. Ecol. Prog. Ser.* (in press).

5.   Pade, N.G. *et al*. First results from satellite-linked archival tagging of porbeagle shark, Lamna nasus: Area fidelity, wider-scale movements and plasticity in diel depth changes. *J. Exp. Mar. Biol. Ecol.* **370**, 64-74 (2009).

6.   Sims, D.W., Southall, E.J., Richardson, A.J., Reid, P.C. and Metcalfe, J.D. Seasonal movements and behaviour of basking sharks from archival tagging: no evidence of winter hibernation. *Mar. Ecol. Prog. Ser.* **248**, 187-196 (2003).

7.   Brunnschweiler, J.M., Baensch, H., Pierce, S.J., and Sims, D.W. Deep diving behaviour of a whale shark during long-distance movement in the western Indian Ocean. *J. Fish Biol.* **74**, 706-714 (2009).

8.   Schaefer, K. M., Fuller, D.W. and Block, B.A. Vertical movements and habitat utilization of skipjack (*Katsuwonus pelamis*), yellowfin (*Thunnus albacares*), and bigeye (*Thunnus obesus*) tunas in the equatorial eastern Pacific Ocean, ascertained through archival tag data.

In *Tagging and Tracking of Marine Animals with Electronic Devices, Reviews: Methods and Technologies in Fish Biology and Fisheries* (eds Nielsen, J. L. *et al*.). 121-144 (Springer, 2009).

9. Sims, D.W. *et al*. Satellite tracking the world's largest bony fish, the ocean sunfish *Mola mola* in the North-East Atlantic Ocean. *J. Exp. Mar. Biol. Ecol.* **370**, 127-133 (2009).

10. Cornelius, J.M. and Reynolds, J.F. On determining the significance of discontinuities within ordered ecological data. *Ecology* **72**, 2057-2070 (1991).

11. Sims, D.W., Righton, D. and Pitchford, J.W. Minimizing errors in identifying Lévy flight behaviour of organisms. *J. Anim. Ecol.* **76**, 222-229 (2007).

12. White, E.P., Enquist, B.J. and Green, J.L. On estimating the exponent of power-law frequency distributions. *Ecology* **89**, 905-912 (2008).

13. Shlesinger, M. F. and J. Klafter. Lévy flights versus Lévy walks. In *On Growth and Form* (eds Stanley, H. & Ostrowsky, N.) 279-283 (Kluwer,1986).

14. Viswanathan, G.M. *et al*. Lévy flights and superdiffusion in the context of biological encounters and random searches. *Physics Life Rev.* **5**, 133-150 (2008).

15. Clauset, A., Shalizi, C.R. and Newman, M.E.J. Power-law distributions in empirical data. *SIAM Rev.* **51**, 661-703 (2009).

16. Kagan, Y.Y., Seismic moment distribution revisited: I. Statistical results. *Geophys. J. Int.* **148**, 520-541 (2002).

17. Burnham, K.P. and Anderson, D.R. Multimodel inference - understanding AIC and BIC in model selection. *Sociol. Methods. Res.* **33**, 261-304 (2004).

18. R Development Core Team. R: A Language and Environment for Statistical Computing (R Foundation for Statistical Computing, 2009).

19. Le Fèvre, J. Aspects of the biology of frontal systems. *Adv. Mar. Biol.* **23**, 163-299 (1986).

20.   Zainuddin, M., Kiyofuji, H., Saitoh, K., and Saitoh, S.I. Using multi-sensor satellite remote sensing and catch data to detect ocean hot spots for albacore (*Thunnus alalunga*) in the northwestern North Pacific. *Deep-Sea Res. II* **53**, 419-431 (2006).

21.   Fiedler, P.C. and Bernard, H.J. Tuna aggregation and feeding near fronts observed in satellite imagery. *Cont. Shelf Res.* **7**, 871-881 (1987).

22.   Gallager, S. M., Davis, C.S., Epstein, A.W., Solow, A. and Beardsley, R.C. High-resolution observations of plankton spatial distributions correlated with hydrography in the Great South Channel, Georges Bank. *Deep Sea Res. II* **43**, 1627-1663 (1996).

23.   Zimmerman, R.A. and Biggs, D.C. Patterns of distribution of sound-scattering zooplankton in warm- and cold-core eddies in the Gulf of Mexico, from a narrowband acoustic Doppler current profiler survey. *J. Geophys. Res.-Oceans* **104**, 5251-5262 (1999).

Table S3. Summary of the data used and results of the MLE best fit parameters and model comparison analysis [log-likelihoods (LLH) and Akaike weights (wAIC)]. P, TP and E denote power law, truncated Pareto (power law) and exponential models respectively. Exp denotes the exponential model in the model comparison results. See Supplementary Methods 1.4 for more details.

Species	ID	Section	Total points	Max step length (m)	Best fit distribution	Best fit exponent	Best fit Xmin	Best fit Xmax	TP / P GOF	Exp GOF	TP / P LLH	Exp LLH	TP / P wAIC	Exp wAIC
Big eye tuna	1	Section 1	48881	719										
Big eye tuna	1	Section 2	52801	1531	TP	2.062	15.000	466.000	0.022	0.186	-34989	-36223	1.000	0.000
Big eye tuna	1	Section 3	6001	259	TP	2.012	15.000	259.000	0.036	0.167	-4818	-4946	1.000	0.000
Big eye tuna	1	Section 4	5281	1683	TP	2.213	9.000	1683.000	0.037	0.258	-2657	-2954	1.000	0.000
Big eye tuna	1	Section 5	67321	627										
Big eye tuna	1	Section 6	18721	336	TP	2.022	10.000	297.000	0.027	0.172	-12937	-13505	1.000	0.000
Big eye tuna	1	Section 7	7899	336										
Big eye tuna	2	Section 1	19801	1281										
Big eye tuna	2	Section 2	11521	334	TP	2.189	19.000	334.000	0.032	0.166	-7097	-7332	1.000	0.000
Big eye tuna	2	Section 3	14401	1635	TP	1.938	9.000	1601.000	0.029	0.262	-14885	-15925	1.000	0.000
Big eye tuna	2	Section 4	38881	586	E	0.018	53.000		0.069	0.040	-7217	-7120	0.000	1.000
Big eye tuna	2	Section 5	79201	415	E	0.015	42.000		0.069	0.072	-20058	-19945	0.000	1.000
Big eye tuna	2	Section 6	25921	715	TP	2.548	15.000	715.000	0.027	0.189	-12029	-12425	1.000	0.000
Big eye tuna	2	Section 7	36001	529	TP	1.988	10.000	529.000	0.028	0.185	-30064	-31204	1.000	0.000
Big eye tuna	2	Section 8	33481	422	TP	1.975	5.000	422.000	0.026	0.217	-36913	-39232	1.000	0.000
Big eye tuna	3	Section 1	13072	249	TP	2.752	8.000	249.000	0.041	0.135	-8269	-8325	1.000	0.000
Big eye tuna	3	Section 2	49081	1526	TP	2.129	23.000	677.000	0.026	0.171	-28517	-29182	1.000	0.000
Big eye tuna	3	Section 3	4741	212	E	0.102	2.000		0.158	0.022	-7228	-6801	0.000	1.000
Big eye tuna	3	Section 4	11581	317	TP	2.072	13.000	317.000	0.058	0.095	-9459	-9520	1.000	0.000
Big eye tuna	4	Section 1	7200	302										
Big eye tuna	4	Section 2	33120	301	TP	2.525	18.000	301.000	0.022	0.159	-15726	-16065	1.000	0.000
Big eye tuna	4	Section 3	7200	539										
Big eye tuna	4	Section 4	27360	409										
Big eye tuna	4	Section 5	15841	648	TP	1.863	13.000	262.000	0.031	0.140	-15605	-15892	1.000	0.000
Big eye tuna	5	Section 1	20067	271	TP	2.369	9.000	271.000	0.034	0.208	-11380	-12077	1.000	0.000
Big eye tuna	5	Section 2	15841	281	TP	2.213	9.000	281.000	0.029	0.208	-14620	-15496	1.000	0.000
Big eye tuna	5	Section 3	15426	412										
Big eye tuna	5	Section 4	30241	1541	TP	2.155	13.000	1541.000	0.025	0.238	-25494	-27279	1.000	0.000
Big eye tuna	5	Section 5	5761	271										

Species	ID	Section	Total points	Max step length (m)	Best fit distribution	Best fit exponent	Best fit Xmin	Best fit Xmax	TP / P GOF	Exp GOF	TP / P LLH	Exp LLH	TP / P wAIC	Exp wAIC
Big eye tuna	5	Section 6	15841	695										
Big eye tuna	5	Section 7	12961	363	TP	2.323	18.000	363.000	0.02	0.160	-5819	-5960	1.000	0.000
Big eye tuna	5	Section 8	50761	735	TP	2.636	33.000	395.000	0.02	0.124	-18969	-19080	1.000	0.000
Yellowfin tuna	1	Section 1	6121	316	E	0.037	4.000		0.109	0.073	-11286	-11136	0.000	1.000
Yellowfin tuna	1	Section 2	4321	57	E	0.262	1.000		0.148	0.036	-5587	-5928	0.000	1.000
Yellowfin tuna	1	Section 3	28801	324	TP	1.610	5.000	286.000	0.043	0.175	-34348	-35298	1.000	0.000
Yellowfin tuna	1	Section 4	17281	315	E	0.033	15.000		0.101	0.027	-16697	-16330	0.000	1.000
Yellowfin tuna	1	Section 5	37081	339										
Yellowfin tuna	2	Section 1	23711	370	TP	2.059	11.000	370.000	0.026	0.184	-19744	-20596	1.000	0.000
Yellowfin tuna	2	Section 2	68401	133	E	0.044	4.000		0.123	0.051	-110071	-107593	0.000	1.000
Yellowfin tuna	2	Section 3	50401	1018	E	0.037	8.000		0.107	0.045	-59448	-57663	0.000	1.000
Yellowfin tuna	2	Section 4	10801	370										
Yellowfin tuna	2	Section 5	23041	133	E	0.027	4.000		0.143	0.022	-47195	-45065	0.000	1.000
Yellowfin tuna	2	Section 6	154080	1018										
Yellowfin tuna	3	Section 1	3948	202	TP	2.187	12.000	202.000	0.065	0.212	-2871	-3007	1.000	0.000
Yellowfin tuna	3	Section 2	12961	350	TP	2.071	12.000	333.000	0.047	0.230	-9477	-9946	1.000	0.000
Yellowfin tuna	3	Section 3	86041	414	TP	1.364	3.000	267.000	0.063	0.159	-118329	-121948	1.000	0.000
Yellowfin tuna	3	Section 4	38881	414	TP	1.464	3.000	397.000	0.058	0.291	-48854	-54359	1.000	0.000
Yellowfin tuna	4	Section 1	2521	200	TP	2.235	13.000	200.000	0.052	0.179	-2101	-2175	1.000	0.000
Yellowfin tuna	4	Section 2	36001	327	TP	2.600	18.000	291.000	0.051	0.124	-20834	-21144	1.000	0.000
Yellowfin tuna	4	Section 3	8641	539	TP	2.584	23.000	539.000	0.023	0.181	-5806	-5947	1.000	0.000
Yellowfin tuna	4	Section 4	5761	339	TP	1.743	8.000	339.000	0.07	0.173	-5729	-5995	1.000	0.000
Yellowfin tuna	4	Section 5	10441	331	TP	1.859	11.000	331.000	0.077	0.125	-8706	-8844	1.000	0.000
Yellowfin tuna	5	Section 1	2521	275	TP	1.505	7.000	275.000	0.088	0.268	-3208	-3377	1.000	0.000
Yellowfin tuna	5	Section 2	34081	293	TP	2.931	25.000	231.000	0.029	0.104	-13483	-13546	1.000	0.000
Yellowfin tuna	5	Section 3	4801	334	TP	1.160	2.000	266.000	0.102	0.133	-8162	-8274	1.000	0.000
Yellowfin tuna	5	Section 4	9001	318										
Yellowfin tuna	6	Entire	1058	177	E	0.022	5.380		0.215	0.085	-2825	-2720	0.000	1.000
Black Marlin	1	Section 1	590	204	TP	1.071	5.380	91.450	0.143	0.165	-1661	-1744	1.000	0.000
Black Marlin	1	Section 2	863	349	TP	1.266	5.380	349.670	0.185	0.193	-1808	-1849	1.000	0.000
Blue Marlin	1	Entire	1519	177.522	TP	0.519	5.379	145.000	0.123	0.196	0			
Blue Marlin	2	Entire	1110	177.522										
Blue Marlin	3	Entire	1903	290.491										

Species	ID	Section	Total points	Max step length (m)	Best fit distribution	Best fit exponent	Best fit Xmin	Best fit Xmax	TP / P GOF	Exp GOF	TP / P LLH	Exp LLH	TP / P wAIC	Exp wAIC
Blue Marlin	4	Entire	1302	215.179										
Blue Marlin	5	Entire	1688	107.589	TP	0.442	5.379	80.700	0.145	0.224	0			
Blue Marlin	6	Entire	2174	156.004	TP	0.971	5.379	123.700	0.145	0.152	0			
Blue Marlin	7	Entire	2534	172.143	TP	0.768	5.379	86.100	0.142	0.176	0			
Blue Marlin	8	Entire	2985	209.799	TP	1.092	5.379	166.800	0.122	0.169	-4315	-4484	1.000	0.000
Blue Marlin	9	Entire	2468	129.107										
Blue Marlin	10	Entire	2117	172.143	TP	1.680	21.500	150.000	0.107	0.082	-1404	-1425	1.000	0.000
Blue Marlin	11	Entire	4128	204.42	E	0.027	5.380		0.17	0.133	-7166	-7052	0.000	1.000
Swordfish	1	Entire	1191	597	TP	0.908	5.379	597.100	0.107	0.178	0			
Swordfish	2	Entire	2035	962										
Swordfish	3	Entire	1429	624										
Swordfish	4	Entire	2650	1285	TP	1.223	5.379	1285.600	0.108	0.307	-7385	-8097	1.000	0.000
Ocean sunfish	1	Section 1	305100	145	TP	2.052	7.000	145.000	0.063	0.151	-891	-913	1.000	0.000
Ocean sunfish	1	Section 2	378000	185	TP	1.924	5.000	185.000	0.077	0.232	-675	-714	1.000	0.000
Big Eye Thresher	1	Entire	1440	473	TP	1.329	10.758	435.700	0.118	0.147	-2903	-3003	1.000	0.000
Big Eye Thresher	2	Entire	1492	457	TP	1.195	32.276	457.200	0.116	0.168	-2285	-2350	1.000	0.000
Blue Shark	1	Entire	819	381	E	0.013	5.380		0.126	0.102	-2207	-2201	0.000	1.000
Blue Shark	2	Entire	1211	387	E	0.017	5.380		0.166	0.180	-3488	-3417	0.000	1.000
Blue Shark	3	Entire	1541	387										
Blue Shark	4	Entire	2621	177	TP	0.458	5.379	161.300	0.14	0.205	0			
Blue Shark	5	Entire	2256	532	E	0.012	5.380		0.171	0.151	0			
Blue Shark	6	Entire	4133	430										
Blue Shark	7	Entire	846	333										
Blue Shark	8	Entire	1924	371										
Blue Shark	9	Section 1	29160	121										
Blue Shark	9	Section 2	25920	482	TP	1.886	9.000	167.000	0.063	0.217	-741	-765	1.000	0.000
Blue Shark	9	Section 3	70435	482	P	2.458	12.000		0.066	0.237	-1089	-1162	1.000	0.000
Blue Shark	10	Section 1	653040	122	TP	1.630	6.500	122.000	0.062	0.187	-4254	-4405	1.000	0.000
Blue Shark	10	Section 2	1900800	599	TP	2.190	11.000	599.000	0.038	0.242	-9949	-10696	1.000	0.000
Blue Shark	10	Section 3	864000	200	E	0.040	15.000		0.075	0.062	-1916	-1904	0.000	1.000
Blue Shark	10	Section 4	777600	545	TP	1.972	5.500	545.000	0.056	0.234	-6143	-6642	1.000	0.000
Blue Shark	10	Section 5	2125260	523	TP	1.993	7.500	523.000	0.049	0.206	-9326	-9949	1.000	0.000
Blue Shark	11	Entire	38090	87										
Blue Shark	12	Section 1	121403	132	E	0.047	12.500		0.069	0.055	-2645	-2630	0.000	1.000

Species	ID	Section	Total points	Max step length (m)	Best fit distribution	Best fit exponent	Best fit Xmin	Best fit Xmax	TP / P GOF	Exp GOF	TP / P LLH	Exp LLH	TP / P wAIC	Exp wAIC
Blue Shark	12	Section 2	98699	396	TP	2.316	8.500	396.000	0.054	0.173	-2455	-2563	1.000	0.000
Mako shark	1	Section 1	145	376	E	0.017	16.140		0.121	0.106	-333	-333	0.275	0.725
Mako shark	1	Section 2	1273	398	E	0.018	5.380		0.15	0.108	-4031	-3916	0.000	1.000
Mako shark	1	Section 3	865	338	E	0.021	5.380		0.176	0.129	-2319	-2257	0.000	1.000
Mako shark	1	Section 4	532	355	E	0.016	5.380		0.153	0.078	-1530	-1504	0.000	1.000
Porbeagle	1	Entire	2571721	38.5	E	0.172	7.500		0.079	0.080	-2012	-1951	0.000	1.000
Silky shark	1	Entire	2667	231	E	0.027	5.380		0.187	0.079	-7201	-7101	0.000	1.000
Silky shark	2	Entire	4272	193	E	0.055	21.520		0.229	0.137	-2975	-2839	0.000	1.000
Silky shark	3	Entire	1584	166.7	TP	2.030	16.138	156.000	0.181	0.102	-2217	-2256	1.000	0.000
White tip shark	1	Entire	3405	166	TP	1.839	21.520	129.110	0.12	0.114	-4480	-4546	1.000	0.000
Basking shark	1	Section 1	4784	62	TP	1.463	3.000	62.000	0.102	0.166	-935	-972	1.000	0.000
Basking shark	1	Section 2	4705	72										
Basking shark	2	Section 1	5715	66	TP	1.576	4.000	66.000	0.073	0.182	-3325	-3464	1.000	0.000
Basking shark	2	Section 2	25439	59	TP	1.750	4.000	59.000	0.063	0.137	-9715	-9832	1.000	0.000
Basking shark	2	Section 3	2880	80										
Basking shark	2	Section 4	11521	73	TP	1.379	7.000	73.000	0.134	0.178	-3224	-3338	1.000	0.000
Basking shark	3	Section 1	26770	160.5	TP	1.596	5.500	159.000	0.064	0.214	-7597	-8007	1.000	0.000
Basking shark	3	Section 2	27360	138.5										
Basking shark	3	Section 3	42120	161	TP	1.776	7.500	146.000	0.081	0.233	-9741	-10331	1.000	0.000
Basking shark	4	Section 1	51385	100										
Basking shark	4	Section 2	12960	182	E	0.030	14.000		0.121	0.104	-2933	-2891	0.000	1.000
Basking shark	4	Section 3	213892	168	TP	2.414	18.000	168.000	0.058	0.127	-12712	-12735	1.000	0.000
Basking shark	5	Section 1	43437	186										
Basking shark	5	Section 2	236425	72	E	0.107	32.000		0.244	0.244	-275	-206	0.000	1.000
Basking shark	6	Section 1	24258	112	TP	1.820	12.000	112.000	0.121	0.180	-4836	-4874	1.000	0.000
Basking shark	6	Section 2	17281	120	E	0.039	16.000		0.085	0.105	-2340	-2304	0.000	1.000
Basking shark	6	Section 3	5761	140										
Basking shark	6	Section 4	5761	132										
Basking shark	6	Section 5	11521	116										
Basking shark	6	Section 6	5224	156	TP	1.732	14.000	156.000	0.137	0.179	-405	-413	0.999	0.001
Whale shark	1	Section 1	1753	80	TP	2.023	5.379	59.200	0.368	0.264	-2529	-2610	1.000	0.000
Whale shark	1	Section 2	721	1285	E	0.012	5.380		0.135	0.012	0			
Whale shark	1	Section 3	4828	1285										

For a few sections where the estimated exponent for the truncated Pareto distribution was < 1 it was not possible to calculate the log-likelihood. When this occurred (in 8 sections), then the Akaike weights could not be calculated.

Table S4. Kolmogorov-Smirnov goodness of fit values, log-likelihoods and Akaike weights for key sections analysed and shown in figures (denoted in first column) or in the spatial analysis (Fig. 3 main paper). For explanation of model comparison values in table columns see legend to Table S3 and Supplementary Methods 1.4 for details.

Figure	Species	ID	Section	Best fit distribution	Best fit exponent	Best fit Xmin	Best fit Xmax	TP / P GOF	Exp GOF	TP / P LLH	Exp LLH	TP / P wAIC	Exp wAIC	Gamma GOF
3, S3, S4	Big eye tuna	1	Section 4	TP	2.213	9.0	1683.0	0.037	0.258	-2657	-2954	1.000	0.000	0.242
3, S6	Big eye tuna	2	Section 2	TP	2.189	19.0	334.0	0.032	0.166	-7097	-7332	1.000	0.000	0.105
S6	Big eye tuna	2	Section 3	TP	1.938	9.0	1601.0	0.029	0.262	-14885	-15925	1.000	0.000	0.196
S6	Big eye tuna	2	Section 4	E	0.018	53.0		0.069	0.040	-7217	-7120	0.000	1.000	
3, S6	Big eye tuna	2	Section 5	E	0.015	42.0		0.069	0.072	-20058	-19945	0.000	1.000	
S6	Big eye tuna	2	Section 6	TP	2.548	15.0	715.0	0.027	0.189	-12029	-12425	1.000	0.000	0.185
3, S6	Big eye tuna	2	Section 7	TP	1.988	10.0	529.0	0.028	0.185	-30064	-31204	1.000	0.000	0.136
	Big eye tuna	2	Section 8	TP	1.975	5.0	422.0	0.026	0.217	-36913	-39232	1.000	0.000	0.148
3, S3, S4	Big eye tuna	3	Section 3	E	0.102	2.0		0.158	0.022	-7228	-6801	0.000	1.000	
	Big eye tuna	5	Section 4	TP	2.155	13.0	1541.0	0.025	0.238	-25494	-27279	1.000	0.000	0.233
3, S3, S4	Yellowfin tuna	1	Section 1	E	0.037	4.0		0.109	0.073	-11286	-11136	0.000	1.000	
	Yellowfin tuna	1	Section 3	TP	1.610	5.0	286.0	0.043	0.175	-34348	-35298	1.000	0.000	0.144
3, S3, S4	Yellowfin tuna	1	Section 4	E	0.033	15.0		0.101	0.027	-16697	-16330	0.000	1.000	
	Yellowfin tuna	2	Section 1	TP	2.059	11.0	370.0	0.026	0.184	-19744	-20596	1.000	0.000	0.175
	Yellowfin tuna	2	Section 2	E	0.044	4.0		0.123	0.051	-110071	-107593	0.000	1.000	
	Yellowfin tuna	2	Section 3	E	0.037	8.0		0.107	0.045	-59448	-57663	0.000	1.000	
3, S3, S4	Yellowfin tuna	2	Section 5	E	0.027	4.0		0.143	0.022	-47195	-45065	0.000	1.000	
3, S3, S4	Yellowfin tuna	3	Section 3	TP	1.364	3.0	267.0	0.063	0.159	-118329	-121948	1.000	0.000	0.112
3, S3, S4	Yellowfin tuna	3	Section 4	TP	1.464	3.0	397.0	0.058	0.291	-48854	-54359	1.000	0.000	0.160
S3, S4	Yellowfin tuna	4	Section 4	TP	1.743	8.0	339.0	0.07	0.173	-5729	-5995	1.000	0.000	0.154
3, S3, S4	Yellowfin tuna	4	Section 5	TP	1.859	11.0	331.0	0.077	0.125	-8706	-8844	1.000	0.000	
3, S3, S4	Yellowfin tuna	5	Section 1	TP	1.505	7.0	275.0	0.088	0.268	-3208	-3377	1.000	0.000	0.203
	Yellowfin tuna	5	Section 3	TP	1.160	2.0	266.0	0.102	0.133	-8162	-8274	1.000	0.000	0.081
3, S3, S4	Yellowfin tuna	6	Entire	E	0.022	5.4		0.215	0.085	-2825	-2720	0.000	1.000	
S3, S4	Mola mola	1	Section 2	TP	1.924	5.0	185.0	0.077	0.232	-675	-714	1.000	0.000	0.173
1, 3, S3, S4	Blue Shark	9	Section 2	TP	1.886	9.0	167.0	0.063	0.217	-741	-765	1.000	0.000	0.185
2, S4	Blue Shark	9	Section 3	P	2.458	12.0		0.066	0.237	-1089	-1162	1.000	0.000	0.214
2, 3, S4	Blue Shark	10	Section 1	TP	1.630	6.5	122.0	0.062	0.187	-4254	-4405	1.000	0.000	0.157

Figure	Species	ID	Section	Best fit distribution	Best fit exponent	Best fit Xmin	Best fit Xmax	TP / P GOF	Exp GOF	TP / P LLH	Exp LLH	TP / P wAIC	Exp wAIC	Gamma GOF
2	Blue Shark	10	Section 2	TP	2.190	11.0	599.0	0.038	0.242	-9949	-10696	1.000	0.000	0.215
1, 2, 3, S4	Blue Shark	10	Section 3	E	0.040	15.0		0.075	0.062	-1916	-1904	0.000	1.000	
2, 3, S4	Blue Shark	10	Section 4	TP	1.972	5.5	545.0	0.056	0.234	-6143	-6642	1.000	0.000	0.182
3, S3, S4	Blue Shark	10	Section 5	TP	1.993	7.5	523.0	0.049	0.206	-9326	-9949	1.000	0.000	0.179
3, S3, S4	Blue Shark	12	Section 2	TP	2.316	8.5	396.0	0.054	0.173	-2455	-2563	1.000	0.000	0.180
S9	Silky shark	2	Entire	E	0.055	21.520		0.229	0.137	-2975	-2839	0.000	1.000	
S3,S4,S9	Silky shark	3	Entire	TP	2.030	16.138	156.000	0.181	0.102	-2217	-2256	1.000	0.000	0.160

Foraging success of biological Lévy flights recorded in situ

Nicolas E. Humphries[a,b], Henri Weimerskirch[c], Nuno Queiroz[a,d], Emily J. Southall[a], and David W. Sims[a,e,f,1]

[a]Marine Biological Association of the United Kingdom, The Laboratory, Citadel Hill, Plymouth PL1 2PB, United Kingdom; [b]School of Marine Science and Engineering, Marine Institute, University of Plymouth, Drake Circus, Plymouth PL4 8AA, United Kingdom; [c]Centre d'Études Biologiques de Chizé, Centre National de la Recherche Scientifique, 79360 Villiers en Bois, France; [d]CIBIO-Universidade do Porto, Centro de Investigação em Biodiversidade e Recursos Genéticos, Campus Agrário de Vairão, Rua Padre Armando Quintas, 4485-668 Vairão, Portugal; [e]Ocean and Earth Science, National Oceanography Centre, University of Southampton, Waterfront Campus, European Way, Southampton SO14 3ZH, United Kingdom; and [f]Centre for Biological Sciences, Building 85, University of Southampton, Highfield Campus, Southampton SO17 1BJ, United Kingdom

It is an open question how animals find food in dynamic natural environments where they possess little or no knowledge of where resources are located. Foraging theory predicts that in environments with sparsely distributed target resources, where forager knowledge about resources' locations is incomplete, Lévy flight movements optimize the success of random searches. However, the putative success of Lévy foraging has been demonstrated only in model simulations. Here, we use high-temporal-resolution Global Positioning System (GPS) tracking of wandering (*Diomedea exulans*) and black-browed albatrosses (*Thalassarche melanophrys*) with simultaneous recording of prey captures, to show that both species exhibit Lévy and Brownian movement patterns. We find that total prey masses captured by wandering albatrosses during Lévy movements exceed daily energy requirements by nearly four-fold, and approached yields by Brownian movements in other habitats. These results, together with our reanalysis of previously published albatross data, overturn the notion that albatrosses do not exhibit Lévy patterns during foraging, and demonstrate that Lévy flights of predators in dynamic natural environments present a beneficial alternative strategy to simple, spatially intensive behaviors. Our findings add support to the possibility that biological Lévy flight may have naturally evolved as a search strategy in response to sparse resources and scant information.

optimal foraging | organism | predator-prey | telemetry | evolution

Theoretically, in situations where animals possess limited or no information on the whereabouts of resources, a specialized random walk known as a Lévy flight can yield encounters with sparsely and randomly distributed targets (e.g., prey) more efficiently than random walks such as Brownian motion (1, 2), which are efficient where prey is abundant (3) and probably more predictable (4, 5). Lévy flight, in which movement displacements (steps) are drawn from a probability distribution with a power-law tail (a Pareto-Lévy distribution), describes a search pattern composed of many small-step 'walk clusters' interspersed by longer relocations. This pattern is repeated across all scales, such that $P(l) \sim l^{-\mu}$, with $1 < \mu \leq 3$ where l is the flight length (move-step-length), and μ the power-law exponent. Simple model simulations of Lévy search generally describe a forager moving along consecutive step lengths drawn from a power law distribution, such that when randomly and sparsely distributed prey is detected within a "sensory" field, the current step length is terminated, the prey is consumed and then a new random direction and step length are selected (3). These Lévy search-model simulations indicate an optimal exponent of $\mu \approx 2$ for the power-law move-step frequency distribution, leading to searches that increase the probability of a forager encountering new prey patches (1–3). In recent years, Lévy flight or Lévy walk patterns approaching the theoretically optimal value of $\mu \approx 2$ have been identified in movements of diverse organisms, from microbes to humans (1–6). Consequently, it has been proposed (1, 6) that because Lévy flights can optimize search efficiencies, natural selection should have led to adapta-

tions for Lévy flight foraging—the so-called Lévy flight foraging (LFF) hypothesis. Nevertheless, despite a burgeoning literature describing theoretical advantages of adopting Lévy flight search patterns (e.g., 1), and empirical evidence of such patterns among diverse organisms (1–6), the actual prey capture success of Lévy flights in the natural environment compared with other search patterns has not been demonstrated. Without this datum, it remains unclear how compelling the LFF hypothesis might be for explaining an adaptive basis for random search patterns in wild animals.

Lévy flight movement patterns in animals were first suggested for foraging ants (7) and identified in the activity patterns of *Drosophila* (8) reared in the laboratory. However, of singular importance was the first observation of theoretically optimal ($\mu \approx 2$) Lévy flight in the foraging movements of a free-ranging animal, the wandering albatross (9), which introduced the possibility that optimal Lévy strategies were widespread in nature. This possibility was then confirmed by numerous empirical studies (1, 6). Over the last few years, however, a significant number of these studies have been overturned (10–12) on account of the use of inappropriate statistical methods for identifying putative power-law behavior in move-step-length frequency distributions. The most significant overturning (12) was that of the original observation (9) of Lévy flights in wandering albatross, where long move steps were wrongly attributed to searching, and where the absence of power-law-distributed move steps in wandering albatross and other species cast some doubt (13, 14) on the strength of evidence for biological Lévy flights in general.

Recent, statistically robust, empirical studies have now identified Lévy flights in individual insects (8), jellyfish (15), sharks, tuna, billfish, turtles, and penguins (4, 5, 16), and in the population movement patterns of shearwaters (17). Interestingly, Lévy patterns did not occur at all times in marine predators (4, 5, 15); rather, their occurrence was dependent on environmental context—such as prey-sparse distributions—as predicted by theory (3). However, in none of the studies was the foraging success measured; such a measure represents the ultimate test of whether Lévy flight might represent an advantage to the forager. Given that albatrosses often forage on squid and fish prey they catch at the surface in highly heterogeneous habitats (18), it is reasonable to assume that a search strategy aimed at increasing the chance of encountering sparse prey, such as Lévy flight, may be present. Therefore, using appropriate datasets and robust statistical

APPLIED PHYSICAL SCIENCES

ECOLOGY

methods, we tested (*i*) whether Lévy flight search patterns were present in albatrosses, and (*ii*) whether Lévy flights do result in successful foraging trips compared with another strategy, such as a Brownian walk, as predicted by the LFF hypothesis.

Results and Discussion

High-temporal resolution GPS transmitters (19) that report an accurate geographical position approximately every 1 or 10 s were used to track the foraging movements of 27 *Diomedea exulans* and 61 *Thalassarche melanophrys* in the southern Indian Ocean during incubating or chick brooding periods (*SI Appendix, SI Materials and Methods*). The general pattern of foraging movements of the two species was different, with *T. melanophrys* concentrating searches closer to the shelf edge (Fig. 1 *A–C*), whereas trips of *D. exulans* were either mostly in neritic (shelf <2,000 m depth) or oceanic waters (>2,000 m) (Fig. 2 *A* and *B*). Individual foraging tracks showed a similar complex pattern at increasing scales that was reminiscent of the scale-invariant (fractal) patterns of Lévy flights (e.g., Fig. 1*A*). For a generalized searcher undertaking a Lévy walk, the turning points along the track are the points

Fig. 1. GPS trackings of albatross foraging indicate scale-invariant patterns. (*A*) GPS foraging track of a black-browed albatross (BBA46) off the Kerguelen Islands, Southern Indian Ocean, viewed across large (100 s km; *Left*) to small (10 s m; *Right*) scales showing similar patterns of trajectory complexity at all scales. Background color denotes bathymetry in m. Each red square denotes area covered by panel adjacent right. (*B*) Foraging track of a black-browed albatross (BBA33) with flight steps between landings best approximated by a truncated Lévy distribution ($\mu = 1.28$), with movements principally in deep shelf and oceanic habitats. Red square denotes area shown in (*C*). (*C*) Foraging track of BBA35, best approximated by an exponential distribution, was more spatially intensive in shelf and shelf edge habitats. Color denotes water depth, with bathymetric contours identifying neritic shelf waters <2,000 m and oceanic waters >2,000 m. (*D*) Time series profile of flight speeds of a GPS tracked black-browed albatross showing how landing locations and surface resting times were identified.
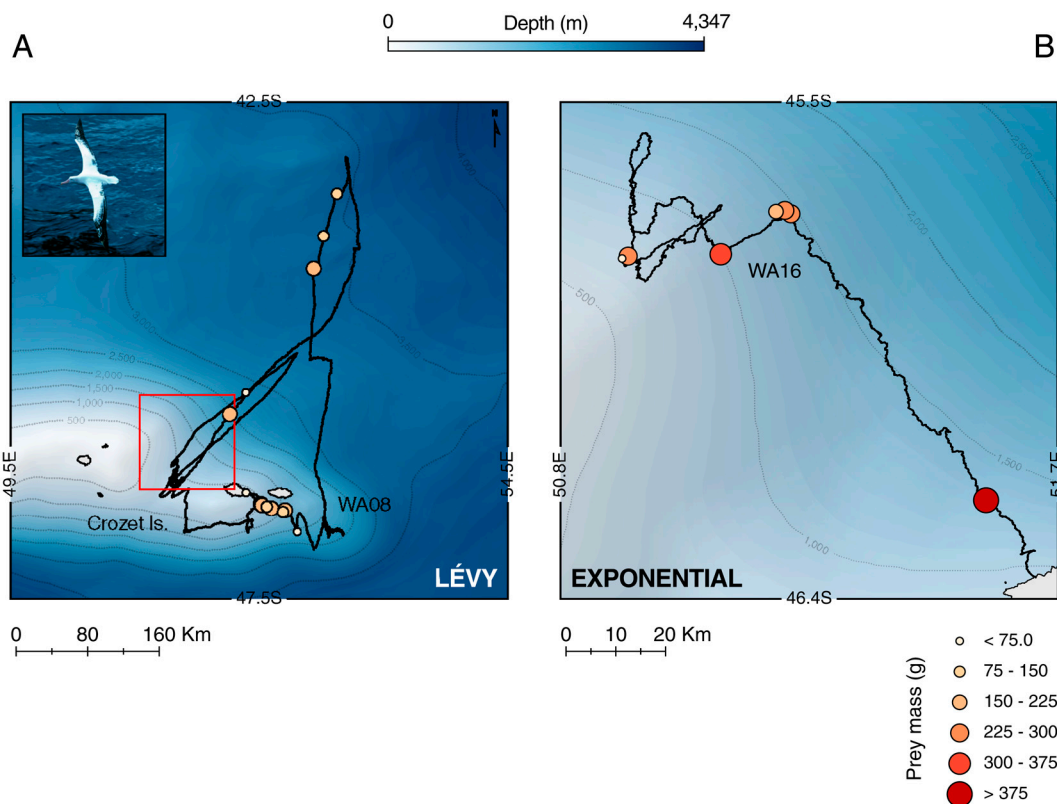
Humphries et al.

Fig. 2. Different types of wandering albatross GPS tracks and prey capture contrasts between Lévy and exponential patterns. (*A*) Foraging track, prey capture locations, and prey masses of wandering albatross WA08 during an 89 h foraging trip approximated by a Lévy pattern ($\mu = 1.25$) occurring principally over deep shelf edge (1,000–2,000 m) and oceanic waters (>2, 000 m). Captures totalled 3.5 kg, but prey were generally solitary and taken further apart, indicating prey sparse habitats. Red square denotes area shown in (*B*). (*B*) Foraging movements by wandering albatross WA16 during which it captured 1.8 kg of prey in 21.5 h when over shallow shelf (500–1,000 m) and shelf edge habitats during landings best described by an exponential distribution (Brownian pattern). Numerous prey items were often taken in a single landing, indicating a greater abundance of prey.

visited by a Lévy flight (20)—in our case, the sea-landing locations of albatrosses. Therefore, we calculated flight steps as the distances between consecutive landings on the sea surface for each individual albatross from each individual time series of flight speeds (Fig. 1*D*; *SI Appendix, SI Materials and Methods*) and calculated whether the truncated power law (Pareto-Lévy) (21) or exponential (Brownian) distributions best fit the observed data. Our purpose was not to test which was the best fit of all possible distributions, but rather to test whether Lévy flight or Brownian walk behavior was present (5).

Using Maximum Likelihood Estimation (MLE) for model parameter fitting and Akaike's Information Criteria weights (*w*AIC) for model selection (*SI Appendix, SI Materials and Methods*), we found strong support for individual bird movements approximating truncated Lévy flight (power law) and Brownian (exponential) search patterns in both black-browed and wandering albatrosses (Fig. 3 *A*–*D*; *SI Appendix, SI Results*). Lévy flights occurred in 22 (38%) individual *T. melanophrys* and 4 (15%) *D. exulans* (Figs. 1*B* and 2*A* and *SI Appendix,* Fig. S4), whereas exponential (Brownian type) movements were exhibited by 11 (18%) and 7 (26%) birds, respectively (Figs. 1*C*, 2*B*, and *SI Appendix,* Fig. S5). A significant proportion of trajectories (41% *T. melanophrys*; 59% *D. exulans*) were not fitted by either distribution and were of more complex form, which may represent tracks having both Lévy and Brownian features, as might be expected if similar time is spent by a bird in both shelf and oceanic habitats (see below). (*SI Appendix, SI Results,* Table S9, and Fig. S6). The lower proportion of Lévy best fits in the *D. exulans* data was likely due to the much lower number of landings per km (and therefore flight steps) for individual birds of this species compared to *T. melanophrys*, as more data points are required to iden-

tify power-law distributions clearly (11) (*SI Appendix, SI Results*). The μ values of truncated power-law fits were within the range of values consistent with the LFF hypothesis ($1 < \mu \leq 3$), but were lower than the theoretical optimum for nondestructive search ($\mu \approx 2$) where prey is distributed in revisitable patches and is only temporarily depleted (1). We calculated mean exponent values of 1.27 and 1.19 for black-browed and wandering albatrosses, respectively. These lower exponents are consistent with optimal Lévy flight search patterns ($\mu \to 1$) expected under the LFF hypothesis when encountered prey are consumed (destructive search) and not available to subsequent searches (nonrevisitable patches) (1, 4, 22); this predicts optimal searches when fewer prey are sparsely distributed (e.g., single prey; see prey capture results below in Table 1).

Clearly our results are at odds with the study of Edwards, et al. (12), which concluded, on the basis of analysis of a new high resolution dataset, that wandering albatrosses do not exhibit Lévy flight search patterns. To address these apparently conflicting results we reanalyzed the published data of Edwards, et al. (12), which comprised the times (as a proxy for distances) between consecutive landings during foraging trips of 20 wandering albatrosses fitted with wet/dry data loggers at Bird Island, South Georgia in 2004. The study pooled individual datasets and did not test for truncated power-law distributions in individual bird move-step data, so it was unclear whether individual birds exhibited Lévy flight patterns. Repeating the robust statistical methods described here with, first, the pooled data, we found better support for a truncated power-law best fit than for an exponential fit (*SI Appendix,* Table S13 and Fig. S11). This rather different result to that found by Edwards, et al. (12) can be attributed to Edwards et al. testing for a pure, rather than truncated power law (*SI Appendix, SI Results and Discussion*). Repeating the analysis

Fig. 3. Albatrosses exhibit truncated Lévy flight patterns of landing locations. Examples of MLE parameter fitting and *w*AIC model selection showing truncated Lévy best fits to GPS-flight-speed derived landing locations of black-browed (*A–C*) and wandering (*D*) albatrosses, and (*E–H*) for previously published (12) wet/dry logger-derived landing times of wandering albatross (*SI Appendix, SI Results*).

with individual bird data, we found strong support for Lévy flight search patterns, with the truncated Lévy distribution accounting for best fits in 45% of bird tracks analyzed and exponential best fits for only 15% (Fig. 3 *E–H*, *SI Appendix*, Figs. S11 and S12, *SI Results*). This significant difference highlights the extent to which the pooling of heterogeneous data can obscure individual movement patterns. The close agreement with results from our Crozet Island birds is interesting because the data of Edwards, et al. (12) were collected from South Georgia (South Atlantic Ocean) and with move steps between landings estimated by a different method to ours, which suggests that Lévy patterns may be widespread in this species.

A significant gap in our knowledge is whether Lévy flights actually confer the advantages to foragers that have been theorized (1). We were able to test whether Lévy flights yield sufficient prey gain compared with Brownian behavior—as expected under the LFF hypothesis—by using 11 GPS and 18 satellite-tracked wandering albatrosses fitted with stomach temperature loggers that recorded the timing and estimated mass of the prey captured (23–25). In contrast to GPS tracked individuals, whose time spent on water is measured from flight speed, landing locations of satellite-tracked birds were detected by a wet/dry logger attached to one of the bird's legs; the time between consecutive landings is shown to approximate the distance flown (*SI Appendix, SI Results*). Analysis showed that *D. exulans* with Lévy patterns landed a greater number of times during a foraging trip than Brownian foragers, although the number of prey captures per km flown was similar between Lévy and Brownian foragers, as was the total mass of prey consumed per trip (Table 1). Wandering albatrosses that showed statistically reliable approximations to a Lévy flight achieved net energy gains despite longer foraging trips further from the nest. We calculated that *D. exulans* showing Lévy behavior ingested an average of 1.46 kg of prey per day, which is sufficient to exceed daily energy requirements (26) by nearly fourfold (Table 1). Hence, Lévy flight search patterns by albatrosses represent a viable alternative strategy, compared with Brownian movements, for attaining net energy gain.

The apparent success of Lévy flights in albatrosses is consistent with expectations under the LFF hypothesis. Furthermore, an assumption of the hypothesis is that Lévy flight search is optimal where prey are sparsely and randomly distributed. Hence, we tested the corollary that greater heterogeneous resources are expected where birds exhibit Lévy flight patterns, whereas more homogeneous resources are expected where Brownian patterns are identified (4, 5). We tested for biological heterogeneity in black-browed albatross described as having Lévy ($n = 22$) or Brownian movement patterns ($n = 11$) by extracting time-referenced chlorophyll 'a' concentrations at landing locations as a proxy for resource availability in areas visited (*SI Appendix*, Fig. S10 *A* and *B*). During individual trips by *T. melanophrys*, concentrations of resources were significantly more variable for the Lévy pattern than for individuals exhibiting Brownian patterns, confirming the theoretical prediction of longer distances between abundant resources where Lévy behavior is observed (*SI Appendix*, Fig. S10 *C* and *D*). In addition, the sea-surface areas where *T. melanophrys* exhibited movements modeled by Lévy flights were located over significantly deeper water depths than those having Brownian patterns (*SI Appendix, SI Results*), which supports the prediction that Lévy flights may be more advantageous in oceanic waters ($>2,000$ m) or the deep shelf edge (1,500–2,000 m) where albatross prey are sparse, compared to the shallower shelf edge where resources are more abundant (24). To support this prediction, we found for *D. exulans* that Lévy patterns comprised landing locations in both neritic and oceanic zones, but that prey captures occurred mainly in shelf edge or oceanic habitats (72% of capture events; *SI Appendix*,

Table 1. Foraging performance of wandering albatrosses showing Lévy or Brownian movement patterns, means ($\pm$1 s.d.) for 13 birds

	No. landings	Distance flown (km)	Total prey mass captured (kg)*	Mass captured per landing (g)	Mass per capture (g)	Total mass per day (kg d^{-1})	Energy ingested per day (kJ kg^{-1} d^{-1})†	Factorial increase of ingested energy per day over daily energy requirements‡
Truncated Lévy ($n = 7$)	**34.6(13.8)**	1,151.9(660.9)	3.74(1.53)	97.9(37.7)	346.4(170.9)	1.46(0.86)	734.8(390.5)	3.68(2.49)
Exponential (Brownian) ($n = 6$)	**15.5(7.5)**	699.1(556.5)	4.18(2.37)	352.6(304.9)	296.1(126.8)	2.53(0.56)	1,364.8(491.0)	7.69(3.12)

Means in bold indicate significant difference between pattern types (truncated Lévy vs exponential): number of landings (*t*-test), $t = 3.01$, $p < 0.02$. All other comparisons not significant at $p = 0.05$.

*Prey capture data from stomach temperature loggers was available for six Lévy and four Brownian birds. Of the 10 birds, landing patterns for five of them (four Levy, one Brownian) were calculated from times between landings recorded by wet/dry loggers (24) rather than distances from GPS-derived landing locations (*SI Appendix*, Supporting Results 2.5).

†*D. exulans* feed mainly on squid. An energy value of Antarctic squid of 4.64 kJ g^{-1} wet weight was used (29).

‡Daily energy requirement of 157 kJ kg^{-1} d^{-1} was an average determined from heart rate telemetry during the brooding period and validated with indirect calorimetry of oxygen consumption (26).

SI Results) (Fig. 2*A*). Prey distribution in habitats visited appears sparse because prey capture during Lévy movements was typified by consumption of solitary, larger prey items that were further apart (lower intake per landing, with more unsuccessful landings), compared to Brownian patterns where numerous smaller items were ingested within a single landing in prey abundant areas (higher intake per landing) (Table 1) (Fig. 2*B*). For the majority of trackings where Brownian patterns described landings of *D. exulans*, prey captures were in more productive neritic waters (76%), although on occasion a high density prey patch was encountered in oceanic habitat, where multiple prey capture events occurred within a highly localized area (*SI Appendix, SI Results*), a finding predicted by the LFF hypothesis. Taken together, these results suggest Lévy patterns of both species occurred in prey-sparse and thus less resource-predictable habitats.

Our analyses of albatross foraging tracks indicate a significant proportion (31%) of Lévy flight patterns among 126 individuals from two species, overturning a principal conclusion of the study by Edwards, et al. (12). An important result in this study was that foraging albatrosses undertaking Lévy flight-modeled search patterns have comparatively high energy gains despite foraging in more heterogenic environments. Although several modeling studies demonstrate that Lévy searches confer foraging advantages in certain types of environment (for review see ref. 1), our study quantifies empirically the foraging success of biological Lévy flights in a free-ranging organism. We also found evidence that Lévy-flight modeled movements for both species were theoretically optimal and occurred in more prey-sparse habitat; such habitat dependence is predicted by the LFF hypothesis. It is possible that albatrosses exhibit movement patterns approximated by Lévy flights as a response to unpredictable habitat such as the oceanic environment, where prey are larger but also highly patchy in their distribution (24, 25). Similarly, albatross movements may emerge as Brownian motion when foraging in more predictable environments, such as shelf edges where prey availability is more likely to be concentrated. Thus, our results may explain the field observation that albatrosses show high site fidelity to more predictable shelf waters, but in the unpredictable oceanic habitat, rarely return to the same coarse scale sites (25). In addition to Lévy and Brownian patterns, we found evidence of more complex movements (*SI Appendix*, Tables S9, S12; Figs. S6, S9) that were perhaps a result of switching between behaviors during single trips by individual birds. Recent analyses of predatory marine fish (4, 5) have found similar links between Lévy patterns and habitats with sparsely distributed resource fields, including switching behavior by individuals, indicating that Lévy flight patterns may be a solution to the search problem for diverse animals occupying unpredictable environments.

A Lévy-flight specialized random walk is the most efficient behavior to find sparse, unpredictable prey patches when information is incomplete (1), that is, when local clues such as olfactory trails are absent. It is not unreasonable to assume that there are occasions when albatrosses and other predators will not have access to such clues, or where experience may not help, such as when they are in new or highly dynamic environments. Under such conditions, an innate movement process could account for the movement patterns we observed in albatrosses, and could apply more generally. Although there is no clear evidence of an innate Lévy process driving movements of vertebrates, experimental studies have shown that in featureless environments *Drosophila* activity patterns are well approximated by a Lévy flight (8, 27). Furthermore, *Drosophila* with silenced parts of the brain's mushroom body, or modified dopaminergic signaling—circuitry linked to decision-making—show disrupted activity patterning and behavioral burstiness, where burstiness is described as heavy-tailed distributions of move or pause times (28). Such evidence for neurophysiological pattern generation linked to decision-making behavior, taken together with our results showing Lévy movements of albatrosses can yield high energy gains in resource-sparse habitats, raises the question of whether an innate stochastic search process based on Lévy flight foraging has naturally evolved in organisms.

Materials and Methods

Study Animals. Animal-attached GPS tags provided time-stamped location datasets for 61 black-browed albatrosses (*Thalassarche melanophrys*) brooding chicks on Kerguelen Island (49.35 °S 70.22 °E) and 27 wandering albatrosses (*Diomedea exulans*) incubating or brooding chicks on Possession Island (46.40 °S 51.76 °E) in the Crozet Islands archipelago. Between 2002 and 2010, birds were equipped just before taking off for the sea with GPS loggers attached with adhesive tape on the back feathers; the total mass of devices (between 20 and 45 g according to the season and species) was far below the recommended 3% threshold. In addition, some wandering albatrosses were also induced to swallow stomach loggers recording temperature from which prey capture events are estimated. Details of deployment procedures and studies are given in *SI Appendix, SI Materials and Methods*.

Flight Profiles. Each individual bird time series of GPS locations was divided into 1 min intervals, and for each interval, an average speed was calculated. If the average speed of an interval was above the threshold flight speed of 10 km h^{-1} and 90% of the data points comprising the interval were also above the threshold, the interval was categorized as in-flight; otherwise it was categorized as at rest. A flight step was calculated for each series of contiguous in-flight intervals; all single interval (i.e., 1 min) flight steps were ignored. For each flight step the move-step-length was calculated as the great circle distance between the points of take-off and landing.

MLE Analysis and Model Selection. For each individual bird flight profile dataset (calculated as per above), parameters for exponential and truncated Pareto (TP) distributions were estimated using MLE and log-likelihoods (and Akaike weights) were calculated for both the fitted distribution (TP or exponential) and the paired competing distribution (exponential or TP). Where AIC favored the fitted TP over the competing exponential, but the fitted exponential was favored over the competing TP (which can arise because of the slightly different ranges of the dataset over which the distributions are fitted), an adjusted goodness of fit (GOF) value, based on the *KS*-D statistic, was used for model selection. Using AIC or GOF, datasets were categorized as (*i*) TP, where AIC supported TP and either AIC or GOF rejected the exponential, the exponent fell in the Lévy range ($1 < \mu \le 3$) and the fit spanned at least 1.5 orders of magnitude of the data range; (*ii*) exponential, where AIC or GOF supported exponential and AIC or GOF rejected the competing TP; or (*iii*) mixed-model, where none of the above applied or where the TP fit was supported by AIC/GOF but covered <1.5 orders of magnitude of the data range. See *SI Appendix, SI Methods and Results* for detailed descriptions.

1. Viswanathan GM, Luz MGE, Raposo EP, Stanley HE (2011) *The Physics of Foraging: An Introduction to Random Searches and Biological Encounters* (Cambridge University Press, New York).
2. Bartumeus F, Catalan J (2009) Optimal search behavior and classic foraging theory. *J Phys A-Math Theor* 42:1–12.
3. Viswanathan GM, et al. (1999) Optimizing the success of random searches. *Nature* 401:911–914.
4. Sims DW, Humphries NE, Russell WB, Bruce BD (2012) Lévy flight and Brownian search patterns of a free-ranging predator reflect different prey field characteristics. *J Anim Ecol* 81:432–442.

5. Humphries NE, et al. (2010) Environmental context explains Lévy and Brownian movement patterns of marine predators. *Nature* 465:1066–1069.

6. Viswanathan GM, Raposo EP, da Luz MGE (2008) Lévy flights and superdiffusion in the context of biological encounters and random searches. *Phys Life Rev* 5:133–150.

7. Shlesinger MF, Klafter J (1986) Lévy walks versus Lévy flights. *On Growth and Form*, eds H Stanley and N Ostrowsky (Kluwer, Dordrecht), pp 279–283.

8. Cole BJ (1995) Fractal time in animal behavior: the movement activity of *Drosophila*. *Anim Behav* 50:1317–1324.

9. Viswanathan GM, et al. (1996) Lévy flight search patterns of wandering albatrosses. *Nature* 381:413–415.

10. Edwards AM (2011) Overturning conclusions of Lévy flight movement patterns by fishing boats and foraging animals. *Ecology* 92:1247–1257.

11. Sims DW, Righton D, Pitchford JW (2007) Minimizing errors in identifying Lévy flight behavior of organisms. *J Anim Ecol* 76:222–229.

12. Edwards AM, et al. (2007) Revisiting Lévy flight search patterns of wandering albatrosses, bumblebees and deer. *Nature* 449:1044–1048.

13. Travis J (2007) Ecology: Do wandering albatrosses care about math? *Science* 318:742–743.

14. Buchanan M (2008) Ecological modelling: the mathematical mirror to animal nature. *Nature* 453:714–716.

15. Hays GC, et al. (2012) High activity and Lévy searches: jellyfish can search the water column like fish. *P Roy Soc B: Biol Sci* 279:465–473.

16. Sims DW, et al. (2008) Scaling laws of marine predator search behavior. *Nature* 451:1098–1102.

17. Bartumeus F, et al. (2010) Fishery discards impact on seabird movement patterns at regional scales. *Curr Biol* 20:215–222.

18. Weimerskirch H (2007) Are seabirds foraging for unpredictable resources? *Deep-Sea Res Pt II* 54:211–223.

19. Weimerskirch H, et al. (2002) GPS tracking of foraging albatrosses. *Science* 295:1259.

20. Shlesinger MF, Zaslavsky GM, Klafter J (1993) Strange kinetics. *Nature* 363:31–37.

21. Mantegna RN, Stanley HE (1994) Stochastic process with ultraslow convergence to a gaussian: the truncated Lévy flight. *Phys Rev Lett* 73:2946–2949.

22. Santos MC, Raposo EP, Viswanathan GM, da Luz MGE (2004) Optimal random searches of revisitable targets: crossover from superdiffusive to ballistic random walks. *Europhys Lett* 67:734–740.

23. Weimerskirch H, Doncaster CP, Cuenotchaillet F (1994) Pelagic seabirds and the marine environment: foraging patterns of wandering albatrosses in relation to prey availability and distribution. *P Roy Soc B: Biol Sci* 255:91–97.

24. Weimerskirch H, Gault A, Cherel Y (2005) Prey distribution and patchiness: factors in foraging success and efficiency of wandering albatrosses. *Ecology* 86:2611–2622.

25. Weimerskirch H, Pinaud D, Pawlowski F, Bost CA (2007) Does prey capture induce area-restricted search? A fine-scale study using GPS in a marine predator, the wandering albatross. *Am Nat* 170:734–743.

26. Weimerskirch H, et al. (2002) Heart rate and energy expenditure of incubating wandering albatrosses: basal levels, natural variation, and the effects of human disturbance. *J Exp Biol* 205:475–483.

27. Maye A, Hsieh CH, Sugihara G, Brembs B (2007) Order in spontaneous behavior. *PLoS ONE* 2:e443.

28. Sorribes A, Armendariz BG, Lopez-Pigozzi D, Murga C, de Polavieja GG (2007) The origin of behavioral bursts in decision-making circuitry. *PLoS Comput Biol* 7:e10045.

29. Clarke A, Prince PA (1980) Chemical composition and calorific value of food fed to mollymauk chicks *Diomedea melanophris* and *Diomedea chrysostoma* at Bird-Island, South Georgia. *Ibis* 122:488–494.

Supporting Information for "Foraging success of biological Lévy flights recorded *in situ*"

Contents

1   Supporting Methods

2   Supporting Results and Discussion

3   Reanalysis of 2004 Albatross data

4   References

List of supporting tables

List of supporting figures

1 Supporting Methods

1.1 Study animals and tags

Global Positioning System (GPS) tags were used to collect movement data from 61 black browed (*Thalassarche melanophrys*) and 27 wandering albatross (*Diomedea exulans*). A summary of the original GPS datasets is given in Table S1. Eleven of these birds were also fitted with a stomach temperature logger. Details of deployment procedures for GPS tags and stomach temperature loggers (for determining the timing of prey capture and estimating prey mass ingested) are given in Weimerskirch *et al.* (1-3). For the prey capture study we also analysed 17 individual location time series of wandering albatross that were each fitted with an Argos satellite transmitter, a wet/dry logger on one leg and were induced to swallow a stomach temperature logger. Full details of procedures and studies are given in Weimerskirch *et al.* (4), the results of the MLE analysis of these 17 additional flight profiles are given in section 2.5 below.

1.2 Processing of GPS time series data

The data obtained from the GPS tags are a time series of geographic locations at intervals of between a few seconds to several minutes, depending on both tag configuration and the time taken for the tag to acquire sufficient satellites to compute a location. This high resolution data captures the complex swooping flight path performed by the bird as it soars over the wave crests (5). Our intention was to test whether the bird flight steps that link periods of rest on the water or possible feeding events follow either a Lévy or exponential distribution. An exponential distribution might be expected if the movement pattern was essentially Brownian, resulting from a Poisson process; a Lévy pattern could suggest an optimal foraging search pattern such as a Lévy flight (6), which would emerge from a bird conducting a Lévy walk since the turning points (landings for resting or feeding) in a Lévy walk are a Lévy flight (7). Alternatively, a Lévy (heavy-tailed) pattern could arise by random movements across a fractal distribution of prey patches (8-10). Because the tags did not include a salt water switch (wet/dry logger) we determined whether the bird was in flight or at rest from variations in flight speed. Periods of time spent resting on the sea surface and drifting with the current would have low speeds,

whereas flight speeds would be necessarily higher. We used a speed threshold of 10 km h^{-1} (11) above which the bird was most probably in flight and below which the bird was most likely at rest (or feeding) on the water. The first processing step converted the time series of locations into a series of movement steps using the Haversine equation to calculate great circle distances, from which, together with the time intervals, average speeds were calculated. The undulating form of the flight path results in sudden changes in speed and would produce a complex flight profile if each move step below the threshold were taken to be a rest step, and each step above the threshold as a flight step (Figure S1, upper grey plot). Therefore, the second processing step converted the movement steps into a flight profile, where unrealistically short periods of time, either at rest or in flight, were ignored. The time series was divided into one minute intervals and an average speed was computed for each interval (Figure S1, upper blue plot). If the speed was below the 10 km h^{-1} threshold then the interval was considered to be a rest interval. However, if more than 90% of the steps included in the interval had a speed above the threshold then the decision was reversed and the interval was set to be a flight interval. In the same way, intervals originally considered to be in flight because the average speed was above the threshold would be reversed and become rest intervals if 90% of the steps in the interval had speeds below the threshold. This reduces the bias associated with steps with unusually high or low speeds. Finally, to remove short-term transient changes in speed from the flight profile, any single rest or flight intervals were also ignored, as indicated by arrows in Figure S1. The resulting flight profile accurately captures the clear bimodal pattern of activity and rest indicated by the raw tag data (Figure S1, grey line) while removing the noise inherent in the bird's complex flight. From each flight profile (Figure S1, lower plot) the flight step lengths were calculated as the great circle distance from the start and end locations of flight steps using the Haversine equation. Additionally, for comparison, the total distance travelled (summed from individual step lengths) and the flight times were calculated. The data processing of GPS locations therefore generated three separate sets of data for each bird, representing three different aspects of the calculated flight profile, all of which are suitable for analysis using Maximum Likelihood Estimation (MLE): (1) move step lengths between consecutive landings, (2) total distance travelled between consecutive landings, and (3)

time between consecutive landings. After this flight profile analysis, three flight profiles comprised only two flight steps and were therefore discarded (BBA28, BBA36 and BBA56), leaving 85 flight profiles available for further analysis.

Table S1: Summary of the original GPS location data used to calculate the flight profiles.

BBA is black-browed and WA is wandering albatross.

Reference	Points	Elapsed Time (hours)	Length (m)	Min Step (m)	Max Step (m)	No of flight steps
BBA01	2638	47.83	640345	0.58	2677.48	41
BBA02	2528	46.25	935469	1.08	1992.37	37
BBA03	2432	46.64	752561	0.45	2354.88	41
BBA04	732	37.69	306117	3.72	10847.04	24
BBA05	1424	24.78	449560	0.89	1339.30	25
BBA06	1516	26.78	727512	1.40	2504.82	18
BBA07	4792	83.93	1425396	0.45	308381.90	70
BBA08	853	15.60	404979	0.45	2680.43	12
BBA09	2503	44.80	652106	0.50	1771.48	46
BBA10	2117	36.98	777877	1.77	2270.50	24
BBA11	3170	59.25	1167475	0.73	3911.72	77
BBA12	1392	24.98	534236	2.08	1884.21	49
BBA13	703	18.11	513686	4.80	12499.82	12
BBA14	2294	41.94	741684	0.45	2668.50	51
BBA15	3433	60.87	861308	0.45	2066.58	46
BBA16	3457	67.88	1407061	1.32	3516.70	97
BBA17	1311	24.00	434634	3.43	5656.79	15
BBA18	2512	46.49	810655	0.45	2889.89	54
BBA19	240	12.16	111097	0.89	2456.46	13
BBA20	565	33.19	543329	3.06	8530.54	16
BBA21	655	33.69	736786	1.32	5419.73	23
BBA22	1806	96.95	1477311	0.33	8464.50	52
BBA23	1663	87.35	1309014	0.33	11372.01	22
BBA24	1521	27.58	579787	0.78	2425.25	35
BBA25	14774	48.62	1566633	0.18	2451.97	29
BBA26	8690	28.53	1214995	0.36	3529.26	9
BBA27	15059	47.99	1245957	0.13	1037.72	19
BBA28	160	2.61	38018	0.63	21267.48	2
BBA29	16852	49.38	1508445	0.29	1060.35	32
BBA30	17106	50.81	1866018	0.11	7154.09	20
BBA31	9612	38.87	1000653	0.18	5467.32	20
BBA32	8567	30.28	835572	0.29	2754.65	11
BBA33	15535	48.01	1355576	0.22	1663.76	33
BBA34	11377	36.17	1237470	0.29	8207.48	17
BBA35	2744	8.76	235204	0.23	1122.48	7
BBA36	5680	22.64	917187	1.71	3974.96	2
BBA37	22450	69.68	2240907	0.18	2702.88	49
BBA38	8708	42.86	363093	0.13	715.15	33
BBA39	4904	19.99	527722	0.29	1705.60	7
BBA40	9471	34.55	823298	0.22	4456.25	9

Reference	Points	Elapsed Time (hours)	Length (m)	Min Step (m)	Max Step (m)	No of flight steps
BBA41	5224	21.98	511339	0.31	3483.31	14
BBA42	7496	27.63	810469	0.13	3090.90	18
BBA43	21833	66.11	2197770	0.13	22959.36	35
BBA44	12259	38.18	988215	0.18	14807.79	27
BBA45	14917	49.63	1305995	0.22	12442.33	36
BBA46	24158	79.80	1287188	0.07	3244.49	68
BBA47	13285	43.89	1867030	0.13	379082.90	30
BBA48	6440	21.44	301416	0.13	7796.18	8
BBA49	10485	35.43	1082602	0.11	11769.75	9
BBA50	1918	5.37	175063	0.53	601.17	6
BBA51	15706	56.66	791716	0.13	2355.02	16
BBA52	19543	69.02	1694744	0.13	7467.27	38
BBA53	7075	21.56	719796	0.18	2177.53	30
BBA54	12727	44.97	1293197	0.22	3698.27	26
BBA55	13599	44.68	1121769	0.07	3167.87	34
BBA56	570	2.14	90557	0.66	1696.93	2
BBA57	3550	10.25	402538	0.23	514.57	6
BBA58	10384	33.21	1242367	0.23	3031.86	17
BBA59	6056	22.60	547045	0.30	1832.12	35
BBA60	10451	32.40	1040653	0.31	1279.98	14
BBA61	3257	11.46	404602	0.49	1986.44	9
WA01	8609	18.70	427702	0.22	12839.40	14
WA02	6993	18.38	514517	0.08	32056.53	10
WA03	27734	37.48	1371064	0.11	11292.90	16
WA04	27423	43.38	1046134	0.23	105668.40	15
WA05	9887	30.74	1449278	0.34	906.95	9
WA06	22488	78.56	2531244	0.19	12147.15	34
WA07	7399	32.52	631939	0.19	1029.00	5
WA08	28672	89.26	2426064	0.14	17363.29	39
WA09	9629	29.19	967481	0.27	2033.50	9
WA10	13985	44.43	1395147	0.19	13507.16	15
WA11	7572	24.95	311985	0.14	1026.84	5
WA12	23566	72.77	2951930	0.08	29393.30	27
WA13	16350	48.79	1424881	0.15	1961.04	20
WA14	7212	31.40	897982	0.30	4382.00	7
WA15	7284	30.38	332189	0.19	3195.47	12
WA16	4602	21.53	350554	0.27	914.56	11
WA17	27696	90.39	3398509	0.11	3540.00	21
WA18	13777	52.35	1358927	0.11	1901.25	8
WA19	12224	41.97	1503415	0.27	1646.33	6
WA20	12881	41.31	757913	0.14	5110.63	14
WA21	31197	90.42	3994637	0.11	1206.78	40
WA22	23064	71.10	2046603	0.24	1800.14	42
WA23	29659	88.48	4718301	0.20	26374.45	27
WA24	30209	86.92	3287408	0.08	2666.38	18
WA25	23086	73.83	2476751	0.14	9196.77	23
WA26	24906	76.24	2212841	0.11	5116.33	17
WA27	2864	8.15	319635	0.30	1118.82	4

Figure S1. Flight speed profile of black-browed albatross 29 showing how flight and rest times were identified. Upper plot: Grey line shows flight speeds computed from the raw GPS tag data; blue line shows average speeds for one minute intervals; red reference line indicates the 10 km h^{-1} speed threshold. Lower plot shows the resulting flight profile comprising periods of flight (grey) or rest (white). Green arrows indicate intervals where the speed threshold decision has been overridden.

1.3   Maximum Likelihood Estimation (MLE) Analysis

In the following sections the term 'dataset' is used to refer to a set of move step lengths computed from a single flight profile of a bird, as described above. This term accurately reflects the nature of the data, which is simply a list of calculated step lengths and cannot correctly be termed a time series.

It is important to recognise that, regardless of the computations performed to determine the best fitting distribution, it is essential to select candidate distributions that are meaningful in terms of the hypothesis being tested. In this study, the hypothesis to be tested is the Lévy flight foraging hypothesis (LFF), where three distributions are most relevant: power law, exponential and truncated power law. Exponential distributions produce move step lengths with normal diffusion (i.e. Brownian movements), whereas power laws produce super-diffusive movements which have been shown previously to optimise encounter rates under conditions of sparse prey availability (12). Because natural movement data is inevitably bounded, pure power law fits are rare and therefore, in the first instance, only truncated power law and exponential distributions are of interest. Other distributions may well exist that provide better fits to the data, but these would not be consistent in terms of the hypothesis being tested and are therefore not considered further in this study. The methodology used here to determine the best fit

distribution is based on that described in Humphries *et al.* (13 Supplementary 1.4) with some additional refinements made here to improve robust model selection.

The Maximum Likelihood Estimation (MLE) methodology employed was that described by Clauset *et al.* (14) with, in this study, truncated Pareto (truncated power law) and exponential distributions being tested. Briefly, the appropriate MLE equation was used to derive an exponent with the initial x_{min} parameter set to the minimum value found in the dataset. A best fit dataset was generated with the estimated parameters and a Kolmogorov-Smirnov (KS) test was used to determine the goodness of fit (the KS D statistic). To determine the best fit value for the x_{min} parameter the calculation was repeated with increasing values for x_{min} taken from the dataset with the value that resulted in the best (lowest) KS-D statistic being retained as the best fit value. When fitting a truncated Pareto distribution the method was repeated to also derive a best fit value for the x_{max} parameter, so for the truncated Pareto distribution both the x_{min} and x_{max} parameters were fitted in the same way. There were two departures from the method as implemented in the programming code given in Clauset *et al.* (14). Firstly, once values for x_{min} and x_{max} had been derived, the dataset was reduced to include only values between those lower and upper bounds. The resulting dataset therefore contained only the step lengths fitting the proposed distribution and it was this that was used to produce plots of $\log_{10}$ rank *vs* $\log_{10}$ step-length; however, for purposes of clarity, the full set of observations were plotted so that the extent of the fit over the data range was evident. Secondly, rather than test all values in the dataset as possible candidates for x_{min} or x_{max}, the iterative search routine was halted once five consecutive worse fits had been found to avoid the problem of fitting to a very small sub-set of the data, a problem exacerbated by complex biological data and exponent estimation (see section 1.2 above). The aim of fitting the lower and upper bounds was to find the distribution that best fit most of the data, rather than select a small sub-set of the data that was a very good fit to a particular distribution.

The MLE analysis requires two equations for each distribution to be tested. One is the MLE equation for the distribution and is used to estimate the exponent. The other is a random number generator (RNG) and is used to generate best-fit datasets. Table S2 gives the equations that were used for each distribution. The power law MLE and the power-law and exponential RNG equations were obtained from Clauset *et al.* (14), the truncated Pareto MLE equation was from White *et al.* (15) and the truncated Pareto RNG was from Kagan (16). The MLE equation for the truncated Pareto distribution has no closed form solution and is therefore solved numerically by finding the value for â that minimises y in the equation:

$$y = \frac{\overline{-\ln x} - 1}{(-\hat{a} + 1)} + \frac{\left(x_{\max}^{-\hat{a}+1} \ln x_{\max} - x_{\min}^{-\hat{a}+1} \ln x_{\min}\right)}{\left(x_{\max}^{-\hat{a}+1} - x_{\min}^{-\hat{a}+1}\right)}$$

Table S2: The MLE and RNG equations used in the analysis.

	MLE equations
Power-law	$\hat{a} = 1 + n \left(\sum_{i=1}^{n} \ln \frac{x_i}{x_{\min}} \right)^{-1}$
Exponential	$\hat{a} = n \left(\sum_{i=1}^{n} (x_i - x_{\min}) \right)^{-1}$
Truncated Pareto	$\overline{\ln} x = \frac{-1}{(-\hat{a}+1)} + \frac{x_{\max}^{-\hat{a}+1} \ln x_{\max} - x_{\min}^{-\hat{a}+1} \ln x_{\min}}{x_{\max}^{-\hat{a}+1} - x_{\min}^{-\hat{a}+1}}$ See note below and text
	Random number equations (in all cases r represents a uniform random number in the interval (0,1)
Power-law	$x = x_{\min}(1 - r)^{-1/(a-1)}$
Exponential	$x = x_{\min} - \frac{1}{a} \ln(1 - r)$

Truncated Pareto	$$x = x_{\min}\left\{ r\left[1 - \left(\frac{x_{\max}}{x_{\min}}\right)^{1-a} \right] + \left(\frac{x_{\max}}{x_{\min}}\right)^{1-a} \right\}^{1/(1-a)}$$

Note: The MLE equation for the truncated Pareto distribution has no closed form solution (15) and must therefore be solved numerically (see text).

1.4   Model selection

To use Akaike Information Criteria weights (*w*AIC), or Akaike weights, as an objective model selection method it is necessary to compute log-likelihoods (LLH) for both of the competing distributions. In this study the competing distributions fitted to data were the exponential and the truncated Pareto (TP). The LLH equations for these distributions, respectively, are given as:

$$llhe = n(\ln \cdot \lambda + \lambda \cdot x_{\min}) - \left(\lambda \cdot \sum(x)\right)$$

$$llhTP = n \ln\left(\frac{\mu - 1}{\left(x_{\min}^{1-\mu}\right) - \left(x_{\max}^{1-\mu}\right)} \right) - \mu \cdot \sum \ln x$$

The methodology used to estimate the exponents and parameters of these two distributions frequently results in different $x_{\min}$ and $x_{\max}$ values, thus resulting in fitting the two distributions to different ranges of the original data. Consequently, it is not possible to compute separately comparable LLHs from the same fitted distributions. Here we address this by dividing the analysis into two stages, whereby LLHs and Akaike weights for both distributions are computed from each fitted dataset. First, we compute the LLH for the fitted TP distribution and using the same dataset (defined by the $x_{\min}$ and $x_{\max}$ parameters) compute the LLH for the competing exponential distribution fitted to that same data. From these LLHs we compute *w*AIC, which can be compared in the usual way to perform the first stage in model selection (17). The result of this first stage might be that the TP distribution is favoured over the competing exponential distribution *for that range of the data*. The second stage tests this more completely by repeating the calculations for the reverse scenario: for this we calculated   the best fit exponential distribution to the original data, then proceeded to fit the competing TP distribution to

that data range over which the exponential was best fitted. This provides a second comparison of wAIC that can be used confidently to rule out the exponential distribution if it was not selected over the TP distribution during the first or second stages. Therefore, using this two stage method we only consider a dataset to be fitted by the TP distribution if wAIC favours the fitted TP over the competing exponential (stage 1), and favours the competing TP over the fitted exponential (stage 2).

This method suffices when the results of the wAIC analysis are unambiguous for stages 1 and 2. However, because the distributions can be fitted to slightly different ranges of the data it is possible for the wAIC results to conflict, whereby the TP fitting favours the competing exponential and *vice versa*. To resolve these conflicts we used the goodness of fit of the two fitted distributions. Because the Kolmogorov-Smirnov test was used as part of the fitting process we made use of the D statistic as a measure of goodness of fit. There is a requirement to select the distribution that not only fits the observations closely, but also which fits as much of a dataset (for a single bird) as possible. For example, a distribution that is a very good fit but to only 10% of the data set (and might as a consequence have a low D-statistic) should be rejected in favour of a distribution with a slightly worse D statistic (i.e. higher), but which fits significantly more of the dataset. Therefore, in this study the GOF was adjusted to account for how much of the original dataset was fitted by the distribution, using the equation $D_{adj} = D * (\log(\text{Total Steps}) / \log(\text{Fitted Steps}))$ where D is the KS-D statistic. Taking the log of total and fitted steps serves to reduce the impact of a difference of just a few points. If the fit is to the entire dataset then the result is D; hence, the less of the data fitted by the best fit distribution the poorer (larger) the resulting GOF value becomes. Adjusting the D statistic in this way allows a better comparison between distributions fitted to different ranges of the dataset.

The decision process we used in this study is summarised in Table S3. For datasets where the wAIC decision is to be classed as a best fit TP, there are the additional requirements that the estimated exponent μ falls within the Lévy range ($1 < \mu \leq 3$), and that the range of data fitted (i.e. $x_{max} - x_{min}$) should span at least 1.5 orders of magnitude. Candidate TP datasets that fail these requirements are assigned to the Mixed-model

category since it is assumed that such data may represent more complex behaviour patterns, e.g. a mixture of Lévy and Brownian strategies.

Table S3: The simple "truth-table" used to perform model selection.

TP denotes a truncated Pareto-Lévy distribution.

wAIC values				Result
Fitted TP	Competing exponential	Fitted exponential	Competing TP	
1	0	0	1	TP
0	1	1	0	Exponential
1	0	1	0	Resolve using GOF
0	1	0	1	Mixed-model

The decision process used for model selection is given in detail in Figure S2 below, and the decisions are further explained as follows:

A. Does wAIC support the fitted TP over the alternate exponential?

B. Does wAIC support the fitted exponential over the alternate TP?

C. Does the adjusted GOF support exponential over TP?

D. Does wAIC reject the fitted exponential in favour of the alternate TP?

E. Does the adjusted GOF reject exponential in favour of TP?

F. Is the TP exponent in the range 1.0 to 3.0?

G. Does the fitted TP range (i.e. x_{min} to x_{max}) span at least 1.5 orders of magnitude?
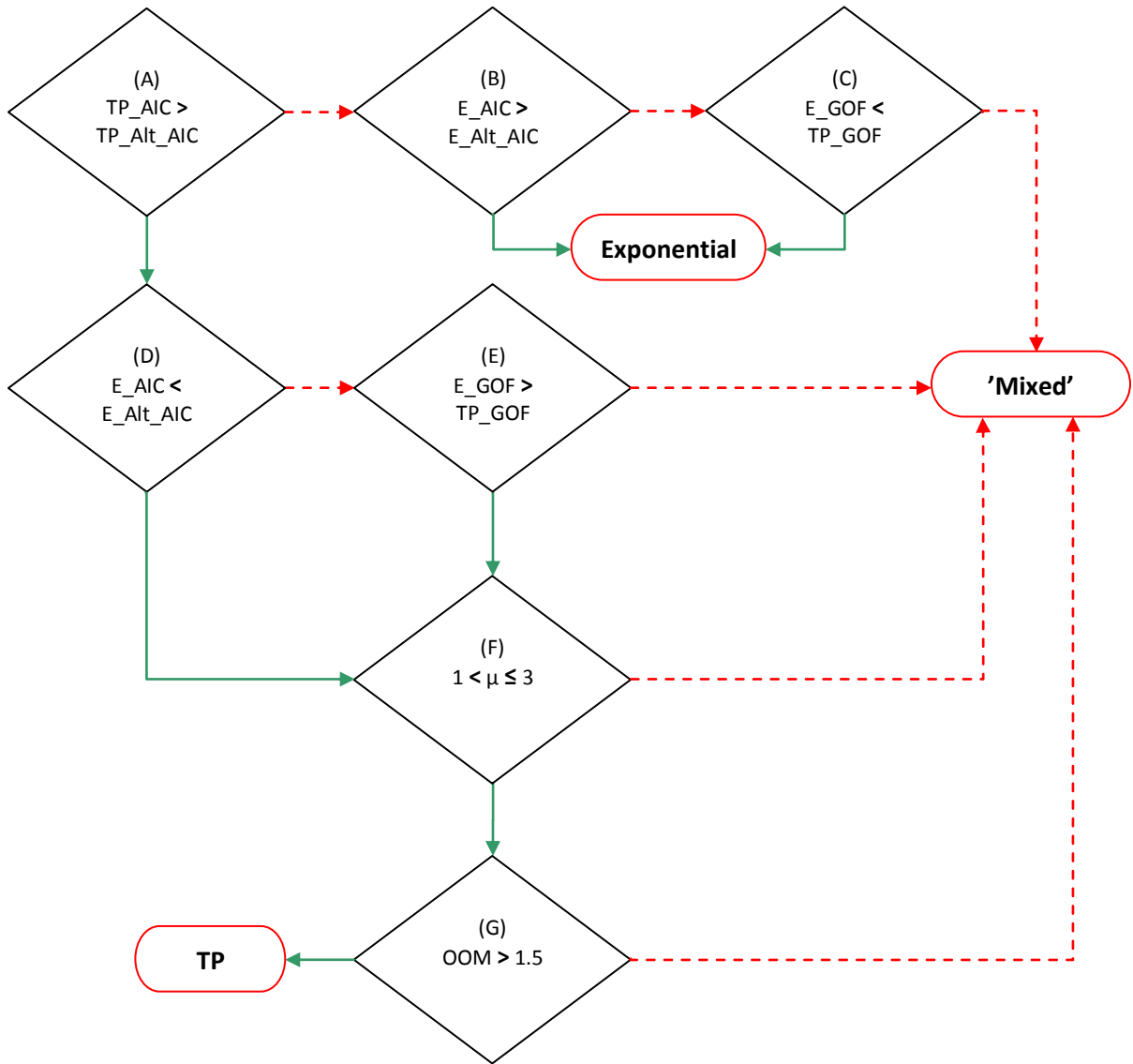
Figure S2. The decision process used for model selection. The process begins at question (A) with green lines being followed for positive responses and red dashed lines for negative responses. A truncated power law (TP) fit is only concluded when there is considerable certainty that it is the correct conclusion. OOM signifies orders of magnitude.

The outcome of this model selection process was that each dataset was sorted into one of the three categories (TP, exponential or mixed-model) based on Akaike weights, a valid Lévy exponent and a sufficient range of fit in terms of the orders of magnitude over which data was fitted. Thus, all the criteria must be met and there must be unequivocal support from AIC weights for an individual bird dataset to be placed in the TP category,

and hence being considered as consistent with the LFF hypothesis. This methodology is appropriately robust because model selection is strict and entirely objective. Nevertheless, this process did not remove the need to perform a final check by scrutinising the model fits to the data on ranked step length plots (e.g. Figure S3). This final visual check is important because Akaike weights do not confirm the goodness of fit, but merely help to decide which of the competing distributions is least bad. Thus, it is entirely feasible for both distributions to have very poor fits to the underlying observations but wAIC will still select one poor model fit over another slightly worse fit. The model fitting and selection methodology used in this study can be applied to any appropriate data and with any suitably relevant distributions. As such it may have wider applicability, particularly in the study of movement data where a conceptual framework already exists in terms of the LFF hypothesis and other movement models (18, 19).

1.5   Model selection validation

The model selection methodology described in 1.1 above was validated using simulations to determine whether the method was sufficiently accurate in assigning known move distributions to their correct category. Simulated datasets were generated comprising 50 move steps drawn from a truncated Pareto (TP) distribution, or 50 move steps from an exponential distribution, or 100 steps comprising a 50:50 mixture of both; 100 datasets being generated in each case giving 300 datasets for analysis. If the model selection methodology is robust and accurate for identifying truncated Lévy walks when present, our expectation from this validation is that TP distributions will be unambiguously identified as TP and not erroneously identified as having been drawn from an exponential distribution. The results of the validation analysis are shown in Table S4. It is evident that none of the pure truncated Pareto distribution (TP) datasets were wrongly assigned as exponential, and none of the pure exponential datasets were wrongly assigned as TP. Although a large percentage of the TP and exponential datasets were classified as mixed (59% and 65% respectively), we considered it to be more important to reduce the number of misclassifications at the cost of losing some datasets from further analysis. The majority of the mixed datasets were classified as mixed model (81%), as expected, with 18 datasets being classified as TP and only one as exponential. With the mixed data it is

probable that in some cases the TP move steps will be the predominant feature and in others the exponential. However, the presence of some longer steps in the TP distributions tends to rule out their classification as exponential.

The relatively low number of unambiguous classifications was attributed to the low number of steps in these datasets which is known to reduce the accuracy of the analysis as described above. To confirm this, we repeated the validation using datasets with 250 steps, the results of which are given in Table S5. It is clear from this further analysis that with more steps the percentage of correct model assignment increases, hence the accuracy becomes greater. We found, as before, that there were no incorrect identifications of either TP or exponential datasets, but increasing the move step number from 50 to 250 increased the correct identification of known TP datasets to 91% and exponential datasets to 84%.

Table S4: Results of the model selection validation tests with 50 steps.

	Resulting category		
Input Data	TP	Exponential	Mixed
TP	41	0	59
Exponential	0	35	65
Mixed	18	1	81

Table S5: Results of the model selection validation tests with 250 steps.

	Resulting category		
Input Data	TP	Exponential	Mixed
TP	91	0	8
Exponential	0	84	16
Mixed	14	1	86

2 Supporting Results and Discussion

2.1 MLE results

Detailed results from the MLE fitting procedure for the flight step lengths are given in Table S7 (truncated power law, TP, fits), Table S8 (exponential fits), Table S9 (mixed model fits). Of the 85 datasets available for analysis 26 were found to be best fit by the TP and 24 by the exponential distribution. The remaining 35 datasets produced model fits that could not be classed robustly as TP or exponential and were therefore classified as

'mixed model' according to the decision process described above. Of the TP model best fits to empirical data only four were wandering albatross (WA01, WA08, WA17 and WA22); species differences that might lead to this discrepancy are discussed in Supporting Results 2.3. Of the 18 exponential model best fits, 7 were wandering and 11 were black-browed albatross. There was a significant correlation between the number of steps (lengths between landings) in an individual bird dataset and the likelihood that the dataset will be fitted by either truncated power law (Pareto-Lévy) or exponential distributions (Mann-Whitney Rank Sum Test; T = 201.5, $p < 0.001$, n(small)= 18 n(large)= 26). Generally, smaller datasets were more likely to yield best model fits to the exponential distribution. This is illustrated by the box plot in Figure S3. It seems likely therefore that the low numbers of steps in the wandering albatross datasets may well explain why these gave principally exponential best fits since larger datasets will have a greater chance of containing longer step lengths, if they were exhibited by the albatrosses. Although this bias affects the results in terms of the number of individuals exhibiting movements approximated by TP and exponential distributions, it does not affect the test of the LFF conducted here, which is to determine whether albatrosses do indeed show movement patterns best approximated by a Lévy flight pattern.

The average number of points comprising datasets best fitted by the TP distribution was ~41 (n = 26; median = 38.5), yet all of the exponential fits were to datasets with fewer than 42 steps (maximum 29, mean ~15, median = 12.5, n = 18). While the numbers of steps available for this analysis are lower than has been considered ideal from simulation studies (see 20), we analysed individual albatross trajectories rather than pooling multiple individuals' step lengths, which occurs usually in an attempt to increase n number (for an example of pooling albatross step lengths see 21). The problem with pooling data from several individuals is that different patterns of movement by different individuals may emerge as a Lévy flight without any one individual displaying such a pattern (22). Although the datasets used here were of relatively low n number, they each described the movement pattern of an individual albatross and provided appropriate ranges of move step data spanning several orders of magnitude in some cases, which can counteract the effect of a lower number of steps. Hence, we found there were clear and reliable best fits

of the TP distribution to the albatross movement data. For example, BBA2 in Figure S3 provided 37 steps for analysis yet yielded a robust best fit to the TP distribution over 2.45 orders of magnitude in move step length.
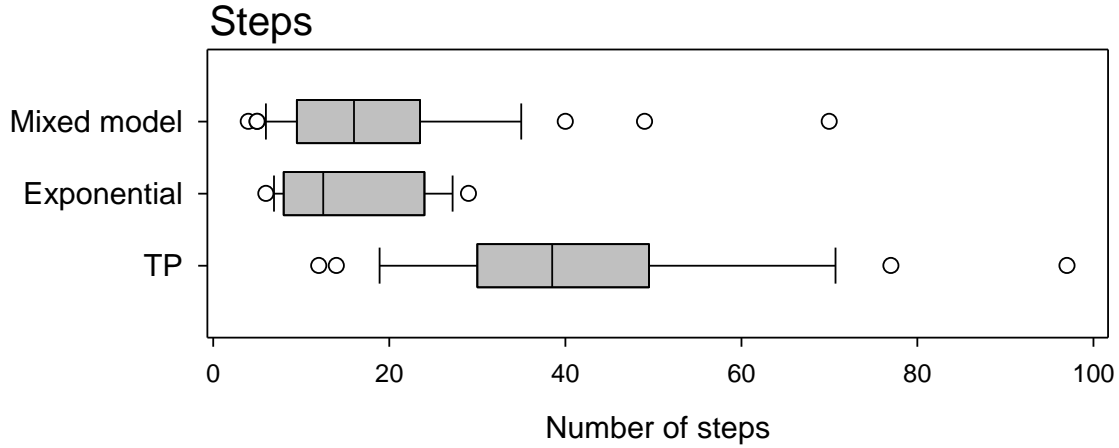
Figure S3. MLE Fitting correlations in flight step length data. Boxes show 25th to 75th percentiles; whiskers show the 10th and 90th percentiles. There is a statistically significant difference ($p < 0.001$) between the exponential and the TP groups.

2.2 Comparison of MLE results using steps, distances and times

The main focus of our analysis was on the step lengths calculated as great circle distances between the start and end of flights (straight line distances between consecutive landings), where the landings between flights are considered to be the turning points in a Lévy walk. Two other measures were calculated from the flight profile; cumulative distances were calculated as the sum of the individual steps comprising a flight, and times were calculated from the start and end times of each flight. For a direct comparison these datasets for each individual bird were analysed in the same way as the move steps. It was hypothesised that neither of these measures would provide as many best fits to a truncated power law (Pareto-Lévy) distribution because the distances include many complex movements associated with the bird's soaring flight, while the times do not take account of the variations in the bird's speed and so do not properly reflect the distance travelled. Table S6 shows a summary of the best fitting results for the three different data sets. As expected the distance and time measures produce slightly fewer TP best fits (25 and 23 respectively, compared to 26 for the step lengths). There were 39 datasets where the analysis results are the same for all data types (12 TP, 8 exponential and 19 mixed

model). Overall, therefore, it seems that distances and times between consecutive landings can be considered to be reasonable proxies for step length measurements used to test the LFF hypothesis, although it should be noted that not all Lévy patterns will be detected by these proxies.

Table S6. Summary of fitted distributions to the three different sets of data

Fitted distribution	Steps	Distances	Times
TP	26	25	23
Exponential	18	17	25
Mixed model	41	43	37

2.3 Species differences between black-browed and wandering albatross datasets

The MLE analysis of individual bird datasets for step lengths revealed clear species differences. Four of the 27 (15%) wandering albatross datasets were found to be best fitted by a TP distribution whereas 22 out of 61 black browed albatross datasets were fitted by the distribution (38%). Ten of the 24 exponential best fits were to wandering albatross movement datasets (42%), in addition to 14 of the 35 mixed model tracks (40%). One possibility for the species difference was that fewer TP best fits were found because the wandering albatross datasets comprised on average only about half the number of flight steps than black-browed albatross individual datasets (Mann-Whitney Rank Sum Test: BBA median = 24, $n = 58$; WA median = 15, $n = 27$, $p = 0.005$). This difference in number of landings estimated during wandering albatross GPS trackings has been shown to affect the likelihood of finding a good fit to a TP distribution (section 2.1 above). However, the difference in the number of flight steps suggests that the two species behave differently because the duration that wandering albatrosses were tracked for was similar to those of black-browed albatross tracks (Mann-Whitney Rank sum test: BBA median = 37.9 h, $n = 58$; WA median = 43.4 h, $n = 27$, $p = 0.137$). If their foraging behaviour or feeding event frequencies were similar it may be expected that both species might land with similar frequency if tracks were of similar duration. This interpretation is consistent with previous observations on the foraging behaviour of the two species (23-25).

18

From the flight profiles calculated here we find a mean landing rate of 0.75 h^{-1} for the black-browed and 0.34 h^{-1} for wandering albatrosses. While these figures are lower than those found by Waugh and Weimerskirch (26), where a figure of 1.35 flight steps h^{-1} was found for wandering albatross, it is still in general agreement with the observation that wandering albatrosses make fewer flight steps and spend more time on the water than other, smaller species. Clearly, the landing frequency will be dependent on the foraging environment and the availability of prey, with richer areas resulting in more frequent landings. This might indicate that the birds in this study were foraging in areas (or at times) of sparser prey availability than those studied by Waugh and Weimerskirch (26).

In the following tables Comp AICw refers to the competing distribution. In some cases (unusually high or low TP exponents) it is not possible to calculate log-likelihoods and in other cases (fewer than 5 fitted steps) it is not possible to calculate Akaike weights, values are therefore shown as --.

Table S7. Truncated Pareto (TP) fits for flight step distributions

Reference	Steps	Min Step	Max Step	Xmin	Exponent	Xmax	Exp AICw	Exp Comp AICw	TP AICw	TP Comp AICw	Exp Fit	TP Fit	Fitted steps	Orders of magnitude
BBA16	97	103	90018	344	1.35	65495	0.00	1.00	1.00	0.00	0.335	0.052	80	2.28
BBA11	77	61	75555	244	1.33	58867	0.09	0.91	1.00	0.00	0.171	0.062	67	2.38
BBA46	68	21	85913	323	1.30	47717	0.20	0.80	1.00	0.00	0.162	0.123	52	2.17
BBA18	54	30	87001	732	1.28	31986	0.18	0.82	1.00	0.00	0.171	0.051	42	1.64
BBA22	52	569	119532	728	1.34	119532	0.66	0.34	1.00	0.00	0.178	0.083	49	2.22
BBA14	51	19	131879	137	1.13	52015	0.01	0.99	1.00	0.00	0.309	0.067	46	2.58
BBA37	49	70	107824	129	1.26	33017	0.01	0.99	1.00	0.00	0.204	0.084	38	2.41
BBA09	46	178	73229	1938	1.44	70914	0.08	0.92	1.00	0.00	0.274	0.100	24	1.56
BBA15	46	56	75897	95	1.07	68676	0.07	0.93	1.00	0.00	0.159	0.122	42	2.86
WA22	42	119	94364	983	1.04	37622	0.04	0.96	0.96	0.04	0.246	0.097	33	1.58
BBA03	41	110	60098	469	1.29	15664	0.00	1.00	0.99	0.01	0.345	0.076	29	1.52
BBA01	41	25	126983	313	1.30	126983	0.69	0.31	1.00	0.00	0.161	0.129	33	2.61
WA08	39	364	265214	2104	1.25	265214	0.55	0.45	1.00	0.00	0.165	0.103	31	2.10
BBA52	38	40	158908	1321	1.31	158908	0.82	0.18	1.00	0.00	0.122	0.086	26	2.08
BBA02	37	216	151350	543	1.11	151350	0.00	1.00	1.00	0.00	0.298	0.130	32	2.45
BBA45	36	47	162559	233	1.28	140678	0.00	1.00	1.00	0.00	0.298	0.105	30	2.78
BBA59	35	51	123722	315	1.52	79569	0.00	1.00	1.00	0.00	0.534	0.080	27	2.40
BBA55	34	94	116256	972	1.46	116256	0.00	1.00	1.00	0.00	0.339	0.104	22	2.08
BBA33	33	59	106320	2539	1.28	106320	0.15	0.85	0.99	0.01	0.187	0.092	24	1.62
BBA47	30	174	376409	309	1.37	376409	0.00	1.00	1.00	0.00	0.552	0.109	28	3.09
BBA53	30	185	169608	267	1.46	19799	0.11	0.89	1.00	0.00	0.295	0.141	23	1.87
BBA54	26	430	147638	3853	1.03	147638	0.41	0.59	0.89	0.11	0.247	0.147	16	1.58
BBA05	25	121	110475	121	1.10	110475	0.91	0.09	1.00	0.00	0.236	0.084	24	2.96
WA17	21	3128	640030	12547	1.45	640030	0.66	0.34	1.00	0.00	0.264	0.117	18	1.71
WA01	14	83	57494	83	1.03	57494	0.00	0.00	1.00	0.00	0.476	0.158	13	2.84
BBA13	12	453	95362	1328	1.00	95362	0.17	0.83	0.83	0.17	0.251	0.126	9	1.86

Table S8. Exponential fits for flight step distributions

Reference	Steps	Min Step	Max Step	Xmin	Exponent	Exp AICw	Exp Comp AICw	TP AICw	TP Comp AICw	Exp Fit	TP Fit	Fitted steps	Orders of magnitude
BBA25	29	217	82855	606	6.46E-05	0.87	0.13	0.46	0.54	0.088	0.105	24	2.14
WA23	27	416	657713	7205	7.44E-06	0.78	0.22	1.00	0.00	0.110	0.123	20	1.96
WA12	27	545	442310	13758	1.08E-05	0.79	0.21	0.99	0.01	0.089	0.091	14	1.51
BBA44	27	139	70814	19547	6.79E-05	0.96	0.04	0.43	0.57	0.198	0.089	8	0.56
BBA21	23	838	79991	1447	4.73E-05	0.54	0.46	0.98	0.02	0.121	0.138	18	1.74
BBA30	20	706	227013	45408	2.57E-05	0.88	0.12	0.03	0.97	0.090	0.151	13	0.70
WA24	18	774	354412	42323	8.96E-06	0.64	0.36	0.02	0.98	0.173	0.174	13	0.92
BBA51	16	91	105091	91	5.13E-05	0.54	0.46	0.14	0.86	0.137	0.167	15	3.06
BBA19	13	348	21110	2299	2.04E-04	1.00	0.00	0.26	0.74	0.319	0.111	5	0.96
WA15	12	2707	52412	2707	7.66E-05	0.83	0.17	0.22	0.78	0.188	0.251	11	1.29
WA16	11	104	67625	104	6.65E-05	0.67	0.33	0.00	1.00	0.104	0.298	10	2.81
WA05	9	2471	402166	90015	9.81E-06	1.00	0.00	0.00	1.00	0.273	0.273	5	0.65
BBA49	9	666	191927	7010	1.81E-05	1.00	0.00	0.09	0.91	0.273	0.204	5	1.44
BBA48	8	765	43379	765	4.68E-05	0.76	0.24	0.02	0.98	0.305	0.193	7	1.75
WA18	8	387	441150	387	8.43E-06	0.76	0.24	0.03	0.97	0.153	0.193	7	3.06
BBA39	7	1379	43882	1379	5.07E-05	0.94	0.06	0.00	1.00	0.362	0.242	6	1.50
BBA35	7	756	9727	756	3.09E-04	0.99	0.01	0.01	0.99	0.181	0.181	6	1.11
BBA50	6	105	21844	105	1.34E-04	1.00	0.00	--	--	0.223	0.323	5	2.32

Table S9. Mixed model flight step distributions

Reference	Steps	Min Step	Max Step	Exp Xmin	Exp Exponent	TP Xmin	TP Exponent	TP Xmax	Exp AICw	Exp Comp AICw	TP AICw	TP Comp AICw	Exp Fit	TP Fit	TP Orders of magnitudes	Exp Orders of magnitudes
BBA07	70	92	43848	229	1.41E-04	225	0.91	21728	0.00	1.00	1.00	0.00	0.138	0.066	1.99	2.28
BBA12	49	52	70669	52	1.64E-04	237	1.87	3340	0.00	1.00	0.44	0.56	0.586	0.097	1.15	3.13
WA21	40	2386	348474	2386	1.78E-05	16910	1.73	348474	1.00	0.00	0.96	0.04	0.155	0.123	1.31	2.16
BBA43	35	35	91744	237	4.59E-05	35	0.78	91744	0.17	0.83	1.00	0.00	0.109	0.119	3.42	2.59
BBA24	35	136	52189	1058	6.33E-05	136	0.96	32329	0.10	0.90	1.00	0.00	0.148	0.070	2.38	1.69
WA06	34	144	242265	2331	2.01E-05	11679	1.05	146353	0.84	0.16	0.72	0.28	0.079	0.055	1.10	2.02
BBA38	33	92	35748	577	1.88E-04	420	1.16	11042	0.02	0.98	0.85	0.15	0.183	0.083	1.42	1.79

Reference	Steps	Min Step	Max Step	Exp Xmin	Exp Exponent	TP Xmin	TP Exponent	TP Xmax	Exp AICw	Exp Comp AICw	TP AICw	TP Comp AICw	Exp Fit	TP Fit	TP Orders of magnitudes	Exp Orders of magnitudes
BBA29	32	125	60158	680	5.26E-05	281	0.89	60158	0.04	0.96	1.00	0.00	0.136	0.102	2.33	1.95
BBA04	24	586	56878	586	1.30E-04	1350	1.15	13797	0.36	0.64	0.55	0.45	0.220	0.114	1.01	1.99
BBA10	24	260	119171	651	5.45E-05	260	0.80	12612	0.00	1.00	0.97	0.03	0.284	0.114	1.69	2.26
WA25	23	633	384623	22188	8.52E-06	10365	1.25	170763	0.49	0.51	0.48	0.52	0.210	0.105	1.22	1.24
BBA23	22	803	90633	803	3.51E-05	7288	1.28	86467	0.12	0.88	0.80	0.20	0.145	0.128	1.07	2.05
WA13	20	320	140636	320	2.19E-05	45090	0.77	140636	0.17	0.83	0.11	0.89	0.107	0.180	0.49	2.64
BBA31	20	49	95834	6537	2.33E-05	1661	0.93	95834	0.47	0.53	0.97	0.03	0.303	0.147	1.76	1.17
BBA27	19	544	60266	5073	4.59E-05	4339	4.00	8149	0.33	0.67	0.00	1.00	0.223	0.274	0.27	1.07
BBA42	18	488	62765	548	6.04E-05	1123	0.89	62765	0.21	0.79	0.73	0.27	0.130	0.142	1.75	2.06
BBA06	18	315	92777	5664	2.87E-05	3066	1.31	92131	0.44	0.56	0.89	0.11	0.292	0.194	1.48	1.21
BBA58	17	126	143584	21770	2.76E-05	126	0.92	143584	0.96	0.04	1.00	0.00	0.208	0.128	3.06	0.82
WA26	17	1174	417106	64834	1.15E-05	1174	0.75	97896	0.93	0.07	0.64	0.36	0.143	0.123	1.92	0.81
BBA34	17	252	130486	1572	3.19E-05	12155	1.75	123557	0.16	0.84	0.18	0.82	0.153	0.170	1.01	1.92
BBA20	16	1756	69325	1756	5.43E-05	9025	-0.18	17064	0.33	0.67	0.09	0.91	0.205	0.167	0.28	1.60
WA03	16	53	174220	180	1.35E-05	53	-0.34	205	0.00	1.00	0.25	0.75	0.361	0.204	0.59	2.99
WA10	15	1074	68428	1396	4.50E-05	1074	0.86	68428	0.22	0.78	0.90	0.10	0.162	0.073	1.80	1.69
BBA17	15	222	60606	222	6.39E-05	11773	3.29	33758	0.02	0.98	0.01	0.99	0.220	0.199	0.46	2.44
WA04	15	21	135047	135	2.30E-05	21	0.90	135047	0.01	0.99	1.00	0.00	0.205	0.147	3.81	3.00
WA20	14	477	71643	477	3.54E-05	12878	0.87	71643	0.27	0.73	0.30	0.70	0.158	0.115	0.75	2.18
BBA41	14	502	50948	502	8.82E-05	4922	1.39	50948	0.23	0.77	0.17	0.83	0.158	0.159	1.01	2.01
BBA60	14	1930	65805	1930	4.94E-05	8264	1.12	65805	0.41	0.59	0.26	0.74	0.158	0.229	0.90	1.53
BBA08	12	308	87517	3501	4.47E-05	308	0.90	87517	0.80	0.20	0.79	0.21	0.149	0.094	2.45	1.40
BBA32	11	957	104025	957	5.12E-05	957	0.81	31411	0.38	0.62	0.35	0.65	0.208	0.121	1.52	2.04
WA02	10	78	119567	78	3.13E-05	36728	2.61	119567	0.17	0.83	--	--	0.233	0.415	0.51	3.18
BBA61	9	646	65872	646	4.28E-05	646	0.87	49975	0.35	0.65	0.42	0.58	0.264	0.161	1.89	2.01
BBA40	9	406	85597	406	3.54E-05	47717	2.83	85597	0.37	0.63	--	--	0.264	0.667	0.25	2.32
BBA26	9	770	192692	770	1.32E-05	141268	4.15	192692	0.13	0.87	--	--	0.264	0.667	0.13	2.40
WA09	9	4739	158782	121526	7.75E-05	121526	718.22	121865	--	--	--	--	0.396	0.000	0.00	0.12
WA14	7	43280	106342	77463	8.97E-05	77463	108.67	78915	--	--	--	--	0.351	0.000	0.01	0.14
BBA57	6	3670	21990	3670	8.50E-05	11716	-2.45	21990	1.00	0.00	--	--	0.445	0.323	0.27	0.78
WA19	6	2795	343588	151222	1.34E-05	151222	2.34	343588	--	--	--	--	0.544	0.544	0.36	0.36
WA11	5	233	31330	233	1.00E-04	4444	1.98	31330	--	--	--	--	0.290	0.488	0.85	2.13
WA07	5	1336	147270	1336	1.38E-05	1336	0.76	147270	--	--	--	--	0.580	0.290	2.04	2.04

Reference	Steps	Min Step	Max Step	Exp Xmin	Exp Exponent	TP Xmin	TP Exponent	TP Xmax	Exp AICw	Exp Comp AICw	TP AICw	TP Comp AICw	Exp Fit	TP Fit	TP Orders of magnitudes	Exp Orders of magnitudes
WA27	4	17908	35046	28545	3.08E-04	28545	1.00	35046	--	--	--	--	1.000	1.000	0.09	0.09

2.4   Ranked step-length plots for black browed and wandering albatross data
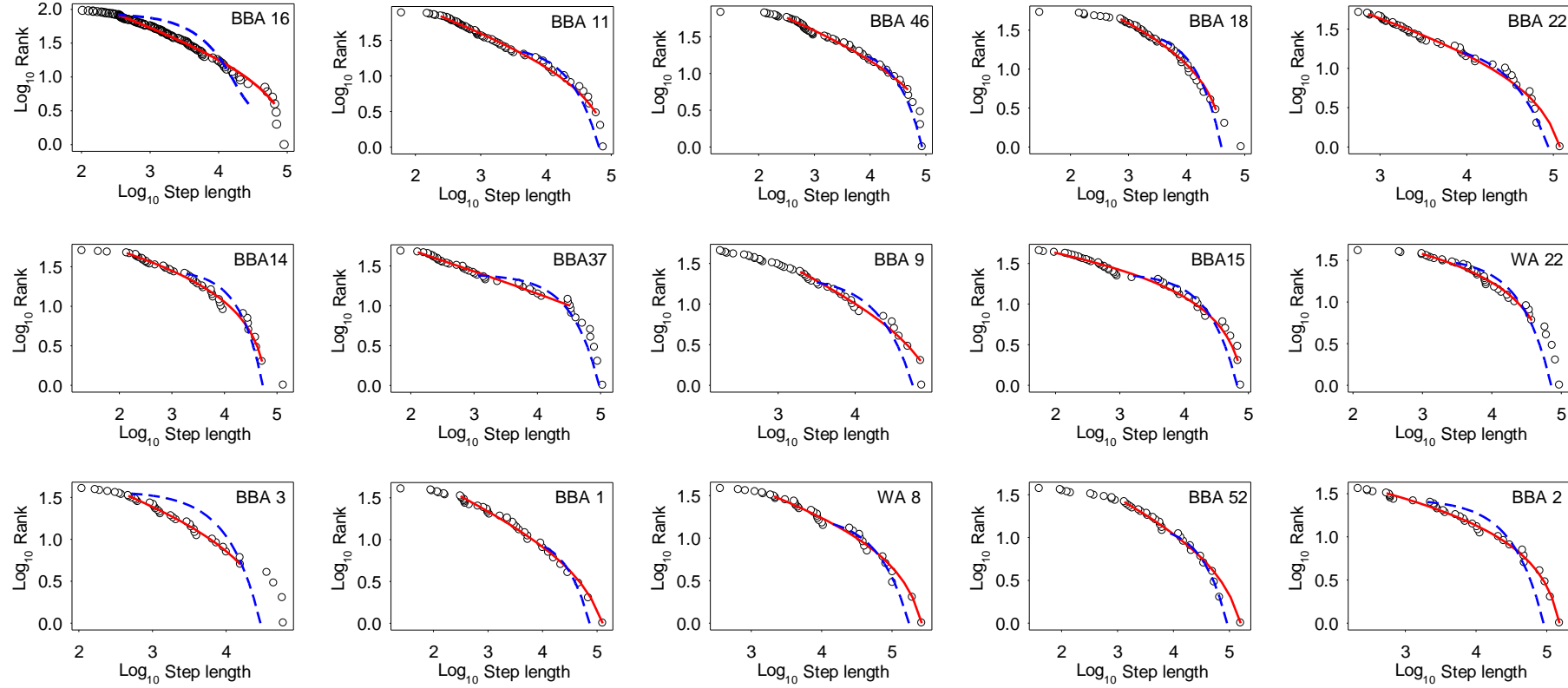

Figure S4. Ranked step length plots for best fits to TP distributions for albatross flight steps. Black circles are step lengths; red line is the best fit TP distribution; blue dashed line is the competing exponential distribution. Not including plots given in Figure 2a-d.
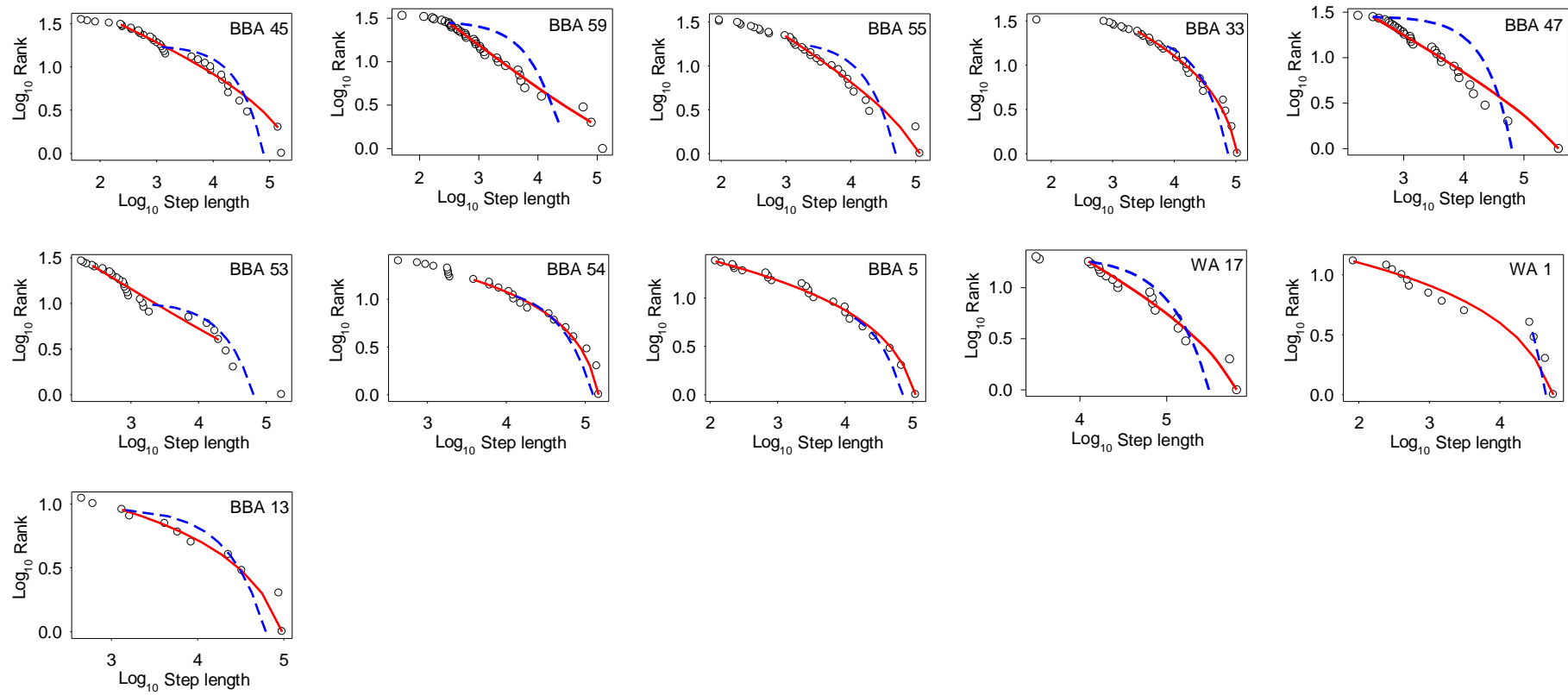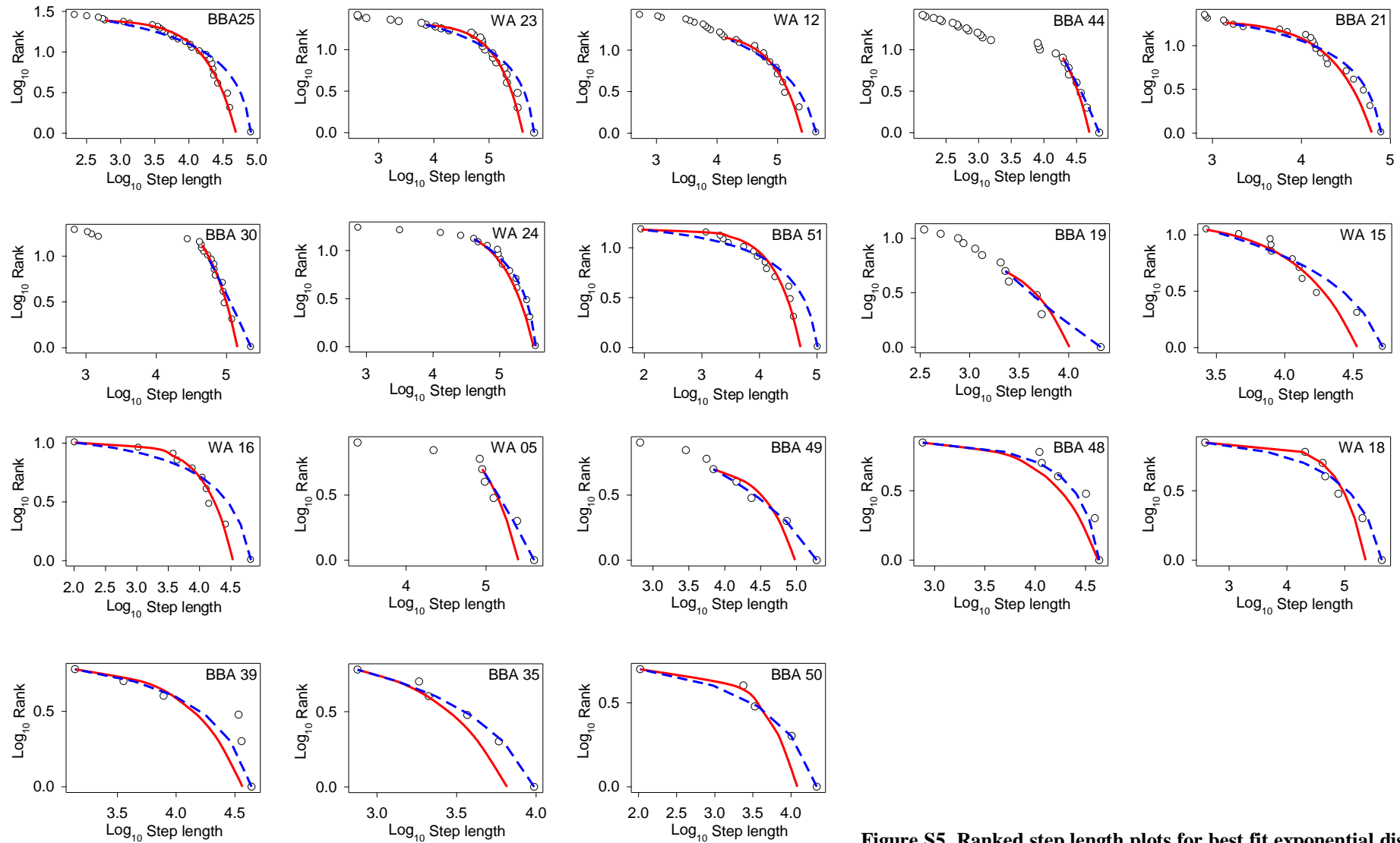
Figure S4 (Continued)

Figure S5. Ranked step length plots for best fit exponential distributions for albatross flight steps. Black circles are step lengths; red line is the competing exponential distribution; blue dashed line is the alternate TP distribution.
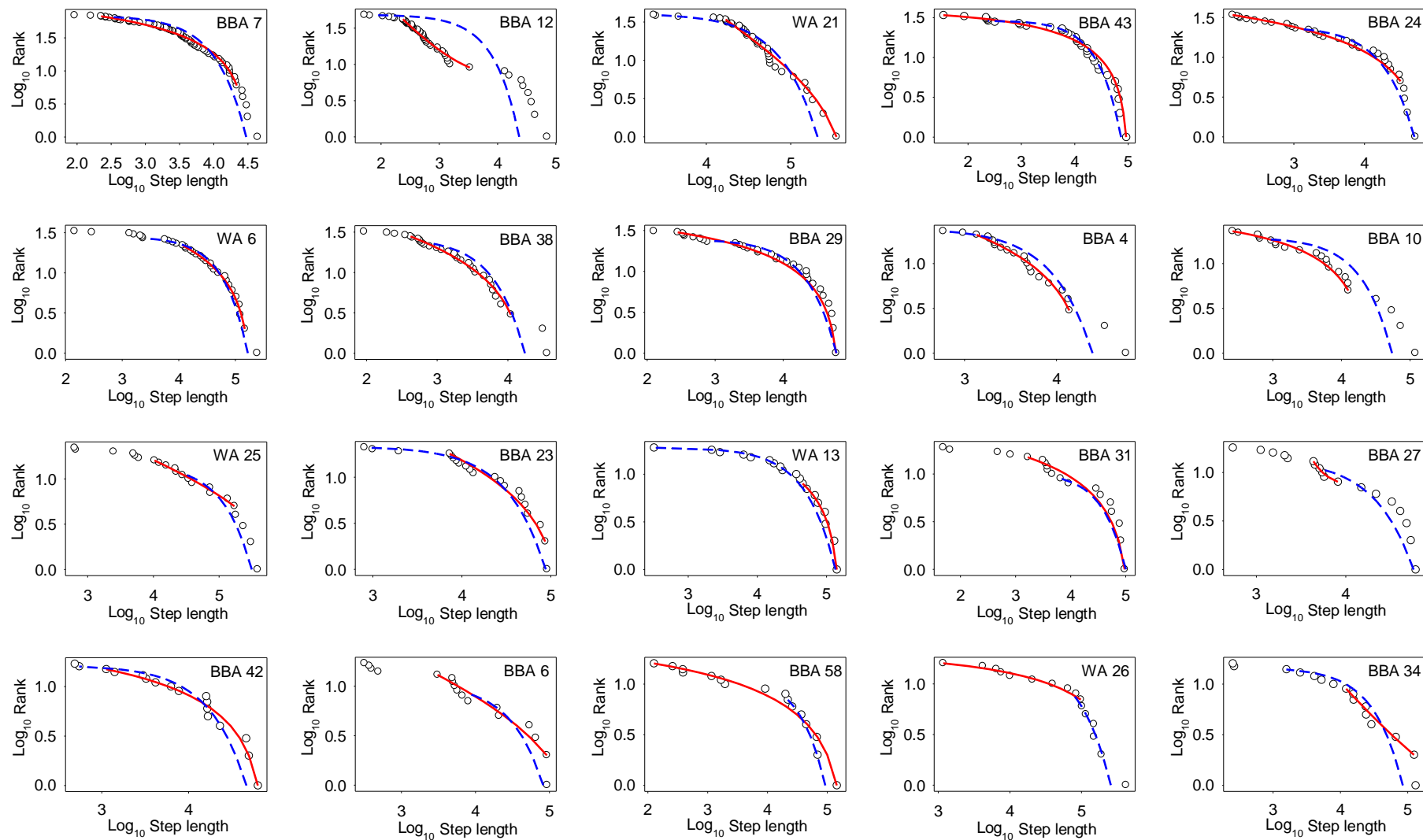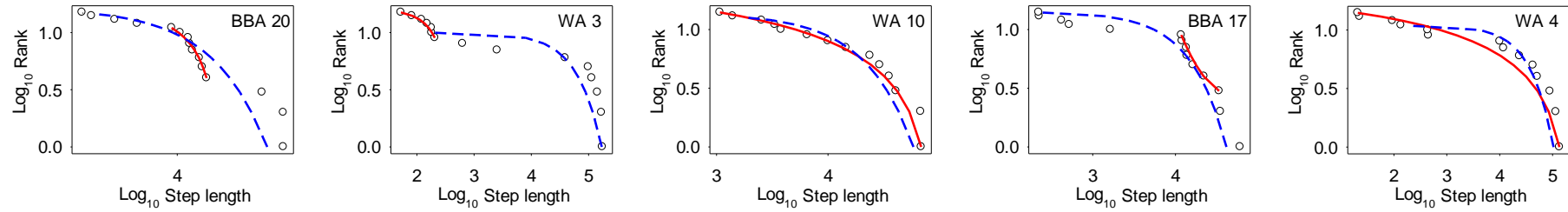
Figure S6. Ranked step length plots for mixed model fits for flight steps as determined by *w*AIC and GOF. Black circles are step lengths; red line is the best fit TP distribution; blue dashed lines are the best fit exponential distribution. Plots with fewer than 15 points not shown.

2.4 MLE Analysis of wet-dry logger data

To support the analysis of the prey capture patterns further data was obtained from 17 wandering albatrosses tagged in 1998, 1999 and 2001. Landing times of these birds were known as they had been fitted with wet-dry loggers as well as stomach temperature loggers. Flight times were analysed using the same MLE and model selection methodology used for the other birds in this study. The results of the analysis are given below.

Table S10: Truncated Pareto (TP) fits for flight step distributions

Reference	Steps	Min Step	Max Step	Xmin	Exponent	Xmax	Exp AICw	Exp Comp AICw	TP AICw	TP Comp AICw	Exp Fit	TP Fit	Fitted steps	Orders of magnitude
WA39	53	424	207885	424	1.05	94120	0.60	0.40	1.00	0.00	0.142	0.061	50	2.35
WA40	47	281	287843	4597	1.16	196604	0.64	0.36	0.99	0.01	0.107	0.060	36	1.63
WA45	36	113	126514	135	1.11	53049	0.03	0.97	1.00	0.00	0.224	0.094	24	2.59
WA41	28	187	236327	187	1.03	236327	0.71	0.29	1.00	0.00	0.289	0.175	24	3.10

Table S11: Exponential fits for flight step distributions

Reference	Steps	Min Step	Max Step	Xmin	Exponent	Exp AICw	Exp Comp AICw	TP AICw	TP Comp AICw	Exp Fit	TP Fit	Fitted steps	Orders of magnitude
WA38	21	312	69387	312	5.13E-05	0.65	0.35	0.63	0.37	0.152	0.225	20	2.35

Table S12: Mixed model flight step distributions

Reference	Steps	Min Step	Max Step	Exp Xmin	Exp Exponent	TP Xmin	TP Exponent	TP Xmax	Exp AICw	Exp Comp AICw	TP AICw	TP Comp AICw	Exp Fit	TP Fit	TP Orders of magnitude	Exp Orders of magnitude
WA34	35	115	190528	125	2.27E-05	115	0.78	190528	0.00	1.00	1.00	0.00	0.134	0.128	3.22	3.18
WA43	30	76	262529	114	1.21E-05	43832	1.44	229857	0.40	0.60	0.44	0.56	0.109	0.167	0.72	3.36
WA31	30	10	191508	68	2.50E-05	2197	0.71	113910	0.03	0.97	0.90	0.10	0.146	0.134	1.71	3.45
WA37	30	57	173184	2946	2.64E-05	115	0.95	173184	0.33	0.67	1.00	0.00	0.141	0.080	3.18	1.77
WA30	22	177	80188	883	3.34E-05	177	1.34	1060	--	--	0.24	0.76	0.557	0.251	0.78	1.96
WA44	21	358	267037	2366	1.23E-05	358	0.92	267037	0.25	0.75	1.00	0.00	0.165	0.102	2.87	2.05
WA32	19	775	176911	6821	1.82E-05	6821	1.16	160244	0.24	0.76	0.59	0.41	0.223	0.128	1.37	1.41

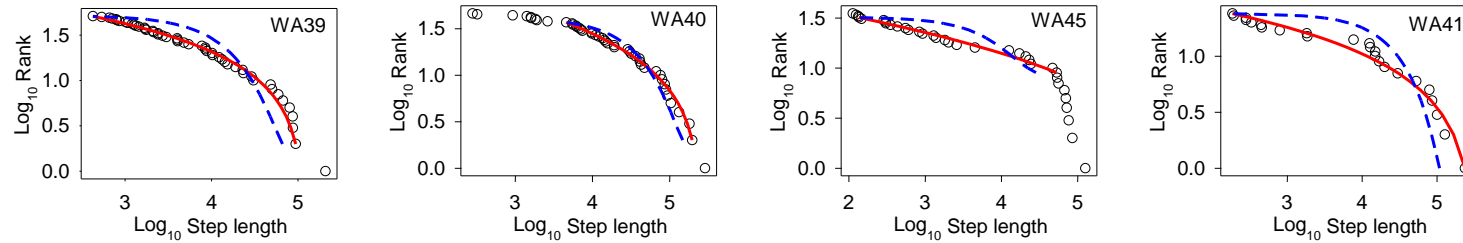| Reference	Steps	Min Step	Max Step	Exp Xmin	Exp Exponent	TP Xmin	TP Exponent	TP Xmax	Exp AICw	Exp Comp AICw	TP AICw	TP Comp AICw	Exp Fit	TP Fit	TP Orders of magnitude	Exp Orders of magnitude
WA46	14	108	108715	542	3.23E-05	108	0.91	35160	0.26	0.74	0.63	0.37	0.229	0.194	2.51	2.30
WA42	13	555	38827	13164	1.34E-04	555	0.93	38827	1.00	0.00	0.81	0.19	0.239	0.172	1.85	0.47
WA35	10	159	132601	159	3.77E-05	20546	4.79	23909	0.31	0.69	--	--	0.233	0.699	0.07	2.92
WA33	8	1235	81093	4610	4.36E-05	1235	1.27	81093	--	--	0.40	0.60	0.375	0.153	1.82	1.25
WA36	4	910	69134	910	3.34E-05	22381	1.00	69134	--	--	--	--	0.421	1.000	0.49	1.88

Figure S7: Truncated Pareto (TP) fits for flight step distributions from wet dry logger data
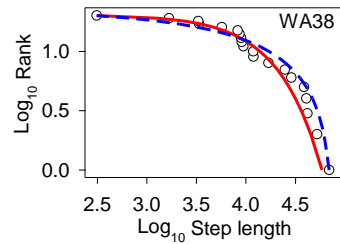

Figure S8: Exponential fit for flight step distributions from wet dry logger data
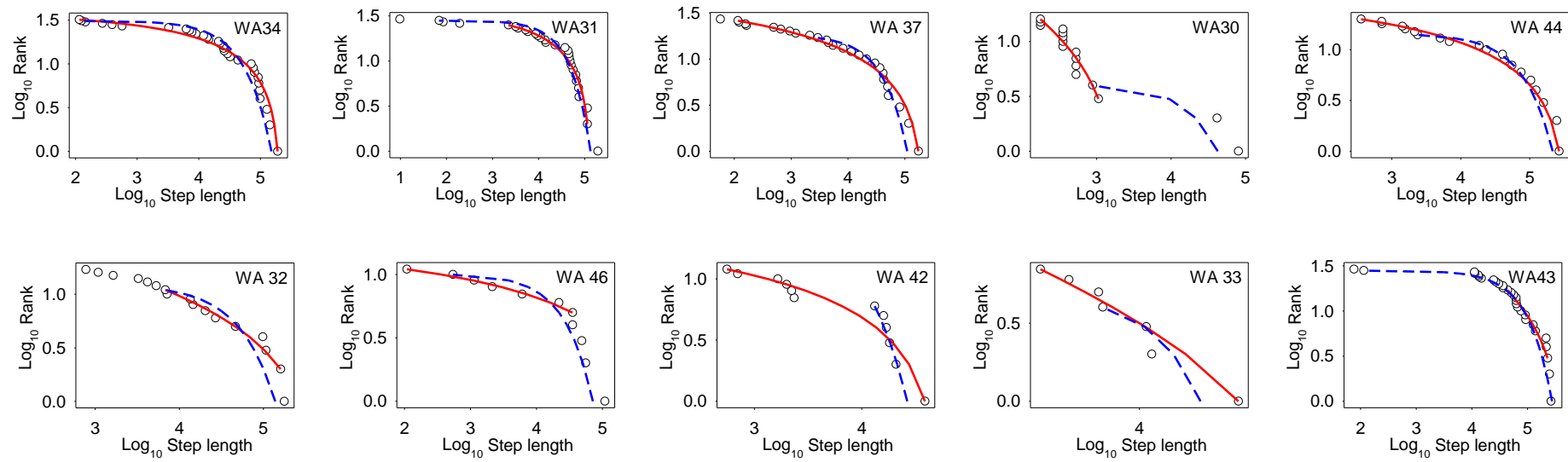
Figure S9: Mixed model fits for flight step distributions from wet/dry logger data. Two shortest plots not show.

2.5 Habitat dependence of Lévy and Brownian movements

Having identified the presence of Lévy and Brownian patterns in the landing distributions of both black-browed and wandering albatrosses (sections 2.1 – 2.5), we next tested whether search patterns were associated with particular habitats. The Lévy flight foraging (LFF) hypothesis (19, 27) predicts that Lévy patterns should occur where resource distributions are sparse and Brownian patterns where resources are more abundant. To test this for albatrosses we calculated the water depths at each landing location as a proxy for habitat type and compared these between birds showing Lévy and Brownian patterns. The Kerguelen and Crozet Islands in the southern Indian Ocean are remote islands with three principal bathymetric domains: namely, shelf waters (depth < 200 m), slope waters (200 to 2000 m; including deep shelf-edge waters, 1500 to 2000 m), and oceanic waters (> 2000 m) (4). Shelf and slope waters are together termed neritic waters (< 2000 m). Therefore, water depth indicates habitat types that have different productivities and resource distributions; for example, primary productivity at the Kerguelen Islands has higher concentrations in neritic waters (Fig. S7A,B) and the squid prey of albatrosses at Crozet are found closer together in neritic than in oceanic waters (4).

Analysis shows that black-browed albatrosses exhibiting a Lévy pattern landed on average over deeper water (mean 520.3 m, S.D. 522.5, random data reduction from $n = 958$ to $n = 165$) than those individuals exhibiting a Brownian pattern (mean 396.8 m, S.D. 561.9, $n = 165$) (t test: t = -2.07, $P < 0.05$). Comparing the 25 deepest habitat depths over which surface landings occurred, confirmed that birds showing Lévy patterns occupied deeper slope waters than Brownian birds (Mann-Whitney test: $W = 524$, $P < 0.05$).

The landing locations of GPS-tracked wandering albatrosses exhibiting a Lévy pattern and for which prey capture data were available, were associated with significantly deeper water habitats than those showing Brownian patterns (Lévy, mean habitat depth 1587.4 m, S.D. 934.3, $n = 23$, random data reduction to match Brownian, with mean 958.3 m, S.D. 601.9, $n = 23$; t test, $t = -2.71$, $P < 0.01$). This is consistent with Lévy search patterns occurring more frequently in deep shelf edge and oceanic habitats than Brownian patterns which occurred mainly in shallow shelf and shelf edge habitats. There were several exceptions to this general pattern. For example, the pattern of landings of albatross WA18 was best described by an exponential distribution, although the prey capture data showed that some 24 of the 25 capture events recorded occurred in oceanic habitat. Mapping the prey capture locations along the track showed that 22 prey capture events took place during 7 landings within a very localised area (45 x 20 km). This shows that WA18 encountered a very abundant patch or patches of prey in

oceanic habitat and because short distances occurred between landings as a result, the dominant pattern found for this bird was best described by Brownian motion. This demonstrates that although Lévy patterns of wandering albatrosses were generally dependent on deep shelf edge and oceanic habitats, a Brownian pattern may dominate when particularly high concentrations of prey are found regardless of habitat. This finding is consistent with predictions of the LFF hypothesis.
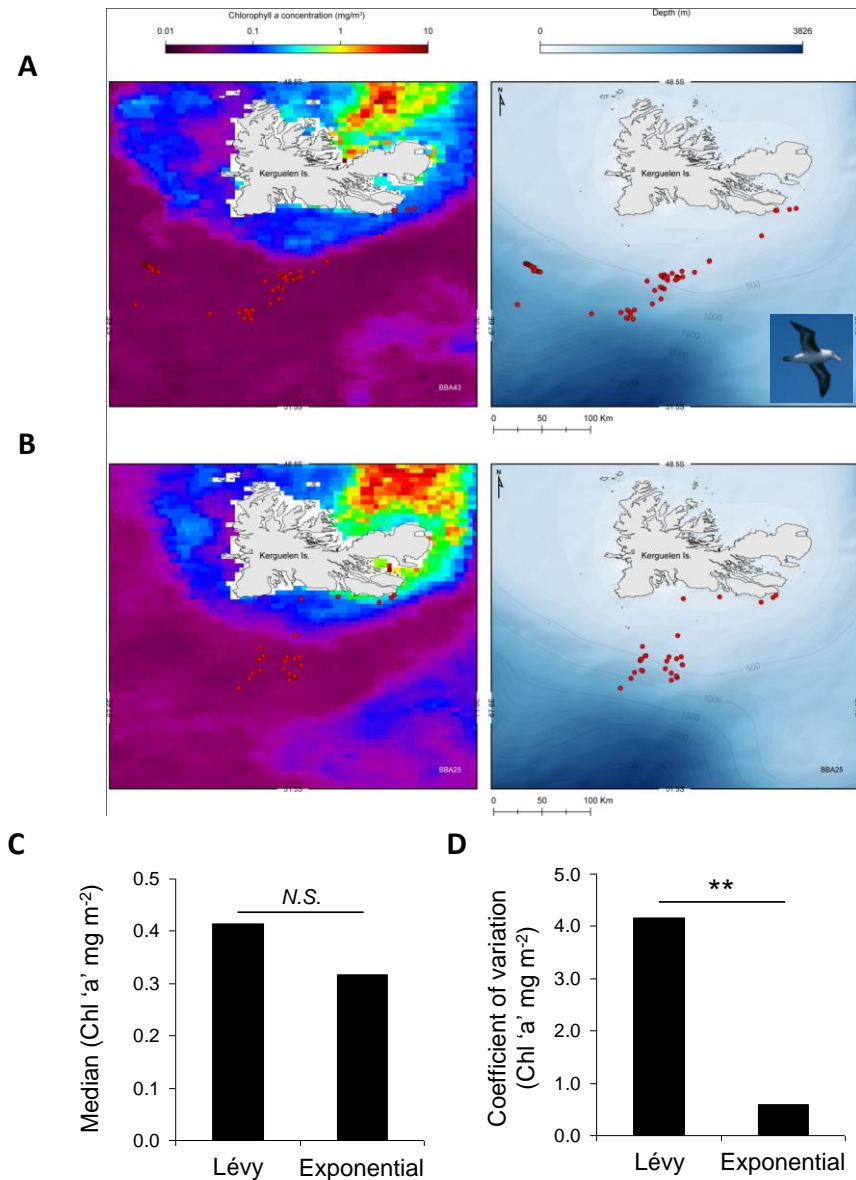
Figure S10. Lévy flight patterns encounter greater environmental heterogeneity. Examples of (*A*) truncated Lévy and (*B*) exponential distributions of distances between landing locations (red circles) for two different black-browed albatrosses off Kerguelen Island and in relation to the distribution of chlorophyll 'a' concentrations, where warm colours represent higher concentrations of primary productivity. (*C*) Median abundance of environmental resources was similar, however (*D*) the variance was over seven times greater during truncated Lévy search patterns of *T. melanophrys* than for exponential (Brownian) foraging patterns. This indicates shelf edge and oceanic habitats supporting Lévy searches by albatrosses were highly heterogeneous compared with shallower habitat where Brownian search occurred; see teext for explanation of habitat differences. N.S. denotes non significance at the 5% level. Test for equal variances in chlorophyll 'a' at Lévy and exponential landing locations: $n = 151$ per group, Levene's test, W = 26.95, $P < 0.001$. ** denotes $P < 0.001$.

3 Reanalysis of 2004 Albatross data

Our analysis of albatross movements from high-resolution GPS tracking of birds foraging in the southern Indian Ocean indicate the presence of movement patterns approximated by Lévy flights and Brownian motion. However, a previous study by Edwards et al. (21) corrected an error in tracking data of wandering albatrosses recorded in 1992 in the Southern Ocean (foraging from Bird Island, South Georgia) (28). Analysis of new data from foraging wandering albatrosses collected in 2004 also contributed to the conclusion that wandering albatrosses do not conduct Lévy flights and, as a consequence therefore, the evidence for biological Lévy flights was weaker, at that time, than previously thought. Nevertheless, the paper by Edwards et al. (21) did not test the LFF hypothesis explicitly on individual albatross tracks. Even though 20 individual wandering albatross wet/dry logger-recorded flight times collected in 2004 were analysed (21)(Supporting Figures S3-S5), MLE fits of the truncated power law distribution to these data were not estimated. Hence, the conclusion that wandering albatross do not exhibit movement patterns consistent with Lévy flights can be considered premature in the absence of statistically robust fitting of an alternative model (e.g. truncated power law distribution) to the ones fitted by Edwards et al. (21) (i.e. exponential and shifted gamma distributions). Therefore, we tested the LFF hypothesis by fitting truncated power law distributions to the data given in Edwards et al. (21) Figures S3-S5.

The 20 datasets in Edwards et al. (21) comprising time steps in seconds of wandering albatrosses tracked with wet/dry loggers in 2004 were kindly provided for reanalysis here by A. M. Edwards and R. A. Phillips. The data required no pre-processing by us and was subject to identical analysis to the albatross data we described previously (see section 1.3), with the one difference being that the correction for discrete data was used as described in Clauset et al. (14). In the original paper (21), the data was pooled and was fitted to a gamma distribution without fitting the x_{min} parameter. Therefore in our study, as well as analysing the datasets separately for individual birds, the datasets were again pooled and were analysed both with and without fitting the x_{min} and x_{max} parameters to provide a direct comparison with Figures S3, S4 and S5 in the original Supplementary Information (21); the pooled results are shown with the reference 2004_P (pooled) and 2004_PNF (pooled no fitting), respectively.

For 20 individual datasets, we found 11 best fits to the truncated power law (TP) distribution and 3 best fits to the exponential distribution with 8 datasets being classified as mixed. Hence, we find good support for the truncated power law (Pareto-Lévy) distribution approximating the

movement pattern of wandering albatrosses. Although we also find support for the exponential distribution it was less prevalent than the truncated power law fit. These results are consistent with other studies analysing the complex behavioural data of marine predators (13, 29), where some individual animal datasets provide good support for Lévy movement while others are best supported by an exponential (i.e. Brownian) movement pattern. It is proposed that the observation of both Lévy and Brownian patterns reflects the complex range of behaviours exhibited by different animals at different times.

Our results of this reanalysis of published data are at odds with the conclusions drawn in the paper by Edwards et al. (21), where no support was found for power law distributed move steps (flight times). It should be noted that in the latter paper no attempt was made to fit a power or truncated power law to either the pooled or individual datasets so no comparison similar to that reported here was possible. As an example, wandering albatross 2004_5 was found here to be best fit by a TP distribution; indeed from visual inspection it seems clear from the plot of this data in Figure S11 in Edwards et al. (21) that the TP best fit we found better describes the empirical data than the shifted gamma or exponential fits shown in the original Supplementary Figure S3. Individual bird 2004_3 (Figure S11)(21) provides another example: in our analysis a best fit to the TP distribution was found for this dataset comprising only 29 data points. With the limited size of individual datasets in terms of data points for MLE analysis available here compared to previous studies (e.g. 13, 29), it is also relevant to note that although the MLE methodology finds best fit values for x_{min} and x_{max}, in nearly all the datasets we analysed the x_{max} fitted value was also the maximum value in the data. Therefore, the best fits presented here are fits to most of the dataset in each case since very few data were not included in the best fit model using the method of Clauset et al. (14).

Our results with the pooled data of 20 wandering albatrosses from 2004 are also interesting and contrast with those of Edwards et al. (21). With both analysis methods (i.e. fitting of x_{min} and x_{max} and no fitting) the pooled data was best fit by a TP distribution. However, when best fitting is performed there is a conflict between the wAIC values for the exponential and TP best fits, which was here resolved by the GOF value which favoured the TP distribution. However, there is a serious problem with pooling datasets comprising complex movement data, as Edwards et al (21) have done. While pooling homogenous data can result in more powerful statistical testing (30), this is not the case with complex heterogeneous data. The datasets analysed in this study describe movements from individual animals, each of which are likely to be behaving and moving in different ways. Pooling such data confuses these individual movements and can have unpredictable results, such as concluding the presence of Lévy flight when it is not

36

exhibited by any one individual, and concluding Brownian motion even though an individual in the pool may have a very different behaviour pattern (e.g. 22, 31). This difference can be seen in the comparison of the MLE results obtained with the pooled data and an individual dataset such as 2004_11, both shown in Figure S11, where it is clear that not only does the individual data fit a TP distribution but the difference in the observed step lengths is quite noticable. Therefore, for an unbiased test of whether albatrosses exhibit movements approximated by Lévy flights it was preferable to analyse individual movement trajectories by fitting both truncated power law and exponential distributions. In summary, we find no support for the conclusion of Edwards et al. (21) questioning the strength of the evidence for biological Lévy flights and find that this was both incorrect and premature.

3.1 2004 Data reanalysis: MLE results

In the following tables, Comp AIC refers to the competing distribution.

Table S13. Data reanalysis showing TP fits

Reference	Steps	Min Step	Max Step	Xmin	Exponent	Xmax	Exp AICw	Exp Comp AICw	TP AICw	TP Comp AICw	Exp Fit	TP Fit	Fitted steps	Order of magnitude
2004_P	1416	40	53590	40	1.05	23430	1.00	0.00	1.00	0.00	0.105	0.052	1396	2.77
2004_PNF	1416	40	53590	40	1.05	23430	1.00	0.00	1.00	0.00	0.105	0.052	1396	2.77
2004_18	171	40	36130	230	1.10	14280	0.96	0.04	1.00	0.00	0.170	0.047	133	1.79
2004_11	119	40	30190	40	1.22	30190	0.00	1.00	1.00	0.00	0.248	0.102	118	2.88
2004_12	113	40	30410	180	1.16	30410	0.00	1.00	1.00	0.00	0.239	0.055	94	2.23
2004_20	82	40	29490	40	1.01	12430	0.00	1.00	1.00	0.00	0.251	0.092	77	2.49
2004_05	66	40	21210	350	1.44	21210	0.50	0.50	1.00	0.00	0.140	0.104	43	1.78
2004_16	60	40	24380	110	1.42	24380	0.05	0.95	1.00	0.00	0.273	0.074	44	2.35
2004_14	51	40	19430	40	1.59	2590	0.22	0.78	1.00	0.00	0.211	0.187	40	1.81
2004_13	42	40	21070	40	1.21	21070	0.19	0.81	1.00	0.00	0.147	0.123	41	2.72
2004_03	29	50	21760	320	1.13	21760	0.39	0.61	0.97	0.03	0.166	0.099	22	1.83

Table S14. Data reanalysis showing exponential fits

Reference	Steps	Min Step	Max Step	Xmin	Exponent	Exp AICw	Exp Comp AICw	TP AICw	TP Comp AICw	Exp GOF	TP GOF	Fitted steps	Orders of magnitude
2004_08	64	40	53590	70	1.78E-04	1.00	0.00	1.00	0.00	0.097	0.114	54	2.88
2004_07	64	40	35940	320	1.67E-04	0.99	0.01	1.00	0.00	0.062	0.098	37	2.05
2004_17	24	40	20600	230	2.90E-04	0.90	0.10	0.97	0.03	0.122	0.176	18	1.95

Table S15. Data reanalysis showing mixed model fits

Reference	Steps	Min Step	Max Step	Exp Xmin	Exp Exponent	TP Xmin	TP Exponent	TP Xmax	Exp AICw	Exp Comp AICw	TP AICw	TP Comp AICw	Exp Fit	TP Fit	TP Orders of magnitude	Exp Orders of magnitude
2004_15	133	50	40020	720	1.94E-04	110	0.97	14960	0.99	0.01	1.00	0.00	0.080	0.050	2.13	1.74
2004_01	117	40	22660	690	2.47E-04	50	0.96	13980	0.93	0.07	1.00	0.00	0.121	0.045	2.45	1.52

Reference	Steps	Min Step	Max Step	Exp Xmin	Exp Exponent	TP Xmin	TP Exponent	TP Xmax	Exp AICw	Exp Comp AICw	TP AICw	TP Comp AICw	Exp Fit	TP Fit	TP Orders of magnitude	Exp Orders of magnitude
2004_10	73	100	12950	100	4.40E-04	350	1.04	6650	0.99	0.01	0.99	0.01	0.125	0.120	1.28	2.11
2004_06	62	50	10900	180	3.45E-04	50	0.84	10900	0.06	0.94	1.00	0.00	0.127	0.082	2.34	1.78
2004_02	50	40	30500	180	2.25E-04	40	0.74	12230	0.93	0.07	1.00	0.00	0.150	0.084	2.49	2.23
2004_09	40	50	34230	1250	1.06E-04	50	0.90	34230	0.48	0.52	1.00	0.00	0.102	0.077	2.84	1.44
2004_04	34	70	36680	120	2.40E-04	110	0.77	6480	0.02	0.98	0.89	0.11	0.173	0.076	1.77	2.49
2004_19	22	60	15980	330	2.02E-04	60	0.98	15980	0.27	0.73	1.00	0.00	0.167	0.097	2.43	1.69

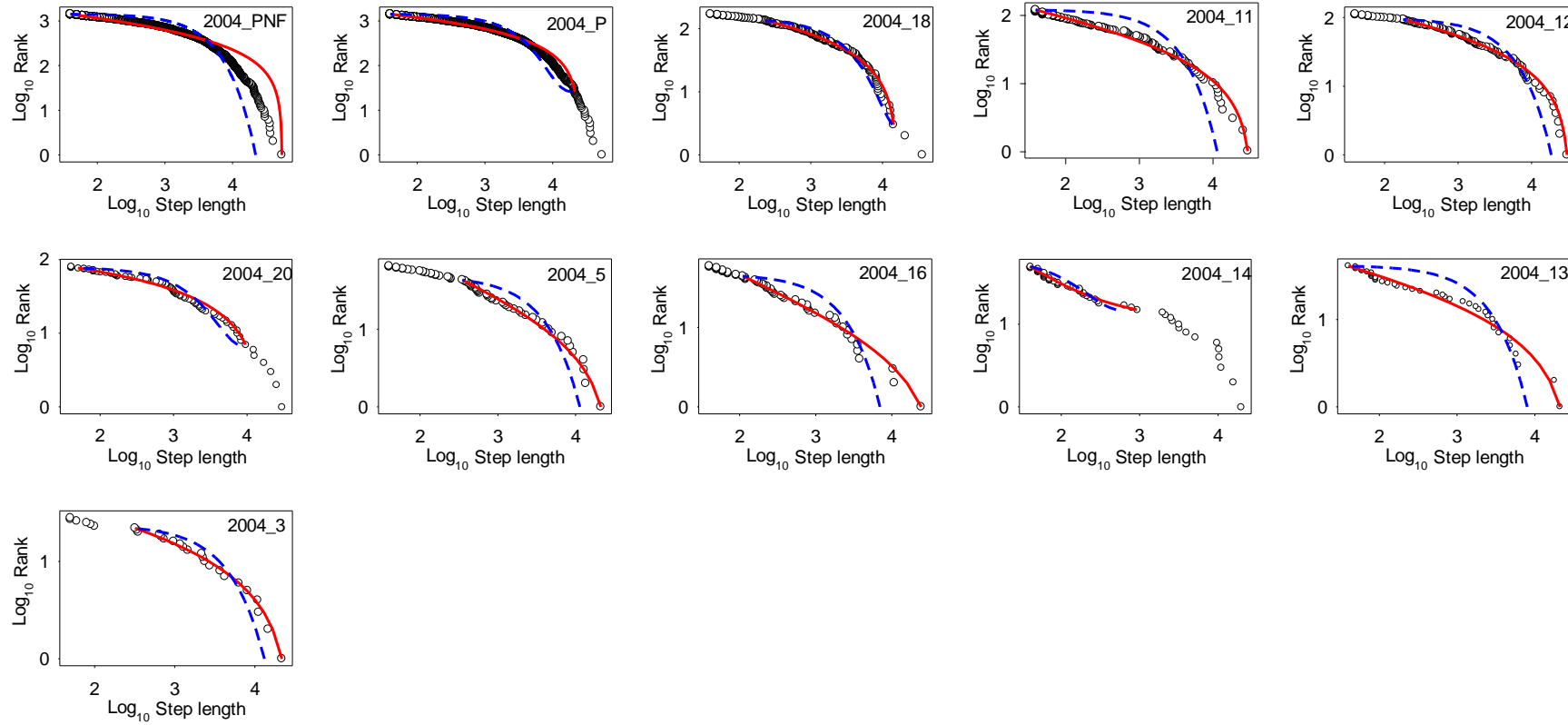## 3.2 2004 Data reanalysis: Ranked step length plots

Figure S11. Truncated Pareto fits from the 2004 reanalysed data. Here the blue dashed line represents the alternate exponential distribution.
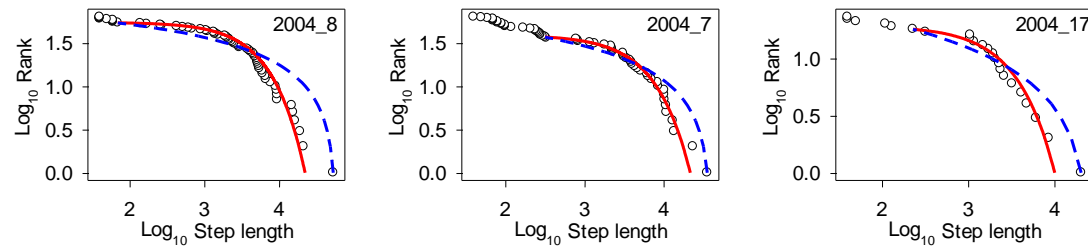
Figure S12. Exponential fits from the 2004 reanalysed data. Red line is the best fit exponential distribution; dashed blue line is the alternate TP.
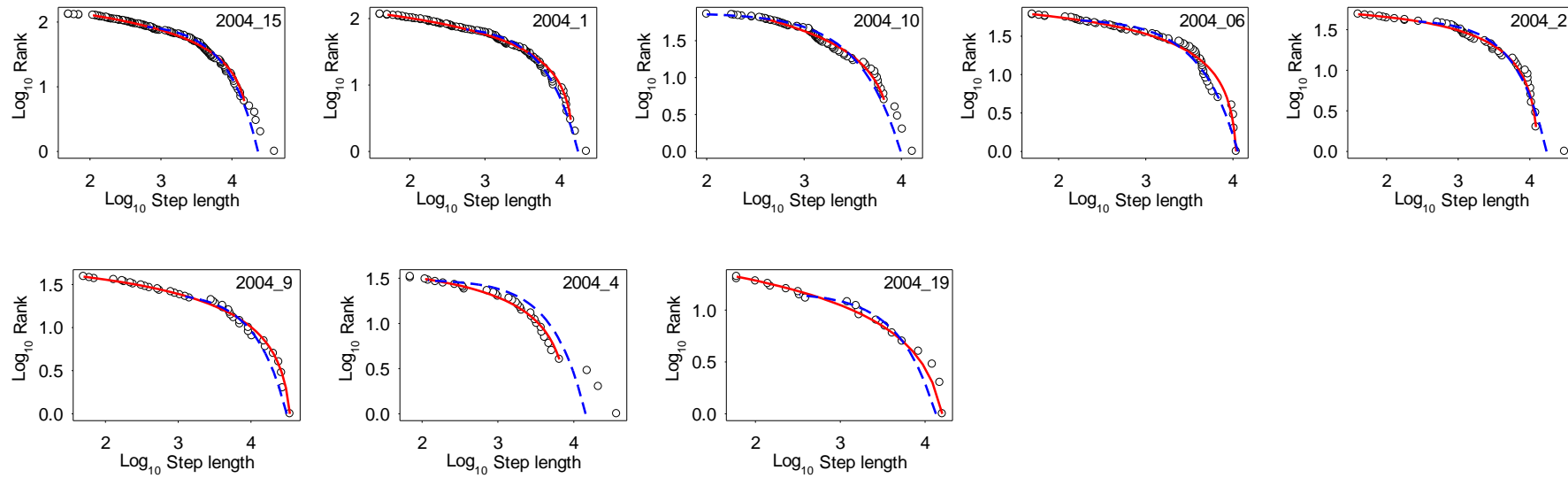

Figure S13. Mixed model fits from the 2004 reanalysed data. The plots show the best fitting TP (red) and best fitting exponential (blue dashed) distributions.

4 References

1. Weimerskirch H, Doncaster CP, & Cuenotchaillet F (1994) Pelagic seabirds and the marine-environment: foraging patterns of wandering albatrosses in relation to prey availability and distribution. *Proc. R. Soc. B: Biol. Sci.* **255,** 91-97.

2. Weimerskirch H*, et al.* (2002) GPS tracking of foraging albatrosses *Science* **295,** 1259.

3. Weimerskirch H, Pinaud D, Pawlowski F, & Bost CA (2007) Does prey capture induce area-restricted search? A fine-scale study using GPS in a marine predator, the wandering albatross. *Am. Nat.* **170,** 734-743.

4. Weimerskirch H, Gault A, & Cherel Y (2005) Prey distribution and patchiness: Factors in foraging success and efficiency of wandering albatrosses. *Ecology* **86,** 2611-2622.

5. Richardson PL (2011) How do albatrosses fly around the world without flapping their wings? *Progress in Oceanography* **88,** 46-58.

6. Bartumeus F, Da Luz MGE, Viswanathan GM, & Catalan J (2005) Animal search strategies: A quantitative. random-walk analysis. *Ecology* **86,** 3078-3087.

7. Shlesinger MF, Zaslavsky GM, & Klafter J (1993) Strange kinetics *Nature* **363,** 31-37.

8. Fritz H, Said S, & Weimerskirch H (2003) Scale-dependent hierarchical adjustments of movement patterns in a long-range foraging seabird. *Proc. R. Soc. B: Biol. Sci.* **270,** 1143-1148.

9. Nams VO (2005) Using animal movement paths to measure response to spatial scale. *Oecologia* **143,** 179-188.

10. Pinaud D & Weimerskirch H (2005) Scale-dependent habitat use in a long-ranging central place predator. *J. Anim. Ecol.* **74,** 852-863.

11. Wakefield ED*, et al.* (2009) Wind field and sex constrain the flight speeds of central-place foraging albatrosses. *Ecol. Monogr.* **79,** 663-679.

12. Bartumeus F, Catalan J, Fulco UL, Lyra ML, & Viswanathan GM (2002) Optimizing the encounter rate in biological interactions: Lévy versus Brownian strategies. *Phys. Rev. Lett.* **88,** 4.

13. Humphries NE*, et al.* (2010) Environmental context explains Lévy and Brownian movement patterns of marine predators. *Nature* **465,** 1066-1069.

14. Clauset A, Shalizi CR, & Newman MEJ (2009) Power-law distributions in empirical data. *SIAM Rev.* **51,** 661-703.

15. White EP, Enquist BJ, & Green JL (2008) On estimating the exponent of power-law frequency distributions. *Ecology* **89,** 905-912.

16. Kagan YY (2002) Seismic moment distribution revisited: I. Statistical results. *Geophys. J. Int.* **148,** 520-541.

17. Burnham KP & Anderson DR (2004) Multimodel inference - understanding AIC and BIC in model selection. *Sociol. Methods. Res.* **33,** 261-304.

18. Bartumeus F (2007) Lévy processes in animal movement: An evolutionary hypothesis. *Fractals* **15,** 151-162.

19. Viswanathan GM, Raposo EP, & da Luz MGE (2008) Lévy flights and superdiffusion in the context of biological encounters and random searches. *Phys. Life Rev.* **5,** 133-150.

20. Sims DW, Righton D, & Pitchford JW (2007) Minimising errors in identifying Lévy flight behaviour of organisms. *J. Anim. Ecol.* **76,** 222-229.

21. Edwards AM*, et al.* (2007) Revisiting Lévy flight search patterns of wandering albatrosses, bumblebees and deer. *Nature* **449,** 1044-1048.

22. Petrovskii S, Mashanova A, & Jansen VAA (2011) Variation in individual walking behavior creates the impression of a Levy flight. *Proc. Natl Acad. Sci. U.S.A.* **108,** 8704-8707.

23. Mackley EK*, et al.* (2010) Free as a bird? Activity patterns of albatrosses during the nonbreeding period. *Mar. Ecol.-Prog. Ser.* **406,** 291-303.

24. Phalan B*, et al.* (2007) Foraging behaviour of four albatross species by night and day. *Mar. Ecol. Prog. Ser.* **340,** 271-286.

25. Weimerskirch H & Guionnet T (2002) Comparative activity pattern during foraging of four albatross species. *Ibis* **144,** 40-50.

26. Waugh SM & Weimerskirch H (2003) Environmental heterogeneity and the evolution of foraging behaviour in long ranging greater albatrosses. *Oikos* **103,** 374-384.

27. Viswanathan GM, Luz MGE, Raposo EP & Stanley HE (2011) *The Physics of Foraging: An Introduction to Random Searches and Biological Encounters* (Cambridge University Press, New York).

28. Viswanathan GM*, et al.* (1996) Lévy flight search patterns of wandering albatrosses. *Nature* **381,** 413-415.

29. Sims DW*, et al.* (2008) Scaling laws of marine predator search behaviour. *Nature* **451,** 1098-1102.

30. Zar JH (1999) *Biostatistical Analysis 4ᵗʰ edition* (Prentice Hall).

31. Codling EA & Plank MJ (2011) Turn designation, sampling rate and the misidentification of power laws in movement path data using maximum likelihood estimates. *Theor. Ecol.* **4,** 397-406.